“गेहूं में नाइट्रोजन उपयोग दक्षता (एनयूई) का फेनोमिक्स और जेनेटिक विश्लेषण”

“PHENOMICS AND GENETIC ANALYSIS OF NITROGEN USE EFFICIENCY (NUE) IN WHEAT (*Triticum aestivum* L.)”

BISWABIPLAB SINGH

DIVISION OF PLANT PHYSIOLOGY

ICAR – INDIAN AGRICULTURAL RESEARCH INSTITUTE

NEW DELHI – 110012

2023

"PHENOMICS AND GENETIC ANALYSIS OF NITROGEN USE EFFICIENCY (NUE) IN WHEAT (*Triticum aestivum* L.)"

BY

BISWABIPLAB SINGH

A Thesis Submitted to the Faculty of the Graduate School,

Indian Agricultural Research Institute, New Delhi,

In partial fulfilment of the requirements

For the award of the degree of

DOCTORATE OF PHILOSOPHY
in
PLANT PHYSIOLOGY

2023

Approved by:

Chairperson	**Dr. Viswanathan Chinnusamy**	
Co-chairperson	**Dr. Lekshmy S.**	
Members	**Dr. Sudhir Kumar**	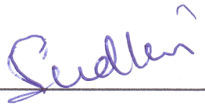
	Dr. Monika Dalal	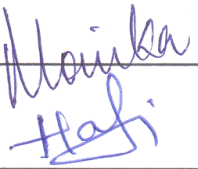
	Dr. Harikrishna	
	Dr. Rabi Narayan Sahoo	

Division of Plant Physiology
ICAR-Indian Agricultural Research Institute,
New Delhi – 110012

Dr. Viswanathan Chinnusamy
Joint Director (Research) &
Principal Scientist

CERTIFICATE

This is to certify that the thesis entitled **"PHENOMICS AND GENETIC ANALYSIS OF NITROGEN USE EFFICIENCY (NUE) IN WHEAT (*Triticum aestivum* L.)"** submitted to the Faculty of the Graduate School, ICAR - Indian Agricultural Research Institute, New Delhi, in partial fulfilment of the requirements for the award of **DOCTORATE of PHILOSOPHY in PLANT PHYSIOLOGY**, embodies the results of the *bona fide* research work carried out by **Mr. BISWABIPLAB SINGH**, **Roll No. 11097** under my guidance and supervision, and that no part of this thesis has been submitted for any other degree or diploma. It is further certified that any help or source of information that has been availed of in this connection has been duly acknowledged by him.

Date: **27/09/2023**

Place: **New Delhi**

(Dr. Viswanathan Chinnusamy)

Chairperson – Advisory committee

ACKNOWLEDGEMENT

It is time to remember all those who made this moment to happen in my life which I dreamt for. I would like to thank Almighty for blessing me with this moment to happen in my life. I acknowledge **I.A.R.I.** for providing the financial support and providing all physical facilities to undertake this work at this premier institute.

Sincere gratitude to my Chairman, **Dr. Viswanathan Chinnusamy, Joint Director (Research),** Indian Agricultural Research Institute. Without his sincere guidance, efforts and involvement, the proposed research couldn't be completed. He nurtured my capabilities and gave me ample freedom to work. His positive attitude and hardworking nature will always inspire me throughout my life.

My sincere gratitude towards the members of the advisory committee comprising of **Dr. Lekshmy S.,** Senior Scientist, Division of Plant Physiology, **Dr. Sudhir Kumar,** Senior Scientist, Division of Plant Physiology, **Dr. Monika Dalal,** Principal Scientist, NIPB, **Dr. Harikrishna,** Scientist, Division of Genetics, **Dr. Rabi Narayan Sahoo,** Principal Scientist, Division of Agricultural Physics, who always helped me in sorting out problems which occurred during the course of investigation.

I am grateful to **Dr. Renu Pandey,** Head & Professor, Division of Plant Physiology, IARI, New Delhi for her ever-willing help and concern, and providing **CHNS** facility.

My sincere gratitude also goes to **Dr. Sudhir Kumar,** Senior Scientist, Division of Plant Physiology ICAR-IARI, New Delhi; **Dr. Harikrishna,** Scientist, Division of Genetics, ICAR-IARI, New Delhi for their precious

suggestions, contribution and thoughts. I am thankful to **Dr. Monika Dalal**, Principal Scientist, ICAR-NIPB for developing and providing the **RILs** used in this study.

I feel grateful to all teaching and non-teaching staffs of Division of Plant Physiology, ICAR-IARI, New Delhi for providing me healthy working environment. My thanks also go to all the members of Nanaji Deshmukh Plant phenomics Centre, ICAR – IARI, New Delhi, including **Dr. Dhandapani R., Dr. Mahesh Kumar and Dr. Madhurima** for their support and help during my research work.

I am especially thankful to my friends: **Satya, Shelly, Ipsita, Sandeep, Payal, Devika, Adhip, and Jyotirmaya** with whom I started my journey at IARI, New Delhi and had a wonderful time. I would also acknowledge my lab members: **Elangovan A, Nguyen Trung Duc, Nidhi, China, Rohit, Harika and Shiva** at Nanaji Deshmukh Plant Phenomics Centre, ICAR-IARI, New Delhi for their support and helping during my research work. I also thank **Swati Goel, Devendra Vasht, Mr. Rahul Tiwari, Mrs. Poonam Gupta, Mr Manish, Mr Sonu Ola, and Mr Pradeep** for their technical assistance.

I am grateful to **my seniors Sukumar Taria, Samir Ranjan Mishra, Soubhagya bhai, Krishna Kumar Jangid, Prince Choyal** for their support in my research work. I am also really grateful to my juniors **Vivek, Swain, Kirti, Nrusingh, Birendra, Naresh, Manoranjan, Manik, Sunny and Dipankar** for their support in my research work and daily life.

I sincerely acknowledge the Molecular stress physiology l*ab* Dr. Santosh Kumar V.V., Chandrapal Viswakarma, Dr. Rakesh Kumar, Dr. Shashank Yadav, Pragya and Dr Shivani for helping me in successful completion of

research work. I would also like to thanks our workers at phenomics, Ramesh, Lavkush, Muna, Parveen, Kanhaiya ji and Pushpender ji, who helped me during my work.

I do express my deep sense of gratitude and indebtedness to **my mother, my father, brothers and sisters** for their affection and encouragement.

Finally, but not the least I would like to remember all those people whose names were difficult to incorporate but were directly or indirectly involved in providing the help and moral support during the entire study period.

I would like to acknowledge **CSIR** for providing fellowship during my Ph.D. study. Also, I would like to thank **NAHEP-CAAST** for providing research grant to carry out part of my research work.

(Biswabiplab Singh)

Date: **27/09.2023**

Place: **New Delhi**

CONTENTS

ACKNOWLEDGEMENT ..... **i**
LIST OF FIGURES ..... **vii**
LIST OF TABLES ..... **xiv**
1 INTRODUCTION **1**
2 REVIEW OF LITERATURE **3**
2.1 Wheat – a major cereal crop in the world 3
2.1.1 Wheat Genetics 4
2.1.2 Nitrogen in agriculture 4
2.1.3 Wheat and nitrogen use 7
2.1.4 Problems associated with nitrogen in agriculture 7
2.2 Effect of nitrogen deficiency in wheat 9
2.3 Nitrogen Use Efficiency (NUE) 10
2.3.1 Nitrogen uptake efficiency (NUpE) 13
2.3.2 Nitrogen utilisation efficiency (NUtE) 13
2.3.3 Nitrogen Harvest Index 14
2.4 Traits influencing N-Uptake Efficiency 14
2.4.1 Root size and morphology related traits 14
2.4.2 Root N transporter systems 15
2.4.3 Interaction with micro-organisms 15
2.5 Traits Influencing N Utilization Efficiency 16
2.5.1 Nitrate assimilation 16
2.5.2 Canopy photosynthetic capacity 17
2.5.3 Post-anthesis N remobilization and senescence dynamics 18
2.5.4 Augmenting grain protein concentration and composition 19
2.6 Phenotyping for NUE 19
2.6.1 Root phenotyping method 19
2.6.2 Canopy phenotyping methods 20
2.6.3 Genetic Diversity in N-use Efficiency and its component traits 20
2.7 Specific traits for potential improvement for NUE 21
2.7.1 Identifying novel genes 21
2.7.2 Targeting specific genes and processes 21
2.8 Selecting for natural variation in NUE 24
2.9 Rationale for improved N economy 24
2.10 Management strategies for improving NUE 24

2.10.1 Advancement in fertilisation 25
2.11 Why high-throughput phenotyping? 26
2.12 High-throughput phenotyping is vital for the future of plant phenotyping 26
2.13 Phenotyping for nitrogen deficiency response and NUE 27
2.14 Linkage map and QTL mapping 33
2.14.1 Genetic map description 33
2.14.2 Construction of genetic map 33
2.14.3 Genetic mapping populations 34
2.14.4 Choice of suitable parents 34
2.14.5 Population Maps 34
2.14.6 Population size 34
2.15 Molecular markers 35
2.15.1 Single-nucleotide polymorphism (SNP) markers 36
2.15.2 Types of SNP array available 36
2.16 Genetic dissection of NUE and component traits 37
2.16.1 QTLs for wheat NUE and its component traits 39
3 MATERIALS & METHODS 41
3.1 Experimental site and setup 41
3.2 Experimental design and plant growth condition 43
3.3 Plant material and mapping population 43
3.4 The 2-factorial experiment 44
3.5 Experimental design for biomass estimation 46
3.6 Image based phenotyping in plant phenomics facility 47
3.7 Image acquisition and analysis 48
3.7.1 Image capturing 48
3.7.2 Image processing 49
3.7.3 RGB, IR and NIR image acquisition and processing 50
3.8 Feature analysis and data transformation for biomass prediction 53
3.9 Modelling for predicting plant biomass 53
3.10 Evaluation of the Models Performance 54
3.11 Manual data collection 54
3.11.1 Phenology parameters: days to booting, days to heading, days to maturity. 54
3.11.2 Agronomical parameters 54
3.11.3 Yield parameters 54
3.11.4 Shoot and grain N concentration measurement: 56
3.12 Nitrogen Use Efficiency Estimation 57
3.13 Semi-automatic seed parameter estimation 57

3.14 Statistical analysis and data visualisation 58
3.14.1 Broad sense heritability (H^2) 58
3.14.2 Donor selection 58
3.15 Genotyping 59
3.15.1 DNA Extraction with Purification Protocol 60
3.16 Linkage map construction and QTL mapping 61
3.17 Identification of putative candidate genes 61
4 RESULTS 62
4.1 Component traits characterization for NUE 62
4.1.1 High throughput phenotyping for NUE component trait characterization 64
4.1.2 Manual phenotyping for component traits of NUE 122
4.1.3 Semi-automated phenotyping for seed trait characterization 134
4.1.4 Donor selection 135
4.2 Genetic basis dissection of nitrogen use efficiency and component traits in wheat 136
4.2.1 Linkage map construction 136
4.2.2 The reliability of the linkage map for QTL mapping 151
4.2.3 QTL mapping for NUE and component traits 151
4.2.4 Effect of QTLs 176
4.3 Candidate gene analysis within major QTL regions 178
5 DISCUSSION 182
5.1 Prediction of plant biomass and leaf area in wheat using machine learning approaches 183
5.2 A HTP approach for characterization of NUE and component traits in wheat 187
5.3 Phenomics analysis of whole plant transpiration and water use in wheat RILs 187
5.4 Phenomics based phenotyping of wheat RILs for NUE and nitrogen deficiency responses 188
5.5 Manual and semi-automatic traits capturing the NUE and N deficiency response 189
5.6 Genetic relationships between kernel size and quality traits 191
5.7 NUE status of wheat RILs 192
5.8 QTLs for NUE and its component traits 192
5.9 Candidate genes underlying major QTLs 194
6 SUMMARY & CONCLUSIONS 196
7 ABSTRACT (English) 201
8 सार 203
9 BIBLIOGRAPHY 205
10 ANNEXURES 243

LIST OF FIGURES

Figure 2.1: Global wheat production trend (FAOSTAT, 2020)..... 3

Figure 2.2: Relationship between the nitrogen sources, uptake, utilization (Raigar et al., 2022)..... 5

Figure 2.3: Regional consumptions of all types of nitrogen fertilizers in 1980 and 2016 (in million metric tonnes)..... 6

Figure 2.4: Nitrogen forms due to microbial activity (Cormier et al., 2016)..... 8

Figure 2.5: Lowering wheat N requirement as a mean to balance N supply and demand (Fradgley et al., 2021)..... 8

Figure 2.6: Strategies to enhance sustainable yield through NUE (Liu et al., 2022)..... 10

Figure 2.7: Characterisation of NUE in wheat (Hawkesford and Griffiths 2019)..... 11

Figure 2.8: NUE determination by different traits (Hawkesford and Riche 2020)..... 12

Figure 2.9: Nitrogen assimilation and uptake in wheat. HATS: High Affinity transporters; LATS: Low affinity transporters (Islam et al., 2021)..... 16

Figure 2.10: DELLA-mediated trade-off between growth and N metabolism. (a) GA lifts DELLA repression of plant growth and N metabolism. (b) In the absence of GA, DELLA accumulation restrains plant growth and N metabolism (Liu et al., 2022)..... 23

Figure 2.11: Framework for Producing Low-N-Requirement Crops (Swarbreck et al., 2019)..... 37

Figure 2.12: Way forward for the development of nitrogen efficient wheat varieties (Hawkesford and Griffiths et al., 2019)..... 38

Figure 3.1:Drone view of Nanaji Deshmukh Plant Phenomics Centre, IARI-ICAR, New Delhi..... 41

Figure 3.2: Photograph of Nanaji Deshmukh Plant Phenomics Centre (NDPPC), IARI-ICAR, New Delhi, India. A) Front aerial view of NDPPC B) Rear-side view of NDPPC at sunset C) Picturesque view of greenhouses of NDPPC..... 42

Figure 3.3: Experiment preparation phase. A) Soil sieving B) Pot filling C) Soil moisture estimation D) Pot transfer..... 43

Figure 3.4: Wheat NUE experiment at NDPPC. A) Seed preparation B) Pot filling with soil by weighing C) Wheat seedling emergence D) First split dose of fertilizer at tillering E) Pot barcoding for identification F) Visual difference between C and N deficiency in RILs..... 44

Figure 3.5: Wheat NUE experiment details. A) Plants showing visual N deficiency and ready to load in the conveyer B) Barcoded plants on moving field conveyer in greenhouses C) Manual data collection D) Wheat at harvesting stage..... 45

Figure 3.6: Imaging and watering facility at NDPPC. A) Wheat NUE experiment in climate-controlled greenhouse B) Individual imaging sensor platforms C) LemnaTec control main system D) Camera

installed inside imaging chambers with light source E) RGB imaging platform F) Automatic weighing and watering station (One inside each four greenhouses and one in imaging area). 47

Figure 3.7: Stagewise phenotypic behavior of RILs under control and nitrogen deficiency. 48

Figure 3.8: Modalities present in LemnaTec systems (A) and image processing pipeline (B). 49

Figure 3.9: Image acquisition process..... 50

Figure 3.10: Checker board for image calibration. 52

Figure 3.11: Yield and grain morphology characterization 55

Figure 3.12: Yield trait estimation in wheat NUE experiment. A) Plants at harvest maturity stage inside greenhouse B) & C) Manual yield parameter recording D) Separate main ear from tiller ear E) Imaging was done of each main ear spike F) Main ear seeds. 55

Figure 3.13: CHNS Analyzer for C and N estimation. A) High precision weighing balance for tissue weighing and packing in tin foils B) The combustion instrument with its attached PC. 56

Figure 3.14: Semi-automated seed analyser setup for seed morphological trait estimation. 57

Figure 3.15: DNA extraction, purification and quantification method. A) Tissue grinding and kept in lysis buffer B) DNA pellet drying after ethanol wash C) Ethanol wash of DNA D) DNA storage E) Genomic DNA presence evaluation F) DNA quantification by Nanodrop. 59

Figure 4.1: Complex trait characterization in wheat. 62

Figure 4.2: Combinatorial approach for wheat N-deficiency response study. 62

Figure 4.3: High-throughput phenotyping of wheat. 63

Figure 4.4: Functionalities of Nanaji Deshmukh Plant Phenomics Centre, New Delhi, India. 65

Figure 4.5: Phenome characterization of NUE in wheat. 67

Figure 4.6: Figure 4.6: Data analysis and modelling pipeline for biomass prediction by i-Traits. A) Digital imaging-based plant phenotyping by visible (or color) and near-infrared sensors (NIR). B) Image datasets were saved in data server and processed through LemnaGrid for feature extraction. C) Phenotypic data were subjected to quality check to remove low-quality data and classified into two categories such as architectural and physiological traits (Commonly referred as i-Traits). D) All the i-Traits were described by per plant basis and combined with manually measured data such as fresh weight (FW), dry weight (DW) and shoot area. E) Now the data matrix with all i_Traits and manual traits were used to predict biomass by HTPmod (a shiny based application) using eight machine learning method developed by Chen *et.al* (2019). F) The results of aal the models were interpreted by R^2, PCC and RMSRE value..... 68

Figure 4.7: Characterization of all the i-Traits by phenotypic analysis for both experiments (Experiment 1 and Experiment 2). A, B) Principal component analysis of all the i-Traits for experiment 1 and experiment 2 respectively. Four PCs represented here which captured approximately all the variation in

the data. Variance proportion explained by the PCs is shown in parentheses. Individuals are represented by orange dots and traits are represented by green lines. C, D, E) Differences in the FW, DW and shoot area across experiments represented by box plot analysis. 70

Figure 4.8: Assessment of trait similarity between i-Traits across experiments. A) Canonical correlation analysis of i-Traits based on experiment 1 (Top) and B) experiment 2 (Bottom). Heatmap plot is organized by both architectural and physiological traits represented by two highlighted boxes. Top box represents Architectural traits and bottom box represents physiological traits. 71

Figure 4.9: Pearson's correlation coefficients (PCC) in each experiment were calculated to assess the relationship between i-Traits and manual traits. The PCC were consistent in both experiments and most of the features were having more than 0.5 positive or negative correlation coefficients with FW, DW and shoot area. A, B) PCC between FW and i-Traits in experiment 1 and 2 respectively. C, D) PCC between DW and i-Traits in experiment 1 and 2 respectively. E, F) PCC between shoot area and i-Traits in experiment 1 and 2 respectively. 72

Figure 4.10: Nondestructive estimation of above ground plant biomass (AGPB) with i-Traits, using predmod in HTPmod. Scatter plots of observed FW vs predicted FW values using 8 prediction models based on machine learning methods BLASSO, BRNN, GLMNET, GP-Poly, MARS, RF, RIDGE and SVR. The prediction models were evaluated by Pearson's correlation coefficient (*r*), its corresponding *P*-value, R^2 and RMSRE. A and B) Prediction of FW in experiment 1 and 2 respectively. C) Evaluation of the model performance of each regression model used for AGPB prediction. 74

Figure 4.11: Non destructive estimation of DW by using i-Traits. A and B) Prediction of DW in experiment 1 and 2 respectively. C) Summary of the predictive power of each regression model. 75

Figure 4.12: Nondestructive estimation of shoot area by using i-Traits. A and B) Prediction of shoot area in experiment 1 and 2 respectively. C) Summary of the predictive power of each regression model. 76

Figure 4.13: Estimation of predictive power and relative importance of features (i-Traits) used in regression models. Bayesian-LASSO (BLASSO) model was used for wheat FW, DW and shoot area prediction, using i-Traits from two independent experiments. But as both experiments performed relatively similar with respect to prediction power and relative importance, experiment 1 information is presented here for the ease of understanding. A, C and E) Relative importance of i-Traits used for FW, DW and shoot area prediction respectively. B, D and F) Predictive power of i-Traits used for FW, DW and shoot area prediction respectively. 78

Figure 4.14: Phenomics Traits Extraction. 80

Figure 4.15: Heritability of morphometric traits of 5 stages under control conditions (Stage 1, 2, 3, 4, and 5 are 60, 70, 80, 90 and 100 DAS, respectively). 89

Figure 4.16: Heritability of morphometric traits of 5 stages under nitrogen deficiency conditions (Stage 1, 2, 3, 4, and 5 are 60, 70, 80, 90 and 100 DAS, respectively). 90

Figure 4.17: Heritability of biomass related traits of 5 stages under control (a) and nitrogen deficiency (b) conditions (Stage 1, 2, 3, 4, and 5 are 60, 70, 80, 90 and 100 DAS, respectively). 91

Figure 4.18: Heritability of color related traits of 5 stages under control conditions (Stage 1, 2, 3, 4, and 5 are 60, 70, 80, 90 and 100 DAS, respectively). 92

Figure 4.19: Heritability of color related traits of 5 stages under nitrogen deficiency conditions (Stage 1, 2, 3, 4, and 5 are 60, 70, 80, 90 and 100 DAS, respectively). 93

Figure 4.20: Heritability of RGB based vegetation indices of 5 stages under control conditions (Stage 1, 2, 3, 4, and 5 are 60, 70, 80, 90 and 100 DAS, respectively). 94

Figure 4.21: Heritability of RGB based vegetation indices of 5 stages under nitrogen deficiency conditions (Stage 1, 2, 3, 4, and 5 are 60, 70, 80, 90 and 100 DAS, respectively). 95

Figure 4.22: Boxplots of morphometric i-Traits representing the stage wise progression of morphometric traits and the effect of nitrogen deficiency over plant age. Each box represents one morphometric i-Trait. 98

Figure 4.23: Boxplots of colour related i-Traits showing the stage wise progression of colour related traits and the effect of nitrogen deficiency over plant age. 102

Figure 4.24: Boxplots of Biomass related and intensity related traits. 103

Figure 4.25: Boxplots of RGB based vegetation indices showing the treatment effect and stage wise progression of phenotypic profiles of RILs. 107

Figure 4.26: Principal component analysis of i-Traits explaining the phenotypic differences between control and nitrogen deficiency condition at a) 60 DAS b) 70 DAS c) 80 DAS d) 90 DAS e) 100 DAS. The red colour and green colour represented by control and nitrogen deficiency plants respectively. 109

Figure 4.27: Principal component analysis showing 4 principal components of all i-Traits and representing the phenotypic differences between control and nitrogen deficiency at a) 60 DAS b) 70 DAS c) 80 DAS d) 90 DAS e) 100 DAS. The orange and blue dots represent the N-deficiency and control plants, respectively, and the green lines represent all the i-Traits. 110

Figure 4.28: Trait contribution to a) PC1 b) PC2 c) PC3. 111

Figure 4.29: Trait similarity between i-Traits under different treatments at stage 1 (60 DAS). A) Control condition B) Nitrogen deficiency. The 4 rectangular black boxes represent 4 i-Trait classes, morphometric, color, intensity and indices related traits (Top to bottom) 113

Figure 4.30: Trait similarity between i-Traits under different treatments at stage 2 (70 DAS). A) Control condition B) Nitrogen deficiency. The 4 rectangular black boxes represent 4 i-Trait classes, morphometric, color, intensity and indices related (Top to bottom). 114

Figure 4.31: Trait similarity between i-Traits under different treatments at stage 3 (80 DAS). A) Control condition B) Nitrogen deficiency. The 4 rectangular black boxes represent 4 i-Trait classes, morphometric, color, intensity and indices related (Top to bottom). 115

Figure 4.32: Trait similarity between i-Traits under different treatments at stage 4 (90 DAS). a) Control condition b) Nitrogen deficiency. The 4 rectangular black boxes represent 4 i-Trait classes, morphometric, color, intensity and indices related (Top to bottom).....116

Figure 4.33: Trait similarity between i-Traits under different treatments at stage 5 (100 DAS). a) Control condition b) Nitrogen deficiency. The 4 rectangular black boxes represent 4 i-Trait classes, morphometric, color, intensity and indices related (Top to bottom).....117

Figure 4.34: Unsupervised colour class characterization of whole plant pixels to evaluate plant nitrogen status. A) Status under control condition B) Status under nitrogen deficiency. The red box represents the greenness related colour classes and the blue boxes represents the yellowness related colour classes. The red and blue arrow represents the value gradient.....120

Figure 4.35: Graphical representation of water use of wheat RILs at day (Left) and night (Right) time under control and nitrogen deficiency condition. This shows the effect of nitrogen deficiency on the water use (ml)/PSA (m2) in wheat RILs at day and night time. The red circles represent the RILs have contrasting day and night time transpiration.....121

Figure 4.36: Graphical representation of plant physiological, phenological and morphological traits recorded manually.....123

Figure 4.37: Yield trait characterisation of wheat plants by manual method. 124

Figure 4.38: Frequency distribution of phenology related traits in wheat RILs. Black arrow and red arrow represent parental value under control condition and nitrogen deficiency condition, respectively. 125

Figure 4.39: Frequency distribution of flag leaf related traits, SPAD value traits, tiller number, leaf number and plant height.....126

Figure 4.40: Frequency distribution and box plot representation of grain, biomass nitrogen content and grain protein content showing the effect of nitrogen deficiency.....127

Figure 4.41: Frequency distribution and box plot representation of NHI, UI, NUE, NUpE and NUtE traits showing the nitrogen deficiency effect. 128

Figure 4.42: Frequency distribution of biomass related traits in all the RILs.....129

Figure 4.43: Frequency distribution of spike related traits in all the RILs. 130

Figure 4.44: Frequency distribution of yield related traits in all the RILs.....130

Figure 4.45: Effect of nitrogen deficiency over main ear and tiller ear with respect to grain weight and grain number of wheat RILs. A) Grain weight (GW) B) Grain number (GN). 131

Figure 4.46: Comparison of main ear, tiller ear and all ear for N stress effect evaluation A) Average grain weight/spike B) Total grain weight/plant C) Average chaff weight/spike D) Total chaff weight/plant.....132

Figure 4.47: Comparison of main ear, tiller ear and all ear for N stress effect evaluation A) Average grain number/spike B) Thousand Kernel Weight C) Total grain number/plant D) Panicle Harvest Index. 133

Figure 4.48: Semi-automatic seed trait characterization in wheat RILs. 134

Figure 4.49: Frequency distribution and effect estimation of nitrogen deficiency on seed morphometric parameters in wheat. 135

Figure 4.50: MGIDI selection index. 135

Figure 4.51: Linkage map construction for RAJ 3765 × HD 2329 population. 137

Figure 4.52: Proportion or number of matching recombinant inbred lines sharing same genotypic information. Histogram of the proportion of markers for which pairs of individuals have matching genotypes. 138

Figure 4.53: Graphical representation of genotypic data. a) Marker segregation ratio b) Plot of number of genotyped markers for each individual (left panel) and number of genotyped individuals for each marker (right panel). 139

Figure 4.54: Graphical representation of markers on 21 chromosomes in 355 RILs (a) before correction and (b) after correction. The red color represents alleles from parent A (RAJ 3765), blue color represents allele from parent B (HD 2329), and white color represents missing information. The black square box showing the duplicate individuals and individuals with higher missing values (white spots). Black vertical lines indicate the boundaries between chromosomes. Recombination blocks are clearly defined in (b) as compared to (a). 140

Figure 4.55: Genetic linkage maps constructed for the RIL population derived from the cross RAJ 3765×HD 2329. Linkage groups corresponding to the 21 wheat chromosomes are shown in x-axis. The y-axis shows genomic distances in cM. 141

Figure 4.56: Detailed representation of linkage group 1A, 1B and 1D (Left to right). 144

Figure 4.57: Detailed representation of linkage group 2A, 2B and 2D (Left to right). 145

Figure 4.58: Detailed representation of linkage group 3A, 3B and 3D (Left to right). 146

Figure 4.59: Detailed representation of linkage group 4A, 4B and 4D (Left to right). 147

Figure 4.60: Detailed representation of linkage group 5A, 5B and 5D (Left to right). 148

Figure 4.61: Detailed representation of linkage group 6A, 6B and 6D (Left to right). 149

Figure 4.62: Detailed representation of linkage group 7A, 7B and 7D (Left to right). 150

Figure 4.63: Number of QTLs detected under different conditions and at different growth stages. .. 152

Figure 4.64: QTL interaction with plant age under control conditions. 170

Figure 4.65: QTL interaction with plant age under nitrogen deficiency conditions. 171

Figure 4.66: Multiple number of QTLs expressed at each stage for different traits. 173

Figure 4.67: Allelic effect of 4 important QTLs detected for grain N percent (A), NutE (B), UI (C & D). 177

Figure 4.68: Allelic effect of 2 important QTLs detected for spikelet number (A & B) and panicle harvest index (C). 178

Figure 4.69:In-silico expression analysis of potential candidate genes underlying NUE QTLs. 181

LIST OF TABLES

Table 2.1: High-throughput phenotyping for nitrogen response studies in plants. 30

Table 2.2:QTLs and genes identified in wheat related to NUE. 40

Table 3.1: Properties of soil used in the experiment. 42

Table 3.2: Nitrogen use efficiency formula. 57

Table 4.1: Phenomics facility in India. 66

Table 4.2: List of all HTP traits. 81

Table 4.3: Summary statistics of linkage map of RAJ 3765×HD 2329. 142

Table 4.4: Major QTLs identified for i-Traits under control conditions. 153

Table 4.5: Major QTLs identified for i-Traits under Nitrogen deficiency conditions. 158

Table 4.6: Major QTLs identified for i-Traits under N:C ratio conditions. 163

Table 4.7: Selected QTLs from all i-Traits, manual and semi-automatic traits with LOD >10 and PVE > 10. 165

Table 4.8: Candidate genes within 4 NUE QTLs. 178

1 INTRODUCTION

Wheat (*Triticum aestivum* L.) is the most commonly cultivated cereal in the world, accounting for 20% of total calories and protein in the global human diet and its second largest food crop in the world (Shiferaw *et al*., 2011). To maintain the food security, wheat demand is expected to rise by 60% by 2050 to feed the expected world population of about 9 billion (https://www.wheatinitiative.org/strategic-research-agenda). India also needs to double the food production by 2050. This increase in production must be achieved mainly through increase in crop productivity per unit area. The major food crops namely rice, wheat, maize and soybean currently produce nearly two-thirds of global agricultural calories. Currently the growth rates of yield in these top four crops are increasing at the rate of 1.0, 0.9, 1.6, and 1.3% per year, respectively. This is less than the required growth rate of 2.4% per year to double food production by 2050 (Ray *et al.*, 2013).

Nitrogen (N) is an essential nutrient, and often the most critical yield-limiting factor in crop production (Tilman *et al.*, 2002). One of the major inputs for crop production is Nitrogen (N) fertilizer, and thus to double to food production, significantly higher amount of N fertilizers is required. Among the crops, wheat received the highest amount of N fertilizers, with 18.2% of global use, followed by maize with 17.8% and rice with 15.2% (Heffer *et al.*, 2013). About 21% of the fertilizers used in Indian agriculture is used by wheat crop. Of the total fertilizers used in wheat, about 73% are nitrogenous fertilizers (FAO, 2005). A 50-year global N budget evaluation in cereal production systems showed that approximately 44.6% of N harvested by wheat crops was derived from applied fertiliser-N, suggesting that the majority of applied N was not used by wheat crops (Lassaletta *et al.*, 2014). It is estimated that only 30%–50% of applied N is taken up by crops, and the unused N is lost to the environment which cause soil, water and air pollution (West *et al.*, 2014; Han *et al*., 2015). Therefore, it is necessary to increase wheat yield in an economically and environmentally friendly manner such as breeding wheat with improved NUE and designing variety-specific recommendations of N fertilizer management. Breeding crops with improved NUE can help increase crop productivity with less N Fertilizer input (Hirel *et al.*, 2011; Han *et al.*, 2015). For this donor for component traits of NUE and genes/QTLs need to be identified in wheat. Several authors (Cormier *et al.*, 2016; Islam *et al.*, 2021; Saini *et al.*, 2021) have reviewed the genetic control of N use-related traits and strategies for improving NUE in wheat.

The advances in the genomics during the past one decade offer great potential for genetic enhancement in yield and adaptability of crops. With the availability of next generation sequencing and automated genotyping technologies, generating accurate genotypic data for a large set of germplasm and breeding population has become easier. However, a limitation in using the genomic information for crop improvement is the costly and time-consuming processes of deciphering the phenotype that arises from the interaction of genome with environment. Conventional phenotyping methods are laborious,

time consuming and not very precise. Thus, phenotyping is the major bottleneck that limits utilization of the power of genomics for identification and use of novel genotypes, high-resolution linkage mapping, genome-wide association mapping and training genomic selection models for crop improvement.

The multi-disciplinary science of phenomics, the sensor aided non-destructive high throughput automated acquisition and analysis of high-dimensional phenotypic data on an organism-wide scale, emerged recently to bridge the phenotype-genotype gap to enhance the pace of analytical breeding. Hyperspectral imaging is found to be highly useful to phenotype concentrations of macronutrients nitrogen (N), phosphorus (P), potassium (K), magnesium (Mg), calcium (Ca), and sulfur (S), and micronutrients sodium (Na), iron (Fe), manganese (Mn), boron (B), copper (Cu), and zinc (Zn) in maize (Pandey *et al.*, 2017). The depth of component phenotypic traits and the spatio-temporal dynamic phenotypic data generated in phenomics are enormous and unparallel to the conventional phenotyping (Kumar *et al*., 2016). Using phenomics at the Plant Accelerator (®), The University of Adelaide, Australia, sorghum was analysed for NUE. Color image analysis was found to correlate with foliar nitrogen and chlorophyll (Neilson *et al.*, 2015). In *Brachypodium*, a time series image-based approach coupled with mathematical modeling showed that it can clearly measure the genotypic response to nutrient supply at high resolution than traditional destructive techniques (Poire *et al.*, 2014).

This thesis research intends to use high throughput phenomics approaches for identification of donors and map QTLs in wheat. Therefore, a research proposal on "***Phenomics and genetic analysis of nitrogen use efficiency (NUE) in Wheat***" was undertaken with the following objectives:

Objectives:

i. **To identify superior Recombinant Inbred Lines (RILs) and component traits for NUE in wheat using phenomics approaches**
ii. **To map QTLs for NUE by using linkage mapping**
iii. **To identify candidate genes underlying QTLs for component traits of NUE**

2.1 Wheat – a major cereal crop in the world

Twenty percent of the total calories consumed by humans worldwide comes from wheat (*Triticum aestivum*), the most widely grown grain crop. The fact that wheat can be made into flour for so many different cuisines gives it great significance. Wheat is an important crop since it is a key source of calories and nutrients for people all around the world. There are sufficient amounts of carbohydrates, fiber and minerals such as iron and magnesium in wheat products. Wheat-based products are crucial to the diets of many people all over the world. India would need to increase its food output by 60 percent by 2050 to keep up with the rising demand for wheat as the global population is projected to reach 9 billion by then (https://www.wheatinitiative.org/strategic-research-agenda). Increasing crop productivity per acre is crucial to meet this target for output growth.

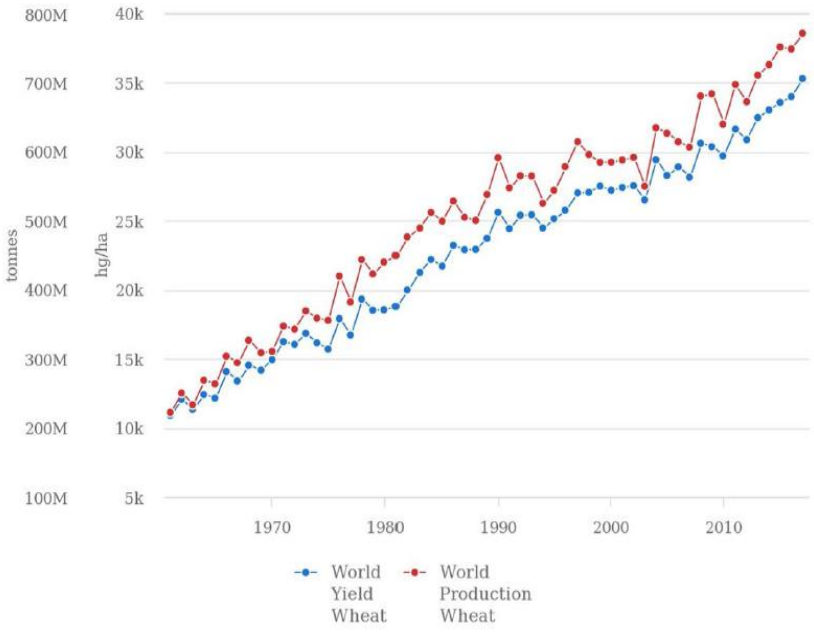

Figure 2.1: Global wheat production trend (FAOSTAT, 2020)

The United Nations Food and Agriculture Organization (FAO) estimates that global wheat production will reach 769 million metric tons in 2020. (FAO, 2021). Some of the world's top wheat producers include China, India, Russia, the USA, and France. The climate and availability of farmable land in these nations make them good locations for wheat production. India is a major player in the global wheat market. India grew approximately 31 million ha of wheat during the 2020-2021 harvest year, yielding over 109 million metric tons (FAO, 2021). To meet the projected food demand of an increasing global population, wheat production will need to increase. By 2050, the United Nations projects that the global population will reach 9.7 billion. According to the UN (2018), wheat output

could be raised to ensure sustained food availability by measures such as better crop management, the introduction of high-yielding cultivars, and the adoption of sustainable agricultural practices.

Over time, significant increases in wheat yields have resulted from better crop varieties, fertilizers, irrigation, and management. The Food and Agriculture Organization (FAO) estimates that yearly worldwide wheat production increased by 1.2% between 2000 and 2018. (FAO, 2019). However, 2.4 percent annual growth rate is necessary to meet the food demand by 2050 (Ray *et al*., 2013). The northern and central regions of India, where the climate and soil are best suited for wheat cultivation, produce the vast majority of India's wheat harvest. Wheat is typically sown in the fall and harvested in the summer in temperate regions. Farms often plant winter wheat as a staple crop. In contrast, countries with milder winters and springs, spring wheat is sown in the winter or spring and harvest it in the summer or autumn.

2.1.1 Wheat Genetics

Wheat's rich genetic basis is the result of thousands of years of evolution. Polyploidy describes wheat, a plant with three chromosomal groups. *Triticum aestivum*, also known as bread wheat, is a hexaploidy wheat species with six complete sets of chromosomes. Wheat's hexaploidy nature increases its genetic diversity and adaptability, making it possible for the plant to flourish in a wide range of settings. Around 10,000 years ago, early human communities began domesticating wild grasses, which eventually led to the development of wheat as a crop. Various types of grass were hybridized through a process of selective cultivation. The hybridization between the two grass species *T. urartu* (the A genome donor), and *T. speltoides* (the B genome donor) gave rise to tetraploid (AABB) wild emmer wheat (*T. turgidum* ssp. *dicoccoides*). Hexaploid bread wheat was created through natural hybridization between a tetraploid wheat species and a diploid wild grass species called *Aegilops tauschii* (Matsuoka, 2011). Bread wheat is hexaploid with AABBDD ($2n = 6x = 42$) genomes. D genome was provided by the *Aegilops tauschii* species, and the A and B were provided by the tetraploid wild emmer wheat (Dubcovsky and Dvorak, 2007).

2.1.2 Nitrogen in agriculture

A high level of agricultural productivity and output is dependent on adequate nitrogen availability, as this macronutrient is needed for plant growth (Tilman *et al*., 2002). Amino acids, proteins, nucleic acids, chlorophyll, and other important plant molecules have N as key constituent. For optimal plant health, robust development, and increased harvest yield and quality, nitrogen is essential. Food production, soil fertility, and global food security can all be improved with more readily available nitrogen (Hirel *et al*., 2011).

The global nitrogen cycle involves complex interactions between the atmosphere, soils, plants and water bodies. The air we breathe consists of about 78% is mostly nitrogen. Molecular nitrogen (N_2)

makes up the vast majority of atmospheric nitrogen, although it is inaccessible to most plants. For plant use, it must undergo microbial conversion to ammonium (NH_4^+) or nitrate (NO_3^-). In the agricultural system, nitrogen can be found in the soil, the plants, and the air. Agricultural systems have multiple nitrogen sources that can be used by plants. Biological nitrogen fixation, mineralization of organic materials, and atmospheric deposition are all natural processes that contribute to nitrogen availability, in addition to the use of nitrogen fertilizers. Ammonium and nitrate are the two most common forms of nitrogen taken up by plants through their roots.

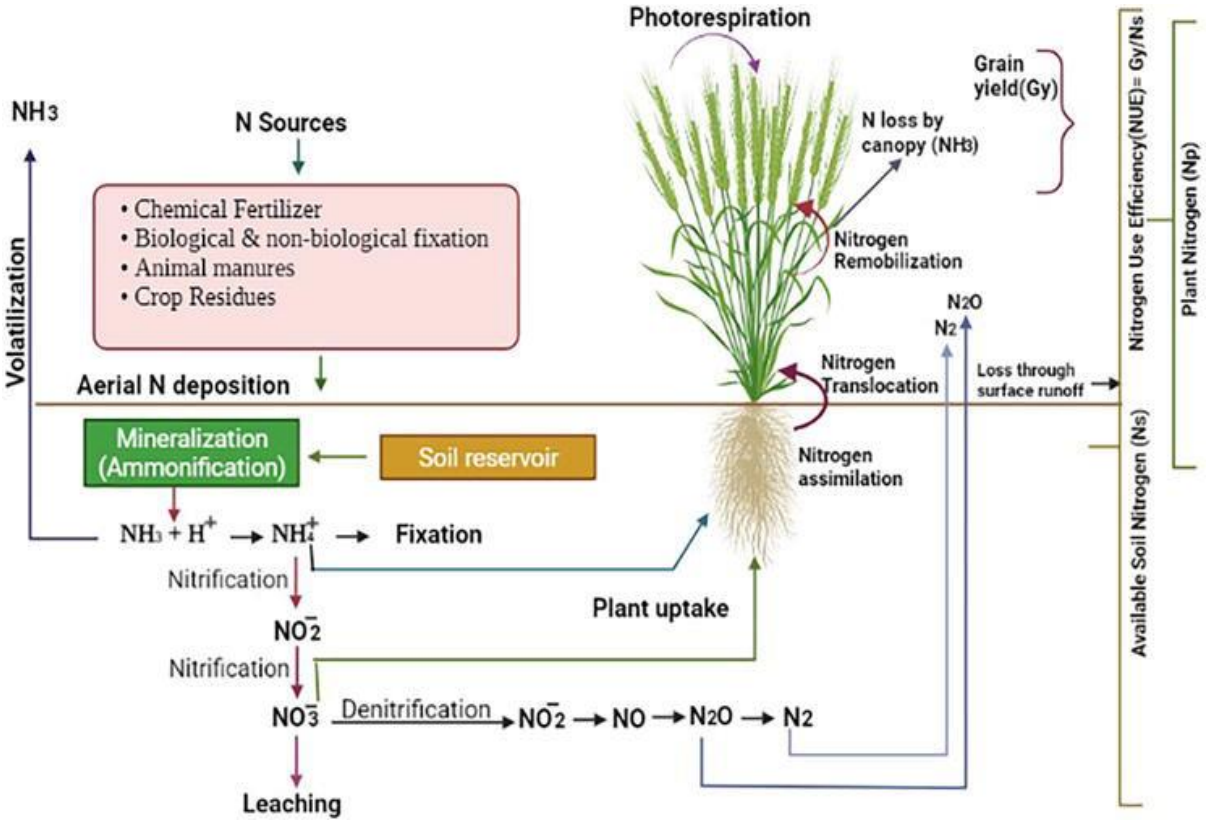

Figure 2.2: Relationship between the nitrogen sources, uptake, utilization (Raigar *et al*., 2022)

One of the major inputs for crop production is Nitrogen (N) fertilizer, and thus to double food production, a significantly higher amount of N fertilizers is required. Among the crops, wheat received the highest amount of N fertilizers, with 18.2% of global use, followed by maize with 17.8% and rice with 15.2% (Heffer *et al*., 2013). About 21% of the fertilizers used in Indian agriculture is used by wheat crop. Of the total fertilizers used in wheat, about 73% are nitrogenous fertilizers (FAO, 2005).

Nitrogen fertilizer use varies globally and within countries. Globally, nitrogen fertilizer consumption has increased over the years. According to the International Fertilizer Association (IFA), global nitrogen fertilizer consumption increased from around 86 million metric tons in 1980 to approximately 120 million metric tons in 2019 (IFA, 2021). In India, nitrogen fertilizer consumption has also increased but at a variable pace over the last four decades. According to the Fertilizer

Association of India (FAI), nitrogen fertilizer consumption in India increased from around 1.75 million metric tons in 1980 to approximately 14.5 million metric tons in 2020 (FAI, 2021). Decade-wise fertilizer consumption data for the last four decades is as follows:

1. 1980s: Global nitrogen fertilizer consumption was around 69 million tons (FAO, 2020).

2. 1990s: Global nitrogen fertilizer consumption increased to approximately 84 million tons (FAO, 2020).

3. 2000s: Global nitrogen fertilizer consumption further rose to about 96 million tons (FAO, 2020).

4. 2010s: Global nitrogen fertilizer consumption reached around 110 million tons (FAO, 2020).

The cost of fertilizer imports in India varies based on international prices, exchange rates, domestic policies, and demand-supply dynamics. As of 2021, IFA estimates suggest that India's annual expenditure on fertilizer imports is around USD 4 billion (IFA, 2021). Globally, the value of nitrogen fertilizer consumption was approximately USD 60 billion in 2019 (IFA, 2021). Fertilizer consumption has shown a generally increasing trend in both global and Indian agriculture over the last four decades. However, the growth rate has slowed down in recent years due to various factors such as changing agricultural practices, environmental concerns, and efforts to improve nutrient use efficiency.

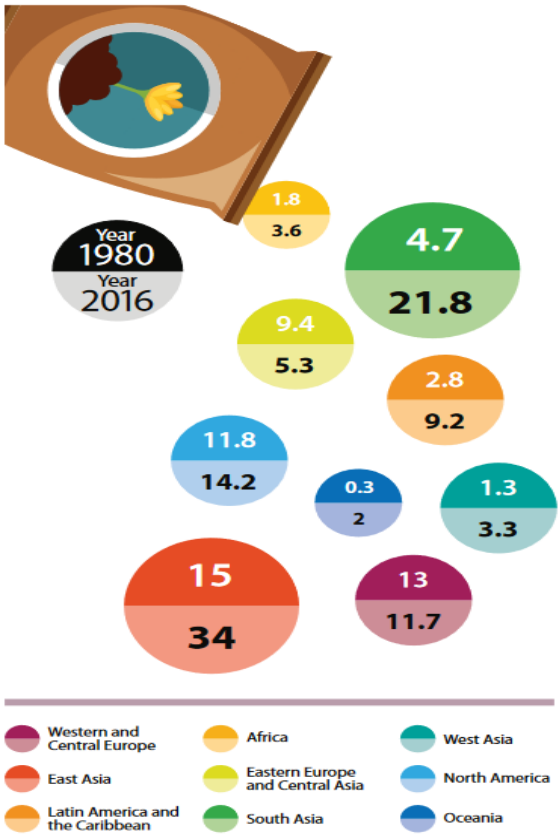

Figure 2.3: Regional consumptions of all types of nitrogen fertilizers in 1980 and 2016 (in million metric tonnes)

2.1.3 Wheat and nitrogen use

In India, wheat is a major crop, and nitrogen fertilizer plays a critical role in its cultivation for achieving optimal yield. Nitrogen management strategies, cropping area, and production levels all have a role in determining India's annual wheat nitrogen fertilizer usage. Wheat's nitrogen needs are highly context-dependent, meaning they change depending on things like soil quality, weather, cultivar, and agricultural techniques. During its vegetative and early reproductive stages, wheat normally requires larger nitrogen inputs. To maximize yield and quality, plants require an adequate supply of nitrogen during key growth stages such as crown root initiation, tillering, stem elongation, and grain formation. The goal of nitrogen fertilizer management is to apply nitrogen at rates and times that are optimal for the crop. Low nitrogen levels can decrease yields and lower quality grain.

Global and Indian wheat fertilizer consumption data vary over time. According to the IFA, global nitrogen fertilizer consumption in wheat cultivation increased from around 10.5 million metric tons in 1980 to approximately 21.6 million metric tons in 2019 (IFA, 2021). In India, nitrogen fertilizer consumption in wheat cultivation increased from around 0.75 million metric tons in 1980 to approximately 6 million metric tons in 2020 (FAI, 2021).

2.1.4 Problems associated with nitrogen in agriculture

Leaching, volatilization, and denitrification are all ways that nitrogen can be lost from farming systems. Nitrate ions are washed out of the root zone and into the groundwater supply via leaching when there is an excess of precipitation or irrigation. Fertilizers containing ammonium can be lost to the atmosphere by a process called volatilization, in which the fertilizer is broken down into ammonia gas. Denitrification is the process by which nitrates are broken down into nitrogen gas by microorganisms under anaerobic conditions and then released into the atmosphere (Robertson and Vitousek, 2009).

A 50-year global N budget evaluation in cereal production systems showed that approximately 44.6% of N harvested by wheat crops was derived from applied fertilizer-N, suggesting that the majority of applied N was not used by wheat crops (Lassaletta *et al*., 2014). It is estimated that only 30%–50% of applied N is taken up by crops, and the unused N is lost to the environment which causes soil, water, and air pollution.

Several problems might arise from overusing nitrogen in farming. Water bodies can be contaminated by nitrogen runoff and leaching, leading to eutrophication and subsequent damage to aquatic ecosystems. Air pollution is exacerbated by the release of nitrogen compounds, which can produce smog and potentially dangerous nitrogen oxides.

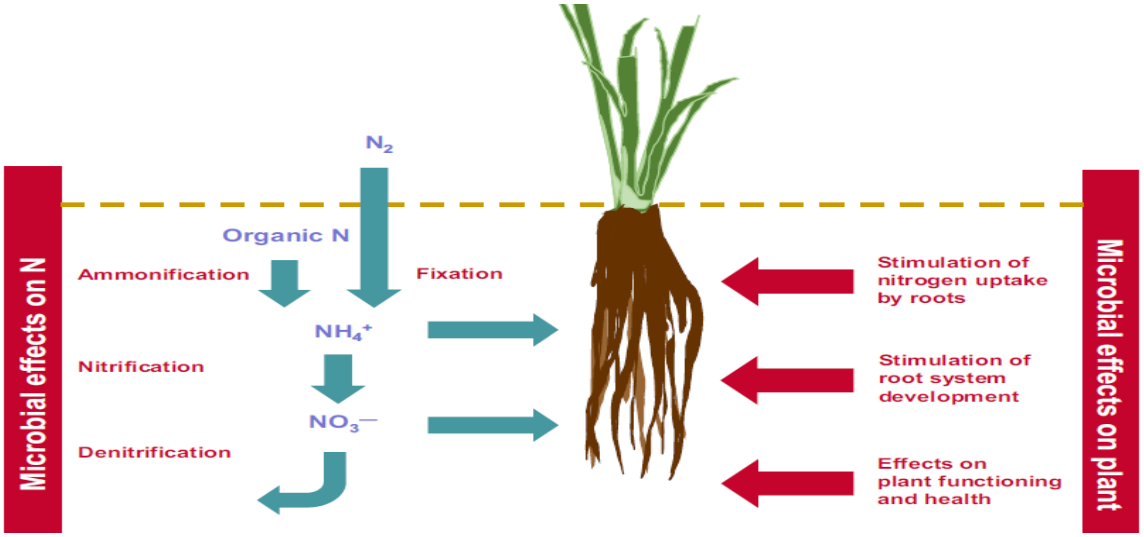

Figure 2.4: Nitrogen forms due to microbial activity (Cormier *et al.*, 2016)

Excessive nitrogen application or poor management techniques can also cause climate change and soil degradation by increasing emissions of greenhouse gases like nitrous oxide. Soil health, microbial communities, and biodiversity loss are just a few of the things that can be negatively impacted by an imbalance in nitrogen levels.

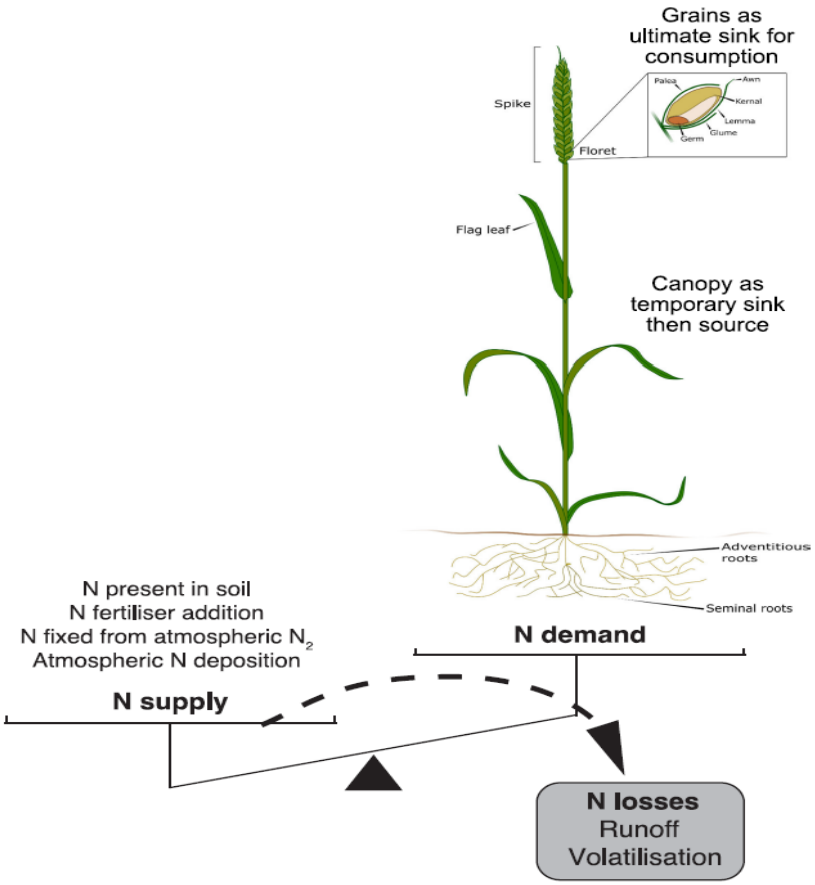

Figure 2.5: Lowering wheat N requirement as a mean to balance N supply and demand (Fradgley *et al.*, 2021)

The nitrogen utilization efficiency of a farm is measured by how much of the nitrogen fertilizer is absorbed and used by the crops. Soil and crop type, climate, nutrient management strategies, when fertilizer is applied, and other variables all affect nitrogen use efficiency to varying degrees. Enhancing nitrogen use efficiency and decreasing nutrient losses can be accomplished by better nutrient management practices such as applying fertilizer at the right time, using the right amount, and employing enhanced-efficiency fertilizers. To minimize losses, lessen our ecological footprint, and maximize agricultural yields, the nitrogen use efficiency must be increased.

2.2 Effect of nitrogen deficiency in wheat

Low levels of nitrogen (N) in arable soils globally hinder agricultural productivity. This constraint has been greatly alleviated by the discovery of synthetic N fertilizers, as well as the adoption of high-yielding crop types and irrigation in some regions of the world, all of which are major components of the green revolution. In places where farmers can afford to supplement N, huge amounts of N fertilizer are applied to maximize crop productivity. Contrary to popular belief, most crop plants typically use just a small portion (40%) of the applied N (Kant *et al*., 2011), with the remainder lost to the environment. This leads to increased crop production costs as well as severe worldwide environmental harm due to eutrophication of water habitats and gaseous loss to the atmosphere (Gao *et al*., 2012). Improving crop N use efficiency (NUE) through a mix of devising methods for enhanced crop management practices, genomics, genetics, and conventional and modern genomic breeding is critical to reducing costs and addressing pollution concerns.

Crop production declines once nitrogen (N) levels are reduced, indicating that N is a key element in crop growth (Uhart *et al*., 1995; Wang *et al*., 2017). Under nitrogen deficiency, plant growth and development were severely affected, suggesting a possible negative effect on plant biomass (Liu *et al*., 2020). The stress of N deprivation is promptly detected by plants, and they respond through a variety of physiological and metabolic processes. The loss of photosynthetic capacity leads to the biggest negative effects on plant growth and development (Boussadia *et al*., 2010). Plants suffering from N deficiency all had lower chlorophyll and other pigment concentrations (Laza *et al*., 1993; Nakano *et al*., 1997). The decrease in plant height, number of leaves, and shoot fresh weight were reported under low nitrogen conditions in wheat (Cormier *et al*., 2014). The reduction in grain yield, No. of grains per spike, flag leaves size and grain protein contents were severely affected by N-limiting conditions (Wang *et al*., 2021). The root activity can be considerably enhanced by nitrogen fertilizer (Wang *et al*., 2022), however excessive nitrogen fertilizer negatively affects the root activity (Xu *et al*., 2018). According to Wang *et al*. (2022), wheat roots displayed lower root length density (RLD), root volume density (RVD), and root mass density (RMD) under low N fertilizer condition than high N fertilizer condition.

Nitrogen (N), phosphorus (P) and potassium (K) deficiencies promote lateral root growth to uptake more nutrients (Sun *et al*., 2016; Zhao *et al*., 2016). Therefore, it is necessary to study root

response under low nitrogen stress **(**Lv *et al*., 2021**).** In addition, low-N stress stimulated protein biosynthesis, increased the activity of important N absorption enzymes, and eventually improved root growth (Lv *et al*., 2021). Moreover, Wang *et al*. (2009) suggested that low availability of N in the soil increases root biomass.

2.3 Nitrogen Use Efficiency (NUE)

The efficiency with which plants absorb and use nitrogen provided to them is what is meant by "Nitrogen use efficiency (NUE)". Soil composition, crop species, weather, management strategies, nitrogen application, and other factors all affect NUE. To maximize agricultural output while minimizing losses and negative environmental effects, greater efficiency in nitrogen utilization is essential. Several scientific methods exist for increasing wheat's nitrogen utilization efficiency. Precision nutrient management, nitrogen delivery techniques tailored to individual sites, nitrogen treatments timed to coincide with crop demands, and nitrogen fertilizer rate optimization based on soil testing and crop nutrient needs are all examples of best management practices. Cover crops that fix nitrogen, crop rotations, and biological nitrogen fixation are all ways to lessen the need for synthetic fertilizers and boost nitrogen use efficiency (Kant *et al*., 2011).

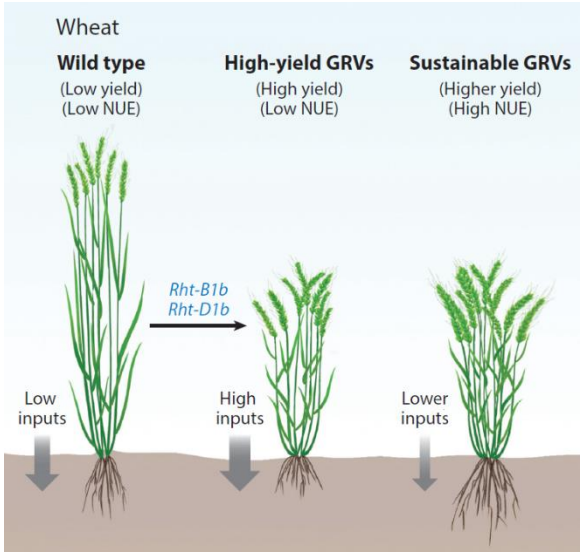

Figure 2.6: Strategies to enhance sustainable yield through NUE (Liu *et al*., 2022)

Nitrogen use efficiency can be calculated by dividing grain biomass by the plant's total amount of available nitrogen (N) (Moll *et al*., 1982). It is divided into two components as Nitrogen uptake efficiency (NUpE) and NUtE (nitrogen utilization efficiency) (Barraclough *et al*., 2010). NUpE can be calculated by the total amount of N in the above-ground plant biomass divided by the total amount of available nitrogen in the soil. NUtE can be calculated as grain dry mass divided total amount of nitrogen in the above-ground plant biomass at harvest. However, in the case of pre-modern cultivars with poor HI, biomass production per unit of N was more (Hawkesford, 2017). Fertilizer use efficiency (FUE)

imitates the recovery of N in the crop as a fraction of fertilizer applied N (Raun and Johnson, 1999). The largest sink for nitrogen is grain protein, which is an indicator of grain nitrogen content. Moreover, remobilization efficiency from the canopy during senescence largely affects grain protein concentration (GPC). Thus, enhancing remobilization efficiency without any yield penalty would be an efficient strategy to enhance the NUE (Islam *et al*., 2012). However, with an increase in yield, GPC decreases as a consequence of dilution by photo-assimilates (Hawkesford *et al*., 2014). However, it has been reported that some of the wheat cultivars possess greater capacity of NUE without any yield penalty (Latshaw *et al*., 2016).

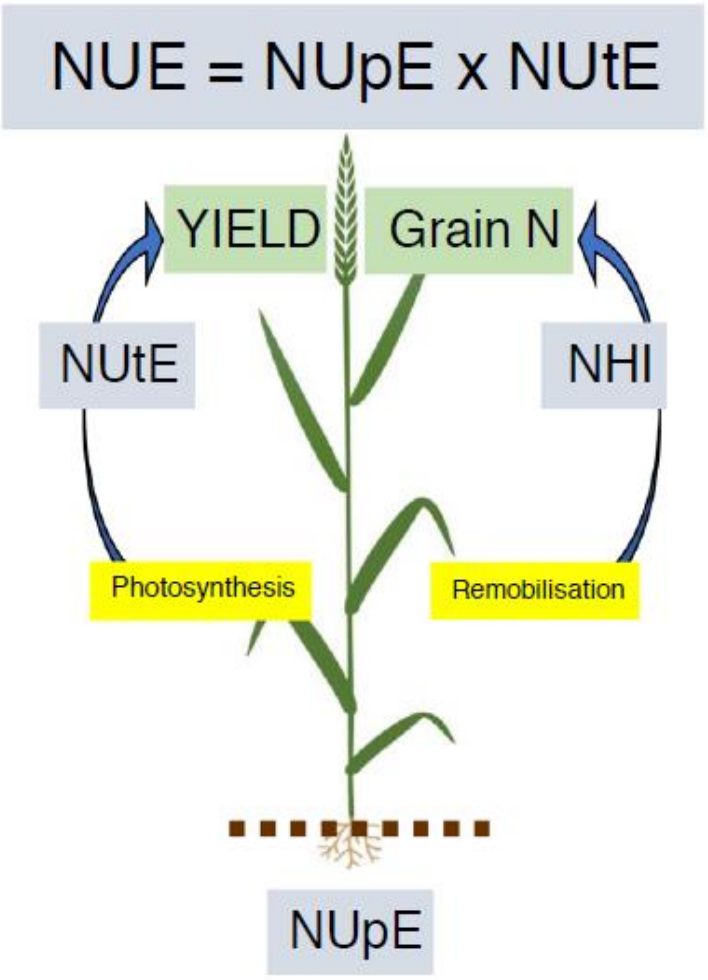

Figure 2.7: Characterisation of NUE in wheat (Hawkesford and Griffiths 2019)

Improving nitrogen use efficiency in wheat can be achieved through various scientific approaches. These include:

1. Site-specific nutrient management (SSNM): Using soil testing and crop modeling to determine precise nitrogen requirements based on specific field conditions and crop demands.

2. Precision agriculture: Employing technologies such as remote sensing, GIS (geographic information systems), and sensor-based systems for real-time monitoring and targeted nutrient application.

3. Nitrogen management practices: Adopting best management practices such as split application, applying nitrogen at different growth stages, and adjusting rates based on crop growth and soil conditions.

4. Enhanced efficiency fertilizers: Using controlled-release fertilizers or inhibitors that slow down nitrogen release or reduce nitrogen losses, thereby increasing efficiency.

5. Improved agronomic practices: Incorporation of nitrogen-fixing cover crops, use of controlled-release fertilizers and use of improved irrigation practices.

6. Crop genetics: Developing wheat varieties with enhanced nitrogen use efficiency traits through breeding and genetic engineering approaches. Use of biological nitrogen inhibitors (BNI) introgressed varieties etc.

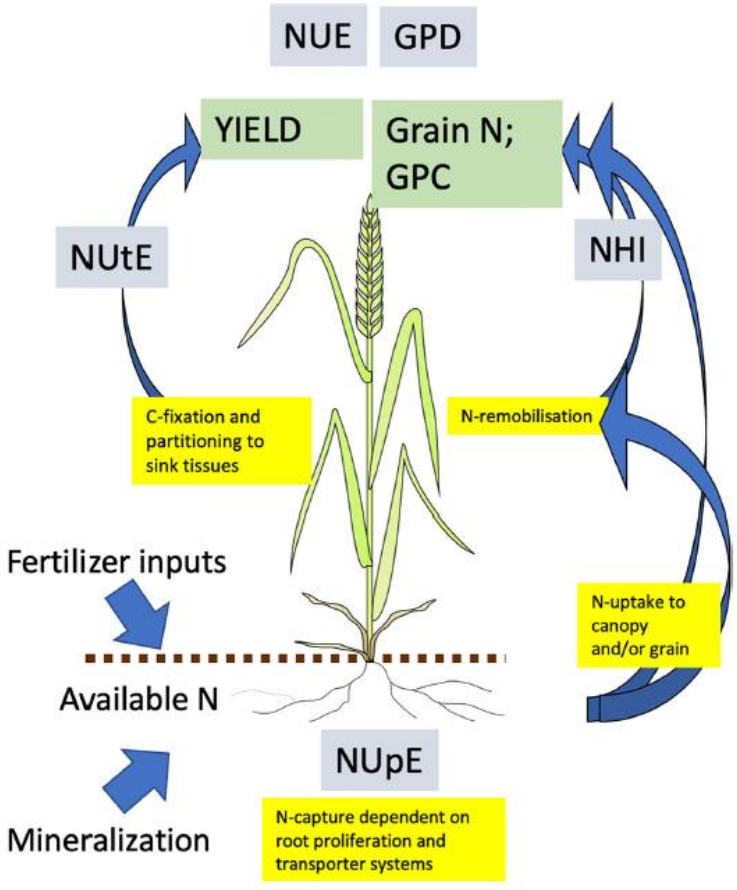

Figure 2.8: NUE determination by different traits (Hawkesford and Riche 2020)

All of these methods are geared toward helping wheat get the most out of its nitrogen fertilization efforts by maximizing uptake and minimizing losses. Different agronomic and management approaches will assist increase wheat crop yield and productivity, but NUE improvement will always lag behind unless wheat's genetic potential to efficiently utilize nutrient resources is enhanced. The potential exists, thanks to recent developments in wheat genetics, to create varieties with enhanced NUE. Wheat germplasm with improved NUE component trait features, such as increased nitrogen uptake, utilization, and remobilization within the plant, can be identified and selected through breeding programs. Traits including those involved in nitrogen assimilation, remobilization of nitrogen during grain filling, and efficiency of nitrogen usage under different environmental conditions are all important for characterization. Marker-assisted selection and genetic engineering are two examples of molecular breeding approaches that help speed up the creation of nitrogen-efficient wheat variants (Foulkes *et al*., 2009).

2.3.1 Nitrogen uptake efficiency (NUpE)

Nitrogen uptake efficiency is (NUpE) defined as the amount of nitrogen taken up by plant as a function of available N in soil. Available soil N includes soil N, fertilizer applied, and atmospherically fixed nitrogen in the soil. Generally, nitrogen uptake is calculated based on the above-ground part, and no account is taken for below ground rooting zone. Nitrogen is taken up by plants throughout their life cycle from seedling establishment to grain filling stage. During grain filling stages, canopy senescence and its remobilization of N contribute to grain nitrogen. In this process, nitrate transporter and amino acid transporter play a critical role. Nitrogen transport is catalyzed by large gene families including nitrate, ammonium, and amino acid transporter in plants (Buchner and Hawkesford, 2014).

2.3.2 Nitrogen utilisation efficiency (NUtE)

Nitrogen utilisation efficiency (NUtE) is defined as grain yield per unit of N taken up. Nitrogen taken up during the vegetative phase is utilized for canopy establishment and to maintain the functional composition of photosynthetic apparatus. At this juncture, the canopy will determine the photosynthetic capacity through carbon fixation, consequently enhancing the yield. During canopy maturation, N stored in vegetative tissue is mobilized to grain by compromising photosynthetic capacity. Thus, photosynthetic capacity reflects the NUtE, which can be explored for genetic variation present in the population (Prins *et al*., 2016). An alternative approach is transgenic manipulation of basic photosynthetic efficiency, with the aim of increasing C fixation without the need for further N investment in canopy or photosynthetic machinery (Parry *et al*., 2011).

2.3.3 Nitrogen Harvest Index

The NHI is the fraction of N recovered in the final grain fraction as a function of the total N taken up. However, NHI is insensitive to N input (Barraclough *et al*., 2010). Most of the grain nitrogen is derived from the canopy nitrogen and mobilisation of stored nitrogen in the vegetative part during canopy maturation. Moreover, the efficiency of these traits is affected by environmental conditions (Barbottin *et al*., 2005) and canopy senescence (Derkx *et al*., 2012).

2.4 Traits influencing N-Uptake Efficiency

2.4.1 Root size and morphology related traits

Root architecture and other physiological factors that influence the roots' capacity to take available N from the soil may influence NUpE. Despite being affected by environmental factors, plant root architecture, in particular root surface area, root biomass and root length have been found to impact NUpE (Islam *et al*., 2021). Nitrogen uptake during the post-anthesis stages is more rely on root depth and density of the root system (Foulkes *et al*., 2009). Limited availability of nitrogen can enhance the partitioning of resources like photosynthates for root development for efficient absorption, which may also limit the shoot biomass and yield (Garnett *et al*., 2009). The main source of nitrogen, nitrate, readily permeates the soil profile, so the genetic potential for quicker and earlier uptake is crucial to achieving higher NUE. This may be due to faster root growth during the early vegetative stage, which would allow for the capture of nitrate before it leaves the rooting profile (Guo *et al*., 2019).

Primary approaches to increase NUpE include (i) enhancing the expression of nitrogen transporter (Hawkesford, 2012) and (ii) targeting the genes involved in the root architecture (Garnett *et al*., 2009). The capacity of the root for uptake depends on the degree to which the root extends its absorption area, which is determined by complex root morphology (Han *et al*., 2015). Primary root traits to improve for enhanced N capture include rooting depth and rooting density (Foulkes *et al*. 2009). Further, developments in root architecture could concentrate on root proliferation at depth in wheat, and a deeper relative distribution of roots could be a component of an ideotype to maximize N capture (Carvalho *et al*. 2014). Root length density is also a potential trait that can contribute to N capture at a lower depth (Reynolds *et al*., 2007). However, greater variation in root system size has been reported in wheat (Hoad *et al*. 2001; Ehdaie and Waines 2003; Ford *et al*. 2006). Root morphological characteristics such as root mass and depth, root axis length, and lateral branching have been studied in relation to NUE (Yadav *et al*., 1997; Shen *et al*., 2001; Horii *et al*., 2006). Although the improvement of field phenotyping through the use of various scanners appears promising, these techniques are presently only effective under artificially controlled conditions, and more labor-intensive techniques (Han *et al*., 2015).

2.4.2 Root N transporter systems

Anhydrous ammonia, urea, ammonium sulfate, and ammonium nitrate are the commercial mineral forms of N that are frequently used to fertilize crops in the majority of nations (Robertson and Vitousek 2009; Andrews *et al*., 2013). Organic or inorganic N is given to the plant, NO_3^- is the principal source of N for the majority of crop species (Gioseffi *et al*., 2012). Although metabolic processes such as photorespiration, phenylpropanoid metabolism, use of N transport chemicals, and amino acid catabolism can produce NH_4^+, the majority of the NH_4^+ integrated by the plant into organic molecules comes from NO_3^- reduction (Lea and Miflin, 2011).

There are essentially three separate NO_3^- transport systems in higher plants, and they each function differently depending on the amount of NO_3^- in the root environment. The first one is an inducible high-affinity transport system (iHATS) that is activated in the presence of low concentrations of NO_3^- that range from 1 to 200 µM (Siddiqi *et al*., 1990). The second is a constitutively expressed high-affinity transport system (cHATS), which is active even when NO_3^- is not present. The third one is represented by a non-saturable low-affinity transport system (LATS), which is active in the 0.5–1 mM concentration range and dominates when NO_3^- in the external medium surpasses 250 µM (Siddiqi *et al*., 1990). Until now, four protein families have been identified as NO_3^- transporter families including NRT1, NRT2, CLC, SLAC1/SLAH (Fan *et al*., 2017). Nevertheless, only the members of NRT1 and NRT2 families are involved in root NO_3^- uptake, where NRT1 operate in low affinity influx and NRT2 operates in high affinity influx (Tsay *et al*., 2007). In the case of ammonium ion, AMT family, which is part of a larger group of NH_4^+ permeases of the Ammonium Transporter / Methylammonium Permease / Rhesus (AMT/MEP/Rh) family play a critical role in root absorption (McDonald and Ward, 2016). However, there is less information available for root NO_3^- and NH_4^+ absorption and their regulation (Islam *et al*., 2021). Plants also possess different isoforms of transporter, which are differentially regulated at species roles like root absorption, and internal partitioning. Moreover, transporter for foliar-applied urea is also reported (Duan *et al*., 2015). Therefore, proper phenotyping for root nitrogen uptake is critical to identify QTLs involved in root NO_3^- and NH_4^+ absorption.

2.4.3 Interaction with micro-organisms

There are several organic substrates released by plant roots including exudates, organic acids and sugars, and various rhizo-deposits (Nguyen, 2003). This produces the rhizosphere, a specific portion of soil in contact with roots that is conducive for the growth of microorganisms. Major contributors to the availability of N for plant roots are soil microorganisms in the rhizosphere (Richardson *et al*., 2009). On the one hand, microbial competition may lower the amount of nitrogen (N) that is available to roots because different soil bacteria and fungi employ nitrate and ammonium as N sources (Nelson and Mele, 2006) and/or denitrify nitrate to produce gaseous N (Herold *et al*., 2012). Although plants can suppress denitrification by producing inhibitory secondary metabolites, this property has not yet been identified

in cultivated cereals (Bardon *et al*., 2014). On the other hand, microbial mineralization of organic N, which results in ammonium in the rhizosphere, increases N availability. This calls for an increase in protozoan predators, bacterial, and fungal decomposers, as well as mycorrhizal fungi (Atul-Nayyar *et al*., 2009) and protozoan decomposers (Bonkowski, 2004). This priming effect in wheat increases at the flowering stage (Cheng *et al*., 2003).

2.5 Traits Influencing N Utilization Efficiency

2.5.1 Nitrate assimilation

After being taken up by the root, nitrate is reduced to nitrite in the cytosol by nitrate reductase, which is positively regulated by the nitrate and light and downregulated by reversible phosphorylation during the dark period (Kaiser *et al*., 2011). Thereafter, NO_2^- is transported to the chloroplast, where it is converted into NH_4^+ (Sakakibara *et al*., 2012). NH_4^+ is incorporated into glutamate by the action of two enzymes as Glutamine synthetase (GS) and Glutamine:2-oxoglutarate aminotransferase (GOGAT). Glutamate and glutamine serve as amino group donors for other amino acids and nitrogen-containing molecules such as DNA and RNA synthesis (Lea and Miflin, 2011). Glutamate can also be generated by the incorporation of NH_4^+ with glutamate by cation of glutamate dehydrogenase (GDH) (Lea and Miflin, 2011). However, number of experiments demonstrated that 95% of NH_4^+ is provided by the action of GS/GOGAT pathways (Lea and Miflin, 2011). It was also shown that when the root and leaf cells are deprived of carbon, GDH operates in the direction of deamination of glutamate to 2-oxoglutarate and NH_4^+ (Labboun *et al*., 2009; Fontaine *et al*, 2012).

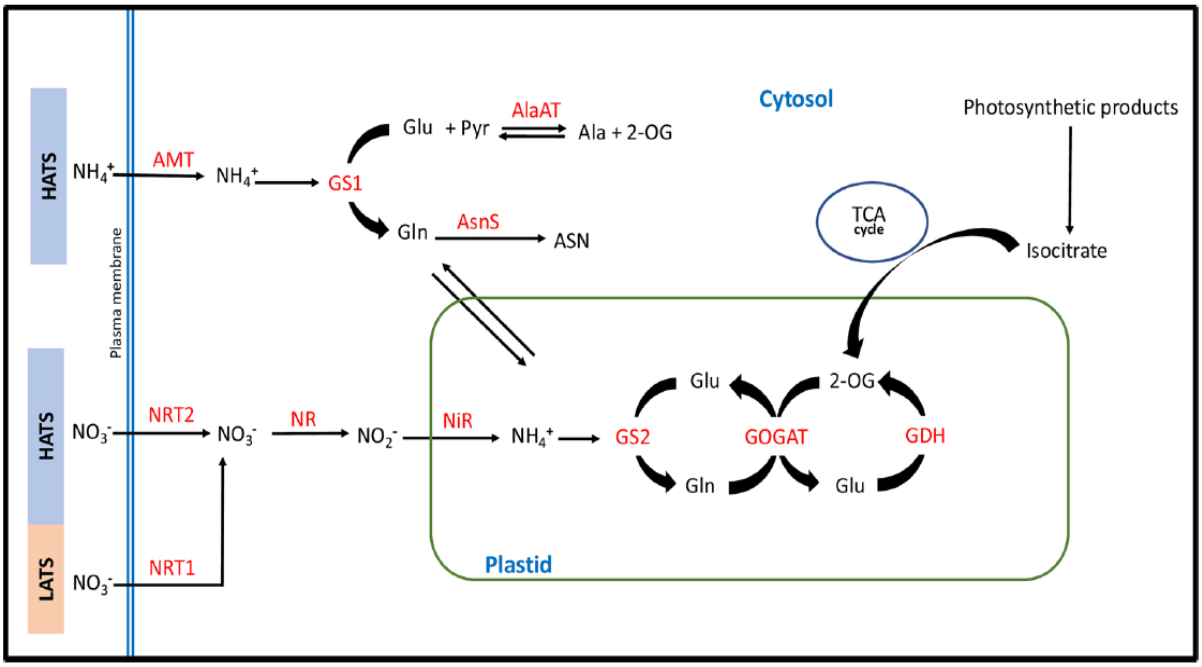

Figure 2.9: Nitrogen assimilation and uptake in wheat. HATS: High Affinity transporters; LATS: Low affinity transporters (Islam *et al*., 2021)

The process of nitrate reduction requires NADH/NADPH as electron donors. Two genes encoding nitrate reductase (NR) have been reported in wheat. The activity of NR genes in wheat is genetically controlled and potential for higher NUtE if N is not a limiting factor (Boisson *et al*., 2005). It has been reported that overexpression of *NR* genes in tobacco increased the protein content without further increase in N fertilizer supply, suggesting its role in NUE (Anjana *et al*., 2001). However, no detailed information is currently available for the allelic variation of the *NR* gene in wheat (Islam *et al*., 2021). As compared to *NR* genes, the *NIR* gene involved in the reduction of nitrate to nitrite is less well known. *NIR* genes also have been reported in maize (Beatty and Good, 2018) and tobacco (Nakano *et al*., 2012).

Two groups of glutamine synthetase (GS) have been reported, out of which GS1 is localized in the cytosol and involved NH_4^+ assimilation in root and res-assimilation of NH_4^+ generated through protein turnover. GS2 is localized in leaves chloroplast and involved in the assimilation of photorespiratory ammonium and the assimilation of NH_4^+ derived from NO_3^- reduction in plastids (Nemeth *et al*., 2018). N-efficient winter wheat cultivar has been demonstrated to have higher expression of *TaGS1* at post-anthesis and *TaGS2* at pre-anthesis stages as compared to N-inefficient cultivars (Zhang *et al*., 2017). Diversity in the genetic potential of GS in regulating N assimilation and yield or yield-contributing traits of wheat has been widely reported (Gadaleta *et al*., 2011; Gao *et al*., 2019) suggesting the potential for improving NUE through traditional breeding strategies. Similarly, GOGAT enzymes which are operating in conjugation with GS, have been reported to be conserved in hexaploidy wheat (Nigro *et al*., 2017) and it has been reported that genes *NADH-GOGAT-3A* and *NADH-GOGAT-3B* are involved in higher grain protein in durum wheat (Nigro *et al*., 2013). Remarkably, one NUE QTL has also been conserved at the same orthologous loci as the *GOGAT* gene on wheat chromosome 3B, rice chromosome 1, sorghum chromosome 3, and maize chromosomes 3 and 8 (Quraishi *et al*., 2011).

2.5.2 Canopy photosynthetic capacity

During the vegetative stage, about 75% of the leaf nitrogen is present in mesophyll cells, mainly in the chloroplastic Rubisco (Evans, 1983) and it is playing an essential role in photosynthesis (Imai *et al*., 2008). Thus, enhancing photosynthetic efficiency per unit of N can improve NUE. This can be possible by either increasing the efficiency of Rubisco or increasing the efficiency of radiation capture.

The photosynthetic process is affected by various factors which include (i) radiation interception per unit of N and (ii) leaf photosynthesis per unit of leaf N (Cormier *et al*., 2016). Enhancing photosynthetic efficiency has the potential to improve yield or reduce input, thereby probably having a role in NUE (Hawkesford, 2014). Increased NUE will result from a canopy that is more effective use of less nitrogen while maintaining the same capacity for carbon fixation. By targeting the natural genetic variation of crops, NUE can be improved (Gaju *et al*., 2016) and an alternative approach would be

transgenic manipulation of photosynthetic machinery (Parry *et al*., 2011; Prins *et al*, 2016). There may be possible ways to improve photosynthetic efficiency by exploiting natural variations of the processes involved in enhancing photosynthetic efficiency and by targeting RuBP regeneration or catalytic properties of Rubisco (Parry *et al*., 2007; Reynolds *et al*., 2009). An alternative approach is the introduction of C_4 cycle mechanism and cyanobacterial CO_2 concentration mechanism in plants (Parry and Hawkesford, 2010). Genetic variation of leaf area indices in relation to photosynthetic efficiency has been reported in wheat, which can be targeted for the improvement of NUE (Silva-Pérez *et al*., 2020). Heritability scoring of traits related to photosynthetic efficiency indicates that NUE can be improved through targeted traits breeding (Laperche *et al*., 2006).

Responses under limited nitrogen conditions include reduce leaf area and leaf expansion rate, decline in leaf N and chlorophyll content, and reduce photosynthesis per unit leaf area (Monneveux *et al*., 2005). This in turn reduces radiation interception and radiation use efficiency (RUE), hence biomass and yield. Radiation capture efficiency can be improved by increasing the leaf area index and light extinction coefficient and by decreasing the specific leaf N (SLN) (Bonelli and Andrade, 2020). A model showed that when N was limited, a 1-2 gm^{-2} decrease in SLN might result in a 10-15% rise in NUE (Semenov *et al*., 2007). In cereal crops, leaf angle is the most important limiting factor to light attenuation, thereby contributing to photosynthesis per unit of N, which also affects to light extinction coefficient (Islam *et al*., 2021). It is reported that modern wheat cultivars at anthesis achieve full light interception with a green leaf index (GAI) of 6 (Gaju *et al*., 2014), thus only possible way to enhance light interception at pre-anthesis stages is at stem elongation phases. However, the enhancement of fractional light interception may be possible through an increase in specific leaf nitrogen area (SLN) and higher light extinction coefficient. For modern-day wheat cultivars, the light extinction coefficient is 0.55 for photosynthetically active radiation, which is for erect and semi-erect leaf angles (Cormier *et al*., 2016). The light extinction coefficient is also affected by the vertical distribution of N with respect to light in the canopy. However, Information on genetic variability in the canopy's vertical distribution of nitrogen in relation to light is scarce (Bertheloot *et al*., 2008; Moreau *et al*., 2012).

2.5.3 Post-anthesis N remobilization and senescence dynamics

Under ideal conditions, leaf lamina stores 35-42% of N in the above-ground portion, 14-20% in the leaf sheath, 20-31% in true stem, and 16-23% in ear in wheat (Barraclough *et al*., 2014). Theoretically, a high maximum rate of N uptake and a greater NUpE could be favored by a true stem's strong capacity to absorb N before flowering (Foulkes *et al*., 2009). There are reports of genetic variations in the stem N concentration at anthesis in wheat (Critchley, 2001; Pask, 2009; Barraclough *et al*., 2014, Gaju *et al*., 2014). Apart from the stem capacity to store nitrogen, the staygreen capacity of crops is also contributing towards NUpE. It is also observed that there was a lesser translocation rate of nitrogen from leaf to grain, making “stay-green” phenotypes in sorghum hybrid (Borrell and

Hammer, 2000). It is also demonstrated that the onset and rate of leaf senescence were explained by a supply-demand framework for N dynamics, in which initially grain N demands were fulfilled by stem N and later on from leaf nitrogen (Van Oosterom *et al*., 2010). Under low N conditions, a positive association was shown between the effectiveness of post-anthesis N remobilization and the start of the fast phase of canopy senescence (Gaju *et al*., 2014). Therefore, Stay-green trait is mostly genetically controlled which provides the opportunity to be utilized to increase the N uptake efficiency through breeding. Wider genetic variations in the stay-green phenotype of hexaploid wheat have been documented, and several QTLs have also been reported (Christopher *et al*. 2018; Kamal *et al*., 2019). Transcription factor genes like NAMB1 (Uauy *et al*., 2006), WRKY and NAC (Derkx *et al*., 2012) have been reported to influence staygreen traits for yield enhancement. It is important to note that the commencement of the rapid phase of canopy senescence and post-anthesis N remobilization efficiency exhibit a positive association (Gaju *et al*., 2014). Thus, the slower rate of N reallocation in stay-green genotypes is associated with lower NHI. However, this can be achieved by enhancing nitrogen uptake from the soil during grain filling stages (Mirosavljević *et al*., 2020).

2.5.4 Augmenting grain protein concentration and composition

Structural and metabolic proteins are present in the cell of endosperm in cereal grain, where the predominant protein fraction in this tissue is the gluten storage proteins, comprising a mixture of monomeric gliadins and polymeric glutenins. A specific balance between gliadin and glutenin is required, as glutenin is required for dough elasticity and gliadin is required for dough viscosity for ease in biscuit making (Cormier *et al*., 2016). Differences in the ability to synthesize proteins play a role in the grain protein's qualitative composition (Ravel *et al*., 2009), whereas the rate, duration, and grain protein quantitative composition can be modified by environmental conditions. However, an inverse correlation between grain protein concentration and yield was also reported (Oury *et al*. 2003; Oury and Godin 2007). This physiological basis of an inverse relationship between grain protein concentration and yield was reported to be a competition of C and N for energy and N dilution effect imparted by carbon-based compounds (Acreche and Slafer, 2009). Because the majority of grain N originates from remobilization (Gaju *et al*., 2014), rather than from post-anthesis uptake, mechanisms to enhance reserve N accumulation in the canopy and efficiency of N remobilization should also be addressed in the genetic improvement of grain protein deviation, which is the deviation of regression between grain protein from grain yield (Hakwesford, 2014).

2.6 Phenotyping for NUE

2.6.1 Root phenotyping method

Root trait gene identification and selection in breeding programs continue to be hampered by a lack of high-throughput and large-scale phenotyping approaches (Fiorani and Schurr, 2013). Most root

phenotyping approaches rely on seeding grown on germination paper or in growth pouches (Hund *et al*., 2009; Bai *et al*., 2013). These laboratories-based screening methods are very difficult to reproduce in field conditions (Passioura 2006, 2010; Poorter *et al*., 2012) due to the interaction between soil conditions and genotypes under study. Some of the promising techniques for root phenotyping methods are rhizotron (Lobet *et al*. 2011; Nagel *et al*. 2012; Richard *et al*. 2015). In addition to that, non-destructing imaging includes X-ray computed tomography (Gregory *et al*. 2003, Lontoc-Roy *et al*. 2006, Hargreaves *et al*. 2009, Mooney *et al*. 2012, Mairhofer *et al*., 2013), magnetic resonance imaging (Metzner *et al*., 2015) and mini-rhizotrons (Lontoc- Roy *et al*., 2006, MacFall and Johnson 2012, Poorter *et al*., 2012, Vamerali *et al*., 2012).

2.6.2 Canopy phenotyping methods

Acquiring high-throughput precise phenotypes on thousands of breeding lines is a critical bottleneck in boosting wheat's yield and N stress tolerance. Spectral reflectance to assess biomass, canopy size, and N content is a promising technology for high-throughput field phenotyping. The spectral reflectance indices (SRI) measure the ability of a canopy to absorb and reflect solar radiation at different wavelengths according to its structural and physiological features. Normalised difference vegetation index (NDVI) is one of the most extensively used SRIs, and it is based on the relative reflectance in the visible (400-700 nm) and near-infrared (700-1100 nm) due to the absorption of light by chlorophyll and related pigments (Araus *et al*., 2001). SRI has been developed to measure crop biomass (Babar *et al*., 2006), green canopy area (Aparicio *et al*., 2002), leaf chlorophyll (Babar *et al*., 2006), staygreen (Lopes and Reynolds, 2012), grain yield (Gutierrez-Rodriguez *et al*., 2004, Gutierrez *et al*., 2010a, b). Apart from spectral-based indices, remote-sensing technologies have been used for field-based phenotyping such as chlorophyll fluorescence imaging to measure photosynthesis (Romer *et al*., 2011), and infrared thermometry for canopy photosynthesis (Saint Pierre *et al*., 2010). Laser image detection and ranging (Lidar) is another remote-sensing tool that is now being utilised for field-based phenotyping in cereals to survey directly the 3D distribution of canopies. This technology provides accurate estimates of crop height, cover, canopy structural properties (Lefsky *et al*., 2002, Omasa *et al*. 2007, Hosoi and Omasa 2009), crop biomass, and N content (Eitel *et al*., 2014).

2.6.3 Genetic Diversity in N-use Efficiency and its component traits

Under high and low N input supply conditions, multiple studies throughout the world have found genetic connections between grain production and NUE components. Most of studies have indicated that uptake efficiency contributed more toward NUE at low N status than at higher N status (Ortiz-Monasterio *et al*., 1997; Le Gouis *et al*., 2000). However, Dhugga and Waines (1989) reported uptake efficiency was the most important contributor to NUE at all nitrogen status conditions. Studies have also demonstrated that genetic gains in NUE with breeding under low N supply have been related

mainly to improvements in NUpE in spring wheat (Ortiz-Monasterio *et al*., 1997; Muurinen *et al*., 2006) and NUtE in winter wheat (Brancourt-Hulmel *et al*., 2003).

Early root growth, root branching, and biomass are among the N uptake-related features that are significantly influenced by genotypic diversity (Sinha *et al*., 2020). It has been reported that root density most often remains below the critical level for optimum nitrate uptake (Ford *et al*., 2007; Reynolds *et al*., 2007). This indicates that there is a substantial scope for improving nitrogen uptake. However, research progress in exploring the genetic advantage of root-related traits has been slow because of the difficulties in screening for root variation in the field (Whalley *et al*., 2017). Furthermore, the most popular strategy to minimise phenotyping issues has been to examine the root systems of immature seedlings. Indirect selection approaches can be used for the selection of nutrient uptake as lower canopy temperature is indicative of higher root uptake capacity, although this uptake capacity is also correlated with higher stomatal conductance (Bai *et al*., 2013).

Genetic potentiality of dep rooting system from diploid wild species of *Triticum tauschii* (D genome) has been transferred to synthetic wheat cultivar (Reynolds *et al*., 2007). Deep root system of tall landraces in China and Iran was also reported (Sun *et al*., 2020). There is a lack of studies on the gene responsible for desirable traits for root traits (Islam *et al*., 2021). Gene for root traits identified in other cereals crops might be useful for wheat breeding for root traits, for example, RHT1 and RHT3 in maize (Hochholdinger *et al*., 2009) and DRO1 in rice (Uga *et al*., 2013). However, root architecture and its N uptake-related functional characteristics are probably multigenic, making it challenging to pinpoint genetic potential.

2.7 Specific traits for potential improvement for NUE

2.7.1 Identifying novel genes

Transcriptomic analysis is gaining popularity for the identification of candidate genes involved in NUE or response (Hawkesford 2014). This approach has been applied to identify species steps in senescence (Howarth *et al*., 2008) or grain filling (Hansen *et al*., 2009) and in roots and shoots in relation to nitrate supply for model plants such as tomato (Wang *et al*., 2001) and Arabidopsis (Wang *et al*., 2003). More sophisticated genotype-environment trait correlations will be needed to whittle down potential genes from the large number of responsive genes that have been identified; yet, explicit attribution of identified genes to determining traits of interest has not generally been successful (Hawkesford, 2014).

2.7.2 Targeting specific genes and processes

Targeted crucial genes have been identified as potential improvements to NUE (McAllister *et al*., 2012). Most of the targeted genes for genetic improvement rely on N uptake or nitrogen assimilatory

pathways and it is rate limiting also. However, the modified expression of alanine aminotransferase was reported to have a marked effect on plant NUE (Good *et al*., 2007; Shrawat *et al*., 2008). , the exact mechanism for the impact on NUE remains indefinable (Hawkesford 2014).

2.7.2.1 Nitrogen uptake

Effective capture is a need for efficient N utilisation. This is a root feature that is primarily dependent on both root architecture and root functioning. In most agricultural soils, N is absorbed by the roots primarily as nitrate, although it is also taken up as ammonium and, to a lesser extent, as organic N in the form of amino acids. One or more major gene families catalyse each of these forms' uptake and transport across cell membranes, and transport mechanisms are highly developed, with high substrate affinities and expression patterns that are frequently regulated by nutritional control (Williams and Miller, 2001; Garnett *et al*., 2013). Two families of nitrate transporters have been characterized, the low-affinity type and the high-affinity type (Daniel-Vedele *et al*., 1998; Williams and Miller, 2001). However, at the macroscopic level, breeding opportunities for better nitrogen uptake may emerge in terms of root architecture and proliferation. Due to the difficulty of doing research root architecture in the field, most of it has been conducted in laboratories using a variety of artificial systems. Furthermore, virtuous alternative measurements for root function in the field may offer useful screening mechanisms such as total N taken up as a function of available N (NUpE), the most evident field-based measurement, which is only partially a function of yield.

2.7.2.2 Nitrogen assimilation

The foremost step in nitrogen assimilation in plants is the reduction of absorbed nitrate to ammonium by consecutive action of nitrate reductase and nitrite reductase. Thereafter, ammonium is assimilated into glutamine and glutamate catalysed by Glutamine synthetase (GS) and Glutamine:2-oxoglutarate aminotransferase (GOGAT). Especially, there are numerous glutamine synthetase isoforms, and they are highly tissue-specific (Bernard *et al*., 2008; Swarbreck *et al*., 2011). One important role of glutamine synthetase in photosynthetic tissue is in the refixation of ammonia released during photorespiration or senescence processes (Mattsson and Schjoerring, 1996; Swarbreck *et al*., 2011). There is a scope for the identification of genetic diversity of expression patterns of this gene family.

2.7.2.3 DELLA protein and NUE

It is a well-known fact that high-yielding semi-dwarf varieties of wheat and rice are based GA deficiency and GA-insensitive DELLA protein, respectively. GA targets DELLA protein for degradation. The DELLA protein is a negative regulator of plant height and nitrogen metabolism (Liu *et al*., 2022).

In rice, GROWTH-REGULATING FACTOR4 (GRF4) is known to be regulating N-uptake and its assimilation. However, rice DELLA protein, SLENDER RICE1 (SLR1) inhibits GRF4 mediated N uptake by inhibiting functional interaction of GRF4 with its transcription co-activator GRF-INTERACTING FACTOR1 (GIF1). Hence, an abundance of GRF4 enhanced the N uptake and its NUE, whereas DELLA protein reduced N uptake and its assimilation in high-yielding green revolution varieties (Li *et al*., 2008). DELLA accumulation is associated with reduced N acquisition and accumulation (Gooding *et al*., 2012). It is reported that both *sd1* and *Rht-B1b* alleles reduced N uptake (Li *et al*., 2018). Furthermore, the activities of glutamine synthetase (GS) and nitrate reductase (NR) are reduced in sd1 mutants (Li *et al*., 2018).

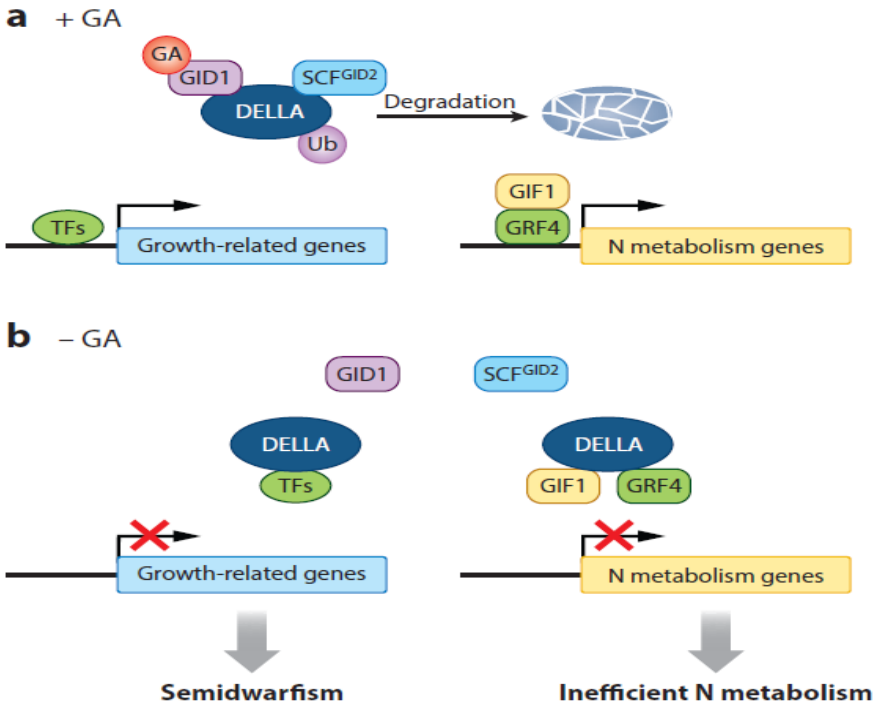

Figure 2.10: DELLA-mediated trade-off between growth and N metabolism. (a) GA lifts DELLA repression of plant growth and N metabolism. (b) In the absence of GA, DELLA accumulation restrains plant growth and N metabolism (Liu *et al*., 2022)

2.7.2.4 Nitrogen harvest index, remobilization, and stay-green phenotypes

It is well known that nitrogen is required for canopy structure and photosynthetic apparatus. In addition, canopy nitrogen is also required for storage protein synthesis during grain filling period. Senescence of the canopy prevents further photosynthetic activity and yield production, but it is necessary for the remobilization of N and other minerals, which are necessary for the grain production. A wider canopy with more N and minerals and a pattern of phased senescence will offer the best balance between ongoing photosynthesis, enough N supplies to the grain, and a maximum NUE overall (Hawkesford, 2014). Moreover, remobilization of N again depends on environmental and genetic

factors. Environmental factor N fertilization delays leaf senescence and increases the leaf N for remobilization. Drought stress aggravates leaf senescence and declines NUE (Barbottin *et al*., 2005). There is substantial genetic variation in the senescence rate in genotypes, which can be exploited for the enhancement of NUE. Stay-green phenotypes will extend the photosynthesis period, which may increase yield; however, delayed or no senescence may negatively affect nutrient remobilization. Improved grain weight, total yield, and improved N uptake have been reported in stay green mutant of durum wheat in glasshouse conditions (Spano *et al*., 2003). Studies also reported that increased leaf senescence rate had a negative impact on yield and extending the grain filling period had little or no impact on yield and N content.

2.8 Selecting for natural variation in NUE

Several studies have indicated significant genetic variations in NUE in cereals (Barraclough *et al*., 2010; Gaju *et al*., 2011). Furthermore, several studies have been conducted for NUpE and NUtE with different levels of nitrogen inputs (Foulkes *et al*., 1998; Van Ginkel *et al*., 2001; Sadras and Lawson, 2013) It is also indicated NUpE and NUtE are major contributors to NUE at low N and higher N status respectively (Ortiz-Monasterio *et al*., 1997). Notable independent variations in NUp and NUt was reported in 39 UK and European modern wheat in different nitrogen levels (Barraclough *et al*., 2010). However, it is well-reported that an increase in yield is correlated with increased NUtE, but not with NUpE for the pre-anthesis dry matter accumulation. This indicated a specific target for genetic improvement must be given for nitrogen uptake at the pre-anthesis stages (Bingham *et al*., 2012). It is obvious that in order to achieve more trait differences, selection should be done at low and high N inputs for both NUpE and NUtE (Hawkesford, 2014).

2.9 Rationale for improved N economy

Wheat crops with low NUE may be associated with: (i) nitrate leaching polluting ground water, (ii) eutrophication of rivers and lakes and (iii) global warming, due to emission of nitrous oxide caused by denitrification of nitrate by soil bacteria and the use of fossil fuels in the manufacture of N fertilizers (Goulding, 2004). Therefore, there is increasing emphasis worldwide in breeding wheat cultivars (Ortiz-Monasterio *et al*., 2001; Guarda *et al*., 2004; Hirel *et al*., 2007; Li *et al*., 2008) and in developing wheat N management strategies (Raun *et al*., 2002; Shanahan *et al*., 2008) for high NUE.

2.10 Management strategies for improving NUE

The major cause for lower nitrogen uptake efficiency is (i) non-synchronization between nitrogenous fertiliser and crop demand (Fageria and Baligar, 2005), (ii) uniform field applications to spatially variable fields (Hurley *et al*., 2004; Koch *et al*., 2004), (iii) use of 'yield based' N recommendations assuming constant efficiency of fertiliser recovery (Sylvester-Bradley *et al*., 1990)

and (iv) failure to take account of year-to-year weather variations (Shanahan *et al*., 2008). Combining N-efficient cultivars with N management practices for high NUE will maximize the practical application of bred-improved characteristics on farms (Foulkes *et al*., 2009).

Future agronomic technology for enhancing uptake efficiency include in-season crop monitoring through ground-based reflectance sensors (Raun *et al*., 2002), leaf chlorophyll meter-based prediction (Lopez-Bellido *et al*., 2004). Furthermore, NUE of the entire agroecosystem will be significantly impacted by the cumulative impacts of management practices on soil quality over time. An important indicator of soil quality is its organic matter content; soils that store carbon in addition to nitrogen, lead to a greater indigenous N supply and lower N fertiliser needs (Cassman *et al*., 2002). Consequently, management strategies that boost soil organic matter will, in most cases, result in improved efficiency in the long run.

2.10.1 Advancement in fertilisation

It is stated that 50% of the yield enhancement is contributed by N fertilizers (Javed *et al*., 2022)**.** However, most of the applied nitrogen is lost through ammonia, denitrification, leaching, and run-off. Therefore, the use of modern fertilizers would be an appropriate method in place of conventional fertilizers (Dass *et al*., 2017). In addition to that, the use of customized fertilizers can enhance the NUE. Customized fertilizers (CF) are multi-nutrient carrier that contains macro and micronutrient forms (Mudalagiriyappa *et al*., 2015). It is reported that the adoption of such fertilizer would enhance the NUE by 40% (Dass *et al*., 2017). The use of nano fertilizers would be a great alternative for enhancing NUE as it releases nitrogen slowly depending up on crop requirements (Mejias *et al*., 2021). Application of NFs enhanced the productivity of crops through the slow and continuous release of nutrients to the roots of plants and thereby increasing NUE (Kah *et al*., 2019). Bio-fertilizers are blends of helpful microorganisms that, either directly or indirectly, stimulate microbial activity and, as a result, speed up the transport and solubilization of nutrients in the soil (Suyal *et al*., 2016). Mycorrhiza has the potential to go deeper in the soil and provide the available form of nutrients to the plant roots thereby increasing the uptake, and providing an opportunity (Abdul Mallik, 2016).

Bio-fertilisers function as organic amendments by breaking down crop residue, controlling harmful insect pests in the soil, and eventually enhancing the soil's resilience and sustainability of the agricultural production system (Sahoo *et al*., 2013). Biochar, charcoal-like materials have been reported to enhance soil fertility and NUE (Majumder *et al*., 2019), attributed due to their higher surface area with pores along with their functional groups (Prommer *et al*., 2014). It has been reported that the application of wheat residues and biochar along with nutrients at 1% and 2% improved soil N and pH (Mierzwa Hersztek *et al*., 2020). In addition to that, precision farming can play a role in precision farming to improve NUE through global positioning systems (GIS), remote sensing, and variable rate applicator technologies (Javed *et al*., 2022). Additionally, several precision farming technologies

including the leaf color chart (LCC), chlorophyll meter, and green seeker are essential in boosting NUE (Dass *et al*., 2015).

2.11 Why high-throughput phenotyping?

Advancements in plant genome sequencing have shown significant strides in recent times, thanks to its cost-effectiveness and ability to handle large amounts of data (Li *et al*., 2018; f Werner, T., 2010; Clarke *et al*., 2016). Despite this progress, the connection between the plant's genotype and its observable characteristics, known as the phenotype, has faced challenges. The plant phenotype encompasses various morphological, physiological, and biochemical traits that provide insights into its structure, composition, and growth (Johannsen, W. *et al*., 1911; Rebolledo *et al*., 2016). This includes not only agronomic features like shape, size, and color but also the plant's physiological conditions throughout its life cycle at different time points.

Conventional phenotyping methods are laborious and time-consuming, making it challenging to collect comprehensive phenotypic data from large groups of plants. Moreover, relying on human measurements introduces subjectivity and the potential for errors, which can affect the accuracy and reliability of the data (Awika *et al*., 2019). Additionally, conventional approaches struggle to continuously monitor phenotypic changes throughout a plant's life cycle. As a solution to these limitations, high-throughput phenotyping has emerged as a promising option to bridge the gap between genotype and phenotype. By overcoming the drawbacks of manual conventional methods, high-throughput phenotyping enables efficient data collection and analysis.

With the development of two essential methods, it is now possible to characterize a whole collection of genes and genomic regions implicated in an N deficiency-induced response across a full growth cycle. First, high-throughput phenotyping techniques built on automatic or semiautomatic platforms have emerged in recent years to characterize a complete set of structural and functional traits of plants (Furbank and Tester, 2011). These high throughput phenotyping methods permit the non-destructive evaluation of phenotypic qualities at numerous stages in a growth cycle, allowing for a more in-depth examination of phenotype generation during development. Second, genetic dissection of these complex traits and relevant component traits by exploring the spatio-temporal data can be done to help disentangle the genetic control of developmental processes of complex traits.

2.12 High-throughput phenotyping is vital for the future of plant phenotyping

Modern imaging techniques for high-throughput phenotyping, including visible light imaging (RGB), hyperspectral imaging, near-infrared, and fluorescence imaging, have proven effective in assessing various aspects of plant growth, biomass, architecture and nutritional status (Muraya *et al*., 2017; Chen *et al*., 2019). These methods primarily rely on non-invasive imaging and spectroscopy to acquire phenotypic data, and advanced computing equipment for real-time analysis of plant growth and

physiological conditions. A typical high-throughput phenotyping platform comprises: a) digital sensors for capturing plant images at multiple time points, b) specially calibrated imaging platforms with hydraulic lift, uniform background, and lighting sources, c) dedicated data storage and processing servers, d) automated imaging software, and e) image processing software.

In comparison to traditional phenotyping approaches, high-throughput phenotyping offers simultaneous data collection for numerous attributes in large plant populations, allowing dynamic observations of plants at various growth stages. Moreover, trait characterization based on spectra or photographs is more objective compared to subjective visual scoring methods. This objectivity minimizes interpretive biases. Additionally, high-throughput phenotyping enables the non-destructive determination of biochemical parameters through modelling, eliminating the need for time-consuming destructive analyses (Xiao *et al*., 2022).

Recent advancements in computer-vision-assisted sensors and analysis tools have significantly improved the reliability and precision of high-throughput plant phenotyping and nitrogen-related studies in crops (Fiorani and Schurr, 2013; Deery *et al*., 2014; Fahlgren *et al*., 2015; Nguyen and Kant, 2018). Digital imaging plays a pivotal role in automating the measurement of plant growth, development, physiology, and the estimation of biochemical components. The non-destructive nature of data capture in digital phenotyping is of utmost importance as it allows for time-series growth measurements, eliminates destructive analyses, and facilitates handling a larger number of genotypes in an experiment.

2.13 Phenotyping for nitrogen deficiency response and NUE

Accurately determining the N level in plants is crucial for effective N management, which involves carefully timing and dosing N fertilizer treatments to meet crop demand and improve crop NUE. Traditional laboratory methods like Kjeldahl digestion, Dumas combustion, and CHNS analyzer are available for quantifying plant N content, offering precise results but proving to be time-consuming, destructive, and challenging to apply when dealing with large plant populations. However, nondestructive sensing and imaging techniques utilizing various sensors and cameras have significantly advanced the efficient and accurate phenotyping of nitrogen level and related crop traits (Muñoz-Huerta *et al*. 2013).

The multi-disciplinary science of phenomics, the sensor-aided non-destructive high throughput automated acquisition and analysis of high-dimensional phenotypic data on an organism-wide scale, emerged recently to bridge the phenotype-genotype gap and enhance the pace of analytical breeding. To begin, in the last several years, high-throughput phenotyping techniques built on automatic or semiautomatic platforms have emerged to characterize a full range of structural and functional traits of plants, from the cellular level to the whole plant or canopy level, both in the lab and in the field (Furbank

and Tester, 2011; Ghanem *et al*.2015; Halperin *et al*., 2017). Hyperspectral imaging is found to be highly useful to phenotype concentrations of macronutrients nitrogen (N), phosphorus (P), potassium (K), magnesium (Mg), calcium (Ca), and sulfur (S), and micronutrients sodium (Na), iron (Fe), manganese (Mn), boron (B), copper (Cu), and zinc (Zn) in maize (Pandey *et al*., 2017). The depth of component phenotypic traits and the spatiotemporal dynamic phenotypic data generated in phenomics are enormous and unparallel to the conventional phenotyping. Using phenomics at the Plant Accelerator (®), The University of Adelaide, Australia, sorghum was analysed for NUE. Color image analysis was found to correlate with foliar nitrogen and chlorophyll (Neilson *et al*., 2015). In *Brachypodium*, a time series image-based approach coupled with mathematical modeling showed that it can clearly measure the genotypic response to nutrient supply at high resolution than traditional destructive techniques (Poire *et al*., 2014).

These innovative techniques are based on the interaction between plant components, such as pigments and inorganic compounds, and electromagnetic radiation in specific spectral regions like visible (400–700 nm), NIR (700–1000 nm), and shortwave infrared (1000–2500 nm) (Fahlgren *et al*., 2015; Mulla, 2013). When plants are exposed to light, they absorb, reflect, emit, transmit, and fluoresce radiation. By analyzing this light interaction, comprehensive information about a plant's structure, biochemistry, and physiological condition can be revealed (Homolová *et al*., 2013). These advancements offer a promising way to facilitate nitrogen-related research in crops efficiently and with precision (Fiorani and Schurr, 2013; Deery *et al*., 2014).

Optical devices have been developed to capture spectral reflectance from plant leaves or canopies, employing data processing and computer visualizations to generate digital plant objects and vegetation indices (VIs) associated with essential plant traits like chlorophyll levels, canopy coverage, N status, biomass, and grain yield (Klukas *et al*., 2014; Filella *et al*., 1995; Pandey *et al*., 2017). For instance, in wheat (*Triticum aestivum* L.) grown under varying N levels in field conditions, canopy chlorophyll content and the normalized difference vegetation index calculated from red and NIR spectral bands show significant correlations with chlorophyll and N content, biomass, and grain yield (Fitzgerald *et al*., 2006).

Two main categories of phenotyping devices and platforms exist: digital imaging and proximal or remote sensing (Table 1). Automated imaging systems, such as visible red-green-blue (RGB), near-infrared (NIR), chlorophyll fluorescence, and hyperspectral cameras, are effectively used for phenotypic screening of various plant species in controlled environmental conditions. Additionally, active and passive optical sensors such as Crop Circle, Green Seeker, YARA N-Sensor, LiDAR, FieldSpec spectrometer, CropScan, and LI-1800, are employed for field phenotyping to assess canopy reflectance and generate vegetation indices that serve as surrogates for chlorophyll content, N status,

biomass, and grain production (Li *et al*., 2008; Tremblay *et al*., 2009; Rambo *et al*., 2010; Eitel *et al*., 2011; Sun *et al*., 2017).

Ground- and aerial-based platforms equipped with multiple sensors and cameras have significantly improved the efficiency and throughput of phenotypic data collection across various crop species, showing great potential for nitrogen-use efficiency (NUE)-related research (Deery *et al*., 2014; Sankaran *et al*., 2015).

Table 2.1: High-throughput phenotyping for nitrogen response studies in plants.

Name and mode of measurement	Sensor type and spectral range	Species	Env	Measured traits	References
Digital imaging					
Scanalyzer 3D (LemnaTec GmbH): ground fixed and fully automated	RGB camera, 400–700 nm; NIR-300 camera, 900–1700 nm; Hyperspectral camera, 550–1700 nm	*Sorghum bicolor*, *Brachypodium, distachyon, Hordeum vulgare, Triticum aestivum, Zea mays*	Controlled Environment	Chlorophyll and water, content, biomass, dynamic growth, leaf,area, plant height, water, content, N content	Poiré *et al*. (2014); Neilson *et al*., (2015); Chen *et al*., (2014); Pandey *et al*., (2017)
HySpex VNIR 1600–160: ground fixed, tractor-mounted and semiautomated	Hyperspectral camera 400–1000 nm	*T. aestivum L.*	Field	Leaf N content	Vigneau *et al*. (2011)
PlantEye (Phenospex): ground fixed and semiautomated	NIR-laser scanner 700–1000 nm	*Brassica napus L., T. aestivum,*	Controlled Environment, field	Chlorophyll fluorescence, leaf area, biomass,	Kjaer and Ottosen, (2015); MaphosaI*et al*. (2016)
Phenoscope: ground fixed and fully automated	RGB camera 400–700 nm	*A. thaliana Heynh.*	Controlled Environment	Shoot growth, shape, biomass	Tisné *et al*. (2013)
Phenosis: ground fixed and fully automated WIWAM: ground fixed and fully automated	RGB camera 400–700 nm	*A. thaliana*	Controlled Environment	Shootgrowth, leaf number, leaf area, shoot growth, leaf area	Granier *et al*. (2006); Skirycz *et al*. (2011)
Proximal or remote sensing					
Crop Circle (HollandScientific Inc.): handheld or tractor-mounted, manual or semiautomated	Multispectral active sensor, three channels: 670 nm, 730 nm,760 nm	*T. aestivum, O. sativa*	Field	VIs, chlorophyll and Ncontent, biomass, grainyield	Erdle *et al*. (2011); Cao *et al*. (2013); Nguyen *et al*. (2016)

Name and mode of measurement	Sensor type and spectral range	Species	Env	Measured traits	References
Green Seeker (NTechIndustries Inc.): handheld or tractor-mounted, manual or semiautomated	Dual-channel activesensor: 656 nm, 774 nm	*T. aestivum, Z. mays*	Field	VIs, chlorophyll and Ncontent, biomass	Hong *et al*. (2007); Erdle *et al*. (2011)
YARA N-Sensor (YaraInternational ASA): handheld or tractor-mounted, manual orsemiautomated	Dual-channel activesensor: 450 nm, 900 nm	*T. aestivum, Z. mays*	Field	VIs, N content, biomass	Tremblay *et al*. (2009)
FieldSpec spectrometer (Analytical SpectralDevices, Inc.): handheld	Hyperspectral passivesensor, multiplechannels from 350 to2500 nm	*T. aestivum*	Field	VIs, N content	Fitzgerald *et al*. (2006); Foster *et al*. (2012)
CropScan (MSR16, CropScan Inc.): handheld	Multichannel passivesensors, 460–950 nm	*Z. mays*	Field	VIs, N content, biomass	Rambo *et al*. (2010)
LI-1800 (LI-COR Inc.): handheld, semiautomated	Multichannel passive sensors, 400–1100 nm	*O. sativa*	Field	VIs, N content	Lee *et al*. (2008)
LiDAR: ground fixed, tractor-mounted, semiautomated	Single-, multi- and hyperspectral sensors, 538–910 nm	*O. sativa, T. aestivum,B. napus, Z. mays*	Controlled Environment, field	VIs, chlorophyll, N, and water content, height, leaf area, biomass	Eitel *et al*. (2011); Deery *et al*. (2014); Sun *et al*. (2017)
Integrated platforms combing sensors and imagers					
Phenomobile (High Resolution Plant Phenomics Centre): tractor mounted and semiautomated	RGB, thermal and hyperspectral cameras, LiDAR, multiple sensors	*T. aestivum, Gossypium sp., Z. mays*	Field	VIs, chlorophyll and N content, crop architecture, height, leaf area, biomass	Deery *et al*. (2014)

Name and mode of measurement	Sensor type and spectral range	Species	Env	Measured traits	References
UAV platforms: aerial mounted, semiautomated	RGB, multispectral cameras	*T. aestivum, Z. mays, Gossypium sp., S. bicolor, H. vulgare*	Field	VIs, emergence, height, growth rate, biomass, grain yield	Sankaran *et al*. (2015); Holman al. (2016); Shi *et al*. (2016)
Field Scanalyzer (Rothamsted Research):ground fixed and fullyautomated	RGB, chlorophyll fluorescence, thermal and hyper-spectral cameras, LiDAR, multiple sensors	*T. aestivum*	Field	VIs, chlorophyll and N content, phenology, crop architecture, height, leaf area, biomass	Virlet *et al*. (2016); Sadeghi-Tehran*et al*. (2017)

RGB, red–green–blue; LiDAR, light detection and ranging; NIR, near infrared; UAV, unmanned aerial vehicle; VI, vegetation index

2.14 Linkage map and QTL mapping

When genes are on different chromosomes or far apart on the same chromosome, they assort separately. The alleles of genes on a chromosome that are near to one another have a tendency to "stick together" and to be inherited collectively (Campbell *et al*., 2008). Mendel's law of independent assortment has the most notable exception, which is a phenomenon known as genetic linkage. During the meiosis phase of sexual reproduction, DNA sequences that are near to one another on a chromosome have a tendency to be inherited together (Purcell *et al*., 2003). Physical proximity between two genetic markers makes it unlikely that they will be separated out onto distinct chromatids during chromosomal crossover. In other words, there is less possibility of recombination between two genes the closer they are to one another on a chromosome.

2.14.1 Genetic map description

The term "genetic map," which includes the terms "classical genetic map" and "molecular genetic map," refers to the reorganization of chromosomes throughout the genome's length. According to the principles of the chain of exchange and the genetic loci exchange hypothesis, the traditional genetic map is created (Burran and DesRochers, 2015; Reece *et al*., 2014). The number of tags on the traditional genetic map is minimal, making it challenging to create a saturated genetic map due to the availability of genetic markers. Additionally difficult is the integration of various genomic maps. Additionally, due to the epistatic interaction of genes, marker-associated features cannot function fully. The traditional genetic mapping application has been severely constrained over the past 50 years due to decreasing efficiency and poor application value. The localization of QTLs, map-based gene cloning, comparative genomic research, molecular marker-assisted breeding, etc. are all based on a molecular genetic map, also known as a linkage map, which is created using DNA markers (Burran and DesRochers, 2015). Since the 1980s, the development of molecular genetic maps has been supported technically by the discovery of DNA molecular markers, enabling accurate QTL mapping.

2.14.2 Construction of genetic map

Chromosome exchange and remodeling are the theoretical cornerstone of genetic map building. The linkage genes on the homologous chromosomes are involved in exchange and restructuring while the genes on the non-homologous chromosomes are independent from one another during meiosis (Botstein *et al*., 1980). The distance between homologous chromosomes and the frequency of gene exchange have been found to be closely correlated. The genetic distance between genes can therefore be determined by the pace of reorganization. According to Tian *et al*. (2015), the process of creating a genetic map primarily entails the following steps: (1) analyzing the genetic variance of the parents; (2) creating a suitable mapping population; (3) testing the polymorphism markers between parents and scanning separation populations; (4) creating linkage groups; and (5) calculating the spacing between

genetic markers. Software that can be used for genetic mapping includes MAPMAKER/Exp ver.3.0 b (Lincoln *et al*., 1993), JoinMAP 4.0 (Van Ooijen and Voorrips, 2006), QTL IciMapping 3.0 (Wang *et al*., 2011), Mapchart 2.1 (Voorrips, 2002) and MergeMap (Vassoler *et al*., 2014).

2.14.3 Genetic mapping populations

The adaptability, size, homozygosity, and genetic diversity of the genetic population are all factors that affect QTL mapping. In the past twenty years, several genetic maps have been constructed and QTLs for controlling yield, quality, and resistance in common wheat have been identified using a variety of mapping populations, including backcross (BC), recombinant inbred line (RIL), near-isogenic lines (NIL), and doubled haploid (DH) populations.

2.14.4 Choice of suitable parents

The genetic distance between the parents should be in the middle, and neither too great nor too small. A hybrid's homologous chromosome pairing may be impacted by a significant discrepancy, which could result in a substantial reduction in crossovers, low recombination rates for loci in the connected segments, biased partitions, and even hybrid sterility. As a result, there would be a sharp decline in confidence. On the other side, a difference that is too small frequently indicates low DNA polymorphism and fewer polymorphic markers, which leads to poor mapping accuracy. Parental purity: Self-crossing can ensure the parents' homozygosity (Tian *et al*., 2015).

2.14.5 Population Maps

A mapping population is frequently created from an F1 hybrid, which is produced when two pure breeding parents with unique alleles cross, and it represents all the genotypes in the family. Theoretically, such a population ought to include both homozygous and heterozygous loci. Temporary populations and permanent populations are the two types of genetic populations used in the creation of genetic maps. According to Silvertown and Charlesworth (2009), the former typically consists of DH, RIL, immortalized F2 (IF2), and NIL, whilst the latter typically consists of F2 and its descendants of F3, F4, and BC lines.

2.14.6 Population size

The size of the mapping population has a significant impact on the precision and efficacy of genetic analysis and QTL detection, particularly on the quantity, estimation and sensitivity of QTLs (Schön *et al*., 2004; Zou *et al*., 2005; Buckler *et al*., 2009). According to Xu (1994), the estimated likelihood ratio test (LOD) value increased with the size of the mapping population while the estimated bias of recombination rate and the biased estimation of the QTL genotypic mean and variance dropped. Furthermore, Beavis (1998) noted that even with a population size of 200 individuals, false-positive

QTLs might still be found. It is advised that the size of the population be chosen based on the purpose of the study and the goal of the research, as building a large genetically segregating population is difficult due to the heavy workload and high cost in the process of establishing a genetic linkage map, trait genetic analyses, and QTL detections. Typically, roughly 200 lines are required for main QTL mapping. The sorts of the population being built should also be taken into account when determining population size. According to Tian *et al*. (2015), the order of population sizes should be F2 > RIL > BC1 > DH in order to get a high mapping accuracy.

2.15 Molecular markers

For a very long time, morphological, physiological, or biochemical markers are frequently utilized to build genetic maps of distinct species. However, these linkage maps frequently have low resolution, low saturation, and great distance between markers, which limits their usefulness for application. The use of nucleotide sequence variants as genetic markers has been made possible by the quick development of molecular biotechnologies. The usage of DNA markers was thought to have begun with the discovery of the restriction fragment length polymorphism (RFLP), which was reported by Botstein *et al*. (1980). Based on the advancement of polymerase chain reaction (PCR) technology, the second-generation marker systems, such as random amplified polymorphic DNA (RAPD) (Joshi and Nguyen, 1993), amplified fragment length polymorphism (AFLP) (Hartl *et al*., 1999) and microsatellite markers (SSR) (Röder *et al*., 1998) were created. These days, third-generation marker systems, such as expressed sequence tag (EST) markers and single nucleotide polymorphism (SNP) markers (Cabral *et al*., 2014) are frequently used to create genetic linkage maps and map QTLs.

Due to its high degree of polymorphism, widespread distribution throughout the genome, low DNA required and ease of automation, SSR markers have been extensively employed in the development of maps. Diversity arrays technology (DArT), a hybridization-based substitute that maximizes the benefits of the parallel nature of the microarray platform, was later developed (Jaccoud *et al*., 2001). In a single test, DArT simultaneously types thousands of loci. Single-nucleotide polymorphisms (SNPs), a common type of genome variation, are present across all genomes (Cadalen *et al*., 1997; Rafalski, 2002). In most species nowadays, SNPs are the preferred marker for phylogenetic analyses, bulked segregant analyses, genome-wide association studies (GWAS) and genomic selection. SNPs are often biallelic while "satellite" polymorphisms are typically multiallelic. SNPs are more useful than SSRs for gene cloning and high-density fine mapping. Because there are many different molecular marker types, it is possible to continuously add new markers to linkage maps, increasing marker density. This suggests that creating high-density genetic maps is essential to understanding the genetic variations of biological traits, especially quantitative traits.

2.15.1 Single-nucleotide polymorphism (SNP) markers

SNPs, which include single-nucleotide transitions, deletions, transversions, and insertions, are single-nucleotide changes that happen inside the coding or non-coding sections of genes in the genome. By comparing DNA sequences to known or reference DNA sequences, SNP discrepancies can be found. The simplest method involves using specific primers to amplify a genome segment by PCR, followed by sequencing the PCR result and nucleotide sequence alignment. As DNA microarray technology developed, SNP emerged as the most significant and useful molecular marker. The most potential third-generation genetic markers are SNPs. Every biological genome has single nucleotide variants, which are the most prevalent type of polymorphism in all biological genomes (Brookes, 1999). SNP is more useful for creating high-density genetic maps, pinpointing target genes and cloning genes than SSR and other more repeat-based sequences. The identification of SNPs by whole-genome transcriptome or reduced-representation sequencing in a variety of groups has been considerably aided by advances in next-generation sequencing (Wang *et al*., 2014). For a variety of economically significant crops and animals, high-density SNP arrays have been created and successfully applied for genetic investigations (Ganal *et al*., 2011; Song *et al*., 2013). The detection of novel genes frequently uses the rice (44 K) and maize (50 and 55 K) SNP array (Tung *et al*., 2010; Zhao *et al*., 2011; Xu *et al*., 2017a; Xu *et al*., 2017b). The ability to screen a large number of SNPs, thanks to advances in next-generation sequencing (NGS) technology, has been leveraged to create high-throughput SNP-typing platforms as BeadExpress (Trebbi *et al*., 2011), KASPar (Allen *et al*., 2011) and Infinium (Cavanagh *et al*., 2013).

2.15.2 Types of SNP array available

A 90K SNP iSelect array containing roughly 90,000 gene-associated SNPs has been described by Wang *et al*. (2014), and it has the potential to provide deep coverage of the wheat genome. The wheat 90K iSelect SNP genotyping array was used to create high-density linkage maps for QTL analysis in wheat (Gao *et al*., 2015; Jin *et al*., 2016; Zhai *et al*., 2016; Wen *et al*., 2017; Hu *et al*., 2021). Additionally, gene-based SNP haplotypes can be found to enhance the selection of targ*et al*leles in breeding programs once genes and QTL have been cloned (Rasheed *et al*., 2016).

To this day, a number of high-density SNP genotyping arrays have been conceived of and put to use for the purpose of marker-assisted breeding in common wheat, for example, the Illumina Wheat 9K iSelect SNP array (Cavanagh *et al.*, 2013), the Illumina Wheat 90K iSelect SNP genotyping array (Wang *et al.*, 2014), the Wheat 15K SNP array (Boeven *et al.*, 2016), the Axiom® Wheat 660K SNP array, the Wheat 55K SNP array, the Axiom® HD Wheat genotyping (820K) array (Winfield *et al.*, 2016), the Wheat Breeders' 35K Axiom array (Allen *et al.*, 2017) and the Wheat 50K Triticum TraitBreed array (Rasheed and Xia, 2019).

Although high-density SNP arrays such as 660K, 820K and 90K chips represent a significant advancement in wheat genotyping, the format does not lend itself well to cost-effective high-throughput genotyping. Additionally, the majority of the markers on these arrays were designed to genotype polymorphisms between wheat and its near relatives and progenitors; as a result, they are of limited direct value to wheat breeders who are specifically interested in comparing hexaploidy germplasm. This is because these markers were designed to genotype polymorphisms between wheat and its near relatives and progenitors. In order to get over these restrictions, 35143 informative markers that are helpful to the breeding community were chosen, and the resulting array is known as the Wheat Breeder's 35K Axiom array.

2.16 Genetic dissection of NUE and component traits

To fulfill the requirement of increasing wheat yield in an economically and environmentally friendly manner, breeding wheat with improved NUE and designing variety-specific recommendations of N fertilizer management is important. Breeding crops with improved NUE can help increase crop productivity with less N Fertilizer input (Hirel *et al*. 2011; Han *et al*. 2015). For this donor for component traits of NUE and genes/QTLs need to be identified in wheat. Mapping quantitative trait loci (QTLs) for complex phenotypes involves linkage mapping based on controlled crossings or genome-wide association studies.

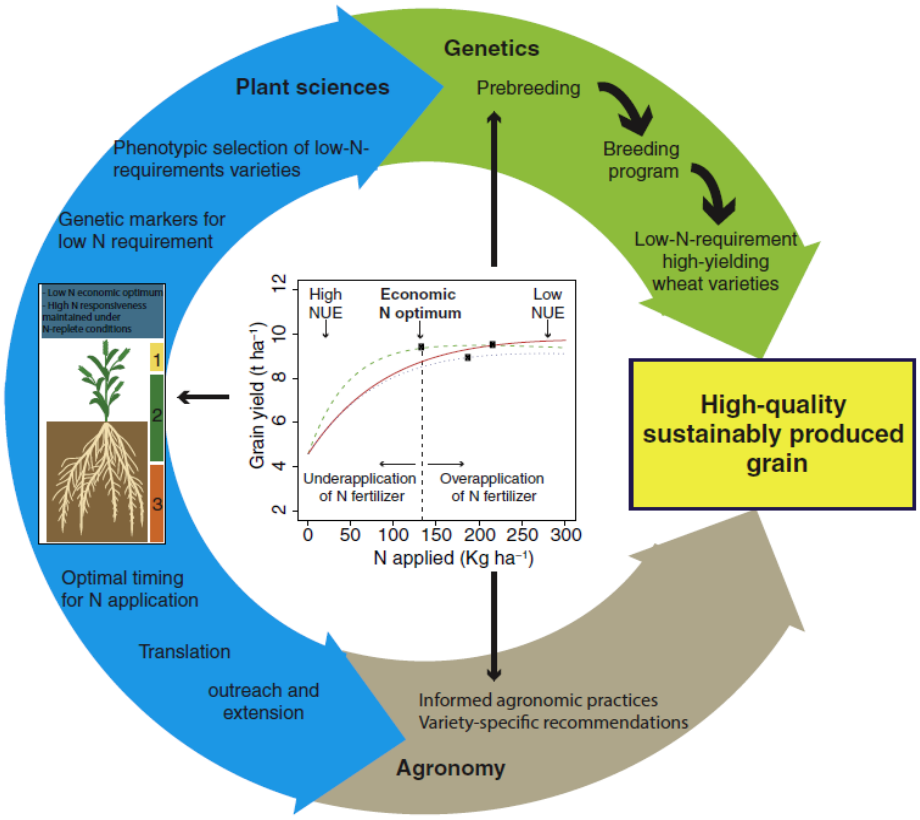

Figure 2.11: Framework for Producing Low-N-Requirement Crops (Swarbreck *et al*., 2019)

The best method of QTL mapping is the use of segregating populations derived from two parents (Biparental mapping population) with contrasting sets of traits. Fixed homozygous lines are produced by single seed descent (SSD) to produce recombinant inbred lines (RILs) or by the production of doubled haploids. These lines have the highest statistical power to detect chromosome regions linked to traits of interest. Numerous QTLs for NUE in rice have been identified (Wei *et al*., 2011). An association mapping panel is another approach to detecting QTLs and it has been used for many studies of NUE to detect QTLs (Cormier *et al*., 2014). Furthermore, the use of multiparent population for QTLs mapping has been carried out to capture more recombination events taking place since the cross are being made like nest associated mapping (NAM) developed in maize and multi-parent advanced generation intercross (MAGIC) developed in wheat (Winfield *et al*., 2016). Soleimani *et al*. (2017) used back cross population to dissect the phosphorus use in barley. Near isogenic line (NILs) populations have been used by Kowalski *et al*. (2016) to map the QTLs of agronomic importance, suggesting possible discovery of NUE research in near future.

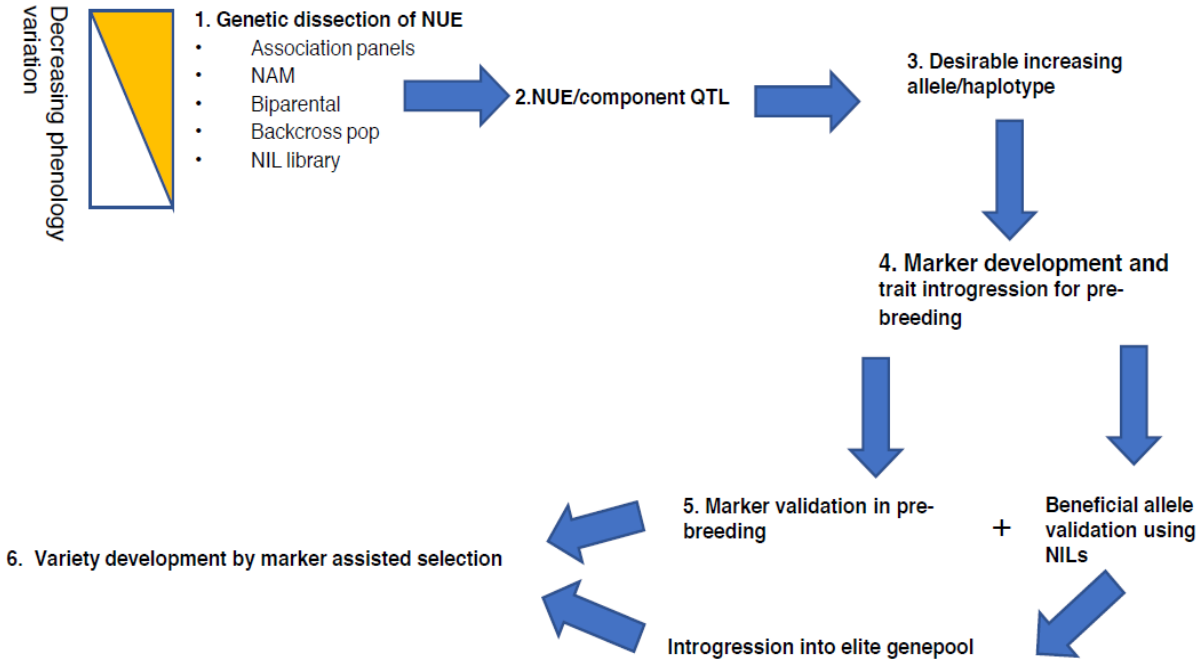

Figure 2.12: Way forward for the development of nitrogen efficient wheat varieties (Hawkesford and Griffiths *et al*., 2019)

Many quantitative trait loci (QTLs) related to wheat grain yield and its components have been mapped by linkage-based QTL mapping method (Nave *et al*., 2016). Through the use of a comparative experimental strategy, several studies have isolated N-responsive QTLs. To map specific QTLs implicated in plant tolerance to N-limited nutritional circumstances, for instance, Laperche *et al*. (2006). Zheng *et al*. (2010) created a mapping population resulting from a crossing between an N stress-tolerant variety and a N stress-sensitive variety and mapped QTLs for important agronomical traits. Zhai *et al*. (2014) and Zhau *et al*. (2015) mapped QTLs for yield related traits under different environments.

Several authors (Cormier *et al*., 2016; Islam *et al*., 2021; Saini *et al*., 2021) have reviewed the genetic control of N use-related traits and strategies for improving NUE in wheat.

2.16.1 QTLs for wheat NUE and its component traits

Nitrogen use efficiency (NUE) in wheat is a complex trait that is affected by the genotype, environment, and management (Hawkesford & Griffiths, 2019; Beres *et al*., 2020; Islam *et al*., 2021). Genetic improvement has a great potential for increasing NUE in wheat (Zhao *et al*., 2023). Foulkes *et al*. (2009) suggested that NUE in wheat crop can be improved genetically at least by 20%. Despite many efforts have been made, till now, no high NUE wheat cultivars had been released or commercialized. However, genetic architecture of NUE traits in wheat have been studied by many research groups throughout the world.

Zhang *et al*. (2019) studied genetic architecture of NUE traits in wheat by constructed a high-density genetic map using a set of 184 recombinant inbred lines (RILs) derived from the cross 'Tainong 18 × Linmai 6' and mapping of NUE related trait viz., 14 seedling traits and 17 maturity traits under hydroponic culture trials with high N (HN), moderate N (MN) and low N (LN) levels in two-time frames, and under field trials with HN and LN levels in two growing seasons. They found a total of 121 QTLs at seedling and 130 QTLs at maturity stages. They also suggested that the morphological/biomass traits and eight yield traits can be used as phenotypic markers for the large-scale screening and selection of NUE donors. Yang *et al*. (2021) reported 12 QTLs detected on chromosomes 1AL (1) in the control, 1DS (2) in high N treatment, 4BL (5) in low and high N treatments, and 7DS (3) and 7DL (1) in low N treatments influencing the root and biomass related traits for N uptake from doubled haploid wheat population consist of 198 lines from the crossed between Yangmai 16 and Zhongmai 895. Total of 7 major QTLs viz., QSnc.2, Qtnc, QRsnc.1, Qsnue.2, QTnue.4, Qgnue and, QAnue.3 were found contributed significantly to NUE in wheat. Among them, three QTLs related to N uptake efficiency (NUpE) included GNC, StNC, and ANC, and three QTLs related to N utilization efficiency (NUtE) traits (GNUE, StNUE, and ANUE). The most stable QTLs (RRS.caas-4DS) on chromosome 4DS, which were related to ratio of root to shoot dry weight trait, was in close proximity of the Rht-D1 gene, and it showed high phenotypic effects, explaining 13.1% of the phenotypic variance.

Brasier *et al*. (2020) found three major QTLs viz., Qnue.151-6A, QNue.151-1D, and QNue.52-7A involved in the assimilation of ammonium into amino acids; indicate a role in seedling vigor; significantly increased NUE under the reduced N rate and resulted in higher NUE, respectively from two bi-parental mapping populations were developed and grown in four site-seasons under low and high N rates.

Total more than 100 QTLs related to NUE estimated using root traits, shoot traits, dry matter, grain yield, agronomic traits, N% in dry matter etc. have been reported in Wheat QTLdb V2.0 (Singh

et al., 2022). Recently, Singh *et al*. (2023) studied the genetic inheritance of NUE using a bi-parental RIL mapping population derived from a cross between high NUE HUW468 and low NUE C306 genotypes and found 36 main effect QTLs explained 6.65–22.89% phenotypic variation spread on 12 chromosomes.

One of the important goals for sustainable wheat production is to decrease N fertilizer input without reducing grain yield. Maintaining or improving N uptake of wheat under low N fertilizer application is a key tackling this problem. Thus, compared to the low-affinity transport system, it seems that the high-affinity transport system has more potential in improving N uptake of wheat under low N supply conditions (Li *et al*., 2022). By overexpression of TaNRT2.1-6B gen previously reported by He *et al*. (2015), Li *et al*. (2022) found that grain yield nitrogen accumulation of wheat under either limited or sufficient N conditions have improved, thus TaNRT2.1-6B gene and the two associated SNP markers as promising powerful tools for breeding wheat cultivars with high N uptake ability and NUE.

Table 2.2:QTLs and genes identified in wheat related to NUE.

No.	QTL/Genes	Description	Ref
1	QSnc.2, Qtnc, QRsnc.1, Qsnue.2, QTnue.4, Qgnue, QAnue.3	Three N uptake efficiency (NUpE) (GNC, StNC, and ANC), and Three N utilization efficiency (NUtE) traits (GNUE, StNUE, and ANUE)	(Zhang *et al.* , 2019)
2	Qnue.151-6A, QNue.151-1D, QNue.52-7A	Involved in the assimilation of ammonium into amino acids; indicate a role in seedling vigor; significantly increased NUE under the reduced N rate and resulted in higher NUE, respectively.	(Brasier *et al.* , 2020)
3	Total of 36 QTLs	13 QTLs for NUE, 13 QTLs for NUpE, and 6 QTLs for NUtE	(Singh *et al.* , 2023)
4	TaNRT2.1-6B gen	Improving N uptake from the soil under both limited and sufficient N conditions	(Li *et al.* , 2022)

3.1 Experimental site and setup

The experiment was conducted at the Nanaji Deshmukh Plant Phenomics Centre (NDPPC), Indian Council of Agricultural Research-Indian Agricultural Research Institute (ICAR-IARI), New Delhi, India (Figure 3.1). The central point of the study area stands at 77.12 0E longitude and 28.08 0N latitude with an average elevation above the mean sea level being 228.61 (750 feet) The location and details of the experimental site is shown in Figure 3.2.

Figure 3.1:Drone view of Nanaji Deshmukh Plant Phenomics Centre, IARI-ICAR, New Delhi

New Delhi, India has a humid subtropical climate, with extremely hot summers and extremely chilly winters. The area is classified as part of the "Trans - Gangetic plains" and "Agroecological Region IV". May and June are reportedly the warmest months of the year, with highs of 43.0°C to 46.0°C; in contrast, January's lows of 4.0°C to 7.0°C mark the beginning of the cold weather season. The active monsoon months (July–September) bring the majority of the capital's yearly rainfall (740 mm), with South-West monsoon rains accounting for 75% of the total.

Figure 3.2: Photograph of Nanaji Deshmukh Plant Phenomics Centre (NDPPC), IARI-ICAR, New Delhi, India. A) Front aerial view of NDPPC B) Rear-side view of NDPPC at sunset C) Picturesque view of greenhouses of NDPPC.

Two types of soil used for the nitrogen use experiment, one is for control treatment plant with normal nitrogen content and one for nitrogen deficiency treatment plants with low nitrogen content. Both the samples are normal with medium organic carbon and pH. The chemical properties of soil like primary nutrients shown in table 3.1.

Table 3.1: Properties of soil used in the experiment.

Soil properties	Methods	Treatment	Mean value
Available N	Kjeldahl (1883)	C	293 kg/ha
		N	209 kg/ha
Available P_2O_5	Olsen and Sommers (1982)	C	602 kg/ha
		N	413 kg/ha
Available K_2O	Toth and Prince (1949)	C	81.9 kg/ha
		N	58.7 kg/ha

C = Control treatment with recommended N; N = N deficiency; no fertilizer nitrogen application

3.2 Experimental design and plant growth condition

Plants were grown in plastic pots filled with 13 kg soil (Figure 3.3). The soil N status measured before sowing. Two treatments with recommended dose of fertilizer with N (120-80-60 kg/ha N-P-K respectively) and recommended dose of fertilizer without N supplication (0-80-60 kg/ha N-P-K respectively) were taken up for this experiment and three replications were done for each wheat RIL and treatment. The plants were grown in pots in ambient conditions till active tillering stage and then shifted to the climate-controlled greenhouses of Nanaji Deshmukh Plant Phenomics Facility (from peak tillering stages till harvesting) in rabi season, 2019-20. Plants were irrigated adequately.

Figure 3.3: Experiment preparation phase. A) Soil sieving B) Pot filling C) Soil moisture estimation D) Pot transfer.

3.3 Plant material and mapping population

Parental lines, *Triticum aestivum* cv. HD 2329 double-dwarf variety with an average height of 90 cm. The ears are dense fully beard with red glumes. Its grains are hard, bold amber. It is susceptible to yellow rust and karnal bunt diseases. It gives average yield about 21 quintals per acre. RAJ 3765 have tolerance to high temperature and rusts and are suitable for normal to very late sowing conditions. From these parental lines RAJ 3765 has a higher NUE than HD 2329. So, a mapping population was developed by single seed descent method (Dr. Monika Dalal, ICAR-National Institute for Plant

Biotechnology, New Delhi) to characterise the genetic basis of NUE and nitrogen deficiency tolerance mechanism in wheat. A total 384 RILs in F_8 generation were taken for both phenotyping and genotyping purpose along with their 2 parents.

3.4 The 2-factorial experiment

1st factor: Wheat recombinant inbred lines (RILs) and parental lines

Plant materials: 384 recombinant inbred lines and 2 parental lines (RAJ 3765 and HD 2329)

2nd factor: Nitrogen levels

+ **Control**: with nitrogen fertilizer supply (N: P: K~120:80:60 kg/ha), well irrigated.

+ **Nstress**: without nitrogen fertilizer supply (N: P: K~0:80:60 kg/ha), well irrigated.

Fertilizer dose: For each pot (1.21g N + 0.6g P_2O_5 + 0.8g K_2O)

(2.7g Urea (46%N) + 3.2g Super Phosphate (16%P_2O_5) + 0.83g Potassium chloride (60% K_2O).

Number of pots: 1200 (1152: 192 RILs x 2 treatments x 3 replications and 48 pots with 3 replications for two treatments of two parents).

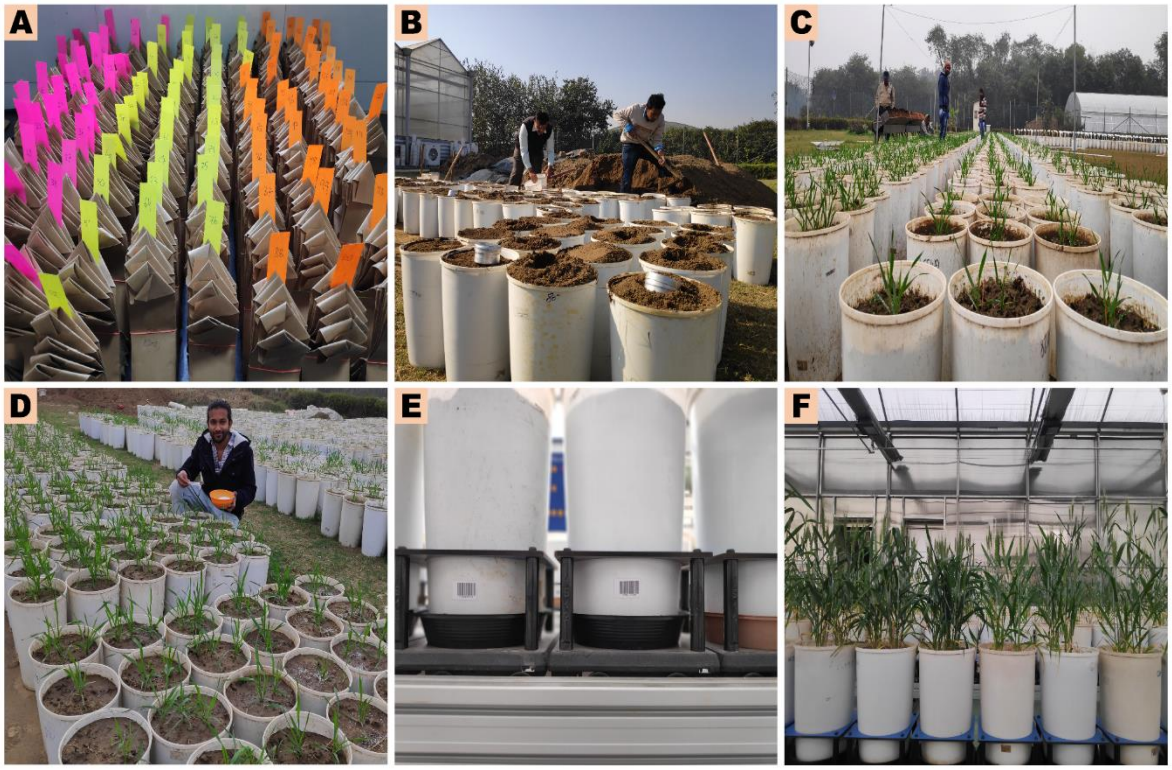

Figure 3.4: Wheat NUE experiment at NDPPC. A) Seed preparation B) Pot filling with soil by weighing C) Wheat seedling emergence D) First split dose of fertilizer at tillering E) Pot barcoding for identification F) Visual difference between C and N deficiency in RILs

Pot size: diameter: 24cm at top, 19cm bottom; height: 36 cm; surface area equal 0.045m^2 containing 13 kg of soil.

Soil preparation: Soil used for this study was not supplied with any N fertilizer around 5 years before transplanting. Soil was prepared with drying in the sun for uniform moisture, sieved it, weeding, mix well to ensure it has to be loose and uniform.

Sowing seeds and seedling emergence: Disease-free seeds were sown in plastic pots on 1st December 2019 and were harvested in April 2020. Healthy wheat seeds of RILs and parents were sown at a depth of 3-5 cm with 4 seeds in each pot and covered with the soil. Recommended fertilizer dose used for Control treatment was 120, 60 and 80 kg NPK/ha, respectively, and for N-deficiency treatment was 0, 60 and 80 kg NPK/ha. Before sowing, basal application of 60P:80K was done for all pots in both the treatments. For control for N was applied in 3 split doses, with 50% N as basal, 25% at tillering and 25% at booting stages. After 7 days of germination 2 plants per pot was kept thereafter till harvesting. Details have been shown in Figure 3.4.

Figure 3.5: Wheat NUE experiment details. A) Plants showing visual N deficiency and ready to load in the conveyer B) Barcoded plants on moving field conveyer in greenhouses C) Manual data collection D) Wheat at harvesting stage.

After 50 days of sowing, 3 uniformed pots per treatment per RIL were loaded and laid out on the conveyor belt system. A randomized complete block design (RCBD) was used where each RIL was replicated 3 times under both Control and Nstress condition. Subsequently, 500 g of white colored polypropylene beads was added to each pot as a cover layer, reducing the evaporation and providing a uniform white background for image analysis. Details have been shown in Figure 3.5.

Greenhouses conditions: The growth conditions in 4 greenhouses were maintain at 24^{o}C during the day and 16^{o}C during the night. The greenhouses were coupled with automatic weighing and watering facility. The greenhouses were made of polycarbonate sheet with 85% transparency. Temperature and relative humidity are measured with the help of data loggers and irrigation is applied using an automatic watering system.

Harvesting: The crop was harvested in April 2020 from the greenhouses as and when the plant attained harvest maturity. The plant was cut close to the ground surface and was placed in an envelope and sun dried for 2-3 days until the weight remained constant for estimating dry biomass of wheat. The whole plant was separated to 3 parts, a) the vegetative foliage part (Straw and leaves) b) main ear separately harvested c) all tiller ear and accordingly data were collected and combined. Then the samples were threshed manually.

3.5 Experimental design for biomass estimation

Two independent experiments were conducted in the Nanaji Deshmukh Plant Phenomics Centre (28°38'31.2"N, 77°09'39.6"E), New Delhi, India, during the winter seasons (Nov-April, Rabi) of 2018 and 2019. In both experiments, wheat germplasm lines and recombinant inbred lines (RILs) of RAJ 3765 x HD 2329 were used. Seeds were sown in pots (0.19 m diameter, 0.4 m high, 15 L volume) containing uniformly filled soil (12.5 Kg per pot). Both experiments differed in genotypes and RILs to validate the model's effectiveness in a wide range of biomass across experiments. Recommended dose of fertilizer (120-80-60 kg/ha N-P-K respectively) was applied to each pot. Well-watered condition was maintained in all the pots and recommended weed, pest and disease control practices were followed. Plants were grown in the natural environment for proper growth and biomass accumulation, and shifted to the greenhouse in phase wise manner to capture the biomass at different vegetative stages (before booting). The idea to capture biomass before booting was due to the fact that after booting the ear creates erroneous result due to its variable weight than leaf and stem. The age of plants was ranging from 30 to 70 days after sowing at the time of imaging. This variability in plant age helped in capturing wider range of FW, DW and SA. Before imaging of the plant, ultra-low weight & solid polypropylene beads were applied just over the soil surface to about 5cm height to arrest direct evaporation from the soil surface, and also for easy segmentation of image. Three hundred plants in 2018 experiment and 154 plants in 2019 experiment were selected for image acquisition using the LemnaTec-Scanalyzer 3D automated phenotyping and imaging platform. Destructive sampling of plants was done to measure

above-ground biomass FW (g), DW (g), and SA (cm2). The SA of the whole plant, along with stem and leaf, was measured by using LI-3100C (LI-COR, Lincoln, NE, USA) automatic leaf area meter.

3.6 Image based phenotyping in plant phenomics facility

The following sensors were used for non-destructive temporal phenotyping of wheat RILs for nitrogen use efficiency and nitrogen deficiency response capture:

RGB Camera: Prosilica GT6600, spectral band: 400-700 nm, sensor: ON Semi KAI-29050 (LemnaTec GmbH, Aachen, Germany). Peak reflectance around 550 nm, due to low absorbance of the pigments in this wavelength region, makes plants look green and enables us to detect plant tissue in RGB images. Analyzing visible light images delivers information about dimensions, morphologic and geometric properties, as well as color distributions.

IR Camera: Pearl eye P-030 LWIR, spectral band: 8000-14000nm, sensor: uncooled microbolometer (LemnaTec GmbH, Aachen, Germany). Thermal energy radiated by an object per second per unit area is proportional to the fourth power of the absolute temperature of the object. With its maintenance-free sensor, a temperature reference element, and a Peltier temperature stabilization, the camera reliably detects temperature differences with top view and side view. Traits like canopy temperature is detected by this sensor.

Figure 3.6: Imaging and watering facility at NDPPC. A) Wheat NUE experiment in climate-controlled greenhouse B) Individual imaging sensor platforms C) LemnaTec control main system D) Camera installed inside imaging chambers with light source E) RGB imaging platform F)

Automatic weighing and watering station (One inside each four greenhouses and one in imaging area).

NIR Camera: Gold eye P-032 SWIR Cool cameras, spectral band: 900-1700nm, sensor: InGaAs (LemnaTec GmbH, Aachen, Germany). Water absorb NIR at 3 bands between 900-1500nm, and thus reflectance is inversely related to water content. Traits can be measured-RWC and leaf thickness.

3.7 Image acquisition and analysis

3.7.1 Image capturing

A LemnaTec Scanalyzer 3D platform (LemnaTec GmbH, Aachen, Germany) was used to phenotype 192 wheat RILs and two parental lines. Plants grew under natural environment condition till tillering stage and in controlled greenhouse conditions till harvesting (Figure 3.6) and were phenotyped at five time points 60 DAS, 70 DAS, 80 DAS 90 DAS and 100 DAS, over the entire experimental phase using the fully automated system consisting of conveyer belts, a weighing and watering station and three imaging sensors (Figure 3.7).

Figure 3.7: Stagewise phenotypic behavior of RILs under control and nitrogen deficiency.

3.7.2 Image processing

Image processing included four main steps:

(1) Preprocessing to prepare the images for segmentation.

(2) Segmentation to divide the image into foreground and background.

(3) Feature extraction: to classify the segmentation result and get a traits list.

(4) Post-processing: to summarize calculated results for each plant.

The analysis was performed in a grid-computing mode to speed up image processing. Analyzed results were exported in csv file format via Lemna Grid functionalities, which can be used for further data inspection. The resulting spreadsheet includes columns for different phenotypic traits and rows for data from different time points. The corresponding metadata is included in the result table as well. Depending on the computing resource available, LemnaGrid can process large-scale image data in a reasonable time ranging from a few hours to a few days.

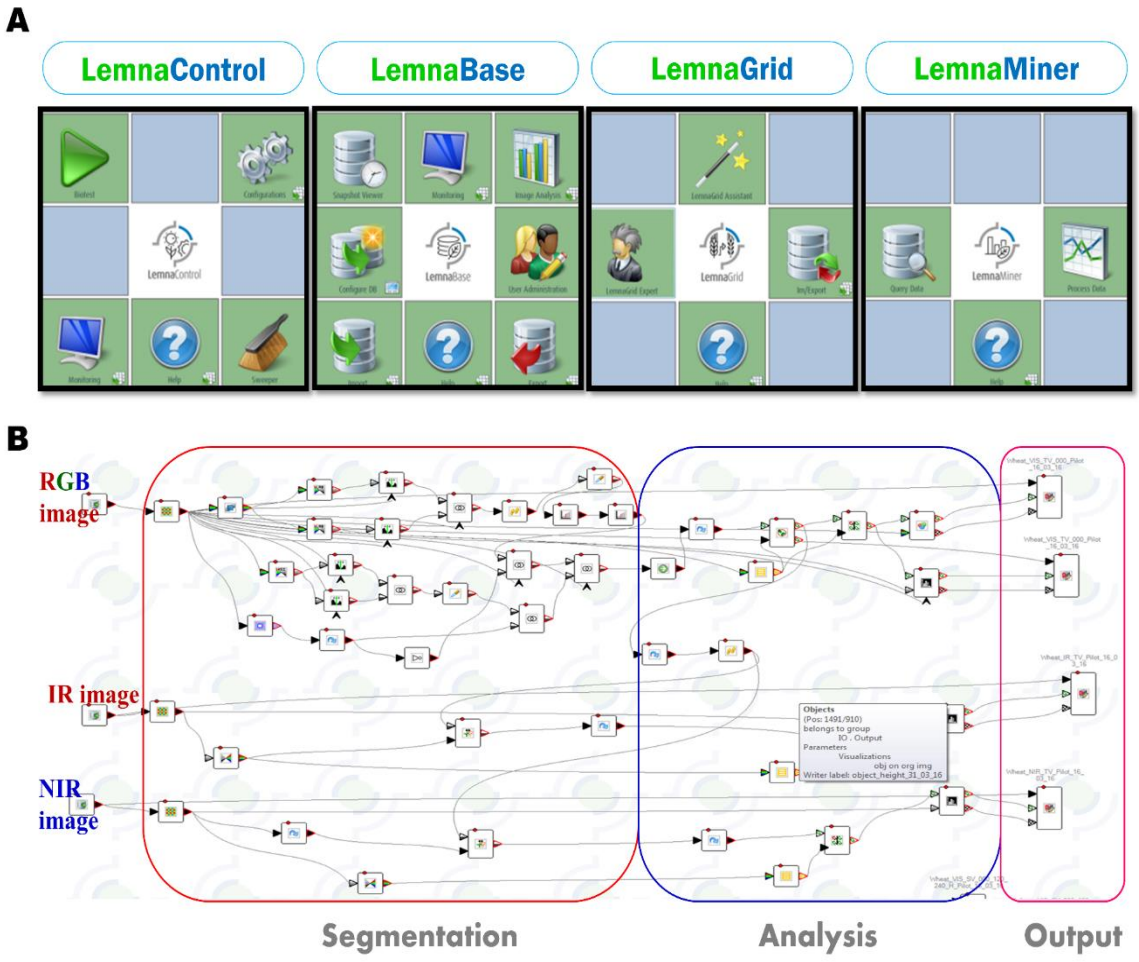

Figure 3.8: Modalities present in LemnaTec systems (A) and image processing pipeline (B).

An image dataset of the size used in this study can be processed within three days on a server PC with 64 gigabytes RAM of system memory using eight central processing unit (CPU) cores. Each plant was characterized by a set of 92 image-derived traits, also referred to as features, which were grouped into three main categories morphometric traits, biomass-related traits, color related traits and RGB based vegetation indices. These traits were defined by considering image information from different cameras (visible light, near infrared, infrared) and imaging side view (0º, 120º, 240º for RGB and one angle for IR and NIR) and top views.

3.7.3 RGB, IR and NIR image acquisition and processing

Nanaji Deshmukh Plant Phenomics Facility is equipped with six different sensors (RGB, IR, NIR, Fluorescence and SWIR & VNIR hyper spectral cameras) and plants are usually imaged sequentially one after the other entering specific chambers installed with said imaging sensors. IR sensor (Model: Pearl eye P-030 LWIR, Allied Vision Technologies GmbH, Germany) were strategically installed just outside greenhouses to acquire thermal image of the plants from both side and top view angles.

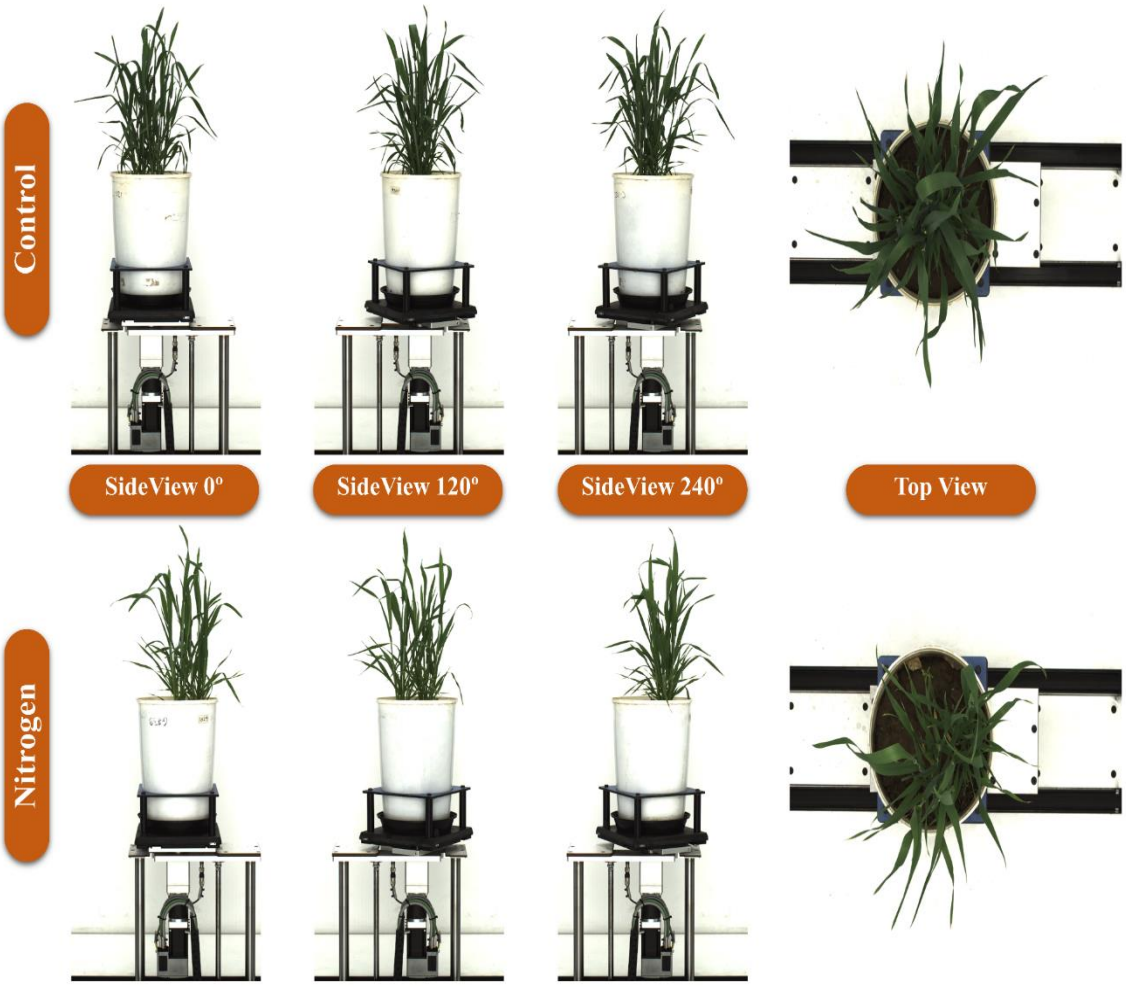

Figure 3.9: Image acquisition process

RGB processing

Plants were imaged once in about 10 days for five times using a Scanalyzer 3D imaging system (LemnaTec GmbH, Aachen, Germany) installed with RGB camera (Prosilica GT6400, spectral band: 400-700 nm, sensor: Allied Vision Technologies GmbH, Germany) using constant fluorescent light source. Twenty-eight mega pixel (6576 (X) * 4384 (Y) resolution) color images were recorded from the top of the plant (top view) and from the side of the plant at three different rotations (0 °, side view 1; 120°, side view 2; 240°, side view 3) as shown in Figure 3.9. The Raw image were acquired with the basic set up of exposure 32,000; gain 25; gamma 100; red white balance 210; blue white red balance 135 along with double door closed option to avoid shadowing effect of side view light source. The recorded images were processed using LemnaGrid software (LemnaTec GmbH). In brief, raw RGB images (12-bit BayerGR8 format) were demosaiced using Adaptive Homogeneity Directed (AHD) algorithm to reconstruct a full color image from the incomplete color output from an image sensor (Figure 3.8). The viewable pixels of these images were segregated in to foreground and background pixels using free form region of interest (ROI) filters. Logical operations such as AND / OR logics were used for combining resultant image of diverse filters whenever required in the pipeline. Edge noise was removed through erosion and dilatation steps before composing all parts identified as plant to one object. Universal convertors were used for converting processed image to object lists or binary image or grey image were ever required in the image processing pipelines. Subsequently, the binary images of our interest (plants) were analyzed for image features that consists of color classification of dark green or brown colored dry leaves. Hue based HSI grey converter with the two-level thresholds 44 to 180 were used for grouping green and brown pixels separately in to 20 bins and histogram was made using pixel intensity ranged between 0-255 values. The size, height, and geometrical dimensions of the object were calculated and all three images were used to estimate the projected shoot area (PSA) of the plant. The calculated PSA were compared with actual plant size determined on the destructively harvested plants. Conversion of pixels from the top view camera accounted for the changing distance effect as the plant grew closer to the camera. The height factor (Centroid) was calculated based center of mass along the y-axis from side view image and multiplied with the factor 1.8 (mm/pixel) to convert pixel to millimeter. The top view-specific constant was calculated by the following (Neilson *et al*.2015; Parent *et al*.2015).

$$Y= 0.00018/1.8*x+0.25$$

Where Y is the top view-specific constant, converting pixel area to millimeters, and x is the mean centroid for the two side view images.

Final calculation of leaf area was achieved by summing all the calibrated side view and top view images. Plant growth rate was calculated using projected shoot area by time (day) in the three time

periods used to calculate growth rates. The variation in color of well fertilized and nitrogen deficit plants were distinguished by using different R, G, B channel-based vegetation indices.

IR processing

IR camera was set up at a distance of 1.5 meter from the plants and the raw image (grey scale 14-bit depth) is acquired with the matrix array size of 480 (x) * 640 (y) pixels. The fully dark imaging chamber was maintained at a temperature of 25ºC during image acquisition to minimize the changes in background temperature. Both top view and side view IR images were taken at 0° angle of the pots that coincide with RGB image settings for further processing. The pipeline for thermal image processing was built using LemnaGrid of LemnaTec Scanalyzer 3D system. The grey scale IR images were first demosaiced and converted into binary images using universal convertor. The common coordinates (x,y) from RGB image and IR grey images were superimposed in order to separate the foreground from the background of IR images. To superimpose two different size (resolution) images, identify common coordinates and resizing the RGB image, image fusion algorithm was used. We conducted a separate checker board experiment (Figure 3.10) 5cm^2 aluminum foils were pasted on a ply board in checker box pattern and spayed with water before RGB and IR image acquisition) to select at least 100 distinguished x, y coordinates for image fusion algorithm. After foreground selection, grey scale intensity was converted in to temperature readings using A/255*16384*0.0075-30 factor as provided in the company (Allied vision technology) operating manual.

Figure 3.10: Checker board for image calibration.

The temperature values were revalidated using hot dry bath at different temperature ranges and regressed for prediction accuracy. The R^2 value of the model was found to be 0.99. After the temperature conversion, pixels intensity (canopy temperature) ranged between 16 to 33ºC were segregated in to 20

bins and major parameters like histogram and mean canopy temperature were mined from the processed IR images.

NIR processing

Similarly, hydration status of the plants was measured using a NIR camera (Model: Gold eye P-032 SWIR cameras, Allied Vision, Exton, USA) with a spatial array size of 508 (x) × 636 (y) pixels. Grey scale NIR image (12 bit) was acquired with the basic camera set up of 2,40,000 exposures; 100 gain; 3400 dark and 2000 IRIS values. As NIR bands (900 to 1700) are sensitive to water absorption wavelength of 1450 nm; plants with high water content showed a low NIR intensity. Two NIR images were acquired per pot, one at 0° from a side-view angle and another from top view angle. Since, it is difficult to delineate the region of interest using NIR grey scale images, response to stress data were obtained by matching RGB and NIR images. To compensate for differences in the image resolution between the two cameras, image matching was performed using the local matching method in 130 matching points. The matched images were cropped to the same size as the NIR images, and only the plant area calculated from the RGB image was extracted to confirm the average water content.

3.8 Feature analysis and data transformation for biomass prediction

After feature extraction, all the features were categorized into four groups: Geometrical features, colour class features, RGB-based indices and near-infrared features. Finally, these features are classified into two major categories namely architectural features (geometric features) and physiological features (colour class, RGB based indices and NIR features). These features were specified by considering the type of imaging sensors (RGB and NIR) and object orientations (side and top views). All the traits were curated for redundancy, processing error, outliers, and non-informativeness by both statistical approach (Multicollinearity removal, poor heritability, etc.) and manual curation. We kept as much variation and informative features as possible to improve the models.

Each experiment dataset was transformed into matrix Xn×m where “n” is the number of plants and “m” is the number of phenotypic traits. Plants represented rows, and different traits represented columns. All missing value plants were discarded for reduction of data analysis complicacy. Before applying regression models, all datasets were normalized as described by Chen *et al*., (2018).

A phenotypic similarity tree was used to see the correlation between all the traits and the similarity between experiments. Principle component analysis was performed on the transformed data matrix Xn×m in the same way as described by (Chen *et al*., 2014) for all the experiments.

3.9 Modelling for predicting plant biomass

After i-Trait selection and phenotypic analysis, the next part was to fit the selected data into the model to predict FW, DW, and SA. We used the open-source tool “HTPmod” for modelling (Chen *et al*.,

2018). In HTPmod (Shiny framework-based application), the module *predMod* contains 16 models constructed with 16 different machine learning methods to regress input features to output traits of interest. We used the default hyperparameters applicable for different machine learning models.

3.10 Evaluation of the Models Performance

Model performance was evaluated using k fold cross-validation method and N-times randomization, where we assigned k and N to 10. So, we adopted a 10-fold cross-validation strategy and ten times randomization for model evaluation by considering the average value. The data set was randomly divided into a training set of 90% of plants and a testing set of the remaining 10% of plants. Then each model was run to predict FW, DW, and SA for the testing data, and then the predicted biomass was compared with the manually measured FW, DW, and SA.

All the regression models were evaluated by the Pearson correlation coefficient (PCC; *r*), the coefficient of determination (R^2) and the root mean squared relative error of cross-validation (RMSRE) between the predicted and observed values

3.11 Manual data collection

3.11.1 Phenology parameters: days to booting, days to heading, days to maturity.

3.11.2 Agronomical parameters

Plant height, tiller number, panicle number, shoot weight and grain yield.

3.11.3 Yield parameters

For assessing the relationship between yield and its components, the parameters like number of panicles per pot, number of grains per panicle and thousand grain weights and grain yield per plant were recorded at maturity (Figure 3.11 and 3.12).

The yield samples were dried to a constant weight and threshed manually, adjusted to 14% grain moisture content and then expressed in g/plant.

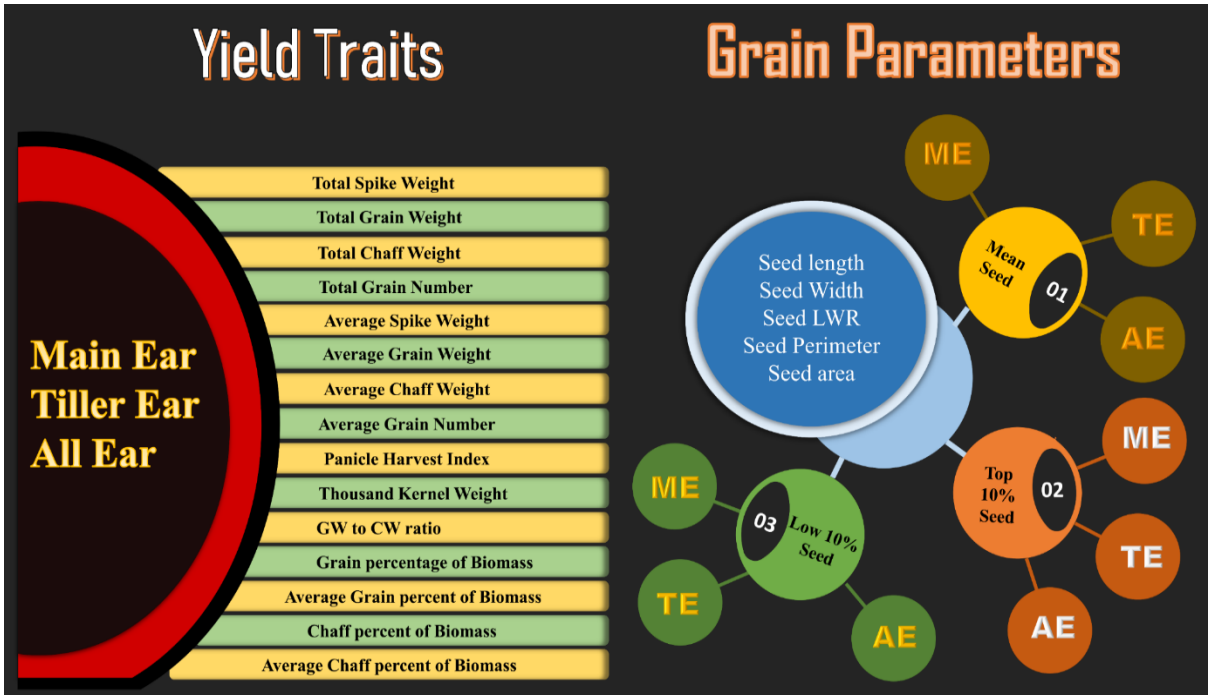

Figure 3.11: Yield and grain morphology characterization

Figure 3.12: Yield trait estimation in wheat NUE experiment. A) Plants at harvest maturity stage inside greenhouse B) & C) Manual yield parameter recording D) Separate main ear from tiller ear E) Imaging was done of each main ear spike F) Main ear seeds.

3.11.4 Shoot and grain N concentration measurement

Clean dehusked seed samples were taken from the main ear seeds to avoid biases for seed selection. A subset of shoot dry biomass samples was ground by a small volume fruit mixer (Sujata Supermix SM 900) and sieved to a fine powder and kept in Eppendorf tubes for storage. Then the fine powder of biomass and seed was packed in tin capsules and weighed with high precision weighing balance (Mettler Toledo).

The tin capsules were then burnt with helium gas by a glass rod containing copper, for estimation of total N% and total C% using CHNS analyzer (EuroVector, EA3000, Italy). Total N content and total C content were estimated by multiplying the nitrogen percentage with biomass and expressed as mg N plant^{-1}. Details have been shown in Figure 3.13.

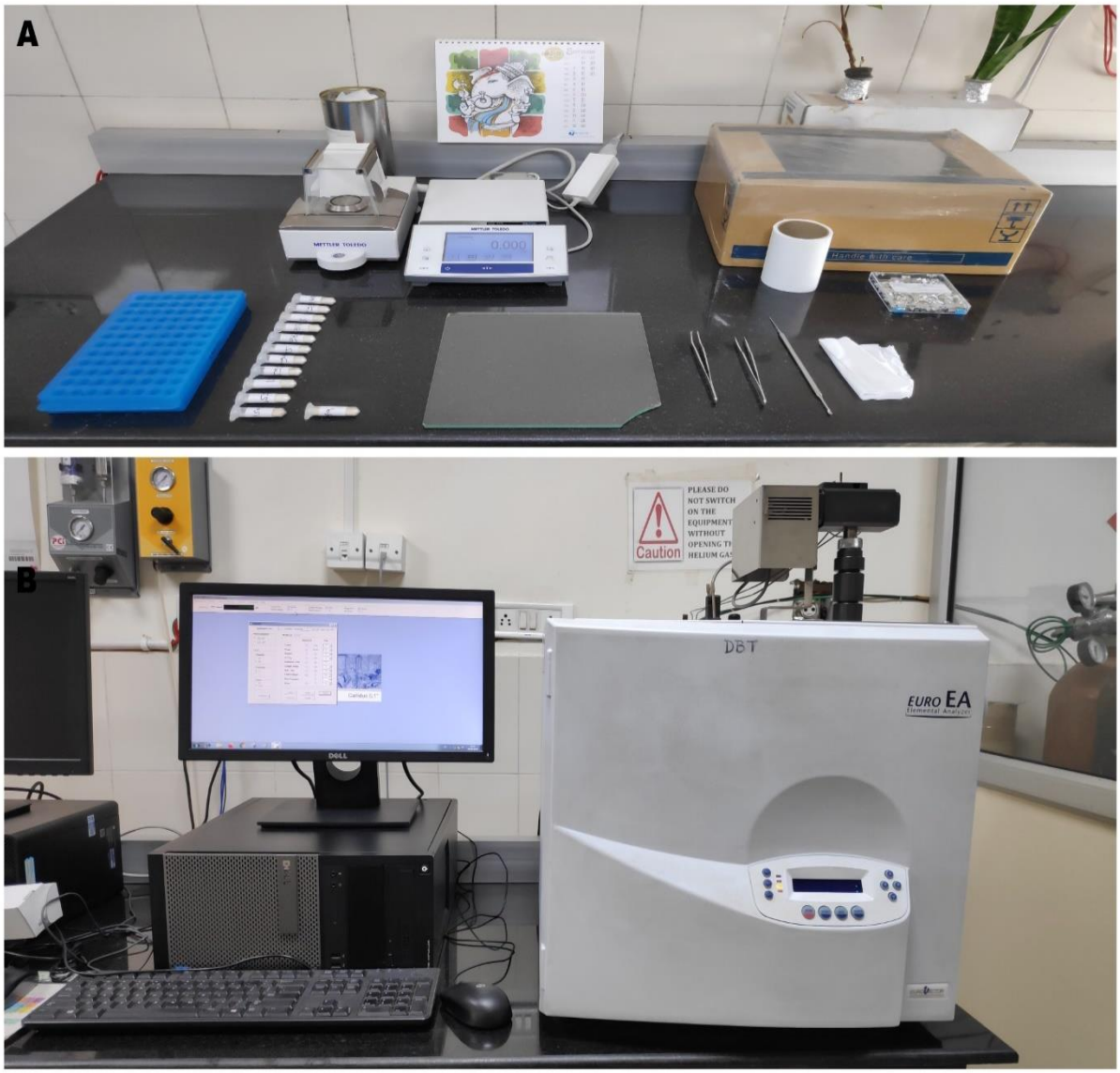

Figure 3.13: CHNS Analyzer for C and N estimation. A) High precision weighing balance for tissue weighing and packing in tin foils B) The combustion instrument with its attached PC.

3.12 Nitrogen Use Efficiency Estimation

Nitrogen Use Efficiency and NUE Index

We used most widely used 6 nitrogen use efficiency related traits.

Table 3.2: Nitrogen use efficiency formula.

Name	Abbreviation	Calculation	Reference
Nitrogen Uptake Efficiency	NUpE	Total nitrogen in plant / Nitrogen supply	Han *et al.*, 2015
Nitrogen Utilization Efficiency	NUtE	Grain yield / Total N in plant	Han *et al.*, 2015
Nitrogen Use Efficiency	NUE	Grain yield / Supplied N	Han *et al.*, 2015
Grain Protein Content	GPC	Grain N content * 5.7	Fujihara *et al.*, 2008
Nitrogen Harvest Index	NHI	Grain N / Total N in plant	Rao *et al.*, 2018
Utilization Index	UI	Above Ground Biomass / AGB N content	Han *et al.*, 2015

3.13 Semi-automatic seed parameter estimation

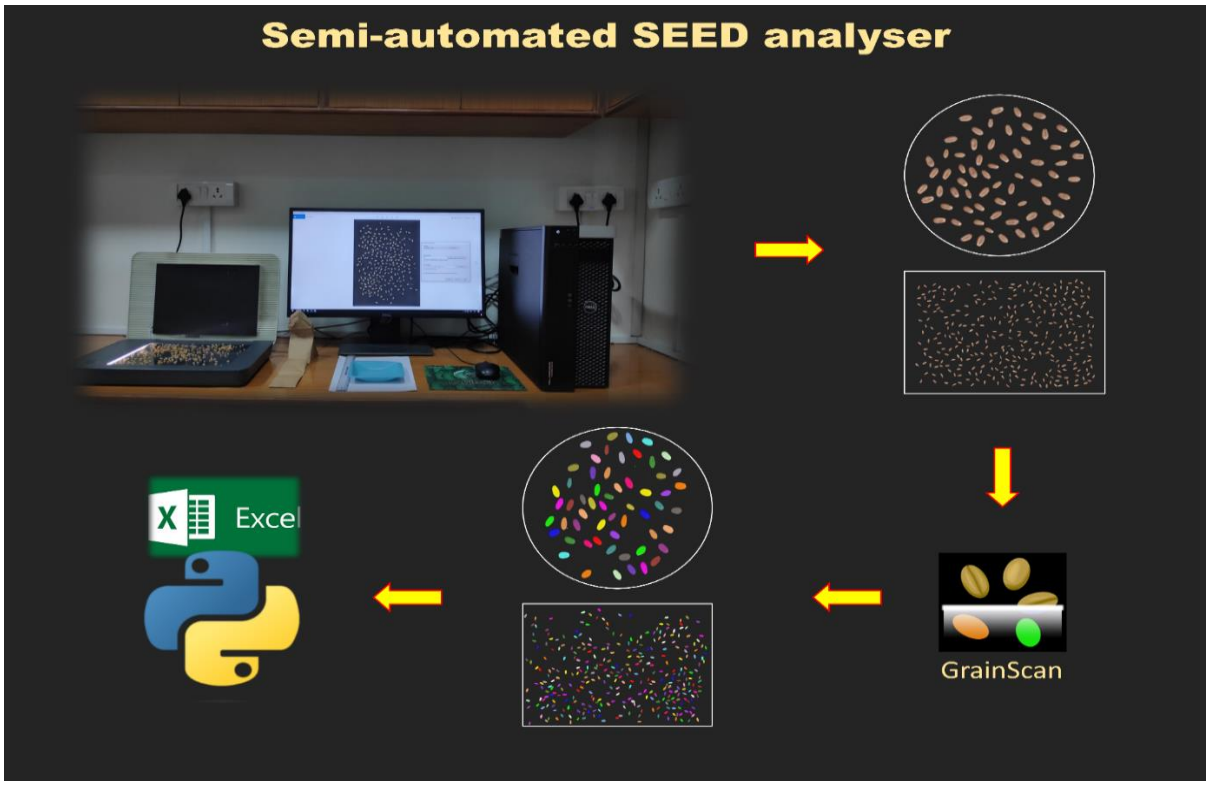

Figure 3.14: Semi-automated seed analyser setup for seed morphological trait estimation.

Different seed morphology-related traits were estimated by imaging the main ear seeds and tiller ear seeds separately (Figure 3.14).

3.14 Statistical analysis and data visualisation

Imaging-derived and manually measured data were checked for outliers by using R "metan" package (Olivoto and Lúcio, 2020) and manually. Extreme replication values and RILs with absurd values were removed from final data analysis. ANOVA and variance components were estimated in R using the "Metan" package.

3.14.1 Broad sense heritability (H^2)

Broad sense heritability (H^2) presented the repeatability of phenotypic was estimated by "Cullis'" broad-sense heritability method (Cullis *et al*., 2006) using R "metan" package. H^2 is widely used to account for the unbalanced scenario that plant breeders face in the single and multi-environment. H^2 is the ratio of total genetic variance (σ^2_g) to total phenotypic variance ($\sigma^2_p = \sigma^2_g + \sigma^2_{gt}/n + \sigma^2_{er}/rn$), The H^2 was calculated as follows: $H^2 = \sigma^2_g / (\sigma^2_g + \sigma^2_{gt}/n + \sigma^2_{er}/rn)$, where + σ^2_g is the variance component estimation for genotypes, + σ^2_{gt} for genotype-by-treatment, + σ^2_{er} for error, + r is the number of replications, + n is the number of treatments.

3.14.2 Donor selection

The selection of donor for NUE in wheat was done by three different selection indices namely, the multitrait genotype-ideotype distance index (MGIDI), Factor analysis and genotype-ideotype distance - Best linear unbiased prediction (FAI-BLUP) and Smith-Hazel index (SH). R "metan" package was used to facilitate the implementation of the different method of index to rank the genotypes based on information of multiple traits as proposed by Olivoto and Nardino (2020). The MGIDI index is computed as follows:

$$MGIDI_i = \sqrt{\sum_{j=1}^{f}(F_{ij} - F_j)^2}$$

Where $MGIDI_i$ is the multi-trait genotype-ideotype distance index for the *i*th genotype; F_{ij} is the score of the *i*th genotype in the *j*th factor ($i = 1, 2, ..., g; j = 1, 2, ..., f$), being g and f the number of genotypes and factors, respectively, and F_j is the *j*th score of the ideotype. The genotype with the lowest MGIDI is then closer to the ideotype and therefore should presents desired values for all the analyzed traits.

3.15 Genotyping

DNA isolation was carried out using the leaves of 14-days-old seedlings grown in pots under natural environment conditions. High molecular weight genomic DNA was extracted using the CTAB method (Murray and Thompson, 1980) with minor modifications given below. DNA quality was checked with the 0.8% agarose gel electrophoresis and DNA nanodrop. The spectrophotometric determination of quality and quantity of total RNA was by done using NanoDrop Nd-1000 UV/Vis Spectrophotometer (Figure 3.16). Genomic DNA was quantified by measuring A_{260} (1 A_{260} = 50 µg) and its quality was assessed by A_{260}/A_{280} and $A_{260}/A_{230}$was in between the range 1.8 to 2.0. 20 ng/µl DNA was used for SNP genotyping. Hybridisation-based SNP chip genotyping of 376 RILs and two parental genotypes was performed using the 35K Axiom® Wheat Breeder's Array of Affymetrix GeneTitan® system according to the procedure described by Affymetrix. Allele calling was carried out using the Affymetrix proprietary software package Axiom Analysis Suite, following the Axiom Best Practices Genotyping Workflow. All the procedures were followed by the guidelines explained in R/qtl (http://www.rqtl.org/tutorials/geneticmaps.pdf), R/ASMap (https://cran.r-project.org/web/packages/ASMap/ASMap.pdf) and ICiMapping software v4.2 tutorials (https://isbreedingen.caas.cn/software/qtllcimapping/294606.htm) to perform all the linkage map analysis and data corrections. All details have been shown in Figure 3.15.

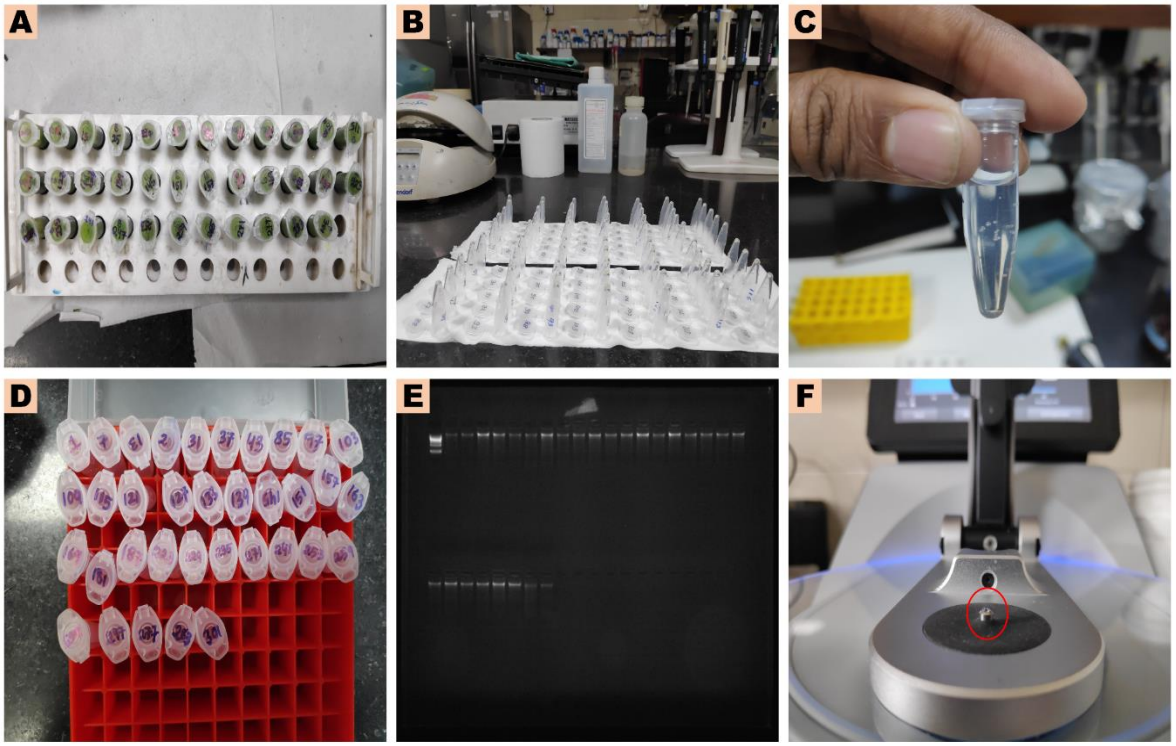

Figure 3.15: DNA extraction, purification and quantification method. A) Tissue grinding and kept in lysis buffer B) DNA pellet drying after ethanol wash C) Ethanol wash of DNA D) DNA storage E) Genomic DNA presence evaluation F) DNA quantification by Nanodrop.

3.15.1 DNA Extraction with Purification Protocol

Step 1: Grinding the tissue

Less sample size: Grind 100-200 mg tissue with liquid nitrogen in pestle and mortar (Mortar and pestle should be ethanol washed) and put the ground tissue in Eppendorf tubes

Larger sample size: Collect healthy young leaves, cut the leaves into small pieces and take 200-300 mg of tissue in an Eppendorf tube, put two sterilized metal balls (one at bottom of tube one at top of tube over the tissue) in the tube. Then use tissue-lyser for grinding with liquid nitrogen. This will be helpful for grinding hundreds of samples easily.

Step 2: Keep 0.8ml CTAB buffer in 2ml Eppendorf tube (Add 0.2 % freshly prepared β-mercaptoethanol). Mix it properly for 30-40 seconds.

Step 3: Keep these in water bath (65 °C for 1hr). Mix the samples by invert mixing in every 15-20 min.

Step 4: Remove the samples from water bath and let it cool down to room temperature. Add equal volume of (24:1 Chloroform: Isoamyl alcohol) in the tubes. Mix by inverting the tubes for 40- 50 seconds.

Step 5: Centrifuge the above tubes at room temperature, 12000 rpm for 15-20 min. Take the supernatant in 2 ml tube (do not take the tissue particles only clear supernatant should be taken).

Step 6: Again, add equal volume of 24:1 Chloroform: Isoamyl alcohol in the tubes. Mix by inverting the tubes for 40- 50 seconds.

Step 7: Centrifuge these tubes at room temperature, 12000 rpm for 15-20 min. And take the upper tissue supernatant phase in 1.5ml tubes without taking any Chloroform: Isoamyl alcohol mixture.

Step 8: Add equal volume of chilled isopropanol and mix it very slowly.

Step 9: Centrifuge the tubes at 4 °C, 12000 rpm for 20-30 min. Decant the solution and dry the pellet.

Step 10: Add 0.5ml Tris (50mM): EDTA (10mM) (5X TE buffer at pH 8.0) to the pellet. Dissolve the pellet slowly.

Step 11: Now, add 5µl RNAse in the tube and keep in incubator (37 °C overnight).

Step 12: Next day add equal volume of phenol: chloroform: isoamylalcohol (25:24:1) in the tube.

Step 13: Centrifuge at room temperature, 12000 rpm for 15-20 min. Take supernatant in 1.5 ml tube (do not take the interphase part).

Step 14: Add equal volume of chloroform: isoamylalcohol (24:1)

Step 15: Centrifuge at room temperature, 12000 rpm for 10 minutes.

Step 16: Take supernatant in 1.5 ml tube and add 2 - 2.5 times chilled ethanol and mix it slowly.

Step 17: Centrifuge at 4 °C, 12000 rpm for 20-30min and decant the solution. Don't let the pellet slip away.

Step 18: Add 0.5ml of 70% ethanol (pellet washing). And let the ethanol dry from the tube.

Step 19: Add 0.1 X TE buffer or DNAse free water (as per your requirement) and let the pellet dissolve.

Step 20: Now the genomic DNA is ready for quality check. Keep it at 4ºC if want to use it soon otherwise can store it at -20ºC.

3.16 Linkage map construction and QTL mapping

The genotypic data for 376 RILs from mapping population with filter SNP marker with significant segregation distortion and >20% missing data were removed. The filtered SNPs marker was used for linkage map construction using the linkage mapping function executed in the QTL IciMapping software v4.2 (Zhang *et al*., 2010). The grouping and ordering of 1749 polymorphic SNP markers were carried out using regression mapping algorithm RECORD (Recombination Counting and Ordering) based on recombination event between adjacent markers. Furthermore, Rippling was done for refinement of the ordered markers on their respective chromosome by sum of adjacent recombination fractions (SARF) algorithm with a default widow size. QTL mapping for WUE QTLs and other traits was performed using inclusive composite interval mapping (ICIM) function applied in the IciMapping software v4.2. The QTL was computed by permutation test involving 1000 runs at signification level of P=0.05. After completion permutation test window size 5 cM and walk speed of 1cM was set to start analysis of inclusive composite interval mapping. For identification of main effect of additive of QTL in each trait, the ICIM-ADD function of the software was utilized. The logarithm of odds (LOD) score peaks >2.5 were used to declare the presence of putative QTL in a given genomic region.

3.17 Identification of putative candidate genes

The candidate genes were searched within QTL region. Firstly, we retrieve the physical position of left and right marker of a selected QTL from online publicly available database, gene based 35K wheat Breeder's array SNP chip (Allen *et al*., 2017). The list of genes and their function annotated using physical position of interval marker of the QTLs by Ensemble Plants. Further we sorted out putative candidate gene-based traits associated gene previously reported gene in literature.

4.1 Component traits characterization for NUE

NUE is a complex trait which is influenced by a number of secondary traits. Mainly NUE takes into consideration of nitrogen content of seed, nitrogen content of biomass, yield and harvest index. These above primary traits are resultant of several yield component traits such as spike characteristics, seed parameters, plant fresh weight, dry weight, leaf area etc. Also plant growth characteristics such as phenology, plant architecture, plant age affects plants response to nitrogen deficiency (Figure 4.1).

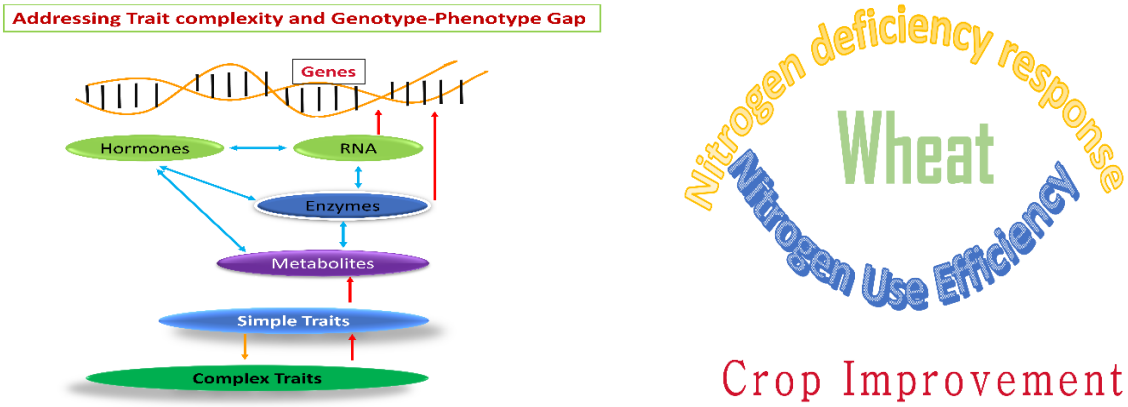

Figure 4.1: Complex trait characterization in wheat.

So, to characterize the dynamics of nitrogen use efficiency and nitrogen deficiency response in wheat, a combination of high throughput phenotyping, semi throughput phenotyping and manual phenotyping approaches were used in this study (Figure 4.2).

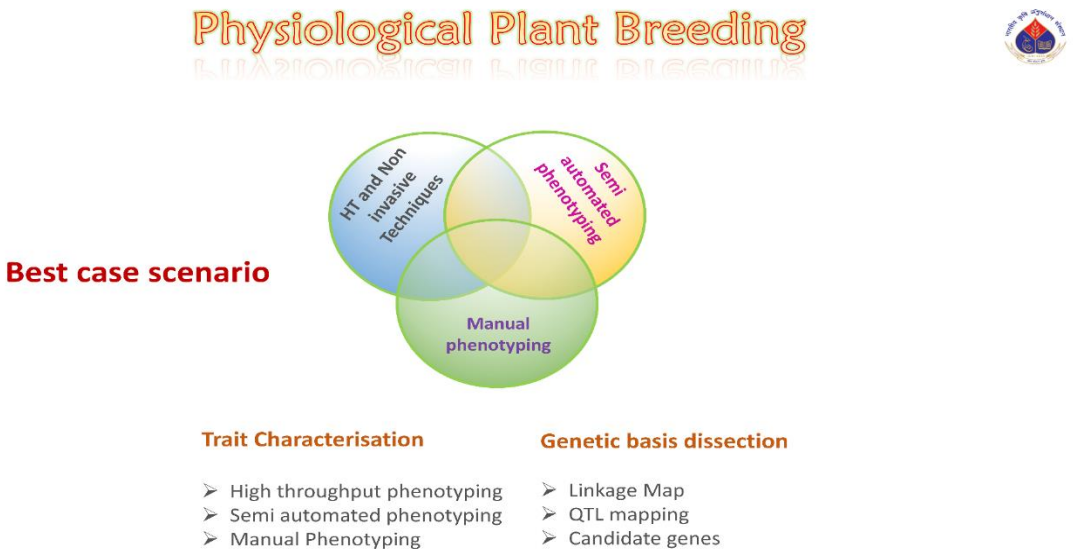

Figure 4.2: Combinatorial approach for wheat N-deficiency response study.

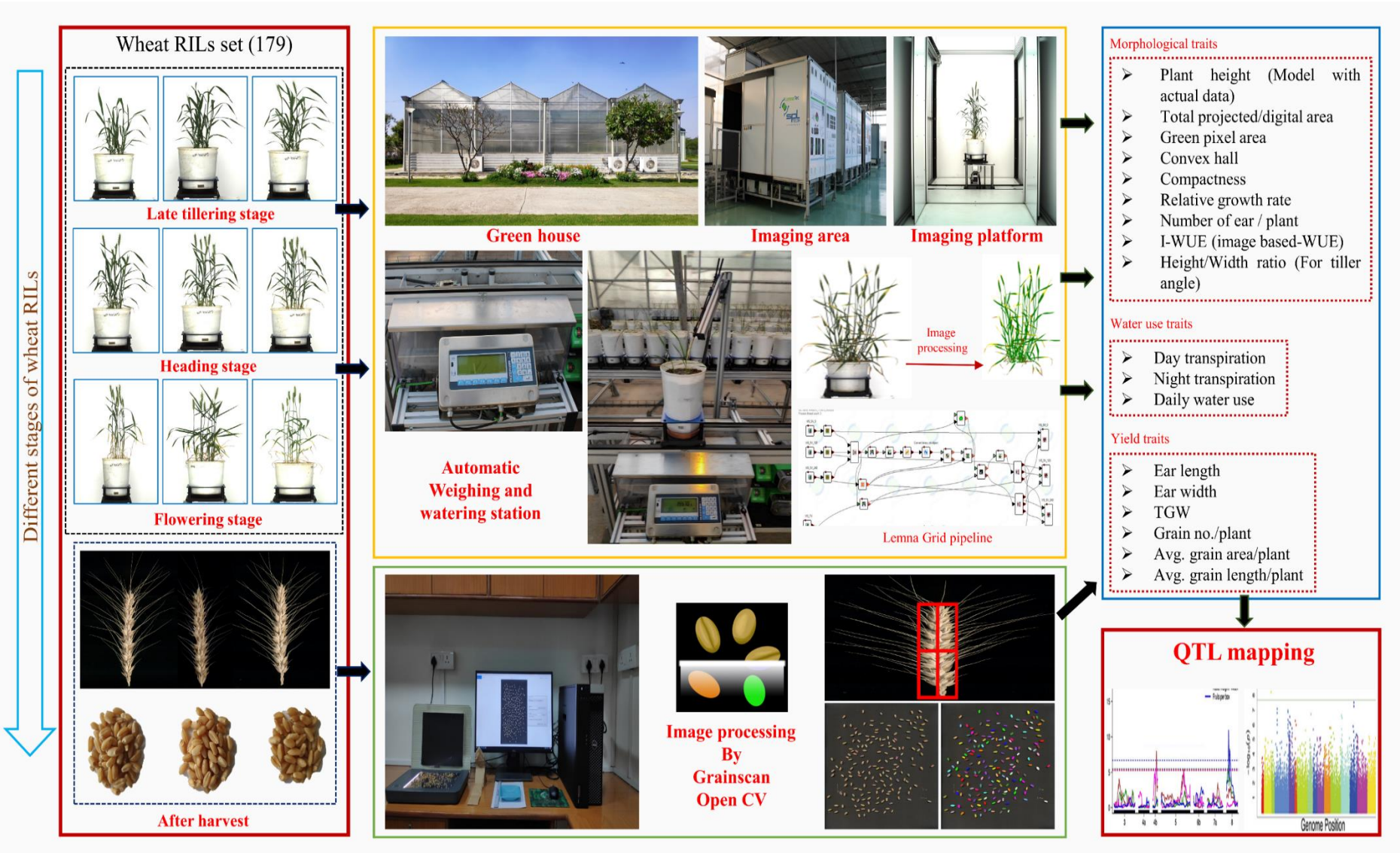

Figure 4.3: High-throughput phenotyping of wheat.

This combinatorial approach will enable multidimensional phenotypic screening of wheat RILs throughout the growth period and after harvest. The high throughput phenotyping system will capture the morphometric, colour related, biomass related and water status related traits, the semi-throughput phenotyping system obtain the seed characteristics and manual phenotyping captures all the yield related parameters, phenology and physiological parameters.

4.1.1 High throughput phenotyping for NUE component trait characterization

We phenotyped 175 RILs using high throughput plant phenotyping platform available at Nanaji Deshmukh Plant Phenomics Centre (NDPPC). Images of all the plants were captured at 60, 70, 80, 90 and 100 DAS to evaluate the NUE and nitrogen deficiency response of plants at different growth phases and the interaction of plant age with nitrogen deficiency treatment (Figure 4.3). Different sensors such as RGB, NIR and IR were used to capture images for trait characterization. This HTP of wheat at multiple growth stages and by multiple sensors leads to generation of parameters covering wide range of plant characteristics, otherwise difficult and tedious to obtain manually (Figure 4.3 and 4.5).

4.1.1.1 Functionalities and design of NDPPC

Nanaji Deshmukh Plant Phenotyping Center (NDPPC) is an advanced high throughput phenotyping facility comprised of four climate-controlled greenhouses aided with multi-sensor high throughput imaging platform (Controlled by LemnaTec Scanalyzer 3D). This is the largest phenotyping facility in India, with respect to number of pots (1200) and number of sensors (7). The climate-controlled greenhouses are equipped with facilities such as controlled temperature, controlled light source and CO_2. Total 1200 carts with RFID tags can be accommodated in all four green houses at particular point of time i.e., 300 carts in each green house (Figure 4.4). The phenotyping platform consists of eight advanced imaging sensors. The detailed information about this facility along with other Indian phenomics facilities is given in Table 1.

The reasons for combining digital imaging facility along with climate-controlled greenhouses was to a) acquire plant phenotypic data on multiple time point noninvasively and in automated high throughput manner, b) reduce climatic variability that possess difficulty in estimating the genotypic effect, environment effect and their interaction effect and c) images from multiple sensors will capture wide range of parameters including physiological, morphological and biochemical characteristics.

The whole facility is automated, the imaging chambers and greenhouses are connected by conveyer belt from all the green houses to imaging chambers but all greenhouses are separated from each other for climate control. The green houses and imaging chamber is connected via automated pneumatic doors and also each sensor is divided by pneumatic doors from each other.

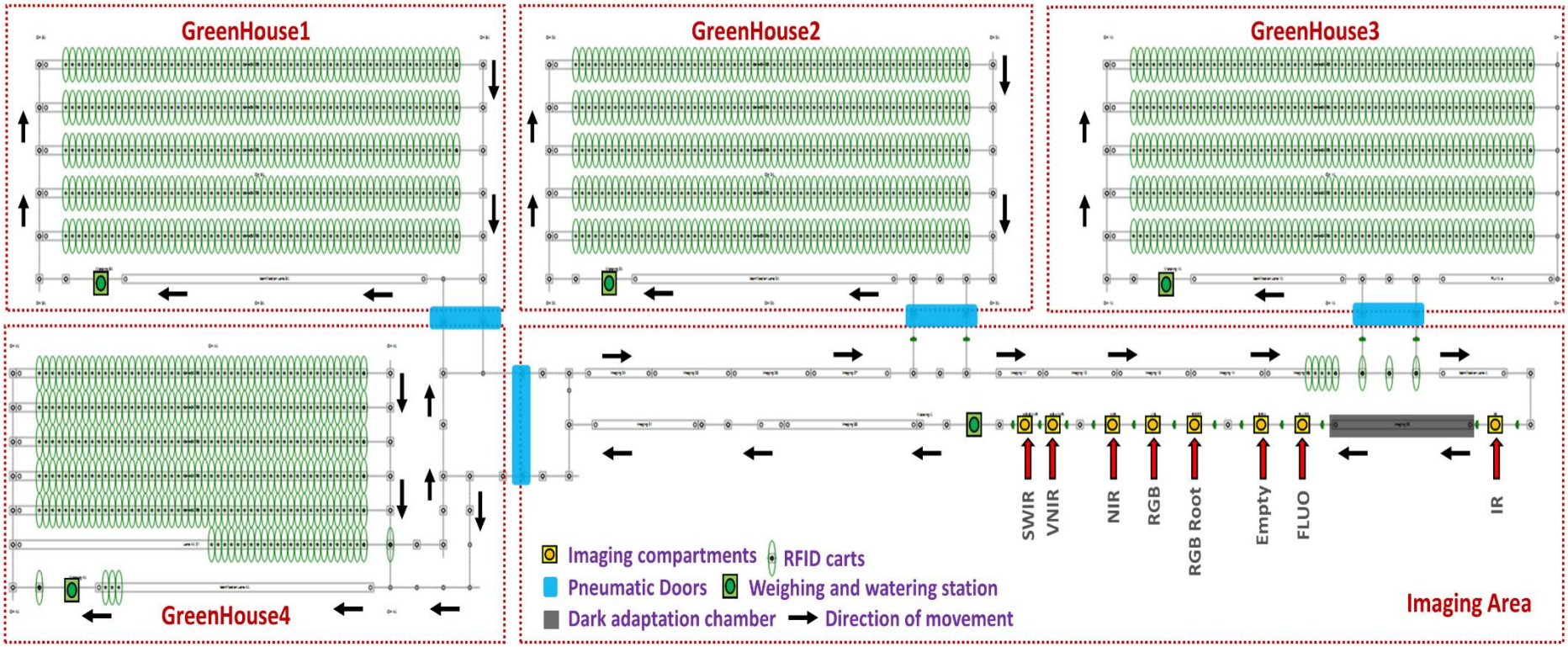

Figure 4.4: Functionalities of Nanaji Deshmukh Plant Phenomics Centre, New Delhi, India.

Table 4.1: Phenomics facility in India.

Name	Year	Capacity
Phenomics Facility, ICAR -Central Research Institute for Dryland Agriculture (ICAR – CRIDA), Hyderabad	2014	+ Scanalyzer system (Lemna Tec) + 240 carts + 3 sensors: RGB, NIR, IR + Automate weighing & watering
Phenomics Facility, ICAR - Indian Institute of Horticultural Research (ICAR-IIHR), Bengaluru	2015	+ Scanalyzer system (Lemna Tec) + 240 carts + 3 sensors: RGB, NIR, IR + Automate weighing & watering
Phenomics Facility, ICAR - National Institute of Abiotic Stress Management (ICAR-NIASM), Baramati	2016	+ Scanalyzer system (Lemna Tec) + 240 cars + 3 sensors: RGB, NIR, IR + Automate weighing & watering
Nanaji Deshmukh Plant Phenomics Center, ICAR – IARI, New Delhi	2017	+ Scanalyzer system (Lemna Tec) + 1200 carts + 7 sensors: 1. Thermal IR imaging (8000 -14000 nm) 2. Chlorophyll fluorescence PSII imaging 3. Empty Chamber for sensor 4. Root RGB imaging (400-700 nm) 5. Visual RGB color imaging (400-700nm) 6. NIR shoot imaging (900-1700nm) 7. VNIR imaging (400-1000 nm) 8. SWIR imaging (1000-2500 nm) + Automate weighing & watering (five stations)

Automatic weighing and watering stations available in each greenhouse and also an additional station is available at the imaging area for broader accessibility. The weighing and watering station is controlled by the LemnaTec system and according to programming of the motor pump, the scaled amount of water is given to different pot present on carts. Greenhouse 1, 2 and 3 have five lanes of conveyer belt system and each lane can contain 60 RFID carts, while Greenhouse 4 has six lanes of conveyer belt system and each lane can contain 50 RFID carts. This lane compartmentalization enables the whole system to be controlled independently and provide flexibility to design experiments. The RFID chipped carts help in assigning barcodes to each cart and capturing the data systematically from the sensors.

In the imaging chamber, eight separate imaging compartments are present and within each compartment different sensors are present. The whole imaging loop consisting of eight sensors, starts with IR sensor, then a dark adaptation tunnel, Fluorescence camera, RGB root camera, RGB shoot sensor, NIR sensor, VNIR sensor and SWIR sensor are present sequentially. All sensors can be accessed independently as per the need of the experiment. Each imaging compartments are equipped with

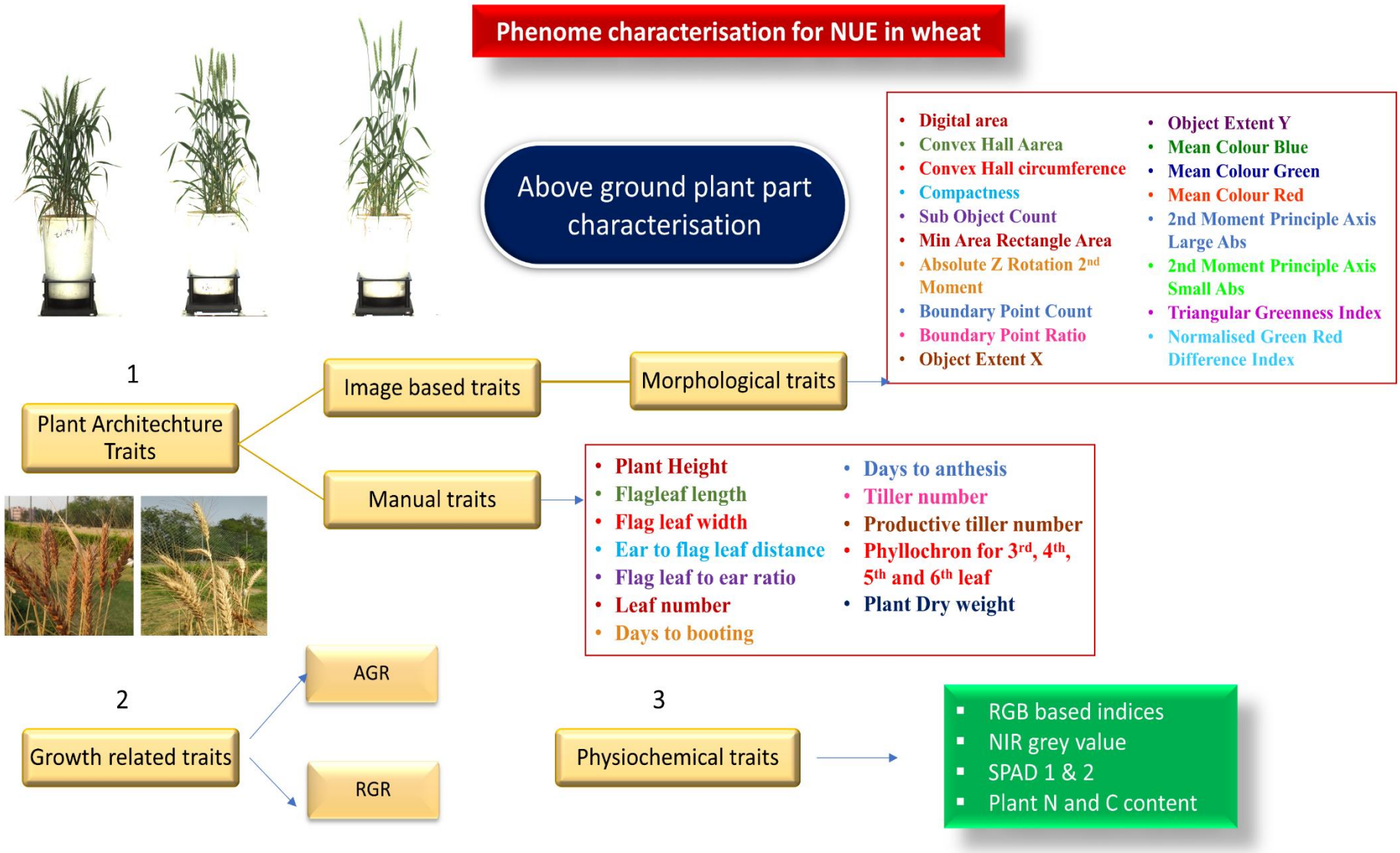

Figure 4.5: Phenome characterization of NUE in wheat.

suitable source of light as per the sensor requirement and contains hydraulic stages for taking image at a requisite height. These hydraulic imaging stations have also the functionalities of rotating the carts at any angle ranging from 0-360º angle. All the compartments have white background for uniform image segmentation required for image processing. After imaging of a pot by all the sensors, it goes back to its respective place in the greenhouse.

4.1.1.2 i-Trait extraction and characterization for biomass prediction

We analysed two image datasets, 1800 images (Experiment 1, 2018) and 924 images (Experiment 2), collected from 300 (Experiment 1) and 154 plants (Experiment 2, 2019), respectively. Each plant was imaged at a single time point by RGB (One top view and three side view images at 0º, 120º and 240º angle) and NIR sensor (One top view and one side view), then plants were harvested to measure FW) and SA immediately, and oven dried to record DW. To increase the variability in biomass range, we conducted our experiment with germplasm and RILs with wider variability in biomass, and phenotyping at different plant growth stages. All the images retrieved from the server and processed by the LemnaGrid image analysis pipeline, which was modified explicitly for mid to large-sized important cereals such as wheat (challenging due to its narrow leaf and compact character), resulting in nearly 200 phenotypic traits extracted from images of each plant (Figure 4.6).

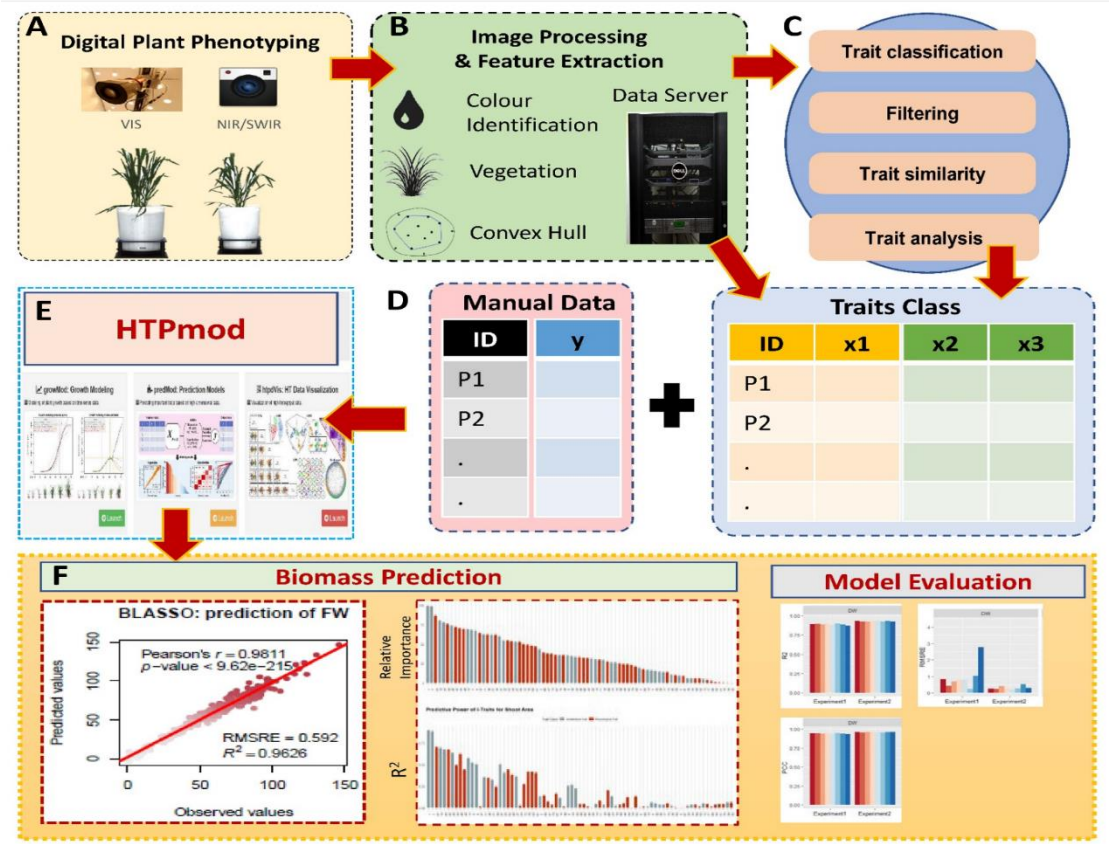

Figure 4.6: Figure 4.6: Data analysis and modelling pipeline for biomass prediction by i-Traits. A) Digital imaging-based plant phenotyping by visible (or color) and near-infrared sensors (NIR).

B) Image datasets were saved in data server and processed through LemnaGrid for feature extraction. C) Phenotypic data were subjected to quality check to remove low-quality data and classified into two categories such as architectural and physiological traits (Commonly referred as i-Traits). D) All the i-Traits were described by per plant basis and combined with manually measured data such as fresh weight (FW), dry weight (DW) and shoot area. E) Now the data matrix with all i_Traits and manual traits were used to predict biomass by HTPmod (a shiny based application) using eight machine learning method developed by Chen *et.al* (2019). F) The results of aal the models were interpreted by R^2, PCC and RMSRE value.

After quality control such as outliers, multicollinearity and manual checking of all the extracted traits, we selected 77 i-Traits which were divided into two major categories of traits such as architectural (35 traits) and physiological (42) traits.

4.1.1.3 Phenotypic profile analysis of plants in both experiments

We observed broader range of phenotypic values in all the traits in both experiments. The phenotypic value of FW, DW, and SA of experiment 1 ranged 0.6-145.86 g, 0.15-27.35g and 18.43-3622.25 cm^2, respectively. In the experiment 2, the FW, DW, and SA ranged 3.3-107.8 g, 0.5-22.2 g, and 26.15- 1434.01 cm^2, respectively (Figures 4.7).

In both experiments, 77 selected i-Traits were analysed. Principal component analysis (PCA) was carried out for both experiments to see the global phenotypic variation present in the population. The top 4 principal components (PCs) of experiment 1 and 2 accounted for 76.56% and 75.02% of the total phenotypic variation explained by i-Traits. The first two PCs clearly distinguished the experiments as the first two PCs of experiment 1 and 2 accounted for 39.41%, 17.77% and, 29.03%, 23.28%, respectively (Figure 4.7).

To access the patterns of trait correlations, we performed the trait similarity analysis based on canonical Pearson's correlation coefficient (Figures 4.8). We observed that the patterns of correlation were similar in both experiments however i-Traits were more correlated in experiment 1 than in experiment 2 as suggested by the intensity of colour in Figures 4.8 but traits across experiments shows similar correlation with each other. Also, the correlation of architectural traits with physiological traits was less, and traits were both positively and negatively correlated in the two experiments. Correlation among the physiological traits as higher than the correlation among the architectural traits.

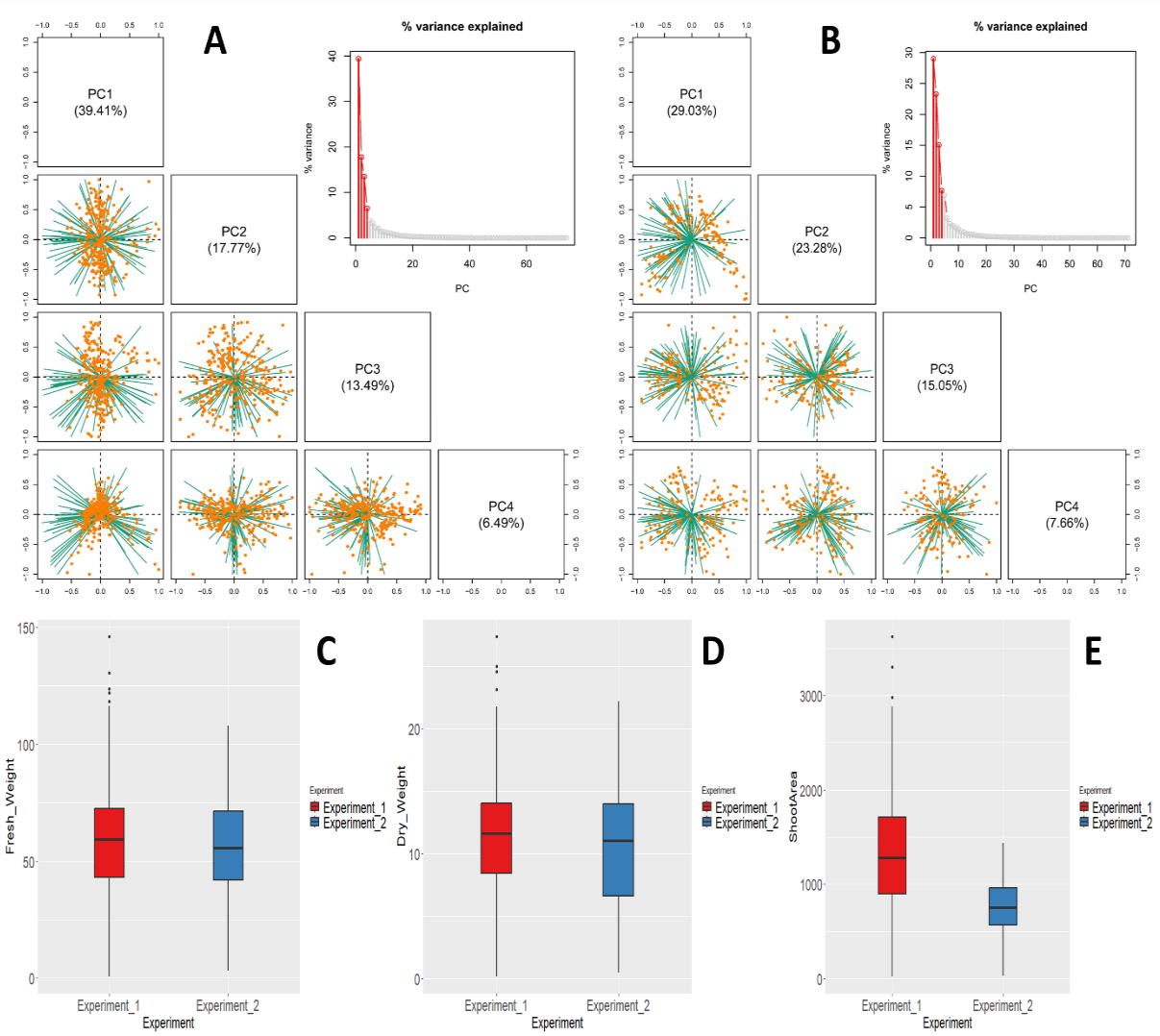

Figure 4.7: Characterization of all the i-Traits by phenotypic analysis for both experiments (Experiment 1 and Experiment 2). A, B) Principal component analysis of all the i-Traits for experiment 1 and experiment 2 respectively. Four PCs represented here which captured approximately all the variation in the data. Variance proportion explained by the PCs is shown in parentheses. Individuals are represented by orange dots and traits are represented by green lines. C, D, E) Differences in the FW, DW and shoot area across experiments represented by box plot analysis.

4.1.1.4 Phenotypic association of i-Traits with FW, DW and shoot area

We further evaluated the association of i-Traits with the manual traits in both experiments to see the relation between i-Traits and manual traits and to observe the biological relevance of predicting biomass from digital image-derived parameters (Figure 4.9). The direct relatedness of architectural traits with biomass is well reported in literature and the physiological traits that we included here having some unique feature that have not been reported earlier such as RGB colour class and RGB indices. The

use of physiological traits in biomass estimation is to incorporate the additional properties presented by NIR grey value (water status of plant), RGB colour class (greenness of different plant pixels) and RGB

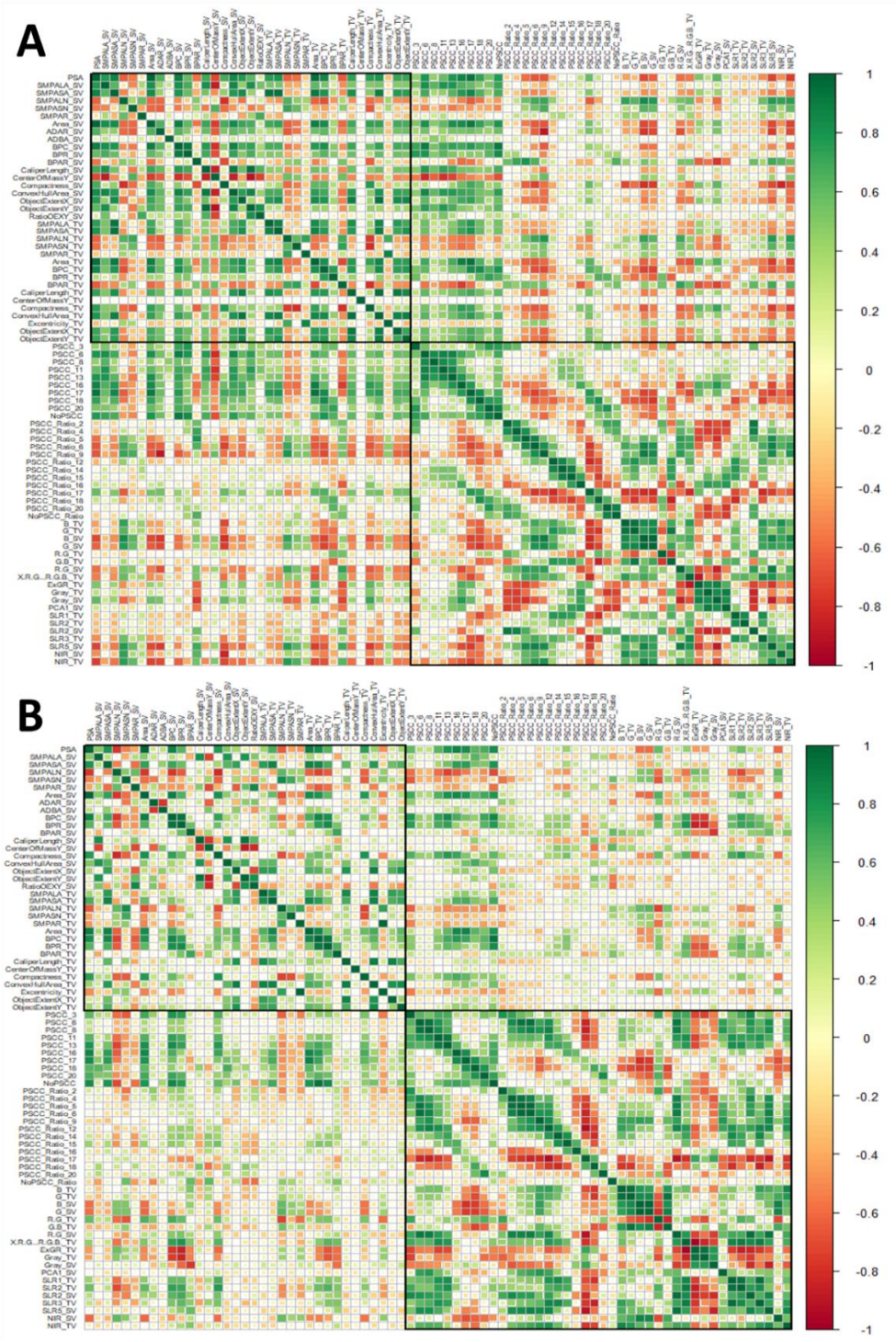

Figure 4.8: Assessment of trait similarity between i-Traits across experiments. A) Canonical correlation analysis of i-Traits based on experiment 1 (Top) and B) experiment 2 (Bottom). Heatmap plot is organized by both architectural and physiological traits represented by two highlighted boxes. Top box represents Architectural traits and bottom box represents physiological traits.

indices (reported vegetation indices). The PCC of the i-Traits with FW, DW and SA in experiment 1 ranged from -0.73 to 0.97, -0.76 to 0.92, and -0.76 to 0.93, respectively. While in the case of experiment 2, the FW, DW and SA correlations with i-Traits ranged from -0.76 to 0.95, -0.74 to 0.93 and -0.73 to 0.95, respectively. Architectural traits had a higher correlation with manual traits, than physiological traits. Among all the traits, PSA and Area_SV had a correlation of >0.9 for FW, DW and SA in both experiments. As expected, both boundary point count and compactness of side view images are also highly correlated with the manual traits. This explains that the biologically relevant traits, such as area and architecture, are highly related to biomass traits. We also found that physiological traits such as colour class correlated with biomass traits. NIR_SV was negatively correlated with FW, DW and SA ranging from -0.36 to -0.68 in both experiments. This also suggests that physiological traits not directly measured as plant architectural traits can also be used as biomass predictors. Indices derived from the mean blue, green and red values of RGB images also correlated with biomass, but the correlations were relatively lower than other traits.

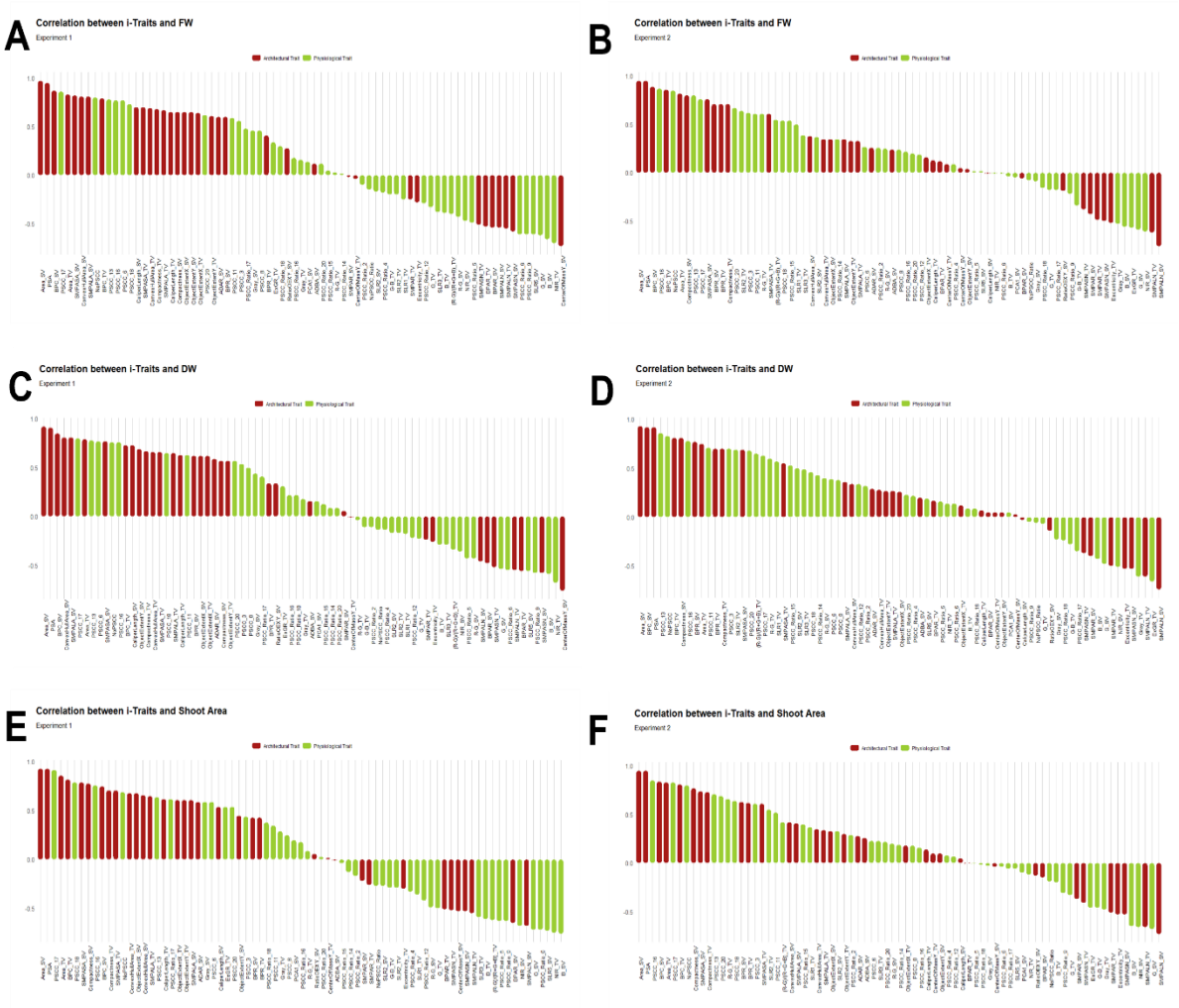

Figure 4.9: Pearson's correlation coefficients (PCC) in each experiment were calculated to assess the relationship between i-Traits and manual traits. The PCC were consistent in both experiments

and most of the features were having more than 0.5 positive or negative correlation coefficients with FW, DW and shoot area. A, B) PCC between FW and i-Traits in experiment 1 and 2 respectively. C, D) PCC between DW and i-Traits in experiment 1 and 2 respectively. E, F) PCC between shoot area and i-Traits in experiment 1 and 2 respectively.

4.1.1.5 Modelling of plant biomass using machine learning methods

HTP is particularly meaningful in dissecting complex genetics of biomass development in plants. The relationship between i-traits and above-ground shoot biomass accumulation were analysed by digital phenotyping data containing structural (e.g., architectural traits) and physiological traits (e.g., colour class, RGB based indices and plant moisture content as reflected by NIR-intensity traits). The results about i-Traits and manual traits suggested that these i-Traits can be very useful in predicting plant biomass-related traits.

To develop the model by machine learning (ML) methods, we used the available open-source tools. We used the *predMod* module from the HTPmod, a R program based shiny application. We used 16 ML methods available in *predMod*. From the 16 models, we found eight models that were consistent for all the manual trait estimations in both the experiments. The selected models were Bayesian LASSO, Bayesian regularized neural networks (BRNN), Lasso and elastic-net regularized generalized linear models (GLMNET), Gaussian process with the polynomial kernel (GP-Poly), multivariate adaptive regression splines (MARS), random forest (RF), ridge regression (RIDGE) and Support vector machines with linear kernel (SVM-Linear).

4.1.1.6 Biomass estimation model performance evaluation

Since our aim was to produce a more generalized model that can use genotypes and RILs to predict the biomass from image traits over multiple time points, the models were tested in both experiments to validate their performance and to evaluate their generalized nature. Analysis was performed with all 16 models, from which eight models that performed better for all the traits irrespective of experiments were selected. Results of all the 16 models showed that the R^2 for FW prediction was between 0.84 to 0.96, DW prediction was between 0.79 to 90 and SA prediction was 0.85 to 0.97 in experiment 1. In experiment 2 the R^2 for FW prediction was between 0.88 to 0.96, DW prediction was between 0.86 to 93 and

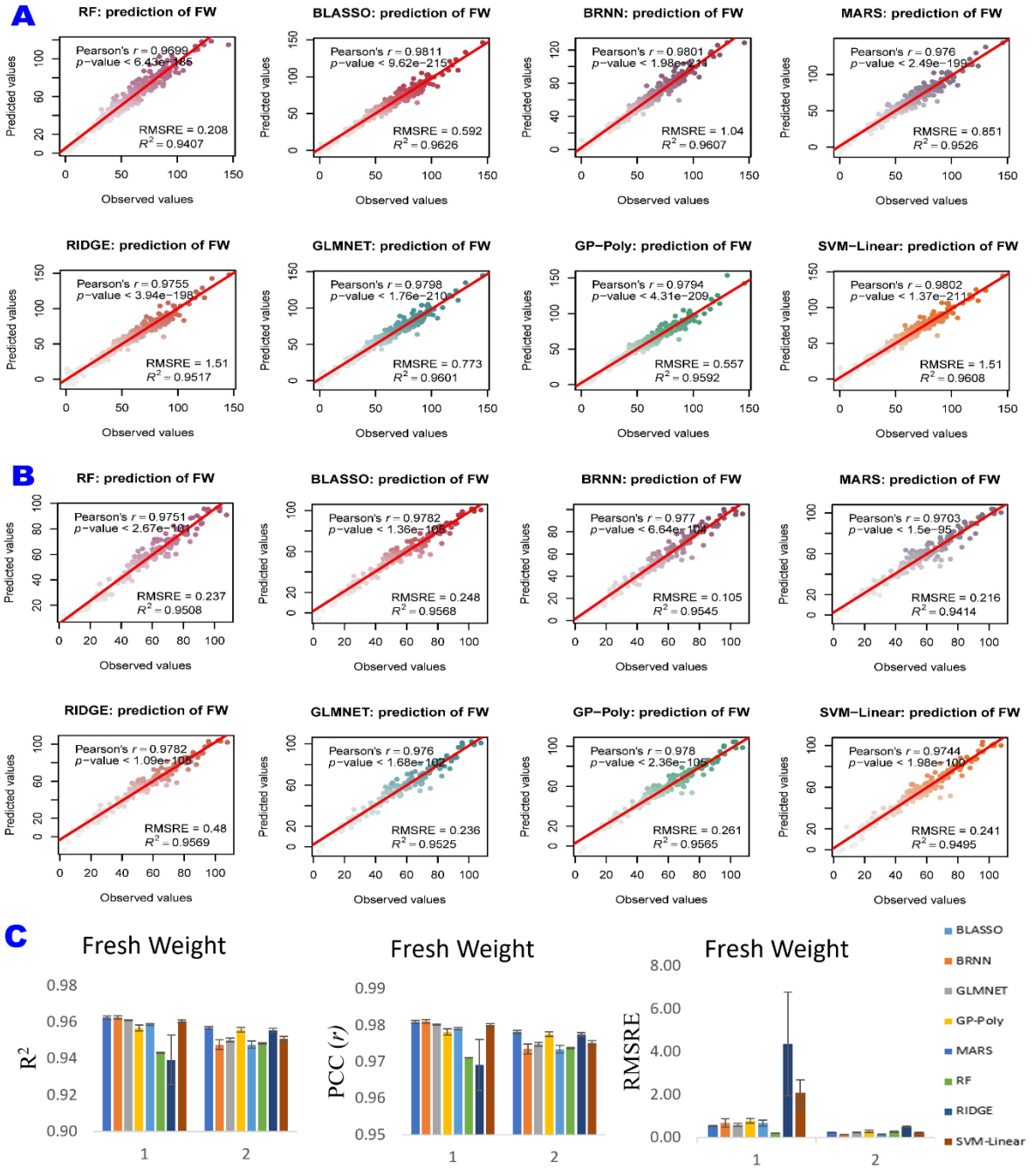

Figure 4.10: Nondestructive estimation of above ground plant biomass (AGPB) with i-Traits, using predmod in HTPmod. Scatter plots of observed FW vs predicted FW values using 8 prediction models based on machine learning methods BLASSO, BRNN, GLMNET, GP-Poly, MARS, RF, RIDGE and SVR. The prediction models were evaluated by Pearson's correlation coefficient (*r*), its corresponding *P*-value, R^2 and RMSRE. A and B) Prediction of FW in experiment 1 and 2 respectively. C) Evaluation of the model performance of each regression model used for AGPB prediction.

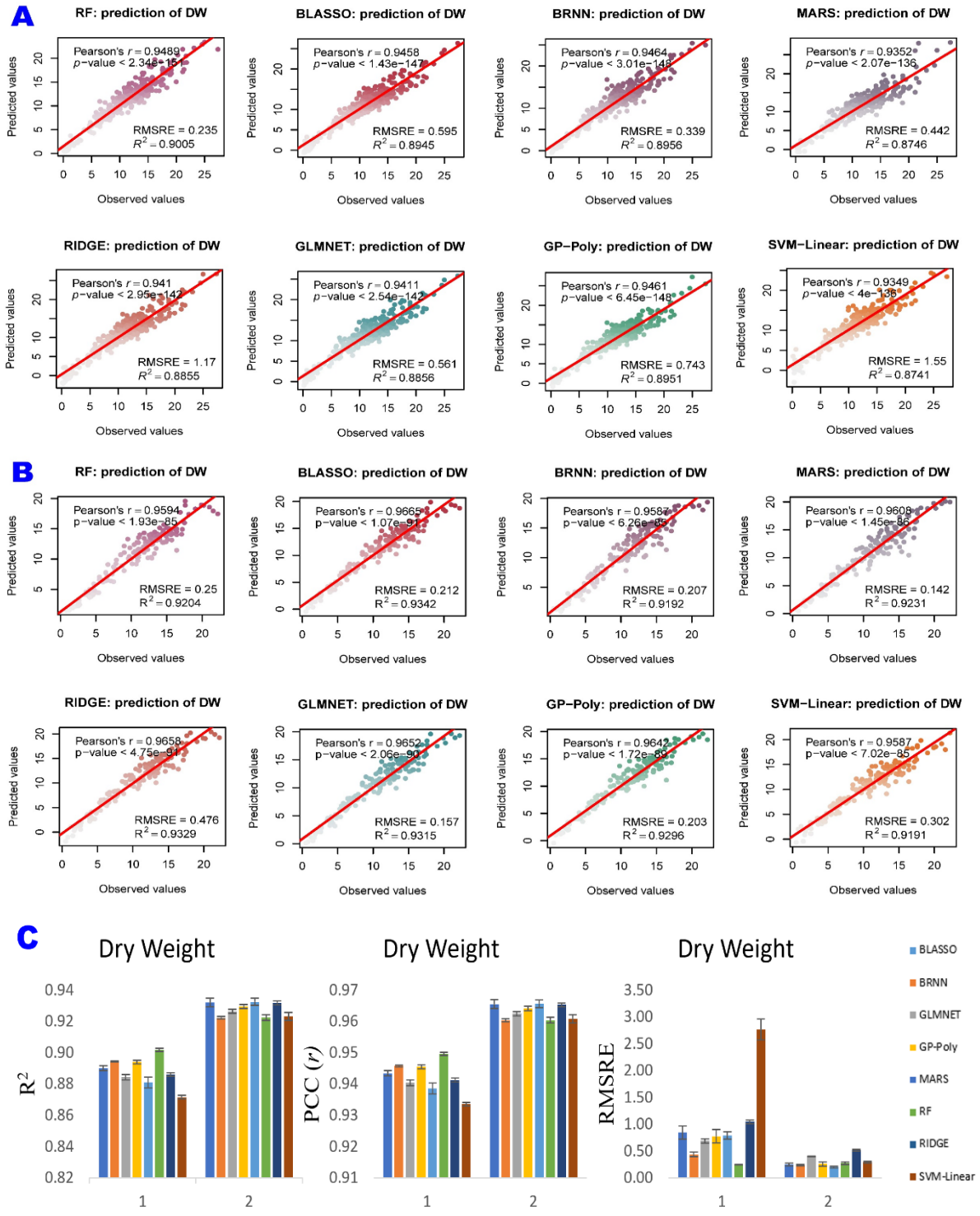

Figure 4.11: Non destructive estimation of DW by using i-Traits. A and B) Prediction of DW in experiment 1 and 2 respectively. C) Summary of the predictive power of each regression model.

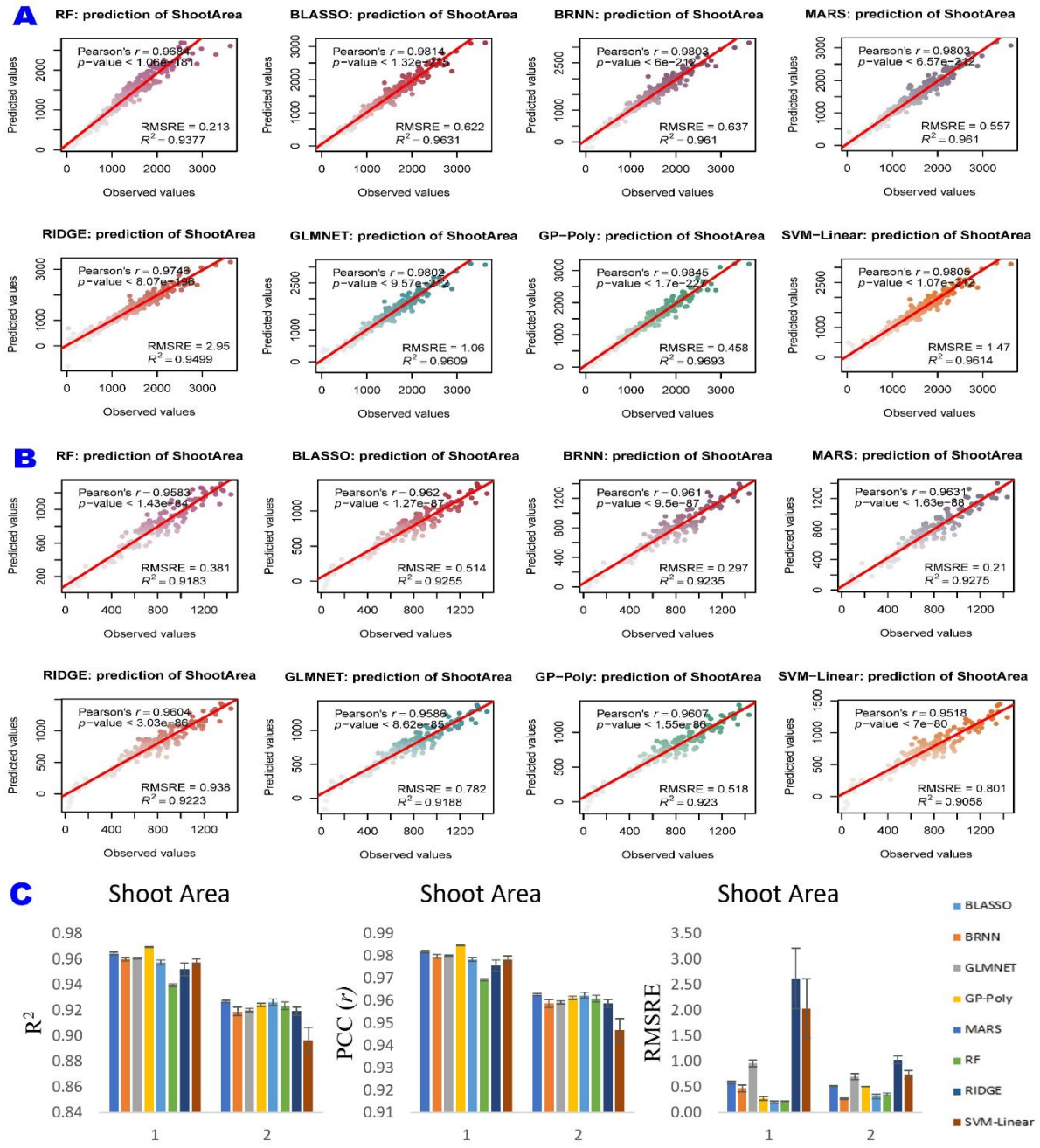

Figure 4.12: Nondestructive estimation of shoot area by using i-Traits. A and B) Prediction of shoot area in experiment 1 and 2 respectively. C) Summary of the predictive power of each regression model.

SA prediction was 0.86 to 0.93. We found that eight models performed relatively better than other eight models. Bayesian Generalized Linear Model (BGLM), Gradient Boosting Machine (GBM), Generalized Linear Model (GLM), Gaussian Process with Radial Kernel (GP-Radial), K-Nearest Neighbors (KNN), Least Absolute Shrinkage and Selection Operator Regression (LASSO), Multivariate Linear Regression (MLR) and Support Vector Machines with Radial Kernel (SVM-Radial) performed with relatively less accuracy than other eight models namely Bayesian LASSO, Bayesian

regularized neural networks (BRNN), Lasso and elastic-net regularized generalized linear models (GLMNET), Gaussian process with the polynomial kernel (GP-Poly), multivariate adaptive regression splines (MARS), random forest (RF), ridge regression (RIDGE) and Support vector machines with linear kernel (SVM-Linear). BGLM, GBM, GLM, GP-Radial, KNN, LASSO, MLR and SVM-Radial had R^2 value for prediction of FW ranged from 0.84 to 0.90, for DW ranged from 0.79 to 0.87 and for SA ranged from 0.85 to 0.95 in experiment 1 (Supplementary data sheet 1). At the same time BLASSO, BRNN, GLMNET, GP-Poly, MARS, RF, RIDGE and SVM-Linear had higher R^2 value of 0.94 to 0.96 for FW, 0.87 to 0.90 for DW and 0.93 to 0.96 for SA prediction in experiment 1 (Figure 4.10, 4.11 and 4.12). Similar condition was there in experiment 2 also. In experiment 2, BGLM, GBM, GLM, GP-Radial, KNN, LASSO, MLR and SVM-Radial had R^2 value of 0.88 to 0.92 for FW, 0.86 to 0.89 for DW and 0.86 to 0.90 for SA prediction (Supplementary data sheet 1). While BLASSO, BRNN, GLMNET, GP-Poly, MARS, RF, RIDGE and SVM-Linear had higher R^2 value of 0.94 to 0.96 for FW, 0.91 to 0.93 for DW and 0.90 to 0.93 for SA prediction in experiment 2 (Figure 4.10, 4.11 and 4.12). We also noticed that these eight models performed better than normal multivariate regression (MLR) model. All eight selected models BLASSO, BRNN, GLMNET, GP-Poly, MARS, RF, RIDGE and SVM-Linear performed relatively similar in terms of estimation accuracy, while we confined the results to select four best-suited models for our experiments namely BLASSO, BRNN, GLMNET and GP-Poly that were with less RMSRE value and with similar estimation accuracy across experiments.

In case of FW estimation, R^2 and *r* value ranged from 0.95 to 0.96 and 0.97 to 0.98 in the two experiments for BLASSO, BRNN, GLMNET and GP-Poly models (Figure 4.10). So, this represents the generalized nature of the estimation, as almost all four models showed similar results. DW's estimation also showed promising results as the R^2 and *r* value ranged from 0.89 to 0.93 and 0.94 to 0.96 in the two experiments (Figure 4.11). In SA estimation, R^2 and *r* value ranged from 0.91 to 0.97 and 0.95 to 0.98 in both the experiments (Figure 4.12). As per these four models, Experiment 1 had slightly higher estimation accuracy than experiment 2 for FW and SA estimation but in the case of the DW, experiment 2 had better performance than experiment 1. RMSRE values were relatively lower in experiment 2 than in experiment 1 in most of the parameters but the difference was not large.

By observing the estimation ability of the models by R^2 and *r* and RMSRE we found out BLASSO, BRNN, GLMNET and GP-Poly were relatively better-performing models in all the traits and across all the experiments. Selecting a single model was interesting due to the relatively similar and better estimation accuracy across models. Nevertheless, BLASSO performed better in all the trait estimations in all the experiments with the highest R^2 and lowest RMSRE values. The R^2 of Bayesian Least Absolute Shrinkage and Selection Operator BLASSO for FW prediction was 0.96 (both year experiments), for DW prediction was 0.90 (Experiment 1) and 0.93 (Experiment 2) and for SA prediction 0.96 (Experiment 1) and 0.93 (Experiment 2). Also, the RMSRE of BLASSO for FW

prediction was 0.53 (Experiment 1) and 0.24 (Experiment 2), for DW prediction was 0.85 (Experiment 1) and 0.25 (Experiment 2) and for SA prediction 0.59 (Experiment 1) and 0.53 (Experiment 2).

4.1.1.7 Evaluation of i-Traits for predictive power and relative importance

For each i-Trait, the predictive power and relative importance were calculated by the degenerate model using the *predMod* module. In both experiments, the predictive power and feature importance of i-Traits were similar, so here we explained the individual capability of each i-Trait as a predictor of biomass in experiment 1 (Figure 4.13). Both predictive power and relative importance of most architectural traits were higher than physiological traits. The top 10 important features contained architectural and physiological traits, but more architectural traits were present than physiological ones. PSA, Area_SV, and BPC_SV have higher predictive power and relative importance among all the i-Traits for FW, DW and SA. Area_SV had R^2 of 0.94 for the estimation of FW, which was highest than the DW (R^2 of 0.79) and shot area (R^2 of 0.89) estimation. Among physiological traits, PSCC_17, 16, 13, NIR_TV and SV, B_SV, G_SV, SLR5_SV, Gray_TV, etc., had higher predictive power and relative importance than other physiological traits. NIR_TV and NIR_SV also had significant predictive power and relative importance ranging from ~0.1 to 0.5 (R^2) and ~5 to 59 % (Inclusive MSE) relative importance. The best predictor i-Trait for FW and DW prediction was Area_SV and for SA prediction was projected shoot area. These results give deep understanding into major determinants of plant biomass and also suggests that along with architectural traits, physiological traits also help to improve estimation accuracy and are determinants of plant growth.

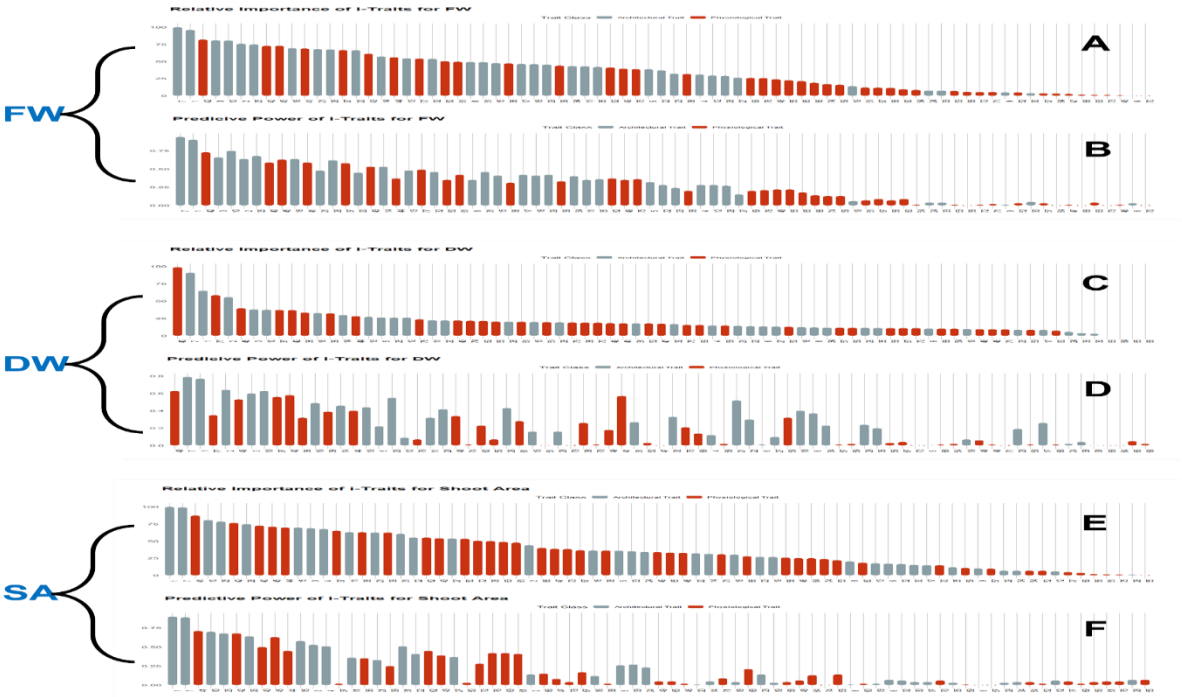

Figure 4.13: Estimation of predictive power and relative importance of features (i-Traits) used in regression models. Bayesian-LASSO (BLASSO) model was used for wheat FW, DW and shoot

area prediction, using i-Traits from two independent experiments. But as both experiments performed relatively similar with respect to prediction power and relative importance, experiment 1 information is presented here for the ease of understanding. A, C and E) Relative importance of i-Traits used for FW, DW and shoot area prediction respectively. B, D and F) Predictive power of i-Traits used for FW, DW and shoot area prediction respectively.

4.1.1.8 Extraction of phenotypic traits from high-throughput phenotyping for NUE component traits

To study the nitrogen use efficiency and N deficiency response of wheat, an experiment was conducted in the controlled greenhouses of NDPPC in rabi season of year 2019-20. A total of 48000 images (~2 TB of data) were collected from 175 RILs, 2 parental genotypes, two treatments (control and nitrogen deficiency) and three biological replications over the whole season at five time points (60, 70, 80, 90, and 100 DAS). Following the data collection, image processing and trait analysis were carried out to understand the underlying physiology in the high-throughput phenotyping data (Figure 4.14). All the images were processed using the inhouse pipeline developed in commercial image processing software LemnaGrid at NDPPC.

This dataset generated ~ 400 raw image derived parameters at each time point. Once all the parameters were extracted from the LemnaGrid through the LemnaMiner mediator database software, into excel sheet, they were arranged and sorted by genotype, treatment and replication wise. From these primary data some secondary derived traits such as RGB based vegetation indices, relative growth rate, absolute growth rate and transpiration use efficiency were calculated. Now from all the extracted parameters high quality traits were selected (Figure 4.14) by removing redundant, noninformative and low heritability traits by analyzing the correlation, clustering, heritability analysis and manual curation of all the traits.

So, after this robust cleaning process we selected 91 high quality i-Traits which were categorized into morphometric, biomass related, colour related, RGB vegetation indices and gray value intensity traits. These above 91 traits were captured at five time points and also 24 secondary derived traits from primary traits were formulated which includes 9 growth rate related traits (5 AGRs and 4 RGRs) and 15 day and night transpiration related traits. Detailed list of traits extracted from HTP is given below (Table 2).

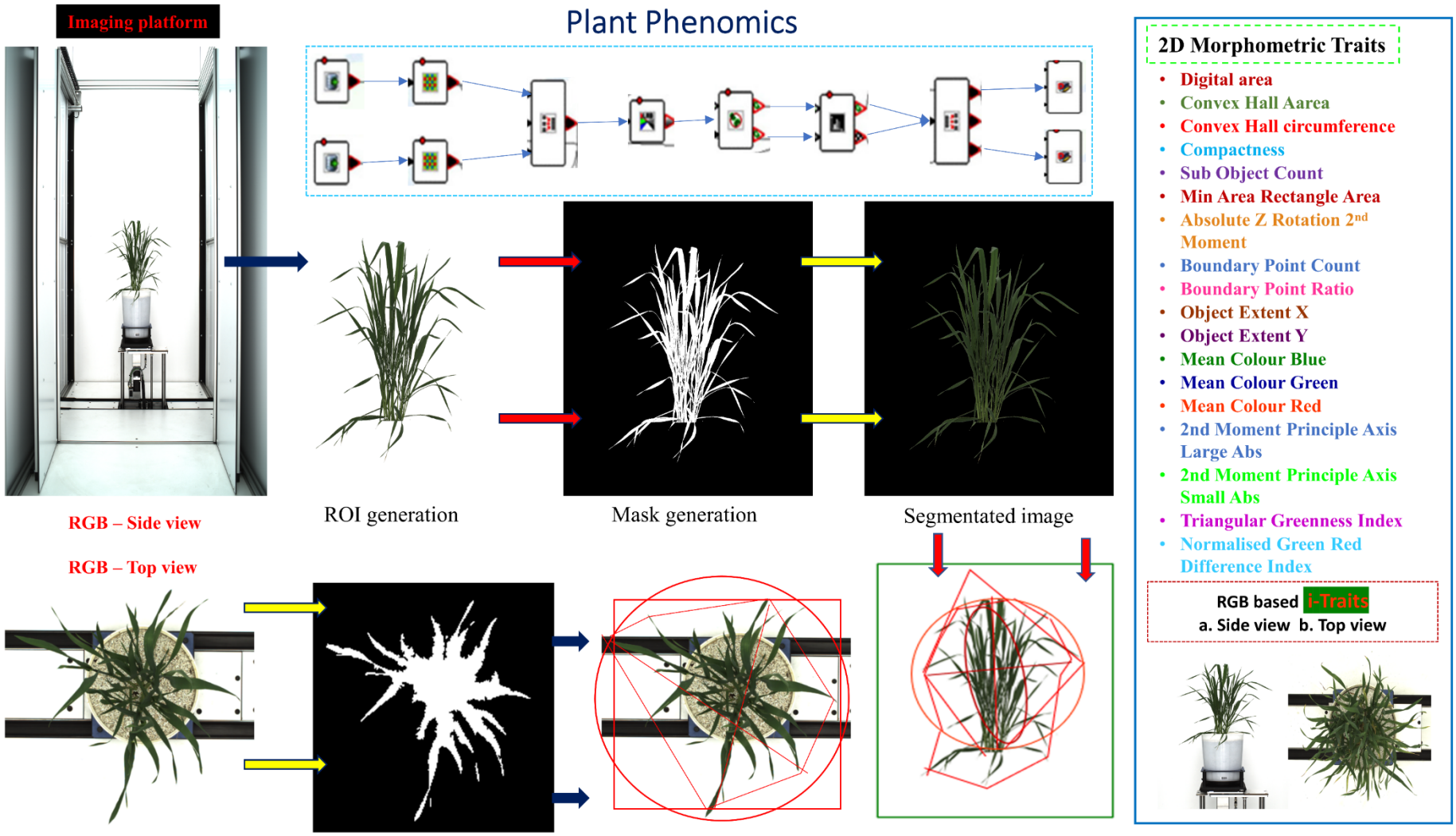

Figure 4.14: Phenomics Traits Extraction.

Table 4.2: List of all HTP traits.

Sl. No	Trait Name	Trait Code	Trait Category	Sensor
1	2ndMomentPrincipleAxisLargeAbs_SV	2MPALA_SV	Mophometric	RGB
2	2ndMomentPrincipleAxisSmallAbs_TV	2MPASA_TV	Mophometric	RGB
3	2ndMomentPrincipleAxisSmallAbs_SV	2MPASA_SV	Mophometric	RGB
4	2ndMomentPrincipleAxisLargeNorm_SV	2MPALN_SV	Mophometric	RGB
5	2ndMomentPrincipleAxisSmallNorm_TV	2MPASN_TV	Mophometric	RGB
6	2ndMomentPrincipleAxisSmallNorm_SV	2MPASN_SV	Mophometric	RGB
7	2ndMomentsPrincipalAxisRatio_SV	2MPAR_SV	Mophometric	RGB
8	BoundaryPointCount_TV	BPC_TV	Mophometric	RGB
9	BoundaryPointCount_SV	BPC_SV	Mophometric	RGB
10	BoundaryPointRoundness_TV	BPR_TV	Mophometric	RGB
11	BoundaryPointRoundness_SV	BPR_SV	Mophometric	RGB
12	CentreOfMassY_SV	cmY_SV	Mophometric	RGB
13	ConvexHullArea_TV	CHArea_TV	Mophometric	RGB
14	ConvexHullArea_SV	CHArea_SV	Mophometric	RGB
15	Circumference_SV	Circumference_SV	Mophometric	RGB
16	Excentricity_SV	Excentricity_SV	Mophometric	RGB
17	ObjectExtentX_SV	ObjectExtentX_SV	Mophometric	RGB
18	ObjectExtentY_TV	ObjectExtentY_TV	Mophometric	RGB
19	ObjectExtentY_SV	ObjectExtentY_SV	Mophometric	RGB
20	MinAreaRectAngle_TV	MARA_TV	Mophometric	RGB
21	AbsolutZRotation2ndMoment_TV	AZR2M_TV	Mophometric	RGB
22	NormalisedZRotation2ndMoment_TV	NZR2M_TV	Mophometric	RGB
23	BoundaryPointsToAreaRatio_TV	BPAR_TV	Mophometric	RGB
24	BoundaryPointsToAreaRatio_SV	BPAR_SV	Mophometric	RGB
25	Compactness_TV	Compactness_TV	Mophometric	RGB
26	Compactness_SV	Compactness_SV	Mophometric	RGB
27	AreaDistributionAboveRelative_SV	ADAR_SV	Biomass	RGB
28	ObjectArea_TV	Area_TV	Biomass	RGB
29	ObjectArea_SV	Area_SV	Biomass	RGB
30	ProjectedShootArea	PSA	Biomass	RGB
31	Biovolume	Biovolume	Biomass	RGB
32	NIRmeangrayintensity_TV	NIR	Intensity	NIR

Sl. No	Trait Name	Trait Code	Trait Category	Sensor
33	NIRmeangrayintensity_SV	NIR	Intensity	NIR
34	InfraRedintensity_TV	IR	Intensity	IR
35	InfraRedintensity_SV	IR	Intensity	IR
36	ProjectedShootColourClass_1	PSCC_1	Colour	RGB
37	ProjectedShootColourClass_2	PSCC_2	Colour	RGB
38	ProjectedShootColourClass_3	PSCC_3	Colour	RGB
39	ProjectedShootColourClass_4	PSCC_4	Colour	RGB
40	ProjectedShootColourClass_5	PSCC_5	Colour	RGB
41	ProjectedShootColourClass_6	PSCC_6	Colour	RGB
42	ProjectedShootColourClass_7	PSCC_7	Colour	RGB
43	ProjectedShootColourClass_8	PSCC_8	Colour	RGB
44	ProjectedShootColourClass_9	PSCC_9	Colour	RGB
45	ProjectedShootColourClass_10	PSCC_10	Colour	RGB
46	ProjectedShootColourClass_11	PSCC_11	Colour	RGB
47	ProjectedShootColourClass_12	PSCC_12	Colour	RGB
48	ProjectedShootColourClass_13	PSCC_13	Colour	RGB
49	ProjectedShootColourClass_14	PSCC_14	Colour	RGB
50	ProjectedShootColourClass_15	PSCC_15	Colour	RGB
51	ProjectedShootColourClass_16	PSCC_16	Colour	RGB
52	ProjectedShootColourClass_17	PSCC_17	Colour	RGB
53	ProjectedShootColourClass_18	PSCC_18	Colour	RGB
54	ProjectedShootColourClass_19	PSCC_19	Colour	RGB
55	ProjectedShootColourClass_20	PSCC_20	Colour	RGB
56	No_ProjectedShootColourClass	No_PSCC	Colour	RGB
57	Mean Blue Intensity_TV	Blue_TV	Colour	RGB
58	Mean Blue Intensity_SV	Blue_SV	Colour	RGB
59	Mean Green Intensity_TV	Green_TV	Colour	RGB
60	Mean Green Intensity_SV	Green_SV	Colour	RGB
61	Mean Red Intensity_TV	Red_TV	Colour	RGB
62	Mean Red Intensity_SV	Red_SV	Colour	RGB
63	(G-B)/(R+G+B) _SV	(G-B)/(R+G+B) _SV	Indices	RGB
64	(R-G)/(R+G+B) _TV	(R-G)/(R+G+B) _TV	Indices	RGB
65	Channel index B _TV	b_TV	Indices	RGB

Sl. No	Trait Name	Trait Code	Trait Category	Sensor
66	Channel index B _SV	b_SV	Indices	RGB
67	Excess blue vegetation index_SV	ExB_SV	Indices	RGB
68	Excess green vegetation index_SV	ExG_SV	Indices	RGB
69	Channel index G _TV	g_TV	Indices	RGB
70	Binary channel index _TV	G/B_TV	Indices	RGB
71	Binary channel index _SV	G/R_SV	Indices	RGB
72	Green minus Red_SV	GMR_SV	Indices	RGB
73	Gray_TV	Gray_TV	Indices	RGB
74	Gray_SV	Gray_SV	Indices	RGB
75	I2_TV	I2_TV	Indices	RGB
76	PCA index_SV	Ipca_SV	Indices	RGB
77	PCA 1_TV	PCA1_TV	Indices	RGB
78	PCA 2_SV	PCA1_SV	Indices	RGB
79	PCA 2_SV	PCA2_SV	Indices	RGB
80	Channel index R_SV	r_SV	Indices	RGB
81	Red minus Blue_TV	R-B_TV	Indices	RGB
82	Red minus Green_TV	R-G_TV	Indices	RGB
83	SCOM_TV	SCOM_TV	Indices	RGB
84	SLR 1_TV	SLR1_TV	Indices	RGB
85	SLR 2_SV	SLR1_SV	Indices	RGB
86	SLR 2_TV	SLR2_TV	Indices	RGB
87	SLR 3_SV	SLR2_SV	Indices	RGB
88	SLR 3_TV	SLR3_TV	Indices	RGB
89	SLR 4_SV	SLR3_SV	Indices	RGB
90	SLR 4_SV	SLR4_SV	Indices	RGB
91	SLR 5_TV	SLR5_TV	Indices	RGB
92	Absolute Growth Rates	AGR1	Growth Rate	RGB
93	Absolute Growth Rates	AGR2	Growth Rate	RGB
94	Absolute Growth Rates	AGR3	Growth Rate	RGB
95	Absolute Growth Rates	AGR4	Growth Rate	RGB
96	Absolute Growth Rates	AGR5	Growth Rate	RGB
97	Relative Growth Rates	RGR1	Growth Rate	RGB
98	Relative Growth Rates	RGR2	Growth Rate	RGB

Sl. No	Trait Name	Trait Code	Trait Category	Sensor
99	Relative Growth Rates	RGR3	Growth Rate	RGB
100	Relative Growth Rates	RGR4	Growth Rate	RGB
101	Water use related traits	AWU_Diurnal	Water Use	Weight
102	Water use related traits	AWU_Day	Water Use	Weight
103	Water use related traits	AWU_Night	Water Use	Weight
104	Water use related traits	PSA_TUE_Diurnal	Water Use	Weight
105	Water use related traits	PSA_TUE_Day	Water Use	Weight
106	Water use related traits	PSA_TUE_Night	Water Use	Weight
107	Water use related traits	Foliage_TUE _Diurnal	Water Use	Weight
108	Water use related traits	Foliage_TUE_Day	Water Use	Weight
109	Water use related traits	Foliage_TUE_Night	Water Use	Weight
110	Water use related traits	PSA_TR_Diurnal	Water Use	Weight
111	Water use related traits	PSA_TR_Day	Water Use	Weight
112	Water use related traits	PSA_TR_Night	Water Use	Weight
113	Water use related traits	Foliage_TR_Diurnal	Water Use	Weight
114	Water use related traits	Foliage_TR_Day	Water Use	Weight
115	Water use related traits	Foliage_TR_Day	Water Use	Weight

The description about each trait have been explained and the derivation of secondary traits also described below. All these 115 i-Traits covers wide range of plant characteristics that was affected by the nitrogen deficiency and have higher heritability which will be also helpful for its genetic basis dissection by linkage mapping approach that we have done in this work. Also, the importance of these traits has been explained category wise along with the extraction formula.

Morphometric Traits:

1. **2nd Moment Principal Axis Large Abs:** $\mu l = S$ (pixelA * rAs^2), rAs is the distance of pixel A from the larger moment axis (through the centre of mass) in direction of the smaller moment axis with the additional condition $\mu 11=0$.
2. **2nd Moment Principal Axis Small Abs:** $\mu s = S$ (pixelA * rAl^2), rAl is the distance of pixel A from the smaller moment axis (through the centre of mass) in direction of the larger moment axis with the additional condition $\mu 11=0$.
3. **2nd Moment Principal Axis Large Norm:** 2nd Moment Principal Axis Large Norm = 2nd Moment Principal Axis Large Abs/Object Area

4. **2nd Moment Principal Axis Small Norm:** 2nd Moment Principal Axis Small Norm = 2nd Moment Principal Axis Small Abs/Object Area
5. **2nd Moments Principal Axis Ratio:** 2nd Moments Principal Axis Ratio = 2nd Moment Principal Axis Large Abs/2nd Moment Principal Axis Small Abs
6. **Boundary Point Count:** Number of all pixels of an object boundary
7. **Boundary Point Roundness:**
   Boundary Point Roundness = (Boundary Point Count) ²/size.
8. **Centre Of Mass Y:** Average y-value (y-position) of all object pixels (all pixel same size). Formula = Centre of Mass X = S pixelA*rAy/Object area. It is the y-value of the crossing point of the two principal axes.
9. **Convex Hull Area:** Convex Hull Area is the area of the smallest object without concave boundary parts
10. **Circumference:** Sum of the direction corrected length of the outer boundary of all sub objects
11. **Eccentricity:** eccentricity = sqr (μ20 -μ02) + 4 * sqr (μ11)/sqr (μ20 + μ02)
12. **Object Extent X:** Length in x-direction of the minimum vertically oriented rectangle covering the object
13. **Object Extent Y:** Length in y-direction of the minimum vertically oriented rectangle covering the object
14. **Min Area Rectangle Angle:** The angle measured describes the angle between 3 o'clock/east and the larger extension side of the rectangle.
15. **Absolut Z Rotation 2nd Moment:** μz = S (pixelA * rA²) rA Euclidian distance from the centre of mass
16. **Normalised Z Rotation 2nd Moment:** μz = (S (pixelA * rA²))/Object Area
17. **Boundary Points to Area Ratio:** Boundary Points to Area Ratio = Boundary Point Count /Object Area (0 to 1 /no unit)
18. **Compactness:** Compactness = Object Area/Convex Hull Area
19. **Area Distribution Above Relative:** Pixels present above
20. **Object Area:** Number of object pixels
21. **Projected Shoot Area:** Sum of Top View and Side View (0º, 120º and 240º) object area
22. **Biovolume:** Estimated digital volume (unit: voxel) that corresponds to a pixel volume. Calculated from all side and top view images as sqrt (average plant side area2 x top plant area)

NIR & IR intensity traits:

23. **NIR mean gray intensity:** Near Infrared intensity for water related traits
24. **Infra-Red intensity:** Representation of canopy temperature

Colour related traits:

25. **Projected Shoot Colour Class:** Object area classified into 20 colour classes and each PSCC represents area of a specific colour class. Colour classification is used to separate all colours of an image into biologically relevant classes defining colour shades or e.g specific effects of nutrient deficiency e.g., chlorosis and senescence
26. **Mean Blue Intensity:** Mean Blue Value of all the pixels
27. **Mean Green Intensity:** Mean Green Value of all the pixels
28. **Mean Red Intensity:** Mean Red Value of all the pixels

RGB based vegetation indices:

29. (G-B)/(R+G+B): (G-B)/(R+G+B)
30. (R-G)/(R+G+B): (R-G)/(R+G+B)
31. **Channel index B:** B/ (R + G + B)
32. **Excess blue vegetation index:** 1.4b − g
33. **Excess green vegetation index:** 2g − r − b
34. **Channel index G:** G/ (R + G + B)
35. **Binary channel index:** B/G
36. **Binary channel index:** R/G
37. **Green minus Red:** G-R
38. **Gray:** 0.2898*red + 0.5870*green + 0.1140*blue
39. **I2:** 0.55 + 11.4((G-B)/(G+B)) - 12.5((R-B)/(R+B)) + 9((R-G)/(R+G))
40. **Principal component analysis index:** 0.994|R − B| + 0.961|G − B| + 0.914|G − R|
41. **PCA 1:** -0.977b + 0.916((G-B)/(G+B)) + 0.995((R-B)/(R+B)) + 0.771 ((R-G)/(R+G))
42. **PCA 2:** 0.999|R-B| + 0.92|G-B| + 0.886|R-G|
43. **Channel index R:** R/(R + G + B)
44. **Red minus Blue:** R-B
45. **Red minus Green:** R-G
46. **SCOM:** 0.25 × ExG + 0.30 × ExGR + 0.33 × CIVE
47. **SLR 1:** -60430 - 0.7316B + 69680b + 112800g + 28270((G-B)/(G+B)) -23890((R-B)/(R+B)) + 68380((R-G)/(R+G))
48. **SLR 2:** -46240 - 2.678B + 1.05G + 52570b + 87420g + 20720((G-B)/(G+B)) -18240((R-B)/(R+B)) + 52500((R-G)/(R+G))
49. **SLR 3:** -25373 + 30106b + 46539g + 12776((G-B)/(G+B)) - 10507((R-B)/(R+B)) +28821((R-G)/(R+G))
50. **SLR 4:** -44312 + 51689b + 81995g + 21751((G-B)/(G+B)) - 18156((R-B)/(R+B)) +50425((R-G)/(R+G))

51. **SLR 5:** 41048 + 46964b + 76841g + 19998((G-B)/(G+B)) - 17173((R-B)/(R+B)) + 47162((R-G)/(R+G))

Growth rate related traits:

52. **Absolute Growth Rate:** Absolute growth rate between germination, 60DAS, 70DAS, 80DAS, 90DAS and 100DAS.
53. **Relative Growth Rates:** Relative growth rate between 60DAS, 70DAS, 80DAS, 90DAS and 100DAS.

Water use related traits:

54. Water use related traits: Average Water Use per day
55. Water use related traits: Average Water Use from morning to evening
56. Water use related traits: Average Water Use from evening to morning
57. Water use related traits: Projected shoot area per ml water transpired_Diurnal
58. Water use related traits: Projected shoot area per ml water transpired_Day
59. Water use related traits: Projected shoot area per ml water transpired_Night
60. Water use related traits: dry wt foliage per ml water transpired_Diurnal
61. Water use related traits: dry wt foliage per ml water transpired_Day
62. Water use related traits: dry wt foliage per ml water transpired_Night
63. Water use related traits: ml of water transpired per PSA_Diurnal
64. Water use related traits: ml of water transpired per PSA_Day
65. Water use related traits: ml of water transpired per PSA_Night
66. Water use related traits: ml of water transpired per dry wt foliage_Diurnal
67. Water use related traits: ml of water transpired per dry wt foliage_Day
68. Water use related traits: ml of water transpired per dry wt foliage_Night

4.1.1.9 Univariate analysis of phenotypic behavior of RILs

Heritability

Broad sense heritability (H^2) of all the i-Traits were observed under control and nitrogen deficiency condition at all the five stages. The average h^2 of all the morphometric traits were 0.78, 0.81, 0.79, 0.80 and 0.83 under control conditions at 60, 70, 80, 90 and 100 DAS, respectively (Figure 4.15). Whereas, the average H^2 of all the morphometric traits were 0.71, 0.72, 0.72, 0.71 and 0.78 under nitrogen deficiency condition at 60, 70, 80, 90 and 100 DAS, respectively (Figure 4.16). There was an average difference of ~10% in the heritability of traits under control and N condition. The H^2 of morphometric traits ranged from 0.49-0.94 and 0.35-0.92 under control and N deficiency conditions, respectively at 60 DAS. At 70 DAS the H^2 of morphometric traits ranged from 0.47-0.96 and 0.25-0.95

under control and N-deficiency conditions, respectively. Also, at 80, 90, and 100 DAS, the H^2 of all the morphometric traits ranged 0.39-0.97 and 0.19-0.96, 0.31-0.98 and 0.17-0.96, and 0.23-0.98 and 0.14-0.96 under control and nitrogen deficiency conditions, respectively. Traits such as ObjectExtentY_TV, MARA_TV, Circumference_SV1, 2MPASN_TV, ADAR_SV were having the lowest h^2 (below 0.7) among the morphometric traits.

The biomass related traits such as Area_TV, Area_SV and Biovolume had H^2 more than 0.6 at all the stages (Figure 4.17) and as the growth period increased the heritability increased from ~0.6 to ~0.9 under both control and N-deficiency conditions. Here also under nitrogen deficiency conditions, the heritability was lower than the control conditions. In case of colour related traits the average H^2 was 0.78, 0.81, 0.84, 0.82 and 0.9 under control conditions (Figure 4.18) and 0.68, 0.72, 0.72, 0.75 and 0.83 under nitrogen deficiency conditions at 60, 70, 80, 90 and 100 DAS, respectively (Figure 4.19). A ~15% reduction of heritability on i-Traits under N-deficiency conditions was observed as compared with that of control conditions. The lower range of H^2 were 0.46-0.71 and 0.51-0.67 for control and N-deficiency conditions, respectively. The RGB based vegetation indices were having H^2 ranging from 0.73-0.97 and 0.49-0.93 under control and N-deficiency treatments, respectively (Figure 4.20 & 4.21). The average H^2 was 0.88, 0.89, 0.9, 0.9 and 0.91 under control conditions and 0.67, 0.76, 0.79, 0.84 and 0.86 under N-deficiency conditions, at 60, 70, 80, 90 and 100 DAS, respectively. IR and NIR traits also have better heritability of above 0.9. Overall, we found all traits possessed higher broad sense heritability than under nitrogen deficiency conditions, and as growth duration progressed the heritability of most of the traits improved.

The figures from Figure 4.15 to Figure 4.21 show the broad sense heritability of morphometric, colour related, biomass related, RGB based indices and intensity based at all the growth stages.

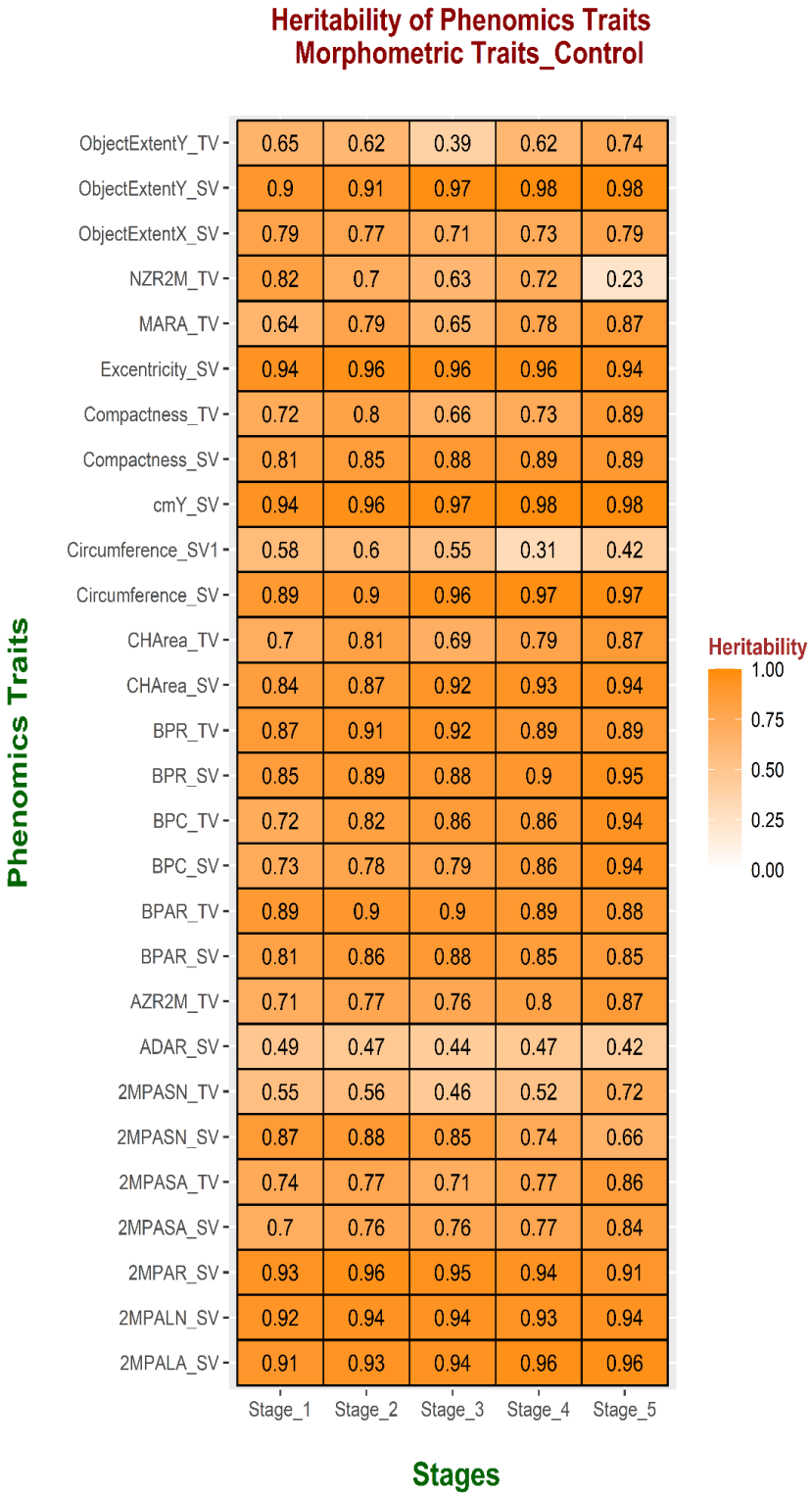

Figure 4.15: Heritability of morphometric traits of 5 stages under control conditions (Stage 1, 2, 3, 4, and 5 are 60, 70, 80, 90 and 100 DAS, respectively).

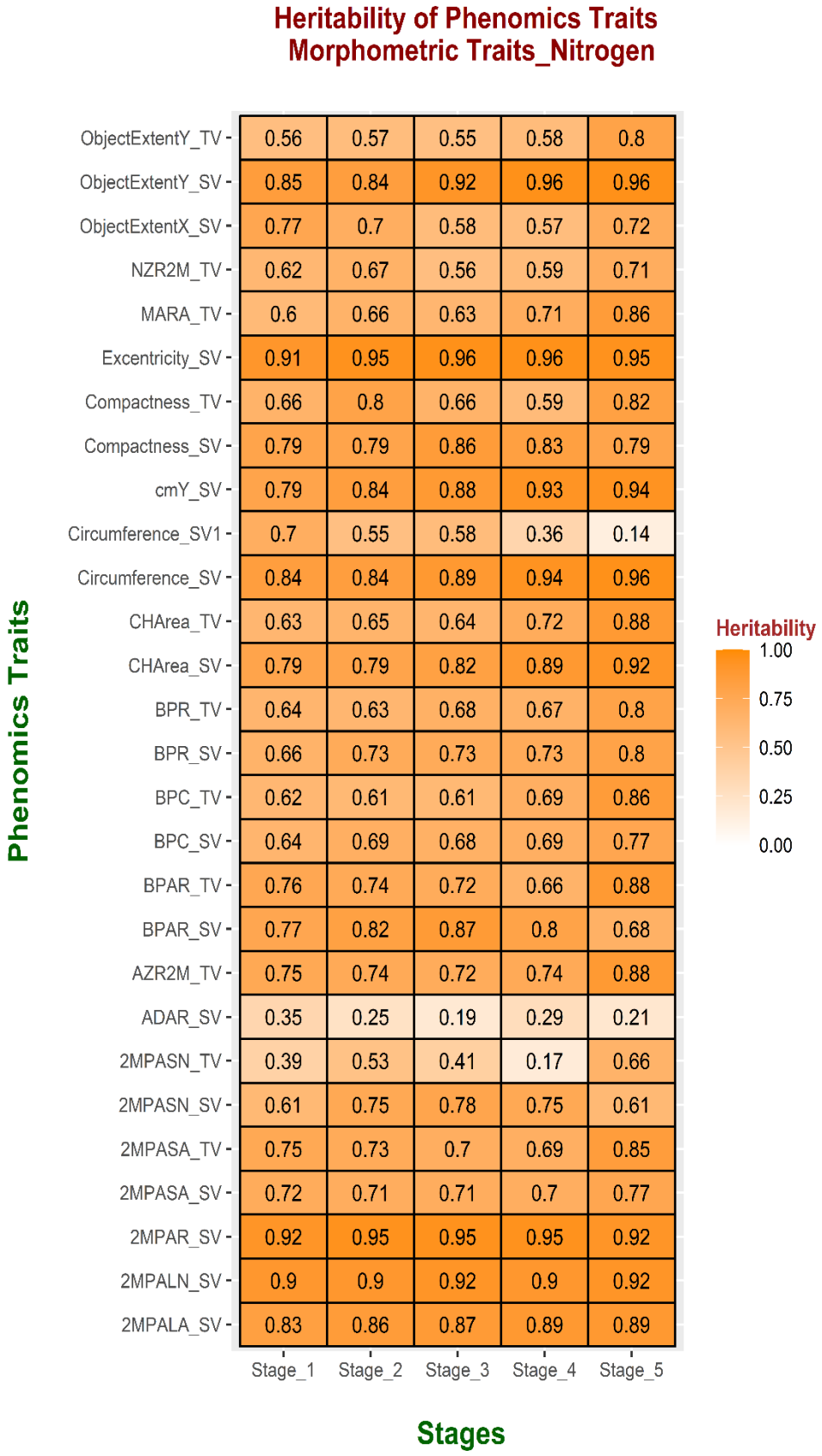

Figure 4.16: Heritability of morphometric traits of 5 stages under nitrogen deficiency conditions (Stage 1, 2, 3, 4, and 5 are 60, 70, 80, 90 and 100 DAS, respectively).

a) b)

Figure 4.17: Heritability of biomass related traits of 5 stages under control (a) and nitrogen deficiency (b) conditions (Stage 1, 2, 3, 4, and 5 are 60, 70, 80, 90 and 100 DAS, respectively).

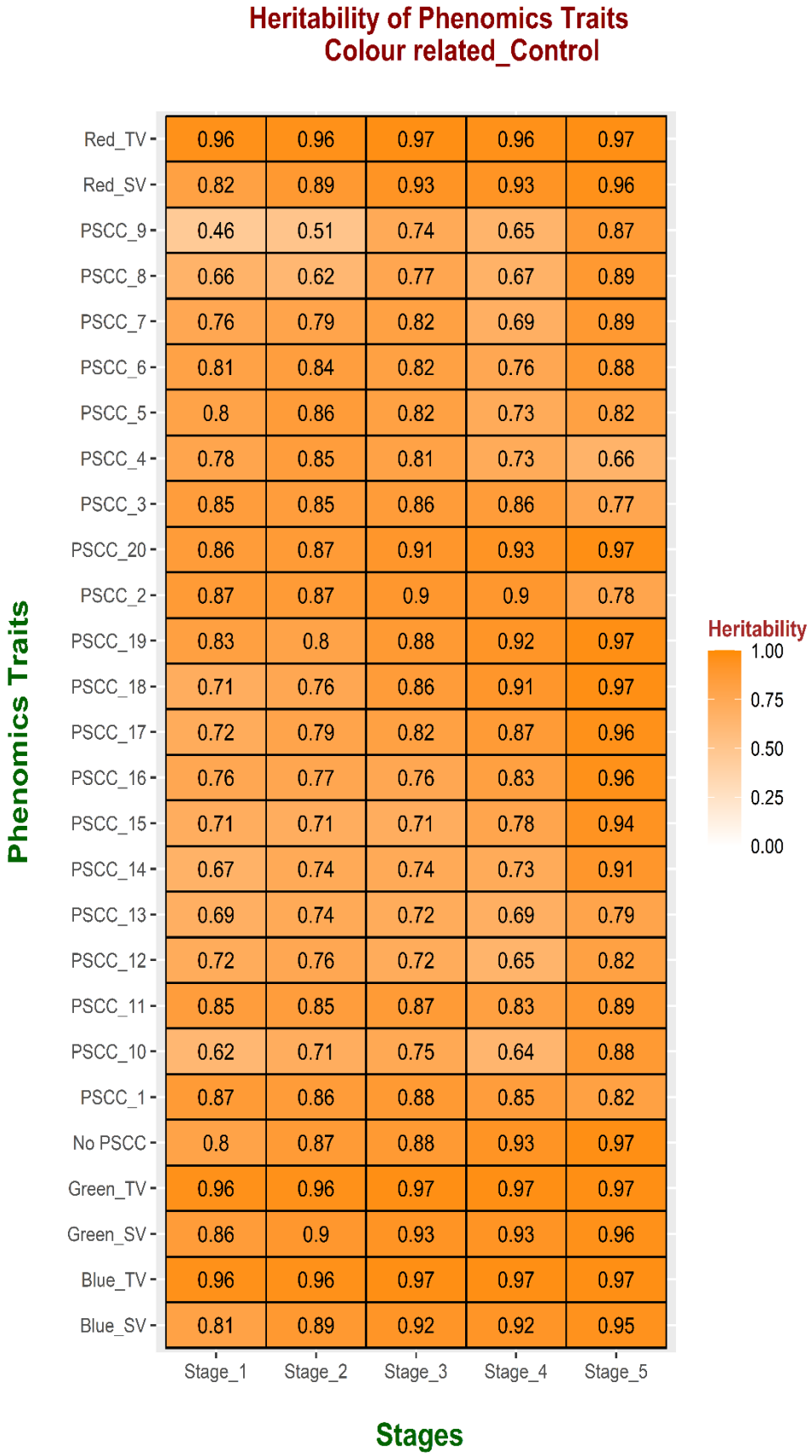

Figure 4.18: Heritability of color related traits of 5 stages under control conditions (Stage 1, 2, 3, 4, and 5 are 60, 70, 80, 90 and 100 DAS, respectively).

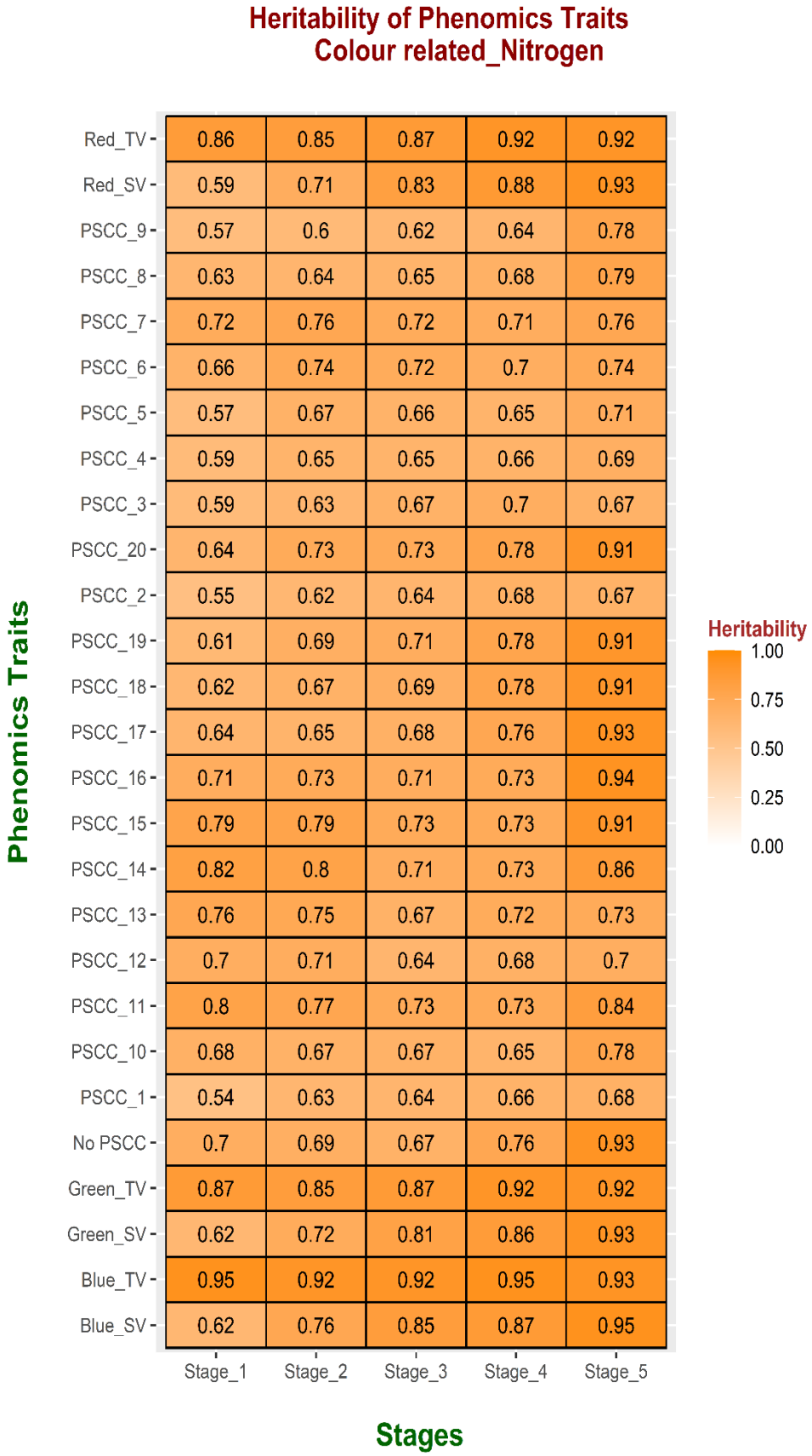

Figure 4.19: Heritability of color related traits of 5 stages under nitrogen deficiency conditions (Stage 1, 2, 3, 4, and 5 are 60, 70, 80, 90 and 100 DAS, respectively).

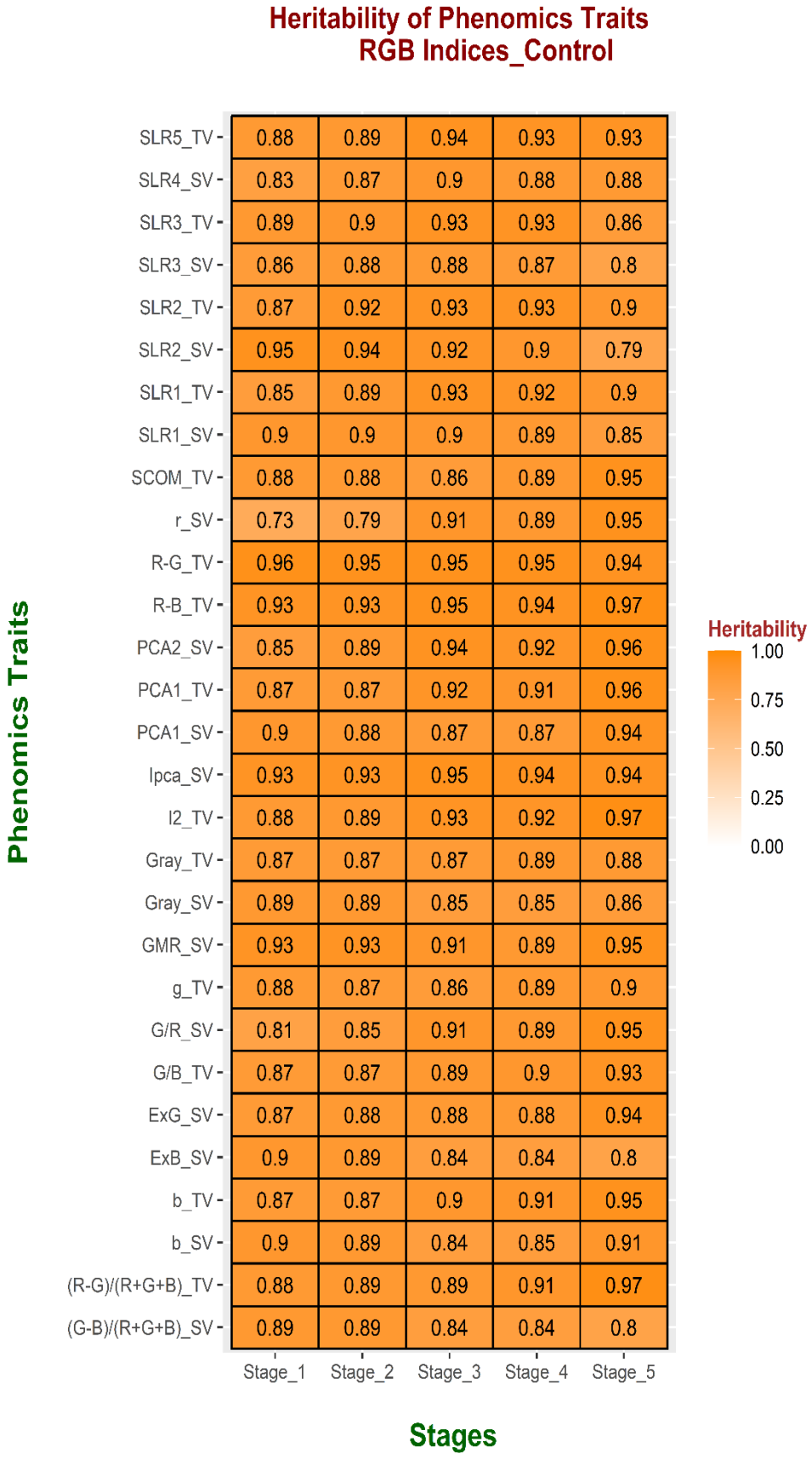

Figure 4.20: Heritability of RGB based vegetation indices of 5 stages under control conditions (Stage 1, 2, 3, 4, and 5 are 60, 70, 80, 90 and 100 DAS, respectively).

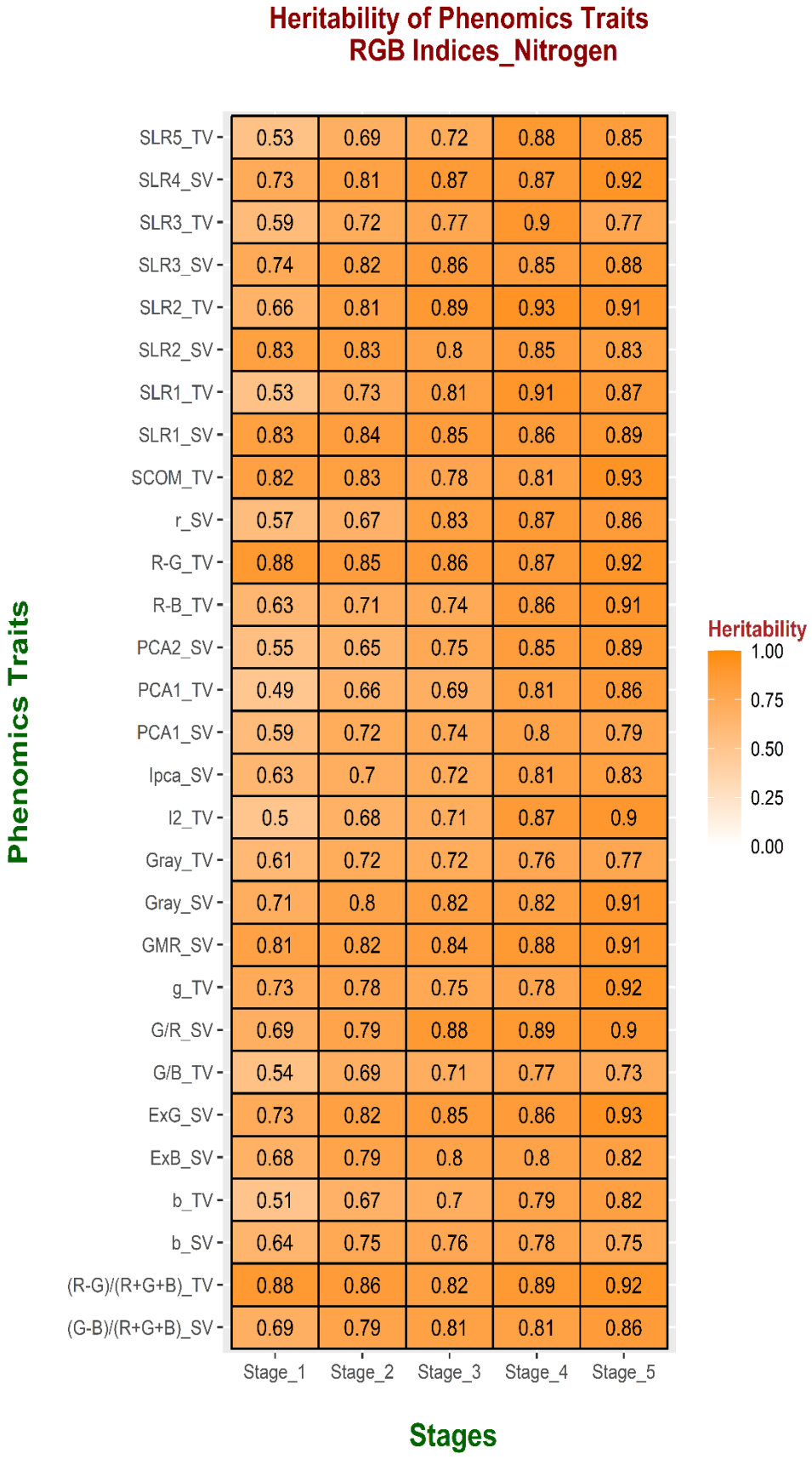

Figure 4.21: Heritability of RGB based vegetation indices of 5 stages under nitrogen deficiency conditions (Stage 1, 2, 3, 4, and 5 are 60, 70, 80, 90 and 100 DAS, respectively).

4.1.1.10 Phenotypic variation under control and N-deficiency conditions in wheat

The graphical representation of all the RILs as box plots explain the range of phenotypic expression, the median and also explains the distribution of individuals along the median. Plotting the box plots of all five stages under both control and nitrogen deficiency conditions give insight into the phenotypic expression profile along the different growth stages and the response of genotypes to nitrogen deficiency over the control plants. Boxplots of all the i-Traits were prepared and presented here category wise (Figure 4.22 to 4.25). In these figures, all Stage 1, 2, 3, 4, and 5 represent 60, 70, 80, 90 and 100 DAS, respectively.

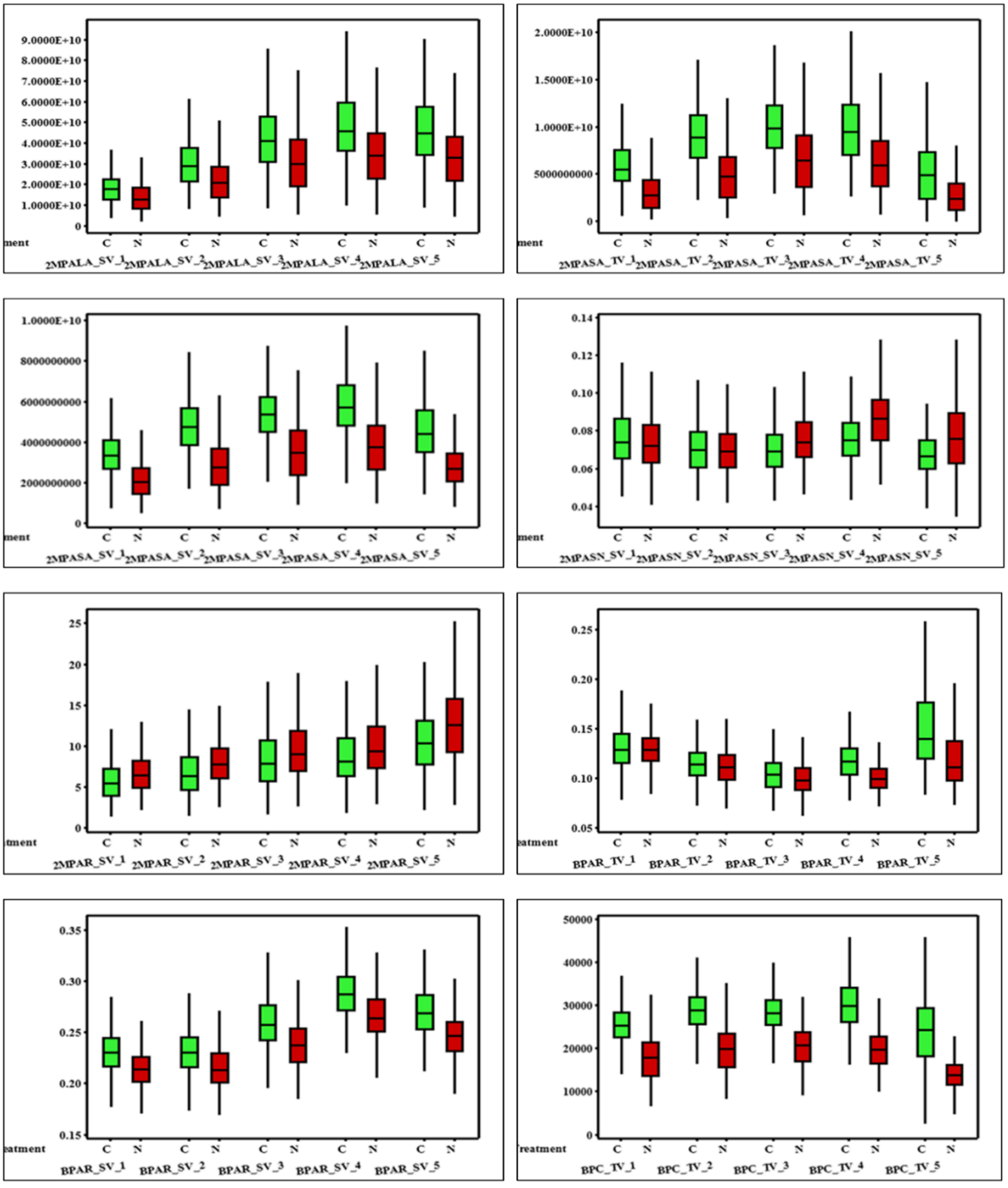

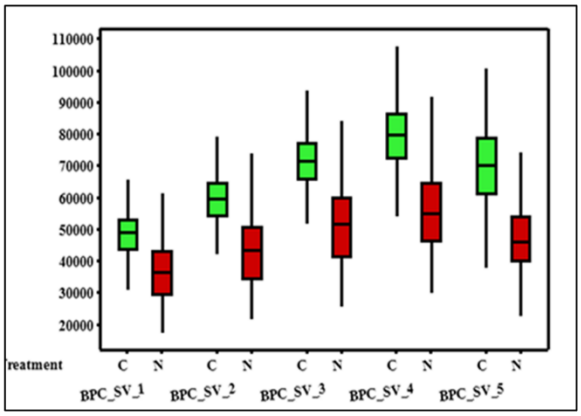
110000
100000
90000
80000
70000
60000
50000
40000
30000
20000
reatment
C N C N C N C N C N
BPC_SV_1 BPC_SV_2 BPC_SV_3 BPC_SV_4 BPC_SV_5

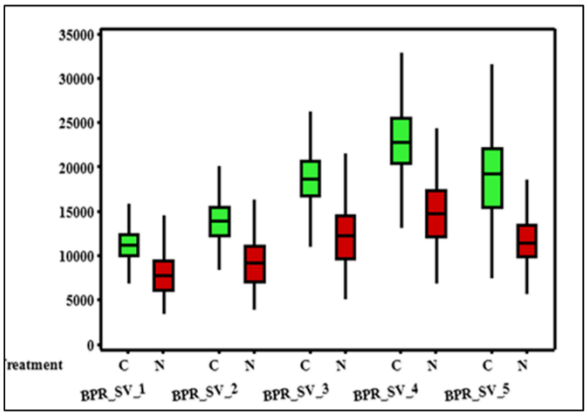
35000
30000
25000
20000
15000
10000
5000
0
reatment
C N C N C N C N C N
BPR_SV_1 BPR_SV_2 BPR_SV_3 BPR_SV_4 BPR_SV_5

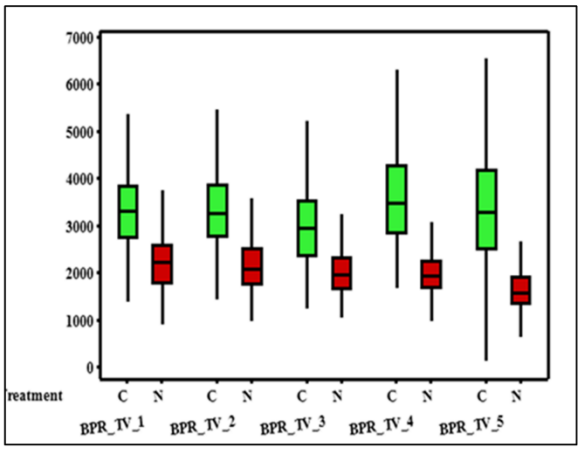
7000
6000
5000
4000
3000
2000
1000
0
reatment
C N C N C N C N C N
BPR_TV_1 BPR_TV_2 BPR_TV_3 BPR_TV_4 BPR_TV_5

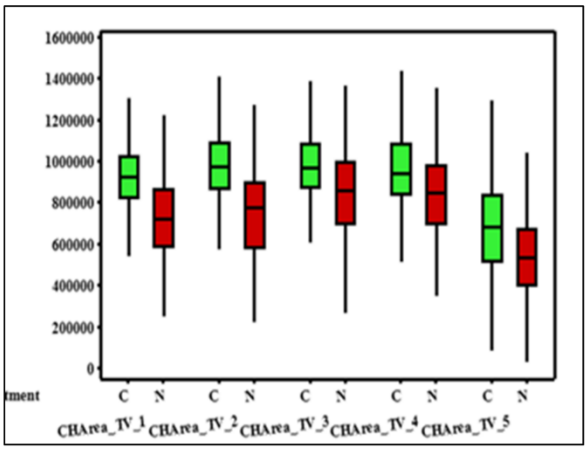
1600000
1400000
1200000
1000000
800000
600000
400000
200000
0
tment
C N C N C N C N C N
CHArea_TV_1 CHArea_TV_2 CHArea_TV_3 CHArea_TV_4 CHArea_TV_5

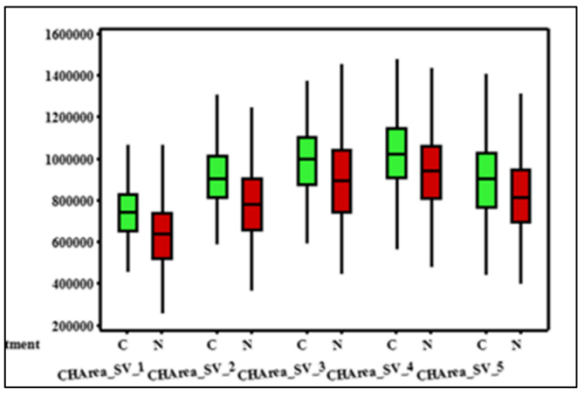
1600000
1400000
1200000
1000000
800000
600000
400000
200000
tment
C N C N C N C N C N
CHArea_SV_1 CHArea_SV_2 CHArea_SV_3 CHArea_SV_4 CHArea_SV_5

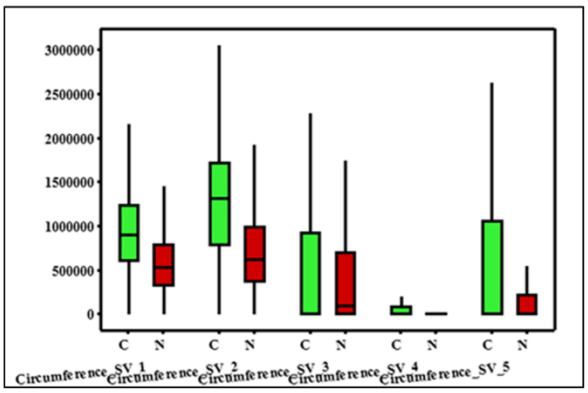
3000000
2500000
2000000
1500000
1000000
500000
0
C N C N C N C N C N
Circumference_SV_1 Circumference_SV_2 Circumference_SV_3 Circumference_SV_4 Circumference_SV_5

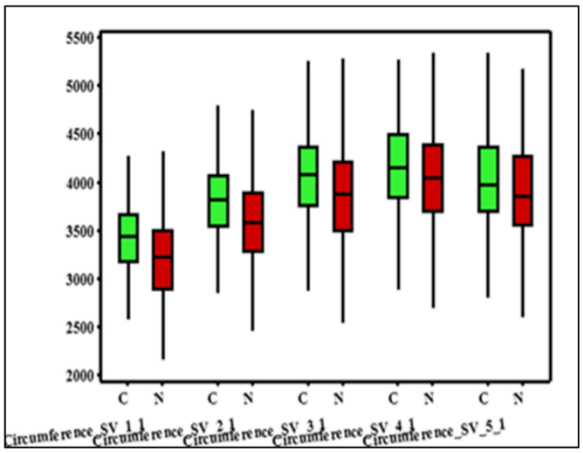
5500
5000
4500
4000
3500
3000
2500
2000
C N C N C N C N C N
Circumference_SV_1_1 Circumference_SV_2_1 Circumference_SV_3_1 Circumference_SV_4_1 Circumference_SV_5_1

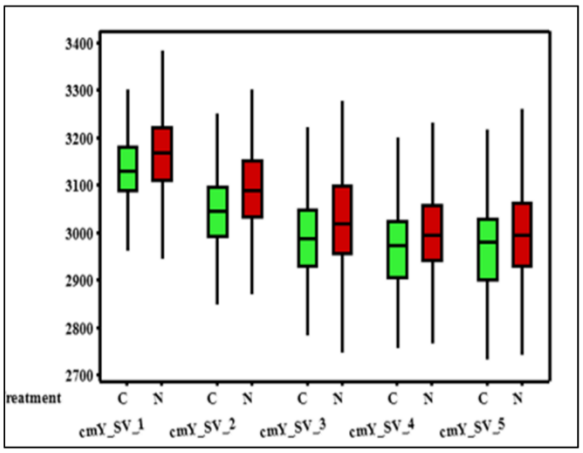
3400
3300
3200
3100
3000
2900
2800
2700
reatment
C N C N C N C N C N
cmY_SV_1 cmY_SV_2 cmY_SV_3 cmY_SV_4 cmY_SV_5

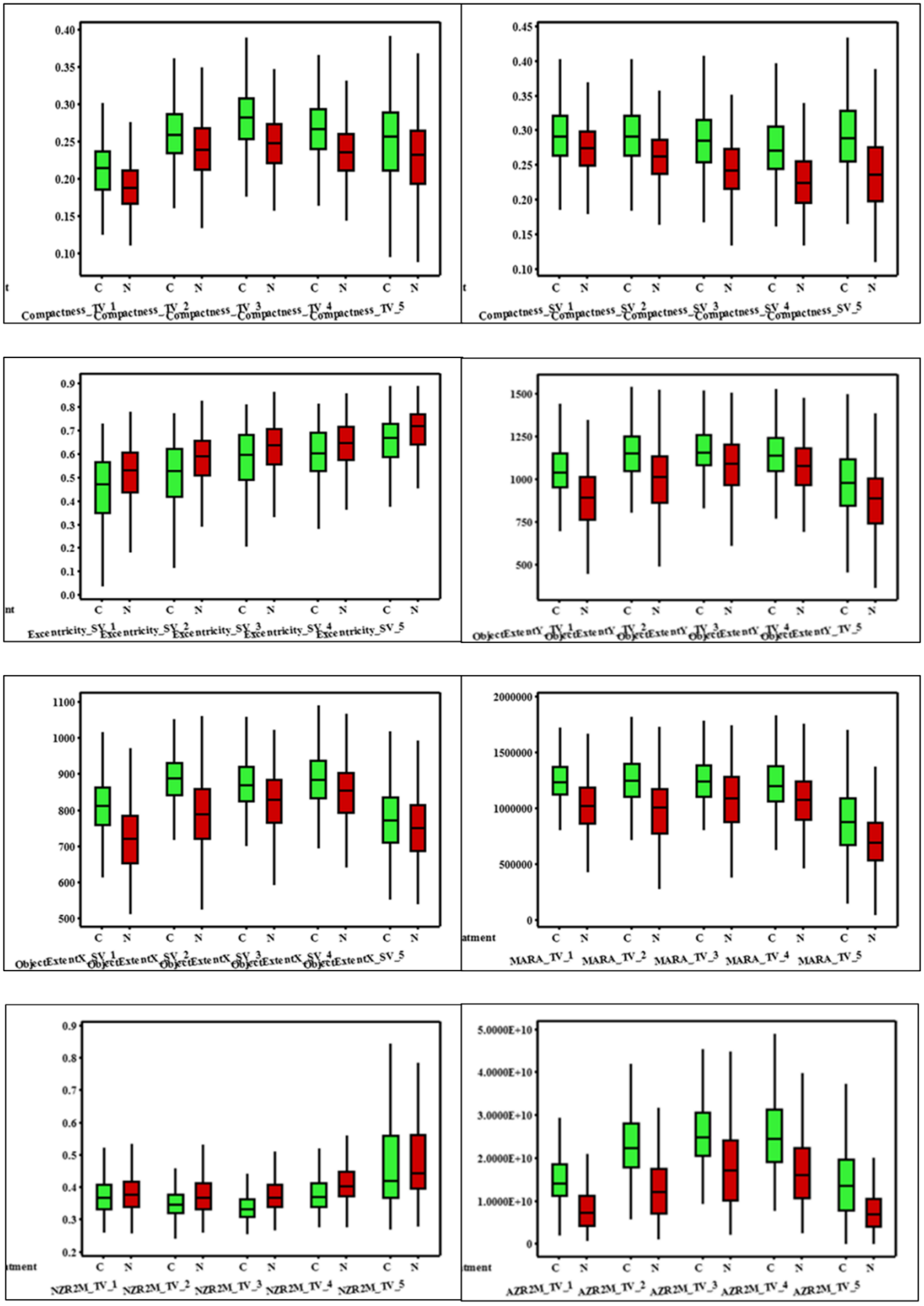

Figure 4.22: Boxplots of morphometric i-Traits representing the stage wise progression of morphometric traits and the effect of nitrogen deficiency over plant age. Each box represents one morphometric i-Trait.

The difference in plot pattern shows the differences in all the morphometric traits and it also suggests that different i-Trait capture different plant nitrogen deficiency effect over time. Traits such as 2MPALA_SV, BPC_SV, BPR_SV and CHArea_SV increased over stage 1-4 but the value decreased in stage 5 under both control and N-deficiency conditions (Figure 4.14). Significant and clearcut effect of nitrogen deficiency was observed at all stages. 2MPASA_TV, 2MPASA_SV and AZR2M_TV traits showed more treatment effect at earlier stages (stage 1, 2 and 3), while their detection ability decreased at later stages (Stage 4 & 5). The 2MPAR_SV showed a different response which showed an increased value progressively at all stages till stage 5 and nitrogen deficiency plants had higher values than the control plants at all stages. BPR_TV showed a highly significant difference between control and N plants at all stages. NZ2RM_TV, Eccentricity_SV, cmY_SV and 2MPAR_SV showed higher values under N deficiency than in control plants and all other traits showed opposite effect (Figure 4.22).

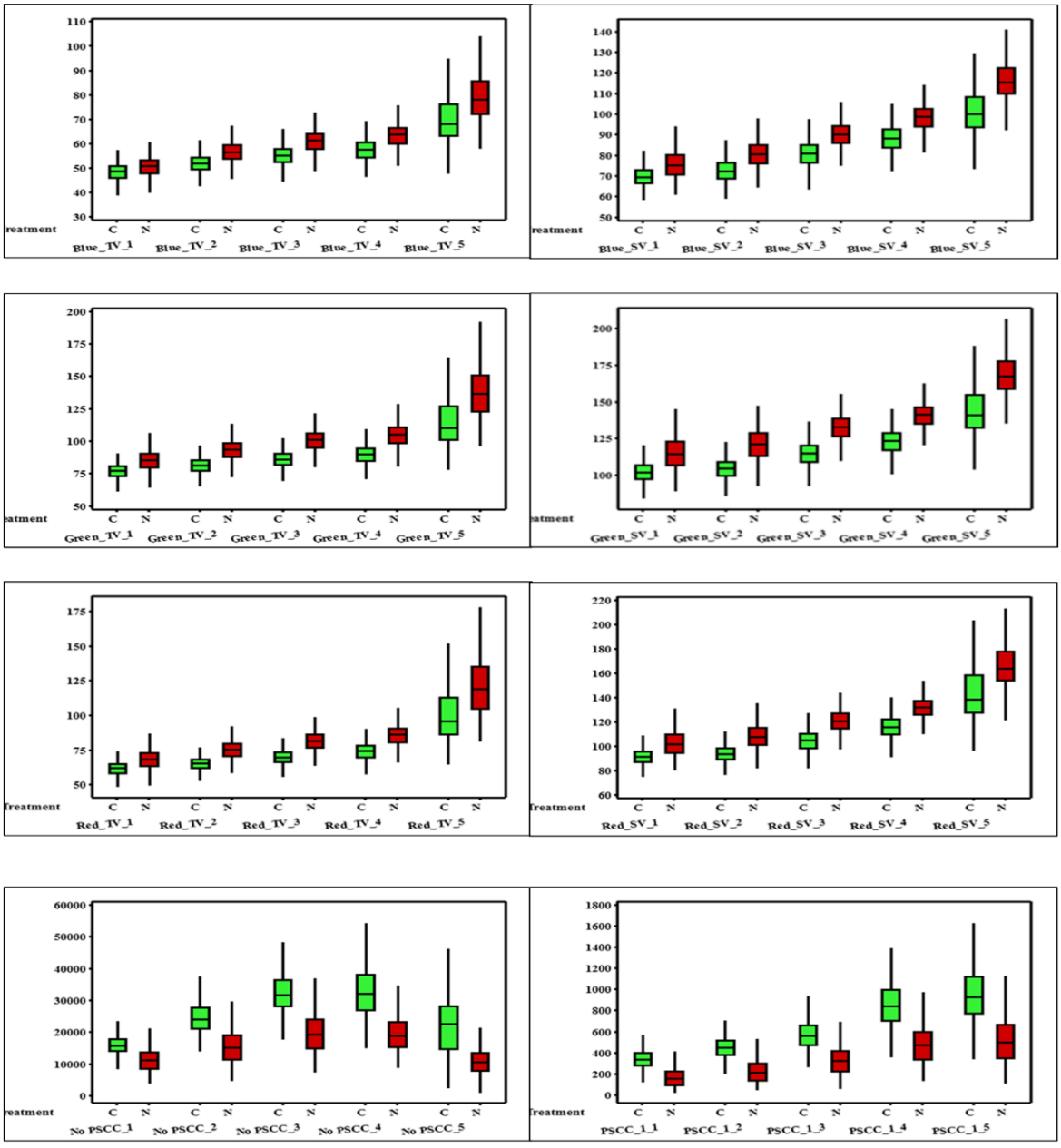

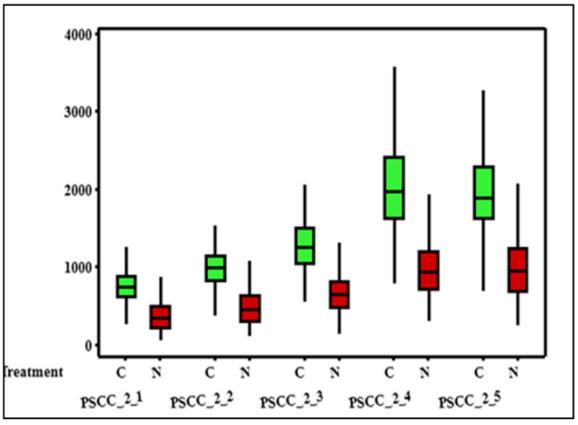
4000
3000
2000
1000
0
Treatment
C N C N C N C N C N
PSCC_2_1 PSCC_2_2 PSCC_2_3 PSCC_2_4 PSCC_2_5

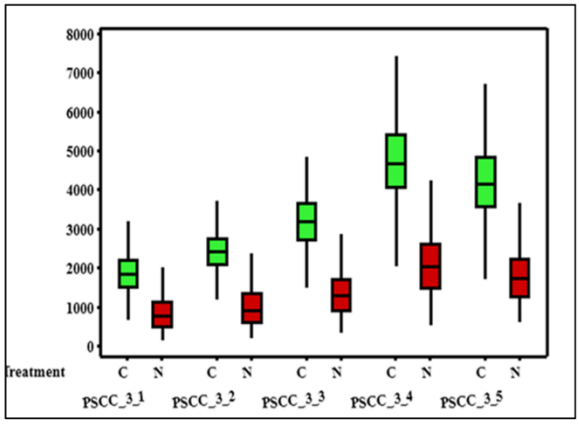
8000
7000
6000
5000
4000
3000
2000
1000
0
Treatment
C N C N C N C N C N
PSCC_3_1 PSCC_3_2 PSCC_3_3 PSCC_3_4 PSCC_3_5

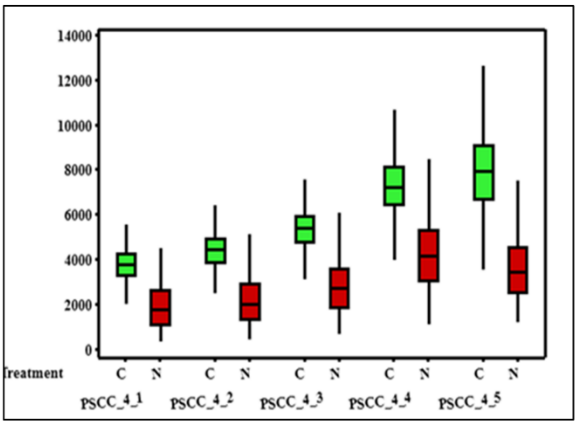
14000
12000
10000
8000
6000
4000
2000
0
Treatment
C N C N C N C N C N
PSCC_4_1 PSCC_4_2 PSCC_4_3 PSCC_4_4 PSCC_4_5

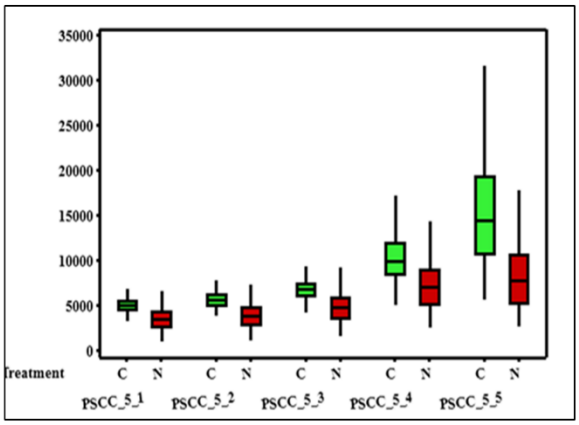
35000
30000
25000
20000
15000
10000
5000
0
Treatment
C N C N C N C N C N
PSCC_5_1 PSCC_5_2 PSCC_5_3 PSCC_5_4 PSCC_5_5

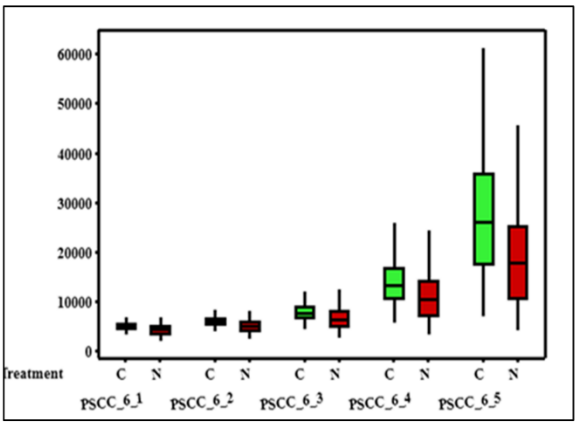
60000
50000
40000
30000
20000
10000
0
Treatment
C N C N C N C N C N
PSCC_6_1 PSCC_6_2 PSCC_6_3 PSCC_6_4 PSCC_6_5

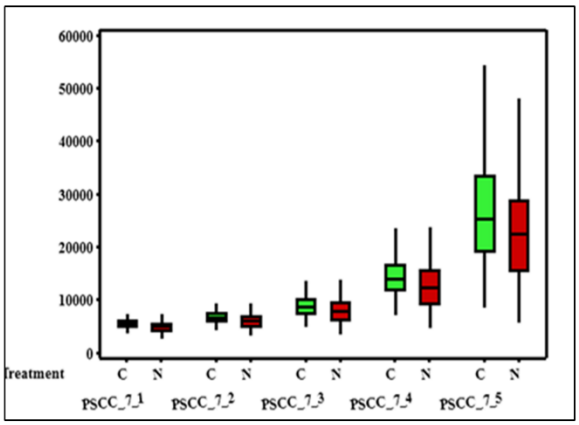
60000
50000
40000
30000
20000
10000
0
Treatment
C N C N C N C N C N
PSCC_7_1 PSCC_7_2 PSCC_7_3 PSCC_7_4 PSCC_7_5

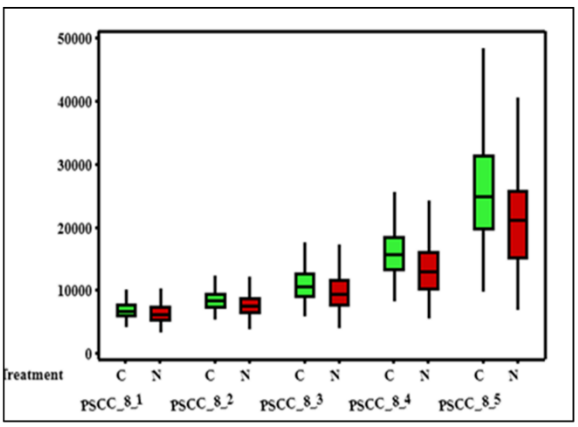
50000
40000
30000
20000
10000
0
Treatment
C N C N C N C N C N
PSCC_8_1 PSCC_8_2 PSCC_8_3 PSCC_8_4 PSCC_8_5

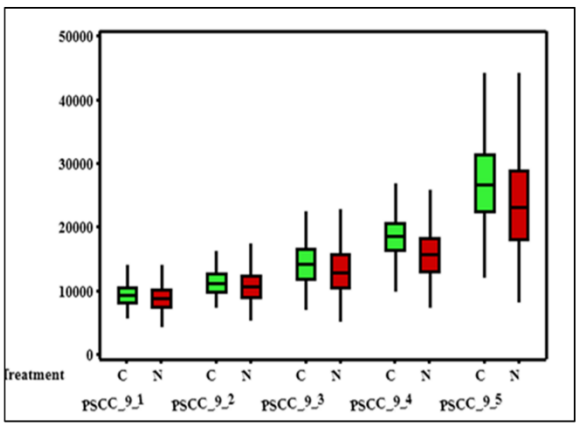
50000
40000
30000
20000
10000
0
Treatment
C N C N C N C N C N
PSCC_9_1 PSCC_9_2 PSCC_9_3 PSCC_9_4 PSCC_9_5

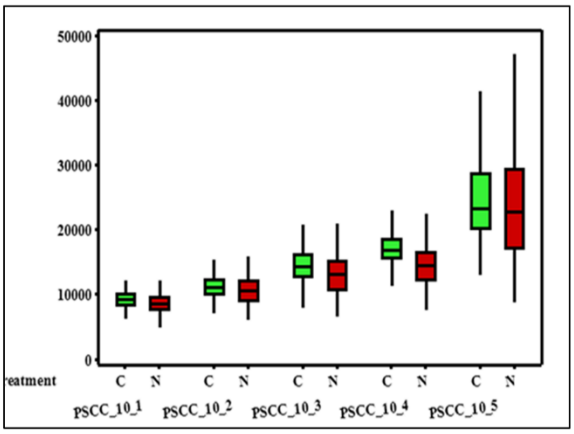
50000
40000
30000
20000
10000
0
C N C N C N C N C N
PSCC_10_1 PSCC_10_2 PSCC_10_3 PSCC_10_4 PSCC_10_5

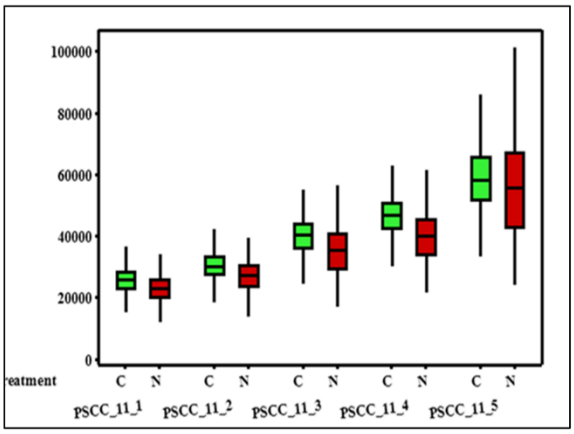
100000
80000
60000
40000
20000
0
C N C N C N C N C N
PSCC_11_1 PSCC_11_2 PSCC_11_3 PSCC_11_4 PSCC_11_5

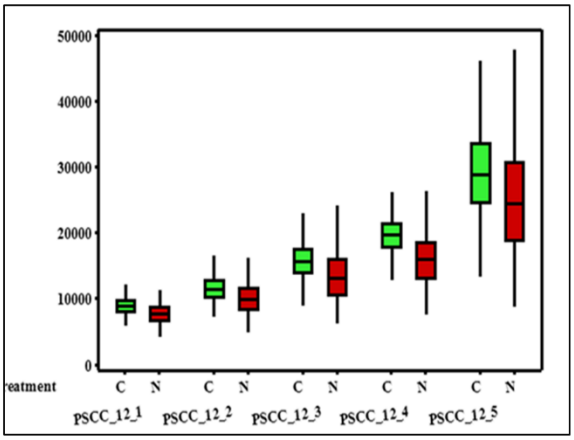
50000
40000
30000
20000
10000
0
C N C N C N C N C N
PSCC_12_1 PSCC_12_2 PSCC_12_3 PSCC_12_4 PSCC_12_5

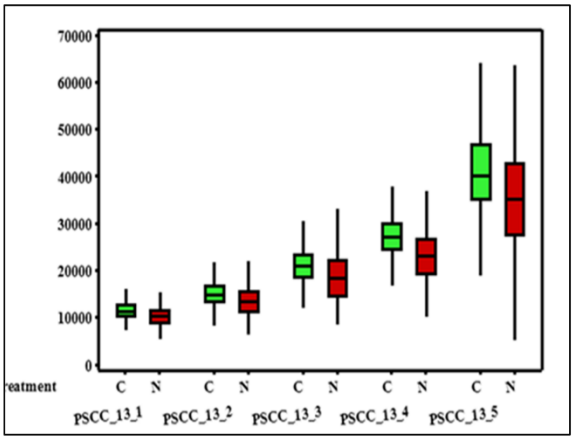
70000
60000
50000
40000
30000
20000
10000
0
C N C N C N C N C N
PSCC_13_1 PSCC_13_2 PSCC_13_3 PSCC_13_4 PSCC_13_5

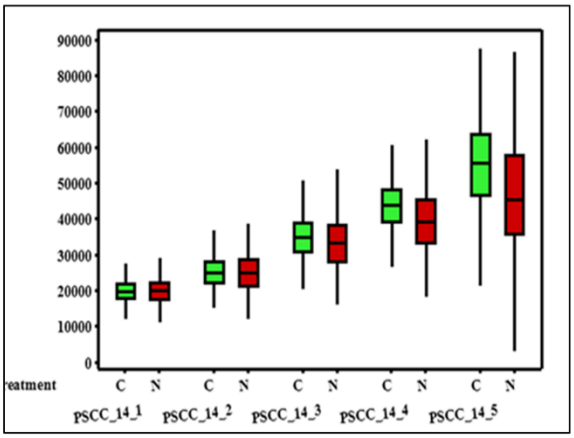
90000
80000
70000
60000
50000
40000
30000
20000
10000
0
C N C N C N C N C N
PSCC_14_1 PSCC_14_2 PSCC_14_3 PSCC_14_4 PSCC_14_5

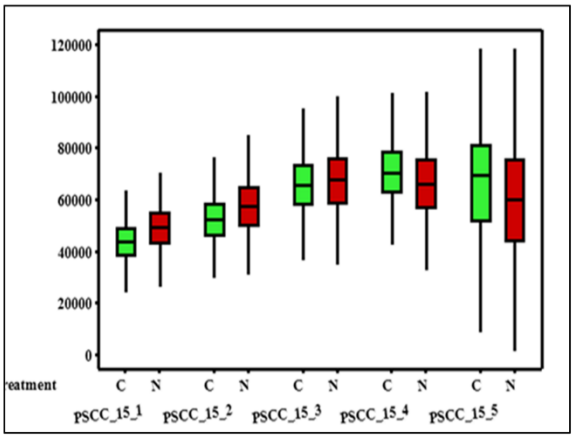
120000
100000
80000
60000
40000
20000
0
C N C N C N C N C N
PSCC_15_1 PSCC_15_2 PSCC_15_3 PSCC_15_4 PSCC_15_5

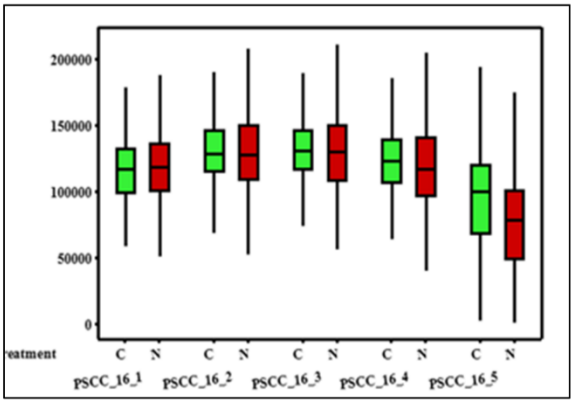
200000
150000
100000
50000
0
C N C N C N C N C N
PSCC_16_1 PSCC_16_2 PSCC_16_3 PSCC_16_4 PSCC_16_5

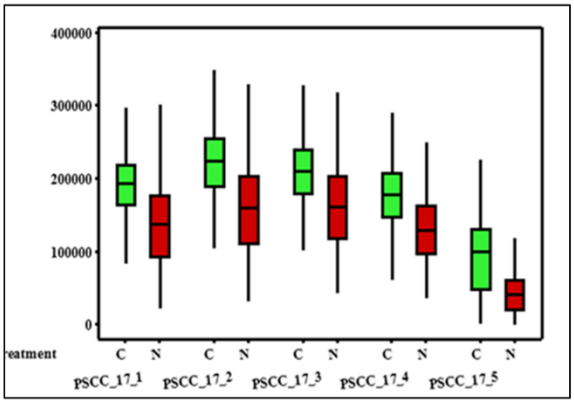
400000
300000
200000
100000
0
C N C N C N C N C N
PSCC_17_1 PSCC_17_2 PSCC_17_3 PSCC_17_4 PSCC_17_5

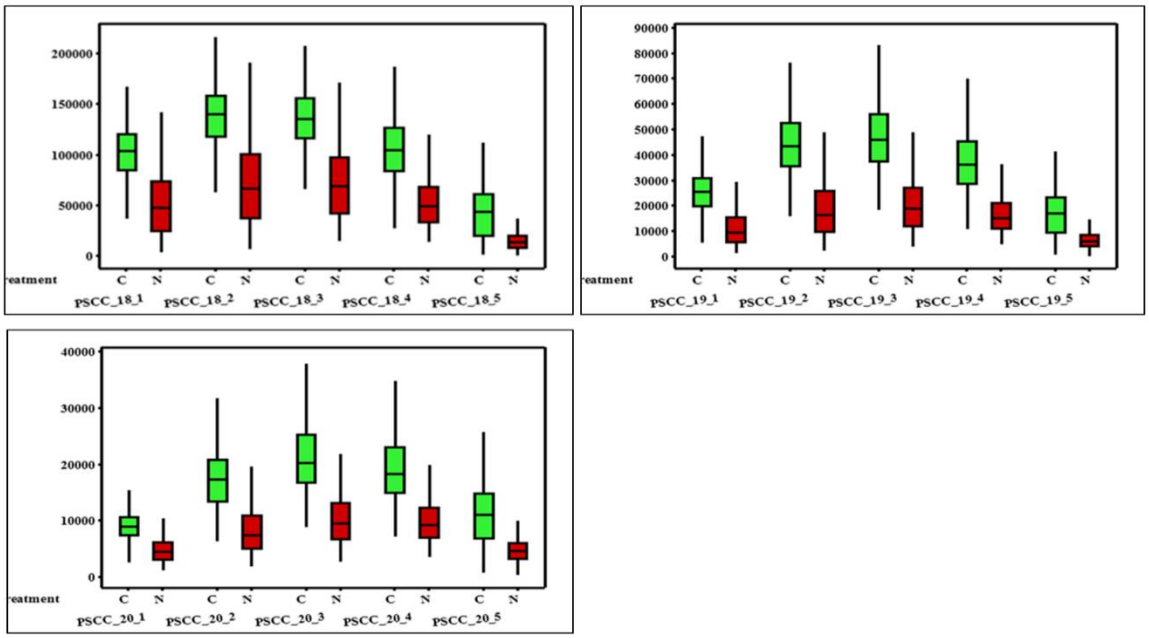

Figure 4.23: Boxplots of colour related i-Traits showing the stage wise progression of colour related traits and the effect of nitrogen deficiency over plant age.

The red, green and blue intensity related traits of both side and top view suggested a progressive increase in all stages and the plants under N deficiency had higher intensity values than the control plants (Figure 4.23). The difference between control and N-deficiency is clearly visible from the box plots at all stages. PSCC_1, 2, 3, and 4 had similar behavior where the values increased over time in both treatments, but decreased at last stage and control plants had higher values than N-deficiency plants at all stages. Also, the phenotypic range increased over time as the plant area increased. PSCC_5, 6 and 7 behaved similarly and increased progressively at all stages, their phenotypic range increased over time and control plants had significantly higher values than N-deficiency plants. PSCC_8, 9, 10, 11, 12, 13 and 14 showed similar patterns with each other and they had significantly higher values than other PSCC_1-7. These colour class traits increased over time and control had higher values than N-deficiency treatment. The PSCC_15-20 were having significantly higher values than other PSCCs and they increased till stage 3 and then decreased (Figure 4.23).

Biomass related traits such as Biovolume, PSA, Area_TV and Area_SV had similar patterns which increased till stage 3 and then declined. These traits showed clearcut reduction in biomass under nitrogen deficiency conditions (Figure 4.24). But it showed that Biovolume and PSA which combines both side view and top view plant area captures the whole plant variation than any part of the plant alone. NIR value increased till stage 3 and then decreased in later stages and nitrogen deficient plants had higher values than the control plants. IR values were very inconsistent with reference to stages, as tissue temperature is mainly determined by the temperature and VPD rather than the age per se (Figure 4.24).

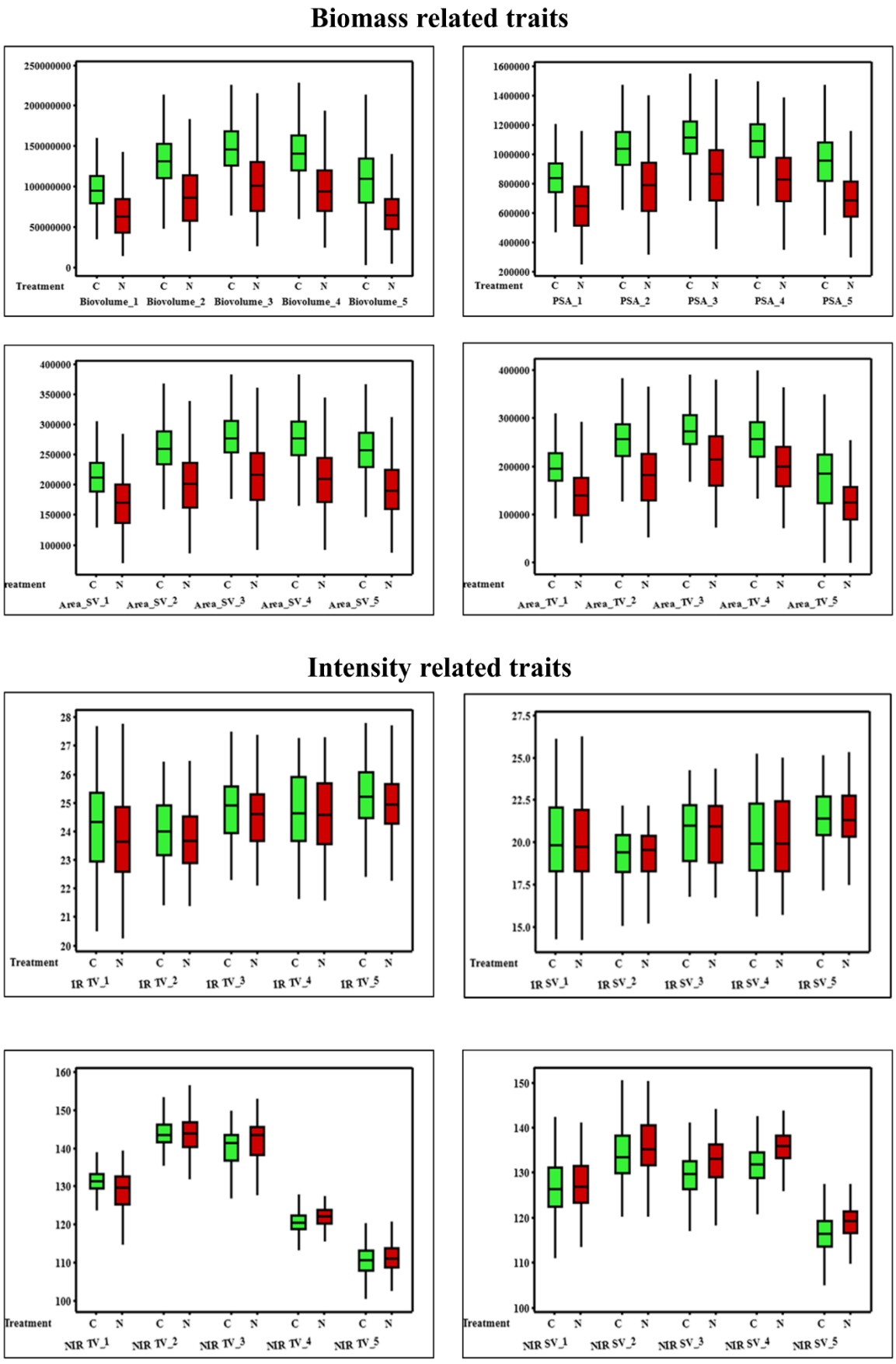

Figure 4.24: Boxplots of Biomass related and intensity related traits.

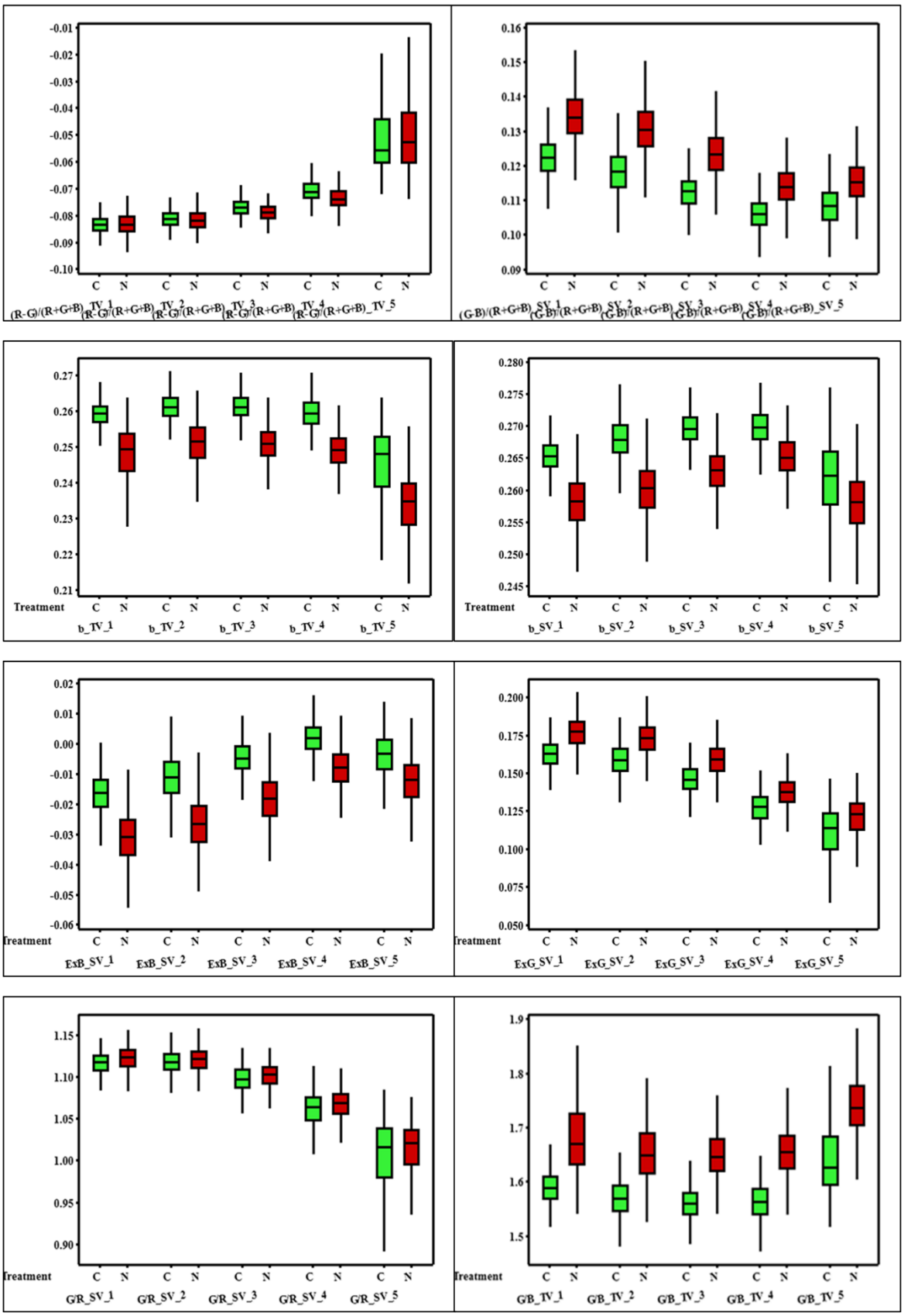
(R-G)/(R+G+B)_TV_1
(R-G)/(R+G+B)_TV_2
(R-G)/(R+G+B)_TV_3
(R-G)/(R+G+B)_TV_4
(R-G)/(R+G+B)_TV_5
(G-B)/(R+G+B)_SV_1
(G-B)/(R+G+B)_SV_2
(G-B)/(R+G+B)_SV_3
(G-B)/(R+G+B)_SV_4
(G-B)/(R+G+B)_SV_5
Treatment
C N
b_TV_1
b_TV_2
b_TV_3
b_TV_4
b_TV_5
b_SV_1
b_SV_2
b_SV_3
b_SV_4
b_SV_5
ExB_SV_1
ExB_SV_2
ExB_SV_3
ExB_SV_4
ExB_SV_5
ExG_SV_1
ExG_SV_2
ExG_SV_3
ExG_SV_4
ExG_SV_5
G/R_SV_1
G/R_SV_2
G/R_SV_3
G/R_SV_4
G/R_SV_5
G/B_TV_1
G/B_TV_2
G/B_TV_3
G/B_TV_4
G/B_TV_5

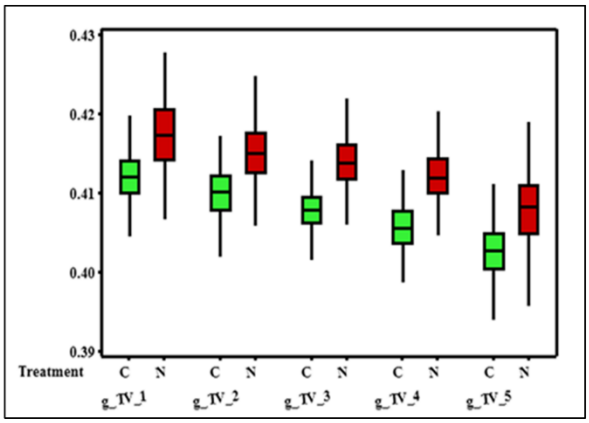
0.43
0.42
0.41
0.40
0.39
Treatment
C N C N C N C N C N
g_TV_1 g_TV_2 g_TV_3 g_TV_4 g_TV_5

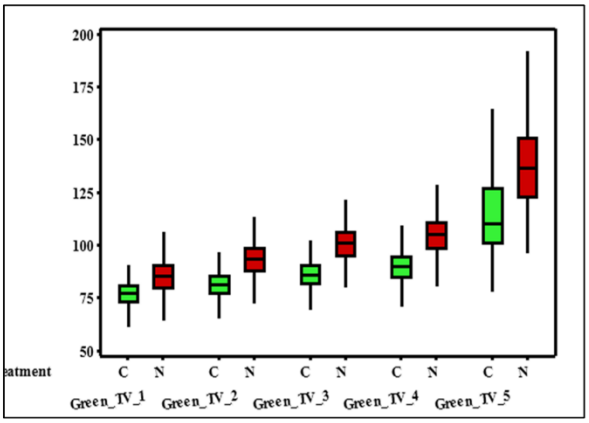
200
175
150
125
100
75
50
eatment
C N C N C N C N C N
Green_TV_1 Green_TV_2 Green_TV_3 Green_TV_4 Green_TV_5

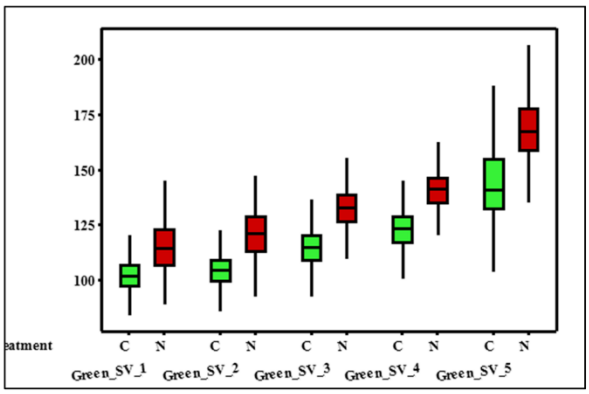
200
175
150
125
100
eatment
C N C N C N C N C N
Green_SV_1 Green_SV_2 Green_SV_3 Green_SV_4 Green_SV_5

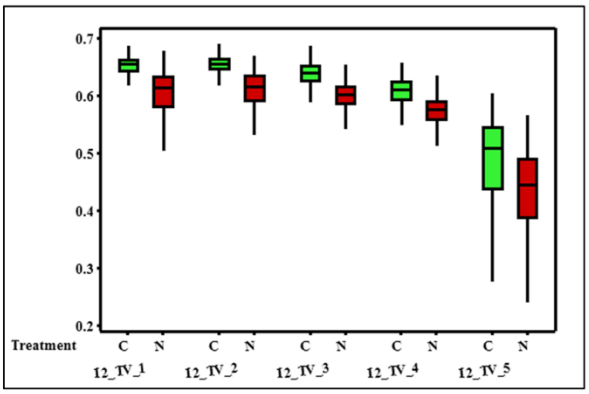
0.7
0.6
0.5
0.4
0.3
0.2
Treatment
C N C N C N C N C N
12_TV_1 12_TV_2 12_TV_3 12_TV_4 12_TV_5

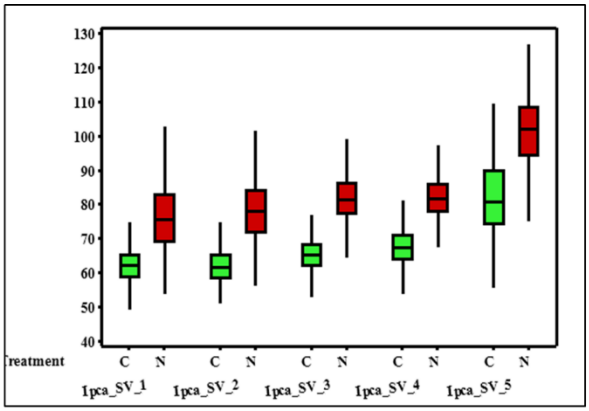
130
120
110
100
90
80
70
60
50
40
Treatment
C N C N C N C N C N
1pca_SV_1 1pca_SV_2 1pca_SV_3 1pca_SV_4 1pca_SV_5

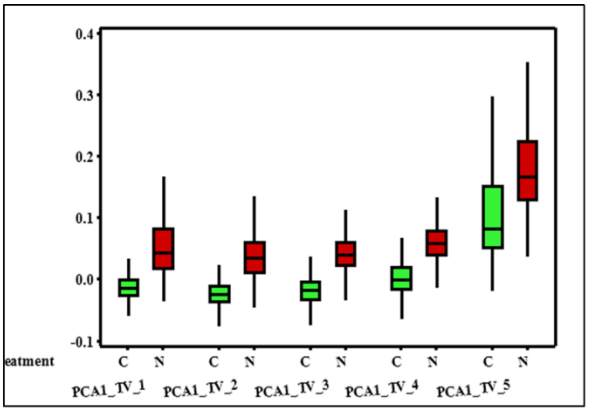
0.4
0.3
0.2
0.1
0.0
-0.1
eatment
C N C N C N C N C N
PCA1_TV_1 PCA1_TV_2 PCA1_TV_3 PCA1_TV_4 PCA1_TV_5

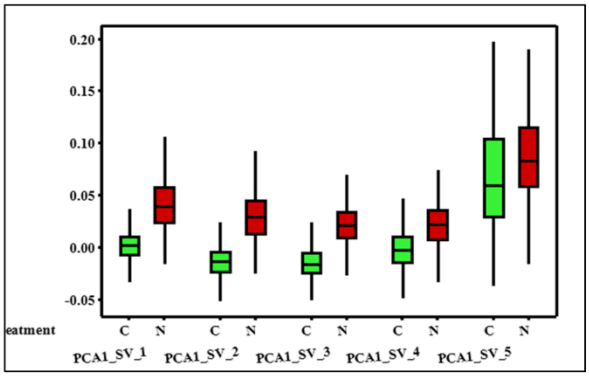
0.20
0.15
0.10
0.05
0.00
-0.05
eatment
C N C N C N C N C N
PCA1_SV_1 PCA1_SV_2 PCA1_SV_3 PCA1_SV_4 PCA1_SV_5

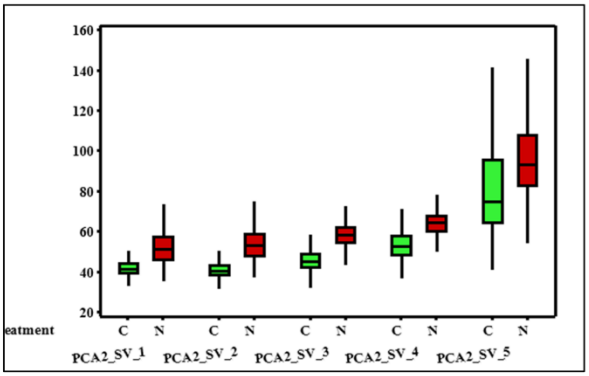
160
140
120
100
80
60
40
20
eatment
C N C N C N C N C N
PCA2_SV_1 PCA2_SV_2 PCA2_SV_3 PCA2_SV_4 PCA2_SV_5

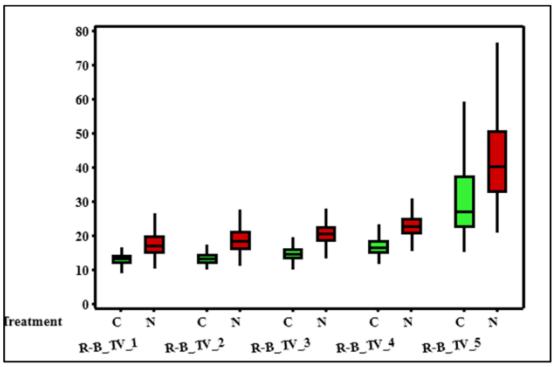
80
70
60
50
40
30
20
10
0
Treatment
C N C N C N C N C N
R-B_TV_1 R-B_TV_2 R-B_TV_3 R-B_TV_4 R-B_TV_5

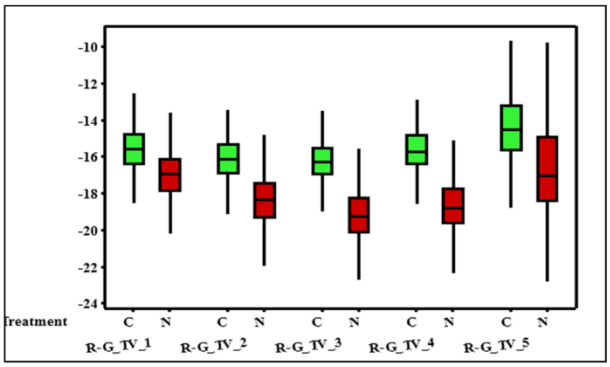
-10
-12
-14
-16
-18
-20
-22
-24
Treatment
C N C N C N C N C N
R-G_TV_1 R-G_TV_2 R-G_TV_3 R-G_TV_4 R-G_TV_5

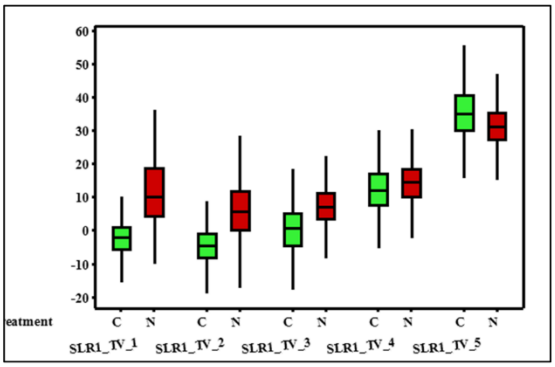
60
50
40
30
20
10
0
-10
-20
eatment
C N C N C N C N C N
SLR1_TV_1 SLR1_TV_2 SLR1_TV_3 SLR1_TV_4 SLR1_TV_5

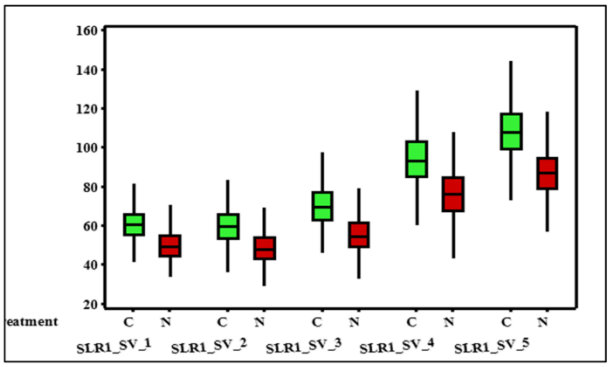
160
140
120
100
80
60
40
20
eatment
C N C N C N C N C N
SLR1_SV_1 SLR1_SV_2 SLR1_SV_3 SLR1_SV_4 SLR1_SV_5

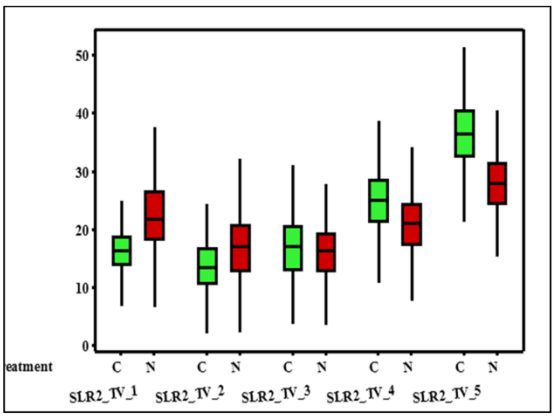
50
40
30
20
10
0
eatment
C N C N C N C N C N
SLR2_TV_1 SLR2_TV_2 SLR2_TV_3 SLR2_TV_4 SLR2_TV_5

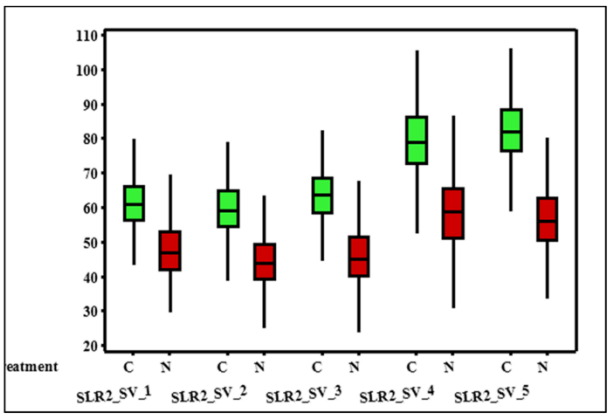
110
100
90
80
70
60
50
40
30
20
eatment
C N C N C N C N C N
SLR2_SV_1 SLR2_SV_2 SLR2_SV_3 SLR2_SV_4 SLR2_SV_5

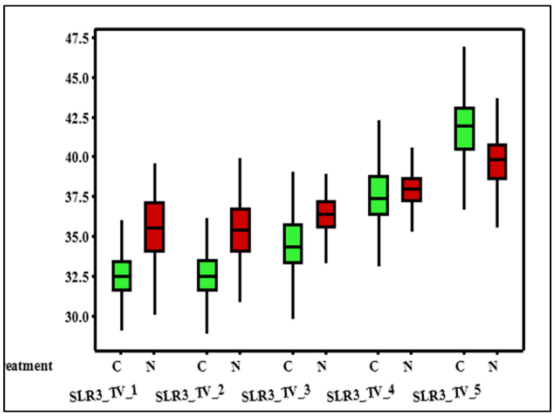
47.5
45.0
42.5
40.0
37.5
35.0
32.5
30.0
eatment
C N C N C N C N C N
SLR3_TV_1 SLR3_TV_2 SLR3_TV_3 SLR3_TV_4 SLR3_TV_5

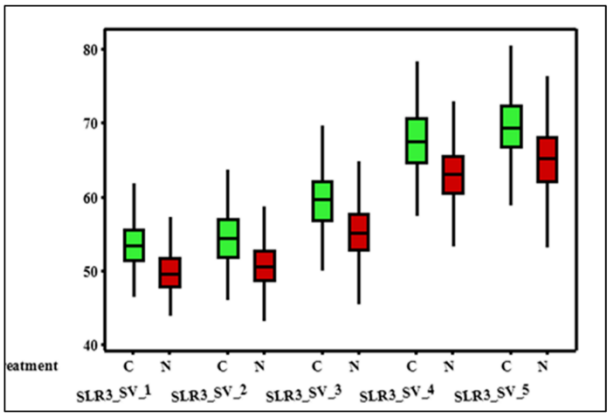
80
70
60
50
40
eatment
C N C N C N C N C N
SLR3_SV_1 SLR3_SV_2 SLR3_SV_3 SLR3_SV_4 SLR3_SV_5

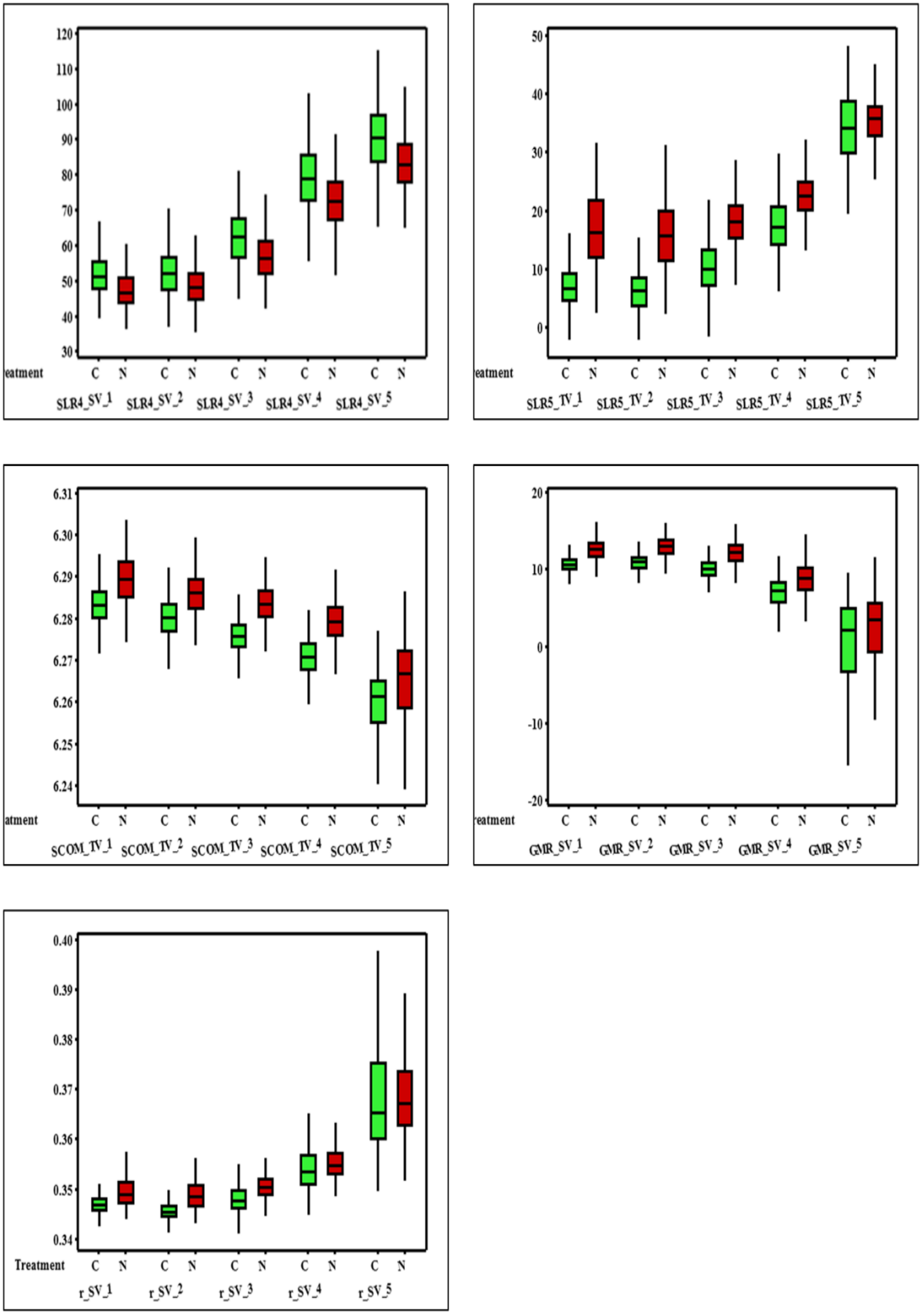

Figure 4.25: Boxplots of RGB based vegetation indices showing the treatment effect and stage wise progression of phenotypic profiles of RILs.

The vegetation indices extracted from RGB intensity values showed different temporal trend and contrasting nitrogen deficiency response (Figure 4.25). Traits like had higher values in control than nitrogen plants and traits like had lower values in control plants than nitrogen deficiency plants. Some indices like showed progressive increase trend over time and some like showed decreasing trend over time and some traits like had peculiar trend over time (Figure 4.25).

4.1.1.11 Multivariate analysis of i-Traits reflecting nitrogen deficiency responses

Principal component analysis

To capture the phenotypic variation among the population and to explore the ability of i-Traits to reflect the nitrogen deficiency responses, principal component analysis (PCA) of all the i-Traits was carried out at all stages (Figure 4.26). PCA of i-Traits at multiple stages suggests how the phenotypic behavior changes according to time and at which stage the phenotypic differences are large between treatments. As nitrogen deficiency response is visible from very start of plant life cycle such as from tillering stage, the PCA showed distinguishable differences between control and nitrogen deficiency at all stages as observed by the clear separation between the red and green ellipse representing control and N-deficient plants, respectively. As the stage progressed the overlapping of ellipse reduced (Figure 4.26).

Cumulative PCs of 4 principal components at all stages explained more than 80% of phenotypic variation, and PC1 and PC2 cumulatively explained 67%, 64%, 60%, 57% and 61% at 60, 70, 80, 90 and 100 DAS, respectively. A marginal reduction in cumulative PCs (PC1 and PC2) was observed after flowering stage (70 DAS). Alone PC1 showed ~47% variability at stage 1 and 2, but the value decreased to ~42% at later stages (Figure 4.27). The PCA biplot at stage 5 was completely dissimilar as at close to maturity plant i-Trait characteristics merge as the plants dry. The spread of red and green dots is scattered at stage 1 and 2 than in later stages where the dots are little clustered which might suggest the changes in phenotypic behaviour is peak at before flowering and after flowering there is not much increase in deficiency response. Also, the distance between centroid showed the difference between control and nitrogen deficiency plants. The presence of centroid outside of other ellipse boundary shows better differences.

Traits like BPC_SV, PSCC_4, 18, 5, 19, 3, 1, BPR_SV, PSA, Biovolume, 2MPASA_SV, BPC_TV, AZR2M_TV, G-B_TV, PCA1_SV and Gray_TV were found significantly contributing to PC1 which includes representative traits from each five trait classes. Red_TV & SV, Green_TV & SV, Blue_TV & SV, 2MPALN_SV, PCA2_SV, PSCC_14 & 15, ObjectExtentY_SV, BPAR_TV traits contributed more to PC2. Hence these i_Traits were able to capture the most phenotypic variation (Figure 4.28).

A. **B.**

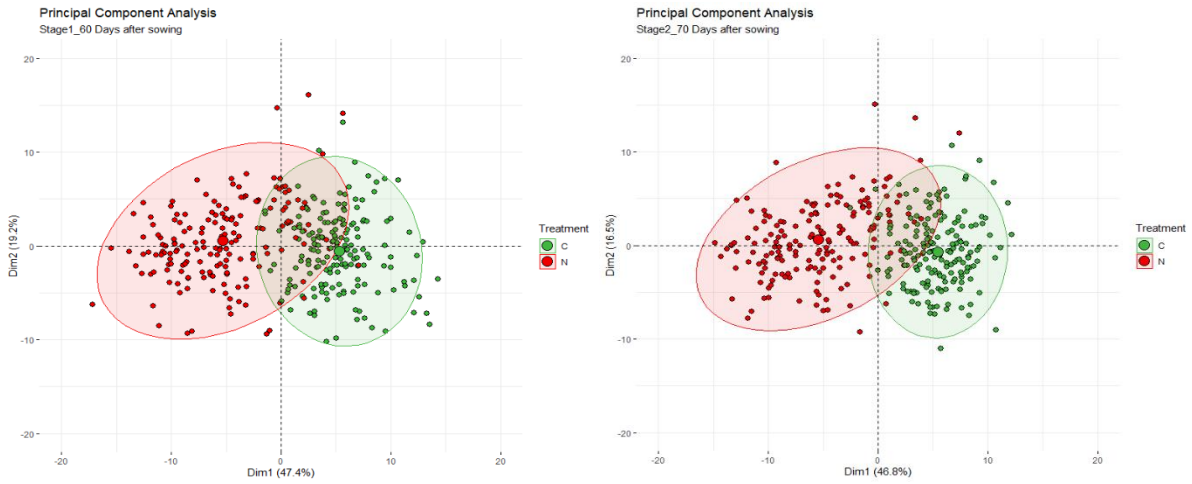

C. **D.**

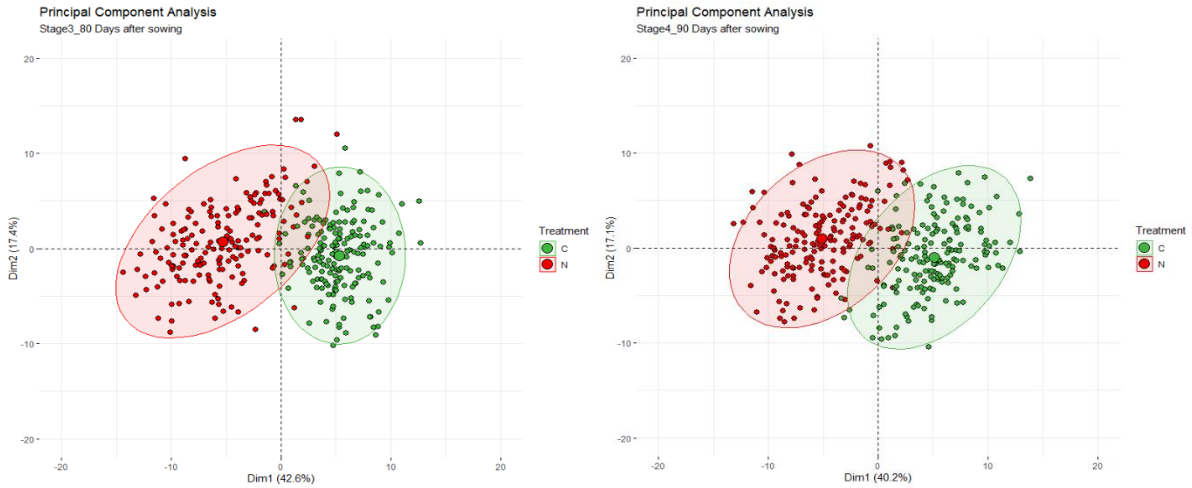

E.

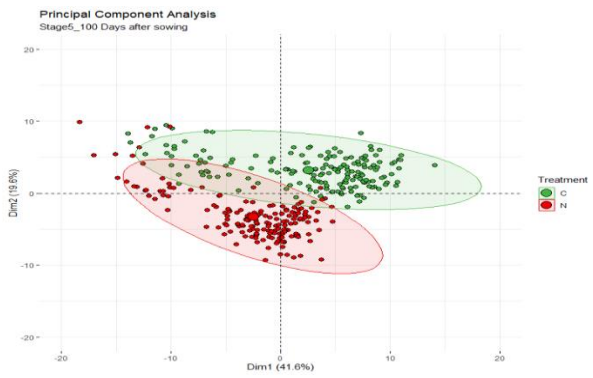

Figure 4.26: Principal component analysis of i-Traits explaining the phenotypic differences between control and nitrogen deficiency condition at a) 60 DAS b) 70 DAS c) 80 DAS d) 90 DAS e) 100 DAS. The red colour and green colour represented by control and nitrogen deficiency plants respectively.

A.

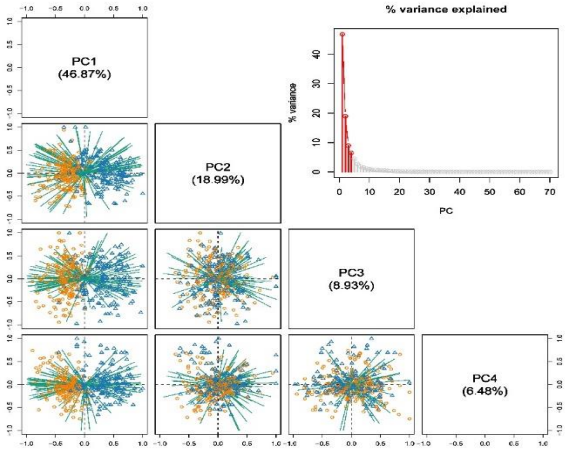

B.

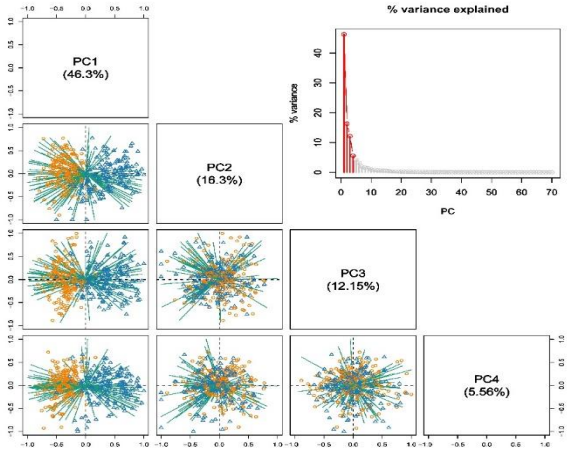

C.

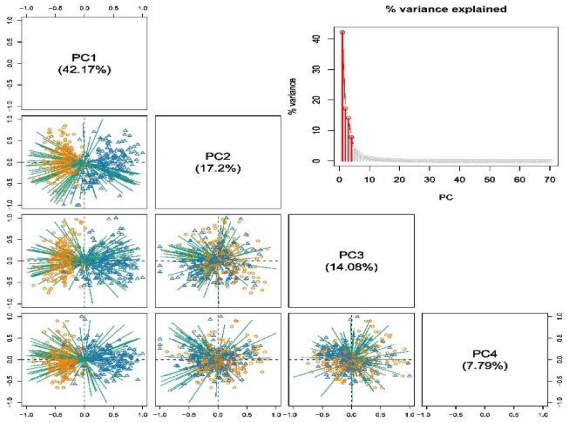

D.

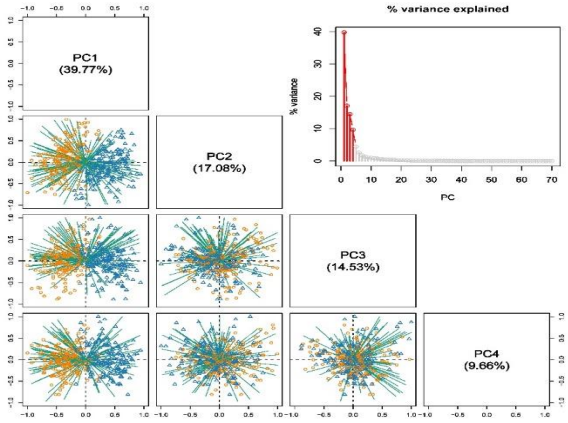

E.

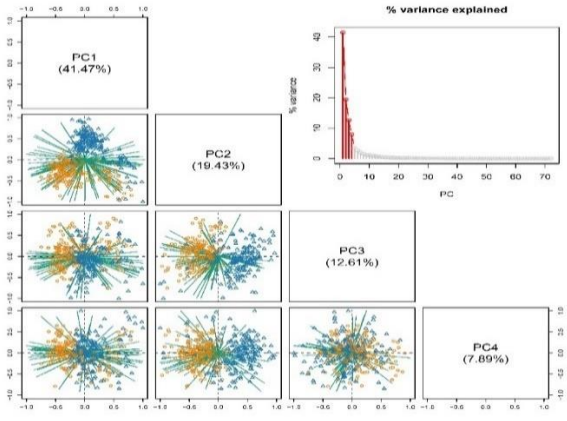

Figure 4.27: Principal component analysis showing 4 principal components of all i-Traits and representing the phenotypic differences between control and nitrogen deficiency at a) 60 DAS b) 70 DAS c) 80 DAS d) 90 DAS e) 100 DAS. The orange and blue dots represent the N-deficiency and control plants, respectively, and the green lines represent all the i-Traits.

A.

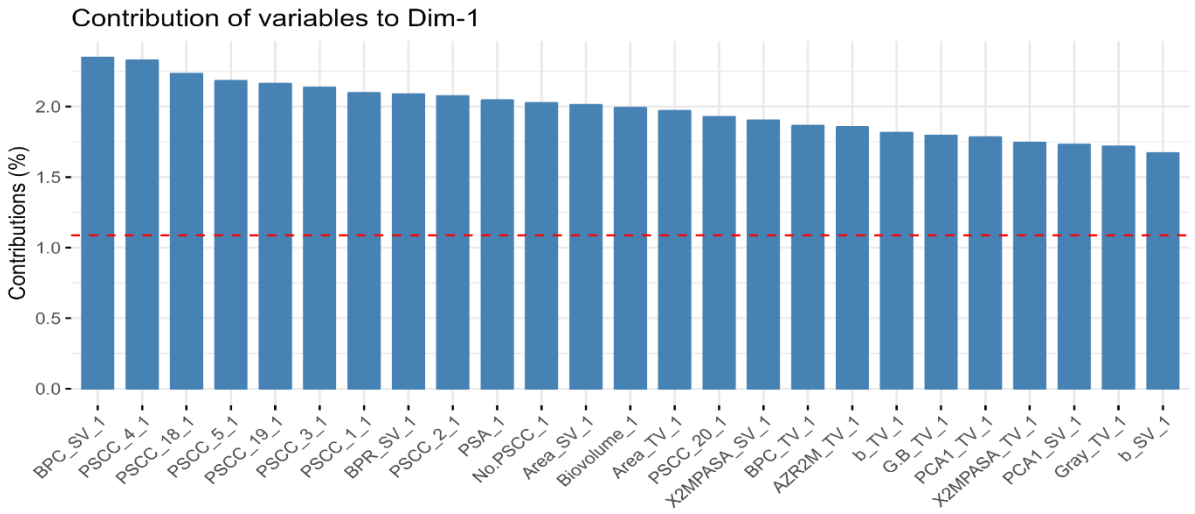

B.

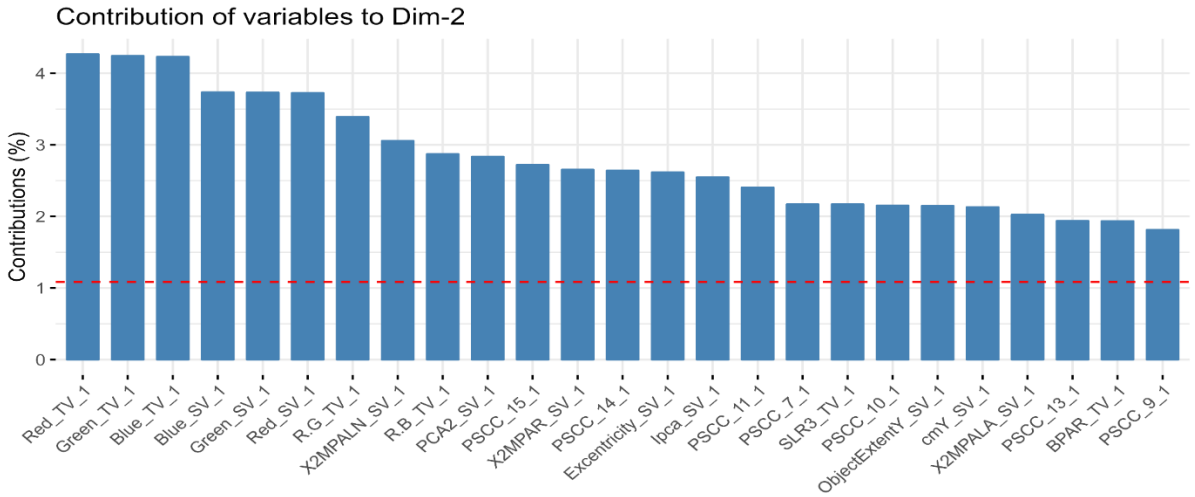

C.

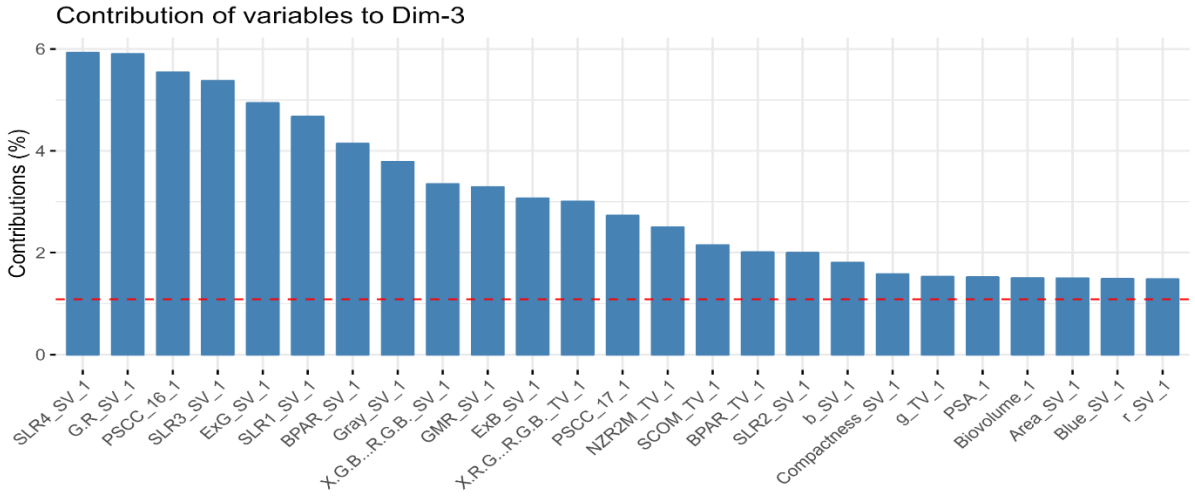

Figure 4.28: Trait contribution to a) PC1 b) PC2 c) PC3.

Trait similarity

To access the patterns of trait correlations, we performed the trait similarity analysis based on canonical Pearson's correlation coefficient. We assessed the similarity between all the i-Traits at all 5 stages and compared the similarity under control and nitrogen deficiency conditions. The correlation between traits were higher under nitrogen deficiency conditions than under control conditions as seen by the intensity of green and red color. As a general pattern we found that the RGB based indices were negatively correlated with morphometric traits and color related traits. Differences in color with in the rectangular cubes suggested that there were different i-Traits explaining variability among the traits and these variabilities might capture different aspects of phenotype. Barring the intensity differences, both control and N deficiency gives some striking similarity in correlation patterns. The correlation pattern was similar at stage 1, 2 and 3, but the differences were observed between stage 1, 2, 3 and stage 4, 5. At stage 5 the similarity patterns changed drastically than other stages due to the maturity phase.

4.1.1.12 Capability of i-Traits to capture nitrogen deficiency response and NUE

Biomass related traits

Effect of nitrogen deficiency was significant in all biomass related traits from the first stage itself. Biovolume showed the highest reduction due to N deficiency. Reduction range of Biovolume due to N deficiency was 30-36 %, reduction in PSA was 21-25 %, reduction in Area_TV was 22-28 % and reduction in Area_SV was 19-25 % in all 5 stages. The CV of Biovolume, PSA, Area_TV and Area_SV was in the range of 21-38 %, 14-20 %, 16-44 % and 14-16 % in all 5 stages (Figure 4.29 to 4.33).

Morphometric traits

We observed that from 28 morphometric traits, in seven traits plants under N deficiency had higher values than control plants, and other 21 traits had lower values under N deficiency. Among morphometric traits 2MPASN_TV, NZR2M_TV, 2MPALN_SV, 2MPASN_SV, 2MPAR_SV, cmY_SV and Eccentricity_SV had negative percent reduction from control plants i.e., N-deficient plants had higher values than the control plants. Rest 21 i-Traits had positive percent reduction from control plants (Figure 4.29 to 4.33), i.e., N deficient plants had lower values than the control plants. The percentage reduction for traits were ranging from as high as 42 % to -25%. Traits like Circumference_SV, 2MPASA_TV & SV, AZR2M_TV, BPR_TV & SV and BPC_TV & SV had reduction of about 30-42% and traits like 2MPALN_SV, 2MPAR_SV and Eccentricity_SV had increase of about 10-25 %. From 28 morphometric traits, 10 traits namely 2MPASN_TV, BPAR_TV, NZR2M_TV, 2MPASN_SV, ADAR_SV, BPAR_SV, cmY_SV, Circumference_SV, ObjectExtentX_SV and ObjectExtentY_SV had <10% difference between control and N deficient treatments (Figure 4.29 to 4.33). The mean CV of all the morphometric traits was 28 and 32 % under control and N deficiency, respectively. Where in stage 1-4 the mean CV was ~ 20 % and 25%, and at

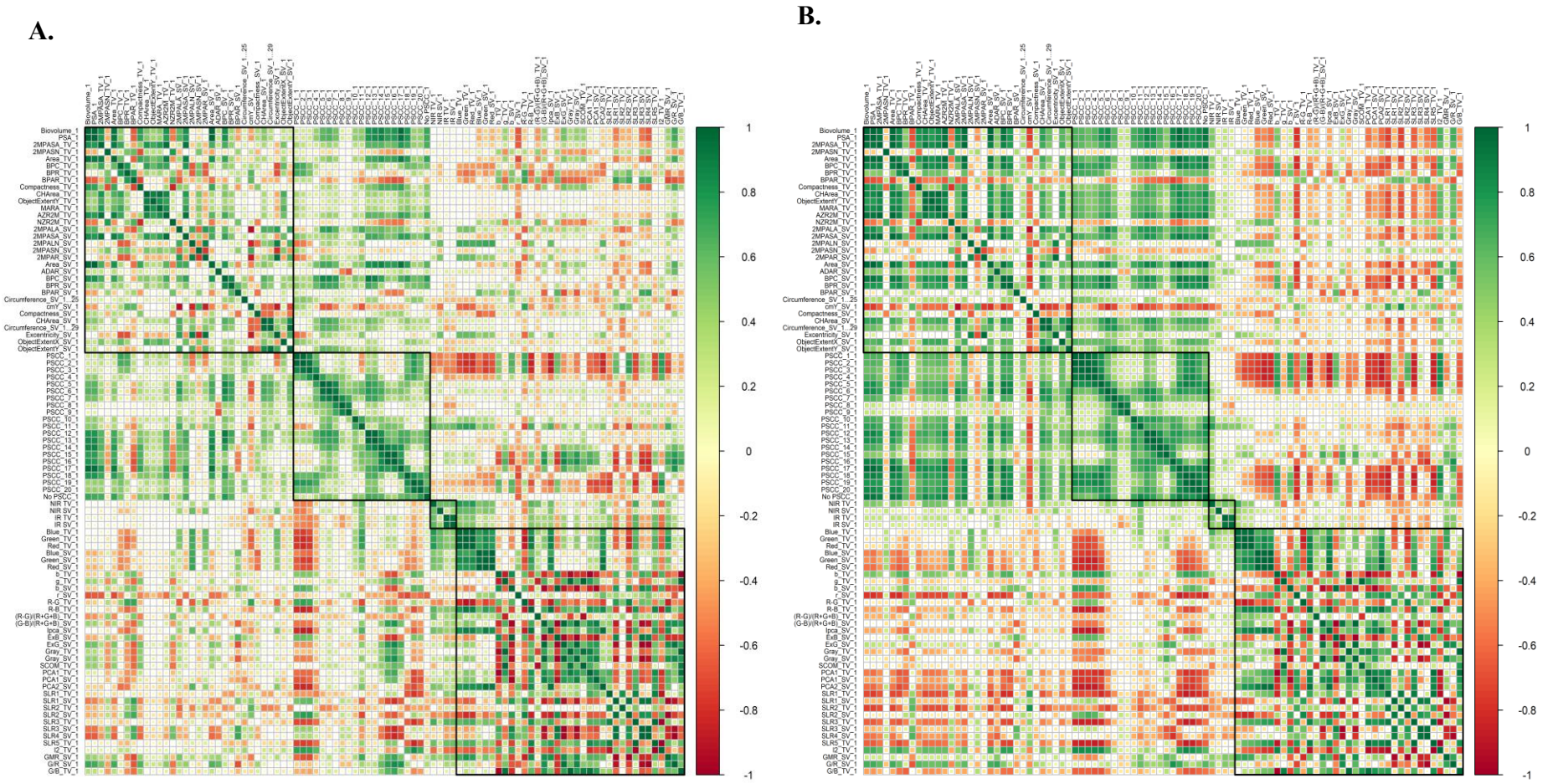

Figure 4.29: Trait similarity between i-Traits under different treatments at stage 1 (60 DAS). A) Control condition B) Nitrogen deficiency. The 4 rectangular black boxes represent 4 i-Trait classes, morphometric, color, intensity and indices related traits (Top to bottom)

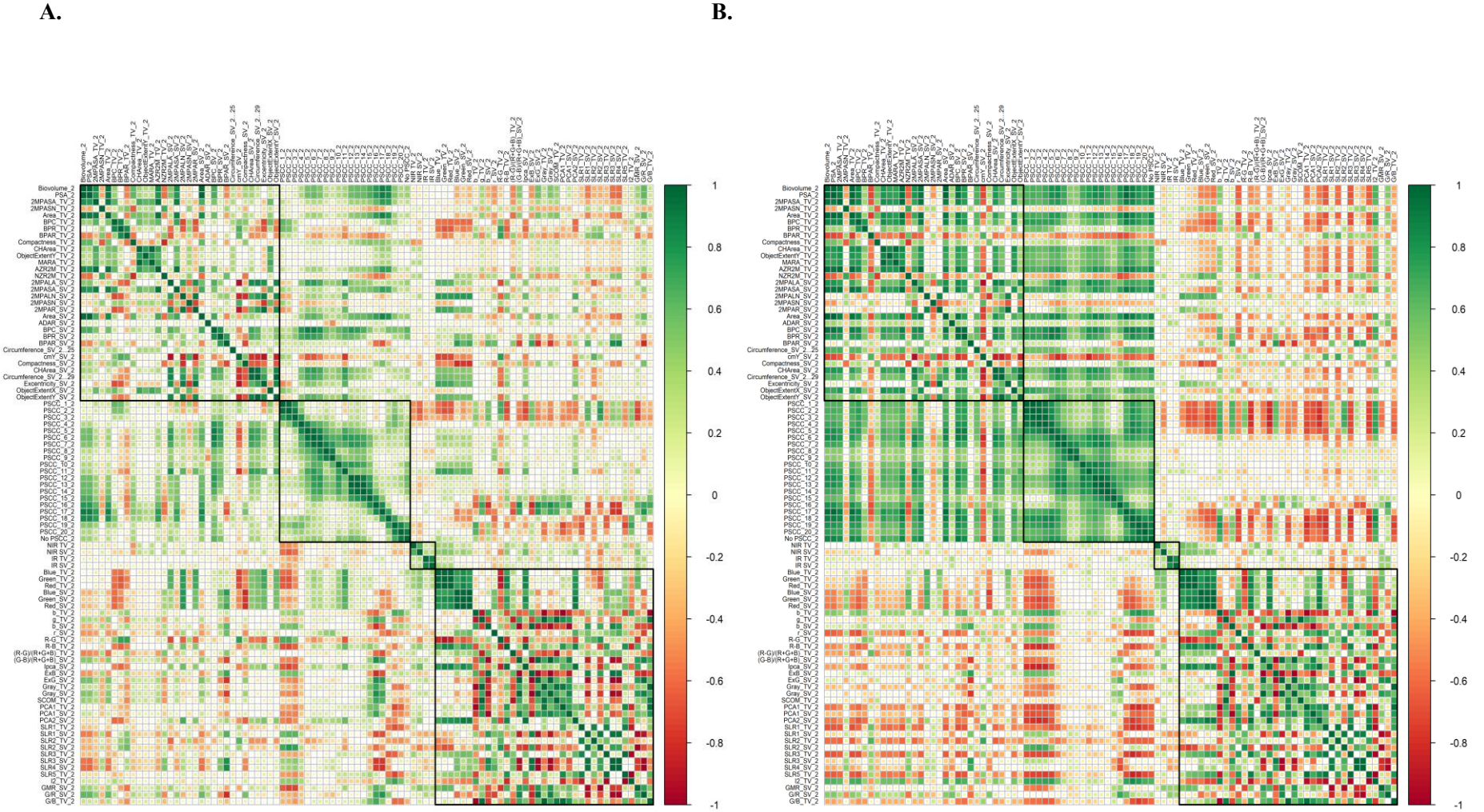

Figure 4.30: Trait similarity between i-Traits under different treatments at stage 2 (70 DAS). A) Control condition B) Nitrogen deficiency. The 4 rectangular black boxes represent 4 i-Trait classes, morphometric, color, intensity and indices related (Top to bottom).

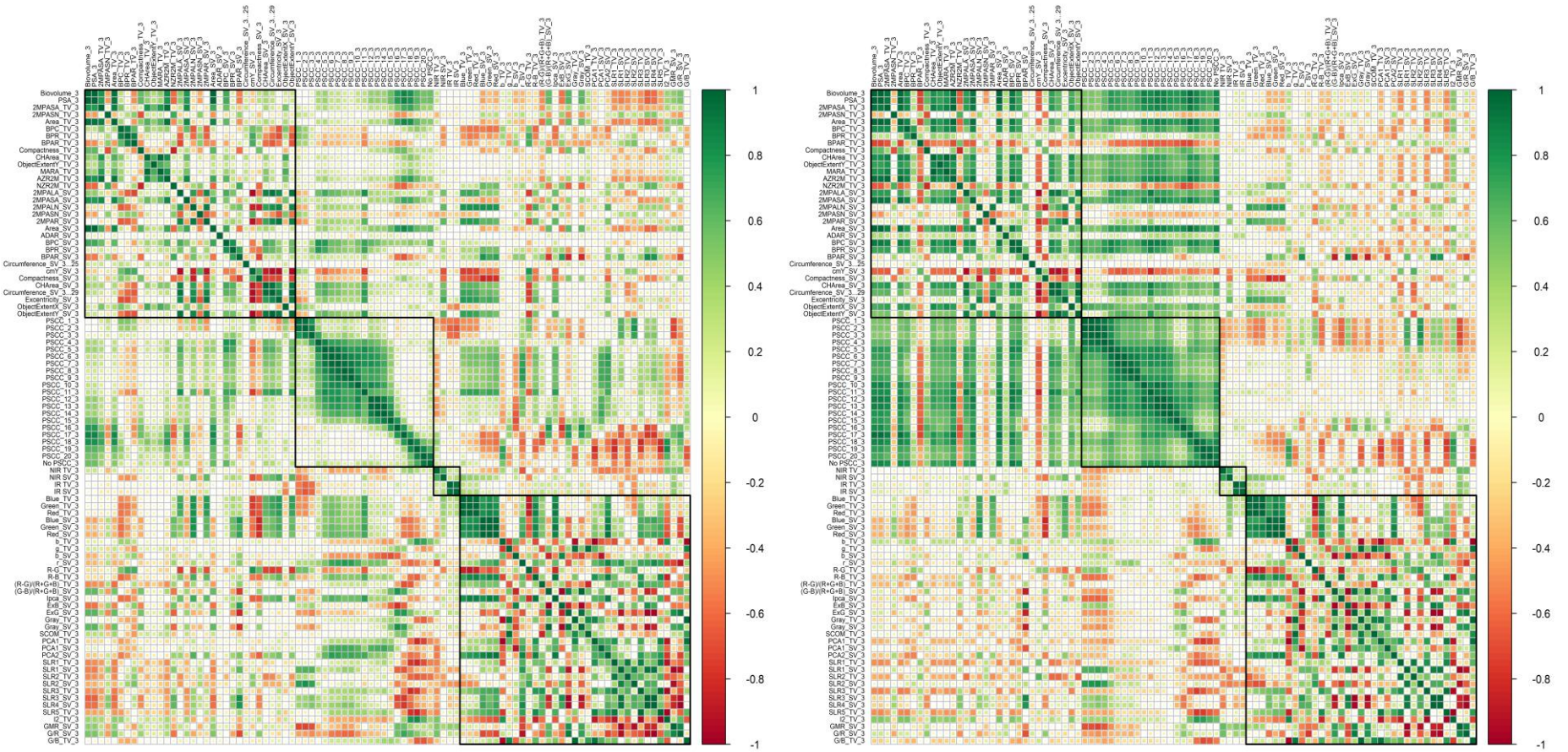

Figure 4.31: Trait similarity between i-Traits under different treatments at stage 3 (80 DAS). A) Control condition B) Nitrogen deficiency. The 4 rectangular black boxes represent 4 i-Trait classes, morphometric, color, intensity and indices related (Top to bottom).

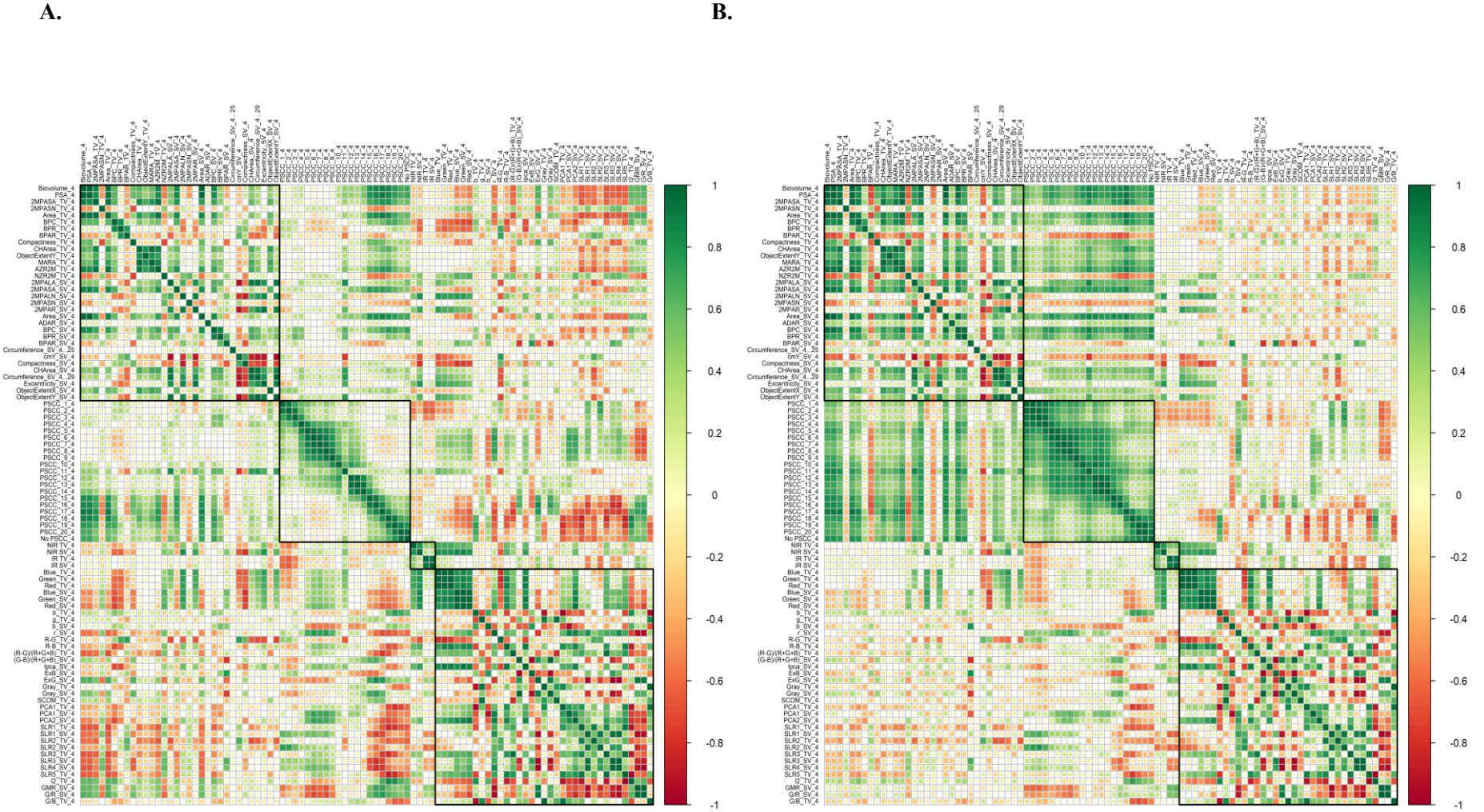

Figure 4.32: Trait similarity between i-Traits under different treatments at stage 4 (90 DAS). a) Control condition b) Nitrogen deficiency. The 4 rectangular black boxes represent 4 i-Trait classes, morphometric, color, intensity and indices related (Top to bottom).

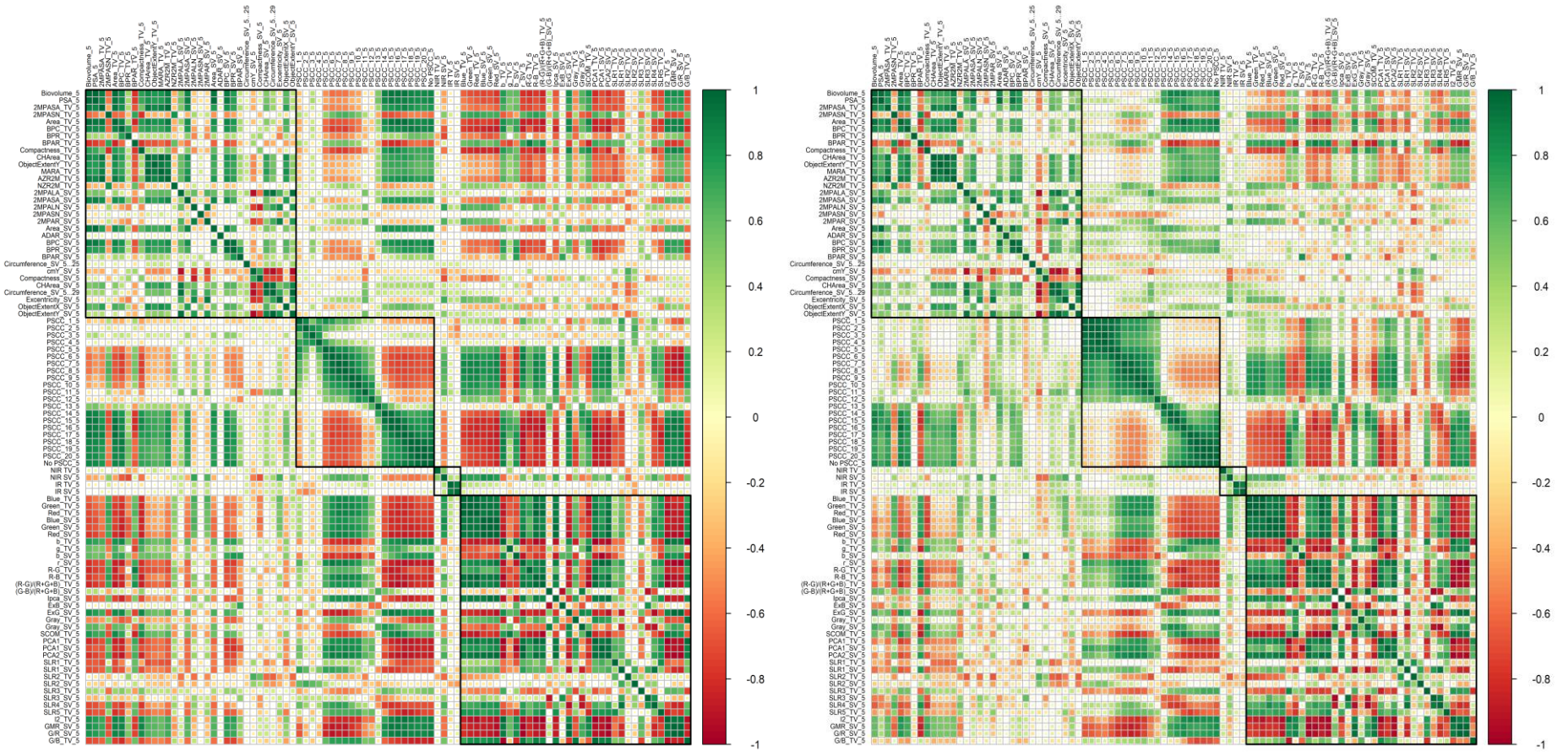

Figure 4.33: Trait similarity between i-Traits under different treatments at stage 5 (100 DAS). a) Control condition b) Nitrogen deficiency. The 4 rectangular black boxes represent 4 i-Trait classes, morphometric, color, intensity and indices related (Top to bottom).

stage 5 the CV was 29 % and 31% under control and N deficiency, respectively (ANNEXURE 4). The range of CV under control and N stress conditions was ~0.2-42 % and ~0.4-70%, respectively at stage 1-4 but at stage 5 the range was ~0.3-81.3% and 0.4-121%, respectively.

Colour class traits

Colour classes showed highly significant reduction due to N deficiency. The reduction percent range was -2 % to 57%. Traits like PSCC_19, 3, 18, 20 and 2 had reduction of about 50-57 % and PSCC_11, 9, 10, 14, 16 and 15 had <10% reduction in N deficient plants than that of control plants. The mean CV of all the colour class related traits was 24 and 36 % under control and N deficiency, respectively (ANNEXURE 4). Where in stage 1-4 the mean CV was ~ 21 % & 34% and at stage 5 the CV was 38 % & 47 % under control and N deficiency, respectively. The range of CV under control and N stress conditions was ~12-35 % and ~0.4-60%, respectively, at stage 1-4, but at stage 5 the range was ~19-63% and 33-69%, respectively, under control and N deficiency (ANNEXURE 4).

RGB based Vegetation Indices

The Red_TV & SV, Green_TV & SV and Blue_TV & SV intensity values were observed to identify the differentiate the treatments. In all these traits the intensity values were higher under N deficiency treatment than that of control plants. The range of percentage difference of Red_TV & SV, Green_TV & SV and Blue_TV & SV intensity values were 10-16 % (ANNEXURE 4). Within all the RGB derived indices the range of percentage difference was 37 to -55 %. Traits like GMR_SV, SLR2_SV, PCA1_SV, SLR1_SV, SLR4_SV, I2_TV and SLR3_SV had higher positive difference and traits like IPCA_SV, PCA2_SV, R-B_TV, SLR1_TV, ExB_SV, SLR5_TV and PCA1_TV had negative percentage difference between control and N deficiency plants. G/B_TV, ExG_SV, (G-B)/(R+G+B)_SV, R-G_TV, Ipca_SV, PCA2_SV had less than 10% difference between control and N stress treatments (ANNEXURE 4).

4.1.1.13 Feature identification for traits contributing to yield and plant nitrogen status

To select the major informative i-Traits contributing to yield and plant nitrogen level, the Random Forest machine learning model was used to all the i-Traits at different time points. Then as per the trait contribution details of all i-Traits, the topmost important traits which highly contributed to yield and plant nitrogen level were selected. Major i-Traits such as BPC_SV & TV, Comapactness_SV & TV, PSA, Area_SV and 2MPASA_TV are among the top morphometric traits contributed to yield and nitrogen level responses. Among colour related traits Blue_SV, PSCC_3, 4, 5, 17, 18, 19, and 20 have contributed to both the traits. RGB based indices like r_SV, SLR2_SV, GMR_SV and PCA1_SV are the major contributors to the yield and nitrogen level response of wheat. By analysing the effect of trait contribution over plant age, it was found that i-Traits at stage 3 and 4 were contributing majorly to manual traits than the i-Traits at early stage 1 and 2. PSA of all stages were contributing to both the

traits due to the fact that biomass is a contributing factor to yield. But other than biomass, other morphometric traits were also determining factor for plant yield and nitrogen status.

4.1.1.14 Colour class related traits explaining the whole plant colour status

Colour class characterization gave interesting insight into whole plant response to nitrogen deficiency. We classified whole plant pixels into 20 colour classes by unsupervised classification approach. Then we observed how these colour classes behaved according to progress in plant age and nitrogen status of plants (Figure 4.34). We found that PSCC_16, 17 and 18 are greenness related colour class and these values decreased as the plant age progressed and they had lower values under nitrogen deficiency conditions.

Traits such as PSCC_5, 6, 7, 10, 11, 12, 13 and 14 are yellowness or senescence related colour class, as their value increased with the progression of plant age and had higher values under N deficiency conditions than that of control plants. PSCC_15 was constant in all stages under both treatments. PSCC_1, 2, 3 and 4 had <1 % pixels at all stages, and PSCC_11, 14, 15, 16, 17 and 18 represented higher percentage of whole plant pixels (Figure 4.34).

4.1.1.15 Phenotypic variation profile of RILs represented by i_Traits

Coefficients of variation (CV) differed strongly between image traits (0.06 to 78.81%). Around 75 % image traits have CV higher than N stress conditions. The mean difference of CV under control condition and nitrogen deficiency conditions was about 18%. Highest CV was calculated for 2MPASA_TV_1 (69.16%), 2MPASA_TV_2 (63.27%), 2MPASA_TV_5 (78.58%), AZR2M_TV_1 (64.36%), AZR2M_TV_5 (71.66%), Circumference_SV_2 (74.36%), PSCC_17_5 (68.68%), PSCC_18_1 (61.51%), PSCC_18_5 (66.32%), PSCC_19_1 (63.33%) and PSCC_19_2, (61.01%) across treatments.

The lowest CVs were determined ADAR_SV_2(0.43%), ADAR_SV_3 (0.38%), ADAR_SV_4 (0.39%), ADAR_SV_5 (0.41%), Gray_SV_1 (0.47%), Gray_SV_2 (0.5%), Gray_SV_3 (0.47%), Gray_SV_4 (0.4%), Gray_TV_3 (0.45%), Gray_TV_4 (0.45%), Gray_TV_5 (0.46%), SCOM_TV_1 (0.09%), SCOM_TV_2 (0.08%), SCOM_TV_3 (0.07%), SCOM_TV_4 (0.08%) and SCOM_TV_5 (0.22%) different treatments (ANNEXURE 4).

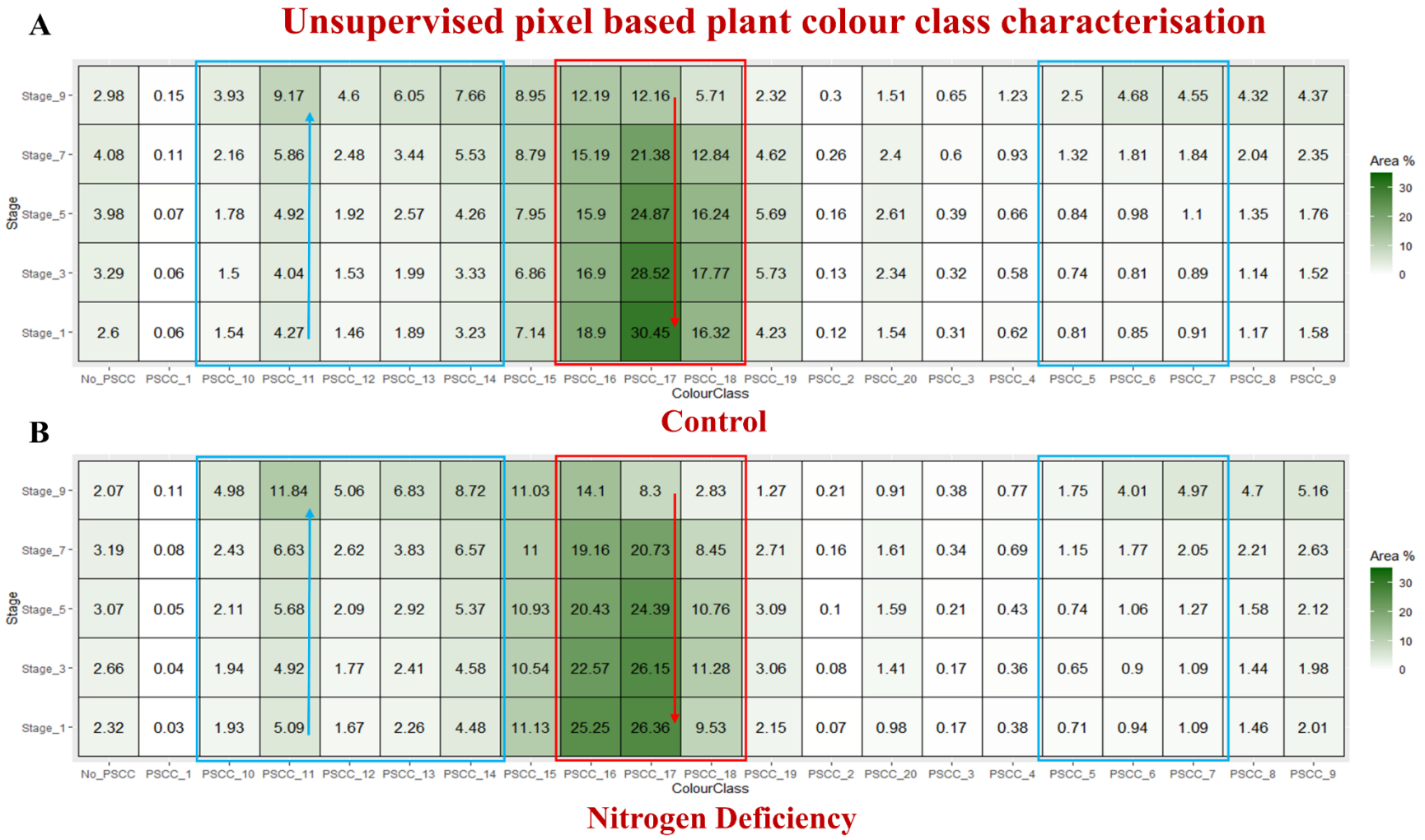

Figure 4.34: Unsupervised colour class characterization of whole plant pixels to evaluate plant nitrogen status. A) Status under control condition B) Status under nitrogen deficiency. The red box represents the greenness related colour classes and the blue boxes represents the yellowness related colour classes. The red and blue arrow represents the value gradient.

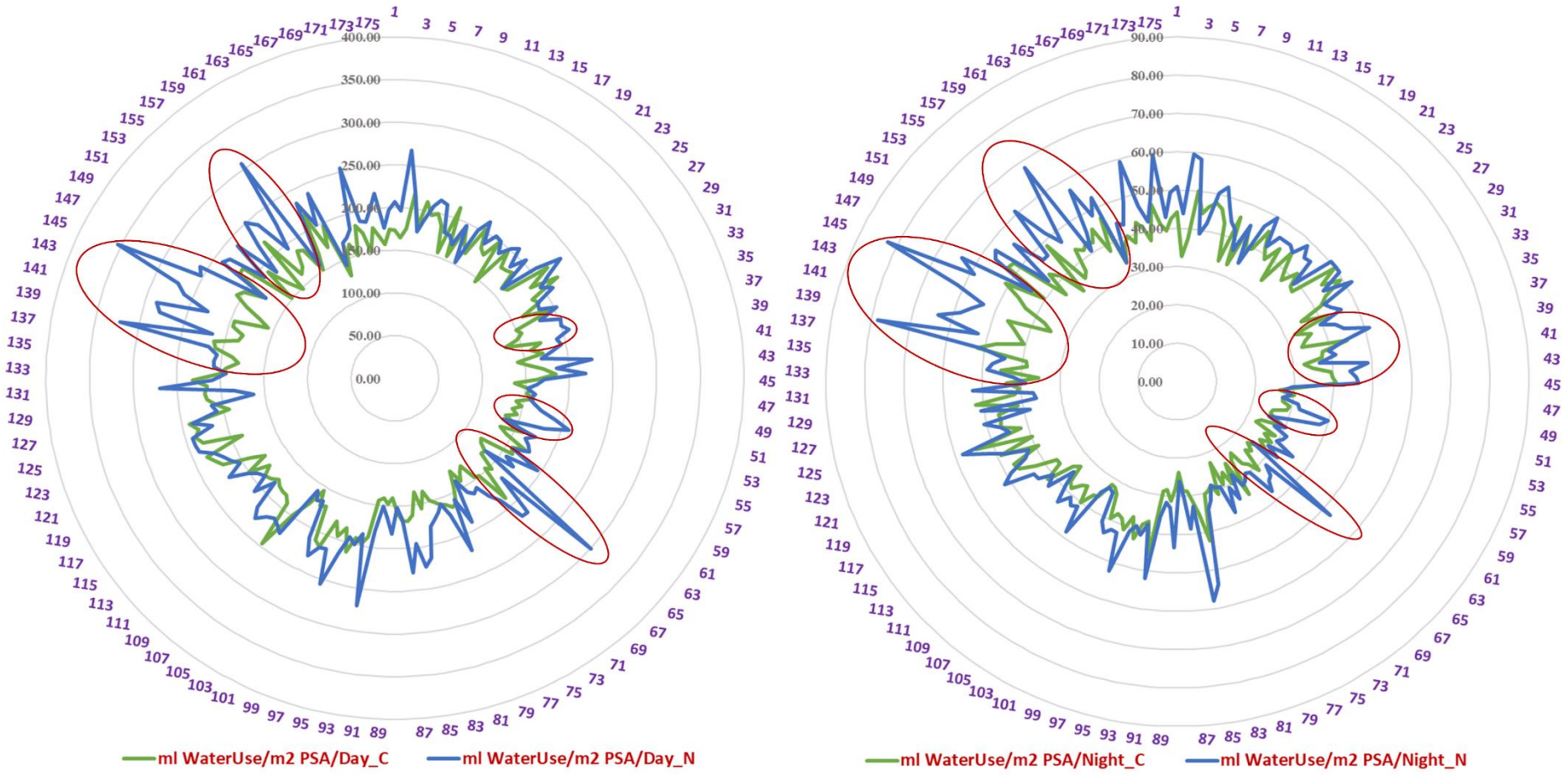

Figure 4.35: Graphical representation of water use of wheat RILs at day (Left) and night (Right) time under control and nitrogen deficiency condition. This shows the effect of nitrogen deficiency on the water use (ml)/PSA (m2) in wheat RILs at day and night time. The red circles represent the RILs have contrasting day and night time transpiration.

4.1.1.16 Effect of nitrogen deficiency on whole plant transpiration

The mean water use (ml)/PSA (m^2) of the RILs was 176 ml and 202 ml at day, and 38 ml and 43 ml at night under control and N stress conditions, respectively (Figure 4.35). Comparison of the water use/PSA (m^2) under control and N stress conditions of all the RILs revealed that there was 13% increase in mean water use/PSA (m^2) under nitrogen deficiency in both day and night time transpiration. In 121 RILs the water use (ml)/PSA (m^2) was high under nitrogen deficiency conditions than that of control, 13 RILs had lower water use (ml)/PSA (m^2) under nitrogen deficiency conditions than that of control. Only 41 RILs had <5% difference in water use/PSA (m^2) between the treatments.

The range of water use/PSA (m^2) under control condition was 121 to 246 ml and 54 to 22 mL at day and night time, respectively. Under N stress conditions, the phenotypic range of water use/PSA (m^2) was 133 to 354 ml, and 24 to 82 ml at day and night time, respectively (Figure 4.35). We also found that most of the RILs which were transpiring more water use/PSA (m^2) during the day were also transpiring more water use/PSA (m^2) in the night time under both control and nitrogen deficiency conditions. But interestingly some RILs had contrasting day and night transpiration as shown in red circles in Figure 4.35.

4.1.2 Manual phenotyping for component traits of NUE

To capture the nitrogen deficiency response and measure the NUE related traits, manual traits such as flag leaf traits, biomass traits, phenology, leaf emergence rate, tiller number, leaf number, SPAD value, ear number, ear length, seed number, TKW, grain yield, spikelet density, spikelet number, grain number HI and PHI were recorded. Plant architecture traits such as plant height was observed along with plant nitrogen use efficiency related traits (Figure 4.36 & 4.37).

4.1.2.1 Effect of nitrogen level to the phenology

The days to booting and days to anthesis of all the RILs under control and nitrogen deficiency conditions were recorded. Mean days to booting under control and nitrogen deficiency was 67 and 69 days, respectively which was not significant. Also, no significant difference was not observed for days to anthesis between control and nitrogen deficiency. Both parents had similar mean time taken for booting and anthesis. The range of days to booting and anthesis was 62 DAS to 74 DAS and 70 DAS to 82 DAS, respectively (Figure 4.38).

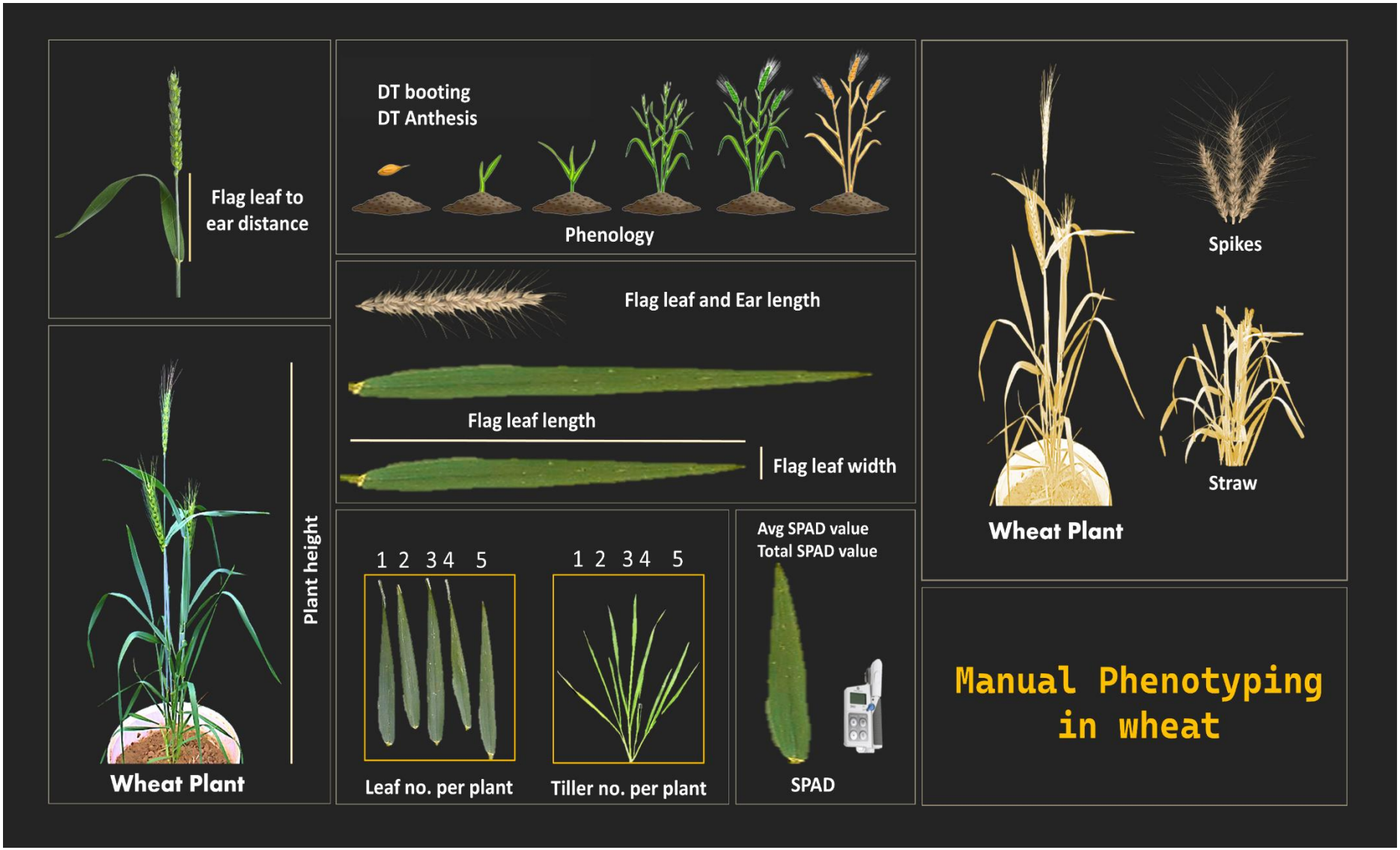

Figure 4.36: Graphical representation of plant physiological, phenological and morphological traits recorded manually.

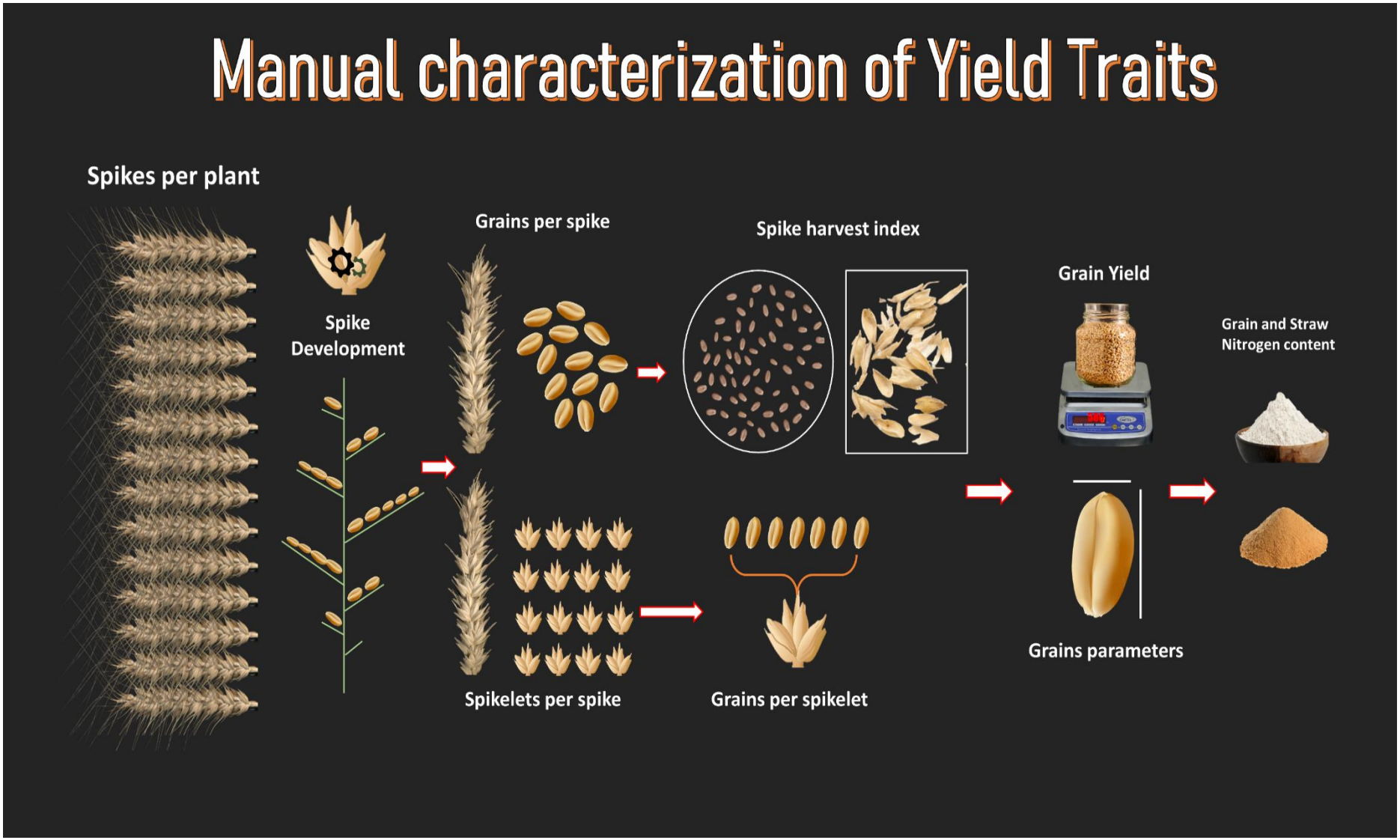

Figure 4.37: Yield trait characterisation of wheat plants by manual method.

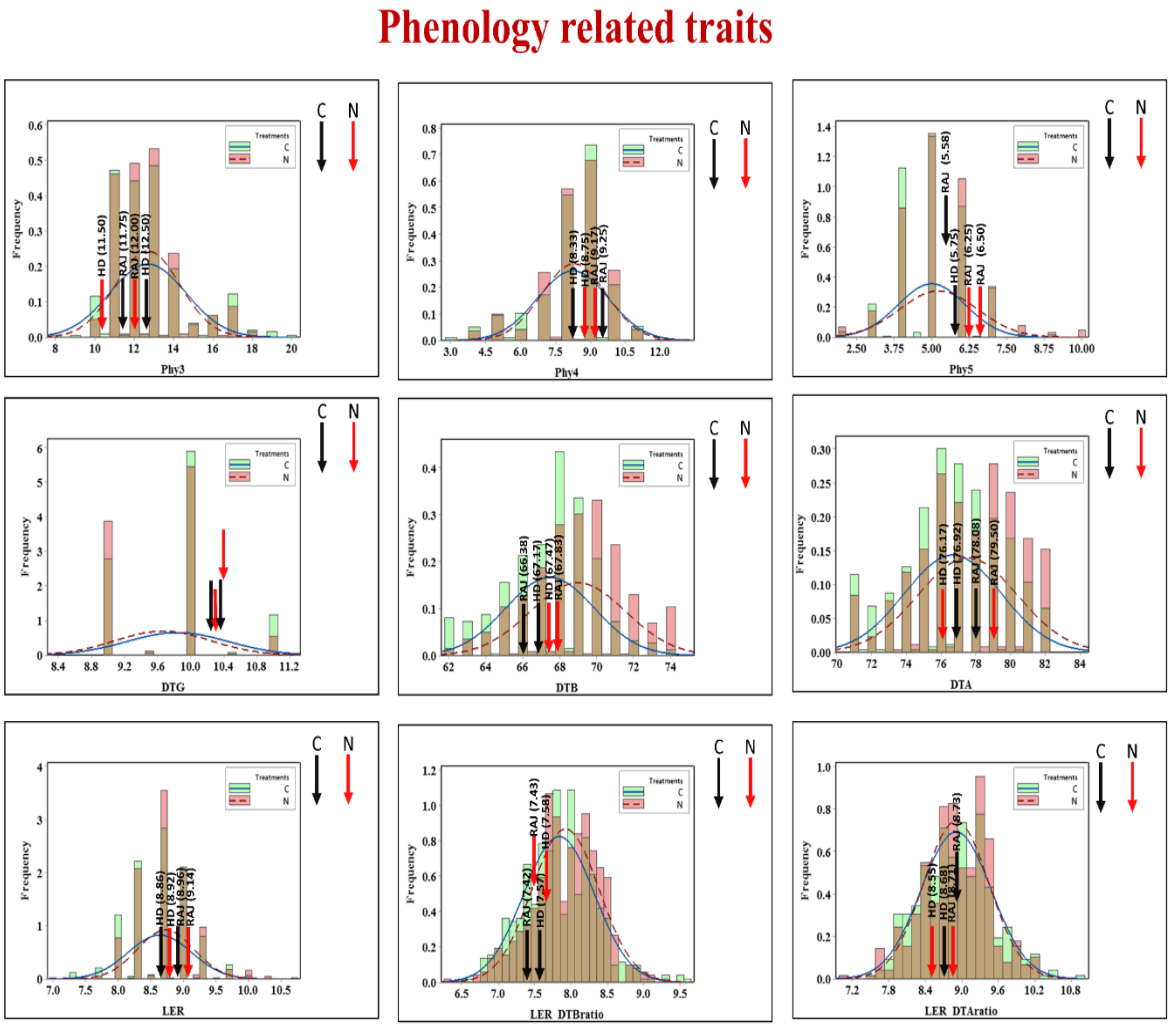

Figure 4.38: Frequency distribution of phenology related traits in wheat RILs. Black arrow and red arrow represent parental value under control condition and nitrogen deficiency condition, respectively.

4.1.2.2 Effect of nitrogen levels on the physiological traits

The flag leaf is a major contributor of photosynthates for seed development. It was observed that nitrogen deficiency conditions reduced the flag leaf length and width was reduced by 17 % and 10 %, respectively. Flag leaf total area and length to width ratio were reduced by 25 % and 9% respectively, due to nitrogen deficiency. Fag leaf length, width and area range was 17-33cm, 1.6-2.2cm and 23-52cm^2 under control condition, 15-30cm, 1.3-2.06cm and 16-41cm^2 under N deficiency conditions, respectively (Figure 4.39). Number of leaves at vegetative stage was decreased by nitrogen deficiency by 17 % as compared with the control. The range of leaf number per plant was 22-48 and 17-43 under control and N stress conditions, respectively. The SPAD value had same mean reduction at both vegetative and reproductive stage which is ~13 % in N deficiency as compared with control treatment. We calculated total SPAD value by multiplying the total flag leaf area to average SPAD value at both

vegetative stage and reproductive stage separately, and found that 33 % and 36% reduction at vegetative and reproductive stage, respectively, in N deficiency as compared with control treatment (Figure 4.39).

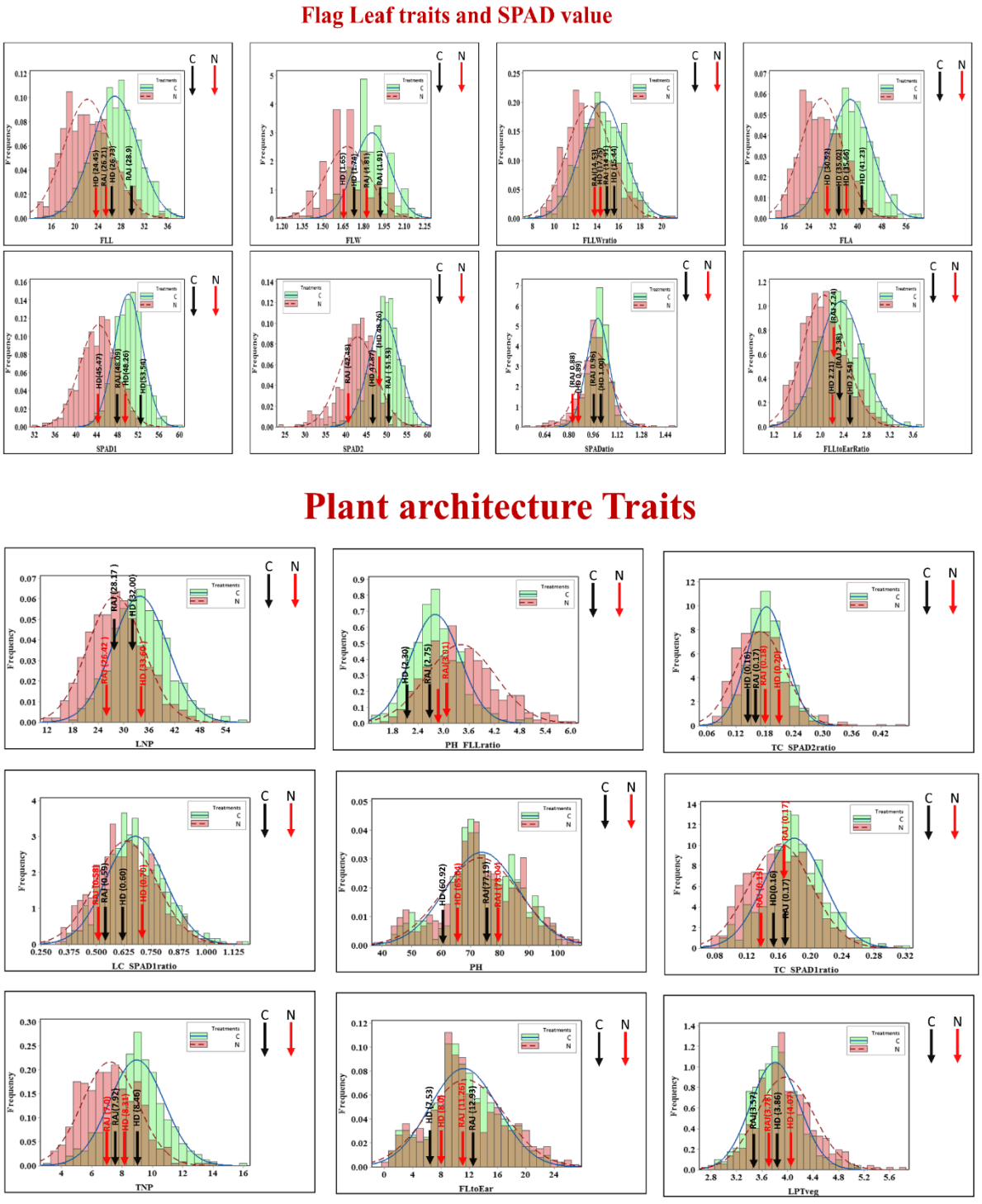

Figure 4.39: Frequency distribution of flag leaf related traits, SPAD value traits, tiller number, leaf number and plant height.

The SPAD value range was 44-56 and 39-56 under control conditions, and 36-50 and 27-56 under nitrogen deficiency condition at vegetative and reproductive stages, respectively. Tiller number reduced

by about 17 % due to nitrogen deficiency conditions. There was no significant reduction in plant height under nitrogen deficient condition. Tiller number varied from 5-13 under control, and 4-11 under nitrogen deficiency among the RILs (Figure 4.39).

4.1.2.3 NUE of RILs

Eight nitrogen related traits were recorded under both control and nitrogen deficiency conditions for all the RILs and parents. Straw and chaff nitrogen, and grain nitrogen percentage was reduced by 33 % and 26 % due to nitrogen deficiency. Grain protein content decreased 5 % in nitrogen deficient plants. The nitrogen harvest index showed non-significant differences between control and nitrogen deficiency plants (Figure 4.40). There was about 28 % increase in utilisation index of plants under nitrogen deficiency as compared with the control plants. The range of grain N % was from 2.24-4.15 and 1.56-3.26 under control and N deficiency condition, respectively. The straw N % range was 0.69-1.78 and 0.42-1.45 under control and N deficiency conditions, respectively (Figure 4.40). The range of GPC was 12-24 % under control condition and 8-20 % under N stress condition but mean GPC was 17 % and 12 % under control and N deficiency condition respectively.

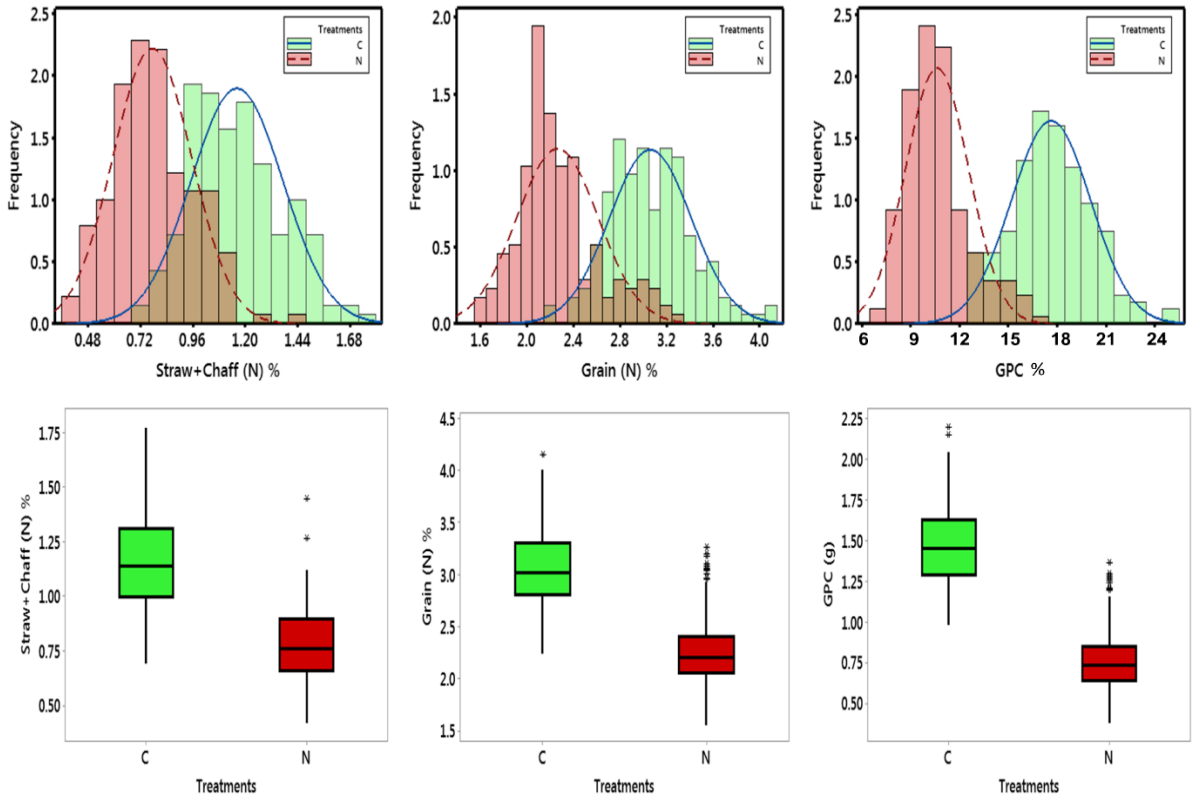

Figure 4.40: Frequency distribution and box plot representation of grain, biomass nitrogen content and grain protein content showing the effect of nitrogen deficiency.

The range of NUpE, NUtE and NUE was 0.19-0.42 gN in plant/gN supplied, 18.84-31.85 g grain/gN in plant and 4.55-10.32 g grain/gN supplied under control conditions (Figure 4.41). Under

nitrogen deficiency conditions, the range of NUpE, NUtE and NUE was 0.58-2.02 gN in plant/gN supplied, 21.22-49.11 g grain/gN in plant and 17.14-68.22 g grain/gN supplied, respectively. Due to no additional supply of N in the nitrogen deficiency, the value of NUE, NUpE and NUtE increased many folds but their value compared by normalising the data (Figure 4.41).

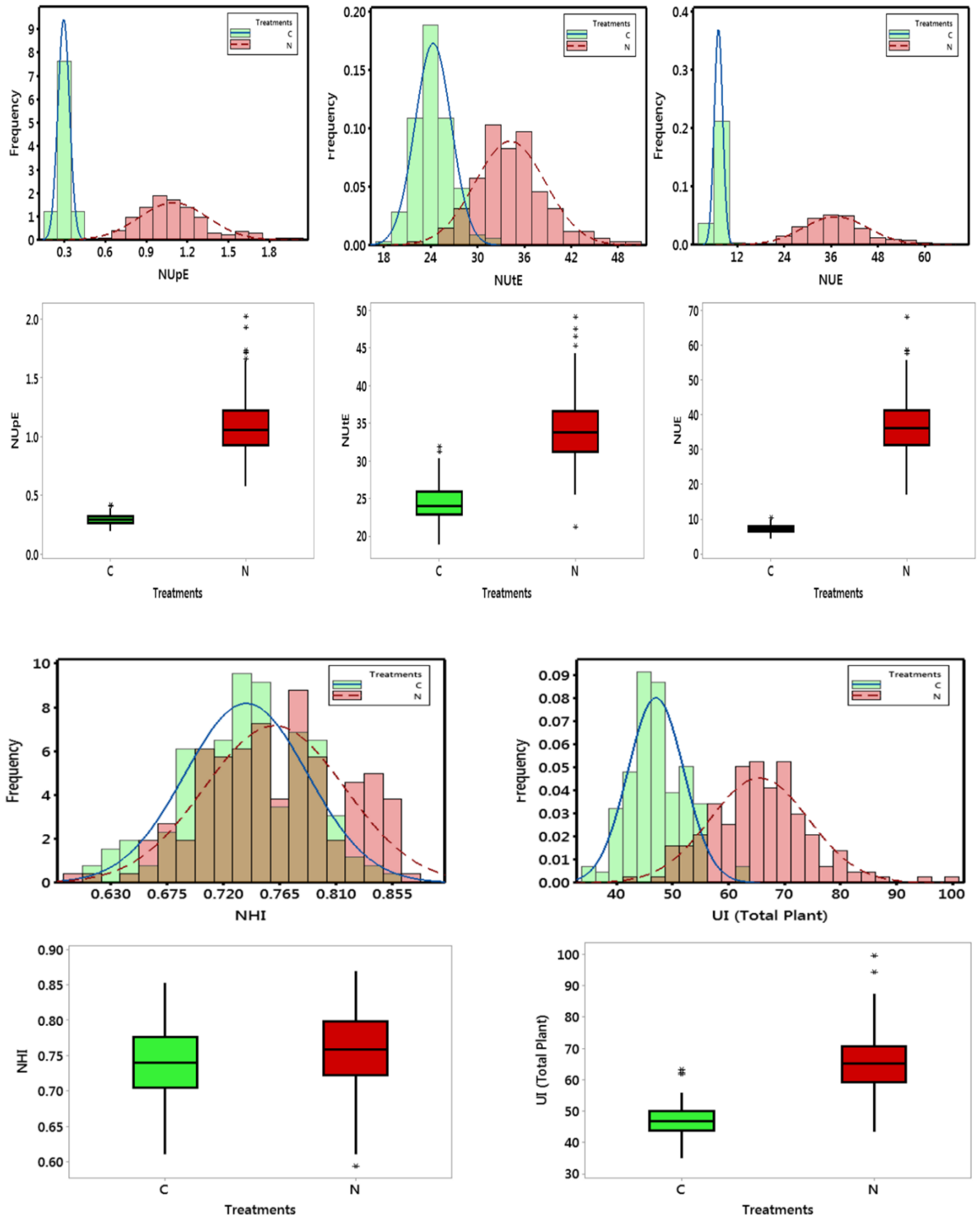

Figure 4.41: Frequency distribution and box plot representation of NHI, UI, NUE, NUpE and NUtE traits showing the nitrogen deficiency effect.

4.1.2.4 Effect of nitrogen levels on biomass, grain yield and its components

Straw, Total_Biomass, Total Ear and HI were reduced by 24, 27, 27 and 0.64 %, respectively, due to nitrogen deficiency. The phenotypic range of straw and chaff, total biomass, total ear and HI was 7-16g, 21-44g, 5-14g and 0.38-0.57 under control condition, and 4-14g, 11-34g, 4-10g and 0.38-0.59 under N stress conditions, respectively (Figure 4.42). ANOVA showed significant variation in all these traits.

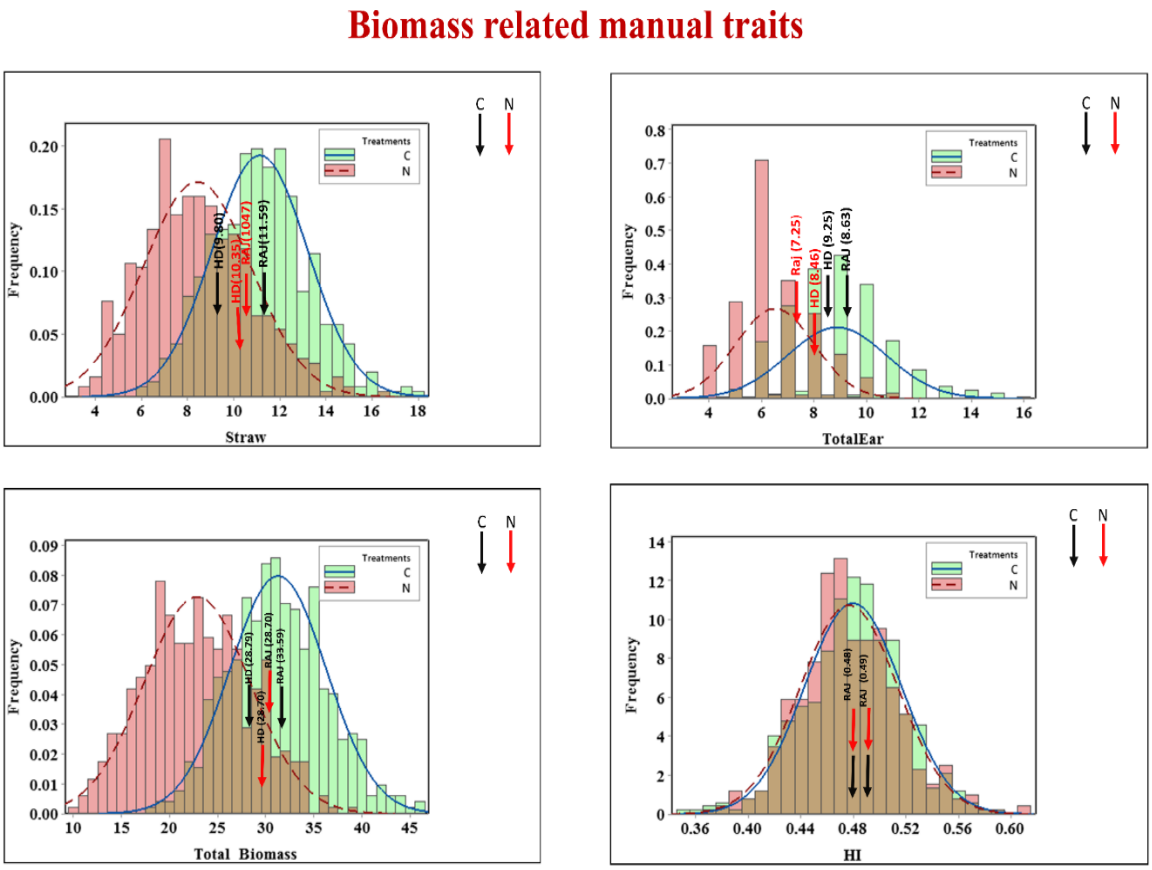

Figure 4.42: Frequency distribution of biomass related traits in all the RILs.

Different spike related traits were recorded. Spike length (SL), spikelet number per spike (SNS), sterile spikelets per spike (SSN), grains per spikelet (GPS), spikelet density (SD) and spikelet fertility index (SFI) were in the range of 9-13cm, 16-24, 0.3-8, 1.8-3.4, 1.4-2.3 and 47-103 under control, and 8-13cm, 16-24, 0.6-6.8, 1.7-3.1, 1.4-2.7 and 53-118 under N stress, respectively (Figure 4.43). The percent difference between control and N stress for SL, SNS, SSN, GPS, SD and SFI was 6%, -1%, 17%, 6%, -7% and -6%, respectively. This showed that under nitrogen deficiency the mean value of SNS, SD and SFI increased than the control treatment.

Total spike weight (SW), grain weight (GW) and chaff weight (CW) were recorded in all the RILs. The phenotypic range of SW, GW and CW was 13-28g, 10-21g and 3-7g under control, and 7-

21g, 5-16g and 1.5-5g under nitrogen deficiency, respectively (Figure 4.43 and 4.44). There was 28, 27 and 30 % reduction of SW, GW and CW under N deficiency as compared with control conditions. The range of total grain number per plant (TGN), panicle harvest index (PHI) and thousand kernel weight (TKW) was 201-558, 0.64-0.83 and 24-58g under control, and 155-408, 0.65-0.85 and 27-54g under N deficiency conditions, respectively (Figure 4.43 and 4.44). The reduction in TGN was 27% due to nitrogen deficiency, but in TKW the reduction was 1% and in PHI there was 1% increase in mean value in N deficiency than the control treatment.

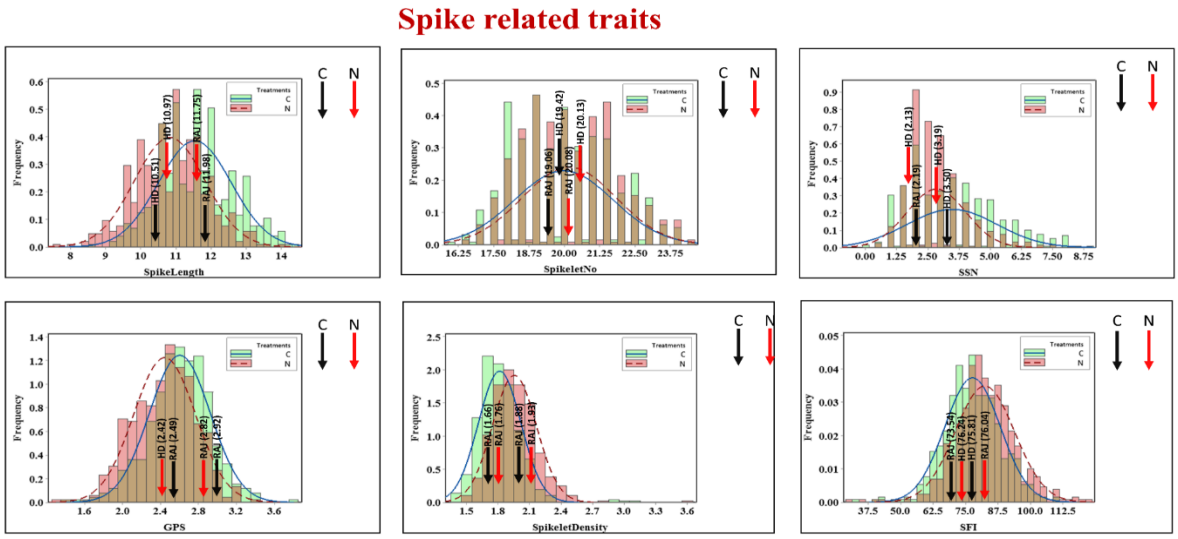

Figure 4.43: Frequency distribution of spike related traits in all the RILs.

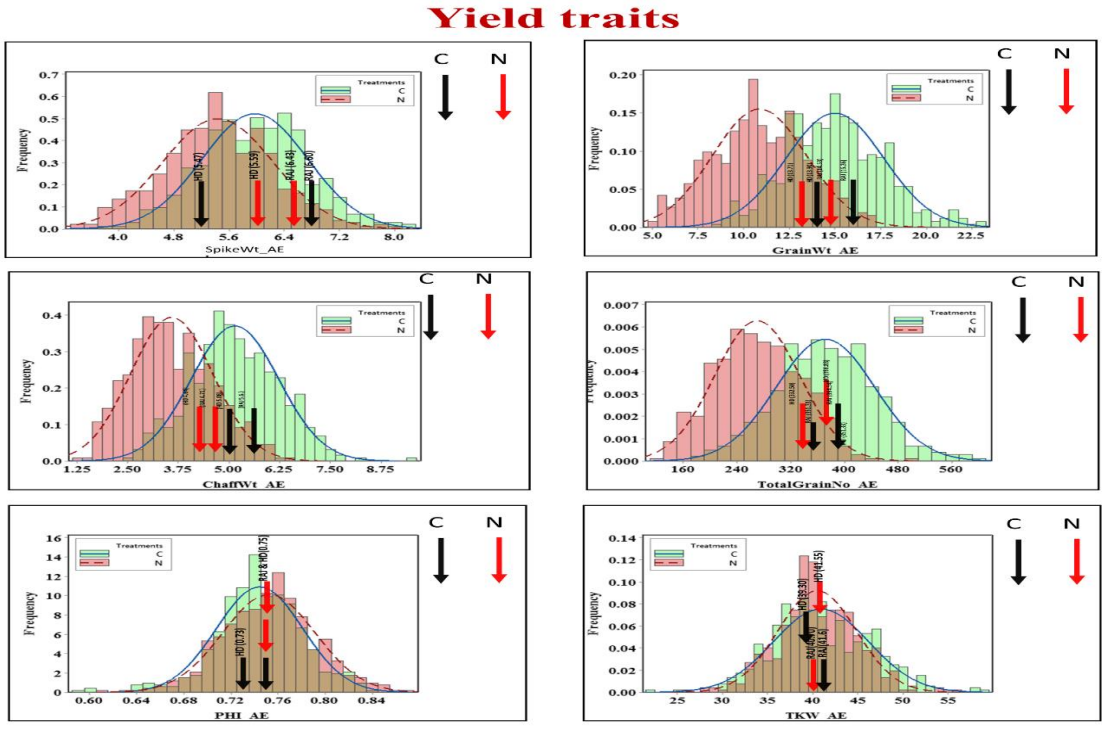

Figure 4.44: Frequency distribution of yield related traits in all the RILs.

4.1.2.5 Effect of nitrogen levels on main ear and tiller ear traits

To evaluate the effect of nitrogen deficiency on the main ear and tiller ear, we compared the yield related traits of main ear and tiller ear to identify RILs in which the main ear is close to the tiller ear (Figure 4.45).

A.

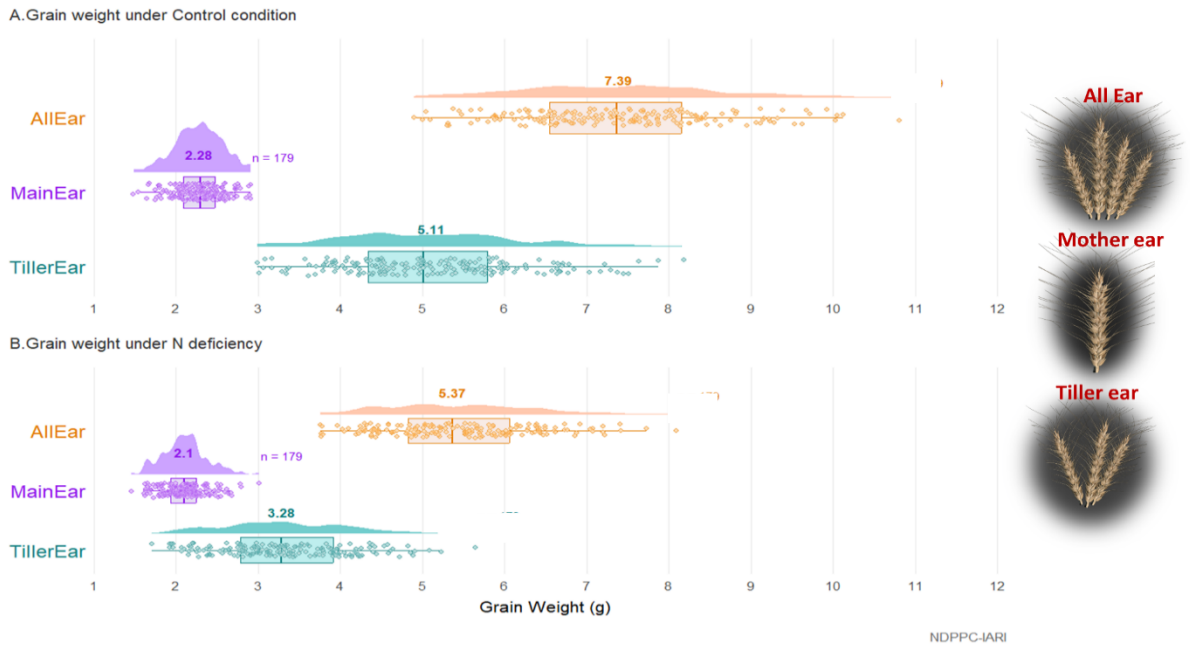

B.

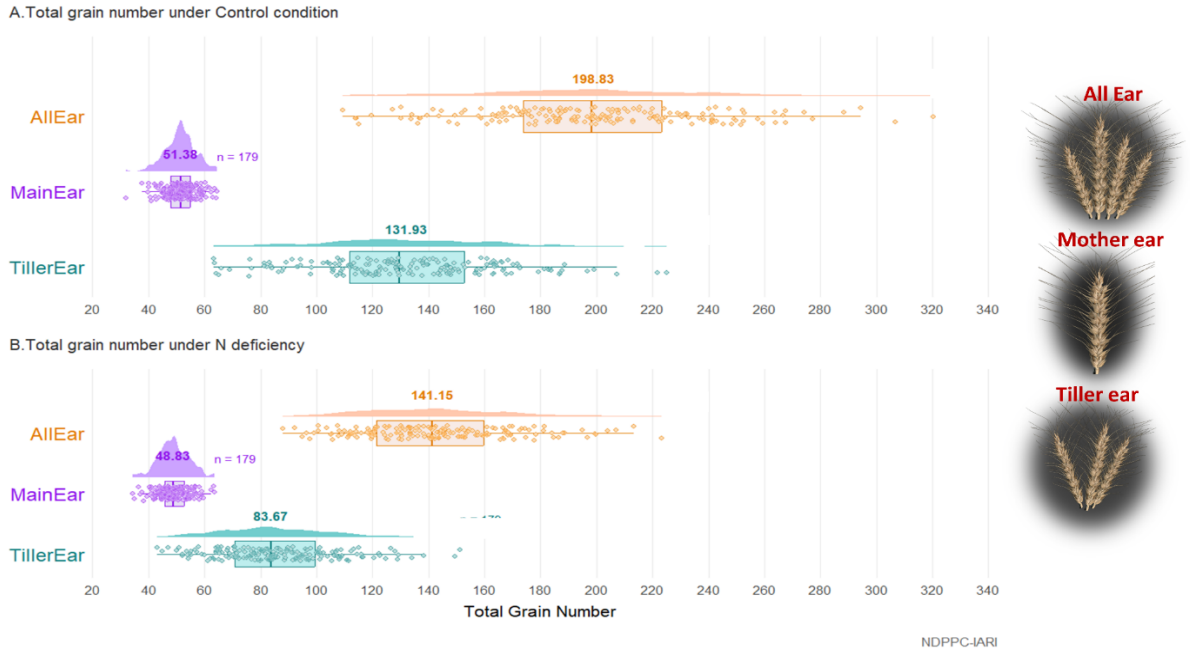

Figure 4.45: Effect of nitrogen deficiency over main ear and tiller ear with respect to grain weight and grain number of wheat RILs. A) Grain weight (GW) B) Grain number (GN).

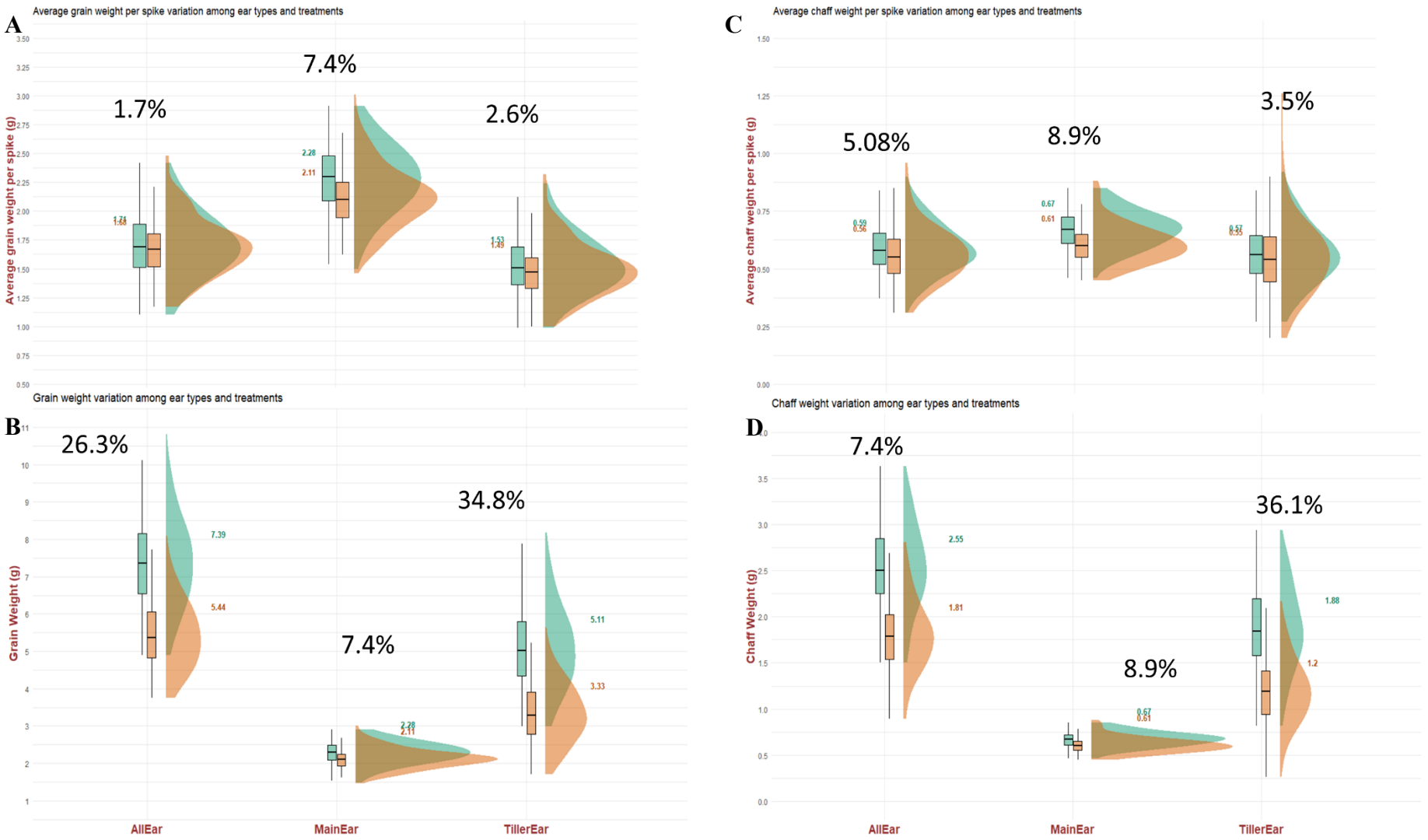

Figure 4.46: Comparison of main ear, tiller ear and all ear for N stress effect evaluation A) Average grain weight/spike B) Total grain weight/plant C) Average chaff weight/spike D) Total chaff weight/plant.

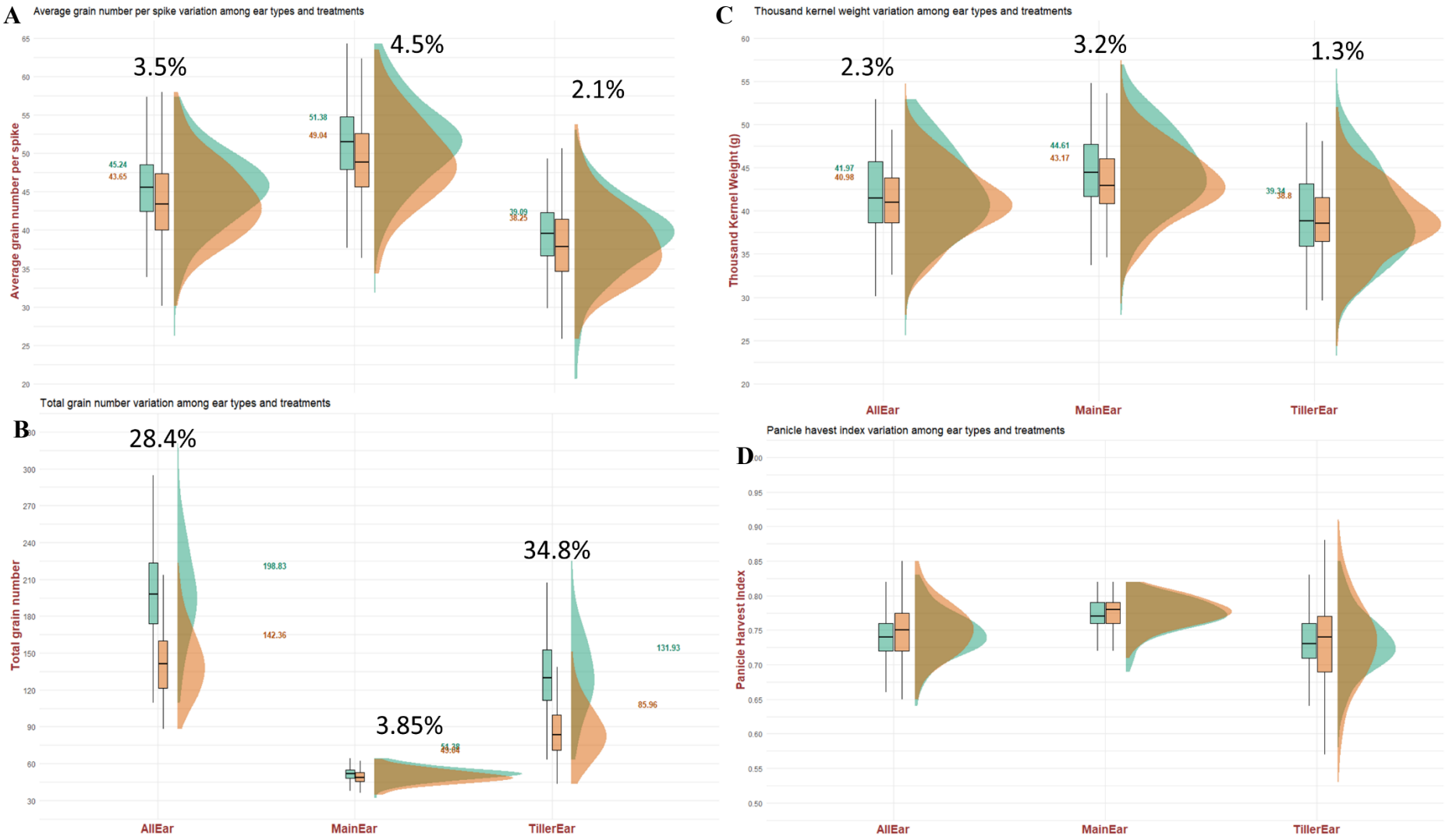

Figure 4.47: Comparison of main ear, tiller ear and all ear for N stress effect evaluation A) Average grain number/spike B) Thousand Kernel Weight C) Total grain number/plant D) Panicle Harvest Index.

We found that the overall mean value of all ear (AE), main ear (ME) and tiller ear (TE) grain weight was 7.39g, 2.28g and 5.11g under control, and 5.37g, 2.1g and 3.28g under N stress conditions, respectively. The difference in GW and GN of AE is created due to the tiller ear mainly as the number of tillers was affected by 17 % due to N deficiency (Figure 4.46 and 4.47).

Comparison of the average GW, GN, PHI and TKW of main ear and tiller ear in all the RILs revealed that that there was 7.4%, 8.9%, 4.5% and 3.2 % average reduction of GW, CW, GN and TKW due to N deficiency in a single main ear, and 2.6%, 3.5%, 2.1% and 1.3% reduction in a single tiller ear under nitrogen deficiency condition, respectively. In PHI the difference was less between control and N deficiency of about 1% but here there was increase in value under nitrogen deficiency than control (Figure 4.46 and 4.47).

4.1.3 Semi-automated phenotyping for seed trait characterization

We characterized seed parameters by semi-automated seed analyser where we took the image of all seeds of main ear and tiller ears separately, and after processing the images, we estimated the seed traits such as seed area, seed length, width, perimeter and length width ratio. We recorded all these traits for main ear and tiller ear in all the RILs (Figure 4.48 & 4.49).

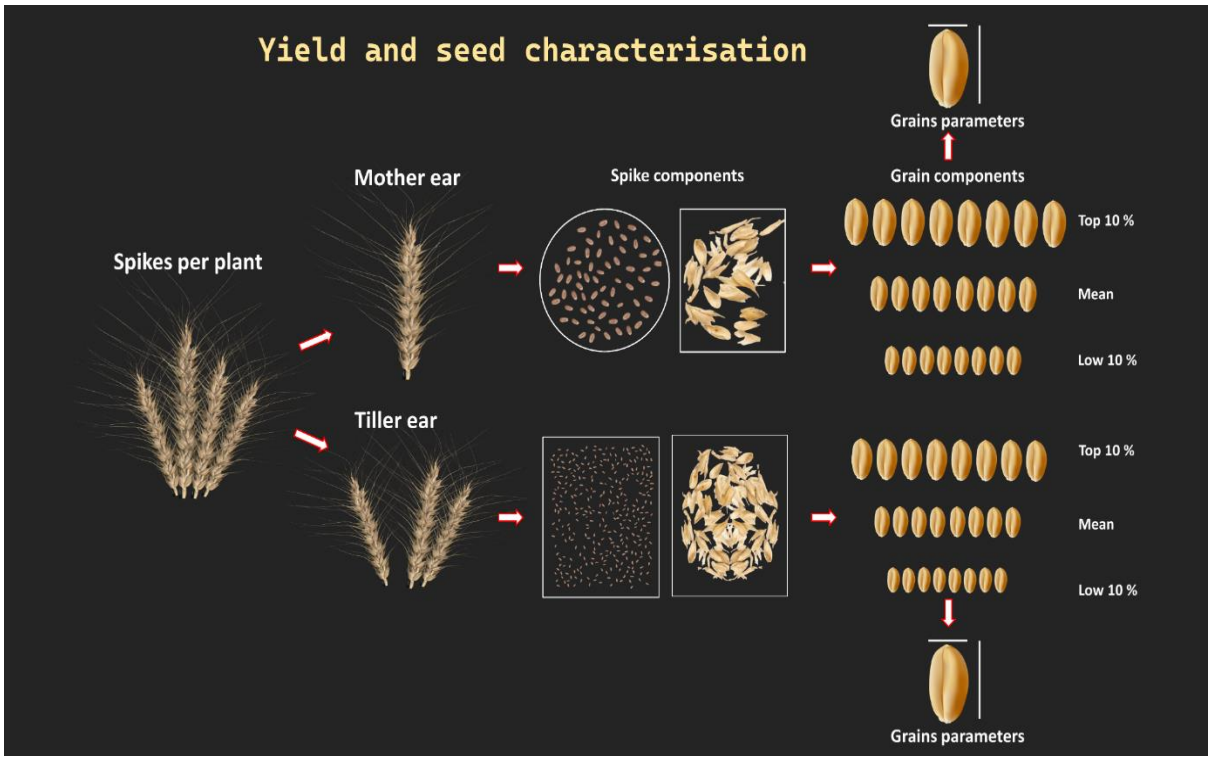

Figure 4.48: Semi-automatic seed trait characterization in wheat RILs.

All the seed morphometric parameters distributed normally and both parents had significant difference between them under both conditions. The overlapping of seed width frequency distribution of control plants with N stress was more.

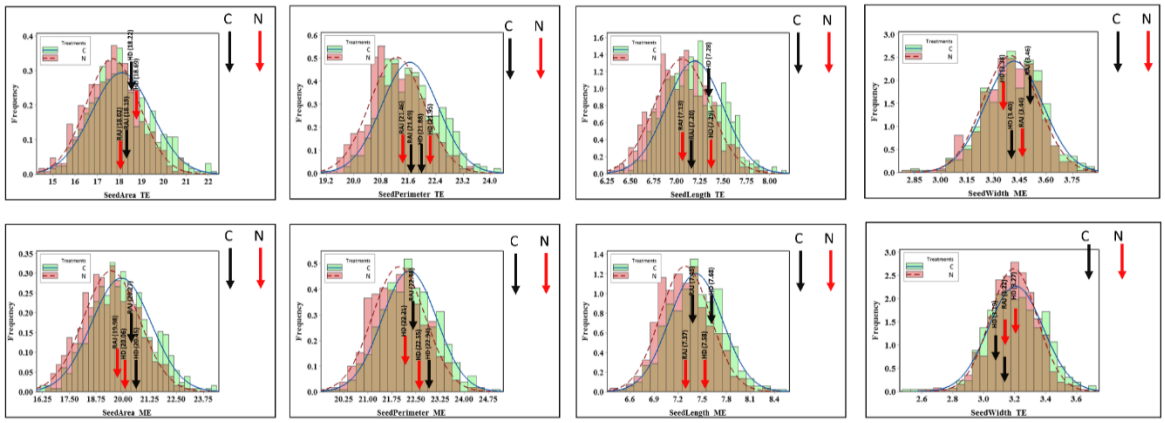

Figure 4.49: Frequency distribution and effect estimation of nitrogen deficiency on seed morphometric parameters in wheat.

4.1.4 Donor selection

We selected better RILs with higher yield, NUE and grain N concentration by MGIDI, a multivariate selection index. By implementing 15% selection intensity we selected 25 RILs with higher value for all three traits (Figure 4.50).

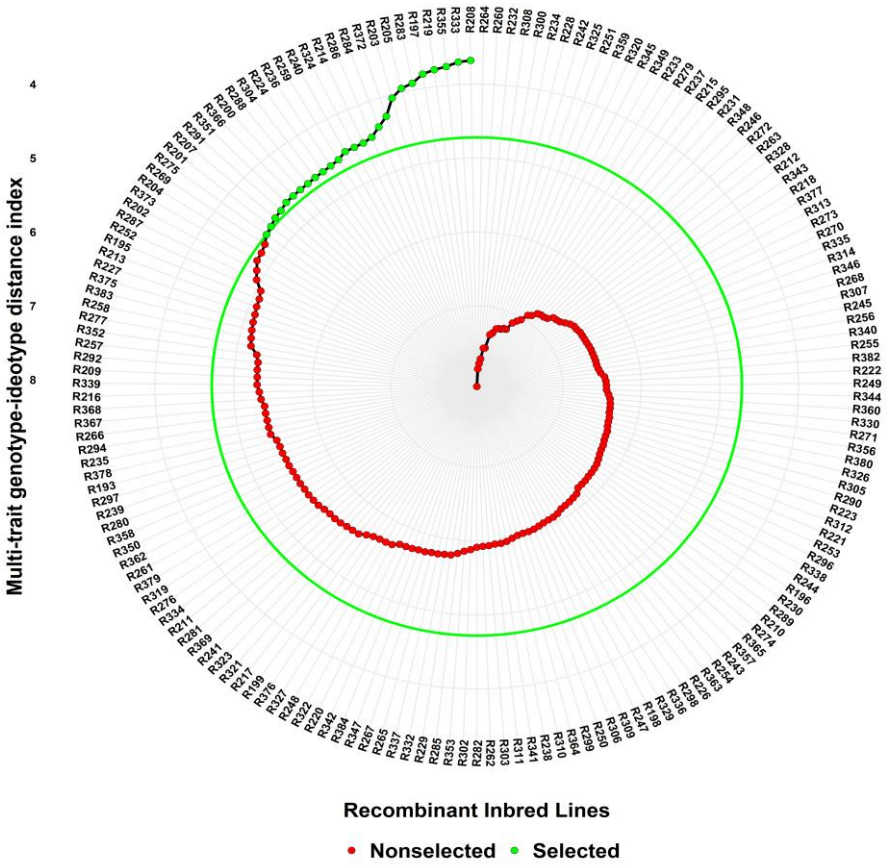

Figure 4.50: MGIDI selection index.

4.2 Genetic basis dissection of nitrogen use efficiency and component traits in wheat

NUE progress will always be constrained without enhancing the plant's genetic potential to efficiently use nitrogen, even though agronomic advancements will continue to be crucial. Wheat genotypes that sustain yield under moderate or intense nitrogen deficiency conditions can adapt to low input systems. Genetic dissection of the genomic region responsible for NUE related agronomic and physiological traits have immense importance in the development of climate-resilient and resource use efficient varieties.

To date, limited quantitative trait loci (QTL) for both yield and its response to N deficiency in wheat have been documented. Detection of genotypes and underlying QTLs for maintaining yields at low N levels are of value in wheat breeding programs designed to increase N-deficiency tolerance. We used a mapping population of RAJ 3765 × HD 2329 to identify the genomic regions associated with NUE and its component traits.

4.2.1 Linkage map construction

We genotyped 376 RILs plus the parental lines (Two replicate), by Axiom Wheat35K SNP array (Figure 4.51). The Axiom Wheat35K SNP array, also known as the 'Wheat Breeders Array', contains 35,143 SNP probes selected from Wheat820K SNP array. This new array with a large number of genome-wide polymorphic co-dominant markers for genotyping at lower cost and less computational load, has been used in several QTL studies. We aimed to prepare a subset of SNP markers from the genotyped 35K Breeder's array (Allen *et al*., 2017) under strict quality controls and extensive manual curation.

Construction of linkage map is an iterative process and till a high density, uniformly distributed markers map is prepared without any distortions, the process continues. Primary responsibility of a linkage map construction is to select good quality markers as per the population requirements. So, to select good quality SNPs from our 35K Breeder's array SNPs chipset, criteria following criteria were followed: -

- Select polymorphic marker between parents
- Chi square test for segregation distortion (alleles biased towards either parent) were done
- Segregation distortion markers tend to be clustered and hence to be removed (3 or more markers, segregation distorted regions)
- Remove SNPs with >20% missing values
- Remove SNPs that mapped into multiple locations
- Remove SNPs that parental genotype differs for replications
- Remove SNPs that one or both parents have no genotype calls

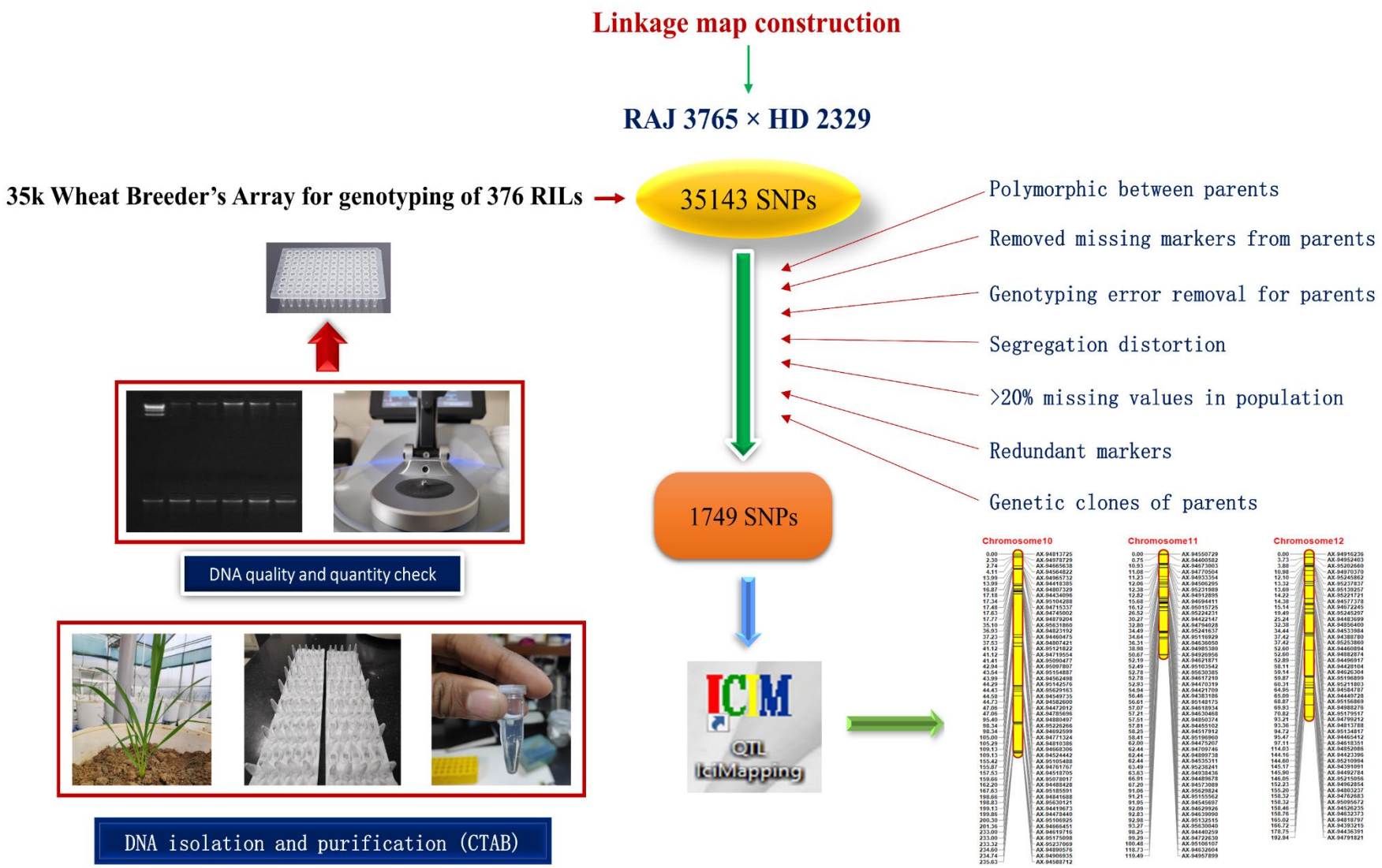

Figure 4.51: Linkage map construction for RAJ 3765 × HD 2329 population.

- Identify duplicate individuals and remove
- Check individuals genotype frequencies
- Binning of markers to remove redundancy

We used R packages R/ASMap2 and R/qtl1 to inspect the genotypic data and remove the low-quality markers and RILs to ensure that high-quality markers and genotypes are being used to construct a final linkage map. After removing lines based on high rate of missing or heterozygous observations, high similarity, high number of double crossovers and genotype similar to parents, 355 met the threshold and were used to create the genetic map. Stringent filtering removed low-quality markers and left around 4000 markers as input for linkage analysis.

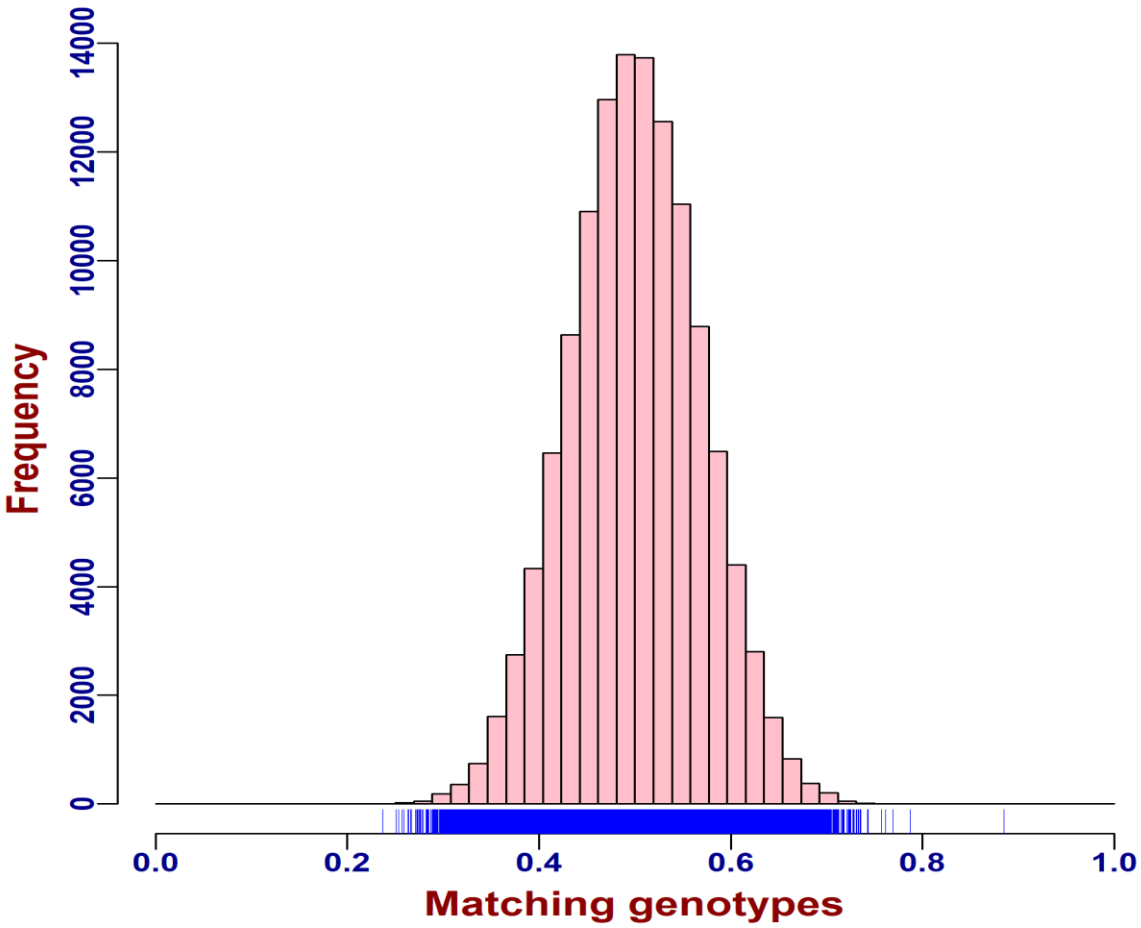

Figure 4.52: Proportion or number of matching recombinant inbred lines sharing same genotypic information. Histogram of the proportion of markers for which pairs of individuals have matching genotypes.

We compared the RILs between all pairs of individuals, in order to reveal pairs with unusually similar genotypes, which may indicate sample duplications. Function *comparegeno* in R/qtl was used to compare the genotypes for all pairs of lines to identify duplicate genotypes (Figure 4.52). The function *geno.image* was used to visualize and plot the genotypes for 355 RILs. Genotypic markers

were tested for segregation distortion (deviation expected 1:1 ratios) by Chi-squared tests. Significant distorted markers (Chi-square Test, $p < 0.01$) that deviate from expected 1:1 allelic ratio as assumed in bi-parental populations were identified and dropped using *geno.table* and *drop.markers* commands in R/qtl.

a)

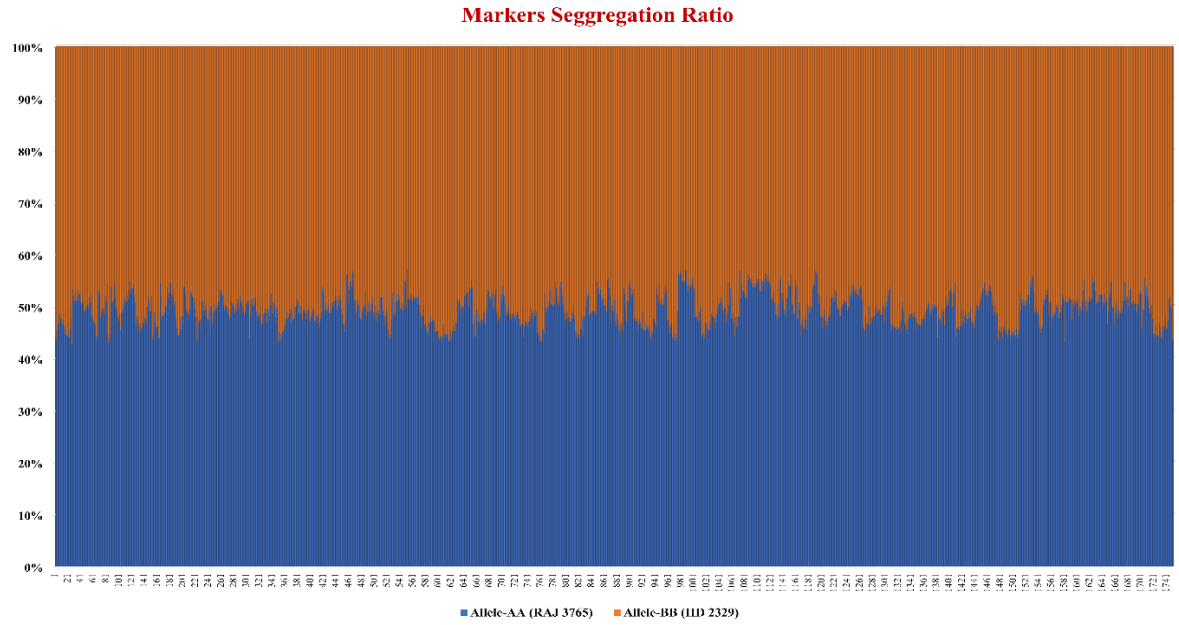

b)

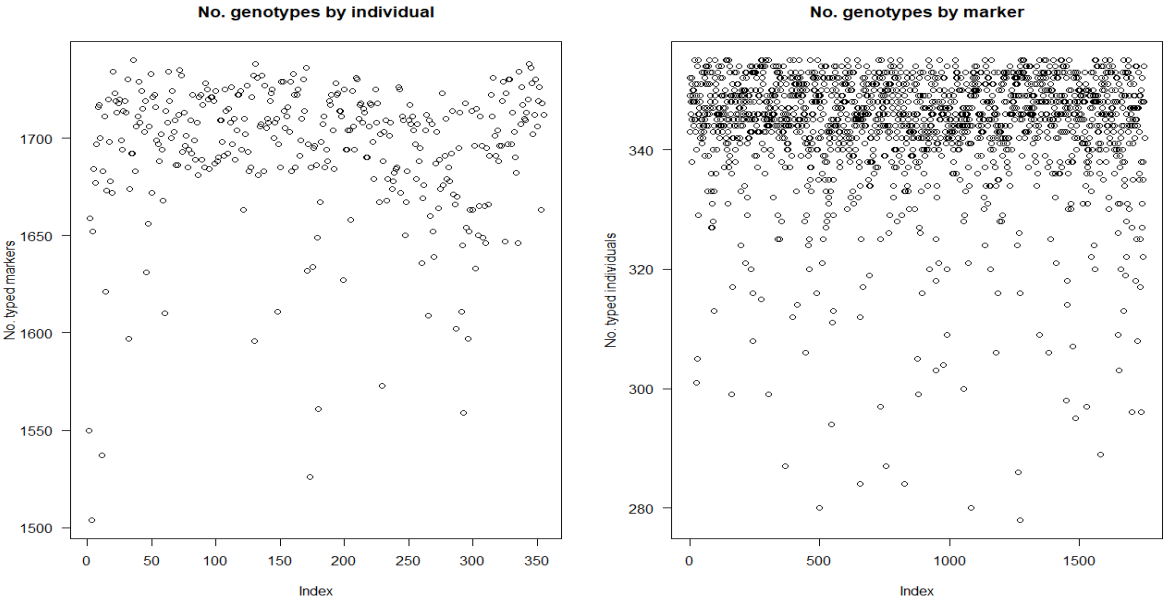

Figure 4.53: Graphical representation of genotypic data. a) Marker segregation ratio b) Plot of number of genotyped markers for each individual (left panel) and number of genotyped individuals for each marker (right panel).

Furthermore, for efficient linkage map construction and diagnosis, R/ASMap package was used to check for genotyping errors or elevated number of double recombinants. For the calculation and profiling of statistics (number of single crossovers and number of double crossovers) for genotypes, functions *statGen()* and *profileGen()* were used in R/ASMap. Similarly, *statMark()* and *profileMark()* functions were used for the calculation and profiling of statistics (double cross overs and allele proportions) associated with the markers.

a)

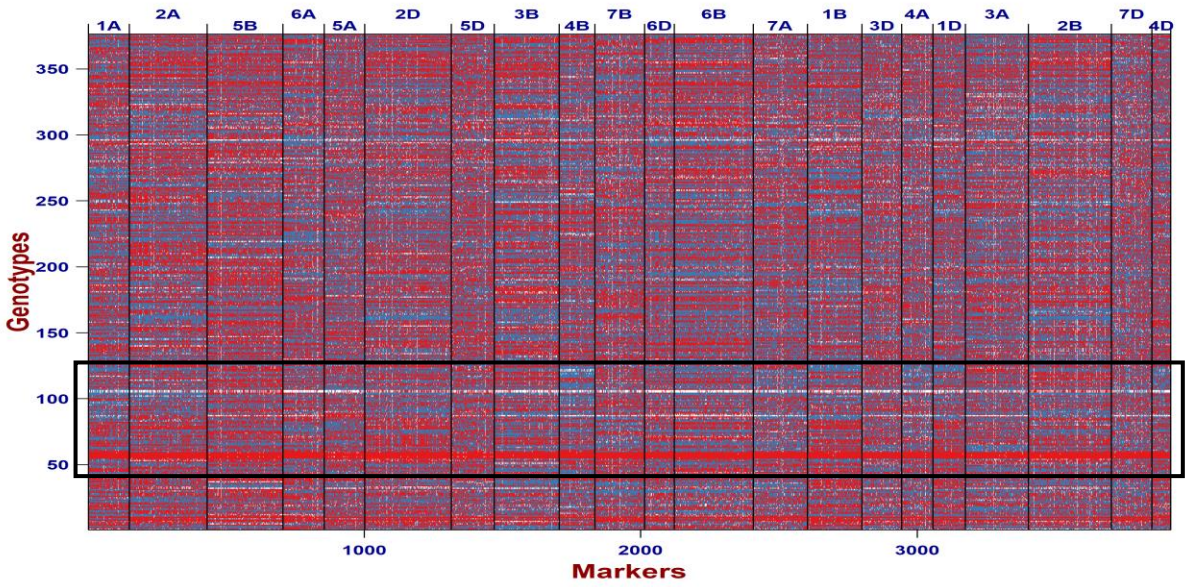

b)

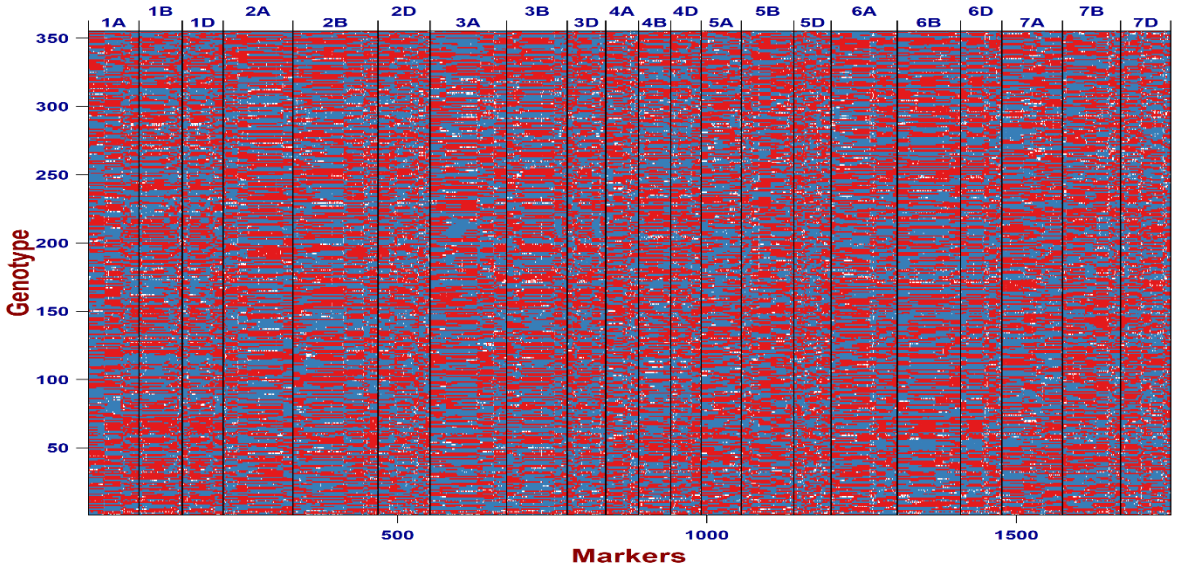

Figure 4.54: Graphical representation of markers on 21 chromosomes in 355 RILs (a) before correction and (b) after correction. The red color represents alleles from parent A (RAJ 3765),

blue color represents allele from parent B (HD 2329), and white color represents missing information. The black square box showing the duplicate individuals and individuals with higher missing values (white spots). Black vertical lines indicate the boundaries between chromosomes. Recombination blocks are clearly defined in (b) as compared to (a).

Genotypes and markers with inflated single crossovers and double crossovers were dropped using *drop.markers* and subset functions. After error correction and construction of final linkage map, all 355 genotypes were again visualized using function *geno.image* in R/qtl. Markers or genotypes with a high proportion of missing information could indicate problems with the linkage map. Markers missing from >20% individuals and genotype with >20% markers missing markers were removed. Pairwise marker linkages were studied to look for switched alleles. Alleles will be considered switched (A ↔ B) if they are tightly associated with other markers, but with recombination fractions (RFs) well above 0.5. To check for switched alleles, *checkAlleles* function was used in R/qtl, and no apparently problem was found in genotypic data.

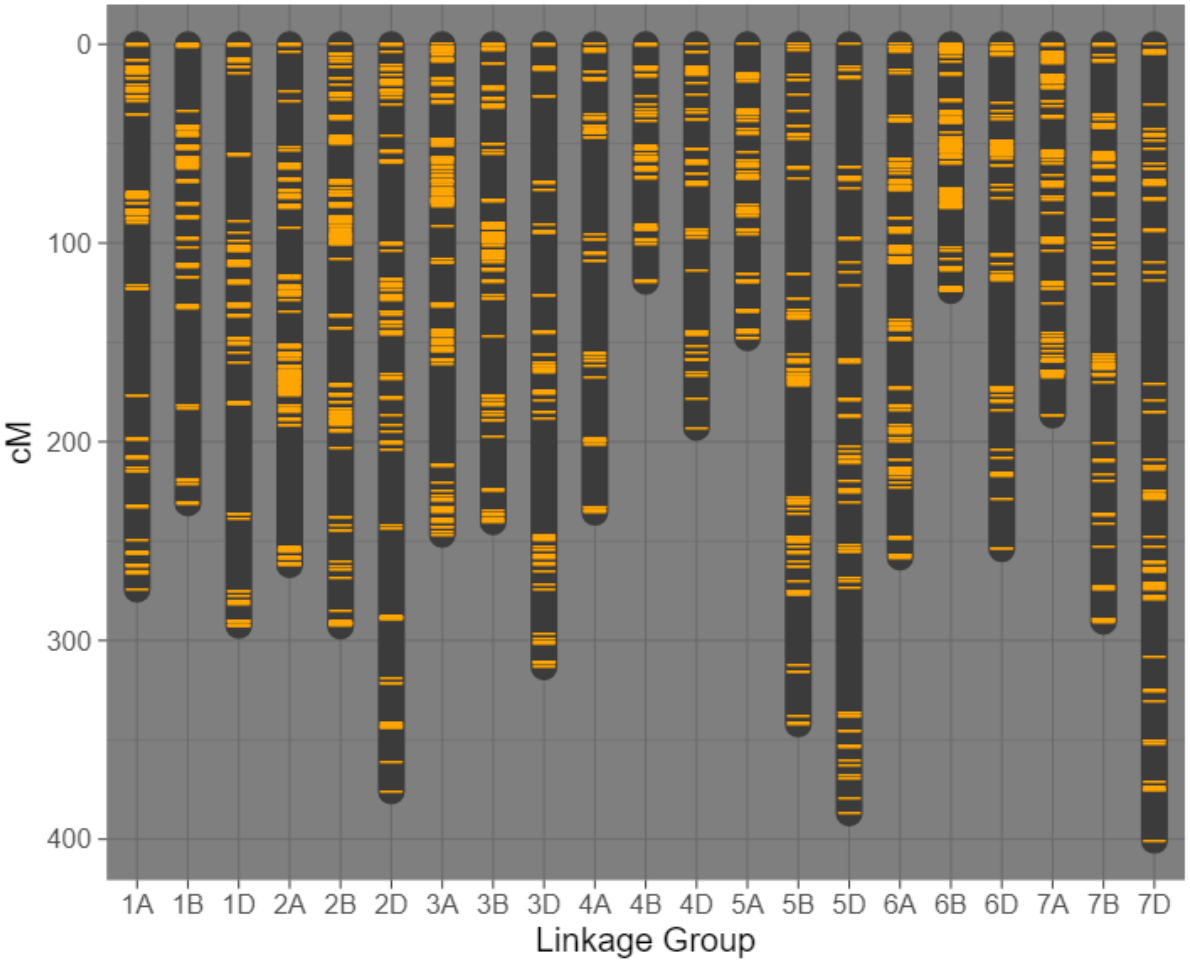

Figure 4.55: Genetic linkage maps constructed for the RIL population derived from the cross RAJ 3765×HD 2329. Linkage groups corresponding to the 21 wheat chromosomes are shown in x-axis. The y-axis shows genomic distances in cM.

Redundant markers were binned based on their pattern of segregation in the RIL population using the BIN function in IciMapping 4.1. Markers sharing segregation with at least one other were retained, and one marker was chosen to represent each bin (the marker with the least missing data, or a random marker when percentages of missing data were equal). In total 1749 markers and 355 RILs were kept from total of ~4000 markers and 376 RILs from the genotypic data after all the filtering process for final construction of linkage map. Genotypes were also visualized in Excel, and each allele was color coded using conditional formatting in Excel-2016 to display the data and check for any double recombinants. Markers were ordered using the Kosambi mapping function in the "MAP" tool in IciMapping 4.1 and a LOD score ≥ 3 after preliminary analysis. The linkage map was visualised in a single plot to compare the length and marker distribution in all the linkage groups in R (Figure 4.55) and in detailed plots by ICiM plots (Figure 4.56 to 4.62).

Table 4.3: Summary statistics of linkage map of RAJ 3765×HD 2329.

Chromosome ID	Markers	Marker %	LG Length (cM)	cM/Marker
LG-1A	82	4.69	274.32	3.35
LG-1B	70	4.00	230.99	3.30
LG-1D	66	3.77	292.52	4.43
LG-2A	113	6.46	262.04	2.32
LG-2B	137	7.83	292.93	2.14
LG-2D	84	4.80	375.90	4.48
LG-3A	124	7.09	246.80	1.99
LG-3B	98	5.60	240.46	2.45
LG-3D	62	3.54	313.47	5.06
LG-4A	53	3.03	235.63	4.45
LG-4B	52	2.97	119.49	2.30
LG-4D	49	2.80	192.94	3.94
LG-5A	65	3.72	147.88	2.28
LG-5B	85	4.86	342.14	4.03
LG-5D	60	3.43	386.96	6.45
LG-6A	107	6.12	258.23	2.41
LG-6B	102	5.83	124.15	1.22
LG-6D	67	3.83	254.08	3.79
LG-7A	98	5.60	186.79	1.91
LG-7B	94	5.37	290.56	3.09
LG-7D	81	4.63	400.70	4.95
A Genome	**642**	**36.71**	**1611.69**	**2.51**

B Genome	**638**	**36.48**	**1640.72**	**2.57**
D Genome	**469**	**26.82**	**2216.57**	**4.73**
Whole Genome	**1749**	**100.00**	**5468.98**	**3.35**

Finally, a high-density linkage map was constructed for RAJ 3765×HD 2329 population of 355 individuals with 1749 binned markers spanned over a total of 5,468 cM. Individual linkage group averaged 260 cM, ranging from 119 cM (Chromosome 4B) to 400 cM (Chromosome 7D). The average marker per chromosome was 83, ranging 49 (Chromosome 4D) to 137 (Chromosome 2B). The average cM/marker was 3.35 in the whole genome, ranging from 1.22 (Chromosome 6B) and 6.45 (Chromosome 5D). The chromosome 6B was having the highest number of markers per cM and chromosome 5D was having lowest number of markers per cM. Marker percentage was highest in chromosome 2B (7.83%) and lowest in chromosome 4D (2.8%). The A genome was covering 1611.69 cM, B genome was covering 1640.72 cM and D genome was covering 2216.57 cM by 642, 638 and 469 number of markers, respectively. The D genome was little inflated due to the smaller number of markers present and distribution was not evenly present. In the A genome the cM/marker length was 2.51, in B genome it was 2.57 and in D genome it was 4.73. It showed that marker density was higher in the A and B genome than in D genome. A genome had 36.71% markers, B genome had 36.48% and D genome had 26.82% markers.

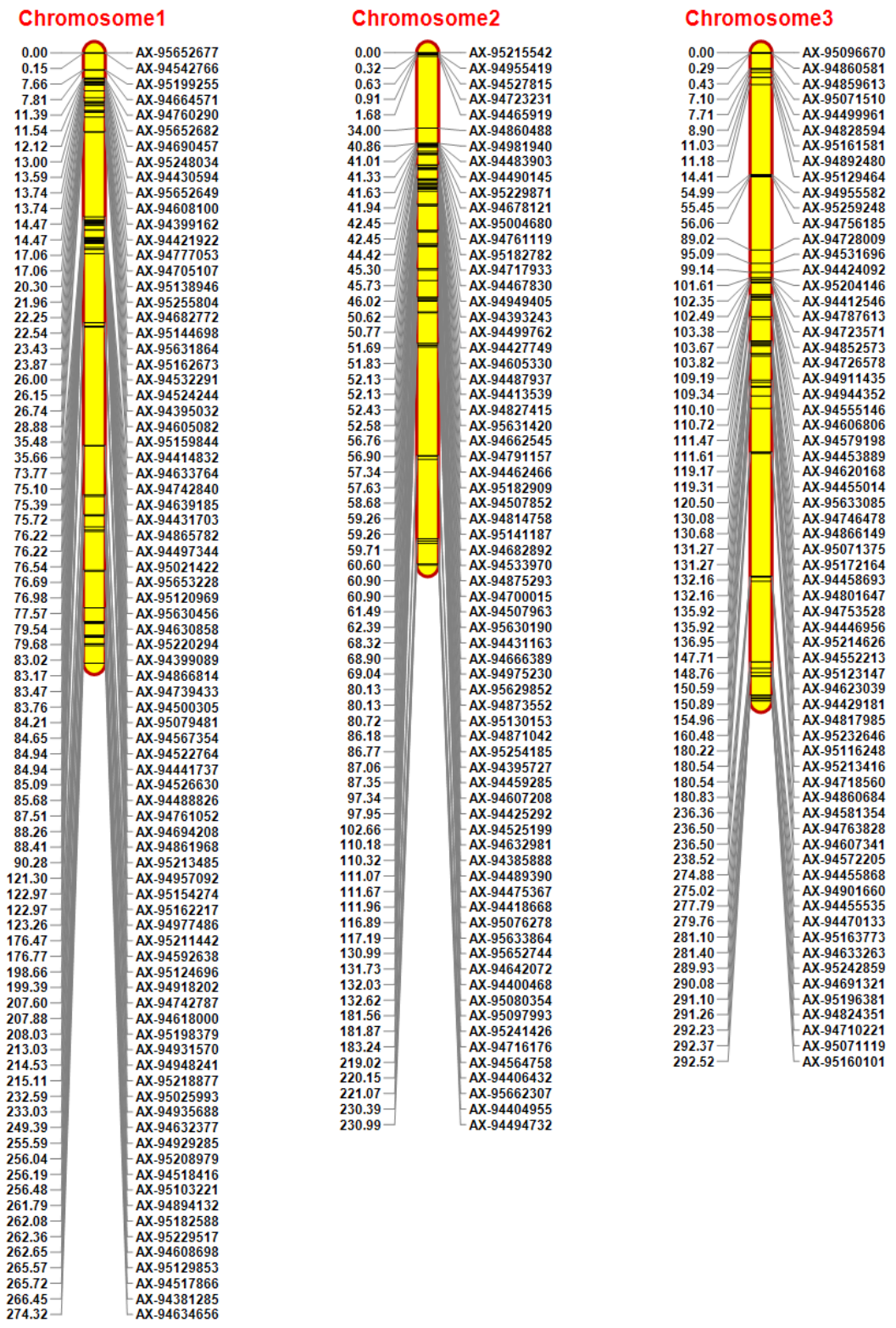

Figure 4.56: Detailed representation of linkage group 1A, 1B and 1D (Left to right).

Figure 4.57: Detailed representation of linkage group 2A, 2B and 2D (Left to right).

Figure 4.58: Detailed representation of linkage group 3A, 3B and 3D (Left to right).

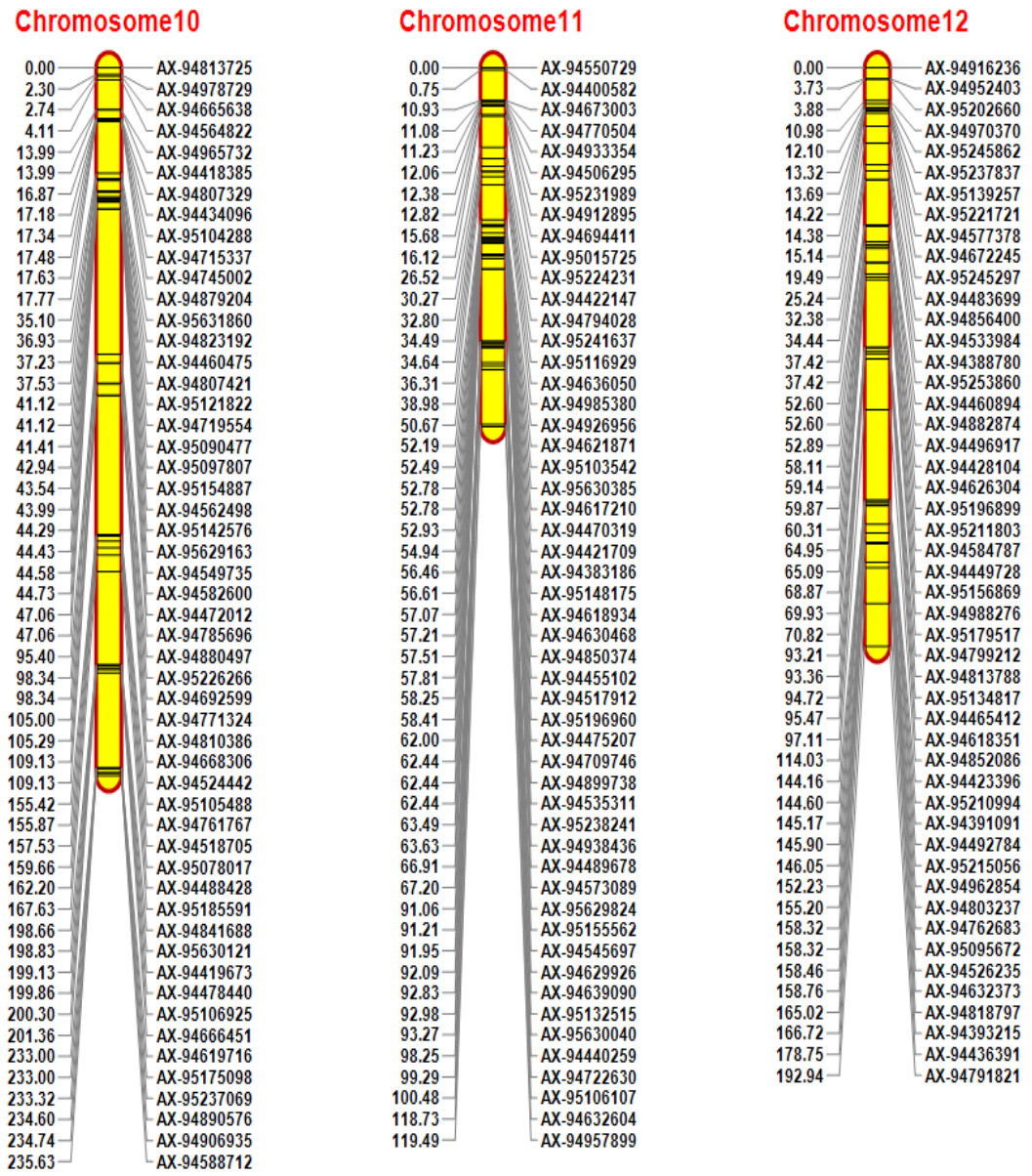

Figure 4.59: Detailed representation of linkage group 4A, 4B and 4D (Left to right).

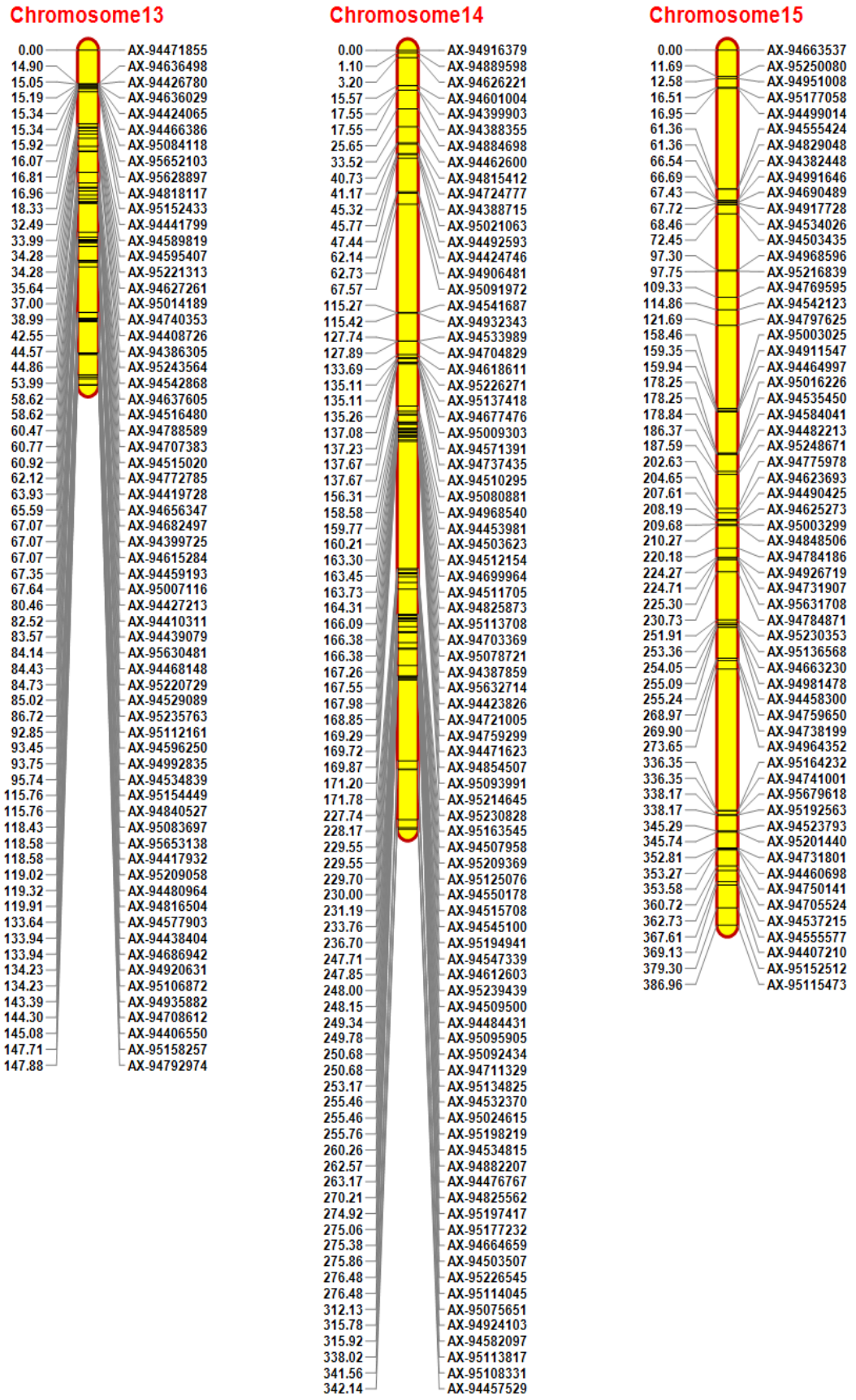

Figure 4.60: Detailed representation of linkage group 5A, 5B and 5D (Left to right).

Figure 4.61: Detailed representation of linkage group 6A, 6B and 6D (Left to right).

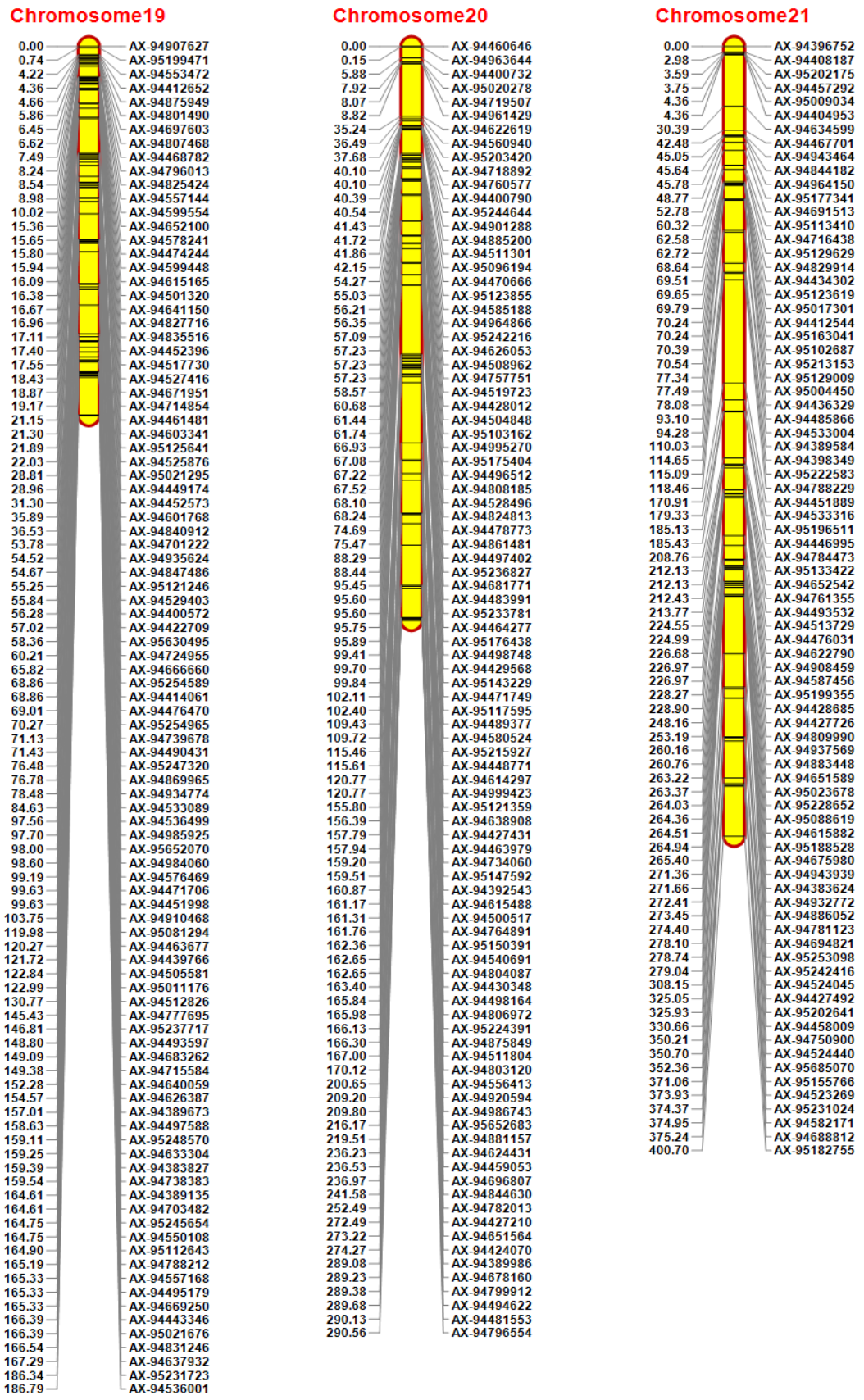

Figure 4.62: Detailed representation of linkage group 7A, 7B and 7D (Left to right).

4.2.2 The reliability of the linkage map for QTL mapping

Once a high-density linkage map is developed using high-throughput SNP markers, we wanted to make sure how accurate is the linkage map regarding for QTL mapping purposes. To evaluate the accuracy and reliability of a linkage map for QTL mapping, QTL analysis was performed for plant height under field and greenhouse condition. The main purpose to study plant height was to evaluate the quality of the high-density linkage map for further mapping purpose. We found a consistent QTL under both control and nitrogen deficiency condition in both field and greenhouse condition, namely *QpH.iari-4D*. Under field condition this QTL was having LOD value of 9.6 and 7.5 in control and nitrogen deficiency conditions with PVE of 14.4 and 12.4, respectively. Similarly, under greenhouse condition by phenomics we identified same QTL for plant height. Mapping QTL of plant height exactly on previously reported Rht region i.e., 4D, indicates linkage map constructed of high quality and reliable for QTL mapping experiments. This also emphasizes the relevance of phenomics based traits in field conditions.

4.2.3 QTL mapping for NUE and component traits

Composite interval QTL mapping by IciMapping v4.2 of all the phenomics, manual and semi-manual traits revealed a total of 554 QTLs (>3 LOD value and with 1000 permutation) on all 21 chromosomes, of which 349 QTLs were detected for phenomics traits, and 205 QTLs detected for manual and semi-manual traits. The identification of large number of QTLs were important to dissect the genetic basis of NUE related traits and nitrogen deficiency response by assessing the individual and interaction QTL effect by also by observing the pleiotropic nature and QTL × plant age interaction of the QTLs.

4.2.3.1 QTLs for Phenomics traits

In phenomics related traits, we found QTLs for most of the traits and QTLs were present in all stages. We found a total of 171 QTLs for all phenomics traits at all 5 stages under control conditions, among them 124 QTLs were unique QTLs (detected for one trait only) and 47 QTLs were pleiotropic QTLs (same QTL was identified for different traits). From these 171 QTLs, 48 QTLs were major QTLs (>3 LOD value and >10 PVE), which consisted of 22 unique and 26 multi trait QTLs. A total of 71 QTLs were found under nitrogen deficiency in all phenomics traits in 5 stages, from them 33 were unique QTLs and 38 were multi trait QTLs. Among 71 QTLs, 28 major QTLs which includes 3 unique QTLs and 25 multi trait QTLs. To identify QTLs for nitrogen deficiency response the ratio of nitrogen deficiency to control trait value was used for QTL mapping and we found 25 nitrogen response related QTLs, which includes 20 unique and 5 multi trait QTLs. In these 25 QTLs, 6 were major QTLs which includes 2 unique and 4 multi trait QTLs. These nitrogen response related QTLs have great importance which give insight into the genetic basis of plant response to nitrogen deficiency. Thus, phenomics

approach helped to bring out these QTLs to dissect the genetic basis of the nitrogen deficiency response characteristics of wheat. All details have been shown in Figure 4.63.

Phenomics QTLs

Control				Nitrogen				N response			
	Unique	Multi trait	Total		Unique	Multi trait	Total		Unique	Multi trait	Total
All QTL	124	47	171	All QTL	33	38	71	All QTL	20	5	25
Major QTL	22	26	48	Major QTL	3	25	28	Major QTL	2	4	6
	Total QTL	Major QTL			Total QTL	Major QTL			Total QTL	Major QTL	
Stage 1	33	11		Stage 1	26	11		Stage 1	12	2	
Stage 2	25	10		Stage 2	25	10		Stage 2	7	3	
Stage 3	47	20		Stage 3	27	16		Stage 3	5	2	
Stage 4	20	9		Stage 4	31	12		Stage 4	6	1	
Stage 5	21	14		Stage 5	17	8		Stage 5	5	1	
	Total QTL	Major QTL			Total QTL	Major QTL			Total QTL	Major QTL	
Stage 1	63	23		Stage 1	45	17		Stage 1	16	2	
Stage 2	52	19		Stage 2	54	24		Stage 2	20	6	
Stage 3	83	35		Stage 3	64	38		Stage 3	18	9	
Stage 4	45	23		Stage 4	69	28		Stage 4	16	2	
Stage 5	35	24		Stage 5	35	22		Stage 5	6	1	

Manual QTLs

	Control	Nitrogen	N response
	Total	Total	Total
All QTL	62	71	20
Major QTL	22	26	4

Total QTLs - 349 (Phenomics) + 205 (Manual) = 554

Figure 4.63: Number of QTLs detected under different conditions and at different growth stages.

Under control conditions, total QTLs found to be highest (47) in stage 3, while under nitrogen deficiency conditions, total QTLs number found to be highest in stage 4 (31). Under N response, the highest number of QTLs were found in stage 1 (12). The number of major QTLs were same at stage 1 and 2 under both condition (11 and 10 QTLs) and then it peaked at stage 3 (20 QTLs for control and 16 QTLs for N stress) in both control and N stress condition and then declined at stage 4 and 5 from stage 3.

We identified a total of 82 major QTLs in all 3 conditions for phenomics traits which included all types of traits such as morphometric, biomass related traits and colour related indices. Among these 82 major QTLs, 7 were pleiotropic QTLs which were associated with multiple traits found on 2B, 4B and 4D chromosomes. These 82 major QTLs were found in 17 chromosomes. Among major QTLs under control and N deficiency conditions, the highest number of QTLs were found on chromosome 4D (14 QTLs for control and 12 QTLs for N stress). The common major QTLs between control and N-deficiency were on chromosome 4B (1 QTL), 4D (5 QTLs) and 2D (1 QTL).

Table 4.4: Major QTLs identified for i-Traits under control conditions.

Traits	Chromosome	Position	LeftMarker	RightMarker	LOD	PVE (%)
AreaDistributionAboveRelative_SV_3_C	2A	158	AX-94386216	AX-94466314	5.07	17.37
AreaDistributionAboveRelative_SV_3_C	2A	52	AX-94391321	AX-94896508	3.89	17.37
R-G_TV_1_C, 2ndMomentsPrincipalAxisRatio_SV_2_C, Green_TV_3_C, Red_TV_3_C, INT_TV_3_C	4D	167	AX-94393215	AX-94436391	3.95-6.13	10.45-12.38
PSCC_2_3_C	2A	151	AX-94417025	AX-94521851	24.02	14.98
AreaDistributionAboveRelative_SV_3_C	1D	101	AX-94424092	AX-95204146	3.82	17.37
BoundaryPointsToAreaRatio_SV_1_C, AreaDistributionAboveRelative_SV_3_C	6B	77	AX-94444292	AX-95242894	6.84-21.82	16.11-17.37
2ndMomentPrincipleAxisSmallAbs_SV_1_C	4D	68	AX-94449728	AX-95156869	7.73	13.4
Ipca_SV_1_C,I1_SV_1_C	2B	195	AX-94472688	AX-94511149	10.31-10.78	10.72-11.20
AreaDistributionAboveRelative_SV_3_C	3A	239	AX-94495777	AX-94410925	9.53	17.37
2ndMomentPrincipleAxisSmallAbs_TV_2_C	6D	49	AX-94498408	AX-94909377	6.34	10.12
Blue_TV_3_C, R-G_TV_3_C, INT_TV_3_C, Compactness_SV_4_C, R-G_TV_4_C, SLR2_TV_4_C, Compactness_SV_5_C	4B	92	AX-94545697	AX-94629926	5.08-9.56	10.04-14.91
AreaDistributionAboveRelative_SV_3_C	2A	182	AX-94555534	AX-94390510	8.04	17.37
ConvexHullArea_TV_4_C, MinAreaRectangleArea_TV_4_C	4A	47	AX-94582600	AX-94472012	3.47-4.16	10.07-10.23
ObjectExtentY_TV_2_C, ObjectExtentX_SV_2_C	4D	65	AX-94584787	AX-94449728	4.08	26.06
AreaDistributionAboveRelative_SV_3_C	2A	182	AX-94555534	AX-94390510	8.04	17.37

Traits	Chromosome	Position	LeftMarker	RightMarker	LOD	PVE (%)
CenterOfMassY_SV_1_C,Excentricity_SV_1_C, SLR2_TV_1_C,Blue_TV_2_C,Green_TV_2_C, Red_TV_2_C,SLR2_TV_2_C,INT_TV_2_C	4D	162	AX-94632373	AX-94818797	5.45-6.91	10.41-16.25
BoundaryPointsToAreaRatio_SV_2_C, Compactness_TV_3_C, BoundaryPointsToAreaRatio_SV_3_C, Compactness_TV_4_C, BoundaryPointsToAreaRatio_SV_4_C	2B	291	AX-94635171	AX-94568326	4.86-5.70	12.08-15.14
AreaDistributionAboveRelative_SV_5_C	2B	6	AX-94642093	AX-94787319	4.18	30.93
AreaDistributionAboveRelative_SV_5_C	7A	20	AX-94714854	AX-94461481	4.66	15.46
Blue_TV_1_C,SLR2_SV_5_C	4D	65	AX-94584787	AX-94449728	5.24-6.05	11.54-13.69
RG_TV_2_C,Compactness_SV_3_C,C onvexHullArea_SV_3_C, ConvexHullCircumference_SV_3_C, Blue_TV_3_C,SLR2_TV_4_C	4D	166	AX-94818797	AX-94393215	4.70-8.01	10.41-13.42
PSCC_8_1_C	5B	271	AX-94825562	AX-95197417	4.7	11.8
CenterOfMassY_SV_2_C, 2ndMomentPrincipleAxisLargeAbs_SV_3_C, 2ndMomentsPrincipalAxisRatio_SV_3_C, CenterOfMassY_SV_3_C, Excentricity_SV_3_C, ObjectExtentY_SV_3_C,RG_TV_3_C, SLR2_SV_3_C,BoundaryPointsToAreaRatio_TV_4_, 2ndMomentPrincipleAxisLargeAbs_SV_4_C,	4D	138	AX-94852086	AX-94423396	3.92-10.73	5.85-27.73

Traits	Chromosome	Position	LeftMarker	RightMarker	LOD	PVE (%)
CenterOfMassY_SV_4_C,						
ConvexHullCircumference_SV_4_C,						
Excentricity_SV_4_C,						
ObjectExtentY_SV_4_C,						
RG_TV_4_C,SLR2_SV_4_C,						
2ndMomentPrincipleAxisLargeAbs_SV_5_C,						
2ndMomentsPrincipalAxisRatio_SV_5_C,						
CenterOfMassY_SV_5_C,ConvexHullArea_SV_5_C,						
ConvexHullCircumference_SV_5_C,						
Excentricity_SV_5_C,ObjectExtentY_SV_5_C						
AreaDistributionAboveRelative_SV_3_C	7B	86	AX-94861481	AX-94497402	13.34	17.37
AreaDistributionAboveRelative_SV_5_C	7D	263	AX-94883448	AX-94651589	3.9	15.46
NormalisedZRotation2ndMoment_TV_1_C,	6A	93	AX-94893553	AX-94942005	58.87-88.19	11.49-18.80
PCA2_SV_1_C						
2ndMomentPrincipleAxisSmallAbs_SV_3_C	2B	37	AX-94901457	AX-94395539	5.46	11.46
Excentricity_SV_2_C,ConvexHullArea_SV_4_C	4D	153	AX-94962854	AX-94803237	6.35-6.58	15.58-15.69
2ndMomentPrincipleAxisSmallNorm_TV_1_C,	4D	70	AX-94988276	AX-95179517	5.13-15.97	10.15-26.00
2ndMomentPrincipleAxisLargeNorm_SV_1_C,						
2ndMomentPrincipleAxisSmallNorm_SV_1_C,						
Excentricity_SV_1_C,BoundaryPointCount_TV_2_C,						
2ndMomentPrincipleAxisSmallNorm_SV_2_C,						
Excentricity_SV_2_C,ObjectExtentY_SV_2_C,						
2ndMomentPrincipleAxisLargeNorm_SV_3_C,						
Excentricity_SV_3_C,Excentricity_SV_4_C,						

Traits	Chromosome	Position	LeftMarker	RightMarker	LOD	PVE (%)
2ndMomentPrincipleAxisLargeNorm_SV_5_C, Excentricity_SV_5_C						
AreaDistributionAboveRelative_SV_3_C	6D	71	AX-94998023	AX-94958771	6.5	17.37
Circumference_SV_5_C	6B	10	AX-95013982	AX-94448837	3.97	10.06
AreaDistributionAboveRelative_SV_5_C	1B	133	AX-95080354	AX-95097993	5.2	15.46
BoundaryPointCount_TV_1_C, BoundaryPointRoundness_TV_1_C, 2ndMomentsPrincipalAxisRatio_SV_1_C, 2ndMomentPrincipleAxisLargeNorm_SV_2_C, 2ndMomentsPrincipalAxisRatio_SV_2_C, 2ndMomentPrincipleAxisSmallNorm_SV_3_C, 2ndMomentsPrincipalAxisRatio_SV_3_C, 2ndMomentPrincipleAxisLargeAbs_SV_4_C, 2ndMomentPrincipleAxisLargeNorm_SV_4_C, 2ndMomentsPrincipalAxisRatio_SV_4_C, CenterOfMassY_SV_4_C, ConvexHullCircumference_SV_4_C, ObjectExtentY_SV_4_C, 2ndMomentPrincipleAxisLargeAbs_SV_5_C, CenterOfMassY_SV_5_C, ConvexHullArea_SV_5_C, ConvexHullCircumference_SV_5_C, ObjectExtentY_SV_5_C,SLR2_TV_5_C,	4D	77	AX-95179517	AX-94799212	4.96-10.68	10.55-27.90
NIRSV_3_C	4D	95	AX-95134817	AX-94465412	8.06	12.99

Traits	Chromosome	Position	LeftMarker	RightMarker	LOD	PVE (%)
2ndMomentPrincipleAxisSmallAbs_TV_2_C	4D	60	AX-95196899	AX-95211803	7.74	12.55
2ndMomentPrincipleAxisSmallAbs_TV_1_C, AbsoluteZRotation2ndMoment_TV_1_C	4B	59	AX-95196960	AX-94475207	6.43-6.80	10.34-10.83
ConvexHullArea_TV_1_C, ObjectExtentY_TV_1_C, MinAreaRectangleArea_TV_1_C, AbsoluteZRotation2ndMoment_TV_2_C, 2ndMomentPrincipleAxisSmallAbs_SV_2_C	4D	64	AX-95211803	AX-94584787	7.46-9.04	13.23-16.85
2ndMomentsPrincipalAxisRatio_SV_4_C	4D	151	AX-95215056	AX-94962854	6.62	15.42
NIRTV_5_C	5A	85	AX-95220729	AX-94529089	4.89	14.69
AreaDistributionAboveRelative_SV_5_C	2D	304	AX-95242359	AX-94470776	4.25	30.93
AreaDistributionAboveRelative_SV_3_C	6B	80	AX-95257962	AX-94883234	4.38	17.37
2ndMomentPrincipleAxisSmallAbs_TV_1_C, ConvexHullArea_TV_1_C, ObjectExtentY_TV_1_C, AbsoluteZRotation2ndMoment_TV_1_C	6A	47	AX-95628663	AX-94531473	4.40-4.95	10.09-10.91
MinAreaRectangleArea_TV_2_C	6A	60	AX-95652375	AX-94490584	5.18	10.66
PSCC_1_3_C	2B	170	AX-95652707	AX-94790270	36.48	18.06
BoundaryPointsToAreaRatio_SV_5_C	2D	338	AX-95683514	AX-95016766	5.81	14.24

Table 4.5: Major QTLs identified for i-Traits under Nitrogen deficiency conditions.

TraitID	Chromosome	Position	LeftMarker	RightMarker	LOD	PVE (%)
2ndMomentPrincipleAxisSmallNorm_SV_1_N	6A	192	AX-94431190	AX-94575839	65.58	15.47
2ndMomentPrincipleAxisSmallNorm_SV_4_N	2B	138	AX-94464385	AX-94578476	5.09	10.11
ConvexHullArea_SV_5_N	4D	96	AX-94465412	AX-94618351	55.72	14.35
2ndMomentPrincipleAxisSmallNorm_SV_2_N	4B	67	AX-94489678	AX-94573089	9.62	20.24
SLR2_TV_3_N, BoundaryPointRoundness_SV_4_N, ConvexHullArea_SV_4_N, SLR2_TV_4_N,ObjectExtentY_TV_5_N	4B	92	AX-94545697	AX-94629926	4.71-8.00	10.75-11.34
INT_TV_4_N	4B	87	AX-94573089	AX-95629824	6.16	11.88
Gray_TV_4_N	4D	100	AX-94618351	AX-94852086	4.31	10.58
Blue_TV_2_N, Green_TV_2_N, RG_TV_2_N, INT_TV_2_N, Blue_TV_3_N, Green_TV_3_N, Red_TV_3_N, Green_SV_3_N, R-G_TV_3_N, INT_TV_3_N, Blue_TV_4_N, Green_TV_4_N,	4D	161	AX-94632373	AX-94818797	4.12-10.34	10.48-15.16

TraitID	Chromosome	Position	LeftMarker	RightMarker	LOD	PVE (%)
Green_SV_4_N, INT_TV_4_N						
Ipca_SV_3_N	6B	48	AX-94752965	AX-95242074	5.1	10.96
2ndMomentPrincipleAxisLargeNorm_SV_1_N, Excentricity_SV_1_N, SLR2_TV_3_N, SLR2_TV_4_N	4D	158	AX-94803237	AX-94762683	4.88-10.98	11.43-15.60
2ndMomentPrincipleAxisLargeNorm_SV_1_N, CenterOfMassY_SV_3_N, ConvexHullArea_SV_5_N	4D	94	AX-94813788	AX-95134817	4.60-68.02	10.34-21.17
R-G_TV_1_N	4D	166	AX-94818797	AX-94393215	4.52	10.13
Excentricity_SV_2_N, ObjectExtentY_SV_3_N, 2ndMomentPrincipleAxisLargeAbs_SV_4_N, CenterOfMassY_SV_4_N, ConvexHullCircumference_SV_4_N, ObjectExtentY_SV_4_N, 2ndMomentPrincipleAxisLargeAbs_SV_5_N, CenterOfMassY_SV_5_N, ConvexHullCircumference_SV_5_N, ObjectExtentY_SV_5_N	4D	140	AX-94852086	AX-94423396	5.06-7.82	11.97-23.66
PCA1_SV_1_N	2B	292	AX-94852490	AX-95244768	4.67	11.88
NIRTV_5_N	5B	63	AX-94906481	AX-95091972	4.35	10.56
2ndMomentPrincipleAxisSmallNorm_SV_4_N	4B	66	AX-94938436	AX-94489678	8	16.23

TraitID	Chromosome	Position	LeftMarker	RightMarker	LOD	PVE (%)
SLR2_SV_5_N	4D	155	AX-94962854	AX-94803237	6.84	12.4
2ndMomentsPrincipalAxisRatio_SV_1_N, Excentricity_SV_1_N, 2ndMomentPrincipleAxisLargeNorm_SV_2_N, 2ndMomentsPrincipalAxisRatio_SV_2_N, ConvexHullCircumference_SV_2_N, Excentricity_SV_2_N,ObjectExtentY_SV_2_N, 2ndMomentPrincipleAxisLargeNorm_SV_3_N, Excentricity_SV_3_N, 2ndMomentPrincipleAxisLargeNorm_SV_5_N, 2ndMomentsPrincipalAxisRatio_SV_5_N, Compactness_SV_5_N, Excentricity_SV_5_N	4D	70	AX-94988276	AX-95179517	4.51-19.73	10.93-16.22
BoundaryPointsToAreaRatio_TV_2_N, BoundaryPointsToAreaRatio_SV_2_N, BoundaryPointsToAreaRatio_TV_3_N, BoundaryPointRoundness_TV_4_N	2D	342	AX-95016766	AX-95654169	5.18-8.23	10.30-18.58
PSCC_15_1_N	2B	280	AX-95126899	AX-95137042	5.18	12.33
NIRSV_3_N	4D	95	AX-95134817	AX-94465412	5.9	10.72
b_SV_1_N, ExG_SV_1_N, Gray_SV_1_N	2B	288	AX-95137042	AX-94494621	5.56-6.45	13.89-15.73
2ndMomentPrincipleAxisSmallNorm_SV_1_N, Ipca_SV_2_N,Gray_TV_2_N,	6B	46	AX-95160166	AX-94829211	4.32-57.33	10.61-13.81

TraitID	Chromosome	Position	LeftMarker	RightMarker	LOD	PVE (%)
PCA2_SV_2_N,I1_SV_2_N,						
Blue_SV_3_N,Green_SV_3_N,						
Red_SV_3_N,b_TV_3_N,						
g_TV_3_N,R-B_TV_3_N,						
(R-G)/(R+G+B)_TV_3_N,						
(G-B)/(R+G+B)_TV_3_N,						
(G-B)/(R+G+B)_SV_3_N,Gray_TV_3_N,						
PCA1_TV_3_N,PCA2_SV_3_N,						
I1_SV_3_N,INT_SV_3_N						
2ndMomentsPrincipalAxisRatio_SV_2_N,						
Excentricity_SV_2_N,						
2ndMomentPrincipleAxisLargeAbs_SV_3_N,						
2ndMomentPrincipleAxisSmallNorm_SV_3_N,						
2ndMomentsPrincipalAxisRatio_SV_3_N,						
Excentricity_SV_3_N,						
2ndMomentPrincipleAxisLargeAbs_SV_4_N,						
2ndMomentPrincipleAxisLargeNorm_SV_4_N,	4D	91	AX-95179517	AX-94799212	4.54-15.84	10.29-28.62
2ndMomentsPrincipalAxisRatio_SV_4_N,						
CenterOfMassY_SV_4_N,Compactness_SV_4_N,						
ConvexHullCircumference_SV_4_N,						
Excentricity_SV_4_N,ObjectExtentY_SV_4_N,						
R-G_TV_4_N,						
2ndMomentPrincipleAxisSmallAbs_TV_5_N,						
ConvexHullArea_TV_5_N,						

TraitID	Chromosome	Position	LeftMarker	RightMarker	LOD	PVE (%)
MinAreaRectangleArea_TV_5_N,						
AbsoluteZRotation2ndMoment_TV_5_N,						
2ndMomentPrincipleAxisLargeAbs_SV_5_N,						
CenterOfMassY_SV_5_N,						
ConvexHullCircumference_SV_5_N,						
ObjectExtentY_SV_5_N,SLR1_TV_5_N,						
SLR2_TV_5_N						
CenterOfMassY_SV_3_N,	4D	148	AX-95215056	AX-94962854	4.61-5.63	10.57-13.82
ConvexHullArea_SV_4_N						
BoundaryPointRoundness_TV_1_N,	2D	343	AX-95654169	AX-94976248	6.62-10.6	15.16-22.29
BoundaryPointsToAreaRatio_TV_1_N,						
BoundaryPointsToAreaRatio_SV_1_N,						
BoundaryPointRoundness_TV_2_N,						
BoundaryPointRoundness_TV_3_N						
PSCC_14_1_N,PSCC_15_2_N,	2D	327	AX-95683514	AX-95016766	4.66-6.00	11.24-14.57
Compactness_TV_3_N						

Table 4.6: Major QTLs identified for i-Traits under N:C ratio conditions.

TraitID	Chromosome	Position	LeftMarker	RightMarker	LOD	PVE (%)
NIRSV_1_CN	6B	75	AX-94531156	AX-94878401	11.89	10.57
2ndMomentPrincipleAxisLargeNorm_SV_2_CN, BoundaryPointRoundness_TV_5_CN	7D	109	AX-94533004	AX-94389584	4.64-5.07	10.71-11.16
r_SV_2_CN, PCA2_SV_2_CN	6B	47	AX-94599546	AX-94406470	4.11-4.36	10.08-11.10
PSCC_4_3_CN,b_TV_3_CN,R-B_TV_3_CN ,(R-G)/(R+G+B)_TV_3_CN, (G-B)/(R+G+B)_TV_3_CN, (G-B)/(R+G+B)_SV_3_CN, Gray_TV_3_CN,I2_TV_3_CN	6B	48	AX-94752965	AX-95242074	4.14-5.17	10.02-12.72
CenterOfMassY_SV_2_CN, PSCC_4_2_CN,PSCC_5_2_CN, PSCC_18_3_CN,PSCC_18_4_CN, b_TV_4_CN	6B	46	AX-95160166	AX-94829211	4.04-5.18	10.18-11.77
BoundaryPointRoundness_TV_1_CN	4D	71	AX-95179517	AX-94799212	13.22	12.46

Note: The green colour text represents the same loci found for control and nitrogen condition and the red, purple and blue represents the same loci identified in manual traits QTL mapping also.

There were 51 consistent QTLs detected both under control and nitrogen deficiency conditions of which 7 were major pleiotropic QTLs (>3 LOD value and >10 PVE). We also found 2 major common QTLs between N response (N:C ratio) and control treatment, and 3 QTLs (1 major and 2 minor) common between N response (N:C ratio) and nitrogen deficiency treatment. Among the 51 common QTLs, 4 were detected in stage 1, 11 were found in stage 2, 8 were found in stage 3, 13 were detected in stage 4 and 15 were detected in stage 5. There was gradual increase in common QTLs detection as the plant age progressed.

Common QTLs were detected for iTraits namely 2ndMomentPrincipleAxisLargeNorm_SV, 2ndMomentPrincipleAxisSmallNorm_SV, 2ndMomentsPrincipalAxisRatio_SV, b_TV, Blue_TV, CenterOfMassY_SV, ConvexHullArea_SV, ConvexHullCircumference_SV, Excentricity_SV, Green_TV, INT_TV, MinAreaRectangleArea_TV, NIR_SV, ObjectExtentY, PSCC_11, Red_TV and SLR2_TV. Common QTLs for 2ndMomentPrincipleAxisLargeNorm_SV were identified in stage 3, 4 and 5, for 2ndMomentPrincipleAxisSmallNorm_SV in stage 3, for 2ndMomentsPrincipalAxisRatio_SV in stage 1 (2 QTLs), stage 2, 3 and 4 (1 QTL) and stage 5 (2 QTLs), for b_TV in stage 4, for Blue_TV in stage 2, for CenterOfMassY_SV in stage 1, 4 (2 QTLs) and 5 (2 QTLs), for ConvexHullArea_SV and TV in stage 4 and 5, respectively, for ConvexHullCircumference_SV in stage 2, 4 (2 QTLs) and 5 (2 QTLs), for Excentricity_SV in stage 1, 2, 3, 4 and 5 (2 QTLs), for Green_TV and INT_TV in stage 2, MARA_TV in stage 5, NIR_SV in stage 3 (2 QTLs), ObjectExtentY_SV in stage 2 (3 QTLs), stage 3, Stage 4 (2 QTLs) and stage 5 (2 QTLs), for PSCC_11 in stage 4, for Red_TV in stage 2 and for SLR2_TV in stage 2, 3, 4 and 5 (2 QTLs) were detected.

Table 4.7: Selected QTLs from all i-Traits, manual and semi-automatic traits with LOD >10 and PVE > 10.

QTL Grp	QTL Name	TraitID	Trait Type	Trait description	Chromosome	Position	Left Marker	Right Marker	LOD	PVE (%)	Add	Left CI	Right CI
	QSp.N. iari-2B	Spikeletno._C	**Manual**	Spikelet number per ear	**2B**	45	AX-94395539	AX-95258478	**13.37**	**13.41**	-0.627	40.5	46.5
	QUi.iari-5A	UI_TotalPlant_NC	**NUE related**	Utilisation efficiency of plant	**5A**	43	AX-94408726	AX-94386305	**3.32**	**8.95**	0.0364	39.5	44.5
	QPscc2.iari-2A	PSCC_2_3_C	**Phenomics**	colour class of plant	**2A**	151	AX-94417025	AX-94521851	**24.02**	**14.98**	222.531	149.5	151.5
	QBpar.iari-6B	BoundaryPointsToAreaRatio_SV_1_C	**Phenomics**	density of plant, biomass density, plant architecture	**6B**	77	AX-94444292	AX-95242894	**21.82**	**16.11**	0.013	76.5	77.5
QC_1	***QI1.iari-2B***	I1_SV_1_C	**Phenomics**	vegetation indices	**2B**	195	AX-94472688	AX-94511149	**10.78**	**11.20**	-2.088	194.5	196.5
QC_1	***QIpca.iari-2B***	Ipca_SV_1_C	**Phenomics**	vegetation indices	**2B**	195	AX-94472688	AX-94511149	**10.31**	**10.72**	-2.318	194.5	197.5
QC_1	***QSLwrL.iari-2B***	LWR_Low30_TE_CN	**Manual**	seed length width ratio, yield	**2B**	195	AX-94472688	AX-94511149	**32.63**	**8.42**	-0.047	194.5	196.5
	QStraw.iari-4B	Straw_N	**Manual**	plant biomass content_straw and chaff	**4B**	67	AX-94489678	AX-94573089	**14.76**	**12.95**	-1.039	65.5	67.5
	QNir.iari-6B	NIRSV_1_CN	**Phenomics**	NIR intensity-water-related	**6B**	75	AX-94531156	AX-94878401	**11.89**	**10.57**	-0.007	74.5	75.5
	QSLwrL.iari-3B	LWR_Top5_AE_N	**Manual**	seed length width ratio,yield	**3B**	227	AX-94591588	AX-94847389	**26.14**	**21.32**	0.069	224.5	229.5
	QSc.iari-6B	SeedCount_TE_N	**Manual**	Seed number per plant, yield	**6B**	47	AX-94599546	AX-94406470	**16.66**	**9.11**	28.424	46.5	47.5
	QSLwrL.iari-3A	LWR_Top5_AE_N	**Manual**	seed length width ratio, yield	**3A**	19	AX-94626189	AX-94769054	**16.88**	**11.16**	-0.050	18.5	20.5
QC_2	***QBlue.iari-4D***	Blue_TV_3_N	**Phenomics**	colour related	**4D**	161	AX-94632373	AX-94818797	**10.15**	**16.29**	1.924	158.5	163.5
QC_2	***QR-G.iari-4D***	R-G_TV_3_N	**Phenomics**	vegetation indices	**4D**	162	AX-94632373	AX-94818797	**10.34**	**19.72**	-0.580	158.5	164.5

	QUi.iari-7D	UI_TotalPlant_C	**NUE related**	Utilisation efficiency of plant	**7D**	170	AX-94788229	AX-94451889	**3.43**	**8.67**	-1.5209	145.5	174.5
	QSlr2.iari-4D	SLR2_TV_3_N	**Phenomics**	vegetation indices	**4D**	158	AX-94803237	AX-94762683	**10.98**	**15.60**	-2.023	155.5	158.5
	QOeY.iari-4D	ObjectExtentY_SV_5_C	**Phenomics**	plant height, gibberellins, morphology etc	**4D**	139	AX-94852086	AX-94423396	**10.73**	**27.73**	129.503	131.5	144.5
	QSp.N.iari-2B	Spikeletno._N	**Manual**	Spikelet number per ear	**2B**	292	AX-94852490	AX-95244768	**10.85**	**10.81**	0.531	291.5	292
	QADAR.iari-7B	AreaDistributionAboveRelative_SV_3_C	**Phenomics**	biomass, leaf area, LAI	**7B**	86	AX-94861481	AX-94497402	**13.34**	**17.37**	0.000	75.5	88.5
	QADAR.iari-7A	AreaDistributionAboveRelative_SV_3_C	**Phenomics**	biomass, leaf area, LAI	**7A**	0	AX-94907627	AX-95199471	**11.29**	**17.37**	0.000	0	0.5
	QNutE.iari-7A	NUtE_C	**NUE related**	Nitrogen utilisation efficiency	**7A**	119	AX-94910468	AX-95081294	**3.76**	**9.59**	-0.7343	110.5	120.5
	QLWRseed.iari-2A	LWR_Low30_TE_CN	**Manual**	seed length width ratio, yield, seed morphology	**2A**	177	AX-94940052	AX-94555534	**43.52**	**13.40**	0.059	176.5	177.5
QC_3	***Q2Mpasn.iari-4D***	2ndMomentPrincipleAxisSmallNorm_SV_1_C	**Phenomics**	plant architecture, biomass distribution, morphology	**4D**	70	AX-94988276	AX-95179517	**14.30**	**24.72**	0.008	68.5	70.5
QC_3	***Q2Mpasn.iari-4D***	2ndMomentPrincipleAxisSmallNorm_SV_2_C	**Phenomics**	plant architecture, biomass distribution, morphology	**4D**	70	AX-94988276	AX-95179517	**14.18**	**26.00**	0.007	68.5	70.5
QC_3	***QCHC.iari-4D***	ConvexHullCircumference_SV_2_N	**Phenomics**	plant area, morphology, growth, biomass	**4D**	70	AX-94988276	AX-95179517	**19.73**	**13.03**	-270.754	69.5	70.5
QC_3	***QOeY.iari-4D***	ObjectExtentY_SV_2_C	**Phenomics**	plant height, gibberellins, morphology etc	**4D**	70	AX-94988276	AX-95179517	**15.97**	**16.72**	-109.000	69.5	70.5
QC_3	***QOeY.iari-4D***	ObjectExtentY_SV_2_N	**Phenomics**	plant height, gibberellins, morphology etc	**4D**	70	AX-94988276	AX-95179517	**18.20**	**16.22**	-122.326	69.5	70.5
QC_4	***Qcompactness.iari-6A***	Compactness_SV_3_N	**Phenomics**	plant density, plant thickness, biomass distribution,erect	**6A**	190	AX-95010403	AX-94431190	**10.13**	**13.39**	0.017	186.5	192.5
QC_4	***Qcompactness.iari-6A***	Compactness_SV_4_N	**Phenomics**	plant density, plant thickness, biomass distribution,erect	**6A**	191	AX-95010403	AX-94431190	**11.38**	**11.73**	0.018	186.5	192.5
QC_5	***QSdensity.iari-7A***	SpikeletDensity_C	**Manual**	number of spikelets per cm of spike, spike morphology	**7A**	129	AX-95011176	AX-94512826	**11.55**	**20.60**	-0.086	126.5	132.5

QC_5	***QSp.N.iari-7A***	Spikeletno._C	**Manual**	Spikelet number per ear	**7A**	130	AX-95011176	AX-94512826	**25.36**	**31.15**	-0.953	128.5	130.5
QC_5	***QSp.N.iari-7A***	Spikeletno._N	**Manual**	Spikelet number per ear	**7A**	130	AX-95011176	AX-94512826	**26.52**	**35.14**	-0.957	127.5	133.5
QC_6	***Q2Mpaln.iari-4D***	2ndMomentPrincipleAxisLargeNorm_SV_4_C	**Phenomics**	plant architecture, biomass distribution, morphology	**4D**	78	AX-95179517	AX-94799212	**10.68**	**21.97**	-0.111	71.5	84.5
QC_6	***Q2Mpasn.iari-4D***	2ndMomentPrincipleAxisSmallNorm_SV_3_C	**Phenomics**	plant architecture, biomass distribution, morphology	**4D**	76	AX-95179517	AX-94799212	**10.62**	**23.26**	0.006	71.5	82.5
QC_6	***Q2Mpasn.iari-4D***	2ndMomentPrincipleAxisSmallNorm_SV_3_N	**Phenomics**	plant architecture, biomass distribution, morphology	**4D**	76	AX-95179517	AX-94799212	**12.46**	**26.10**	0.007	71.5	81.5
QC_6	***Q2Mpar.iari-4D***	2ndMomentsPrincipalAxisRatio_SV_1_C	**Phenomics**	plant morphology, density, thickness	**4D**	78	AX-95179517	AX-94799212	**13.12**	**27.90**	-1.213	72.5	83.5
QC_6	***Q2Mpar.iari-4D***	2ndMomentsPrincipalAxisRatio_SV_3_N	**Phenomics**	plant morphology, density, thickness	**4D**	81	AX-95179517	AX-94799212	**12.02**	**26.84**	-2.056	73.5	88.5
QC_6	***Q2Mpar.iari-4D***	2ndMomentsPrincipalAxisRatio_SV_4_N	**Phenomics**	plant morphology, density, thickness	**4D**	81	AX-95179517	AX-94799212	**14.81**	**26.95**	-2.443	75.5	87.5
QC_6	***QBPR.iari-4D***	BoundaryPointRoundness_TV_1_CN	**Phenomics**	plant density, plant thickness, biomass distribution,erect	**4D**	71	AX-95179517	AX-94799212	**13.22**	**12.46**	-0.087	69.5	76.5
QC_6	***Qecc.iari-4D***	Excentricity_SV_4_N	**Phenomics**	plant density, plant thickness, biomass distribution,erect	**4D**	83	AX-95179517	AX-94799212	**15.84**	**28.62**	-0.076	77.5	88.5
QC_6	***QFL.Ear.iari-4D***	FLtoEarlength_C	**Manual**	flag leaf to ear distance, sugar transport, plant height	**4D**	75	AX-95179517	AX-94799212	**17.49**	**31.59**	-2.834	69.5	80.5
QC_6	***QFL.Ear.iari-4D***	FLtoEarlength_N	**Manual**	flag leaf to ear distance, sugar transport, plant height	**4D**	80	AX-95179517	AX-94799212	**17.07**	**28.40**	-3.645	74.5	85.5
QC_6	***QVI.iari-4D***	SLR1_TV_5_N	**Phenomics**	vegetation indices	**4D**	77	AX-95179517	AX-94799212	**11.47**	**20.17**	3.006	70.5	82.5
	QGrainN.iari-1A	Grain_N%_C	**NUE related**	Grain Nitrogen percentage	**1A**	0	AX-95652677	AX-94542766	**3.35**	**8.45**	0.1027	0	0.5
	QPSCC1.iari-2B	PSCC_1_3_C	**Phenomics**	colour class of plant	**2B**	170	AX-95652707	AX-94790270	**36.48**	**18.06**	-121.671	167.5	171.5

QC_7	***QBpar.iari-2D***	BoundaryPoints ToAreaRatio_S V_1_N	**Phenomics**	density of plant, biomass density, plant architecture	**2D**	343	AX-95654169	AX-94976248	**10.86**	**22.29**	-0.007	341.5	343.5
QC_7	***QPHI.iari-2D***	PHI_ME_N	**Manual**	yield, spike trait, panicle harvest index	**2D**	343	AX-95654169	AX-94976248	**37.38**	**24.10**	-0.020	341.5	343.5

Similarly, common QTLs between Nitrogen response (N:C ratio) and control were 2ndMomentsPrincipalAxisRatio_SV in stage 2 (LOD: 3.9-4.6 and PVE 9.7-11.8) on Chromosome 4D and BoundaryPointRoundness_TV in stage 1 (LOD: 7.79-13.22 and PVE 12.46-17.63). The 3 common QTLs between N response and N stress were 2ndMomentsPrincipalAxisRatio_SV in stage 1 (LOD: 3.39-6.44 and PVE 6.99-13.15), PSCC_12 in stage 5 (LOD: 3.41-3.52 and PVE 7.58-8.21) and PSCC_8 in stage 3 (LOD: 3.76-4.13 and PVE 8.19-9.08).

The QTLs with LOD value more than 10 and phenotypic variation explained (PVE) more than 10 were selected for further analysis. There were 14 QTLs for i-Traits that were having value above the described threshold and they were located on chromosome 2A, 2B, 2D, 4D, 6A, 6B, 6D, 7A and 7B. There were 9 were single trait QTLs and 5 were multi trait QTLs. The single trait QTLs were *QPscc2.iari-2A* (LOD: 24.02 and PVE: 14.98), *QBpar.iari-6B* (LOD: 21.82 and PVE: 16.11), *QNir.iari-6B* (LOD: 11.89 and PVE: 10.57), *QSlr2.iari-4D* (LOD: 10.98 and PVE: 15.60), *QOeY.iari-4D* (LOD: 10.73 and PVE: 27.73), *QADAR.iari-7B* (LOD: 13.34 and PVE: 17.37), *QADAR.iari-7A* (LOD: 11.29 and PVE: 17.37), *QPSCC1.iari-2B* (LOD: 36.48 and PVE: 18.06) *and QBpar.iari-2D* (LOD: 10.86 and PVE: 22.29).

Among the 5 multi trait QTLs, one QTL was on chromosome 2B for two RGB based vegetation indices traits namely *QI1.iari-2B* (LOD: 10.78 and PVE: 11.20) and *QIpca.iari-2B* (LOD: 10.31 and PVE: 10.72), one was on chromosome 4D for two RGB based vegetation indices traits namely *QBlue.iari-4D* (LOD: 10.15 and PVE: 16.29) and *QR-G.iari-4D* (LOD: 10.34 and PVE: 19.72) and one more was on chromosome 4D for three morphometric trait namely 2MPASN_SV (Stage 1 & 2), ConvexHullCircumference_SV (Stage 2) and ObjectExtentY_SV (Stage 2 - Control & N stress) and the QTLs name were *Q2Mpasn.iari-4D* (LOD: 14.30 and PVE: 24.72), *Q2Mpasn.iari-4D* (LOD: 14.18 and PVE: 26), *QCHC.iari-4D* (LOD: 19.73 and PVE: 13.03), *QOeY.iari-4D* (LOD: 15.97 and PVE: 16.72), *QOeY.iari-4D* (LOD: 18.20 and PVE: 16.22). From remaining two QTLs, one was present on chromosome 6A for Compactness_SV (Stage 3 & 4) namely *Qcompactness.iari-6A* (LOD: 10.13 and PVE: 13.39) and *Qcompactness.iari-6A* (LOD: 11.38 and PVE: 11.73) and one more was present on chromosome 4D for five morphometric traits and one RGB indices namely *Qcompactness.iari-6A, Qcompactness.iari-6A, Q2Mpaln.iari-4D, Q2Mpasn.iari-4D, Q2Mpasn.iari-4D, Q2Mpar.iari-4D, Q2Mpar.iari-4D, Q2Mpar.iari-4D, QBPR.iari-4D, Qecc.iari-4D, QVI.iari-4D* with LOD value ranging from 10.62 to 15.84 and PVE ranging from 12 to 28.

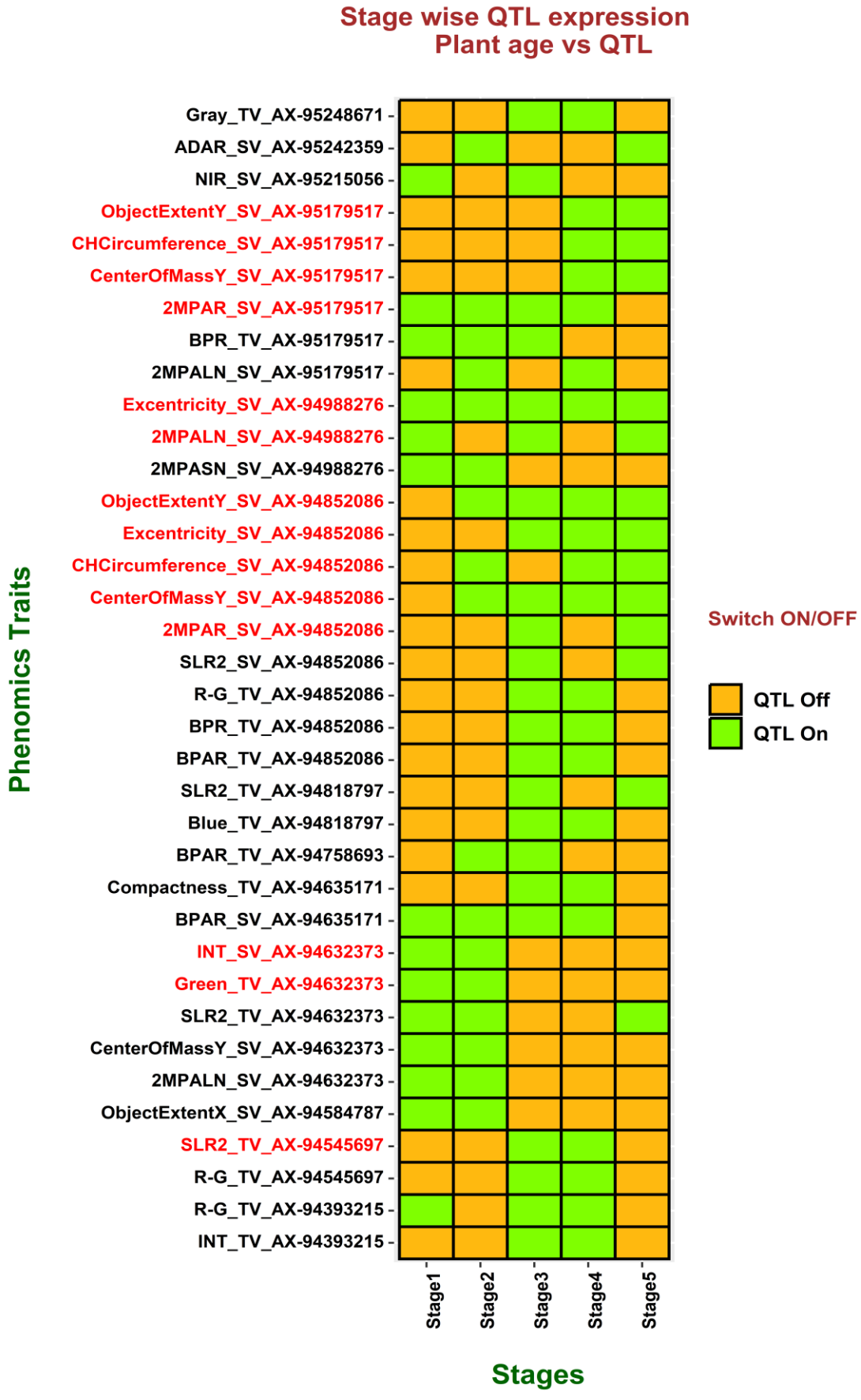

Figure 4.64: QTL interaction with plant age under control conditions.

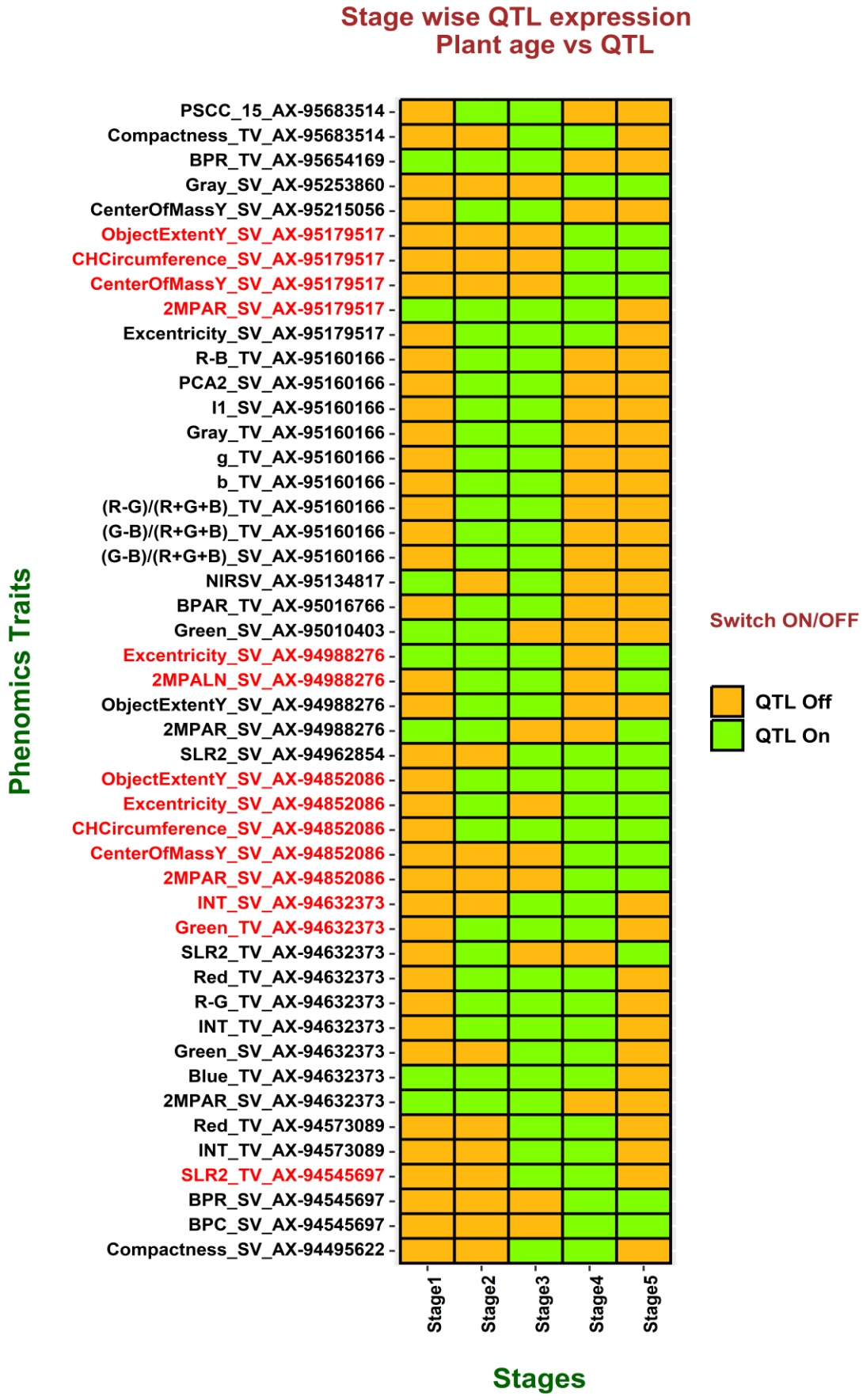

Figure 4.65: QTL interaction with plant age under nitrogen deficiency conditions.

4.2.3.2 Plant age and QTL interaction detected by phenomics traits

To see the interaction of QTLs and plant age we selected those i-Traits QTLs which were expressed more than once in 5 stages and plotted them stage wise to see how their appearance occurred throughout the plant life and also highlighted the common QTLs between control and N deficiency (Figure 4.64 and 4.65). Total 36 and 47 QTLs were identified which expressed in two or more times in 5 stages of plants under control and N stress conditions, respectively, on chromosome 2B, 2D, 3B, 4B, 4D, 5D, 6A, 6B and 6D. Among these highest number of QTLs was observed in chromosome 4D (56 QTLs), followed by 6B (9 QTLs), 4B (7 QTLs), 2D (5 QTLs), 2B (2 QTLs) and one QTL each on 3B, 5D, 6A and 6D (Figure 4.64). Among the QTLs that expressed in multiple stages, 14 common QTLs for both the conditions were present on chromosome 4D and 4B (Figure 4.64 and 4.65). The QTLs which expressed in first two stages are regarded as early-stage QTLs, and those expressed in the later 3 stages were regarded as late-stage QTLs. As per the interaction effect of QTLs to plant age under control conditions from 36 QTLs, we identified 8 early-stage (Expressed in at least 2 stages among stage 1-3), transient (Appeared then disappeared) QTLs and 15 late-stage (Expressed in at least 2 stages among stage 3-5) transient QTLs. We also found 3 consistent stable QTLs (Expressed in at least 3 stages successively among stage 1-5) and 3 transient stable QTLs (Expressed in at least 3 stages among stage 1-5) for i-Traits namely BPR_TV, Eccentricity_SV & SLR2_TV and 2MPALN_SV, CHCircumference_SV and R-G_TV, respectively. Then there were 5 deterministic stable QTLs (Expressed consecutively in at least 4 or 5 stages among stage 1-5) for i-Traits namely 2MPAR_SV, Eccentricity_SV, ObjectExtentY_SV, CentreOfMassY_SV and BPAR_SV. Also, there were 2 inconsistent transient QTL expresses one time at early-stage (first 2 stage) and another time at last-stage (last 2 stage).

In case of nitrogen deficiency conditions, there were 47 QTLs among which 17 were early-stage transient QTLs, 15 were late-stage transient QTLs, 7 consistent stable QTLs, 3 transient stable QTLs and 5 deterministic stable QTLs. The 5 deterministic stable QTLs were for traits like 2MPAR_SV, Eccentricity_SV, ObjectExtentY_SV, CHCircumference_SV and Blue_TV on chromosome 4D (Figure 4.65). There were 4 common deterministic stable QTLs between control and nitrogen deficiency conditions which were for 2MPAR_SV, Excentricity_SV, ObjectExtentY_SV and CHCircumference_SV on chromosome 4D.

To see the QTL detection ability of a plant under different growth stages by observing the phenotypic effect of plants and traits, we plotted QTLs detected at each stage of plant for a set of image-based traits where we observed multiple QTLs at different time points. When we plotted the i-Traits stagewise we observed that among 22 and 21 i-traits under control and N stress conditions, 14 traits were common between both conditions.

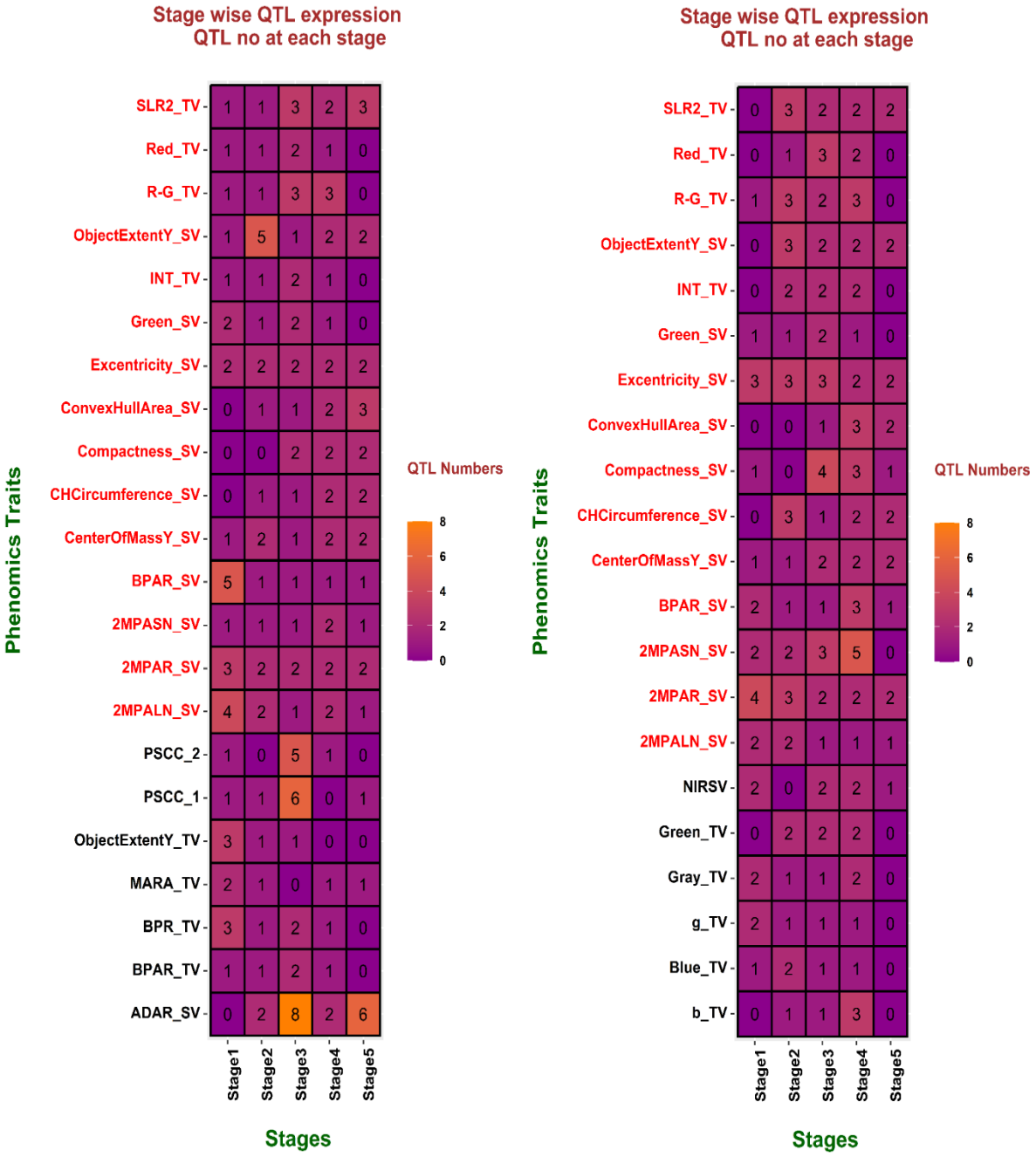

Figure 4.66: Multiple number of QTLs expressed at each stage for different traits.

Under control conditions, high number of QTLs were observed in ADAR_SV, ObjectExtentY_SV, 2MPAR_SV SLR2 and low number of QTLs were found in BPAR_TV_C, INT_TV_C, MARA_TV_C, ObjectExtentY_TV_C. Traits such as BPAR_SV, 2MPAR_SV, 2MPALN_SV, ObjectExtentY_TV and BPR_TV had higher number of QTLs in the first stages and traits such as ADAR_SV, PSCC_1 & 2, SLR2_TV, R-G_TV had higher number QTLs at stage 3 (Figure 4.66). Under N stress conditions, Eccentricity_SV, 2MPAR_SV, 2MPASN_SV, SLR2_TV and R-G_TV had high number of QTLs, while b_TV, Blue_TV, g_TV and Green_SV had lower number of QTLs.

4.2.3.3 QTLs for manual and semi-automatic traits

We identified 62 QTLs under control conditions, 71 QTLs under N stress conditions and 20 QTLs for N-response related traits. From these QTLs, 22 were major QTLs under control condition, 26 were major QTLs under N stress condition and 4 were nitrogen responsive QTLs. From the major QTLs, 15 were common between control and N stress. First, we mapped QTLs identified for calculated NUE, NUpE and NutE traits under both conditions, and we found four QTLs namely *QUi.iari-5A* (LOD: 3.32 & PVE: 8.95), *QUi.iari-7D* (LOD: 3.43 & PVE: 8.67), *QNutE.iari-7A* (LOD: 3.76 & PVE: 9.59) and *QGrainN.iari-1A* (LOD: 3.35 & PVE: 8.45).

The major effect QTLs (LOD >3 and PVE >10) were selected for detailed analysis and further consideration and discussed below. Among the manual traits, we found many univariate QTLs and some multivariate or pleiotropic QTLs for major physiological traits such as flag leaf traits, spike traits, seed traits, tiller and leaf traits, phenology, SPAD and biomass. For phenology related traits we found one QTL common for both days to booting and anthesis on chromosome 2A under control condition, and one more QTL for days to anthesis on chromosome 2B under N stress condition.

For flag leaf related traits, we found about 6 QTLs, among them 2 were for flag leaf length, flag leaf width and length width ratio. The flag leaf length QTLs were on chromosome 2B (LOD: 4 & PVE: 10) and 2A (LOD: 3 & PVE: 12), flag leaf width QTLs were on chromosome 2D but at different locus (QTL1 - LOD: 7 & PVE: 17, QTL2 - LOD: 4 & PVE: 11) and flag leaf length and width ratio QTLs were on chromosome 2B (LOD: 4 & PVE: 10) and 6D (LOD: 4 & PVE: 10) under control and N stress, respectively.

We found some important major effect QTLs for spike related traits. There were 6 QTLs present for traits namely spikelet number per spike, sterile spikelet number, spikelet fertility index, grains per spikelet, spike weight, spike length, spikelet density. Two pleiotropic QTLs were found on chromosome 7A and 2B. The QTL on chromosome 7A was found for spikelet number per spike, sterile spikelets per spike, grains per spikelet and spikelet density under both control and N stress conditions. There were 3 major QTLs found for spikelet number on chromosome 2B (Two different loci, one under control and one under N stress) and 7A (One loci for control and N stress both). Spike length QTL was found on chromosome 2B under control condition with LOD value 3.4 and PVE 10. For average spike weight per plant, we found two QTLs on chromosome 2B, one under control and one under N stress with LOD value 4.8 & PVE 10.4%, and LOD value 5.7 and PVE value 13.2%, respectively. One QTL was found for sterile spikelet number and grain number per spike at chromosome 3A (one loci) with LOD value 4.9 and PVE value 10.3 %. Spikelet fertility index QTL was found on chromosome 5B with LOD 4.5 and PVE 10.7%.

We found one pleiotropic QTL at chromosome 4D (Position 138 cM) for plant height, leaf number per plant and tiller number per plant under both control and N stress with LOD value 4-9 and PVE value 13-28. Similarly, one more pleiotropic QTL was found on same chromosome 4D but at different locus (Position 75 cM) for plant height, leaf number per plant and tiller number per plant under nitrogen stress. Another pleiotropic QTL was found on chromosome 2D for flag leaf width under control, panicle harvest index and grain percentage of spike under nitrogen stress condition with LOD 7-38 and PVE 17-24%.

There was a seed trait related QTL on chromosome 3A identified for seed area and perimeter with LOD 4-6.7 and PVE 10-15 %. Seed number per plant QTL was found on chromosome 7D for N:C ratio (N response QTL) with LOD 4 and PVE 10%. One more pleiotropic QTL was found for seed traits such as seed width and seed length width ratio on chromosome 2B under both control and N stress condition with LOD 4-10 and PVE 10-18 %.

There were 15 common major effect QTLs among all the major QTLs between control and N stress conditions. But the 15 QTLs were collocated in 7 genetic loci. Those QTLs were identified for seed area, ear length, flag leaf to ear distance, grains per spikelet, leaf number per plant, seed length width ratio, seed perimeter, plant height, spikelet density, spikelet number, sterile spikelet number and tiller number per plant.

4.2.3.4 Selected major and stable QTLs from phenomics and manual traits

We selected some important major QTLs for manual traits with LOD value >10 and PVE value >10 and found about 11 QTLs for spikelet number, seed length width ratio, straw and chaff content per plant, seed number per plant, spikelet density, flag leaf to ear distance and panicle harvest index. There was a major stable pleiotropic QTL namely *QSp.N.iari-7A* (LOD: 25 & PVE: 35) found at chromosome 7A which was found for spikelet number under both control and N stress conditions and for spikelet density under control condition. Two more QTLs were detected for spikelet number namely *QSp.N.iari-2B* (LOD: 13.37 & PVE: 13.41) and *QSp.N.iari-2B* (LOD: 10.85 & PVE: 10.81) at two different locations on chromosome 2B under control and N stress, respectively. A QTL for flag leaf to ear distance namely *QFL.Ear.iari-4D* (LOD: 17 & PVE: 31) was found on chromosome 4D at the position where QTLs for plant height was also detected. For panicle harvest index a major QTL *QPHI.iari-2D* (LOD: 37 & PVE: 24) was detected on chromosome 2D. There was one QTL for seed number per plant detected on chromosome 6B namely *QSc.iari-6B* (LOD: 16.88 & PVE: 11.16) and one QTL for plant straw and chaff content on chromosome 4B namely *QStraw.iari-4B* (LOD: 14.76 & PVE: 12.95). There were four QTLs on chromosome 2A, 2B, 3A and 3B for seed length width ratio for nitrogen response and control treatment, respectively.

Similarly, for phenomics traits, we selected some important major effect QTLs with LOD value >10 and PVE value >10 and found about 14 QTLs for PSCC_1 & 2, BPAR_SV, I1_SV, Ipca_SV, NIR_SV, Blue_TV, R-G_TV, SLR2_TV, ObjectExtentY_SV, ADAR_SV, 2MPASN_SV, CHCircumference_SV, Compactness_SV, 2MPALN_SV, 2MPAR_SV, BPR_TV and Excentricity_SV, SLR1_TV. Two colour class related QTLs namely *QPscc1.iari-2B* (LOD: 36 & PVE: 18) and *QPscc2.iari-2A* (LOD: 24 & PVE: 15) were identified on 2B and 2A chromosome for PSCC_1 and PSCC_2, respectively. Two QTLs for BPAR_SV for control and N stress conditions on chromosome 6B and 2D, respectively, and the QTLs were *QBpar.iari-6B* (LOD: 21.8 & PVE: 16.1) and *QBpar.iari-2D* (LOD: 10.8 & PVE: 22.2). One QTL was found for NIR_SV for N:C ratio on chromosome 6B, namely *QNir.iari-6B* (LOD: 11.8 & PVE: 10.5). For compactness we found *QCompactness.iari-6A* (LOD: 11 & PVE: 13) under N deficiency at stage 3 and 4. Two QTLs for ADAR_SV were found at 7A and 7B namely *QADAR.iari-7A* (LOD: 11.2 & PVE: 17.3) and *QADAR.iari-7B* (LOD: 13.3 & PVE: 17.3) under control condition.

One pleiotropic i-Trait based QTL was identified on chromosome 4D for 2MPALN_SV, 2MPASN_SV (Control and N stress both), 2MPAR_SV (Stage 1, 3 & 4), BPR_TV, Excentricity_SV and SLR1_TV, and we named the QTL as *QMpar.iari-4D* (LOD: 14 & PVE: 28). One more pleiotropic QTL was found on chromosome 4D but at different loci than previous one, for 2MPASN_SV, CHCircumference_SV and ObjectExtentY_SV which was named *Q2Mpasn.iari-4D* (LOD: 14 & PVE: 26).

4.2.4 Effect of QTLs

To see the effect of some important QTLs, we plotted both the alleles and phenotypes and observed the significance level by Mann-Whitney test. We found that the effect of 4 NUE related QTLs, panicle harvest index and two spikelet number related QTLs.

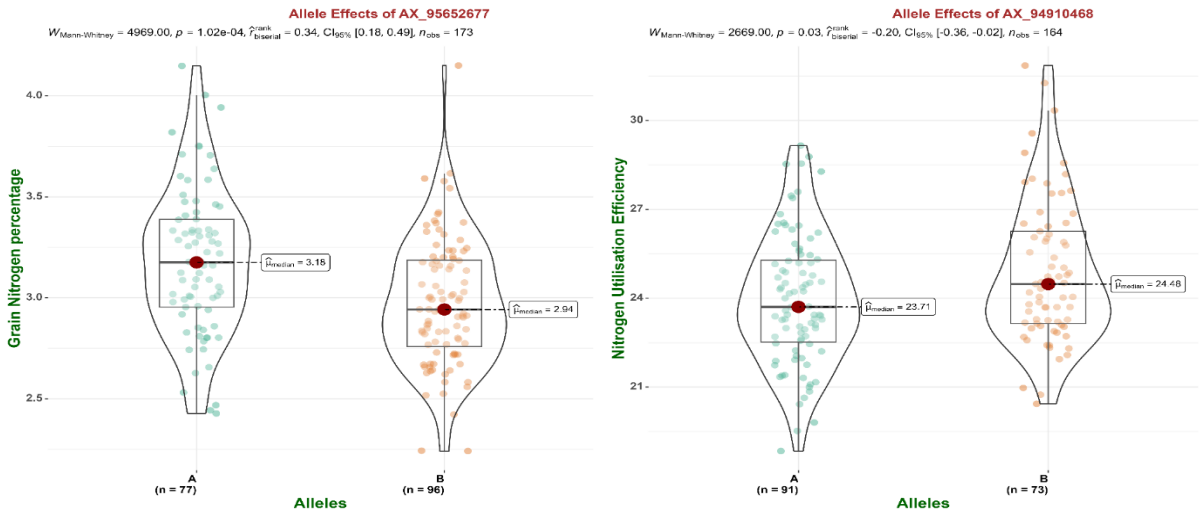

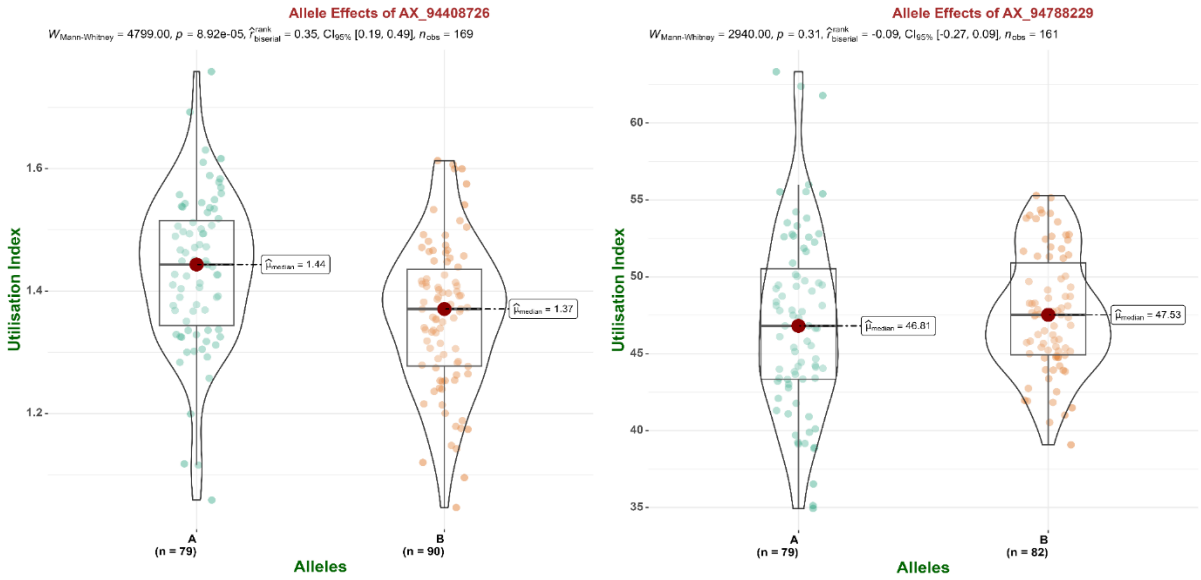

Figure 4.67: Allelic effect of 4 important QTLs detected for grain N percent (A), NutE (B), UI (C & D).

From the QTL effect analysis, the allelic contribution of both parents for the difference in phenotypic effect were analyzed. Here, A allele is from RAJ 3765 and B allele is from HD 2329. For all these major effect QTLs the difference between A and B allele was significant. In case of utilisation index at 5A chromosome, grain nitrogen percentage and panicle harvest index, the A allele had positive effect and B allele had negative effect on phenotype (Figure 4.67 and 4.68). But in case of spikelet number and NutE the A allele had negative effect and B allele had positive effect on phenotype.

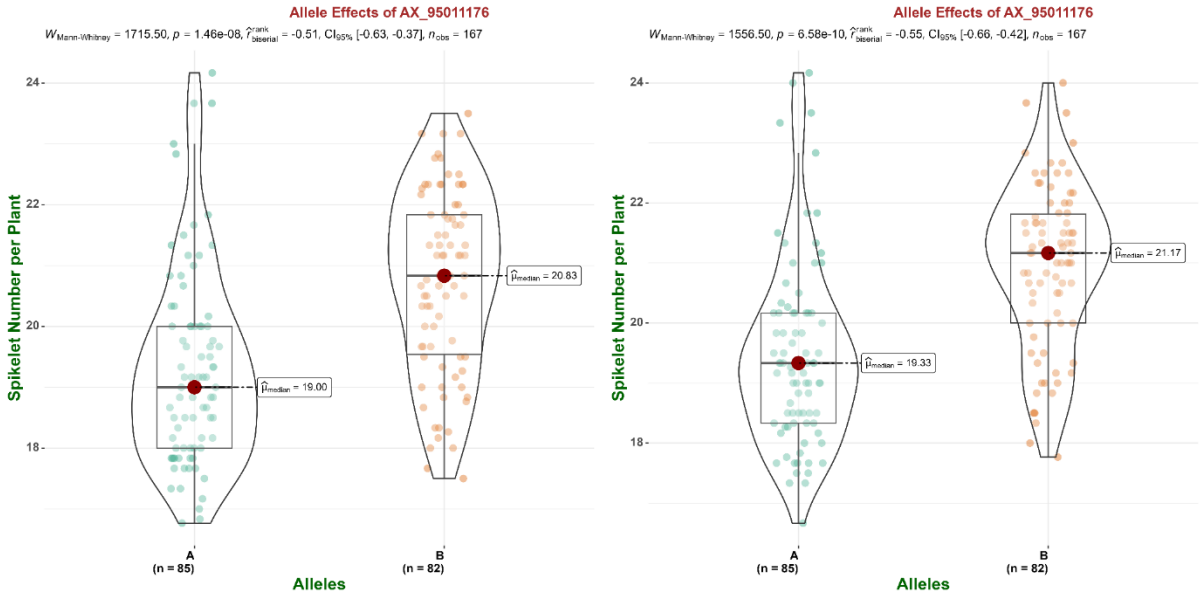

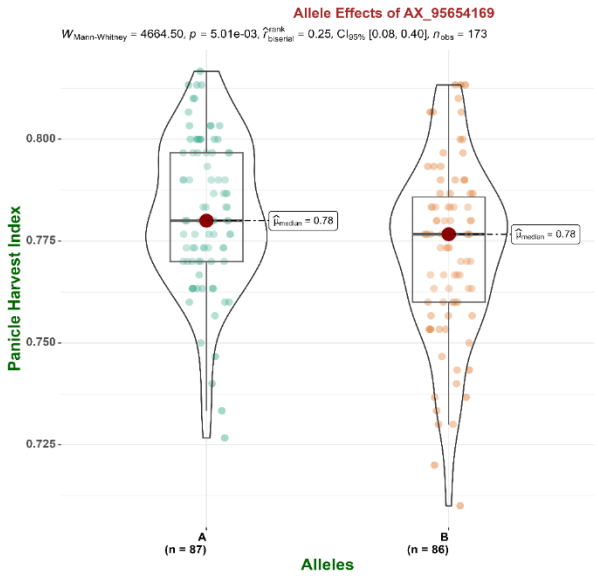

Figure 4.68: Allelic effect of 2 important QTLs detected for spikelet number (A & B) and panicle harvest index (C).

4.3 Candidate gene analysis within major QTL regions

The candidate genes identified for major NUE QTLs by analysing the QTL region between the left and right marker physical position. First, we identified candidate genes (CG) within the four NUE related QTLs. Where we found 8 potential CGs for grain N percentage, 9 CGs for utilisation index on 7D, 23 CGs for NutE and 5 CGs for utilisation index on 5A.

Table 4.8: Candidate genes within 4 NUE QTLs.

GeneID	QTL name	Gene description
TraesCS1A02G443400	***QGrainN.iari-1A***	nucleic acid binding
TraesCS1A02G443100	***QGrainN.iari-1A***	ATP binding
TraesCS1A02G444000	***QGrainN.iari-1A***	extracellular region
TraesCS1A02G443700	***QGrainN.iari-1A***	RNA binding
TraesCS1A02G443200	***QGrainN.iari-1A***	regulation of photoperiodism, flowering
TraesCS1A02G443600	***QGrainN.iari-1A***	nucleolus, protein binding
TraesCS1A02G443500	***QGrainN.iari-1A***	zinc ion binding, carbonate dehydratase activity
TraesCS1A02G443900	***QGrainN.iari-1A***	galactose metabolic process, UDP-glucose 4-epimerase activity
TraesCS7D02G030700	***QUi.iari-7D***	Glutathione transferase
TraesCS7D02G122600	***QUi.iari-7D***	Glutamyl-tRNA reductase
TraesCS7D02G152400	***QUi.iari-7D***	Glutathione peroxidase
TraesCS7D02G188400	***QUi.iari-7D***	Glutathione S-transferase U10
TraesCS7D02G247800	***QUi.iari-7D***	3-hydroxy-3-methylglutaryl coenzyme A reductase
TraesCS7D02G269600	***QUi.iari-7D***	3-hydroxy-3-methylglutaryl coenzyme A synthase
TraesCS7D02G281200	***QUi.iari-7D***	Glutamyl-tRNA reductase-binding protein, chloroplastic
TraesCS7D02G431500	***QUi.iari-7D***	Glutathione synthetase

TraesCS7D02G444100	***QUi.iari-7D***	Glutamate receptor
TraesCS7A02G435700	***QNutE.iari-7A***	IAA-amino acid hydrolase
TraesCS7A02G436200	***QNutE.iari-7A***	DNA repair protein REV1
TraesCS7A02G437900	***QNutE.iari-7A***	Histone H2A
TraesCS7A02G439300	***QNutE.iari-7A***	Copper transport protein CCH
TraesCS7A02G442500	***QNutE.iari-7A***	Glutathione synthetase
TraesCS7A02G442900	***QNutE.iari-7A***	Histone H3
TraesCS7A02G446300	***QNutE.iari-7A***	Mitochondrial intermediate peptidase, mitochondrial
TraesCS7A02G446400	***QNutE.iari-7A***	Probable cytosolic iron-sulfur protein assembly protein CIAO1 homolog
TraesCS7A02G446800	***QNutE.iari-7A***	Protein SCO1 homolog 1, mitochondrial
TraesCS7A02G446900	***QNutE.iari-7A***	Auxin response factor
TraesCS7A02G447300	***QNutE.iari-7A***	Synaptotagmin-3
TraesCS7A02G448000	***QNutE.iari-7A***	Cytochrome b6-f complex subunit 6
TraesCS7A02G448400	***QNutE.iari-7A***	rRNA N-glycosidase
TraesCS7A02G450200	***QNutE.iari-7A***	Glycosyltransferase
TraesCS7A02G450500	***QNutE.iari-7A***	Putative beta-glucosidase 41
TraesCS7A02G451200	***QNutE.iari-7A***	E3 ubiquitin-protein ligase
TraesCS7A02G452800	***QNutE.iari-7A***	DNA polymerase alpha subunit B
TraesCS7A02G452900	***QNutE.iari-7A***	Peroxidase
TraesCS7A02G454300	***QNutE.iari-7A***	Carbonic anhydrase
TraesCS7A02G455200	***QNutE.iari-7A***	Glutamate receptor
TraesCS7A02G455300	***QNutE.iari-7A***	Cytochrome P450 like protein
TraesCS7A02G455800	***QNutE.iari-7A***	Serine/threonine-protein kinase
TraesCS7A02G455900	***QNutE.iari-7A***	DNA repair protein RAD51 homolog 4
TraesCS5A02G349300	***QUi.iari-5A***	Flavin-containing monooxygenase
TraesCS5A02G347400	***QUi.iari-5A***	Cytokinin riboside 5'-monophosphate phosphoribohydrolase
TraesCS5A02G349100	***QUi.iari-5A***	Protein DETOXIFICATION
TraesCS5A02G348400	***QUi.iari-5A***	Flavin-containing monooxygenase
TraesCS5A02G347700	***QUi.iari-5A***	Sulfotransferase

A QTL for utilisation index, *QUi.iari-5A* was present in chromosome 5A between AX-9440872 (Left) - AX-94386305 (Right). There were 5 candidate genes namely TraesCS5A02G34930 (Flavin-containing monooxygenase), TraesCS5A02G347400 (Cytokinin riboside 5'-monophosphate phosphoribohydrolase), TraesCS5A02G349100 (Protein detoxification), TraesCS5A02G348400 (Flavin-containing monooxygenase) and TraesCS5A02G347700 (Sulfotransferase) between the left and right markers. The *QGrainN.iari-1A* mapped in this study for grain nitrogen percentage found between the marker interval AX-95652677 and AX-94542766 harbors candidate genes such as TraesCS1A02G443400 (a nucleic acid binding protein), TraesCS1A02G443700 (RNA binding protein), TraesCS1A02G443200 (associated with regulation of photoperiodism and flowering), TraesCS1A02G443600 (associated with nucleolus), TraesCS1A02G443500 (zinc ion binding protein) and TraesCS1A02G443900 (galactose metabolic process and UDP-glucose 4-epimerase activity).

The QTL identified for nitrogen utilisation index, *QUi.iari-7D* was mapped between AX-94788229 and AX-94451889, and the potential candidate genes present within the region includes TraesCS7D02G030700 (Glutathione transferase), TraesCS7D02G122600 (Glutamyl-tRNA reductase,) TraesCS7D02G152400 (Glutathione peroxidase), TraesCS7D02G188400 (Glutathione S-transferase U10), TraesCS7D02G247800 (3-hydroxy-3-methylglutaryl coenzyme A reductase), TraesCS7D02G281200 (Glutamyl-tRNA reductase-binding protein), TraesCS7D02G431500 (Glutathione synthetase), TraesCS7D02G444100 (Glutamate receptor). The QTL for nitrogen utilisation efficiency, QNutE.iari-7A mapped between AX-94910468 and AX-95081294, harbors the candidate genes TraesCS7A02G435700 (IAA-amino acid hydrolase), TraesCS7A02G442500 (Glutathione synthetase), TraesCS7A02G446900(Auxin response factor), TraesCS7A02G447300 (Synaptotagmin-3), TraesCS7A02G448000 (Cytochrome b6-f complex subunit 6), TraesCS7A02G454300 (Carbonic anhydrase), TraesCS7A02G455200 (Glutamate receptor) and TraesCS7A02G455800 (Serine/threonine-protein kinase).

Based on functional annotations, we identified several genes present within the 2 markers of qtl *QSp.N.iari-7A*, that are associated with plant growth and development. For instance, TraesCS7A02G469300 is associated with a Potassium transporter, TraesCS7A02G470400 for a molybdenum cofactor sulfurase, TraesCS7A02G470900 for Conserved oligomeric Golgi complex component-related / COG complex component-like protein, TraesCS7A02G473900 encoding for phosphoglycerate kinase, TraesCS7A02G475600 for Auxin response factor, TraesCS7A02G477300 associated with Probable ubiquitin conjugation factor E4, TraesCS7A02G478100 probably encoding a glyceraldehyde-3-phosphate dehydrogenase, TraesCS7A02G480700 associated with Mg-protoporphyrin IX chelatase and TraesCS7A02G481500 for allantoate deiminase.

Another major effect QTL for panicle harvest index also harbored potential candidate genes such as TraesCS2D02G491200 (auxin response factor), TraesCS2D02G502100 (glucose-6-phosphate 1-epimerase), TraesCS2D02G500600 (glutamine synthetase), TraesCS2D02G502900S (squamosa promoter-binding-like protein 8), TraesCS2D02G497400 (molybdopterin biosynthesis protein CNX1), TraesCS2D02G484700 (serine/threonine-protein kinase) and TraesCS2D02G489700 (WRKY45-like transcription factor).

We performed the *in silico* expression analysis of the candidate genes identified in the four-nitrogen use efficiency related QTLs (Figure 4.69). We found that genes TraesCS1A02G443400, TraesCS1A02G443700, TraesCS1A02G443900, TraesCS7D02G030700, TraesCS7D02G152400, TraesCS7A02G439300, TraesCS7D02G442900, TraesCS7D02G281200, TraesCS7A02G454300, TraesCS7A02G45520, TraesCS7A02G446900 had differential expression and good expression pattern and value in different growth stages and treatments. So, these genes could be used for further study.

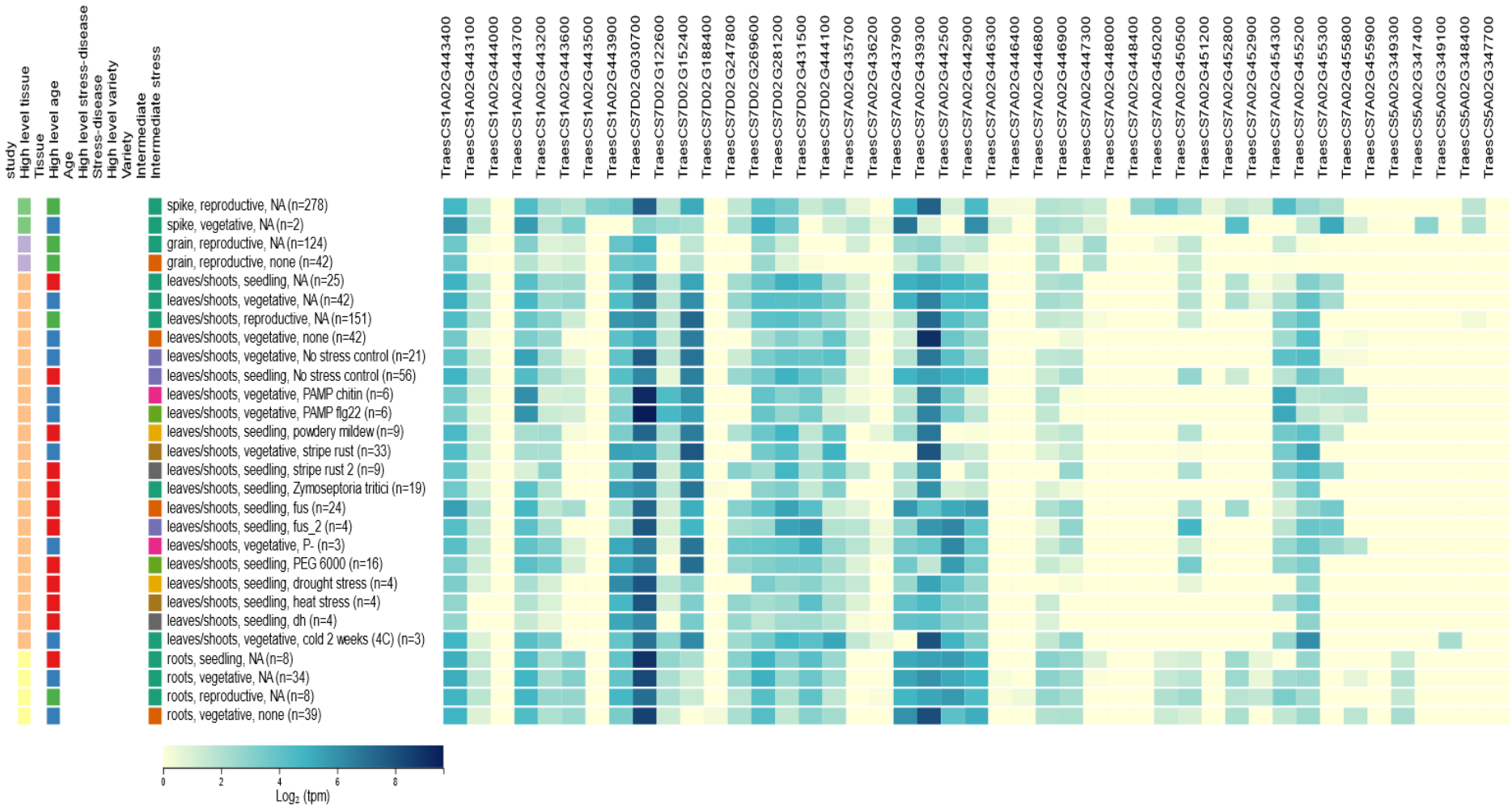

Figure 4.69:In-silico expression analysis of potential candidate genes underlying NUE QTLs.

Modern cereal cultivars rely heavily on nitrogenous inputs to reach their yield potential. However, the nitrogen use efficiency (NUE) of wheat is poor and the recovery of applied nitrogen (N) in cereal production is low, between 30-50 % (Sandhu *et al*., 2021). Crop production declines once nitrogen (N) levels are reduced, indicating that N is a key element in crop production (Wang *et al*., 2017). Under nitrogen deficiency, plant growth and development were severely affected, suggesting a possible negative effect on plant biomass (Liu *et al*., 2020). The stress of N deprivation is promptly detected by plants, and they respond through a variety of physiological and metabolic processes. The loss of photosynthetic capacity is one of those processes that has the biggest negative effects on plant growth and development (Boussadia *et al*., 2010).

A two-fold increase in food production required more than a seven-fold increase in N fertilizer application over the past 40 years, producing immense waste and pollution (Hirel *et al*., 2007). Therefore, understanding the mechanisms of how N influences the yield and quality of wheat grain is of great significance for N fertilizer management. Improving NUE in wheat (*Triticum aestivum* L.) has so far proved difficult due to the complexity of NUE and a lack of phenotyping resolution to identify superior NUE genotypes.

Most mapping studies have instead focused on traditional phenotypes obtained manually at a specific point of time, generally at the mature stage, with characteristics of relative simplicity and the serious difficulty of large-number sampling. Phenotyping of plant by only manual traditional methods made it nearly impossible to perform vertical analyses to dissect temporal behavior of plant phenotypes with additional disadvantages of manual methods are being destructive, high labour cost, low efficiency, and high time consumption.

Wheat growth and development is a dynamic process which varies at different pace throughout the life cycle, and the acquisition of phenotypes at the end time point or at any single time point will never represent the complexity of functional physiological phenotypes. Also, acquisition of phenotypes at the end time point or at any single time point greatly affected by human activities, which are frequently obtained at the expense of integrity with destructive methods. It is now possible, thanks to the development of high-throughput phenotypic facilities, to get phenotype features with a high degree of accuracy. This may be accomplished by assuring high throughput and conducting tests in a non-destructive manner at a number of distinct time periods.

In this study, we developed a strategy to combine high throughput phenotyping, manual phenotyping and semi-automated phenotyping for utilizing the advantages of HTP i.e., the acquisition and analysis of image-based phenomes from the individual to organ level during the whole growth

period, and to capture the phenotypes that is out of context for HTP (Covered by manual and semi-automated phenotyping) in wheat to evaluate the nitrogen deficiency response and NUE.

5.1 Prediction of plant biomass and leaf area in wheat using machine learning approaches

Since nitrogen plans key role in biomass production, dissection of this complex traits over a different growth phase of plant will immensely help dissect genetic basis of biomass production and nitrogen use efficiency. Although earlier several models have been developed to predict biomass from RGB image, it is very challenging to find a model performing stable across experiments. Hence in this work, biomass prediction from RGB and NIR images of wheat germplasm and Recombinant Inbred Lines (RILs) of RAJ 3765xHD 2329 was taken up. The image-based traits (i-Traits) containing geometric features, RGB based indices, RGB colour classes and NIR features were categorized into architectural traits and physiological traits. Total 77 i-Traits were selected for prediction of biomass and leaf area consisting of 35 architectural and 42 physiological traits.

Aided by multiple imaging sensors and computer vision optimization by machine learning methods, high throughput phenotyping has emerged as a major technology helping to dissect plant biological characters unseen before (Kumar at al., 2016; Singh *et al*., 2016; Strock *et al*., 2022). So, gathering multi-dimensional data over multiple time points at multiple organ levels is the critical component of HTP, which has boosted crop improvement programs (Roth *et al*., 2021; Pérez-Valencia *et al*., 2022). Harvest index has been a critical trait for cereal breeders for decades in crop improvement programs, which is closely related to the ability of the plant to accumulate plant biomass and convert it into yield (Chao *et al*., 2019; Porker *et al*., 2020). Since, already we have reached a plateau in improving harvest index, for further improvement in yield, we must improve biomass. We need to characterize accurate biomass of plants at different stages to identify genes working at different phenological stages for biomass production (Chang *et al*., 2019; Chen *et al*., 2020; Rabab *et al*., 2021). Also, data at multiple time points are needed for the functional mapping of plant biomass accumulation. Functional mapping can be a powerful tool to reveal transient and deterministic quantitate trait loci (QTLs) for a complex trait such as biomass (Wu & Lin, 2006; Camargo *et al*., 2018; Jiang *et al*., 2019; Lyra *et al*., 2020). Plant leaf area is a critical physiological parameter which determine the ability of plant to produce economic yield and also it helps to determine the plant leaf area index which is an important conventional physiological trait used for plant developmental studies (Wu *et al*., 2022). Leaf area index (LAI), is a critical parameter of wheat growth, can provide dynamic information during wheat growth phases and closely associated with crop biomass and yield. So, shoot area estimation by non-destructive methods will definitely help to the plant science community in the future. As per our knowledge no work has been done particularly for image-based shoot area estimation by validating with actual shoot area in wheat as it has a compact plant architecture. Traditionally, biomass measurement has been done by destructive methods, which is laborious and time-consuming. Also, one of the other major lacuna

was the inability to take data points at multiple time scales (Tackenberg, 2007; Buxbaum *et al*., 2022). Therefore, to address this major bottleneck, automated, non-destructive biomass estimation by digital imaging method is gaining importance since the evolvement of high throughput phenotyping (Golzarian *et al*., 2011; Rahaman *et al*., 2017; Chen *et al*., 2018; Buxbaum *et al*., 2022).

Several studies in the recent past have developed different models for biomass estimation, but their applicability in other in-house experiments has not been tested widely. Golzarian *et al*., (2011) and Chen *et al*., (2018) predicted biomass in wheat at the age of 15 to 43 days after sowing and in barley at the age of 27 to 58 days after sowing respectively, where crop biomass is not very high and overlapping of leaves are less. But it is challenging to predict the biomass of wheat plant at peak vegetative growth. Also, different crops pose different plant architecture such as leaf distribution, tiller numbers overlapping of leaves etc. which affects the biomass prediction model accuracy. So, a robust and open-source model that excludes the need for repeated destructive measurement is the need of the hour for any high throughput phenotyping facility worldwide. To address this, we conducted an experiment to estimate wheat biomass and related traits non-destructively in the largest phenomics facility in India, Nanaji Deshmukh Plant Phenomics Centre (NDPPC). We aimed to develop a pipeline to predict plant FW, DW and SA non-destructively by open-source tools, which can be used in future experiments by different researchers. We conducted two experiments in consecutive years to see if the models work equally well in different datasets.

The selection of predictor variables for the estimation of a trait is necessary. In the past, single i-trait based biomass estimation (Tackenberg, 2007; Golzarian *et al*., 2011; Campbell *et al*., 2015) and modified experiments with multiple traits have been carried out (Yang *et al*., 2014; Rahaman *et al*., 2017; Chen *et al*., 2018). Previous studies have suggested that combining multiple traits such as vegetation indices and plant-height information can improve biomass estimates (Bendig *et al*., 2015; Han *et al*., 2019). Reports have shown that multiple traits and multi-sensor-based estimation of biomass have more accuracy and biological meaning (Chen *et al*., 2018) which includes different categorical features such as geometric or architectural traits, colour based and NIR based physiological traits. NIR reflectance have been reported to determine water status of plants (Nielson *et al*., 2015; Jin *et al*., 2017). As two plants having same plant architecture but different water status will differ in their fresh weight due to the differences in water status. By taking a leaf out of the literature review of non-destructive plant biomass, we selected both RGB and NIR-based traits for our study. We included architectural, colour class based, mean red, blue and green-based indices and mean grey values to improve the estimation accuracy and make a robust model. We selected 77 high-quality i-Traits by removing redundant, non-informative traits using statistical and manual methods. Both experiments 1 and 2 have differed in phenotypic responses as accessed by principal component and box plot analysis (Figure 3) which emphasizes the independent nature of experiments. So, this will help in understanding the generalised nature of the models across experiments.

We predicted FW, DW and SA using 77 i-Traits by 16 machine learning methods which was available in open-source tool "HTPmod". To validate the results, we also ran all the models in another dataset (experiment 2) with the same i-Traits for the estimation of FW, DW and SA. The estimation accuracy was consistent in both experiments which suggests that all those models were generalized in nature and selecting a particular model will not discriminate much accuracy. By observing the predictive power, PCC and RMSRE, we found eight models to be performing relatively similar with higher estimation accuracies. We included multivariate adaptive regression splines (MARS), random forest (RF) and support vector machine-Radial regression (SVR) in our selected eight models as they had accurate biomass predicting ability (Chen *et al*., 2018). All the predictive models worked accurately for FW, DW and SA in both experiments. But we found that eight models namely BGLM, GBM, GLM, GP-Radial, KNN, LASSO, MLR and SVM-Radial performed relatively poor than other eight models namely BLASSO, BRNN, GLMNET, GP-Poly, MARS, RF, RIDGE and SVM-Linear. Here it is interesting to see that simple multivariate linear regression was in the relatively poor performing group which suggests that use of complex machine learning model improved the accuracy of prediction than simple MLR model (Chen *et al*., 2018). The main reasons for the difference in the prediction accuracy of different machine learning models depends upon factors such as model assumption parameters, model architecture, overfitting of model, sensitivities to extreme values, collinearity present within the data set, complexity of the model and number of samples (Ogutu *et al*., 2012; Arruda *et al*., 2015; Esposito *et al*., 2020; Adak *et al*., 2021). From all the 16 models four models performed relatively poor than other models namely BGLM, GP-Radial, KNN and SVM-Radial. BGLM model is less suited for small scale data and affected by multicollinearity (Koehrsen, 2018), GP-Radial has problem of scalability, representational power and targeted optimisation (Hensman *et al*., 2013; Krauth *et al*., 2016), KNN mostly used on classification and detection based problems and has limitations of poor performance under high dimensionality and sensitive to extreme values (Uddin *et al*., 2022) and SVM-Radial has sensitivities to extreme values, collinearity and more helpful for classification problems. Although these are very good machine learning algorithms cited in literature and worked well under different datasets but in our dataset and type of data, they performance were hampered.

However, for general use and model selection purposes, we made the more stringent model selection with respect to robustness, predictive power, PCC and RMSRE for ease of use in future experiments. The four models BLASSO, BRNN, GLMNET and GP-Poly were consistent across the experiments in FW, DW and SA estimation with relatively similar predictive power, PCC and RMSRE value. These four models had higher R2 and PCC value and lower RMSRE value than other models. The estimation accuracies of these models were at par with the accuracy that have been reported (Neumann *et al*., 2015; Rahaman *et al*., 2017; Chen *et al*., 2018) in literature and also the reproducibility of the accuracy was validated by the results from our second experiment. Also, the validation of actual leaf area to predicted SA has been a unique feature of this undertaken research. Among all these models

we found BLASSO to be the best model in terms of high accuracy and low RMSRE value for all the biomass and related trait prediction and was also stable and interpretable across experiments. BLASSO had highest R2 value and PCC value for both year experiment and lowest RMSRE value among all models. BLASSO is a popular high dimensional data analysis method. It can perform regularization and variable selection at the same time. This can increase the precision of predictions and interpretation of a problem (Vasquez *et al*., 2016). It has major advances in terms of assumptions regarding the sample distribution as it is independent of normality of sample distribution, very efficient in handling large data set and dimensionality also helps to overcome underfitting of model data. So, with the help of this model along with multi-sensor dataset, we were able to predict FW, DW and SA accurately in wheat.

Our results showed that by using open-source tools, we can predict FW, DW and SA of wheat plant accurately in any in-house experiment. The estimation accuracy of all the traits, such as FW, DW, and SA, across both experiments was consistent with past studies (Golzarian *et al*., 2011; Campbell *et al*., 2015; Neilson *et al*., 2015; Neumann *et al*., 2015; Rahaman *et al*., 2017; Chen *et al*., 2018). It also reflected how individual trait impact estimation by analysis of the relative importance and predictive power of each trait. The critical features such as PSA, Area_SV, BPC_SV, PSCC_17, 16, 13, NIR_TV, SV, B_SV, G_SV, SLR5_SV and Gray_TV, which had consistently higher predictive power and more significant correlation with FW, DW and SA can be used as a surrogate for biomass accumulation and dissection of their genetic basis in crop improvement programs. As biomass is a complex trait showing both spatio-temporal variations upon different environments, its characterization can be done using the above-said i-Traits and models effectively at multiple time points.

There was not any major limitation of this study but found some interesting challenges which can be addressed by conducting further research. This study was conducted in the controlled greenhouse conditions so the models selected here have to be tested to predict the biomass under field condition to check the generalised nature of the models. Increase in number of samples and testing of models in different abiotic stress conditions will give deeper insights into biomass modelling. As we have witnessed increase in prediction accuracy was achieved by multiple sensor data, use of advanced hyperspectral sensor data and LIDAR sensor data in further research can give new insight into prediction accuracy of machine learning models.

We developed the biomass and leaf area estimation model using the Bayesian Least Absolute Shrinkage and Selection Operator (BLASSO) machine learning method with high accuracy, which will be helpful to future researchers in predicting biomass and leaf area with high accuracy and robustness. We used the broad genotypic base to include all possible variations in the biomass estimation model to make it more robust. In order to bring out novelty in our research, we used 16 machine-learning models to identify the best estimation model. Wide range of phenotypic variations were taken into consideration by mixing genotypes and recombinant inbred lines (RILs) at different phenological stages. We predicted

SA with higher accuracy in wheat crop having compact plant architecture which had not been validated earlier. We considered consecutive-year data set to evaluate the model replicability. We found Bayesian Least Absolute Shrinkage and Selection Operator (BLASSO) to be the best model which gives prediction accuracy of 0.96 for FW, 0.90 for DW and 0.96 for SA. So, this model can be used as a generic model to predict the vegetative stage biomass and leaf area in wheat. The use of leaf area for estimation of conventional physiological parameters such as leaf area index will be useful in crop improvement programmes. As unique research, it included many biologically relevant image-based traits, including NIR mean gray value, RGB colour class data and mean RGB-derived indices. This work showed the vast potential for future applicability in discovering novel QTLs for biomass and growth-related traits at different phenological stages. Precise phenotyping of biomass at multiple time points in the plant life cycle will serve as a seed for the functional mapping of dynamic traits. It also has future implications in characterizing and quantifying nutrient deficiency effects at the different phenological time scale.

5.2 A HTP approach for characterization of NUE and component traits in wheat

This study describes the development of a robust, high-throughput, and reliable plant phenotyping method using automated digital imaging technology, which can be used to efficiently screen a diverse range of wheat RILs population derived from RAJ 3765 × HD 2329 for NUE enhancement during the whole plant life cycle in a controlled environment. The development of N-efficient wheat varieties by molecular breeding will undoubtedly contribute to a more effective use of nitrogen fertilizer (Cormier *et al*., 2016).

However, NUE is a multi-gene trait, and the fact that there aren't any accurate phenotyping methods right now is a big factor in how well NUE genetic improvement programmes. These methods will help successfully screen breeding populations, phenotype-training populations for genomic selection, and evaluate breeding lines (Cabrera-Bosquet *et al*., 2012; Araus *et al*., 2018; Campbell *et al*., 2018). Therefore, wheat breeders will benefit from the accessibility of effective phenotyping approaches that can characterize and quantify various NUE features. Our findings show that a plant phenomics controlled environment wheat growth evaluation technique is practical and reproducible for NUE and Nitrogen deficiency response research. The outcomes also showed that the digital RGB imaging unit of the automated plant phenotyping platform had a similar level of success in screening wheat varieties for NUE features as it did in the field.

5.3 Phenomics analysis of whole plant transpiration and water use in wheat RILs

Automated weighing and watering and PSA data were used for calculation of whole plant transpiration and partitioned in to day time and night time transpiration in wheat RILs. Since in this study, we have shown that PSA is a good predictor of shoot area by using Bayesian Least Absolute

Shrinkage and Selection Operator (BLASSO) to be the best model which gives prediction accuracy of 0.96 R2, we used PSA directly for calculating whole plant transpiration. We found that the mean transpiration during day time of the RILs increased from 176 mL H_2O/m^2 PSA in N-sufficient condition to 202 mL H_2O/m^2 PSA/day under N-deficient condition, similarly nocturnal transpiration increased from 38 to 43 mL H_2O/m^2 PSA/night in N-deficient condition as compared to control conditions (Figure 4.35). Interestingly, the % contribution of mean night time transpiration and mean day time transpiration to the mean total transpiration of wheat RILs were 18% and 72% respectively, both under control and N-deficiency conditions, and night time transpiration is about 21% of the day time transpiration. Previous studies have shown that night-time transpiration can be substantial, accounting from 5 to 30% of the daytime water loss in different crops (Rawson and Clarke, 1988; Caird *et al*., 2007; Rogiers *et al*., 2013; Even *et al*., 2018). In an earlier study with wheat Cv. Han6172 showed that night time transpiration was about 10.7% (Lu *et al*., 2023). Another study in wheat showed that, it varies from 15-55% depending upon the VPD (Schoppach *et al*., 2014). However, these are short duration studies as compared with this study. Further, earlier no studies have been conducted on whole plant transpiration with long duration experiment in wheat under N-deficient conditions. This study, showed that the transpiration requirement of wheat increases by 15% under N-deficiency conditions. N-deficiency reduced straw nitrogen by 33% in this study, which might have reduced Rubisco content photosynthetic ability. Further studies are required to understand why reduction in N status increased transpiration rate. However, the ratio of night/day transpiration rate was not altered significantly for the mean of RILs.

5.4 Phenomics based phenotyping of wheat RILs for NUE and nitrogen deficiency responses

In the present study, we used phenomics based i-Traits covering different level of plant phenotypes such as morphometric traits, colour related traits, biomass related traits, intensity related and RGB based vegetation indices were used to study NUE and N deficiency responses of wheat. Phenomics based traits have been used for evaluation of water use traits, drought response and salinity stress (Chen *et al*., 2014, Yang *et al*., 2014, Al Tamimi *et al*., 2016, Guo *et al*., 2018). These i-Traits allows physiological and morphological traits to be quantified non-destructively at temporal resolution throughout the plant whole life cycle. Images have valuable digital characteristics that might potentially give phenotypes beyond those measured by standard manual phenotyping. With the development of plant phenomics, phenotypes may be assessed in a non-destructive manner, with less room for human error.

Yang *et al*., (2014) classified different phenomics traits into biomass, morphology, colour and texture related traits to capture drought response in rice. Chen *et al*. (2014) classified phenotypic traits into four groups geometric traits, color-related traits, fluorescence-related traits, and NIR-related traits in drought experiment in barley. Al Tamimi *et al*., (2016) used i-Traits for salinity response capture in rice. Guo *et al*. (2018) combing GWAS and HTP to dissecting genetic mechanism under drought

condition using 507 rice accessions. Phenotyping twenty maize inbred lines under two levels of water and nitrogen supply (control and stress) and combined nitrogen and water deficit, Dodig *et al*. (2019) divided image-derived traits into four groups: manual traits (collected manually) architectural (length, area, shape, structure), physiological included fluorescence-based and color-related traits and biomass-related traits. So, to capture different aspect of plant phenotype we classified the selected 91 i-Traits into 26 morphometric, 4-biomass related, 4-intensity based, 21 colour related, 35 RGB based vegetation indices traits to evaluate the NUE and nitrogen deficiency response.

These all types of traits are categorized and selected from a pool of phenomics traits on the basis of their ability to detect nitrogen deficiency response (Yang *et al*., 2014; Guo *et al*., 2018; Dodig *et al*., 2019,) correlation with NUE related traits, heritability value, covering important aspect of phenotype (manual curation) of plants and contributing to principal components. We used the RGB based vegetation indices to capture the N deficiency response as previous studies have suggested the use of vegetation indices as potential traits (Gholizadeh *et al*., 2011; Saberioon *et al*., 2014; Ac *et al*., 2015; Ghasemi *et al*., 2017).

The heritability of these traits and the frequency distribution of i-Traits were used to assess the suitability of these traits for mapping purpose. The ANOVA suggested the genotype effect, environment effect and genotype and environment interactions were significant for all the traits (Annexure 4). The average broad sense heritability (H^2) of all the morphometric traits were 0.71, 0.72, 0.72, 0.71 and 0.78 under nitrogen deficiency condition at 60, 70, 80, 90 and 100 DAS respectively. There was an average difference of ~10% in the heritability of traits under control and N deficiency condition. However, trait heritability within treatments and the magnitude of genotype × treatment interactions are key factors when comparing breeding strategies, i.e., direct or indirect selection high N and low N environment (Annicchiarico *et al*., 2010). The heritability of all traits ranged from 0.5 to 0.9, indicating that most of these traits were mainly determined by genetic factors.

5.5 Manual and semi-automatic traits capturing the NUE and N deficiency response

The biparental population used in the present study exhibited sufficient variability for NUE, NUpE and NUtE, and their components traits as shown by ANOVA (Annexure 5). The statistical analysis of the phenotypic data gathered on NUE and its component traits also showed that the data followed a normal distribution with transgressive segregation, indicating that the population was appropriate for the research. In addition, the presence of transgressive segregation in a mapping population suggests that favorable QTLs were present in the population.

There are a variety of characteristics that should be present in N-efficient wheat materials, but the ones that stand out the most include early vigour, total biomass, grain yield, harvest index, grain nitrogen content, tiller number, flag area, flag chlorophyll content, and grain protein (Nguyen and Kant,

2018). To a large extent, wheat grain yield is determined by the quantity of carbohydrate stored in the leaves and stems prior to anthesis, and researchers have shown that the more biomass accumulates during vegetative development, the greater the DW and GY will be at harvest (Reynolds *et al*., 2009; Li *et al*., 2013).

Nitrogen deficiency is a major problem that restricts development, yield and quality of wheat (Salvagiotti and Miralles, 2008; Masclaux-Daubresse *et al*., 2010; Liu *et al*., 2020b). Plant height, tillering, flag leaf area, spike and seed characteristics, and grain total N content were all negatively affected by chronic nitrogen deprivation in wheat (Curci *et al*., 2017).

Nitrogen (N) supply level significantly influences the yield and NUE traits of crops. In our study, most of the yield traits (Grain weight, Grain no., TGW, Spikelet No., PHI, Spike length, Spikelet Density, GWS, GNS, CWS and Total Biomass) and the NUpE traits (GNC, StNC and ANC) were significantly decreased with low N input. These results are similar to previous studies (Guo *et al*., 2012; Xu *et al*., 2014; Cui *et al*., 2016).

We found reduction in SPAD value, biomass, number of leaves per plant, number of tillers per plant in our study. Plants suffering from N deficiency all had lower chlorophyll and other pigment concentrations (Laza *et al*., 1993; Nakano *et al*., 1997). The decrease in plant height, number of leaves, and shoot fresh weight were reported under low nitrogen conditions (Li *et al*., 2016). The reduction in grain yield, number of grains per spike, flag leaves size and grain protein contents were severely affected by N-limiting conditions (Wang *et al*., 2021).

We found reduction in grain nitrogen content, protein content and grain yield in nitrogen deficiency in this study. A previous report in Croatian growing conditions showed similar reductions at LN for GY (10%), GPC (13%), and GNY (21%) in a set of 19 European wheat cultivars (Šarčević *et al*., 2014). Previously, Cormier *et al*. (2013) reported significant G × N for GY, GPC, and several NUE traits, and significant G × N interactions for GY and other agronomic traits have also been reported in several other wheat studies (Barraclough *et al*., 2010; Gaju *et al*., 2011). Hitz *et al*. (2016) suggested that the existence of G × N interaction could be useful for breeders, allowing differentiation of performance between two N environments.

According to previous studies, the parameters of the images of a wheat canopy were combined and processed interactively; the correlation between the obtained characteristic parameters and both the chlorophyll content of leaves and nitrogen content of plants was more significant (Zheng *et al*., 2018a). A number of studies showed that Spike length is positively correlated with biomass per plant, harvest index and grain yield (Donmez *et al*., 2001). Spike length also has a strong correlation with spike compactness, even though the correlation is usually negative (Ma *et al*., 2007). In line with this study, Tyagi *et al*., (2020) noted significant variation in plant height (PH), NSPS, BY and HI among wheat

cultivars. Tufa *et al*., (2022) also found significant genotype by environment interactions for PH and NDVI in wheat under optimum and low N conditions.

It is common practice to use chlorophyll-sensitive vegetation indicators for estimating leaf N content due to the strong correlation between these two variables (Zhou *et al*., 2018; Lu *et al*., 2019). Carbohydrate synthesis is not only influenced by nitrogen buildup in the wheat leaves, but also in the wheat spike (Aranjuelo *et al*., 2013, Sanchez-Bragado *et al*., 2014). The accumulation of carbohydrates and protein throughout the spike growth and filling phase can be influenced by the amount of nitrogen available to the plant (Zahedi *et al*., 2004). Previous research has shown that less nitrogen (N) accumulates in the spike and the grain when the dry matter of the spike is lower (Mi *et al*., 2000). The correlation between spike N content and spike dry matter throughout N levels was also demonstrated (Mueller and Vyn, 2018; Mueller *et al*., 2019). This suggests that the N content of spikes should be proportional to their dry weight (Zhao *et al*., 2021). As a result, the nitrogen (N) content of the spike and the nitrogen (N) content of the leaves can be viewed as two markers of the plant's N status during spike growth.

5.6 Genetic relationships between kernel size and quality traits

In addition to productive spikes per unit area, kernels per spike, and kernel weight, kernel size is another major determinant of wheat yield (Cui *et al*., 2014b). The negative yield-quality correlation has long been a key obstacle in wheat breeding programs designed to simultaneously improve yield and quality (Kunert *et al*., 2007; Suprayogi *et al*., 2009). Consequently, QTLs involved in the control of kernel quality that are also independent of negative effects on grain yield should be identified to improve this characteristic. However, the magnitude and relative contribution of the components to overall genetic variability in NUE varies between experiments. For example, NUpE has been shown to account for a greater proportion of variation in NUE at low as compared to high N levels (Le Gouis *et al*., 2000) as has NutE (Gaju *et al*., 2011), although Dhugga and Waines (1989) found NUpE to be equally important at both levels, similar condition which was observed in this study.

In this study, a negative correlation was found between NUE and grain nitrogen content in wheat RILs. Similarly, a global analysis of published data on NUtE trends in wheat revealed that NUtE and % GN are negatively correlated, and, therefore, increasing GY without penalizing grain protein is challenging (de Oliveira Silva *et al*., 2020). Breeding for reduced % GN in wheat is, however, constrained by commercial demands for high grain protein content. In fact, the results of recent retrospective analyses of the effects of breeding efforts during the past few decades on nitrogen economy of wheat, barley (*Hordeum vulgare* L.), and maize (*Zea mays* L.) clearly indicate that improvements in N-use of modern crop varieties have primarily been the result of a reduction in grain nitrogen % and to a minor degree with gains in NHI (Barraclough *et al*., 2010; Gaju *et al*., 2011; Bingham *et al*., 2012; Ciampitti and Vyn, 2012; Sadras and Lawson, 2013).

In agreement with Sinclair and Rufty (2012), the present results clearly revealed that modern wheat cultivars are very efficient in the use of the accumulated N for producing GY. The observed NHIs were more than 80 % in this study which is similar to previous published data (Barraclough *et al*., 2010; Gaju *et al*., 2011; Pask *et al*., 2012; Hitz *et al*., 2017; Liu *et al*., 2020).

5.7 NUE status of wheat RILs

Wheat plants grown under N stress conditions were found to have higher nitrogen use efficiency than the control condition. The NUpE was recorded to be higher (68.22) under Nstress condition than in control (10.32). Similarly, Nstress plants were found to have higher NUtE (49.11 g grain/gN in plant) than the control in (31.85 g grain/gN in plant). Brasier *et al*., (2020) reported similar results that NUE along with NUpE and NUtE were significantly reduced under higher soil N content over control plants. Higher NHI was recorded in plants grown under Nstress condition than in control plants. Overall, the results of from this study clearly showed that NUE traits of plants grown under Nstress condition was higher than well fertilized plants. Similar results were reported in wheat (Gao *et al*. 2017; Rahman *et al*. 2017) and pea (Perchlik and Tegeder, 2017).

5.8 QTLs for NUE and its component traits

QTL mapping is a valuable method for dissecting complicated quantitative variables like NUE, which is regulated by several genes (Yang *et al*., 2017; Sun *et al*., 2013). Several elements are required for effective QTL mapping of a complex trait, including the selection of contrasting parents, an adequate population size, multi-location testing, and enough genome coverage. QTL is traditionally influenced by environmental variation, with adaptive QTL expressing itself in a given environment or modulating its impact with a change in that environment, whereas constitutive QTL is consistent across environments. QTL analysis offers a wealth of possibilities for establishing links between characteristics. Co-localized QTL for distinct phenotypic features provide evidence of a genetically and functionally related trait. Genetic maps have been used widely for QTL mapping for nitrogen use efficiency traits and agronomic traits under different nitrogenous treatments in wheat. Some QTLs for NUE related traits, yield traits and morphological traits in the present study have also been detected in the same or adjacent marker regions of previous QTLs that have been discussed below.

In this study, 554 QTLs (>3 LOD) were mapped on all 21 chromosomes. Previous research has documented QTLs across all 21 chromosomes for nitrogen use efficiency related and agronomic traits (Guo *et al*. 2012; Monostori *et al*. 2017; Hitz *et al*. 2017; Zhang *et al*. 2019; Ranjan *et al*. 2021). Many prior research has also focused on identifying QTLs for additional N-responsive agronomic and physiological variables (Balyan *et al*. 2016; Ren *et al*. 2017; 2018; Fan *et al*. 2018; Ranjan *et al*., 2021). QTLs for these traits have also been reported on all the 21 wheat chromosomes (Brasier *et al*., 2020).

We found a QTL namely *QUi.iari-5A* for nitrogen utilisation index on chromosome 5A, located at 119 cM. By analysing the physical location of the QTL left and right marker we found that this QTL is present in a QTL for root trait and nitrogen utilisation efficiency mapped earlier (Monostori *et al*., 2017; Xiong *et al*., 2019). A QTL for utilisation index namely *QUi.iari-7D* mapped on chromosome 7D at position 170 cM in this study. Earlier study has also reported QTLs for NUE and NUtE on chromosome 7D near this genetic locus that we reported here (Brasier *et al*., 2020). The QTL for nitrogen utilisation efficiency namely *QNutE.iari-7A* was found on chromosome 7A at position 119 cM. This QTL is present within 17Mb region of a previously reported QTL for nitrogen utilisation efficiency and biomass related QTL (Sun *et al*., 2013; Xiong *et al*., 2019). A QTL for grain nitrogen content was identified on chromosome 1A from 591426563 to 592093187 (physical position) namely *QGrainN.iari-1A*. This QTL is located near QTLs for traits such as root length, grain nitrogen content, grain number in previous studies (Xiong *et al*., 2019).

We have characterized NUE and its components by measuring different traits such as biomass, flag leaf, yield, etc. In earlier studies, NUE has also been estimated using root traits, shoot traits, dry matter, grain yield, reproductive/agronomic traits, N% in dry matter, etc. (wheat QTLdb; Singh *et al*. 2021). QTLs for dry matter have also been considered relevant for NUpE and those for photosynthesis may be relevant for NUtE. Some of the main effect QTLs detected in the present study for the three traits were located in the same genomic regions, where QTLs were also reported in earlier studies. For instance, four QTLs for NUE were co-located with the genomic regions defined by QTL analysis in the two previous studies (An *et al*. 2006; Brasier *et al*. 2020).

We found three major effect QTLs for spikelet number per spike which were located on chromosome 2B and 7A. The QTL on chromosome 7A is collocated with QTL found for the same trait on same chromosome in previous studies (Luo *et al*. 2016; Zhai *et al*. 2016; Cao *et al*., 2019; Fan *et al*., 2019). The QTL on 2B was mapped in this study was also found with near genomic loci of studies Katkout *et al*., (2014), Fan *et al*., 2019; Ma *et al*., (2019). and Fan *et al*., (2019). We found one major QTL for seed length width ratio on chromosome 2B at position 195 cM. There were also previously reported QTLs for seed length width ratio and seed traits identified in this chromosome previously (Williams *et al*., 2013; Kumar *et al*., 2016; Xin *et al*., 2020). One major effect QTL for panicle harvest index was found on chromosome 2D at position 343 cM with LOD 37 and PVE 24% namely *QPHI.iari-2D*. This is a novel QTL with potential future use. We found a QTL for seed count per plant at chromosome 6B namely *QSc.iari-6B* with very less marker interval both genetic and physical. The genetic distance was between left CI (46.5) to right CI (47.5) and physical distance was from 644476976-644431400. This QTL was found also in previous study for grain yield and seeds per spike traits at same chromosome (Zou *et al*., 2017; Guan *et al*., 2018; Lozada *et al*., 2018).

5.9 Candidate genes underlying major QTLs

A QTL for utilisation index, *QUi.iari-5A* was present in chromosome 5A between AX-9440872 (Left) - AX-94386305 (Right). There were 5 candidate genes in this QTL. One of the candidate gene TraesCS5A02G348400 coding for Flavin-containing monooxygenase was also mapped in a previous study for NDVI at Heading (Khan, 2020). TraesCS5A02G347400 coding for Cytokinin riboside 5'-monophosphate phosphoribohydrolase is another candidate gene in QUi.iari-5A mapped in this study. This gene has been identified as candidate gene by a recent study in a NUE QTL Qnue.ccsu-5A.3 mapped in wheat using the RILs C306*HUW468 (Singh *et al*. 2023). Cytokinin riboside 5'-monophosphate phosphoribohydrolase is a homolog of LOG enzyme in rice which was mapped from *lonely guy* (*log*) mutants deficient in the maintenance of shoot meristems (Kurakawa *et al*., 2007). LOG enzymes are involved in direct activation of cytokinin. Spatio-temporal regulation of cytokinins play important role nitrogen use efficiency (Gu *et al*., 2018). Cytokinin is a positive regulator of NUE in rice as evident from foliar application studies (Zhu *et al*., 2022). Thus, our study also suggests a potential role of LOG genes in NUE in wheat. TraesCS5A02G349100 codes for Protein detoxification Multidrug and toxic compound extrusion (MATE) genes which is located *QUi.iari-5A* mapped in this study. These proteins play a key role in detoxification which may be necessary for senescence associated N mobilization.

Another QTL identified for nitrogen utilisation index, *QUi.iari-7D* was mapped between AX-94788229 and AX-94451889. This QTL harbors candidate genes for glutathione metabolism such as TraesCS7D02G030700 (Glutathione transferase), TraesCS7D02G152400 (Glutathione peroxidase), TraesCS7D02G188400 (Glutathione S-transferase U10) and TraesCS7D02G431500 (Glutathione synthetase). Glutathione has been shown to play a protective role against oxidative stress and thus help nodule nitrogen fixation in soybean (Dalton *et al*., 2009). In a recent study, high glutathione has been shown to reduce nitrate transport and utilization in wheat seedlings (Yang *et al*., 2022). Thus, further analysis of glutathione metabolism in different tissues and N-deficiency and sufficiency conditions will reveal the regulation of NUE by glutathione. The QTL *QUi.iari-7D* also contains TraesCS7D02G444100 coding for Glutamate receptor (GLR). GLR signaling plays key role in several process including carbon and nitrogen metabolism, and amino acid responses (Simon *et al*., 2023).

The QTL for nitrogen utilisation efficiency, *QNutE.iari-7A* mapped between AX-94910468 and AX-95081294 in this study harbors candidate genes such as TraesCS7A02G435700 (IAA-amino acid hydrolase), TraesCS7A02G446900 (Auxin response factor), TraesCS7A02G442500 (Glutathione synthetase), TraesCS7A02G447300 (Synaptotagmin-3, tethering factor of plant endoplasmic reticulum–plasma membrane contact sites), TraesCS7A02G448000 (Cytochrome b6-f complex subunit 6), TraesCS7A02G454300 (Carbonic anhydrase), TraesCS7A02G455200 for Glutamate receptor, TraesCS7A02G455800 (Serine/threonine-protein kinase). One IAA activating gene and one

auxin response factor mapped in this QTL suggest a potential role of auxin in NUE. Recently, auxin has been shown to positively regulate nitrogen use and yield in rapeseed (Lou *et al*. 2023).

Based on functional annotations, we identified several genes present within the 2 markers of QTL *QSp.N.iari-7A*, that are associated with plant growth and development. This includes TraesCS7A02G469300 (Potassium transporter), TraesCS7A02G470400 (molybdenum cofactor sulfurase), TraesCS7A02G475600 (Auxin response factor), TraesCS7A02G477300 (ubiquitin conjugation factor E4), TraesCS7A02G480700 (Mg-protoporphyrin IX chelatase) and TraesCS7A02G481500 (Allantoate deiminase). Among these, Mo cofactor sulfurase are directly involved in N-metabolism as molybdenum cofactor (Moco) is key component of Nitrate reductase (NR) enzyme (Mendel, 2022). As discussed above, auxin may also play a role.

Another major effect QTL for panicle harvest index, *QPHI.iari-2D*, also harbored some potential candidate genes within the left right marker interval such as TraesCS2D02G491200 (auxin response factor), TraesCS2D02G500600 (glutamine synthetase), TraesCS2D02G502900S (squamosa promoter-binding-like protein 8), and TraesCS2D02G489700 (WRKY45-like/WRKY70-like transcription factor). Interestingly, glutamine synthetase which is directly involved in ammonia assimilation in plants was found in this QTL. Earlier study showed ferredoxin-dependent glutamate synthase (OsFd-GOGAT) play a key role leaf senescence and the nitrogen remobilization in rice (Zeng *et al*., 2016). Earlier, the TraesCS2D02G489700/WRKF-70 like gene has been shown to be upregulated by iron deficiency stress in wheat (Wang *et al*., 2020), and was also mapped in GWAS analysis for NUE and yield component traits (Sandhu *et al*. 2023).

This study was aimed at combining automated high throughput sensor and computer-vision aided phenotyping, semi-automated phenotyping and manual phenotyping to evaluate the nitrogen deficiency response and nitrogen use efficiency (NUE) in wheat and mapping QTLs for traits contributing to NUE. A wheat RIL population (175 RILs) developed from the cross between RAJ 3765 × HD 2329 were sown in pots filled with 13 kg of natural field dry soil under recommended Nitrogen (control) and no fertilizer N application (N-deficiency) conditions. Experiment was laid out with 3 biological replications. The plants were grown in pots in ambient conditions till active tillering stage and then shifted to the climate-controlled greenhouses of Nanaji Deshmukh Plant Phenomics Facility and grown till maturity in rabi season 2019-2020. Plants were irrigated by using automated weighing and watering. The whole plant transpiration was measured daily in the morning and evening by using automated weighing stations.

Plants were phenotype by Visual, IR thermal and Near Infra-Red sensors using automated LemnaTec Scanalyzer3D system during 60, 70, 80, 90 and 100 Days After Sowing (DAS). Manual data measurements were taken at different stages of plants to capture the nitrogen deficiency response in physiological and yield traits and NUE. We also used semi-automated phenotyping for estimation seed morphometric parameters and their response to N stress and their relatedness to NUE traits.

A total of 91 good quality i-Traits were selected based on heritability, contribution to principal component and nature of the i-Traits. These 91 i-Traits consist of plants morphometric traits, biomass related traits, colour related traits, NIR intensity related traits, and RGB based vegetation indices, and represented the whole plant spatio-temporal phenotypes.

A novel colour class related traits classification gives insight into the pixel based colour changes due to the nitrogen deficiency and helped in identification of greenness and senescence related colour classes. This method can be used as a high throughput surrogate for manual nitrogen deficiency evaluator such as leaf colour chart (LCC).

Sixteen machine-learning models were evaluated to identify the best estimation model for shoot area and biomass estimation from the RGB color and NIR images. We predicted shoot area with higher accuracy in wheat crop having compact plant architecture We found Bayesian Least Absolute Shrinkage and Selection Operator (BLASSO) to be the best model which gives prediction accuracy of 0.96 for FW, 0.90 for DW and 0.96 for SA. Thus, the BLASSO machine learning method with multimodal images from RGB and NIR will be helpful to future researchers in predicting biomass and leaf area with high accuracy and robustness.

We identified important traits including i-Traits, manual and semi-automatic traits contributing majorly to the complex trait viz., yield and NUE, and these traits can be used for surrogate for yield and

NUE improvement. These traits are namely BPC_SV & TV, Compactness_SV & TV, 2MPASA_TV, PSCC_17, 18, 19 & 20, PSA, Area_SV, r_SV, SLR2_SV, GMR_SV, Blue_SV, TotalBiomass, TotalGrainNo, SPAD1, PHI, HI, SeedArea, TKW, SpikeLength, TotalEar and LeafNo. These traits include different categories of i-Traits and manual traits such as morphometric, colour class, biomass related, RGB indices, plant physiological traits, yield related traits and seed morphometry. This suggests the importance of spatio-temporal phenotyping by combination of phenomics, manual and semi-automatic phenotyping in plants.

We evaluated the effect of nitrogen deficiency over main ear and tiller ear and seed related traits and found that the negative effect of nitrogen deficiency was more in main ear than that on tiller ear in terms of grain weight, chaff weight, grain number and TKW. However, nitrogen deficiency reduced the tiller number of plant significantly which caused the overall reduction in these traits in nitrogen stress plants.

We found that i-Traits namely PSCC 3 4 19 20, SLR2_SV, ExB_SV, BPR_SV, SPAD1, BPC_SV and BPAR_SV, which represents morphometric, colour class and RGB indices, were highly positively correlated with grain N content and negatively correlated with NUE. Also, i-Traits namely Green_SV, PCA1_SV, Gray_SV, (G-B)/(R+G+B)_SV and g_TV were highly negatively correlated with grain N content and positively correlated with NUE. Thus, this study led to the identification of morphometric, colour class as well as RGB based indices which can also be used as surrogate for NUE and nitrogen deficiency responses of plants.

The six most important manual NUE related traits were NUpE, NUtE, NUE, yield and N content in straw and grain which can be used in phenotyping for measuring N responses of plants in future use in crop breeding programme. A negative correlation was found between NUE and grain N content, and NUE and grain yield.

The whole plant transpiration of the RILs during day time increased from 176 mL H_2O/m^2 PSA in N-sufficient condition to 202 mL H_2O/m^2 PSA/day under N-deficient condition, similarly nocturnal transpiration increased from 38 to 43 mL H_2O/m^2 PSA/night in N-deficient condition as compared to control conditions. The % contribution of mean night time transpiration and mean day time transpiration to the mean total transpiration of wheat RILs were 18% and 72%, respectively. This study also showed that the transpiration requirement of wheat increases by 15% under N-deficiency conditions.

Superior RILs with high yield, NUE and grain N concentration namely R275, R201, R207, R295, R351, R366, R200, R288, R304, R224, R236, R259, R240, R324, R214, R286, R284, R372, R203, R205, R283, R197, R219, R355, R333 and R208 were identified by using the multitrait genotype-ideotype distance index (MGIDI). These can be used as donor in future breeding program.

The parents (RAJ 3765 and HD 2329) and 376 RILs were genotyped with 35K wheat breeder's array SNP markers. From this SNP data, a high-density linkage map was constructed for RAJ 3765×HD 2329 population of 355 individuals with 1749 binned markers spanned over a total of 5,468 cM with marker density of 2.84 (marker/cM). The reliability of the linkage map was tested by identifying same stable consistent QTL, *QpH.iari-4D* for plant height under control and N stress condition under both field and phenomics greenhouse condition. This also emphasizes the relevance of phenomics based traits in field conditions. Composite interval QTL mapping by IciMapping v4.2 of all the phenomics, manual and semi-manual traits revealed a total of 554 QTLs (>3 LOD), of which 349 QTLs were detected for phenomics traits, and 205 QTLs detected for manual and semi-manual traits.

We identified QTLs for NUE, NUpE, NutE, nitrogen utilization index (UI) and Grain N content under both N sufficient and N-deficient conditions namely *QUi.iari-5A* (LOD: 3.32 & PVE: 8.95), *QUi.iari-7D* (LOD: 3.43 & PVE: 8.67), *QNutE.iari-7A* (LOD: 3.76 & PVE: 9.59) and *QGrainN.iari-1A* (LOD: 3.35 & PVE: 8.45). There were 15 common major effect QTLs among all the major QTLs between control and N stress conditions. But the 15 QTLs were collocated in 7 genetic loci. Those QTLs were identified for traits such as seed area, ear length, flag leaf to ear distance, grains per spikelet, leaf number per plant, seed length width ratio, seed perimeter, plant height, spikelet density, spikelet number, sterile spikelet number and tiller number per plant.

The following major QTLs with LOD value >10 and PVE value >10 which can be used in future breeding programme: 1) A major stable pleiotropic QTL namely *QSp.N.iari-7A* mapped on chromosome 7A for spikelet number and spikelet density under both control and N stress conditions; 2) A QTL for flag leaf to ear distance namely *QFL.Ear.iari-4D* was mapped on chromosome 4D where at the same position a QTL for plant height was also detected; 3) For panicle harvest index a major QTL *QPHI.iari-2D* was detected on chromosome 2D; 4) one QTL for seed number per plant detected on chromosome 6B namely *QSc.iari-6B* and one QTL for plant straw and chaff content on chromosome 4B namely *QStraw.iari-4B* and 5) there were four QTLs on chromosome 2A, 2B, 3A and 3B for seed length width ratio under control and N-deficiency treatment respectively.

Similarly, for phenomics i-Traits, 14 major effect QTLs with LOD value >10 and PVE value >10 were mapped. One pleiotropic i-Trait QTL QMpar.iari-4D was mapped on chromosome 4D for 2MPALN_SV, 2MPASN_SV (Control and N stress both), 2MPAR_SV (Stage 1, 3 & 4), BPR_TV, Excentricity_SV and SLR1_TV. One more pleiotropic QTL *Q2Mpasn.iari-4D* was found on chromosome 4D for 2MPASN_SV, CHCircumference_SV and ObjectExtentY_SV. Two colour class related QTLs namely *QPscc1.iari-2B* and *QPscc2.iari-2A* for PSCC_1 and PSCC_2 respectively, were mapped on chromosome 2. Two QTLs *QBpar.iari-6B* and *QBpar.iari-2D* for BPAR_SV for control and N stress conditions on chromosome 6B and 2D, respectively, were mapped. One QTL *QNir.iari-6B* was found for NIR_SV for N:C ratio condition on chromosome 6B.

To see the interaction of QTLs and plant age, we selected those i-Traits QTLs which were expressed more than once in 5 stages and also highlighted the common QTLs between control and N deficiency. As per the interaction effect of QTLs to plant age under control condition from 36 QTLs, we identified 8 early-stage (Expressed in at least 2 stages among stage 1-3), transient (Appeared then disappeared) QTLs and 15 late-stage (Expressed in at least 2 stages among stage 3-5) transient QTLs. We also found 3 consistent stable QTLs (Expressed in at least 3 stages successively among stage 1-5), 3 transient stable QTLs (Expressed in at least 3 stages among stage 1-5) and 5 deterministic stable QTLs (Expressed consecutively in at least 4 or 5 stages among stage 1-5). In case of nitrogen deficiency condition there were 47 QTLs among them from which 17 were early-stage transient QTLs, 15 were late-stage transient QTLs, 7 were consistent stable QTLs, 3 were transient stable QTLs and 5 were deterministic stable QTLs.

By performing the *in silico* analysis of the QTL region, candidate genes for NUE related QTLs were identified. The utilization index, Qui.iari-5A, harbours TraesCS5A02G347400 coding for Cytokinin riboside 5'-monophosphate phosphoribohydrolase, a homolog of LONELY GUY (LOG) enzyme. involved in direct activation of cytokinin. Thus, *LOG* gene in in wheat a potential candidate gene for NUE. This QTL also harbours TraesCS5A02G349100 gene coding for Protein detoxification Multidrug and toxic compound extrusion (MATE) protein, suggesting the potential role of detoxification necessary for senescence associated N mobilization.

Genes for glutathione metabolism (TraesCS7D02G030700, Glutathione transferase; TraesCS7D02G152400, Glutathione peroxidase; TraesCS7D02G188400, Glutathione S-transferase U10 and TraesCS7D02G431500 Glutathione synthetase) mapped in nitrogen utilisation index QTL QUi.iari-7D suggests the significance of glutathione and/or its protective role against oxidative stress in regulation of NUE.

The QNUtE.iari-7A QTL harbors candidate genes such as TraesCS7A02G435700 (IAA-amino acid hydrolase) and TraesCS7A02G446900 (Auxin response factor) and TraesCS2D02G491200 (auxin response factor) in QPHI.iari-2D QTL suggest a potential role of auxin in NUE. Aajor effect QTL for panicle harvest index, QPHI.iari-2D harbored glutamine synthetase which is directly involved in ammonia assimilation in plants, and thus NUE. The candidate genes identified in this study can be functionally validated and to elucidate the role of auxin, cytokinin and glutathione signalling in NUE of wheat.

This study demonstrated the power and potential of phenomics for the dynamic's quantitative evaluation crop response to complex traits such as NUE. This study highlights the prospective of HTP and provides an evidence and framework for future studies to combing HTP and genomics to dissect the genetic architecture of complex polygenic traits such as nitrogen use efficiency. This work also showed the vast potential for future applicability in discovering novel QTLs for tissue level trait

dissection for biomass, colour, architecture and growth-related traits at different phenological stages. Precise phenotyping of biomass at multiple time points in the plant life cycle will serve as a seed for the functional mapping of dynamic traits.

PHENOMICS AND GENETIC ANALYSIS OF NITROGEN USE EFFICIENCY (NUE) IN WHEAT (*Triticum aestivum* L.)

Modern wheat cultivars rely heavily on nitrogenous inputs to reach their yield potential. However, the nitrogen use efficiency (NUE) of wheat is poor and the recovery of applied nitrogen (N) in cereal production is as low as 30-50 %. Therefore, understanding the mechanisms of NUE and its contribution to yield and quality of wheat grain is of great significance for N fertilizer management. In this study, we combined high throughput automated sensor and computer vision-aided phenotyping, semi-automated phenotyping and manual phenotyping to evaluate the nitrogen deficiency response and NUE in a wheat RIL population derived from RAJ 3765 × HD 2329. Plants grown in normal recommended nitrogen (Control) and N-deficiency (no fertilizer application) were phenotyped during 60, 70, 80, 90 and 100 days after sowing (DAS) by using Visual, IR thermal and Near Infra-Red imaging sensors using automated LemnaTec Scanalyzer3D system at Nanaji Deshmukh Plant Phenomics Centre, IARI, New Delhi. A total of 91 good quality i-Traits were selected based on heritability, contribution to principal component and nature of the i-Traits for studying the NUE of wheat. A novel colour class related traits classification, and multimodal RGB and NIR based machine learning model for biomass estimation identified in this study will be useful in precision agriculture and phenotyping applications. The nondestructive biomass and whole plant transpiration estimations showed that the % contribution of mean nocturnal transpiration and day time transpiration is 18 and 72 %, respectively to the total transpiration in wheat. Nitrogen deficiency increased the transpiration requirement of wheat 15%. NUE was found to be negatively correlated with grain nitrogen content. Superior RILs with high yield, NUE and grain N concentration namely R275, R201, R207, R295, R351, R366, R200, R288, R304, R224, R236, R259, R240, R324, R214, R286, R284, R372, R203, R205, R283, R197, R219, R355, R333 and R208 were identified by using the multitrait genotype-ideotype distance index (MGIDI). These can be used as donor in future breeding program. The parents (RAJ 3765 and HD 2329) and 376 RILs were genotyped with 35K wheat breeder's array SNP markers. From this SNP data, a high-density linkage map was constructed for RAJ 3765×HD 2329 population of 355 individuals with 1749 binned markers spanned over a total of 5,468 cM with marker density of 2.84 (marker/cM). For phenomics, manual and semi-manual traits, a total of 554 significant QTLs (>3 LOD) were mapped (349 QTLs for phenomics traits and 205 QTLs for manual and semi-manual traits). QTLs for NUE, NUpE, NUtE, UI and Grain N content under both nitrogen sufficient and deficient conditions namely *QUi.iari-5A* (LOD: 3.32 & PVE: 8.95), *QUi.iari-7D* (LOD: 3.43 & PVE: 8.67), *QNUtE.iari-7A* (LOD: 3.76 & PVE: 9.59) and *QGrainN.iari-1A* (LOD: 3.35 & PVE: 8.45) were mapped. A major stable pleiotropic QTL namely *QSp.N.iari-7A* was mapped chromosome 7A for spikelet number and spikelet density under both control and N-deficiency conditions. For panicle harvest index, a major QTL

QPHI.iari-2D was detected on chromosome 2D. One QTL *QSc.iari-6B* for seed number per plant on chromosome 6B and one QTL *QStraw.iari-4B* for plant straw and chaff nitrogen content on chromosome 4B were mapped. Temporal analysis at five different growth stages of the plants revealed dynamic nature of QTLs and identification of temporal QTLs for different traits. Five deterministic stable QTLs were found for i-Traits which were expressed 4-5 times in five stages under both control and N stress conditions. By performing the *in silico* analysis of the QTL region, novel candidate genes coding for Cytokinin riboside 5'-monophosphate phosphoribohydrolase (LONELY GUY), glutathione metabolism, auxin signaling were identified with potential role in NUE and N-deficiency response in wheat. The superior RILs identified and QTLs mapped in this study will be useful in genetic improvement of NUpE and NutE in wheat.

Keywords: Phenomics, NUE, Deterministic QTLs, Wheat, HTP

गेहूं में नाइट्रोजन उपयोग दक्षता (एनयूई) का फेनोमिक्स और जेनेटिक विश्लेषण (*Triticum aestivum* L.)

आधुनिक गेहूं की किस्में अपनी उपज क्षमता तक पहुंचने के लिए नाइट्रोजन इनपुट पर बहुत अधिक निर्भर करती हैं। हालाँकि, गेहूं की नाइट्रोजन उपयोग दक्षता (एनयूई) खराब है और अनाज उत्पादन में लागू नाइट्रोजन (एन) की रिकवरी 30-50% तक कम है। इसलिए, एनयूई के तंत्र और गेहूं अनाज की उपज और गुणवत्ता में इसके योगदान को समझना एन उर्वरक प्रबंधन के लिए बहुत महत्वपूर्ण है। इस अध्ययन में, हमने राज 3765 × एचडी 2329 से प्राप्त गेहूं आरआईएल आबादी में नाइट्रोजन की कमी की प्रतिक्रिया और एनयूई का मूल्यांकन करने के लिए उच्च थ्रूपुट स्वचालित सेंसर और कंप्यूटर दृष्टि-सहायता प्राप्त फेनोटाइपिंग, अर्ध-स्वचालित फेनोटाइपिंग और मैनुअल फेनोटाइपिंग को जोड़ा। सामान्य रूप से उगाए जाने वाले पौधों की सिफारिश की जाती है नाइट्रोजन (नियंत्रण) और एन-कमी (कोई उर्वरक अनुप्रयोग नहीं) को स्वचालित लेम्नाटेक स्कैनलाइज़र 3 डी सिस्टम का उपयोग करके विजुअल, आईआर थर्मल और नियर इंफ्रा-रेड इमेजिंग सेंसर का उपयोग करके बुवाई (डीएएस) के 60, 70, 80, 90 और 100 दिनों के दौरान फेनोटाइप किया गया था। नानाजी देशमुख प्लांट फेनोमिक्स सेंटर, आईएआरआई, नई दिल्ली। गेहूं के एनयूई का अध्ययन करने के लिए आनुवंशिकता, प्रमुख घटक में योगदान और आई-ट्रेट्स की प्रकृति के आधार पर कुल 91 अच्छी गुणवत्ता वाले आई-ट्रेट्स का चयन किया गया था। इस अध्ययन में पहचाने गए बायोमास आकलन के लिए एक उपन्यास रंग वर्ग से संबंधित लक्षण वर्गीकरण, और मल्टीमॉडल आरजीबी और एनआईआर आधारित मशीन लर्निंग मॉडल सटीक कृषि और फेनोटाइपिंग अनुप्रयोगों में उपयोगी होगा। गैर-विनाशकारी बायोमास और पूरे पौधे के वाष्पोत्सर्जन के आकलन से पता चला है कि गेहूं में कुल वाष्पोत्सर्जन में औसत रात्रि वाष्पोत्सर्जन और दिन के समय वाष्पोत्सर्जन का योगदान क्रमशः 18 और 72% है। नाइट्रोजन की कमी से गेहूं की वाष्पोत्सर्जन आवश्यकता 15% बढ़ गई। एनयूई को अनाज की नाइट्रोजन सामग्री के साथ नकारात्मक रूप से सहसंबद्ध पाया गया। उच्च उपज, एनयूई और अनाज एन सांद्रता वाले बेहतर आरआईएल अर्थात् आर275, आर201, आर207, आर295, आर351, आर366, आर200, आर288, आर304, आर224, आर236, आर259, आर240, आर324, आर214, आर286, आर284, आर372, आर203, आर205, आर283, आर197, आर219, आर355, आर333 और आर208 की पहचान मल्टीट्रेट जीनोटाइप-आइडियोटाइप डिस्टेंस इंडेक्स (MGIDI) का उपयोग करके की गई थी। इन्हें भविष्य के प्रजनन कार्यक्रम में दाता के रूप में उपयोग किया जा सकता है। माता-पिता (राज3765 और एचडी2329) और 376 आरआईएल को 35K गेहूं ब्रीडर सरणी एसएनपी मार्करों के साथ जीनोटाइप किया गया था। इस एसएनपी डेटा से, 2.84 (मार्कर/सीएम) के मार्कर घनत्व के साथ कुल 5,468 सीएम पर फैले 1749 बिन्ड मार्करों के साथ 355 व्यक्तियों की आरएजे 3765×एचडी 2329 आबादी के लिए एक उच्च घनत्व लिंकेज मानचित्र का निर्माण किया गया था। फेनोमिक्स, मैनुअल और अर्ध-मैनुअल लक्षणों के लिए, कुल 554 महत्वपूर्ण क्यूटीएल (>3 एलओडी) मैप किए गए थे (फेनोमिक्स लक्षणों

के लिए 349 क्यूटीएल और मैनुअल और अर्ध-मैनुअल लक्षणों के लिए 205 क्यूटीएल)। NUE, NUpE, NUtE, UI और अनाज N सामग्री के लिए नाइट्रोजन पर्याप्त और कमी दोनों स्थितियों में क्यूटीएल अर्थात् *QUi.iari-5A* (LOD: 3.32 और PVE: 8.95), *QUi.iari-7D* (LOD: 3.43 और PVE: 8.67) , *QNUtE.iari-7A* (LOD: 3.76 और PVE: 9.59) और *QGrainN.iari-1A* (LOD: 3.35 और PVE: 8.45) को मैप किया गया। नियंत्रण और एन-कमी दोनों स्थितियों के तहत स्पाइकलेट संख्या और स्पाइकलेट घनत्व के लिए एक प्रमुख स्थिर प्लियोट्रोपिक क्यूटीएल अर्थात् *QSp.N.iari-7A* को क्रोमोसोम 7A मैप किया गया था। पैनिकल हार्वेस्ट इंडेक्स के लिए, क्रोमोसोम 2डी पर एक प्रमुख क्यूटीएल *QPHI.iari-2D* का पता लगाया गया था। गुणसूत्र 6बी पर प्रति पौधे बीज संख्या के लिए एक क्यूटीएल *QSc.iari-6B* और गुणसूत्र 4B पर पौधे के भूसे और भूसी नाइट्रोजन सामग्री के लिए एक क्यूटीएल *QStraw.iari-4B* को मैप किया गया था। पौधों के पांच अलग-अलग विकास चरणों में अस्थायी विश्लेषण से क्यूटीएल की गतिशील प्रकृति और विभिन्न लक्षणों के लिए अस्थायी क्यूटीएल की पहचान का पता चला। आई-ट्रेट्स के लिए पांच नियतात्मक स्थिर क्यूटीएल पाए गए जिन्हें नियंत्रण और एन तनाव दोनों स्थितियों के तहत पांच चरणों में 4-5 बार व्यक्त किया गया था। क्यूटीएल क्षेत्र के सिलिको विश्लेषण में प्रदर्शन करके, गेहूं में एनयूई और एन-कमी प्रतिक्रिया में संभावित भूमिका के साथ साइटोकिनिन राइबोसाइड 5'-मोनोफॉस्फेट फॉस्फोरिबोहाइड्रोलेज़ (लोनली गाइ), ग्लूटाथियोन चयापचय, ऑक्सिन सिग्नलिंग के लिए कोडिंग वाले उपन्यास उम्मीदवार जीन की पहचान की गई। इस अध्ययन में पहचाने गए बेहतर आरआईएल और क्यूटीएल मैप किए गए गेहूं में एनयूपीई और न्यूटई के आनुवंशिक सुधार में उपयोगी होंगे।

कीवर्ड: फेनोमिक्स, एनयूई, नियतात्मक क्यूटीएल, गेहूं, एचटीपी

9 BIBLIOGRAPHY

Abdul Mallik, M. (2000). Association of arbuscular mycorrhizae with some varieties of Tobacco (*Nicotiana tobacum* L.) and its effect on their growth, nutrition and certain soilborne diseases (Doctoral dissertation, Ph. D. Thesis, Bharathidasan Univ., Tiruchirapalli, S. India, 104).

Ač, A., Malenovský, Z., Olejníčková, J., Gallé, A., Rascher, U., & Mohammed, G. (2015). Meta-analysis assessing potential of steady-state chlorophyll fluorescence for remote sensing detection of plant water, temperature and nitrogen stress. *Remote Sensing of Environment*, *168*, 420-436.

Acreche, M. M., & Slafer, G. A. (2009). Variation of grain nitrogen content in relation with grain yield in old and modern Spanish wheats grown under a wide range of agronomic conditions in a Mediterranean region. *Journal of Agricultural Science*, *147*(6), 657-667.

Adak, A., Conrad, C., Chen, Y., Wilde, S. C., Murray, S. C., Anderson II, S. L., & Subramanian, N. K. (2021). Validation of functional polymorphisms affecting maize plant height by unoccupied aerial systems discovers novel temporal phenotypes. *G3*, *11*(6), jkab075.

Agriculture Organization of the United Nations. Economic, & Social Department. (2005). *The State of Food Insecurity in the World, 2005: Eradicating World Hunger-Key to Achieving the Millennium Development Goals*. Food & Agriculture Org.

Allen, A. M., Barker, G. L., Berry, S. T., Coghill, J. A., Gwilliam, R., Kirby, S., ... & Edwards, K. J. (2011). Transcript-specific, single-nucleotide polymorphism discovery and linkage analysis in hexaploid bread wheat (Triticum aestivum L.). *Plant Biotechnology Journal*, *9*(9), 1086-1099.

Allen, A. M., Winfield, M. O., Burridge, A. J., Downie, R. C., Benbow, H. R., Barker, G. L., ... & Edwards, K. J. (2017). Characterization of a Wheat Breeders' Array suitable for high-throughput SNP genotyping of global accessions of hexaploid bread wheat (Triticum aestivum). *Plant Biotechnology Journal*, *15*(3), 390-401.

Al-Tamimi, N., Brien, C., Oakey, H., Berger, B., Saade, S., Ho, Y. S., ... & Negrão, S. (2016). Salinity tolerance loci revealed in rice using high-throughput non-invasive phenotyping. *Nature Communications*, *7*(1), 13342.

Andrews, M., Raven, J. A., & Lea, P. J. (2013). Do plants need nitrate? The mechanisms by which nitrogen form affects plants. *Annals of Applied Biology*, *163*(2), 174-199.

Anjana, Umar, S., Abrol, Y. P., & Iqbal, M. (2011). Modulation of nitrogen-utilization efficiency in wheat genotypes differing in nitrate reductase activity. *Journal of Plant Nutrition*, *34*(6), 920-933.

Annicchiarico, P., Chiapparino, E., & Perenzin, M. (2010). Response of common wheat varieties to organic and conventional production systems across Italian locations, and implications for selection. *Field Crops Research*, *116*(3), 230-238.

Aparicio, N., Villegas, D., Araus, J. L., Casadesus, J., & Royo, C. (2002). Relationship between growth traits and spectral vegetation indices in durum wheat. *Crop Science*, *42*(5), 1547-1555.

Aranjuelo, I., Sanz-Sáez, Á., Jauregui, I., Irigoyen, J. J., Araus, J. L., Sánchez-Díaz, M., & Erice, G. (2013). Harvest index, a parameter conditioning responsiveness of wheat plants to elevated CO2. *Journal of Experimental Botany*, *64*(7), 1879-1892.

Araus, J. L., Casadesus, J., & Bort, J. (2001). *Recent tools for the screening of physiological traits determining yield. Application of Physiology in Wheat Breeding* (No. 631.53 REY. CIMMYT.).

Araus, J. L., Kefauver, S. C., Zaman-Allah, M., Olsen, M. S., & Cairns, J. E. (2018). Translating high-throughput phenotyping into genetic gain. *Trends in Plant Science*, *23*(5), 451-466.

Arruda, M. P., Brown, P. J., Lipka, A. E., Krill, A. M., Thurber, C., & Kolb, F. L. (2015). Genomic selection for predicting Fusarium head blight resistance in a wheat breeding program. *Plant Genome*, *8*(3), eplantgenome2015.01.0003. doi: 10.3835/plantgenome2015.01.0003.

Atul-Nayyar, A., Hamel, C., Hanson, K., & Germida, J. (2009). The arbuscular mycorrhizal symbiosis links N mineralization to plant demand. *Mycorrhiza*, *19*, 239-246.

Awika, H. O., Bedre, R., Yeom, J., Marconi, T. G., Enciso, J., Mandadi, K. K., ... & Avila, C. A. (2019). Developing growth-associated molecular markers via high-throughput phenotyping in Spinach. *Plant Genome*, *12*(3), 190027.

Babar, M. A., Reynolds, M. P., Van Ginkel, M., Klatt, A. R., Raun, W. R., & Stone, M. L. (2006). Spectral reflectance to estimate genetic variation for in-season biomass, leaf chlorophyll, and canopy temperature in wheat. *Crop Science*, *46*(3), 1046-1057.

Bai, C., Liang, Y., & Hawkesford, M. J. (2013). Identification of QTLs associated with seedling root traits and their correlation with plant height in wheat. *Journal of Experimental Botany*, *64*(6), 1745-1753.

Bai, E., Li, S., Xu, W., Li, W., Dai, W., & Jiang, P. (2013). A meta-analysis of experimental warming effects on terrestrial nitrogen pools and dynamics. *New Phytologist*, *199*(2), 441-451.

Balyan, H. S., Gahlaut, V., Kumar, A., Jaiswal, V., Dhariwal, R., Tyagi, S., ... & Gupta, P. K. (2016). Nitrogen and phosphorus use efficiencies in wheat: physiology, phenotyping, genetics, and breeding. *Plant Breeding Reviews, 40*, 167-234.

Barbottin, A., Lecomte, C., Bouchard, C., & Jeuffroy, M. H. (2005). Nitrogen remobilization during grain filling in wheat: genotypic and environmental effects. *Crop Science*, *45*(3), 1141-1150.

Bardon, C., Piola, F., Bellvert, F., Haichar, F. E. Z., Comte, G., Meiffren, G., ... & Poly, F. (2014). Evidence for biological denitrification inhibition (BDI) by plant secondary metabolites. *New Phytologist*, *204*(3), 620-630.

Barraclough, P. B., Howarth, J. R., Jones, J., Lopez-Bellido, R., Parmar, S., Shepherd, C. E., & Hawkesford, M. J. (2010). Nitrogen efficiency of wheat: genotypic and environmental variation and prospects for improvement. *European Journal of Agronomy*, *33*(1), 1-11.

Barraclough, P. B., Lopez-Bellido, R., & Hawkesford, M. J. (2014). Genotypic variation in the uptake, partitioning and remobilisation of nitrogen during grain-filling in wheat. *Field Crops Research*, *156*, 242-248.

Beatty, P. H., & Good, A. G. (2018). Improving nitrogen use efficient in crop plants using biotechnology approaches. *Engineering Nitrogen Utilization in Crop Plants*, 15-35.

Beavis, W. D. (1998). QTL analyses: power, precision, and accuracy, In: Molecular analysis of complex traits. (Paterson, AH ed.).

Bendig, J., Yu, K., Aasen, H., Bolten, A., Bennertz, S., Broscheit, J., ... & Bareth, G. (2015). Combining UAV-based plant height from crop surface models, visible, and near infrared vegetation indices for biomass monitoring in barley. *International Journal of Applied Earth Observation and Geoinformation*, *39*, 79-87.

Beres, B. L., Rahmani, E., Clarke, J. M., Grassini, P., Pozniak, C. J., Geddes, C. M., ... & Ransom, J. K. (2020). A systematic review of durum wheat: Enhancing production systems by exploring genotype, environment, and management (G× E× M) synergies. *Frontiers in Plant Science*, *11*, 568657.

Bernard, S. M., Møller, A. L. B., Dionisio, G., Kichey, T., Jahn, T. P., Dubois, F., ... & Habash, D. Z. (2008). Gene expression, cellular localisation and function of glutamine synthetase isozymes in wheat (Triticum aestivum L.). *Plant Molecular Biology*, *67*, 89-105.

Bertheloot, J., Martre, P., & Andrieu, B. (2008). Dynamics of light and nitrogen distribution during grain filling within wheat canopy. *Plant Physiology*, *148*(3), 1707-1720.

Bingham, I. J., Karley, A. J., White, P. J., Thomas, W. T. B., & Russell, J. R. (2012). Analysis of improvements in nitrogen use efficiency associated with 75 years of spring barley breeding. *European Journal of Agronomy*, *42*, 49-58.

Boeven, P. H., Longin, C. F. H., Leiser, W. L., Kollers, S., Ebmeyer, E., & Würschum, T. (2016). Genetic architecture of male floral traits required for hybrid wheat breeding. *Theoretical and Applied Genetics*, *129*, 2343-2357.

Boisson, M., Mondon, K., Torney, V., Nicot, N., Laine, A. L., Bahrman, N., ... & Le Gouis, J. (2005). Partial sequences of nitrogen metabolism genes in hexaploid wheat. *Theoretical and Applied Genetics*, *110*(5), 932-940.

Bonelli, L. E., & Andrade, F. H. (2020). Maize radiation use-efficiency response to optimally distributed foliar-nitrogen-content depends on canopy leaf-area index. *Field Crops Research*, *247*, 107557.

Bonkowski, M. (2004). Protozoa and plant growth: the microbial loop in soil revisited. *New Phytologist*, *162*(3), 617-631.

Borrell, A. K., & Hammer, G. L. (2000). Nitrogen dynamics and the physiological basis of stay-green in sorghum. *Crop Science*, *40*(5), 1295-1307.

Botstein, D., White, R. L., Skolnick, M., & Davis, R. W. (1980). Construction of a genetic linkage map in man using restriction fragment length polymorphisms. *American Journal of Human Genetics*, *32*(3), 314.

Boussadia, O., Steppe, K., Zgallai, H., El Hadj, S. B., Braham, M., Lemeur, R., & Van Labeke, M. C. (2010). Effects of nitrogen deficiency on leaf photosynthesis, carbohydrate status and biomass production in two olive cultivars 'Meski'and 'Koroneiki'. *Scientia Horticulturae*, *123*(3), 336-342.

Bradski, G. (2000). The opencv library (2000). *Dr. Dobb's Journal of Software Tools*.

Brancourt-Hulmel, M., Doussinault, G., Lecomte, C., Bérard, P., Le Buanec, B., & Trottet, M. (2003). Genetic improvement of agronomic traits of winter wheat cultivars released in France from 1946 to 1992. *Crop Science*, *43*(1), 37-45.

Brasier, K., Ward, B., Smith, J., Seago, J., Oakes, J., Balota, M., ... & Griffey, C. (2020). Identification of quantitative trait loci associated with nitrogen use efficiency in winter wheat. *PLoS One*, *15*(2), e0228775.

Brookes, A. J. (1999). The essence of SNPs. *Gene*, *234*(2), 177-186.

Buchner, P., & Hawkesford, M. J. (2014). Complex phylogeny and gene expression patterns of members of the NITRATE TRANSPORTER 1/PEPTIDE TRANSPORTER family (NPF) in wheat. *Journal of Experimental Botany*, *65*(19), 5697-5710.

Buckler, E. S., Holland, J. B., Bradbury, P. J., Acharya, C. B., Brown, P. J., Browne, C., ... & McMullen, M. D. (2009). The genetic architecture of maize flowering time. *Science*, *325*(5941), 714-718.

Burran, S., and DesRochers, D. (2015). Principles of Biology I Lab Manual. Reece, J. B., Urry, L. A., Cain, M. L., Wasserman, S. A., Minorsky, P. V., and Jackson, R. B.(2014). "Campbell biology," Pearson Boston.

Buxbaum, N., Lieth, J. H., & Earles, M. (2022). Non-destructive plant biomass monitoring with high spatio-temporal resolution via proximal RGB-d imagery and end-to-End deep learning. *Frontiers in Plant Science*, *13*, 758818.

Cabral, A. L., Jordan, M. C., McCartney, C. A., You, F. M., Humphreys, D. G., MacLachlan, R., & Pozniak, C. J. (2014). Identification of candidate genes, regions and markers for pre-harvest sprouting resistance in wheat (Triticum aestivum L.). *BMC Plant Biology*, *14*(1), 1-12.

Cabrera-Bosquet, L., Crossa, J., von Zitzewitz, J., Serret, M. D., & Luis Araus, J. (2012). High-throughput phenotyping and genomic selection: The frontiers of crop breeding converge F. *Journal of Integrative Plant Biology*, *54*(5), 312-320.

Cadalen, T., Boeuf, C., Bernard, S., & Bernard, M. (1997). An intervarietal molecular marker map in Triticum aestivum L. Em. Thell. and comparison with a map from a wide cross. *Theoretical and Applied Genetics*, *94*, 367-377.

Caird, M. A., Richards, J. H., & Donovan, L. A. (2007). Nighttime stomatal conductance and transpiration in C3 and C4 plants. *Plant Physiology*, *143*(1), 4-10.

Camargo, A. V., Mackay, I., Mott, R., Han, J., Doonan, J. H., Askew, K., ... & Bentley, A. R. (2018). Functional mapping of quantitative trait loci (QTLs) associated with plant performance in a wheat MAGIC mapping population. *Frontiers in Plant Science*, *9*, 887.

Campbell, M. T., Knecht, A. C., Berger, B., Brien, C. J., Wang, D., & Walia, H. (2015). Integrating image-based phenomics and association analysis to dissect the genetic architecture of temporal salinity responses in rice. *Plant Physiology*, *168*(4), 1476-1489.

Campbell, N. A., Reece, J. B., Urry, L. A., Cain, M. L., Wasserman, S. A., Minorsky, P. V.,and Jackson, R. B. (2008). Biology eight edition. San Fracisco: Pearson Education Inc,4–5.

Campbell, Z. C., Acosta-Gamboa, L. M., Nepal, N., & Lorence, A. (2018). Engineering plants for tomorrow: how high-throughput phenotyping is contributing to the development of better crops. *Phytochemistry reviews*, *17*, 1329-1343.

Cao, P., Liang, X., Zhao, H., Feng, B., Xu, E., Wang, L., & Hu, Y. (2019). Identification of the quantitative trait loci controlling spike-related traits in hexaploid wheat (Triticum aestivum L.). *Planta*, *250*, 1967-1981.

Cao, Q., Miao, Y., Wang, H., Huang, S., Cheng, S., Khosla, R., & Jiang, R. (2013). Non-destructive estimation of rice plant nitrogen status with Crop Circle multispectral active canopy sensor. *Field Crops Research*, *154*, 133-144.

Carvalho, P., Azam-Ali, S., & Foulkes, M. J. (2014). Quantifying relationships between rooting traits and water uptake under drought in Mediterranean barley and durum wheat. *Journal of Integrative Plant Biology*, *56*(5), 455-469.

Cassman, K. G., Dobermann, A., & Walters, D. T. (2002). Agroecosystems, nitrogen-use efficiency, and nitrogen management. *AMBIO: A Journal of the Human Environment*, *31*(2), 132-140.

Cavanagh, C. R., Chao, S., Wang, S., Huang, B. E., Stephen, S., Kiani, S., ... & Akhunov, E. (2013). Genome-wide comparative diversity uncovers multiple targets of selection for improvement in hexaploid wheat landraces and cultivars. *Proceedings of the National Academy of Sciences*, *110*(20), 8057-8062.

Chang, T. G., Chang, S., Song, Q. F., Perveen, S., & Zhu, X. G. (2019). Systems models, phenomics and genomics: three pillars for developing high-yielding photosynthetically efficient crops. *in silico Plants*, *1*(1), diy003.

Chao, H., Raboanatahiry, N., Wang, X., Zhao, W., Chen, L., Guo, L., ... & Li, M. (2019). Genetic dissection of harvest index and related traits through genome-wide quantitative trait locus mapping in Brassica napus L. *Breeding Science*, *69*(1), 104-116.

Chen, D., Fu, L. Y., Hu, D., Klukas, C., Chen, M., & Kaufmann, K. (2018). The HTPmod Shiny application enables modeling and visualization of large-scale biological data. *Communications Biology*, *1*(1), 89.

Chen, D., Neumann, K., Friedel, S., Kilian, B., Chen, M., Altmann, T., & Klukas, C. (2014). Dissecting the phenotypic components of crop plant growth and drought responses based on high-throughput image analysis. *The Plant Cell*, *26*(12), 4636-4655.

Chen, D., Shi, R., Pape, J. M., Neumann, K., Arend, D., Graner, A., ... & Klukas, C. (2018). Predicting plant biomass accumulation from image-derived parameters. *GigaScience*, *7*(2), giy001.

Chen, J., Zhu, M., Liu, R., Zhang, M., Lv, Y., Liu, Y., ... & Cai, H. (2020). BIOMASS YIELD 1 regulates sorghum biomass and grain yield via the shikimate pathway. *Journal of Experimental Botany*, *71*(18), 5506-5520.

Chen, T. W., Cabrera-Bosquet, L., Alvarez Prado, S., Perez, R., Artzet, S., Pradal, C., ... & Tardieu, F. (2019). Genetic and environmental dissection of biomass accumulation in multi-genotype maize canopies. *Journal of Experimental Botany*, *70*(9), 2523-2534.

Cheng, W., Johnson, D. W., & Fu, S. (2003). Rhizosphere effects on decomposition: controls of plant species, phenology, and fertilization. *Soil Science Society of America Journal*, *67*(5), 1418-1427.

Christopher, M., Chenu, K., Jennings, R., Fletcher, S., Butler, D., Borrell, A., & Christopher, J. (2018). QTL for stay-green traits in wheat in well-watered and water-limited environments. *Field Crops Research*, *217*, 32-44.

Ciampitti, I. A., & Vyn, T. J. (2012). Physiological perspectives of changes over time in maize yield dependency on nitrogen uptake and associated nitrogen efficiencies: A review. *Field Crops Research*, *133*, 48-67.

Clarke, W. E., Higgins, E. E., Plieske, J., Wieseke, R., Sidebottom, C., Khedikar, Y., ... & Parkin, I. A. (2016). A high-density SNP genotyping array for Brassica napus and its ancestral diploid species based on optimised selection of single-locus markers in the allotetraploid genome. *Theoretical and Applied Genetics*, *129*, 1887-1899.

Cormier, F., Faure, S., Dubreuil, P., Heumez, E., Beauchêne, K., Lafarge, S., ... & Le Gouis, J. (2013). A multi-environmental study of recent breeding progress on nitrogen use efficiency in wheat (*Triticum aestivum* L.). *Theoretical and Applied Genetics*, *126*, 3035-3048.

Cormier, F., Foulkes, J., Hirel, B., Gouache, D., Moënne-Loccoz, Y., & Le Gouis, J. (2016). Breeding for increased nitrogen-use efficiency: a review for wheat (*T. aestivum* L.). *Plant Breeding*, *135*(3), 255-278.

Cormier, F., Le Gouis, J., Dubreuil, P., Lafarge, S., & Praud, S. (2014). A genome-wide identification of chromosomal regions determining nitrogen use efficiency components in wheat (*Triticum aestivum* L.). *Theoretical and Applied Genetics*, *127*, 2679-2693.

Critchley, C. S. (2001). *A physiological explanation for the canopy nitrogen requirement of winter wheat* (Doctoral dissertation, University of Nottingham).

Cui, F., Zhao, C., Ding, A., Li, J., Wang, L., Li, X., ... & Wang, H. (2014). Construction of an integrative linkage map and QTL mapping of grain yield-related traits using three related wheat RIL populations. *Theoretical and Applied Genetics*, *127*, 659-675.

Cullis, B. R., Smith, A. B., & Coombes, N. E. (2006). On the design of early generation variety trials with correlated data. *Journal of Agricultural, Biological, and Environmental Statistics*, *11*, 381-393.

Curci, P. L., Aiese Cigliano, R., Zuluaga, D. L., Janni, M., Sanseverino, W., & Sonnante, G. (2017). Transcriptomic response of durum wheat to nitrogen starvation. *Scientific Reports*, *7*(1), 1176.

Dalton, D. A., Boniface, C., Turner, Z., Lindahl, A., Kim, H. J., Jelinek, L., ... & Taylor, C. G. (2009). Physiological roles of glutathione S-transferases in soybean root nodules. *Plant Physiology*, *150*(1), 521-530.

Daniel-Vedele, F., Filleur, S., & Caboche, M. (1998). Nitrate transport: a key step in nitrate assimilation. *Current Opinion in Plant Biology*, *1*(3), 235-239.

Dass, A., Jat, S. L., & Rana, K. S. (2015). Resource conserving techniques for improving nitrogen-use efficiency. *Nutrient use efficiency: from Basics to Advances*, 45-58.

Dass, A., Jinger, D., Kaur, R., Kumar, S. V., & Kumari, K. (2017). Addressing Multinutrient Deficiency. *Indian Farming*, *67*(03), 22-25.

de Oliveira Silva, A., Ciampitti, I. A., Slafer, G. A., & Lollato, R. P. (2020). Nitrogen utilization efficiency in wheat: A global perspective. *European Journal of Agronomy*, *114*, 126008.

Deery, D., Jimenez-Berni, J., Jones, H., Sirault, X., & Furbank, R. (2014). Proximal remote sensing buggies and potential applications for field-based phenotyping. *Agronomy*, *4*(3), 349-379.

Derkx, A. P., Orford, S., Griffiths, S., Foulkes, M. J., & Hawkesford, M. J. (2012). Identification of differentially Senescing mutants of wheat and impacts on yield, biomass and nitrogen Partitioning F. *Journal of Integrative Plant Biology*, *54*(8), 555-566.

Dhugga, K. S., & Waines, J. G. (1989). Analysis of nitrogen accumulation and use in bread and durum wheat. *Crop Science*, *29*(5), 1232-1239.

Dodig, D., Božinović, S., Nikolić, A., Zorić, M., Vančetović, J., Ignjatović-Micić, D., ... & Altmann, T. (2019). Image-derived traits related to mid-season growth performance of maize under nitrogen and water stress. *Frontiers in Plant Science*, *10*, 814.

Donmez, E., Sears, R. G., Shroyer, J. P., & Paulsen, G. M. (2001). Genetic gain in yield attributes of winter wheat in the Great Plains. *Crop science*, *41*(5), 1412-1419.

Duan, J., Tian, H., Drijber, R. A., & Gao, Y. (2015). Systemic and local regulation of phosphate and nitrogen transporter genes by arbuscular mycorrhizal fungi in roots of winter wheat (Triticum aestivum L.). *Plant Physiology and Biochemistry*, *96*, 199-208.

Dubcovsky, J., & Dvorak, J. (2007). Genome plasticity a key factor in the success of polyploid wheat under domestication. *Science*, *316*(5833), 1862-1866.

Ehdaie, B., & Waines, J. G. (2003). 1RS translocation increases root biomass in Veery-type wheat isogenic lines and associates with grain yield. In *Proceedings of the 10th International Wheat Genetics Symposium* (Vol. 2, pp. 693-695). Paestum, Italy: Rome. ISC.

Eitel, J. U., Magney, T. S., Vierling, L. A., Brown, T. T., & Huggins, D. R. (2014). LiDAR based biomass and crop nitrogen estimates for rapid, non-destructive assessment of wheat nitrogen status. *Field Crops Research*, *159*, 21-32.

Eitel, J. U., Vierling, L. A., Long, D. S., & Hunt, E. R. (2011). Early season remote sensing of wheat nitrogen status using a green scanning laser. *Agricultural and Forest Meteorology*, *151*(10), 1338-1345.

Esposito, S., Carputo, D., Cardi, T., & Tripodi, P. (2019). Applications and trends of machine learning in genomics and phenomics for next-generation breeding. *Plants*, *9*(1), 34.

Evans, J. R. (1983). Nitrogen and photosynthesis in the flag leaf of wheat (*Triticum aestivum* L.). *Plant Physiology*, *72*(2), 297-302

Even, M., Sabo, M., Meng, D., Kreszies, T., Schreiber, L., & Fricke, W. (2018). Night-time transpiration in barley (*Hordeum vulgare*) facilitates respiratory carbon dioxide release and is regulated during salt stress. *Annals of Botany*, *122*(4), 569-582.

Fageria, N. K., & Baligar, V. C. (2005). Enhancing nitrogen use efficiency in crop plants. *Advances in Agronomy*, *88*, 97-185.

Fahlgren, N., Gehan, M. A., & Baxter, I. (2015). Lights, camera, action: high-throughput plant phenotyping is ready for a close-up. *Current Opinion in Plant Biology*, *24*, 93-99.

Fan, X., Cui, F., Ji, J., Zhang, W., Zhao, X., Liu, J., ... & Li, J. (2019). Dissection of pleiotropic QTL regions controlling wheat spike characteristics under different nitrogen treatments using traditional and conditional QTL mapping. *Frontiers in Plant Science*, *10*, 187.

Fan, X., Naz, M., Fan, X., Xuan, W., Miller, A. J., & Xu, G. (2017). Plant nitrate transporters: from gene function to application. *Journal of Experimental Botany*, *68*(10), 2463-2475.

Fan, X., Zhang, W., Zhang, N., Chen, M., Zheng, S., Zhao, C., ... & Li, J. (2018). Identification of QTL regions for seedling root traits and their effect on nitrogen use efficiency in wheat (Triticum aestivum L.). *Theoretical and Applied Genetics*, *131*, 2677-2698.

FAO, I. (2019). The state of food and agriculture 2019. Moving forward on food loss and waste reduction. *FAO, Rome*, 2-13.

FAOSTAT (2020). FAO Statistics, Food and Agriculture Organization of the United Nations, Rome Accessed 17-May-2020 http://faostat.fao.org/

FAO, I. (2019). The state of food and agriculture 2019. Moving forward on food loss and waste reduction, 2-13.

Filella, I., Serrano, L., Serra, J., & Penuelas, J. (1995). Evaluating wheat nitrogen status with canopy reflectance indices and discriminant analysis. *Crop Science*, *35*(5), 1400-1405.

Fiorani, F., & Schurr, U. (2013). Future scenarios for plant phenotyping. *Annual Review of Plant Biology*, *64*, 267-291.

Fitzgerald, G. J., Rodriguez, D., Christensen, L. K., Belford, R., Sadras, V. O., & Clarke, T. R. (2006). Spectral and thermal sensing for nitrogen and water status in rainfed and irrigated wheat environments. *Precision Agriculture*, *7*, 233-248.

Fontaine, J. X., Tercé-Laforgue, T., Armengaud, P., Clément, G., Renou, J. P., Pelletier, S., ... & Dubois, F. (2012). Characterization of a NADH-dependent glutamate dehydrogenase mutant of Arabidopsis demonstrates the key role of this enzyme in root carbon and nitrogen metabolism. *Plant Cell*, *24*(10), 4044-4065.

Forde, B. G., & Lea, P. J. (2006). Glutamate in plants: metabolism, regulation, and signalling. *Journal of Experimental Botany*, *58*(9), 2339-2358.

Foulkes, M. J., Hawkesford, M. J., Barraclough, P. B., Holdsworth, M. J., Kerr, S., Kightley, S., & Shewry, P. R. (2009). Identifying traits to improve the nitrogen economy of wheat: Recent advances and future prospects. *Field Crops Research*, 114(3), 329-342.

Foulkes, M. J., Sylvester-Bradley, R., & Scott, R. K. (1998). Evidence for differences between winter wheat cultivars in acquisition of soil mineral nitrogen and uptake and utilization of applied fertilizer nitrogen. *Journal of Agricultural Science*, 130(1), 29-44.

Fradgley, N. S., Bentley, A. R., & Swarbreck, S. M. (2021). Defining the physiological determinants of low nitrogen requirement in wheat. *Biochemical Society Transactions*, 49(2), 609-616.

Fujihara, S., Sasaki, H., Aoyagi, Y., & Sugahara, T. (2008). Nitrogen-to-protein conversion factors for some cereal products in Japan. *Journal of Food Science*, 73(3), C204-C209.

Furbank, R. T., & Tester, M. (2011). Phenomics–technologies to relieve the phenotyping bottleneck. *Trends in Plant Science*, *16*(12), 635-644.

Gadaleta, A., Nigro, D., Giancaspro, A., & Blanco, A. (2011). The glutamine synthetase (GS2) genes in relation to grain protein content of durum wheat. *Functional & Integrative Genomics*, *11*, 665-670.

Gaju, O., Allard, V., Martre, P., Le Gouis, J., Moreau, D., Bogard, M., ... & Foulkes, M. J. (2014). Nitrogen partitioning and remobilization in relation to leaf senescence, grain yield and grain nitrogen concentration in wheat cultivars. *Field Crops Research*, *155*, 213-223.

Gaju, O., Allard, V., Martre, P., Snape, J. W., Heumez, E., LeGouis, J., ... & Foulkes, M. J. (2011). Identification of traits to improve the nitrogen-use efficiency of wheat genotypes. *Field Crops Research*, *123*(2), 139-152.

Gaju, O., DeSilva, J., Carvalho, P., Hawkesford, M. J., Griffiths, S., Greenland, A., & Foulkes, M. J. (2016). Leaf photosynthesis and associations with grain yield, biomass and nitrogen-use efficiency in landraces, synthetic-derived lines and cultivars in wheat. *Field Crops Research*, *193*, 1-15.

Ganal, M. W., Durstewitz, G., Polley, A., Bérard, A., Buckler, E. S., Charcosset, A., ... & Falque, M. (2011). A large maize (Zea mays L.) SNP genotyping array: development and germplasm genotyping, and genetic mapping to compare with the B73 reference genome. *PloS one*, *6*(12), e28334.

Gao, F., Wen, W., Liu, J., Rasheed, A., Yin, G., Xia, X., ... & He, Z. (2015). Genome-wide linkage mapping of QTL for yield components, plant height and yield-related physiological traits in the Chinese wheat cross Zhou 8425B/Chinese Spring. *Frontiers in Plant Science*, *6*, 1099.

Gao, Y. Q., Chen, J. G., Chen, Z. R., An, D., Lv, Q. Y., Han, M. L., ... & Chao, D. Y. (2017). A new vesicle trafficking regulator CTL1 plays a crucial role in ion homeostasis. *PLoS Biology*, *15*(12), e2002978.

Gao, Y., de Bang, T. C., & Schjoerring, J. K. (2019). Cisgenic overexpression of cytosolic glutamine synthetase improves nitrogen utilization efficiency in barley and prevents grain protein decline under elevated CO2. *Plant Biotechnology Journal*, *17*(7), 1209-1221.

Gao, Y., Yu, G., Luo, C., & Zhou, P. (2012). Groundwater nitrogen pollution and assessment of its health risks: a case study of a typical village in rural-urban continuum, China. *PloS one*, *7*(4), e33982.

Garnett, T., Conn, V., & Kaiser, B. N. (2009). Root based approaches to improving nitrogen use efficiency in plants. *Plant, Cell & Environment*, *32*(9), 1272-1283.

Garnett, T., Conn, V., Plett, D., Conn, S., Zanghellini, J., Mackenzie, N., ... & Kaiser, B. N. (2013). The response of the maize nitrate transport system to nitrogen demand and supply across the lifecycle. *New Phytologist*, *198*(1), 82-94.

Ghanem, M. E., Marrou, H., & Sinclair, T. R. (2015). Physiological phenotyping of plants for crop improvement. *Trends in Plant Science*, *20*(3), 139-144.

Ghasemi, H., Esmaeili, M. A., & Mohammadian, R. (2017). Effects of nitrogen on chlorophyll fluorescence and the relationship between chlorophyll content and SPAD values in sugar beet (Beta Vulgaris L.) under drip-tape system. *Journal of Agricultural and Biological Science*, *12*(3), 117-122.

Gholizadeh, A., Amin, M. S. M., Anuar, A. R., Aimrun, W., & Saberioon, M. M. (2011). Temporal variability of SPAD chlorophyll meter readings and its relationship to total nitrogen in leaves within a Malaysian paddy field. *Australian Journal of Basic and Applied Sciences*, *5*(5), 236-245.

Gioseffi, E., de Neergaard, A., & Schjørring, J. K. (2012). Interactions between uptake of amino acids and inorganic nitrogen in wheat plants. *Biogeosciences*, *9*(4), 1509-1518.

Golzarian, M. R., Frick, R. A., Rajendran, K., Berger, B., Roy, S., Tester, M., & Lun, D. S. (2011). Accurate inference of shoot biomass from high-throughput images of cereal plants. *Plant Methods*, *7*, 1-11.

Good, A. G., Johnson, S. J., De Pauw, M., Carroll, R. T., Savidov, N., Vidmar, J., ... & Stroeher, V. (2007). Engineering nitrogen use efficiency with alanine aminotransferase. *Botany*, *85*(3), 252-262.

Gooding, M. J., Addisu, M., Uppal, R. K., Snape, J. W., & Jones, H. E. (2012). Effect of wheat dwarfing genes on nitrogen-use efficiency. *Journal of Agricultural Science*, *150*(1), 3-22.

Goulding, K. W. T. (2004). Minimising losses of nitrogen from UK agriculture. *Journal of the Royal Agricultural Society of England*, *165*, 1-11.

Gregory, P. J., Hutchison, D. J., Read, D. B., Jenneson, P. M., Gilboy, W. B., & Morton, E. J. (2003). Non-invasive imaging of roots with high resolution X-ray micro-tomography. In *Roots: The Dynamic Interface between Plants and the Earth: The 6th Symposium of the International Society of Root Research, 11–15 November 2001, Nagoya, Japan* (pp. 351-359). Springer Netherlands.

Gu, J., Li, Z., Mao, Y., Struik, P. C., Zhang, H., Liu, L., ... & Yang, J. (2018). Roles of nitrogen and cytokinin signals in root and shoot communications in maximizing of plant productivity and their agronomic applications. *Plant Science*, *274*, 320-331.

Guan, P., Lu, L., Jia, L., Kabir, M. R., Zhang, J., Lan, T., ... & Peng, H. (2018). Global QTL analysis identifies genomic regions on chromosomes 4A and 4B harboring stable loci for yield-related

traits across different environments in wheat (*Triticum aestivum* L.). *Frontiers in Plant Science*, *9*, 529.

Guarda, G., Padovan, S., & Delogu, G. (2004). Grain yield, nitrogen-use efficiency and baking quality of old and modern Italian bread-wheat cultivars grown at different nitrogen levels. *European Journal of Agronomy*, *21*(2), 181-192.

Guo, H., Tian, Z., Sun, S., Li, Y., Jiang, D., Cao, W., & Dai, T. (2019). Pre anthesis root growth and nitrogen uptake improved wheat grain yield and Nitrogen Use Efficiency. *Agronomy Journal*, *111*(6), 3048-3056

Guo, Y., Kong, F. M., Xu, Y. F., Zhao, Y., Liang, X., Wang, Y. Y., ... & Li, S. S. (2012). QTL mapping for seedling traits in wheat grown under varying concentrations of N, P and K nutrients. *Theoretical and Applied Genetics*, *124*, 851-865.

Guo, Z., Yang, W., Chang, Y., Ma, X., Tu, H., Xiong, F., ... & Xiong, L. (2018). Genome-wide association studies of image traits reveal genetic architecture of drought resistance in rice. *Molecular Plant*, *11*(6), 789-805.

Gutierrez, M., Reynolds, M. P., & Klatt, A. R. (2010a). Association of water spectral indices with plant and soil water relations in contrasting wheat genotypes. *Journal of Experimental Botany*, *61*(12), 3291-3303.

Gutierrez, M., Reynolds, M. P., Raun, W. R., Stone, M. L., & Klatt, A. R. (2010b). Spectral water indices for assessing yield in elite bread wheat genotypes under well-irrigated, water-stressed, and high-temperature conditions. *Crop Science*, *50*(1), 197-214.

Gutiérrez-Rodríguez, M., Reynolds, M. P., Escalante-Estrada, J. A., & Rodríguez-González, M. T. (2004). Association between canopy reflectance indices and yield and physiological traits in bread wheat under drought and well-irrigated conditions. *Australian Journal of Agricultural Research*, *55*(11), 1139-1147.

Halperin, O., Gebremedhin, A., Wallach, R., & Moshelion, M. (2017). High-throughput physiological phenotyping and screening system for the characterization of plant–environment interactions. *Plant Journal*, *89*(4), 839-850.

Han, L., Yang, G., Dai, H., Xu, B., Yang, H., Feng, H., ... & Yang, X. (2019). Modeling maize above-ground biomass based on machine learning approaches using UAV remote-sensing data. *Plant Methods*, *15*(1), 1-19.

Han, M., Okamoto, M., Beatty, P. H., Rothstein, S. J., & Good, A. G. (2015). The genetics of nitrogen use efficiency in crop plants. *Annual Review of Genetics*, *49*, 269-289.

Hansen, M., Friis, C., Bowra, S., Holm, P. B., & Vincze, E. (2009). A pathway-specific microarray analysis highlights the complex and co-ordinated transcriptional networks of the developing grain of field-grown barley. *Journal of Experimental Botany*, *60*(1), 153-167.

Hargreaves, C. E., Gregory, P. J., & Bengough, A. G. (2009). Measuring root traits in barley (*Hordeum vulgare* ssp. *vulgare* and ssp. *spontaneum*) seedlings using gel chambers, soil sacs and X-ray microtomography. *Plant and Soil*, *316*, 285-297.

Hartl, L., Mohler, V., Zeller, F. J., Hsam, S. L., & Schweizer, G. (1999). Identification of AFLP markers closely linked to the powdery mildew resistance genes Pm1c and Pm4a in common wheat (*Triticum aestivum* L.). *Genome*, *42*(2), 322-329.

Hawkesford, M. J. (2012). Improving nutrient use efficiency in crops. eLS. *Chichester: John Wiley & Sons, Ltd.* doi.*10*(9780470015902), a0023734.

Hawkesford, M. J. (2014). Reducing the reliance on nitrogen fertilizer for wheat production. *Journal of Cereal Science*, *59*(3), 276-283.

Hawkesford, M. J. (2017). Genetic variation in traits for nitrogen use efficiency in wheat. *Journal of Experimental Botany*, *68*(10), 2627-2632.

Hawkesford, M. J., & Griffiths, S. (2019). Exploiting genetic variation in nitrogen use efficiency for cereal crop improvement. *Current Opinion in Plant Biology*, *49*, 35-42.

Hawkesford, M. J., & Riche, A. B. (2020). Impacts of G x E x M on nitrogen use efficiency in wheat and future prospects. *Frontiers in Plant Science*, *11*, 1157.

He, X., Qu, B., Li, W., Zhao, X., Teng, W., Ma, W., ... & Tong, Y. (2015). The nitrate-inducible NAC transcription factor TaNAC2-5A controls nitrate response and increases wheat yield. *Plant Physiology*, *169*(3), 1991-2005.

Heffer, P., Gruère, A., & Roberts, T. (2013). Assessment of fertilizer use by crop at the global level. *International Fertilizer Industry Association, Paris*.

Hensman, J., Fusi, N., & Lawrence, N. D. (2013). Gaussian processes for big data. *arXiv preprint arXiv:1309.6835*.

Herold, M. B., Baggs, E. M., & Daniell, T. J. (2012). Fungal and bacterial denitrification are differently affected by long-term pH amendment and cultivation of arable soil. *Soil Biology and Biochemistry*, *54*, 25-35.

Hirel, B., Le Gouis, J., Ney, B., & Gallais, A. (2007). The challenge of improving nitrogen use efficiency in crop plants: towards a more central role for genetic variability and quantitative genetics within integrated approaches. *Journal of Experimental Botany*, *58*(9), 2369-2387.

Hirel, B., Tétu, T., Lea, P. J., & Dubois, F. (2011). Improving nitrogen use efficiency in crops for sustainable agriculture. *Sustainability*, *3*(9), 1452-1485.

Hitz, K., Clark, A. J., & Van Sanford, D. A. (2017). Identifying nitrogen-use efficient soft red winter wheat lines in high and low nitrogen environments. *Field Crops Research*, *200*, 1-9.

Hoad, S. P., Russell, G., Lucas, M. E., & Bingham, I. J. (2001). The management of wheat, barley, and oat root systems. *Advances in Agronomy*, 74, 193-246.

Hochholdinger, F., & Tuberosa, R. (2009). Genetic and genomic dissection of maize root development and architecture. *Current Opinion in Plant Biology*, *12*(2), 172-177.

Homolová, L., Malenovský, Z., Clevers, J. G., García-Santos, G., & Schaepman, M. E. (2013). Review of optical-based remote sensing for plant trait mapping. *Ecological Complexity*, *15*, 1-16.

Horii, H., Nemoto, K., Miyamoto, N., & Harada, J. (2006). Quantitative trait loci for adventitious and lateral roots in rice. *Plant Breeding*, *125*(2), 198-200.

Hosoi, F., & Omasa, K. (2009). Estimating vertical plant area density profile and growth parameters of a wheat canopy at different growth stages using three-dimensional portable lidar imaging. *ISPRS Journal of Photogrammetry and Remote Sensing*, *64*(2), 151-158.

Howarth, J. R., Parmar, S., Jones, J., Shepherd, C. E., Corol, D. I., Galster, A. M., ... & Hawkesford, M. J. (2008). Co-ordinated expression of amino acid metabolism in response to N and S deficiency during wheat grain filling. *Journal of Experimental Botany*, *59*(13), 3675-3689.

https://www.wheatinitiative.org/strategic-research-agenda

Hu, X., Zhang, Y., Zhang, J., Islam, S., She, M., Zhao, Y., ... & Ma, W. (2021). Consensus genetic linkage map construction based on one common parental line for QTL mapping in wheat. *Agronomy*, *11*(2), 227.

Hund, A., Ruta, N., & Liedgens, M. (2009). Rooting depth and water use efficiency of tropical maize inbred lines, differing in drought tolerance. *Plant and Soil*, *318*, 311-325.

Hurley, T. M., Malzer, G. L., & Kilian, B. (2004). Estimating site-specific nitrogen crop response functions: A conceptual framework and geostatistical model. *Agronomy Journal*, *96*(5), 1331-1343.

IFA Annual Report 2021. (n.d.). www.fertilizer.org.

Imai, K., Suzuki, Y., Mae, T., & Makino, A. (2008). Changes in the synthesis of Rubisco in rice leaves in relation to senescence and N influx. *Annals of Botany*, *101*(1), 135-144.

Islam, M. Z., Sattar, M. A., Ashrafuzzaman, M., Saud, H. M., & Uddin, M. K. (2012). Improvement of yield potential of rice through combined application of biofertilizer and chemical nitrogen. *African Journal of Microbiology Research*, *6*(4), 745-750.

Islam, S., Zhang, J., Zhao, Y., She, M., & Ma, W. (2021). Genetic regulation of the traits contributing to wheat nitrogen use efficiency. *Plant Science*, *303*, 110759.

Jaccoud, D., Peng, K., Feinstein, D., & Kilian, A. (2001). Diversity arrays: a solid-state technology for sequence information independent genotyping. *Nucleic Acids Research*, *29*(4), e25-e25.

Javed, T., Singhal, R. K., Shabbir, R., Shah, A. N., Kumar, P., Jinger, D., ... & Siuta, D. (2022). Recent advances in agronomic and physio-molecular approaches for improving nitrogen use efficiency in crop plants. *Frontiers in Plant Science*, *13*, 877544.

Jiang, L., Sun, L., Ye, M., Wang, J., Wang, Y., Bogard, M., ... & Wu, R. (2019). Functional mapping of N deficiency-induced response in wheat yield-component traits by implementing high-throughput phenotyping. *Plant Journal*, *97*(6), 1105-1119.

Jin, H., Wen, W., Liu, J., Zhai, S., Zhang, Y., Yan, J., ... & He, Z. (2016). Genome-wide QTL mapping for wheat processing quality parameters in a Gaocheng 8901/Zhoumai 16 recombinant inbred line population. *Frontiers in Plant Science*, *7*, 1032.

Jin, X., Shi, C., Yu, C. Y., Yamada, T., & Sacks, E. J. (2017). Determination of leaf water content by visible and near-infrared spectrometry and multivariate calibration in Miscanthus. *Frontiers in Plant Science*, *8*, 721.

Johannsen, W. (1911). The genotype conception of heredity. *American Naturalist*, *45*(531), 129-159.

Joshi, C. P., & Nguyen, H. T. (1993). RAPD (random amplified polymorphic DNA) analysis based intervarietal genetic relationships among hexaploid wheats. *Plant Science*, *93*(1-2), 95-103.

Kah, M., Tufenkji, N., & White, J. C. (2019). Nano-enabled strategies to enhance crop nutrition and protection. *Nature Nanotechnology*, *14*(6), 532-540.

Kaiser, W. M., Planchet, E. and Rumer, S. (2011) Nitrate reductase and nitric oxide. In: C. H. Foyer, and H. Zhang (eds), Annual Plant Reviews, Nitrogen Metabolism in Plants in the Post-genomic Era, 127—146. Wiley-Blackwell, Chichester.

Kamal, N. M., Gorafi, Y. S. A., Abdelrahman, M., Abdellatef, E., & Tsujimoto, H. (2019). Stay-green trait: A prospective approach for yield potential, and drought and heat stress adaptation in globally important cereals. *International Journal of Molecular Sciences*, *20*(23), 5837.

Kant, S., Bi, Y. M., & Rothstein, S. J. (2011). Understanding plant response to nitrogen limitation for the improvement of crop nitrogen use efficiency. *Journal of Experimental Botany*, *62*(4), 1499-1509.

Katkout, M., Kishii, M., Kawaura, K., Mishina, K., Sakuma, S., Umeda, K., ... & Ogihara, Y. (2014). QTL analysis of genetic loci affecting domestication-related spike characters in common wheat. *Genes & Genetic Systems*, *89*(3), 121-131.

Khan, J. (2020). *Deciphering the Genetic Architecture of Spike Fertility, Spike Harvest Index and Complex Physiological Mechanisms to Increase Harvest Index, Yield and Prediction Accuracy in US Soft Wheat Under High and Moderately Drought Environments* (Doctoral dissertation, University of Florida).

Kipp, S., Mistele, B., Baresel, P., & Schmidhalter, U. (2014). High-throughput phenotyping early plant vigour of winter wheat. *European Journal of Agronomy*, *52*, 271-278.

Kjeldahl, J. G. C. T. (1883). Neue methode zur bestimmung des stickstoffs in organischen körpern. *Zeitschrift für analytische Chemie*, *22*(1), 366-382.

Klukas, C., Chen, D., & Pape, J. M. (2014). Integrated analysis platform: an open-source information system for high-throughput plant phenotyping. *Plant Physiology*, *165*(2), 506-518.

Koch, B., Khosla, R., Frasier, W. M., Westfall, D. G., & Inman, D. (2004). Economic feasibility of variable-rate nitrogen application utilizing site-specific management zones. *Agronomy Journal*, *96*(6), 1572-1580.

Koehrsen, W. (2018). Introduction to Bayesian linear regression. *An explanation of the Bayesian approach to linear modeling. Towards Data Sci*, *4*(1).

Kowalski, A. M., Gooding, M., Ferrante, A., Slafer, G. A., Orford, S., Gasperini, D., & Griffiths, S. (2016). Agronomic assessment of the wheat semi-dwarfing gene Rht8 in contrasting nitrogen treatments and water regimes. *Field Crops Research*, *191*, 150-160.

Krauth, K., Bonilla, E. V., Cutajar, K., & Filippone, M. (2016). AutoGP: Exploring the capabilities and limitations of Gaussian process models. *arXiv preprint arXiv:1610.05392*.

Kumar, A., Mantovani, E. E., Seetan, R., Soltani, A., Echeverry-Solarte, M., Jain, S., ... & Mergoum, M. (2016). Dissection of genetic factors underlying wheat kernel shape and size in an elite× non adapted cross using a highdensity SNP linkage map. *The Plant Genome*, *9*(1), plantgenome2015-09.

Kunert, A., Naz, A. A., Dedeck, O., Pillen, K., & Léon, J. (2007). AB-QTL analysis in winter wheat: I. Synthetic hexaploid wheat (*T. turgidum ssp. dicoccoides*× *T. tauschii*) as a source of

favourable alleles for milling and baking quality traits. *Theoretical and Applied Genetics*, *115*, 683-695.

Kurakawa, T., Ueda, N., Maekawa, M., Kobayashi, K., Kojima, M., Nagato, Y., ... & Kyozuka, J. (2007). Direct control of shoot meristem activity by a cytokinin-activating enzyme. *Nature*, *445*(7128), 652-655.

Labboun, S., Tercé-Laforgue, T., Roscher, A., Bedu, M., Restivo, F. M., Velanis, C. N., ... & Hirel, B. (2009). Resolving the role of plant glutamate dehydrogenase. I. in vivo real time nuclear magnetic resonance spectroscopy experiments. *Plant and Cell Physiology*, *50*(10), 1761-1773.

Laperche, A., Brancourt-Hulmel, M., Heumez, E., Gardet, O., & Gouis, J. L. (2006). Estimation of genetic parameters of a DH wheat population grown at different N stress levels characterized by probe genotypes. *Theoretical and Applied Genetics*, *112*(5), 797-807.

Lassaletta, L., Billen, G., Grizzetti, B., Anglade, J., & Garnier, J. (2014). 50-year trends in nitrogen use efficiency of world cropping systems: the relationship between yield and nitrogen input to cropland. *Environmental Research Letters*, *9*(10), 105011.

Latshaw, S. P., Vigil, M. F., & Haley, S. D. (2016). Genotypic differences for nitrogen use efficiency and grain protein deviation in hard winter wheat. *Agronomy Journal*, *108*(6), 2201-2213.

Laza, R. C., Bergman, B., & Vergara, B. S. (1993). Cultivar differences in growth and chloroplast ultrastructure in rice as affected by nitrogen. *Journal of Experimental Botany*, *44*(11), 1643-1648.

Le Gouis, J., Béghin, D., Heumez, E., & Pluchard, P. (2000). Genetic differences for nitrogen uptake and nitrogen utilisation efficiencies in winter wheat. *European Journal of Agronomy*, *12*(3-4), 163-173.

Lea, P. J., & Miflin, B. J. (2011). Nitrogen assimilation and its relevance to crop improvement. *Annu. Plant Reviews. 42*, 1-40.

Lefsky, M. A., Cohen, W. B., Parker, G. G., & Harding, D. J. (2002). Lidar remote sensing for ecosystem studies: Lidar, an emerging remote sensing technology that directly measures the three-dimensional distribution of plant canopies, can accurately estimate vegetation structural attributes and should be of particular interest to forest, landscape, and global ecologists. *BioScience*, *52*(1), 19-30.

Li, J., Nishimura, Y., Zhao, X., & Fukumoto, Y. (2016). Effect of Nitrogen Application on Active Oxygen Species, Senescence, Photosynthesis, and Growth in Cucumber 'Jinchun No. 5'Seedlings. *Japan Agricultural Research Quarterly: JARQ*, *50*(3), 285-292.

Li, M., Wang, T., Zhang, H., Liu, S., Li, W., Abou Elwafa, S. F., & Tian, H. (2022). Tanrt2. 1-6b is a dual-affinity nitrate transporter contributing to nitrogen uptake in bread wheat under both nitrogen deficiency and sufficiency. *Crop Journal*, *10*(4), 993-1005.

Li, Y., Wu, Y., Hernandez-Espinosa, N., & Peña, R. J. (2013). The influence of drought and heat stress on the expression of end-use quality parameters of common wheat. *Journal of Cereal Science*, *57*(1), 73-78.

Li, Y., Xiao, J., Chen, L., Huang, X., Cheng, Z., Han, B., ... & Wu, C. (2018). Rice functional genomics research: past decade and future. *Molecular Plant*, *11*(3), 359-380.

Li, Z., Li, B., & Tong, Y. (2008). The contribution of distant hybridization with decaploid Agropyron elongatum to wheat improvement in China. *Journal of Genetics and Genomics*, *35*(8), 451-456.

Lincoln, S. E., Daly, M. J., & Lander, E. S. (1993). Constructing genetic linkage maps with MAPMAKER/EXP Version 3.0: a tutorial and reference manual. *A Whitehead Institute for Biomedical Research Technical Report*, *3*.

Liu, M., Wu, X., Li, C., Li, M., Xiong, T., & Tang, Y. (2020). Dry matter and nitrogen accumulation, partitioning, and translocation in synthetic-derived wheat cultivars under nitrogen deficiency at the post-jointing stage. *Field Crops Research*, *248*, 107720.

Liu, Q., Wu, K., Song, W., Zhong, N., Wu, Y., & Fu, X. (2022). Improving crop nitrogen use efficiency toward sustainable green revolution. *Annual Review of Plant Biology*, *73*, 523-551.

Liu, X., Wang, S., Deng, X., Zhang, Z., & Yin, L. (2020). Comprehensive evaluation of physiological traits under nitrogen stress and participation of linolenic acid in nitrogen-deficiency response in wheat seedlings. *BMC Plant Biology*, *20*, 1-16.

Lobet, G., Pagès, L., & Draye, X. (2011). A novel image-analysis toolbox enabling quantitative analysis of root system architecture. *Plant Physiology*, *157*(1), 29-39.

Lontoc-Roy, M., Dutilleul, P., Prasher, S. O., Han, L., Brouillet, T., & Smith, D. L. (2006). Advances in the acquisition and analysis of CT scan data to isolate a crop root system from the soil medium and quantify root system complexity in 3-D space. *Geoderma*, *137*(1-2), 231-241.

Lopes, M. S., & Reynolds, M. P. (2012). Stay-green in spring wheat can be determined by spectral reflectance measurements (normalized difference vegetation index) independently from phenology. *Journal of Experimental Botany*, *63*(10), 3789-3798.

Lopez-Bellido, R. J., Shepherd, C. E., & Barraclough, P. B. (2004). Predicting post-anthesis N requirements of bread wheat with a Minolta SPAD meter. *European Journal of Agronomy*, *20*(3), 313-320.

Lou, H., Zhao, B., Peng, Y., El-Badri, A. M., Batool, M., Wang, C., ... & Zhou, G. (2023). Auxin plays a key role in nitrogen and plant density-modulated root growth and yield in different plant types of rapeseed. *Field Crops Research*, *302*, 109066.

Lozada, D. N., Mason, R. E., Sukumaran, S., & Dreisigacker, S. (2018). Validation of grain yield QTLs from soft winter wheat using a CIMMYT spring wheat panel. *Crop Science*, *58*(5), 1964-1971.

Lu, N., Zhou, J., Han, Z., Li, D., Cao, Q., Yao, X., ... & Cheng, T. (2019). Improved estimation of aboveground biomass in wheat from RGB imagery and point cloud data acquired with a low-cost unmanned aerial vehicle system. *Plant Methods*, *15*(1), 1-16.

Lu, Y., Jeffers, R., Raju, A., Kenny, T., Ratchanniyasamu, E., & Fricke, W. (2023). Does night-time transpiration provide any benefit to wheat (*Triticum aestivum* L.) plants which are exposed to salt stress? *Physiologia Plantarum*, *175*(1), e13839.

Luo, W., Ma, J., Zhou, X. H., Sun, M., Kong, X. C., Wei, Y. M., ... & Lan, X. J. (2016). Identification of quantitative trait loci controlling agronomic traits indicates breeding potential of Tibetan semiwild wheat (*Triticum aestivum* ssp. *tibetanum*). *Crop Science*, *56*(5), 2410-2420.

Lv, X., Zhang, Y., Hu, L., Zhang, Y., Zhang, B., Xia, H., ... & Kong, L. (2021). Low-nitrogen stress stimulates lateral root initiation and nitrogen assimilation in wheat: roles of phytohormone signaling. *Journal of Plant Growth Regulation*, *40*, 436-450.

Lyra, D. H., Virlet, N., Sadeghi-Tehran, P., Hassall, K. L., Wingen, L. U., Orford, S., ... & Slavov, G. T. (2020). Functional QTL mapping and genomic prediction of canopy height in wheat measured using a robotic field phenotyping platform. *Journal of Experimental Botany*, *71*(6), 1885-1898.

Ma, J., Qin, N., Cai, B., Chen, G., Ding, P., Zhang, H., ... & Wei, Y. (2019). Identification and validation of a novel major QTL for all-stage stripe rust resistance on 1BL in the winter wheat line 20828. *Theoretical and Applied Genetics*, *132*, 1363-1373.

MacFall, J. S., & Johnson, G. A. (2007). Plants, seeds, roots, and soils as applications of magnetic resonance microscopy. In: R. K. Harris, and R. E. Wasylishen (eds), Encyclopedia of NMR, Vol. 6, 3403-3409. John Wiley & Sons, Chichester, UK.

Mairhofer, S., Zappala, S., Tracy, S., Sturrock, C., Bennett, M. J., Mooney, S. J., & Pridmore, T. P. (2013). Recovering complete plant root system architectures from soil via X-ray μ-computed tomography. *Plant Methods*, *9*(1), 1-7.

Majumder, S., Neogi, S., Dutta, T., Powel, M. A., & Banik, P. (2019). The impact of biochar on soil carbon sequestration: meta-analytical approach to evaluating environmental and economic advantages. *Journal of Environmental Management*, *250*, 109466.

Masclaux-Daubresse, C., Daniel-Vedele, F., Dechorgnat, J., Chardon, F., Gaufichon, L., & Suzuki, A. (2010). Nitrogen uptake, assimilation and remobilization in plants: challenges for sustainable and productive agriculture. *Annals of Botany*, *105*(7), 1141-1157.

Matsuoka, Y. (2011). Evolution of polyploid Triticum wheats under cultivation: the role of domestication, natural hybridization and allopolyploid speciation in their diversification. *Plant and Cell Physiology*, *52*(5), 750-764.

Mattsson, M., & Schjoerring, J. K. (1996). Ammonia emission from young barley plants: influence of N source, light/dark cycles and inhibition of glutamine synthetase. *Journal of Experimental Botany*, *47*(4), 477-484.

McAllister, C. H., Beatty, P. H., & Good, A. G. (2012). Engineering nitrogen use efficient crop plants: the current status. *Plant Biotechnology Journal*, *10*(9), 1011-1025.

McDonald, T. R., & Ward, J. M. (2016). Evolution of electrogenic ammonium transporters (AMTs). *Frontiers in Plant Science*, *7*, 352.

Mejias, J. H., Salazar, F., Pérez Amaro, L., Hube, S., Rodriguez, M., & Alfaro, M. (2021). Nanofertilizers: A cutting-edge approach to increase nitrogen use efficiency in grasslands. *Frontiers in Environmental Science*, *9*, 52.

Mendel, R. R. (2022). The history of the molybdenum cofactor—A personal view. *Molecules*, *27*(15), 4934.

Metzner, R., Eggert, A., van Dusschoten, D., Pflugfelder, D., Gerth, S., Schurr, U., ... & Jahnke, S. (2015). Direct comparison of MRI and X-ray CT technologies for 3D imaging of root systems in soil: potential and challenges for root trait quantification. *Plant Methods*, *11*(1), 1-11.

Mi, G., Tang, L., Zhang, F., & Zhang, J. (2000). Is nitrogen uptake after anthesis in wheat regulated by sink size? *Field Crops Research*, *68*(3), 183-190.

Mierzwa-Hersztek, M., Wolny-Koładka, K., Gondek, K., Gałązka, A., & Gawryjołek, K. (2020). Effect of coapplication of biochar and nutrients on microbiocenotic composition, dehydrogenase activity index and chemical properties of sandy soil. *Waste and Biomass Valorization*, *11*, 3911-3923.

Mirosavljević, M., Momčilović, V., Mikić, S., Trkulja, D., Brbaklić, L., Zorić, M., & Abičić, I. (2020). Changes in stay-green and nitrogen use efficiency traits in historical set of winter barley cultivars. *Field Crops Research*, *249*, 107740.

Moll, R. H., Kamprath, E. J., & Jackson, W. A. (1982). Analysis and interpretation of factors which contribute to efficiency of nitrogen utilization 1. *Agronomy Journal*, *74*(3), 562-564.

Monneveux, P., Zaidi, P. H., & Sanchez, C. (2005). Population density and low nitrogen affects yield-associated traits in tropical maize. *Crop Science*, *45*(2), 535-545.

Monostori, I., Szira, F., Tondelli, A., Árendás, T., Gierczik, K., Cattivelli, L., ... & Vágújfalvi, A. (2017). Genome-wide association study and genetic diversity analysis on nitrogen use efficiency in a Central European winter wheat (*Triticum aestivum* L.) collection. *PLoS One*, *12*(12), e0189265.

Mooney, S. J., Pridmore, T. P., Helliwell, J., & Bennett, M. J. (2012). Developing X-ray computed tomography to non-invasively image 3-D root systems architecture in soil. *Plant and Soil*, *352*, 1-22.

Mudalagiriyappa, B., Raghavendra Goud, B., Ramachandrappa, B. K., & Nanjappa, H. V. (2015). Influence of customized fertilizers on growth and yield of Finger Millet {Eleusine coracana (L.) Gaertn.} in Alfisols of Southern India. *Indian Journal of Dryland Agricultural Research and Development*, *30*(1), 50-54.

Mueller, S. M., & Vyn, T. J. (2018). Physiological constraints to realizing maize grain yield recovery with silking-stage nitrogen fertilizer applications. *Field Crops Research*, *228*, 102-109.

Mueller, S. M., Messina, C. D., & Vyn, T. J. (2019). The role of the exponential and linear phases of maize (*Zea mays* L.) ear growth for determination of kernel number and kernel weight. *European Journal of Agronomy*, *111*, 125939.

Mulla, D. J. Precision Agriculture: Key Advances and Remaining Knowledge Gaps.

Muñoz-Huerta, R. F., Guevara-Gonzalez, R. G., Contreras-Medina, L. M., Torres-Pacheco, I., Prado-Olivarez, J., & Ocampo-Velazquez, R. V. (2013). A review of methods for sensing the nitrogen status in plants: advantages, disadvantages and recent advances. *Sensors*, *13*(8), 10823-10843.

Muraya, M. M., Chu, J., Zhao, Y., Junker, A., Klukas, C., Reif, J. C., & Altmann, T. (2017). Genetic variation of growth dynamics in maize (*Zea mays* L.) revealed through automated non-invasive phenotyping. *Plant Journal*, *89*(2), 366-380.

Muurinen, S., Slafer, G. A., & Peltonen-Sainio, P. (2006). Breeding effects on nitrogen use efficiency of spring cereals under northern conditions. *Crop Science*, *46*(2), 561-568.

Nagel, K. A., Putz, A., Gilmer, F., Heinz, K., Fischbach, A., Pfeifer, J., ... & Schurr, U. (2012). GROWSCREEN-Rhizo is a novel phenotyping robot enabling simultaneous measurements of root and shoot growth for plants grown in soil-filled rhizotrons. *Functional Plant Biology*, *39*(11), 891-904.

Nakano, H., Makino, A., & Mae, T. (1997). The effect of elevated partial pressures of CO2 on the relationship between photosynthetic capacity and N content in rice leaves. *Plant Physiology*, *115*(1), 191-198.

Nakano, S., Takahashi, M., Sakamoto, A., Morikawa, H., & Katayanagi, K. (2012). Structure–function relationship of assimilatory nitrite reductases from the leaf and root of tobacco based on high-resolution structures. *Protein Science*, *21*(3), 383-395.

Nave, M., Avni, R., Ben-Zvi, B., Hale, I., & Distelfeld, A. (2016). QTLs for uniform grain dimensions and germination selected during wheat domestication are co-located on chromosome 4B. *Theoretical and Applied Genetics*, *129*, 1303-1315.

Neilson, E. H., Edwards, A. M., Blomstedt, C. K., Berger, B., Møller, B. L., & Gleadow, R. M. (2015). Utilization of a high-throughput shoot imaging system to examine the dynamic phenotypic responses of a C4 cereal crop plant to nitrogen and water deficiency over time. *Journal of Experimental Botany*, *66*(7), 1817-1832.

Nelson, D. R., & Mele, P. M. (2006). The impact of crop residue amendments and lime on microbial community structure and nitrogen-fixing bacteria in the wheat rhizosphere. *Soil Research*, *44*(4), 319-329.

Németh, E., Nagy, Z., & Pécsváradi, A. (2018). Chloroplast glutamine synthetase, the key regulator of nitrogen metabolism in wheat, performs its role by fine regulation of enzyme activity via negative cooperativity of its subunits. *Frontiers in Plant Science*, *9*, 191.

Neumann, K., Klukas, C., Friedel, S., Rischbeck, P., Chen, D., Entzian, A., ... & Kilian, B. (2015). Dissecting spatiotemporal biomass accumulation in barley under different water regimes using high-throughput image analysis. *Plant, Cell & Environment*, *38*(10), 1980-1996.

Nguyen, C. (2003). Rhizodeposition of organic C by plants: mechanisms and controls. *Agronomie*, *23*(5-6), 375-396.

Nguyen, G. N., & Kant, S. (2018). Improving nitrogen use efficiency in plants: effective phenotyping in conjunction with agronomic and genetic approaches. *Functional Plant Biology*, *45*(6), 606-619.

Nigro, D., Fortunato, S., Giove, S. L., Mangini, G., Yacoubi, I., Simeone, R., ... & Gadaleta, A. (2017). Allelic variants of glutamine synthetase and glutamate synthase genes in a collection of durum wheat and association with grain protein content. *Diversity*, *9*(4), 52.

Nigro, D., Gu, Y. Q., Huo, N., Marcotuli, I., Blanco, A., Gadaleta, A., & Anderson, O. D. (2013). Structural analysis of the wheat genes encoding NADH-dependent glutamine-2-oxoglutarate amidotransferases and correlation with grain protein content. *PLoS One*, *8*(9), e73751.

Ogutu, J. O., Schulz-Streeck, T., & Piepho, H. P. (2012). Genomic selection using regularized linear regression models: ridge regression, lasso, elastic net and their extensions. In *BMC proceedings* (Vol. 6, pp. 1-6). BioMed Central.

Olivoto, T., & Lúcio, A. D. C. (2020). metan: An R package for multi-environment trial analysis. *Methods in Ecology and Evolution*, *11*(6), 783-789.

Olsen, S. R., & Sommers, L. E. (1982). Phosphorus. pp. 403-430. In: A. L. Page, et al. (eds.) *Methods of soil analysis*: Part 2. Chemical and microbiological properties. Agron. Mongr. 9. 2nd ed. ASA and SSSA, Madison, WI.

Omasa, K., Hosoi, F., & Konishi, A. (2007). 3D lidar imaging for detecting and understanding plant responses and canopy structure. *Journal of Experimental Botany*, *58*(4), 881-898.

Ortiz-Monasterio, J. I., Manske, G. G. B., & Van Ginkel, M. (2001). Nitrogen and phosphorus use efficiency. *Application of Physiology in Wheat Breeding*, 200-207.

Ortiz-Monasterio R, J. I., Sayre, K. D., Rajaram, S., & McMahon, M. (1997). Genetic progress in wheat yield and nitrogen use efficiency under four nitrogen rates. *Crop Science*, *37*(3), 898-904.

Oury, F. X. F. X., Berard, P., Brancourt-Hulmel, M., Depatureaux, C., Doussinault, G., Galic, N., ... & Trottet, M. (2003). Yield and grain protein concentration in bread wheat: a review and a study of multi-annual data from a French breeding program. *Journal of Genetics and Breeding*, (57), 59-68.

Oury, F. X., & Godin, C. (2007). Yield and grain protein concentration in bread wheat: how to use the negative relationship between the two characters to identify favourable genotypes? *Euphytica*, *157*(1-2), 45-57.

Pandey, P., Ge, Y., Stoerger, V., & Schnable, J. C. (2017). High throughput in vivo analysis of plant leaf chemical properties using hyperspectral imaging. *Frontiers in Plant Science*, *8*, 1348.

Parent, B., Shahinnia, F., Maphosa, L., Berger, B., Rabie, H., Chalmers, K., ... & Fleury, D. (2015). Combining field performance with controlled environment plant imaging to identify the genetic

control of growth and transpiration underlying yield response to water-deficit stress in wheat. *Journal of Experimental Botany*, *66*(18), 5481-5492.

Parry, M. A. J., Madgwick, P. J., Carvalho, J. F. C., & Andralojc, P. J. (2007). Prospects for increasing photosynthesis by overcoming the limitations of Rubisco. *Journal of Agricultural Science*, *145*(1), 31.

Parry, M. A., & Hawkesford, M. J. (2010). Food security: increasing yield and improving resource use efficiency. *Proceedings of the Nutrition Society*, *69*(4), 592-600.

Parry, M. A., Reynolds, M., Salvucci, M. E., Raines, C., Andralojc, P. J., Zhu, X. G., ... & Furbank, R. T. (2011). Raising yield potential of wheat. II. Increasing photosynthetic capacity and efficiency. *Journal of Experimental Botany*, *62*(2), 453-467.

Pask, A. (2009). *Optimising nitrogen storage in wheat canopies for genetic reduction in fertiliser nitrogen inputs* (Doctoral dissertation, University of Nottingham).

Pask, A. J. D., Sylvester-Bradley, R., Jamieson, P. D., & Foulkes, M. J. (2012). Quantifying how winter wheat crops accumulate and use nitrogen reserves during growth. *Field Crops Research*, *126*, 104-118.

Passioura, J. B. (2006). The perils of pot experiments. *Functional Plant Biology*, *33*(12), 1075-1079.

Passioura, J. B. (2010). Scaling up: the essence of effective agricultural research. *Functional Plant Biology*, *37*(7), 585-591.

Perchlik, M., & Tegeder, M. (2017). Improving plant nitrogen use efficiency through alteration of amino acid transport processes. *Plant Physiology*, *175*(1), 235-247.

Pérez-Valencia, D. M., Rodríguez-Álvarez, M. X., Boer, M. P., Kronenberg, L., Hund, A., Cabrera-Bosquet, L., ... & Eeuwijk, F. A. V. (2022). A two-stage approach for the spatio-temporal analysis of high-throughput phenotyping data. *Scientific Reports*, *12*(1), 3177.

Poiré, R., Chochois, V., Sirault, X. R., Vogel, J. P., Watt, M., & Furbank, R. T. (2014). Digital imaging approaches for phenotyping whole plant nitrogen and phosphorus response in Brachypodium distachyon. Journal of Integrative Plant Biology, 56(8), 781-796.

Poorter, H., Bühler, J., van Dusschoten, D., Climent, J., & Postma, J. A. (2012). Pot size matters: a meta-analysis of the effects of rooting volume on plant growth. *Functional Plant Biology*, *39*(11), 839-850.

Porker, K., Straight, M., & Hunt, J. R. (2020). Evaluation of G× E× M interactions to increase harvest index and yield of early sown wheat. *Frontiers in Plant Science*, 994, 11:994. doi: 10.3389/fpls.2020.00994.

Prins, A., Orr, D. J., Andralojc, P. J., Reynolds, M. P., Carmo-Silva, E., & Parry, M. A. (2016). Rubisco catalytic properties of wild and domesticated relatives provide scope for improving wheat photosynthesis. *Journal of Experimental Botany*, *67*(6), 1827-1838.

Prommer, J., Wanek, W., Hofhansl, F., Trojan, D., Offre, P., Urich, T., ... & Hood-Nowotny, R. C. (2014). Biochar decelerates soil organic nitrogen cycling but stimulates soil nitrification in a temperate arable field trial. *PloS one*, *9*(1), e86388.

Purcell, S., Cherny, S. S., & Sham, P. C. (2003). Genetic Power Calculator: design of linkage and association genetic mapping studies of complex traits. *Bioinformatics*, *19*(1), 149-150.

Quraishi, U. M., Abrouk, M., Murat, F., Pont, C., Foucrier, S., Desmaizieres, G., ... & Salse, J. (2011). Cross-genome map-based dissection of a nitrogen use efficiency ortho-metaQTL in bread wheat unravels concerted cereal genome evolution. *Plant Journal*, *65*(5), 745-756.

Rabab, S., Breen, E., Gebremedhin, A., Shi, F., Badenhorst, P., Chen, Y. P. P., & Daetwyler, H. D. (2021). A New Method for Extracting Individual Plant Bio-Characteristics from High-Resolution Digital Images. *Remote Sensing*, *13*(6), 1212.

Rafalski, A. (2002). Applications of single nucleotide polymorphisms in crop genetics. *Current Opinion in Plant Biology*, *5*(2), 94-100.

Rahaman, M. M., Ahsan, M. A., Gillani, Z., & Chen, M. (2017). Digital biomass accumulation using high-throughput plant phenotype data analysis. *Journal of Integrative Bioinformatics*, *14*(3), 20170028.

Raigar, O. P., Mondal, K., Sethi, M., Singh, M. P., Singh, J., Kumari, A., & Sekhon, B. S. (2022). Nitrogen use efficiency in wheat: genome to field. In *Wheat*. IntechOpen.

Rambo, L., Ma, B. L., Xiong, Y., & Regis Ferreira da Silvia, P. (2010). Leaf and canopy optical characteristics as crop-N-status indicators for field nitrogen management in corn. *Journal of Plant Nutrition and Soil Science*, *173*(3), 434-443.

Ranjan, R., Yadav, R., Jain, N., Sinha, N., Bainsla, N. K., Gaikwad, K. B., & Kumar, M. (2021). Epistatic QTLsPlay a major role in nitrogen use efficiency and its component traits in Indian spring wheat. *Agriculture*, *11*(11), 1149.

Rao, I. S., Neeraja, C. N., Srikanth, B., Subrahmanyam, D., Swamy, K. N., Rajesh, K., ... & Voleti, S. R. (2018). Identification of rice landraces with promising yield and the associated genomic regions under low nitrogen. *Scientific Reports*, *8*(1), 9200.

Rasheed, A., & Xia, X. (2019). From markers to genome-based breeding in wheat. *Theoretical and Applied Genetics*, *132*, 767-784.

Rasheed, A., Wen, W., Gao, F., Zhai, S., Jin, H., Liu, J., ... & He, Z. (2016). Development and validation of KASP assays for genes underpinning key economic traits in bread wheat. *Theoretical and Applied Genetics*, *129*, 1843-1860.

Raun, W. R., & Johnson, G. V. (1999). Improving nitrogen use efficiency for cereal production. *Agronomy Journal*, *91*(3), 357-363.

Raun, W. R., Solie, J. B., Johnson, G. V., Stone, M. L., Mullen, R. W., Freeman, K. W., ... & Lukina, E. V. (2002). Improving nitrogen use efficiency in cereal grain production with optical sensing and variable rate application. *Agronomy Journal*, *94*(4), 815-820.

Ravel, C., Martre, P., Romeuf, I., Dardevet, M., El-Malki, R., Bordes, J., ... & Charmet, G. (2009). Nucleotide polymorphism in the wheat transcriptional activator Spa influences its pattern of expression and has pleiotropic effects on grain protein composition, dough viscoelasticity, and grain hardness. *Plant Physiology*, *151*(4), 2133-2144.

Rawson, H. M., & Clarke, J. M. (1988). Nocturnal transpiration in wheat. *Functional Plant Biology*, *15*(3), 397-406.

Ray, D. K., Mueller, N. D., West, P. C., & Foley, J. A. (2013). Yield trends are insufficient to double global crop production by 2050. *PloS one*, *8*(6), e66428.

Rebolledo, M. C., Peña, A. L., Duitama, J., Cruz, D. F., Dingkuhn, M., Grenier, C., & Tohme, J. (2016). Combining image analysis, genome wide association studies and different field trials to reveal stable genetic regions related to panicle architecture and the number of spikelets per panicle in rice. *Frontiers in Plant Science*, *7*, 1384.

Reece, J. B., Urry, L. A., Cain, M. L., Wasserman, S. A., Minorsky, P. V., & Jackson, R. B. (2014). An introduction to ecology and the biosphere. *Campbell biology. Pearson Education Ine, Boston*, 1164-1165.

Ren, Y., Qian, Y., Xu, Y., Zou, C., Liu, D., Zhao, X., ... & Tong, Y. (2017). Characterization of QTLs for root traits of wheat grown under different nitrogen and phosphorus supply levels. *Frontiers in Plant Science*, *8*, 2096.

Reynolds, M., Dreccer, F., & Trethowan, R. (2007). Drought-adaptive traits derived from wheat wild relatives and landraces. *Journal of Experimental Botany*, *58*(2), 177-186.

Reynolds, M., Foulkes, M. J., Slafer, G. A., Berry, P., Parry, M. A., Snape, J. W., & Angus, W. J. (2009). Raising yield potential in wheat. *Journal of Experimental Botany*, *60*(7), 1899-1918.

Richard, C. A., Hickey, L. T., Fletcher, S., Jennings, R., Chenu, K., & Christopher, J. T. (2015). High-throughput phenotyping of seminal root traits in wheat. *Plant Methods*, *11*(1), 1-11.

Richardson, A. E., Barea, J. M., McNeill, A. M., & Prigent-Combaret, C. (2009). Acquisition of phosphorus and nitrogen in the rhizosphere and plant growth promotion by microorganisms. Plant and Soil, 321, 305-339.

Röder, M. S., Korzun, V., Wendehake, K., Plaschke, J., Tixier, M. H., Leroy, P., & Ganal, M. W. (1998). A microsatellite map of wheat. *Genetics*, *149*(4), 2007-2023.

Rogiers, S. Y., & Clarke, S. J. (2013). Nocturnal and daytime stomatal conductance respond to root-zone temperature in 'Shiraz'grapevines. *Annals of Botany*, *111*(3), 433-444.

Römer, C., Bürling, K., Hunsche, M., Rumpf, T., Noga, G., & Plümer, L. (2011). Robust fitting of fluorescence spectra for pre-symptomatic wheat leaf rust detection with support vector machines. *Computers and Electronics in Agriculture*, *79*(2), 180-188.

Roth, L., Rodríguez-Álvarez, M. X., van Eeuwijk, F., Piepho, H. P., & Hund, A. (2021). Phenomics data processing: A plot-level model for repeated measurements to extract the timing of key stages and quantities at defined time points. *Field Crops Research*, *274*, 108314.

Saberioon, M. M., Amin, M. S. M., Anuar, A. R., Gholizadeh, A., Wayayok, A., & Khairunniza-Bejo, S. (2014). Assessment of rice leaf chlorophyll content using visible bands at different growth stages at both the leaf and canopy scale. *International Journal of Applied Earth Observation and Geoinformation*, *32*, 35-45.

Sadras, V. O., & Lawson, C. (2013). Nitrogen and water-use efficiency of Australian wheat varieties released between 1958 and 2007. *European Journal of Agronomy*, *46*, 34-41.

Sahoo, R. K., Bhardwaj, D., & Tuteja, N. (2012). Biofertilizers: a sustainable eco-friendly agricultural approach to crop improvement. In *Plant acclimation to environmental stress* (pp. 403-432). New York, NY: Springer New York.

Saini, P., Sheikh, I., Saini, D. K., Mir, R. R., Dhaliwal, H. S., & Tyagi, V. (2022). Consensus genomic regions associated with grain protein content in hexaploid and tetraploid wheat. *Frontiers in Genetics*, *13*, 1021180.

Sakakibara, Y., Kimura, H., Iwamura, A., Saitoh, T., Ikegami, T., Kurisu, G., & Hase, T. (2012). A new structural insight into differential interaction of cyanobacterial and plant ferredoxins with nitrite reductase as revealed by NMR and X-ray crystallographic studies. *The Journal of Biochemistry*, *151*(5), 483-492.

Salvagiotti, F., & Miralles, D. J. (2008). Radiation interception, biomass production and grain yield as affected by the interaction of nitrogen and sulfur fertilization in wheat. *European Journal of Agronomy*, *28*(3), 282-290.

Sanchez-Bragado, R., Molero, G., Reynolds, M. P., & Araus, J. L. (2014). Relative contribution of shoot and ear photosynthesis to grain filling in wheat under good agronomical conditions assessed by differential organ δ13C. *Journal of Experimental Botany*, *65*(18), 5401-5413.

Sandhu, N., Kaur, A., Sethi, M., Kaur, S., Sharma, A., Bentley, A. R., ... & Chhuneja, P. (2021). Genetic dissection uncovers genome-wide marker-trait associations for plant growth, yield, and yield-related traits under varying nitrogen levels in nested synthetic wheat introgression libraries. *Frontiers in Plant Science*, *12*, 738710.

Sankaran, S., Khot, L. R., & Carter, A. H. (2015). Field-based crop phenotyping: Multispectral aerial imaging for evaluation of winter wheat emergence and spring stand. *Computers and Electronics in Agriculture*, *118*, 372-379.

Šarčević, H., Jukić, K., Ikić, I., & Lovrić, A. (2014). Estimation of quantitative genetic parameters for grain yield and quality in winter wheat under high and low nitrogen fertilization. *Euphytica*, *199*, 57-67.

Schön, C. C., Utz, H. F., Groh, S., Truberg, B., Openshaw, S., & Melchinger, A. E. (2004). Quantitative trait locus mapping based on resampling in a vast maize testcross experiment and its relevance to quantitative genetics for complex traits. *Genetics*, *167*(1), 485-498.

Semenov, M. A., Jamieson, P. D., & Martre, P. (2007). Deconvoluting nitrogen use efficiency in wheat: a simulation study. *European Journal of Agronomy*, *26*(3), 283-294.

Shanahan, J. F., Kitchen, N. R., Raun, W. R., & Schepers, J. S. (2008). Responsive in-season nitrogen management for cereals. *Computers and Electronics in Agriculture*, *61*(1), 51-62.

Shen, L., Courtois, B., McNally, K. L., Robin, S., & Li, Z. (2001). Evaluation of near-isogenic lines of rice introgressed with QTLs for root depth through marker-aided selection. *Theoretical and Applied Genetics*, *103*, 75-83.

Shiferaw, B., Prasanna, B. M., Hellin, J., & Bänziger, M. (2011). Crops that feed the world 6. Past successes and future challenges to the role played by maize in global food security. *Food Security*, *3*, 307-327.

Shrawat, A. K., Carroll, R. T., DePauw, M., Taylor, G. J., & Good, A. G. (2008). Genetic engineering of improved nitrogen use efficiency in rice by the tissue-specific expression of alanine aminotransferase. *Plant Biotechnology Journal*, *6*(7), 722-732.

Siddiqi, M. Y., Glass, A. D., Ruth, T. J., & Rufty Jr, T. W. (1990). Studies of the uptake of nitrate in barley: I. Kinetics of 13NO3− influx. *Plant Physiology*, *93*(4), 1426-1432.

Silva-Pérez, V., De Faveri, J., Molero, G., Deery, D. M., Condon, A. G., Reynolds, M. P., ... & Furbank, R. T. (2020). Genetic variation for photosynthetic capacity and efficiency in spring wheat. *Journal of Experimental Botany*, *71*(7), 2299-2311.

Silvertown, J., & Charlesworth, D. (2009). *Introduction to plant population biology*. John Wiley & Sons.

Simon, A. A., Navarro-Retamal, C., & Feijó, J. A. (2023). Merging Signaling with Structure: Functions and Mechanisms of Plant Glutamate Receptor Ion Channels. *Annual Review of Plant Biology*, *74*, 415-452.

Sinclair, T. R., & Rufty, T. W. (2012). Nitrogen and water resources commonly limit crop yield increases, not necessarily plant genetics. *Global Food Security*, *1*(2), 94-98.

Singh, A., Ganapathysubramanian, B., Singh, A. K., & Sarkar, S. (2016). Machine learning for high-throughput stress phenotyping in plants. *Trends in Plant Science*, *21*(2), 110-124.

Singh, K., Batra, R., Sharma, S., Saripalli, G., Gautam, T., Singh, R., ... & Gupta, P. K. (2021). WheatQTLdb: a QTL database for wheat. *Molecular Genetics and Genomics*, *296*(5), 1051-1056.

Singh, R., Saripalli, G., Kumar, A., Gautam, T., Singh, S. K., Gahlaut, V., ... & Gupta, P. K. (2023). QTL analysis for nitrogen use efficiency in wheat (*Triticum aestivum* L.). *Euphytica*, *219*(1), 9.

Sinha, S. K., Kumar, A., Tyagi, A., Venkatesh, K., Paul, D., Singh, N. K., & Mandal, P. K. (2020). Root architecture traits variation and nitrate-influx responses in diverse wheat genotypes under different external nitrogen concentrations. *Plant Physiology and Biochemistry*, *148*, 246-259.

Soleimani, B., Sammler, R., Backhaus, A., Beschow, H., Schumann, E., Mock, H. P., ... & Pillen, K. (2017). Genetic regulation of growth and nutrient content under phosphorus deficiency in the wild barley introgression library S42IL. *Plant Breeding*, *136*(6), 892-907.

Song, Q., Hyten, D. L., Jia, G., Quigley, C. V., Fickus, E. W., Nelson, R. L., & Cregan, P. B. (2013). Development and evaluation of SoySNP50K, a high-density genotyping array for soybean. *PloS one*, *8*(1), e54985.

Spano, G., Di Fonzo, N., Perrotta, C., Platani, C., Ronga, G., Lawlor, D. W., ... & Shewry, P. R. (2003). Physiological characterization of 'stay green'mutants in durum wheat. *Journal of Experimental Botany*, *54*(386), 1415-1420.

Strock, C. F., Schneider, H. M., & Lynch, J. P. (2022). Anatomics: High-throughput phenotyping of plant anatomy. *Trends in Plant Science*. 27(6), 520-523.

Sun, J., Shi, S., Gong, W., Yang, J., Du, L., Song, S., ... & Zhang, Z. (2017). Evaluation of hyperspectral LiDAR for monitoring rice leaf nitrogen by comparison with multispectral LiDAR and passive spectrometer. *Scientific Reports*, *7*(1), 40362.

Sun, L., Tian, J., Zhang, H., & Liao, H. (2016). Phytohormone regulation of root growth triggered by P deficiency or Al toxicity. *Journal of Experimental Botany*, *67*(12), 3655-3664.

Sun, X., Liu, D., Zhang, X., Li, W., Liu, H., Hong, W., ... & Zheng, H. (2013). SLAF-seq: an efficient method of large-scale de novo SNP discovery and genotyping using high-throughput sequencing. *PloS one*, *8*(3), e58700.

Sun, Y., Zhang, S., & Chen, W. (2020). Root traits of dryland winter wheat (*Triticum aestivum* L.) from the 1940s to the 2010s in Shaanxi Province, China. *Scientific Reports*, *10*(1), 5328.

Suprayogi, Y., Pozniak, C. J., Clarke, F. R., Clarke, J. M., Knox, R. E., & Singh, A. K. (2009). Identification and validation of quantitative trait loci for grain protein concentration in adapted Canadian durum wheat populations. *Theoretical and Applied Genetics*, *119*, 437-448.

Suyal, D. C., Soni, R., Sai, S., & Goel, R. (2016). Microbial inoculants as biofertilizer. *Microbial Inoculants in Sustainable Agricultural Productivity: Vol. 1: Research Perspectives*, 311-318.

Swarbreck, S. M., Defoin-Platel, M., Hindle, M., Saqi, M., & Habash, D. Z. (2011). New perspectives on glutamine synthetase in grasses. *Journal of Experimental Botany*, *62*(4), 1511-1522.

Swarbreck, S. M., Wang, M., Wang, Y., Kindred, D., Sylvester-Bradley, R., Shi, W., ... & Griffiths, H. (2019). A roadmap for lowering crop nitrogen requirement. *Trends in Plant Science*, *24*(10), 892-904.

Sylvester-Bradley, R., Stokes, D. T., Scott, R. K., & Willington, V. B. A. (1990). A physiological analysis of the diminishing responses of winter wheat to applied nitrogen. 2. Evidence. *Aspects of Applied Biology*, (25), 289-300.

Tackenberg, O. (2007). A new method for non-destructive measurement of biomass, growth rates, vertical biomass distribution and dry matter content based on digital image analysis. *Annals of Botany*, *99*(4), 777-783.

The State of Food and Agriculture 2020. (2020). In The State of Food and Agriculture 2020. FAO. https://doi.org/10.4060/cb1447en.

Tian, J., Chen, G., Zhang, H., Chen, J., Wu, P., & Zhao, Y. (2015). *Genetic Analyses of Wheat and Molecular Marker-Assisted Breeding, Volume 1*. Dordrecht: Springer Netherlands.

Tilman, D., Cassman, K. G., Matson, P. A., Naylor, R., & Polasky, S. (2002). Agricultural sustainability and intensive production practices. *Nature*, *418*(6898), 671-677.

Toth, S. J., & Prince, A. L. (1949). Estimation of cation-exchange capacity and exchangeable Ca, K, and Na contents of soils by flame photometer techniques. *Soil Science*, *67*(6), 439-446.

Trebbi, D., Maccaferri, M., de Heer, P., Sørensen, A., Giuliani, S., Salvi, S., ... & Tuberosa, R. (2011). High-throughput SNP discovery and genotyping in durum wheat (Triticum durum Desf.). *Theoretical and Applied Genetics*, *123*, 555-569.

Tremblay, N., Wang, Z., Ma, B. L., Belec, C., & Vigneault, P. (2009). A comparison of crop data measured by two commercial sensors for variable-rate nitrogen application. *Precision Agriculture*, *10*, 145-161.

Tsay, Y. F., Chiu, C. C., Tsai, C. B., Ho, C. H., & Hsu, P. K. (2007). Nitrate transporters and peptide transporters. *FEBS Letters*, *581*(12), 2290-2300.

Tufa, Z. B., Diriba-Shiferaw, G., Balemi, T., & Tadesse, K. (2022). Improved bread and durum wheat cultivars showed contrasting performances in N-efficiency and N-responsiveness. *International Journal of Agronomy*, *2022*.

Tung, C. W., Zhao, K., Wright, M. H., Ali, M. L., Jung, J., Kimball, J., ... & McCouch, S. R. (2010). Development of a research platform for dissecting phenotype–genotype associations in rice (*Oryza* spp.). *Rice*, *3*, 205-217.

Tyagi, B. S., Foulkes, J., Singh, G., Sareen, S., Kumar, P., Broadley, M. R., ... & Singh, G. P. (2020). Identification of wheat cultivars for low nitrogen tolerance using multivariable screening approaches. *Agronomy*, *10*(3), 417.

Uauy, C., Distelfeld, A., Fahima, T., Blechl, A., & Dubcovsky, J. (2006). A NAC gene regulating senescence improves grain protein, zinc, and iron content in wheat. *Science*, *314*(5803), 1298-1301.

Uddin, S., Haque, I., Lu, H., Moni, M. A., & Gide, E. (2022). Comparative performance analysis of K-nearest neighbour (KNN) algorithm and its different variants for disease prediction. *Scientific Reports*, *12*(1), 6256.

Uga, Y., Sugimoto, K., Ogawa, S., Rane, J., Ishitani, M., Hara, N., ... & Yano, M. (2013). Control of root system architecture by DEEPER ROOTING 1 increases rice yield under drought conditions. *Nature Genetics*, *45*(9), 1097-1102.

Uhart, S. A., & Andrade, F. H. (1995). Nitrogen deficiency in maize: I. Effects on crop growth, development, dry matter partitioning, and kernel set. *Crop Science*, *35*(5), 1376-1383.

United Nations (UN), 2018. United Nations climate change conference in Poland. 2018.

Vamerali, T., Bandiera, M., & Mosca, G. (2012). Minirhizotrons in modern root studies. *Measuring Roots: an Updated Approach*, 341-361.

Van Ginkel, M., Ortiz-Monasterio, I., Trethowan, R., & Hernandez, E. (2001). Methodology for selecting segregating populations for improved N-use efficiency in bread wheat. In *Wheat in a Global Environment: Proceedings of the 6th International Wheat Conference, 5–9 June 2000, Budapest, Hungary* (pp. 611-620). Springer Netherlands.

Van Ooijen, V. (2018). JoinMap® 5, Software for the calculation of genetic linkage maps in experimental populations of diploid species. *Kyazma BV, Wageningen, Netherlands.*

Van Oosterom, E. J., Borrell, A. K., Chapman, S. C., Broad, I. J., & Hammer, G. L. (2010). Functional dynamics of the nitrogen balance of sorghum: I. N demand of vegetative plant parts. *Field Crops Research*, *115*(1), 19-28.

Van Rossum G. (1995). *Centrum voor Wiskunde en Informatica.* Python tutorial, technical report CS-R9526. Amsterdam: University of Amsterdam.

Vasquez, M. M., Hu, C., Roe, D. J., Chen, Z., Halonen, M., & Guerra, S. (2016). Least absolute shrinkage and selection operator type methods for the identification of serum biomarkers of overweight and obesity: simulation and application. *BMC Medical Research Methodology*, *16*(1), 1-19.

Vassoler, G. A., Perin, W. D. A., & Cury, D. (2014). Mergemaps–a computational tool for merging of concept maps. In *Proceedings of the 14th International Conference on Concept Mapping*.

Voorrips, R. (2002). MapChart: software for the graphical presentation of linkage maps and QTLs. *Journal of Heredity*, *93*(1), 77-78.

Wang, B., Lai, T., Huang, W. E., Yang, X. M, Shen, Q. R. (2009). Effect of N fertilizers on root growth and endogenous hormones in strawberry. *Pedosphere,* 19, 86–95. doi: 10.1016/S1002-0160(08)60087-9.

Wang, H. C., Liu, Y., Yang, Y. M., Fang, Y. K., Luo, S., Cheng, H. Y., & Wang, A. J. (2022). Element sulfur-based autotrophic denitrification constructed wetland as an efficient approach for nitrogen removal from low C/N wastewater. *Water Research*, *226*, 119258.

Wang, J., Li, H., Zhang, L., Li, C., & Meng, L. (2011). Users' manual of QTL IciMapping v3. 1. *Institute of Crop Science, CAAS, Beijing, and Crop Research Informatics Lab, Mexico*.

Wang, M., Gong, J., & Bhullar, N. K. (2020). Iron deficiency triggered transcriptome changes in bread wheat. *Computational and Structural Biotechnology Journal*, *18*, 2709-2722.

Wang, R., Okamoto, M., Xing, X., & Crawford, N. M. (2003). Microarray analysis of the nitrate response in Arabidopsis roots and shoots reveals over 1,000 rapidly responding genes and new linkages to glucose, trehalose-6-phosphate, iron, and sulfate metabolism. *Plant Physiology*, *132*(2), 556-567.

Wang, S., Wong, D., Forrest, K., Allen, A., Chao, S., Huang, B. E., ... & Akhunov, E. (2014). Characterization of polyploid wheat genomic diversity using a high-density 90 000 single nucleotide polymorphism array. *Plant Biotechnology Journal*, *12*(6), 787-796.

Wang, Y. H., Garvin, D. F., & Kochian, L. V. (2001). Nitrate-induced genes in tomato roots. Array analysis reveals novel genes that may play a role in nitrogen nutrition. *Plant Physiology*, *127*(1), 345-359.

Wang, Y., Lu, J., Ren, T., Hussain, S., Guo, C., Wang, S., ... & Li, X. (2017). Effects of nitrogen and tiller type on grain yield and physiological responses in rice. *AoB Plants*, *9*(2), plx012.

Wang, Y., Wang, D., Tao, Z., Yang, Y., Gao, Z., Zhao, G., & Chang, X. (2021). Impacts of nitrogen deficiency on wheat (*Triticum aestivum* L.) grain during the medium filling stage: Transcriptomic and metabolomic comparisons. *Frontiers in Plant Science*, *12*, 674433.

Wei, D., Cui, K., Pan, J., Ye, G., Xiang, J., Nie, L., & Huang, J. (2011). Genetic dissection of grain nitrogen use efficiency and grain yield and their relationship in rice. *Field Crops Research*, *124*(3), 340-346.

Wen, W., He, Z., Gao, F., Liu, J., Jin, H., Zhai, S., ... & Xia, X. (2017). A high-density consensus map of common wheat integrating four mapping populations scanned by the 90K SNP array. *Frontiers in Plant Science*, *8*, 1389.

Werner, T. (2010). Next generation sequencing in functional genomics. *Briefings in Bioinformatics*, *11*(5), 499-511.

West, P. C., Gerber, J. S., Engstrom, P. M., Mueller, N. D., Brauman, K. A., Carlson, K. M., ... & Siebert, S. (2014). Leverage points for improving global food security and the environment. *Science*, *345*(6194), 325-328.

Whalley, W. R., Binley, A., Watts, C. W., Shanahan, P., Dodd, I. C., Ober, E. S., ... & Hawkesford, M. J. (2017). Methods to estimate changes in soil water for phenotyping root activity in the field. *Plant and Soil*, *415*, 407-422.

Williams, K., Munkvold, J., & Sorrells, M. (2013). Comparison of digital image analysis using elliptic Fourier descriptors and major dimensions to phenotype seed shape in hexaploid wheat (*Triticum aestivum* L.). *Euphytica*, *190*, 99-116.

Williams, L. E., & Miller, A. J. (2001). Transporters responsible for the uptake and partitioning of nitrogenous solutes. *Annual Review of Plant Biology*, *52*(1), 659-688.

Winfield, M. O., Allen, A. M., Burridge, A. J., Barker, G. L., Benbow, H. R., Wilkinson, P. A., ... & Edwards, K. J. (2016). High-density SNP genotyping array for hexaploid wheat and its secondary and tertiary gene pool. *Plant Biotechnology Journal*, *14*(5), 1195-1206.

World Food and Agriculture – Statistical Yearbook 2021. (2021). In World Food and Agriculture – Statistical Yearbook 2021. FAO. https://doi.org/10.4060/cb4477en

Wu, S., Deng, L., Guo, L., & Wu, Y. (2022). Wheat leaf area index prediction using data fusion based on high-resolution unmanned aerial vehicle imagery. *Plant Methods*, *18*(1), 1-16.

Xiao, Q., Bai, X., Zhang, C., & He, Y. (2022). Advanced high-throughput plant phenotyping techniques for genome-wide association studies: A review. *Journal of Advanced Research*, *35*, 215-230.

Xin, F., Zhu, T., Wei, S., Han, Y., Zhao, Y., Zhang, D., ... & Ding, Q. (2020). QTL mapping of kernel traits and validation of a major QTL for kernel length-width ratio using SNP and bulked segregant analysis in wheat. *Scientific Reports*, *10*(1), 25.

Xiong, H., Guo, H., Zhou, C., Guo, X., Xie, Y., Zhao, L., ... & Liu, L. (2019). A combined association mapping and t-test analysis of SNP loci and candidate genes involving in resistance to low nitrogen traits by a wheat mutant population. *PLoS One*, *14*(1), e0211492.

Xu, C., Ren, Y., Jian, Y., Guo, Z., Zhang, Y., Xie, C., ... & Zou, C. (2017). Development of a maize 55 K SNP array with improved genome coverage for molecular breeding. *Molecular Breeding*, *37*, 1-12.

Xu, G. W., Lu, D. K., Wang, H. Z., & Li, Y. (2018). Morphological and physiological traits of rice roots and their relationships to yield and nitrogen utilization as influenced by irrigation regime and nitrogen rate. *Agricultural Water Management*, *203*, 385-394.

Xu, Y. (1994). Factors influencing the power of QTL mapping: population size. *Journal of Zhejiang Agricultural University*, *6*, 573-578.

Xu, Y., Wang, R., Tong, Y., Zhao, H., Xie, Q., Liu, D., ... & An, D. (2014). Mapping QTLs for yield and nitrogen-related traits in wheat: influence of nitrogen and phosphorus fertilization on QTL expression. *Theoretical and Applied Genetics*, *127*, 59-72.

Yadav, R., Courtois, B., Huang, N., & McLaren, G. (1997). Mapping genes controlling root morphology and root distribution in a doubled-haploid population of rice. *Theoretical and Applied Genetics*, *94*, 619-632.

Yang, D., Zhao, J., Bi, C., Li, L., & Wang, Z. (2022). Transcriptome and proteomics analysis of wheat seedling roots reveals that increasing NH4+/NO3–ratio induced root lignification and reduced nitrogen utilization. *Frontiers in Plant Science*, *12*, 797260.

Yang, W., Guo, Z., Huang, C., Duan, L., Chen, G., Jiang, N., ... & Xiong, L. (2014). Combining high-throughput phenotyping and genome-wide association studies to reveal natural genetic variation in rice. *Nature Communications*, *5*(1), 5087.

Yang, X., Xia, X., Zhang, Z., Nong, B., Zeng, Y., Xiong, F., ... & Li, D. (2017). QTL mapping by whole genome re-sequencing and analysis of candidate genes for nitrogen use efficiency in rice. *Frontiers in Plant Science*, *8*, 1634.

Yang, Y., Amo, A., Wei, D., Chai, Y., Zheng, J., Qiao, P., ... & Hu, Y. G. (2021). Large-scale integration of meta-QTL and genome-wide association study discovers the genomic regions and candidate genes for yield and yield-related traits in bread wheat. *Theoretical and Applied Genetics*, *134*(9), 3083-3109.

Zahedi, M., McDonald, G., & Jenner, C. F. (2004). Nitrogen supply to the grain modifies the effects of temperature on starch and protein accumulation during grain filling in wheat. *Australian Journal of Agricultural Research*, *55*(5), 551-564.

Zeng, D. D., Qin, R., Li, M., Alamin, M., Jin, X. L., Liu, Y., & Shi, C. H. (2017). The ferredoxin-dependent glutamate synthase (OsFd-GOGAT) participates in leaf senescence and the nitrogen remobilization in rice. *Molecular Genetics and Genomics*, *292*, 385-395.

Zhai, H., Feng, Z., Li, J., Liu, X., Xiao, S., Ni, Z., & Sun, Q. (2016). QTL analysis of spike morphological traits and plant height in winter wheat (Triticum aestivum L.) using a high-density SNP and SSR-based linkage map. *Frontiers in Plant Science*, *7*, 1617.

Zhai, H., Lü, S., Wang, Y., Chen, X., Ren, H., Yang, J., ... & Xia, Z. (2014). Allelic variations at four major maturity E genes and transcriptional abundance of the E1 gene are associated with flowering time and maturity of soybean cultivars. *PloS one*, *9*(5), e97636.

Zhai, S., He, Z., Wen, W., Jin, H., Liu, J., Zhang, Y., ... & Xia, X. (2016). Genome-wide linkage mapping of flour color-related traits and polyphenol oxidase activity in common wheat. *Theoretical and Applied Genetics*, *129*, 377-394.

Zhang, J., Liu, Y. X., Zhang, N., Hu, B., Jin, T., Xu, H., ... & Bai, Y. (2019). NRT1. 1B is associated with root microbiota composition and nitrogen use in field-grown rice. *Nature Biotechnology*, *37*(6), 676-684.

Zhang, L., Wang, S., Li, H., Deng, Q., Zheng, A., Li, S., ... & Wang, J. (2010). Effects of missing marker and segregation distortion on QTL mapping in F 2 populations. *Theoretical and Applied Genetics*, *121*, 1071-1082.

Zhang, M., Gao, M., Zheng, H., Yuan, Y., Zhou, X., Guo, Y., ... & Li, S. (2019). QTL mapping for nitrogen use efficiency and agronomic traits at the seedling and maturity stages in wheat. *Molecular Breeding*, *39*, 1-17.

Zhang, Z., Xiong, S., Wei, Y., Meng, X., Wang, X., & Ma, X. (2017). The role of glutamine synthetase isozymes in enhancing nitrogen use efficiency of N-efficient winter wheat. *Scientific Reports*, *7*(1), 1000.

Zhao, B., Ata-Ul-Karim, S. T., Lemaire, G., Duan, A., Liu, Z., Guo, Y., ... & Liu, Z. (2021). Exploring the nitrogen source-sink ratio to quantify ear nitrogen accumulation in maize and wheat using critical nitrogen dilution curve. *Field Crops Research, 274*, 108332.

Zhao, K., Tung, C. W., Eizenga, G. C., Wright, M. H., Ali, M. L., Price, A. H., ... & McCouch, S. R. (2011). Genome-wide association mapping reveals a rich genetic architecture of complex traits in Oryza sativa. *Nature Communications*, *2*(1), 467.

Zhao, L., Yang, Y., Chen, J., Lin, X., Zhang, H., Wang, H., ... & Xiao, J. (2023). Dynamic chromatin regulatory programs during embryogenesis of hexaploid wheat. *Genome Biology*, *24*(1), 1-29.

Zhao, X. H., Yu, H. Q., Jing, W. E. N., Wang, X. G., Qi, D. U., Jing, W. A. N. G., & Qiao, W. A. N. G. (2016). Response of root morphology, physiology and endogenous hormones in maize (*Zea mays* L.) to potassium deficiency. *Journal of Integrative Agriculture*, *15*(4), 785-794.

Zheng, H., Li, W., Jiang, J., Liu, Y., Cheng, T., Tian, Y., ... & Yao, X. (2018). A comparative assessment of different modeling algorithms for estimating leaf nitrogen content in winter wheat using multispectral images from an unmanned aerial vehicle. *Remote Sensing*, *10*(12), 2026.

Zhou, Y., Conway, B., Miller, D., Marshall, D., Cooper, A., Murphy, P., ... & Costa, J. (2018). Quantitative trait loci mapping for spike characteristics in hexaploid wheat. *Plant Genome*, *10*(2), plantgenome2016-10.

Zhu, K., Ren, W., Yan, J., Zhang, Y., Zhang, W., Xu, Y., ... & Yang, J. (2022). Grain yield and nitrogen use efficiency are increased by exogenous cytokinin application through the improvement in root physiological traits of rice. *Plant Growth Regulation*, *97*(1), 157-169.

Zou, F., Gelfond, J. A., Airey, D. C., Lu, L., Manly, K. F., Williams, R. W., & Threadgill, D. W. (2005). Quantitative trait locus analysis using recombinant inbred intercrosses: theoretical and empirical considerations. *Genetics*, *170*(3), 1299-1311.

10 ANNEXURES

ANNEXURE 1: Phenotypic traits measured by manual method

Sl. No.	Trait Code	Organisation Level	Trait Categories	Trait Description
1	Straw	Whole Plant	Biomass Traits	Total straw and chaff amount
2	Total_Biomass	Whole Plant	Biomass Traits	Total Biomass
3	TotalEar	Whole Plant	Biomass Traits	Total Ear number per plant
4	HI	Whole Plant	Biomass Traits	Harvest Index
5	PH	Whole Plant	Plant architecture Traits	Plant height
6	PH_FLLratio	Whole Plant	Plant architecture Traits	Plant height to flag leaf length ratio
7	FLtoEar	Whole Plant	Plant architecture Traits	Flag Leaf to Ear Distance
8	LNP	Whole Plant	Plant architecture Traits	Leaf number per plant
9	TNP	Whole Plant	Plant architecture Traits	Tiller number per plant
10	LPTveg	Whole Plant	Plant architecture Traits	No of leaf per tiller at Vegetative stage
11	LC_SPAD1ratio	Whole Plant	Plant architecture Traits	Leaf Count to SPAD1 ratio
12	LC_SPAD2ratio	Whole Plant	Plant architecture Traits	Leaf Count to SPAD2 ratio
13	TC_SPAD1ratio	Whole Plant	Plant architecture Traits	Tiller Count to SPAD1 ratio
14	TC_SPAD2ratio	Whole Plant	Plant architecture Traits	Tiller Count to SPAD2 ratio
15	FLL	Flagleaf	Flagleaf Traits	Flag Leaf Length
16	FLW	Flagleaf	Flagleaf Traits	Flag Leaf Width
17	FLLWratio	Flagleaf	Flagleaf Traits	Flag leaf length to flag leaf width ratio
18	FLLtoEarRatio	Flagleaf	Flagleaf Traits	Flag leaf length to Ear ratio
19	FLA	Flagleaf	Flagleaf Traits	Flag Leaf Area
20	SPAD1	Flagleaf	Colour Traits	Soil Plant Analysis Development value at vegetative stage
21	SPAD2	Flagleaf	Colour Traits	Soil Plant Analysis Development value at reproductive stage
22	SPADratio	Flagleaf	Colour Traits	Vegetative stage SPAD to Reproductive stage SPAD ratio
23	SPAD1total	Flagleaf	Colour Traits	Total SPAD value of flag leaf at Vegetative stage
24	SPAD2total	Flagleaf	Colour Traits	Total SPAD value of flag leaf at Reproductive stage
25	DTG	Whole Plant	Developmental traits	Days to Germination
26	DTB	Whole Plant	Developmental traits	Days to Booting

27	DTA	Whole Plant	Developmental traits	Days to Anthesis
28	Phy3	Whole Plant	Developmental traits	Phyllochron3
29	Phy4	Whole Plant	Developmental traits	Phyllochron4
30	Phy5	Whole Plant	Developmental traits	Phyllochron5
31	LER	Whole Plant	Developmental traits	Leaf Emergence Rate
32	LER_DTBratio	Whole Plant	Developmental traits	No of leaf in main ear till booting
33	LER_DTAratio	Whole Plant	Developmental traits	No of leaf in main ear till Anthesis
34	SpikeLength	Main Ear	Spike Traits	Spike Length
35	SpikeletNo	Main Ear	Spike Traits	Total Spikelet Numbers per spike
36	SSN	Main Ear	Spike Traits	Sterile Spikelet Number per spike
37	GPS	Main Ear	Spike Traits	Grains per Spikelet
38	SpikeletDensity	Main Ear	Spike Traits	Spikelet Density
39	SFP	Main Ear	Spike Traits	SpikeletFertilityPercentage
40	SFI	Main Ear	Spike Traits	SpikeletFertilityIndex
41	SpikeWt	ME, TE, AE	Yield Traits	Total Spike Weight
42	GrainWt	ME, TE, AE	Yield Traits	Total Grain Weight
43	ChaffWt	ME, TE, AE	Yield Traits	Total Chaff Weight
44	TotalGrainNo	ME, TE, AE	Yield Traits	Total Grain Number
45	GPB	ME, TE, AE	Yield Traits	Grain percentage of Biomass
46	AGPB	ME, TE, AE	Yield Traits	Average Grain percent of Biomass
47	CPB	ME, TE, AE	Yield Traits	Chaff percent of Biomass
48	ACPB	ME, TE, AE	Yield Traits	Average Chaff percent of Biomass
49	AvgSpikeWt	ME, TE, AE	Yield Traits	Average Spike Weight
50	AvgGrainWt	ME, TE, AE	Yield Traits	Average Grain Weight
51	AvgChaffWt	ME, TE, AE	Yield Traits	Average Chaff Weight
52	GWCWratio	ME, TE, AE	Yield Traits	Grain Weight to Chaff Weight
53	PHI	ME, TE, AE	Yield Traits	Panicle Harvest Index
54	TKW	ME, TE, AE	Yield Traits	Thousand Kernel Weight
55	StrawNpercent	Whole plant	Nitrogen related	Nitrogen percentage of straw and chaff

56	GrainNpercent	Whole plant	Nitrogen related	Nitrogen percentage of grain
57	GPC	Whole plant	Nitrogen related	Grain Protein Content
58	NHI	Whole plant	Nitrogen related	Nitrogen Harvest Index
59	UI	Whole plant	Nitrogen related	Utilisation Index
60	NUpE	Whole plant	Nitrogen related	Nitrogen Uptake Efficiency
61	NUtE	Whole plant	Nitrogen related	Nitrogen Utilisation Efficiency
62	NUE	Whole plant	Nitrogen related	Nitrogen Use Efficiency

ANNEXURE 2: Semi-automatic seed parameter estimation

Sl. No.	Trait Code	Organisation Level	Trait Categories	Trait Description
1	AvgGrainNo	ME, TE, AE	Yield Traits	Average Grain Number
2	SeedArea	Grain_ME, TE, AE	Grain Architecture	Average area of each seed
3	SeedArea_Low	Grain_ME, TE, AE	Grain Architecture	Average area of each seed of lower 5 percent seeds
4	SeedArea_Top	Grain_ME, TE, AE	Grain Architecture	Average area of each seed of top 5 percent seeds
5	SeedPerimeter	Grain_ME, TE, AE	Grain Architecture	Average perimeter of each seed
6	SeedPerimeter_Low	Grain_ME, TE, AE	Grain Architecture	Average perimeter of each seed of lower 5 percent seeds
7	SeedPerimeter_Top	Grain_ME, TE, AE	Grain Architecture	Average perimeter of each seed of top 5 percent seeds
8	SeedLength	Grain_ME, TE, AE	Grain Architecture	Average length of each seed
9	SeedLength_Low	Grain_ME, TE, AE	Grain Architecture	Average length of each seed of lower 5 percent seeds
10	SeedLength_Top	Grain_ME, TE, AE	Grain Architecture	Average length of each seed of top 5 percent seeds
11	SeedWidth	Grain_ME, TE, AE	Grain Architecture	Average width of each seed
12	SeedWidth_Low	Grain_ME, TE, AE	Grain Architecture	Average width of each seed of lower 5 percent seeds
13	SeedWidth_Top	Grain_ME, TE, AE	Grain Architecture	Average width of each seed of top 5 percent seeds
14	SeedLWR	Grain_ME, TE, AE	Grain Architecture	Average Length of width ratio of each seed
15	SeedLWR_Low	Grain_ME, TE, AE	Grain Architecture	Average Length of width ratio of each seed of lower 5 percent seeds

16	SeedLWR_Top	Grain_ME, TE, AE	Grain Architecture	Average Length of width ratio of each seed of top 5 percent seeds

ANNEXURE 3: High throughput phenotyping trait description

Sl. No.	Trait Name	Trait Code	Trait Category	Imaging Angle	Sensor	Traits Description
1	2ndMomentPrincipleAxisLargeAbs	2MPALA	Mophometric	SV	RGB	μl = S (pixelA * rAs²), rAs is the distance of pixel A from the larger moment axis (through the centre of mass) in direction of the smaller moment axis with the additional condition μ11=0
2	2ndMomentPrincipleAxisSmallAbs	2MPASA	Mophometric	TV, SV	RGB	μs = S (pixelA * rAl²), rAl is the distance of pixel A from the smaller moment axis (through the centre of mass) in direction of the larger moment axis with the additional condition μ11=0
3	2ndMomentPrincipleAxisLargeNorm	2MPALN	Mophometric	SV	RGB	2ndMomentPrincipleAxisLargeNorm = 2ndMomentPrincipleAxisLargeAbs/ObjectArea
4	2ndMomentPrincipleAxisSmallNorm	2MPASN	Mophometric	TV, SV	RGB	2ndMomentPrincipleAxisSmallNorm = 2ndMomentPrincipleAxisSmallAbs/ObjectArea
5	2ndMomentsPrincipalAxisRatio	2MPAR	Mophometric	SV	RGB	2ndMomentsPrincipalAxisRatio = 2ndMomentPrincipleAxisLargeAbs/2ndMomentPrincipleAxisSmallAbs
6	BoundaryPointCount	BPC	Mophometric	TV, SV	RGB	Number of all pixels of an object boundary
7	BoundaryPointRoundness	BPR	Mophometric	TV, SV	RGB	BoundaryPointRoundness = (BoundaryPointCount)²/size.
8	CentreOfMassY	cmY	Mophometric	SV	RGB	Average y-value (y-position) of all object pixels (all pixel same size). Formula = CentreOfMassX = S pixelA*rAy/Object area. It is the y-value of the crossing point of the two principal axes.
9	ConvexHullArea	CHArea	Mophometric	TV, SV	RGB	ConvexHullArea is the area of the smallest object without concave boundary parts
10	Circumference	Circumference	Mophometric	SV	RGB	Sum of the direction corrected length of the outer boundary of all subobjects
11	Excentricity	Excentricity	Mophometric	SV	RGB	Excentricity = sqr (μ20 -μ02) + 4 * sqr (μ11)/sqr (μ20 + μ02)
12	ObjectExtentX	ObjectExtentX	Mophometric	SV	RGB	Length in x-direction of the minimum vertically oriented rectangle covering the object

13	ObjectExtentY	ObjectExtentY	Mophometric	TV, SV	RGB	Length in y-direction of the minimum vertically oriented rectangle covering the object
14	MinAreaRectAngle	MARA	Mophometric	TV	RGB	The angle measured describes the angle between 3 o'clock/east and the larger extension side of the rectangle.
15	AbsolutZRotation2ndMoment	AZR2M	Mophometric	TV	RGB	μz = S (pixelA * rA²) rA Euclidian distance from the centre of mass
16	NormalisedZRotation2ndMoment	NZR2M	Mophometric	TV	RGB	μz = (S (pixelA * rA²))/ObjectArea
17	BoundaryPointsToAreaRatio	BPAR	Mophometric	TV, SV	RGB	BoundaryPointsToAreaRatio = BoundaryPointCount /ObjectArea (0 to 1 /no unit)
18	Compactness	Compactness	Mophometric	TV, SV	RGB	Compactness = ObjectArea/ConvexHullArea
19	AreaDistributionAboveRelative	ADAR	Biomass	SV	RGB	Pixels present above
20	ObjectArea	Area	Biomass	TV, SV	RGB	Number of object pixels
21	ProjectedShootArea	PSA	Biomass	Combined TV & SV	RGB	Sum of TopView and SideView (2-3 angles) object area
22	Biovolume	Biovolume	Biomass	Combined TV & SV	RGB	Estimated digital volume (unit: voxel) that corresponds to a pixel volume. Calculated from all side and top view images as sqrt (average plant side area2 x top plant area)
24	NIRmeangrayintensity	NIR	Intensity	TV, SV	NIR	Near Infrared intensity for water related traits
25	InfraRedintensity	IR	Intensity	TV, SV	IR	Representation of canopy temprature
23	ProjectedShootColourClass	PSCC_1 to 20	Colour	Combined TV & SV	RGB	Object area classified into 20 colour classes and each PSCC represents area of a specific colour class
26	Mean Blue Intensity	Blue	Colour	TV, SV	RGB	Mean Blue Value of all the pixels
27	Mean Green Intensity	Green	Colour	TV, SV	RGB	Mean Green Value of all the pixels
28	Mean Red Intensity	Red	Colour	TV, SV	RGB	Mean Red Value of all the pixels
29	(G-B)/(R+G+B)	(G-B)/(R+G+B)	Indices	SV	RGB	(G-B)/(R+G+B)
30	(R-G)/(R+G+B)	(R-G)/(R+G+B)	Indices	TV	RGB	(R-G)/(R+G+B)

31	Channel index B	b	Indices	TV, SV	RGB	B/(R + G + B)
32	Excess blue vegetation index	ExB	Indices	SV	RGB	1.4b − g
33	Excess green vegetation index	ExG	Indices	SV	RGB	2g − r − b
34	Channel index G	g	Indices	TV	RGB	G/(R + G + B)
35	Binary channel index	G/B	Indices	TV	RGB	B/G
36	Binary channel index	G/R	Indices	SV	RGB	R/G
37	Green minus Red	GMR	Indices	SV	RGB	G-R
38	Gray	Gray	Indices	TV, SV	RGB	0.2898red + 0.5870green + 0.1140blue
39	I2	I2	Indices	TV	RGB	0.55 + 11.4((G-B)/(G+B)) - 12.5((R-B)/(R+B)) + 9((R-G)/(R+G))
40	Principal component analysis index	Ipca	Indices	SV	RGB	0.994|R − B| + 0.961|G − B| + 0.914|G − R|
41	PCA 1	PCA1	Indices	TV, SV	RGB	-0.977b + 0.916((G-B)/(G+B)) + 0.995((R-B)/(R+B)) + 0.771 ((R-G)/(R+G))
42	PCA 2	PCA2	Indices	SV	RGB	0.999|R-B| + 0.92|G-B| + 0.886|R-G|
43	Channel index R	r	Indices	SV	RGB	R/(R + G + B)
44	Red minus Blue	R-B	Indices	TV	RGB	R-B
45	Red minus Green	R-G	Indices	TV	RGB	R-G
46	SCOM	SCOM	Indices	TV	RGB	0.25 × ExG + 0.30 × ExGR + 0.33 × CIVE
47	SLR 1	SLR1	Indices	TV, SV	RGB	-60430 - 0.7316B + 69680b + 112800g + 28270((G-B)/(G+B)) -23890((R-B)/(R+B)) + 68380((R-G)/(R+G))
48	SLR 2	SLR2	Indices	TV, SV	RGB	-46240 - 2.678B + 1.05G + 52570b + 87420g + 20720((G-B)/(G+B)) -18240((R-B)/(R+B)) + 52500((R-G)/(R+G))
49	SLR 3	SLR3	Indices	TV, SV	RGB	-25373 + 30106b + 46539g + 12776((G-B)/(G+B)) - 10507((R-B)/(R+B)) +28821((R-G)/(R+G))
50	SLR 4	SLR4	Indices	SV	RGB	-44312 + 51689b + 81995g + 21751((G-B)/(G+B)) - 18156((R-B)/(R+B)) +50425((R-G)/(R+G))

51	SLR 5	SLR5	Indices	TV	RGB	41048 + 46964b + 76841g + 19998((G-B)/(G+B)) - 17173((R-B)/(R+B)) + 47162((R-G)/(R+G))
52	Absolute Growth Rate	AGR	Growth Rate	Derived	RGB	
57	Relative Growth Rate	RGR	Growth Rate	Derived	RGB	
61		AWU_Diurnal	Water Use	Derived	Gravimetric	Average Water Use per day
62		AWU_Day	Water Use	Derived	Gravimetric	Average Water Use from morning to evening
63		AWU_Night	Water Use	Derived	Gravimetric	Average Water Use from evening to morning
64		PSA_TUE_Diurnal	Water Use	Derived	Gravimetric	Projected shoot area per ml water transpired_Diurnal
65		PSA_TUE_Day	Water Use	Derived	Gravimetric	Projected shoot area per ml water transpired_Day
66		PSA_TUE_Night	Water Use	Derived	Gravimetric	Projected shoot area per ml water transpired_Night
67		Foliage_TUE_Diurnal	Water Use	Derived	Gravimetric	drywt foliage per ml water transpired_Diurnal
68		Foliage_TUE_Day	Water Use	Derived	Gravimetric	drywt foliage per ml water transpired_Day
69		Foliage_TUE_Night	Water Use	Derived	Gravimetric	drywt foliage per ml water transpired_Night
70		PSA_TR_Diurnal	Water Use	Derived	Gravimetric	ml of water transpired per PSA_Diurnal
71		PSA_TR_Day	Water Use	Derived	Gravimetric	ml of water transpired per PSA_Day
72		PSA_TR_Night	Water Use	Derived	Gravimetric	ml of water transpired per PSA_Night
73		Foliage_TR_Diurnal	Water Use	Derived	Gravimetric	ml of water transpired per drywt foliage_Diurnal
74		Foliage_TR_Day	Water Use	Derived	Gravimetric	ml of water transpired per drywt foliage_Day
75		Foliage_TR_Day	Water Use	Derived	Gravimetric	ml of water transpired per drywt foliage_Night

ANNEXURE 4: Descriptive statistics and ANOVA of HTP traits

	Control				Nitrogen				ANOVA_P-value		
Traits	Mean	CV	Min	Max	Mean	CV	Min	Max	Treatment	Genotype	G×E
Biovolume_1	95503145	25.66	20580343	166532749	66009928	43.15	14109955	178839617	1.7E-93	8.9E-44	6.0E-14
Biovolume_2	132505401	23.47	48103009	236164719	88529294	41.92	20547304	228524561	9.2E-118	5.5E-43	6.6E-19
Biovolume_3	147192182	21.72	64013383	260800996	102132232	39.26	26026794	236739301	2.0E-113	6.4E-44	3.9E-20
Biovolume_4	142262655	24.84	60299392	258168072	96640751	38.04	24746872	239547357	3.2E-128	2.8E-65	1.3E-21
Biovolume_5	106490531	38.72	3147593	213916920	67465736	44.29	4450569	178839472	8.0E-169	1.3E-183	1.0E-32
PSA_1	835636	16.9	308486	1206890	652667	28.08	250615	1269658	4.7E-90	1.8E-35	7.1E-13
PSA_2	1035759	15.53	548905	1527635	787458	27.63	316313	1490327	2.3E-114	2.8E-36	1.8E-16
PSA_3	1110953	14.54	648311	1636352	860639	26.3	356304	1513173	3.6E-113	8.1E-39	1.2E-17
PSA_4	1090749	16.26	629206	1622744	832693	25.35	348946	1534388	9.7E-131	2.6E-58	7.9E-19
PSA_5	946943	20.53	450618	1471778	701877	25.15	298567	1288731	1.3E-173	2.9E-130	1.0E-23
2MPASA_TV_1	5965699963	42.1	632335800	14719390000	3212030820	69.16	202178200	12676700000	4.8E-107	1.9E-59	9.1E-14
2MPASA_TV_2	9302078973	37.04	2274744000	23597730000	5085547828	63.27	412085000	21842250000	1.3E-122	1.7E-54	6.1E-22
2MPASA_TV_3	10235477735	33.06	2929828000	28293120000	6762088379	56.68	635462700	20246580000	1.7E-75	5.1E-43	8.6E-16
2MPASA_TV_4	9940074787	40.37	2669229000	26800270000	6502311346	56.52	736823900	28096040000	7.8E-72	1.1E-59	1.0E-10
2MPASA_TV_5	5254035667	72.44	145104	28276120000	2833809286	78.58	1053319	13844110000	3.8E-82	2.7E-126	1.4E-19
2MPASN_TV_1	0.14748	19	0.08611	0.26648	0.14383	17.72	0.0791	0.23577	1.2E-02	6.0E-17	2.0E-03
2MPASN_TV_2	0.13999	16.36	0.07489	0.22216	0.14234	19.24	0.0768	0.27469	7.5E-02	2.2E-20	3.8E-06
2MPASN_TV_3	0.13319	16.39	0.08168	0.21598	0.14057	19.51	0.06846	0.23983	9.3E-08	2.0E-10	2.6E-04
2MPASN_TV_4	0.14532	17.9	0.08756	0.25844	0.15075	19.51	0.07789	0.259	6.0E-04	2.0E-10	2.6E-01
2MPASN_TV_5	0.19239	81.27	0.07397	2.45734	0.2094	121.11	0.0561	3.2988	8.9E-02	3.3E-51	1.6E-02
Area_TV_1	198734	22.32	63528	321072	142218	37.03	40641	317518	9.5E-103	3.6E-51	6.2E-13
Area_TV_2	255468	19.08	103516	398717	182340	34.79	52582	384029	7.3E-120	2.2E-45	9.6E-19
Area_TV_3	275375	16.28	146391	426081	212586	31.41	73059	429614	7.5E-93	1.3E-39	2.4E-18
Area_TV_4	258794	20.86	132798	449274	201696	29.3	71711	404618	1.7E-95	9.0E-75	3.2E-17
Area_TV_5	170308	44.9	243	350383	123224	45.38	1005	290902	2.2E-129	3.3E-256	3.9E-34

BPC_TV_1	25615	18.43	11973	40366	17786	29.17	6694	36075	4.0E-145	1.0E-33	1.0E-15
BPC_TV_2	29045	17.15	15992	48977	19753	26.94	8354	35231	4.4E-181	1.8E-41	1.9E-22
BPC_TV_3	28684	17.25	16703	47111	20586	23.68	9144	35264	4.2E-173	3.0E-52	9.9E-29
BPC_TV_4	30267	19.35	16331	51409	19936	22.07	9979	36263	6.7E-232	2.4E-73	1.7E-33
BPC_TV_5	23527	36.39	183	50250	13846	31.53	588	32732	6.8E-240	2.8E-185	6.4E-67
BPR_TV_1	3389	26.36	1400.6	6925.1	2271.6	28.39	929.5	4704.6	1.7E-160	4.4E-79	4.4E-28
BPR_TV_2	3386.1	27.02	1458.8	7152.5	2190	26.43	986.7	4263.2	2.0E-199	1.8E-104	2.2E-40
BPR_TV_3	3076.8	31.16	1262.8	8360.9	2042.3	24.2	1057.6	3891.3	3.2E-190	3.3E-128	2.6E-58
BPR_TV_4	3640	29.98	1698	8402.1	2014.7	23.27	997.7	5396.3	8.3E-254	1.5E-95	2.2E-61
BPR_TV_5	3459.8	36.84	137.8	8003.1	1708.2	38.52	272.6	6267.7	4.3E-235	3.9E-96	6.4E-78
BPAR_TV_1	0.13196	16.47	0.07852	0.20349	0.12989	14.34	0.07521	0.18573	5.5E-03	5.4E-117	2.8E-12
BPAR_TV_2	0.11569	16.28	0.07265	0.20126	0.11288	15.97	0.07029	0.19776	6.0E-05	3.3E-105	9.0E-16
BPAR_TV_3	0.10565	17.49	0.06748	0.20335	0.10074	16.51	0.06266	0.16773	5.3E-13	1.4E-99	4.1E-21
BPAR_TV_4	0.11905	17.17	0.07787	0.20959	0.10225	16.15	0.0719	0.18901	2.0E-88	3.1E-86	3.2E-27
BPAR_TV_5	0.16009	40.8	0.0839	0.75309	0.13811	56.59	0.07377	0.653	4.2E-19	1.2E-149	7.8E-13
Compactness_TV_1	0.21377	16.96	0.1048	0.33103	0.1911	17.71	0.11096	0.31081	4.3E-39	7.2E-45	6.0E-11
Compactness_TV_2	0.2611	16.22	0.12453	0.40412	0.24068	17.59	0.13424	0.39619	4.6E-30	5.3E-89	1.2E-09
Compactness_TV_3	0.28224	14.48	0.1693	0.39095	0.25052	15.8	0.13507	0.39566	1.5E-51	2.5E-41	3.2E-06
Compactness_TV_4	0.26808	14.65	0.13383	0.39282	0.23744	15.95	0.13911	0.36386	2.2E-52	8.7E-39	4.8E-10
Compactness_TV_5	0.24232	30.72	0.00781	0.43871	0.2243	30.02	0.0136	0.41277	1.3E-12	6.1E-136	1.2E-06
CHArea_TV_1	931361	16.71	444646	1778230	730485	26.88	250997	1222403	2.1E-90	1.9E-38	2.2E-08
CHArea_TV_2	986659	16.75	576304	1627645	755776	29.09	226666	1446498	7.2E-105	2.5E-47	3.6E-15
CHArea_TV_3	984717	15.87	611172	1637631	845378	26.36	270293	1584294	4.5E-44	2.6E-36	2.1E-09
CHArea_TV_4	973024	19.65	518261	1652748	846126	23.71	350513	1624587	4.0E-44	4.8E-73	3.9E-05
CHArea_TV_5	684706	36.95	31126	1860441	546131	42.02	31514	2067789	6.0E-54	7.0E-145	5.5E-09
ObjectExtentY_TV_1	1053.3	13.98	697	1762	886.71	20.41	447	1351	7.8E-71	1.2E-29	9.4E-06
ObjectExtentY_TV_2	1157.3	12.49	804	1758	1002.1	19.18	490	1630	1.6E-59	2.4E-22	5.6E-10
ObjectExtentY_TV_3	1171.6	11.69	829	1692	1080	16.1	568	1510	1.2E-25	9.0E-14	2.2E-06
ObjectExtentY_TV_4	1153.7	13.65	770	1949	1075.6	15.03	573	1564	3.7E-21	6.4E-34	4.2E-03

ObjectExtentY_TV_5	977.3	23.21	203	1815	880.06	25.32	188	1655	1.1E-22	5.2E-80	4.4E-04
MARA_TV_1	1255205	14.91	674696	2315732	1030202	22.83	428655	1675443	1.6E-77	3.1E-31	6.5E-07
MARA_TV_2	1259598	17.49	717375	2246910	985450	28.85	278987	1732683	6.8E-91	6.3E-50	6.8E-12
MARA_TV_3	1252966	16.63	804971	2124142	1084713	26.34	386952	2056422	6.3E-38	1.5E-34	3.1E-07
MARA_TV_4	1237109	20.16	629148	2138996	1079846	23.65	468733	1984674	2.4E-40	4.3E-69	9.7E-05
MARA_TV_5	892516	37.24	40866	2317189	715003	41.69	49871	2555407	2.0E-49	1.6E-134	4.0E-09
AZR2M_TV_1	15104750670	39.33	1929344000	47518840000	8270282049	64.36	741943600	31956370000	4.0E-111	1.6E-57	6.7E-11
AZR2M_TV_2	23266530276	33.09	5735767000	51948770000	13138514729	58.39	1159661000	46755440000	8.7E-131	3.5E-56	9.5E-23
AZR2M_TV_3	25952536516	29.2	9330806000	69395370000	17742010302	51.6	2107879000	52546150000	6.5E-82	5.8E-51	5.1E-19
AZR2M_TV_4	25939050722	36.79	7778650000	69167830000	17334349198	49.8	2475376000	58722980000	6.4E-85	5.4E-75	1.0E-11
AZR2M_TV_5	14576503681	66.56	3857063	73039290000	8129179571	71.66	2934137	32103160000	1.7E-90	4.5E-136	1.1E-18
NZR2M_TV_1	0.37741	17.49	0.26085	0.67086	0.38263	15.99	0.2582	0.78538	6.2E-02	8.5E-56	2.6E-16
NZR2M_TV_2	0.35376	14.47	0.24217	0.61336	0.37627	16.19	0.26006	0.63308	7.5E-17	1.4E-43	1.7E-09
NZR2M_TV_3	0.34013	12.88	0.25655	0.52353	0.37838	15.65	0.26663	0.67907	9.6E-42	3.5E-25	1.4E-07
NZR2M_TV_4	0.38477	21.08	0.27645	1.29022	0.41344	15.36	0.27682	0.68486	6.9E-16	3.9E-37	3.4E-13
NZR2M_TV_5	0.81	371.91	0.27	65.32	0.779	235.54	0.2797	31.0536	8.2E-01	3.2E-16	6.8E-01
2MPALA_SV_1	18369755057	40.18	3878952600	52032830000	14295649000	54.89	2188164400	55490460000	1.3E-46	1.3E-134	1.6E-15
2MPALA_SV_2	30347348043	39.47	8381224400	86063298000	22880460524	55.57	4448121800	87667970000	5.8E-65	3.7E-157	1.7E-22
2MPALA_SV_3	42667188677	39.44	8795298600	1.02E+11	32820951700	54.81	5745833000	1.14E+11	7.7E-63	2.5E-172	9.4E-23
2MPALA_SV_4	47776355967	36.97	10028640400	97114116000	36674561314	49.86	5585357400	1.04E+11	7.0E-85	3.1E-205	4.5E-25
2MPALA_SV_5	46130050564	37.23	9034340600	99494860000	35034199250	48.86	4733766800	90022668000	4.9E-93	1.5E-210	1.0E-23
2MPASA_SV_1	3492079186	31.52	773641660	7375975000	2179635426	44.22	529782040	5936163400	4.1E-115	3.3E-49	1.1E-12
2MPASA_SV_2	4842781600	29.06	1721910600	11484482800	2917424115	43.38	742394220	8459421200	5.2E-142	3.3E-51	1.8E-19
2MPASA_SV_3	5466683139	25.75	2060751400	12217528000	3609291084	41.36	915559100	10054621200	4.3E-121	2.8E-49	1.4E-20
2MPASA_SV_4	5902167972	27.31	1995733000	13120404000	3862595545	39.53	999647880	10892561000	6.7E-125	9.2E-56	2.1E-15
2MPASA_SV_5	4670754163	33.66	1458202200	10663417200	2851707638	38.21	832078500	11377591600	9.2E-154	7.0E-92	1.4E-22
2MPALN_SV_1	0.4034	28.43	0.17524	0.73538	0.4731	24.62	0.22679	0.99414	5.3E-75	3.3E-193	7.7E-09
2MPALN_SV_2	0.44866	33.18	0.16127	1.09128	0.54495	28.01	0.24614	1.32662	8.9E-88	6.5E-208	3.1E-07
2MPALN_SV_3	0.55451	36.85	0.15563	1.37644	0.687	34.48	0.2358	1.9217	5.2E-87	4.0E-225	6.4E-09

2MPALN_SV_4	0.63148	35.62	0.16446	1.49605	0.829	35.09	0.2922	2.0645	4.5E-104	1.6E-187	5.3E-13
2MPALN_SV_5	0.6965	33.89	0.191	1.5165	0.9374	34.75	0.3085	2.4688	3.2E-134	2.0E-210	1.9E-16
2MPASN_SV_1	0.076931	21.31	0.045334	0.143421	0.074601	21.16	0.04078	0.147794	7.1E-04	5.7E-75	2.7E-08
2MPASN_SV_2	0.071293	20.22	0.043204	0.127884	0.070677	19.71	0.041959	0.135401	2.6E-01	1.6E-102	1.7E-09
2MPASN_SV_3	0.070538	18.88	0.043225	0.118255	0.076132	19.22	0.046399	0.125626	4.2E-23	5.1E-101	4.8E-09
2MPASN_SV_4	0.076796	21.01	0.043358	0.239276	0.086387	18.43	0.051698	0.132555	2.7E-37	3.6E-59	1.0E-13
2MPASN_SV_5	0.068429	19.09	0.031644	0.146488	0.078078	26.3	0.03458	0.196929	2.4E-27	1.3E-30	3.0E-08
2MPAR_SV_1	5.692	40.47	1.45	13.331	6.76	34.2	2.225	16.366	2.6E-52	3.3E-207	2.6E-05
2MPAR_SV_2	6.783	42.69	1.525	16.023	8.172	35.42	2.627	21.518	1.6E-77	5.0E-270	1.5E-11
2MPAR_SV_3	8.386	43.39	1.665	19.163	9.559	39.64	2.723	28.048	5.6E-39	1.7E-269	2.6E-07
2MPAR_SV_4	8.677	39.69	1.838	20.019	10.154	39.92	2.953	26.707	4.6E-50	1.9E-248	8.9E-07
2MPAR_SV_5	10.816	39.65	2.276	34.881	12.951	39.28	2.859	34.5	1.3E-48	1.2E-196	3.9E-11
Area_SV_1	212301	15.96	81653	306222	170150	26.03	69991	317380	8.7E-83	1.3E-32	1.1E-12
Area_SV_2	260097	14.99	140215	381420	201706	25.86	86728	368766	1.3E-109	1.4E-35	2.4E-15
Area_SV_3	278526	14.49	167307	411665	216018	24.99	92214	373841	3.2E-118	8.0E-40	4.2E-17
Area_SV_4	277318	15.55	157616	406394	210332	24.57	92412	376590	4.2E-139	1.8E-53	3.7E-19
Area_SV_5	258878	16.62	147142	390630	192884	23.91	88082	344397	4.0E-165	2.2E-80	5.6E-21
ADAR_SV_1	0.9934	0.31	0.98297	0.99877	0.99175	0.52	0.96839	0.99843	7.3E-12	3.6E-09	2.8E-03
ADAR_SV_2	0.9948	0.26	0.98513	0.9991	0.99333	0.43	0.97509	0.99907	9.3E-13	2.0E-05	6.4E-03
ADAR_SV_3	0.99505	0.23	0.98612	0.99896	0.99387	0.38	0.97844	0.99903	1.6E-10	3.4E-04	2.8E-02
ADAR_SV_4	0.99476	0.24	0.98604	0.99888	0.99338	0.39	0.97734	0.99873	1.7E-13	8.3E-07	7.4E-03
ADAR_SV_5	0.99482	0.25	0.98599	0.99886	0.99338	0.41	0.97552	0.99866	3.0E-13	2.4E-04	2.1E-02
BPC_SV_1	48769	13.68	25657	65885	36513	26.12	17462	66258	3.3E-135	1.3E-36	7.6E-14
BPC_SV_2	59864	12.72	42410	85113	43323	25.86	21920	77255	1.4E-172	7.8E-49	1.3E-15
BPC_SV_3	71773	11.97	48215	100131	51324	24.82	25594	87638	1.2E-188	7.0E-45	3.2E-17
BPC_SV_4	79729	13.62	49540	113992	55647	22.5	30023	92634	3.4E-227	1.8E-67	6.1E-21
BPC_SV_5	69950	18.32	38058	100857	47306	21.48	22744	83909	8.8E-276	3.2E-138	2.2E-39
BPR_SV_1	11311	16.37	6929	18014	7908.1	28.91	3479.1	15562.5	3.6E-168	2.1E-58	8.5E-17
BPR_SV_2	13940	17.08	8438	21724	9396	28.69	3916	18905	4.0E-209	1.0E-90	1.5E-17

BPR_SV_3	18692	15.72	9611	27443	12326	28	5158	22136	1.6E-229	4.3E-86	2.4E-16
BPR_SV_4	23127	16.64	13210	37076	14849	23.38	6957	25325	2.2E-277	3.2E-102	5.6E-24
BPR_SV_5	19099	23.84	7557	31648	11711	22.2	5788	23093	0.0E+00	3.9E-174	6.0E-65
BPAR_SV_1	0.23146	8.98	0.17699	0.31304	0.21528	8.54	0.17078	0.27026	3.8E-72	3.0E-85	2.2E-11
BPAR_SV_2	0.23215	10.37	0.17343	0.31285	0.21578	9.11	0.16978	0.27343	2.7E-72	1.4E-118	3.1E-09
BPAR_SV_3	0.25986	10	0.1904	0.33751	0.23881	10.07	0.18535	0.32627	1.9E-98	3.7E-145	2.7E-07
BPAR_SV_4	0.28947	8.97	0.21509	0.37205	0.26697	8.97	0.20555	0.34969	9.7E-91	1.1E-103	4.1E-11
BPAR_SV_5	0.27041	9.68	0.19227	0.35104	0.24781	9.32	0.18286	0.336	3.7E-83	2.0E-71	1.5E-22
Circumference_SV_1	1054482	98.97	587	14492387	670441	106.22	245	9551516	3.2E-17	1.7E-35	9.2E-05
Circumference_SV_2	1369915	65.25	477	5667446	740812	74.36	154	4176048	2.3E-52	1.5E-22	3.6E-09
Circumference_SV_3	592941	174.33	752	7215154	413670	139.91	306	4391972	4.2E-05	5.2E-23	1.7E-05
Circumference_SV_4	494603	234.21	1227	13386785	261600	270.95	509	7271690	2.6E-05	5.4E-08	1.3E-01
Circumference_SV_5	724383	225.12	835	15881915	349567	281.31	585	9224478	1.1E-06	1.5E-08	2.5E-02
cmY_SV_1	3133.2	2.11	2947.9	3303.9	3169.4	2.57	2937.4	3385.6	1.4E-37	4.1E-128	1.2E-07
cmY_SV_2	3049.5	2.55	2850	3251.9	3090.6	2.93	2819.3	3301.8	6.2E-48	2.8E-172	6.5E-12
cmY_SV_3	2993.9	3.05	2746.7	3249.1	3024.7	3.47	2735	3279.7	2.1E-28	8.5E-214	5.2E-10
cmY_SV_4	2971.6	3.22	2757.8	3239.5	2996.2	3.59	2707.4	3276.6	7.9E-25	2.5E-271	6.2E-11
cmY_SV_5	2975.3	3.36	2735	3239.5	2995.5	3.73	2674.2	3278.3	1.9E-18	2.9E-291	2.0E-10
Compactness_SV_1	0.29296	14.27	0.17456	0.40319	0.27408	14.22	0.11044	0.37508	1.5E-28	2.7E-91	5.9E-08
Compactness_SV_2	0.29289	15.21	0.17294	0.42806	0.26307	14.85	0.16098	0.38453	1.8E-62	1.4E-104	7.6E-09
Compactness_SV_3	0.28884	17.64	0.15764	0.47635	0.24624	17.29	0.13399	0.37169	5.3E-110	1.3E-143	4.1E-12
Compactness_SV_4	0.27863	18.81	0.13879	0.51608	0.2292	19.7	0.13352	0.37238	6.5E-124	1.9E-135	5.9E-16
Compactness_SV_5	0.29554	19.77	0.16458	0.51599	0.23967	23.5	0.10975	0.39833	1.0E-108	2.9E-120	1.2E-10
CHArea_SV_1	743851	16.15	366180	1132115	637717	24.55	260115	1115607	9.9E-66	1.4E-94	9.7E-10
CHArea_SV_2	914728	15.28	588898	1323291	785412	22.65	369355	1337033	7.0E-76	8.2E-102	1.1E-12
CHArea_SV_3	991238	16.11	522688	1375763	894727	22.91	448787	1457714	1.8E-44	1.3E-133	9.4E-13
CHArea_SV_4	1024532	17.41	548753	1547638	936071	20.86	395939	1440733	6.9E-48	7.5E-182	2.2E-09
CHArea_SV_5	904844	20.48	444126	1605771	829715	23.55	402742	2066606	1.2E-43	3.3E-219	8.9E-15
Circumference_SV_1_1	3436.5	10.38	2312.1	4969.4	3224.5	13.5	2168.1	5163.9	6.5E-44	1.0E-129	2.2E-08

Circumference_SV_2_1	3821.2	10.04	2856.4	5036.6	3606.9	12.47	2466.4	5002.6	2.7E-42	2.2E-134	8.8E-09
Circumference_SV_3_1	4055.3	11.15	2690.1	5259.2	3867	13.92	2541.5	5333.6	4.0E-38	5.1E-207	1.9E-14
Circumference_SV_4_1	4147.8	11.01	2814.8	5275.2	4022.3	13.03	2534.7	5341.9	4.0E-28	1.5E-274	4.3E-14
Circumference_SV_5_1	3993.9	12.28	2593.4	5344.4	3892.4	14	2497.5	5842.1	1.8E-22	0.0E+00	3.3E-15
Excentricity_SV_1	0.4492	33.89	0.03642	0.73174	0.51871	22.78	0.14417	0.78065	3.3E-67	5.1E-222	2.5E-13
Excentricity_SV_2	0.50429	30.84	0.04467	0.77378	0.57765	19.69	0.19707	0.82893	2.2E-98	5.9E-280	3.7E-28
Excentricity_SV_3	0.56825	27.19	0.06244	0.81106	0.61512	20.61	0.20862	0.866	4.5E-50	7.7E-299	1.3E-14
Excentricity_SV_4	0.58597	23.04	0.08739	0.81646	0.63178	18.94	0.23339	0.85879	2.9E-55	1.8E-294	2.2E-06
Excentricity_SV_5	0.64911	18.27	0.15159	0.8913	0.69502	15.78	0.22799	0.89005	1.2E-52	2.8E-251	5.6E-06
ObjectExtentX_SV_1	817.94	10.58	599	1101.4	724.72	14.22	512.6	1082.2	2.2E-89	4.2E-80	8.7E-08
ObjectExtentX_SV_2	887.2	7.88	623.4	1108.2	788.18	12.63	515.4	1105.2	3.5E-101	1.0E-50	9.1E-14
ObjectExtentX_SV_3	874.18	7.75	700.4	1059	820.61	10.93	550.6	1022.6	8.5E-38	2.2E-33	2.0E-07
ObjectExtentX_SV_4	887.67	8.63	635.6	1152.4	848.55	9.78	589.2	1087.6	1.3E-22	3.7E-42	7.0E-05
ObjectExtentX_SV_5	776.71	11.53	552.6	1099.6	752.97	12.15	540.2	1363.8	2.0E-09	4.5E-72	1.2E-07
ObjectExtentY_SV_1	1247.5	15.11	729.6	2083.8	1180.2	17.73	703.8	2270.8	2.1E-21	5.3E-141	1.7E-08
ObjectExtentY_SV_2	1411.1	14.92	872.8	2130.4	1356.8	16.02	785.4	2131	9.4E-14	2.3E-152	4.1E-06
ObjectExtentY_SV_3	1551.7	16.36	789.4	2216.4	1490.7	18.43	830.4	2225.4	7.4E-21	1.7E-253	4.5E-13
ObjectExtentY_SV_4	1589.6	15.41	883.4	2202.2	1570.9	17.15	886.6	2239.8	8.4E-05	0.0E+00	5.4E-14
ObjectExtentY_SV_5	1548.5	16.27	845.8	2162.2	1533	17.98	858.2	2213.8	1.5E-03	0.0E+00	4.2E-12
PSCC_1_1	348.53	28.29	93	741.6	166.26	51.36	23	492.8	8.5E-212	4.7E-57	5.9E-23
PSCC_1_2	453.94	23.02	172	873.6	226.22	46.78	45.2	547.8	1.7E-234	5.9E-67	2.5E-14
PSCC_1_3	574.73	23.79	269	1083	329.69	41.07	61.6	917.8	2.6E-197	1.1E-72	7.6E-16
PSCC_1_4	864.91	26.34	358.8	1618.8	484.84	39.38	136.8	1164.6	1.9E-200	2.7E-73	2.4E-18
PSCC_1_5	953.3	28.12	342.8	1762	529.3	44.81	112	1770.4	3.5E-178	3.7E-64	3.3E-18
PSCC_2_1	768.26	27.57	275.6	1580.8	367.03	49.77	59.6	1083.8	1.4E-220	1.3E-59	2.0E-24
PSCC_2_2	998.7	23.78	382.2	1944.2	475	44.62	112	1285.4	5.9E-258	2.3E-70	1.5E-19
PSCC_2_3	1296.4	26.05	562	2772.4	663.7	39.01	146.8	1931.8	2.9E-253	4.3E-91	1.2E-27
PSCC_2_4	2055.9	28.71	789.2	4168.2	979	38.42	317	2271.6	2.8E-278	2.3E-106	1.2E-37
PSCC_2_5	1962.6	27.09	700	4378.8	1004.1	41.22	249.2	3028.8	4.1E-212	4.9E-54	3.0E-20

PSCC_3_1	1890.2	26.11	673.4	3679.8	838.5	51.54	172.2	2898.2	5.7E-244	1.4E-57	2.1E-22
PSCC_3_2	2438.7	21.69	999.8	4121	1015.5	48.66	227.6	3207.8	2.2E-297	2.0E-66	5.2E-16
PSCC_3_3	3205.9	21.44	1502.8	5508.4	1371.6	44.33	349	4529.4	#NUM!	1.1E-74	2.2E-20
PSCC_3_4	4752.4	21.61	2064.2	8497.8	2130.3	40.18	559.6	5455.6	#NUM!	5.1E-81	1.0E-20
PSCC_3_5	4301.7	25.03	1559.8	8883	1848.7	41.32	619.6	6192.8	3.8E-274	2.2E-46	1.1E-25
PSCC_4_1	3799.2	17.32	1424.4	5682.2	1921.4	48.69	374.2	5378.2	6.5E-225	1.8E-33	1.9E-14
PSCC_4_2	4433.9	15.75	2504.2	6594.4	2183.5	46.19	477.8	5384	7.3E-268	4.0E-52	1.2E-15
PSCC_4_3	5401.6	15.05	3151.2	7608.2	2816.4	41.94	716.8	7942	3.8E-257	7.6E-43	2.6E-17
PSCC_4_4	7378	18.84	3989.4	13935.6	4271.4	36.4	1130.8	9718.8	2.7E-208	6.3E-44	5.8E-11
PSCC_4_5	8007.1	23.95	2825.6	17862.8	3751.3	43.47	1237.4	14344.8	1.8E-234	4.4E-36	1.6E-14
PSCC_5_1	4963.6	13.67	2547.8	6844.6	3433.3	33.39	988.8	6621.8	1.8E-146	1.1E-31	5.9E-12
PSCC_5_2	5630.1	14.01	3816	7980.6	3819.6	32.82	1131.8	7327	1.8E-176	1.0E-53	1.6E-16
PSCC_5_3	6841.9	17.1	4188	12166.6	4807.1	36.14	1585.8	12567.8	2.0E-128	1.0E-51	1.6E-11
PSCC_5_4	10443	27.78	5052	21861	7246	39.06	2575	20447	4.2E-93	1.5E-43	7.8E-13
PSCC_5_5	15600	40.51	5647	48158	8565	53.81	2712	35005	7.0E-133	1.4E-72	3.0E-23
PSCC_6_1	5194	13.25	3085.8	6986.6	4373.2	21.73	2150.4	7377.6	1.7E-80	8.5E-55	5.6E-09
PSCC_6_2	6162.2	14.33	4133.6	9268.4	5127	23.76	2576	9909.4	5.1E-89	9.0E-77	2.9E-12
PSCC_6_3	8036.9	22.94	4534.8	17876.4	6790	34.84	2898	19556	1.4E-37	5.2E-70	3.5E-09
PSCC_6_4	14207	33.5	5953	34446	11223	44.32	3436	33446	6.3E-38	1.3E-52	4.5E-15
PSCC_6_5	28387	48.12	7190	83745	19542	58.73	4353	83128	1.3E-62	9.7E-96	1.2E-29
PSCC_7_1	5501.3	13.62	3260.4	8676.2	4961.9	18.86	2698.2	7769.4	5.2E-41	1.4E-63	2.2E-07
PSCC_7_2	6774.8	15.02	4425.4	10396.4	6082.9	21.47	3242.6	11505.6	6.2E-39	1.9E-75	2.3E-08
PSCC_7_3	8986.9	21.92	4998.2	17055.4	8041	29.08	3550	17409	7.5E-23	6.9E-71	2.4E-10
PSCC_7_4	14508	27.2	7130	33851	12657	35.99	4683	33361	7.5E-20	2.5E-48	4.0E-10
PSCC_7_5	27639	42.82	8594	85779	23813	48.49	5817	82995	4.3E-17	5.4E-103	1.0E-18
PSCC_8_1	7042.1	20.26	4230.8	14277.4	6508.7	26.05	3408.8	13510.2	7.4E-12	6.9E-43	1.2E-02
PSCC_8_2	8615.3	19.32	5504	16053.6	7913.6	24.89	3859.8	14842.6	1.9E-14	2.6E-39	1.3E-03
PSCC_8_3	11039	23.11	5939	22490	9843	27.78	4162	19905	1.5E-21	3.3E-53	3.2E-08
PSCC_8_4	16066	23.48	8366	30007	13429	30.41	5657	33556	3.1E-40	6.5E-42	1.5E-09

PSCC_8_5	26559	35.08	9846	71909	22247	43.46	7008	69114	1.8E-31	7.7E-110	3.0E-20
PSCC_9_1	9485.1	19	5660.8	14688	8897.5	21.95	4324.4	14302.2	5.3E-09	5.5E-21	1.7E-03
PSCC_9_2	11382	18.7	7307	17917	10850	22.52	5350	19792	8.1E-06	1.8E-24	3.1E-05
PSCC_9_3	14350	22.49	7056	25265	13200	25.44	5216	22931	3.5E-13	9.4E-43	5.2E-11
PSCC_9_4	18573	17.44	9972	28722	15873	24.6	7393	33002	3.2E-46	1.1E-31	9.9E-11
PSCC_9_5	27514	26.54	12082	54829	24584	36.85	8278	61658	7.6E-19	2.9E-96	3.9E-15
PSCC_10_1	9299.1	12.07	6049.8	13059.8	8699.2	15.26	4988.4	13081.2	2.3E-22	2.1E-38	1.4E-07
PSCC_10_2	11324	14.06	6449	17076	10738	19.17	6154	20165	2.5E-11	8.3E-46	1.1E-08
PSCC_10_3	14545	16.52	8001	21907	13229	22.94	6714	22353	1.4E-23	3.8E-44	4.2E-14
PSCC_10_4	17118	13.27	10171	23869	14726	23.06	7727	32340	5.3E-55	5.5E-32	2.9E-12
PSCC_10_5	24961	25.67	13065	53122	24163	37.55	8851	57581	9.7E-03	5.2E-94	3.9E-16
PSCC_11_1	25842	14.79	15490	37184	23167	18.53	11449	37888	2.9E-55	2.7E-107	2.8E-08
PSCC_11_2	30523	14.09	18637	44553	27391	18.76	13864	50339	1.2E-51	8.0E-91	4.4E-11
PSCC_11_3	40131	14.9	22396	55141	35534	21.81	17367	62551	2.5E-49	5.4E-79	4.2E-13
PSCC_11_4	46477	12.8	30511	63253	40295	20.98	21857	69995	7.6E-70	1.8E-68	5.0E-15
PSCC_11_5	59172	18.78	33567	104429	58053	36.81	24491	176124	7.2E-02	2.1E-110	4.4E-27
PSCC_12_1	8943	14.79	4602.8	13359.6	7756	20.2	4278.6	15265.2	1.7E-59	8.7E-49	2.1E-13
PSCC_12_2	11686	16.68	7409	19767	10086	24.78	4925	22944	3.1E-49	1.4E-55	5.6E-13
PSCC_12_3	15857	16.86	8982	23725	13374	26.49	6309	24157	1.1E-52	1.7E-37	1.5E-12
PSCC_12_4	19731	14.54	11276	31675	16098	25.62	7586	33745	1.2E-79	2.8E-32	8.9E-18
PSCC_12_5	29985	25.62	13464	61587	25323	33.49	8816	66590	1.7E-36	1.0E-68	2.7E-11
PSCC_13_1	11634	15.12	5145	16824	10413	20.21	5597	20557	4.9E-40	3.0E-52	1.3E-16
PSCC_13_2	15251	17.24	8500	26926	13683	25.06	6472	31875	4.2E-29	5.8E-60	1.0E-14
PSCC_13_3	21201	17.29	10092	33948	18617	25.93	8607	33727	3.0E-34	1.8E-41	4.6E-13
PSCC_13_4	27399	15.53	15174	43831	23440	26.93	10260	53283	3.9E-50	3.8E-42	6.4E-20
PSCC_13_5	40838	23.87	8099	73718	35081	33.03	4721	72101	6.0E-32	1.1E-67	1.4E-09
PSCC_14_1	19868	15.04	8346	29464	20250	18.61	10811	36993	8.2E-03	7.1E-69	1.8E-15
PSCC_14_2	25506	17.66	13167	45393	25556	22.17	12298	56753	8.1E-01	2.1E-74	5.6E-14
PSCC_14_3	35183	17.18	15432	55686	33698	22.65	16176	60044	2.0E-06	1.9E-52	2.4E-13

PSCC_14_4	44188	16.09	24222	66465	40099	24.46	18313	93092	6.8E-25	9.5E-49	1.3E-19
PSCC_14_5	53732	30.46	5104	97599	45815	38.32	2511	98608	3.4E-40	4.3E-151	1.8E-13
PSCC_15_1	44127	17.98	16883	68195	49606	18.48	26447	83873	1.9E-43	6.8E-67	3.6E-11
PSCC_15_2	52889	18.07	26043	89415	58155	19.65	26760	105239	8.1E-29	1.4E-69	2.4E-10
PSCC_15_3	65811	16.07	30443	95337	67930	19.22	32969	109943	7.4E-05	1.6E-51	5.2E-15
PSCC_15_4	71107	17.93	42700	121967	66961	21.54	33012	123888	3.4E-12	1.5E-60	1.8E-18
PSCC_15_5	64567	38.45	3354	132431	58712	45.93	1514	179479	2.1E-15	1.6E-203	8.5E-16
PSCC_16_1	117887	21.57	40949	206497	119134	24.33	38988	223477	3.0E-01	2.4E-60	1.4E-08
PSCC_16_2	131571	20.51	64654	213838	129323	24.02	41757	214451	7.6E-02	2.2E-63	4.3E-11
PSCC_16_3	132362	17.57	71386	209417	129681	24.36	44351	223826	3.0E-02	1.1E-53	9.9E-14
PSCC_16_4	124324	21.42	64206	212762	119247	27.6	40275	234941	6.0E-05	3.1E-71	1.0E-14
PSCC_16_5	90357	48.48	2408	194261	75595	55.09	1043	202926	7.6E-45	3.0E-263	1.8E-23
PSCC_17_1	191717	21.64	57734	305548	134448	43.74	21835	313056	9.1E-92	3.7E-37	4.5E-13
PSCC_17_2	223608	21.34	104502	386742	158855	38.61	32721	351861	4.2E-104	5.8E-41	2.9E-20
PSCC_17_3	208898	20.35	102013	328442	161362	35.24	42855	318923	4.6E-78	1.1E-49	1.4E-19
PSCC_17_4	176950	24.28	61750	317728	132227	35.34	35753	311523	9.9E-102	6.0E-92	3.2E-18
PSCC_17_5	91440	58.33	1625	226831	43770	68.68	697	147615	8.2E-240	2.2E-270	4.0E-81
PSCC_18_1	102861	24.77	26536	186746	50351	61.51	4032	150746	1.7E-174	2.1E-32	7.6E-14
PSCC_18_2	138794	21.36	51049	240900	71000	54.9	7226	203085	5.5E-196	1.6E-40	1.2E-18
PSCC_18_3	136566	23.14	66436	255328	72627	48.14	14462	171333	1.9E-212	7.7E-64	2.9E-26
PSCC_18_4	106475	29.5	27769	210842	54055	48.11	13695	152760	1.1E-242	8.4E-124	1.4E-28
PSCC_18_5	42640	62.98	1149	112226	14685	66.32	521	51522	2.3E-304	1.2E-262	######
PSCC_19_1	26528	34.66	5777	55413	11120	63.33	1664	39378	9.7E-203	1.9E-55	8.3E-28
PSCC_19_2	44389	27.62	15935	92285	19053	61.01	2449	68892	5.9E-226	5.0E-61	1.6E-15
PSCC_19_3	47571	29.02	18440	105423	20582	51.76	3954	58237	4.1E-266	5.9E-90	5.9E-34
PSCC_19_4	38073	34.64	10986	83603	17128	47.06	4852	49531	5.9E-274	7.8E-140	1.7E-45
PSCC_19_5	17077	58.41	877	41598	6561	56.16	389	19539	0.0E+00	7.4E-278	######
PSCC_20_1	9579	34.35	2634	22876	4851	47.05	1293	15724.6	1.0E-190	3.6E-68	9.3E-39
PSCC_20_2	18086	35.06	6421	49175	8548	54.57	1882	32296	3.1E-205	1.3E-94	5.2E-23

PSCC_20_3	21735	32.36	8950	49940	10352	45.73	2742	30136	9.1E-250	7.8E-115	3.4E-36
PSCC_20_4	19644	34.25	7170	42598	10034	40.42	3648	25912	1.6E-259	2.9E-155	6.5E-46
PSCC_20_5	10996	53.16	859	25801	4690	50.48	356	12158	0.0E+00	6.4E-281	######
No PSCC_1	16058	19.8	7704	28623	11254	33.06	3942	25423	1.3E-135	1.5E-53	3.5E-19
No PSCC_2	25147	24.58	14028	56870	15670	35.54	4815	39526	2.0E-181	6.3E-76	3.1E-26
No PSCC_3	32832	21.8	17780	62562	19774	31.57	7314	41379	4.2E-225	3.5E-76	2.2E-29
No PSCC_4	33095	25.58	15018	61120	19758	29.9	8839	38317	5.5E-258	1.9E-136	8.3E-42
No PSCC_5	21375	45.15	2537	46365	10660	44.17	986	24593	0.0E+00	3.3E-285	######
NIR TV_1	131.36	2.48	118.53	141.27	128.96	3.94	112.45	139.55	1.1E-47	5.8E-127	6.6E-09
NIR TV_2	144.19	2.88	133.75	158.7	143.74	3.7	126.94	157.86	3.3E-04	1.1E-226	3.7E-10
NIR TV_3	137.9	6.05	115.52	149.97	139.63	6.36	115.47	153.05	7.2E-66	0.0E+00	1.1E-05
NIR TV_4	120.54	2.22	113.29	132	122.02	2.08	113.58	129.72	2.4E-66	6.8E-185	6.0E-16
NIR TV_5	110.55	3.09	96.81	120.38	111.39	3.21	101.11	125.5	3.5E-15	1.8E-187	4.4E-07
NIR SV_1	126.68	4.67	111.14	142.39	127.34	4.4	113.53	141.15	7.2E-11	0.0E+00	9.6E-08
NIR SV_2	134.15	4.27	120.31	151.43	135.95	4.19	120.3	150.41	2.4E-50	0.0E+00	2.3E-09
NIR SV_3	129.17	3.77	113.24	143.27	132.4	3.69	113.86	144.22	6.1E-121	1.1E-263	1.4E-12
NIR SV_4	131.47	3.66	115.2	146.27	135.29	3.05	119.15	143.95	1.5E-132	3.2E-204	8.8E-20
NIR SV_5	116.24	4.09	102.18	129.25	118.91	3.23	105.76	129.97	2.1E-82	1.0E-198	4.3E-26
IR TV_1	24.178	6.92	20.522	27.706	23.699	7.02	20.257	27.791	3.2E-107	0.0E+00	8.2E-23
IR TV_2	23.999	4.77	21.414	26.449	23.735	4.72	21.384	26.491	3.2E-59	0.0E+00	3.2E-19
IR TV_3	24.778	4.29	22.313	27.519	24.523	4.32	22.106	27.389	5.1E-54	0.0E+00	6.7E-10
IR TV_4	24.74	5.43	21.63	27.274	24.611	5.35	21.591	27.319	5.1E-18	0.0E+00	1.7E-09
IR TV_5	25.241	4.39	21.351	28.975	24.97	4.35	21.709	29.144	1.1E-52	0.0E+00	2.4E-20
IR SV_1	19.951	14.25	14.253	26.123	19.908	14.3	14.23	26.298	2.1E-06	0.0E+00	1.1E-23
IR SV_2	19.227	8.81	14.906	22.19	19.229	8.62	15.161	22.166	8.2E-01	0.0E+00	5.8E-43
IR SV_3	20.651	9.33	16.795	24.298	20.628	9.48	16.748	24.374	1.9E-02	0.0E+00	5.8E-37
IR SV_4	20.252	11.46	15.63	25.27	20.312	11.64	15.71	25.016	5.1E-05	0.0E+00	4.4E-24
IR SV_5	21.485	7.98	17.167	25.152	21.481	8.14	17.477	25.326	6.8E-01	0.0E+00	3.2E-15
Blue_TV_1	48.316	7.62	36.972	58.433	50.611	8.36	37.481	62.154	3.8E-105	1.3E-272	1.9E-21

Blue_TV_2	51.877	7.3	41.514	62.23	56.437	7.93	43.905	71.175	9.4E-197	1.8E-227	1.1E-16
Blue_TV_3	55.26	7.75	44.392	68.559	61.092	7.28	48.45	74.519	6.5E-256	2.1E-246	2.1E-16
Blue_TV_4	57.559	8.55	43.032	75.63	63.421	7.86	47.928	78.153	6.8E-267	4.7E-297	7.3E-22
Blue_TV_5	70.826	16.93	47.767	131.574	80.661	17.35	58.005	146.603	1.4E-144	4.6E-264	7.1E-22
Green_TV_1	76.882	7.9	57.565	90.766	85.214	9.51	62.215	113.361	1.9E-174	8.2E-176	3.4E-18
Green_TV_2	81.428	7.43	65.555	101.748	93.423	8.84	71.146	117.618	1.3E-243	4.3E-163	3.3E-15
Green_TV_3	86.268	7.9	69.59	108.825	100.82	7.82	76.38	121.46	0.0E+00	1.3E-189	4.4E-19
Green_TV_4	90.066	8.77	68.636	122.003	105	8.42	80.49	132.92	0.0E+00	1.0E-238	2.2E-20
Green_TV_5	117.16	20.65	78.18	225.77	140.74	18.64	96.55	249.94	2.9E-178	2.1E-250	5.0E-23
Red_TV_1	61.378	8.19	45.314	74.245	68.313	10.2	48.363	93.411	1.6E-165	1.1E-167	1.8E-18
Red_TV_2	65.327	7.66	52.028	82.816	75.134	9.43	57.01	98.158	3.7E-232	2.9E-158	5.3E-17
Red_TV_3	70.056	8.31	55.595	89.539	81.683	8.13	61.887	98.875	5.5E-295	1.3E-189	3.3E-19
Red_TV_4	74.433	9.4	55.324	104.337	86.347	8.93	65.726	112.859	6.4E-304	6.3E-245	1.0E-19
Red_TV_5	103.45	25.34	64.48	222.72	125.26	23.89	81.57	251.1	4.1E-141	1.3E-249	1.3E-21
Blue_SV_1	69.916	7.1	57.118	95.072	76.035	8.73	61.066	102.399	1.1E-85	3.2E-52	4.3E-07
Blue_SV_2	72.759	7.96	59.14	93.559	80.711	8.41	62.057	105.317	4.9E-142	1.5E-101	4.5E-10
Blue_SV_3	80.904	8.43	60.737	101.389	90.277	7.31	68.638	109.874	4.0E-198	3.0E-154	8.8E-14
Blue_SV_4	88.302	7.83	67.981	109.219	98.445	6.47	79.85	118.242	1.5E-226	3.1E-164	8.0E-19
Blue_SV_5	102.21	12.79	73.47	146.22	117.51	10.47	92.4	160.42	1.5E-247	2.3E-268	3.2E-15
Green_SV_1	102.05	6.93	84.22	134.14	115.66	9.54	89.39	155.57	5.5E-139	2.6E-52	1.3E-08
Green_SV_2	104.84	7.28	86.27	130.84	121.33	8.71	92.71	153.46	3.5E-203	8.3E-86	2.0E-11
Green_SV_3	114.57	7.86	87.78	138.9	132.56	6.87	101.75	155.74	5.8E-273	3.0E-141	4.4E-18
Green_SV_4	122.98	7.49	95.8	152	140.74	6.07	114.63	165.44	2.0E-298	5.8E-170	6.2E-22
Green_SV_5	144.49	12.68	104.02	200.48	169.72	9.53	128.22	218.83	4.8E-282	7.5E-251	3.4E-19
Red_SV_1	91.397	7.33	74.771	124.504	103.12	10.23	80.1	143.6	2.3E-115	5.0E-42	4.8E-08
Red_SV_2	93.849	7.95	76.237	120.572	108.31	9.38	81.61	144.09	1.9E-178	1.9E-80	3.2E-11
Red_SV_3	104.51	8.89	77.61	130.83	120.33	7.44	90.66	146.47	1.1E-246	1.7E-150	7.2E-18
Red_SV_4	116.06	8.83	87.79	150.79	131.92	6.59	105.98	159.22	9.2E-259	3.1E-176	4.4E-24
Red_SV_5	144.69	17.06	96.46	220.51	168.72	13.23	121.12	235.13	3.1E-201	7.1E-257	4.6E-20

b_TV_1	0.25904	1.39	0.24403	0.269	0.24824	2.97	0.22788	0.26388	1.7E-167	1.7E-25	1.7E-10
b_TV_2	0.26122	1.42	0.24881	0.27192	0.25108	2.4	0.23421	0.26587	7.5E-211	1.3E-58	2.0E-11
b_TV_3	0.26124	1.39	0.25186	0.27123	0.25092	1.87	0.2373	0.26379	5.8E-276	1.4E-79	5.5E-15
b_TV_4	0.25931	1.65	0.24026	0.27079	0.24909	1.91	0.2313	0.26176	1.1E-285	2.4E-121	1.4E-09
b_TV_5	0.24502	4.47	0.20762	0.26383	0.23391	3.51	0.20777	0.25573	2.0E-178	4.1E-180	5.3E-34
g_TV_1	0.41207	0.73	0.40297	0.42163	0.41737	1	0.4067	0.42772	8.2E-158	3.4E-80	1.7E-11
g_TV_2	0.40995	0.73	0.40202	0.41878	0.41519	0.85	0.40591	0.42484	2.7E-189	3.7E-100	1.7E-11
g_TV_3	0.40775	0.62	0.39938	0.41412	0.41387	0.73	0.40601	0.42192	4.6E-253	1.5E-90	1.0E-08
g_TV_4	0.40564	0.67	0.39869	0.41294	0.41212	0.75	0.403	0.42328	2.5E-273	1.2E-111	1.9E-07
g_TV_5	0.40248	0.88	0.38912	0.41111	0.40696	1.47	0.38538	0.41905	1.7E-136	1.9E-183	1.9E-40
b_SV_1	0.26549	1.13	0.25756	0.27586	0.25813	1.65	0.24573	0.26881	8.4E-212	1.4E-63	9.8E-12
b_SV_2	0.268	1.15	0.25952	0.27749	0.26019	1.71	0.24509	0.2712	2.8E-237	4.9E-95	2.1E-06
b_SV_3	0.26969	0.96	0.2627	0.27775	0.26306	1.4	0.24931	0.27261	3.9E-238	3.8E-77	2.8E-18
b_SV_4	0.26981	1.1	0.26027	0.27845	0.26526	1.27	0.25303	0.27473	2.5E-164	5.8E-90	2.0E-18
b_SV_5	0.26171	2.24	0.24118	0.27605	0.25794	2.08	0.23879	0.27234	2.8E-62	2.0E-105	1.5E-33
r_SV_1	0.34698	0.46	0.3426	0.35337	0.34956	0.85	0.34419	0.36172	3.6E-79	4.1E-26	2.9E-10
r_SV_2	0.34566	0.48	0.3415	0.35167	0.34882	0.76	0.34328	0.35915	3.4E-133	1.8E-46	1.3E-13
r_SV_3	0.34823	0.82	0.34117	0.3575	0.35057	0.64	0.34426	0.35871	1.2E-116	3.2E-149	1.0E-24
r_SV_4	0.35433	1.23	0.34487	0.37107	0.35544	0.97	0.34859	0.37163	5.0E-17	4.0E-147	4.2E-22
r_SV_5	0.36835	2.93	0.3496	0.39784	0.36926	2.48	0.35179	0.39848	1.4E-03	2.4E-193	4.7E-27
R-G_TV_1	-15.503	-7.67	-18.503	-12.251	-16.901	-8.12	-20.883	-13.051	4.0E-173	6.2E-196	6.5E-16
R-G_TV_2	-16.102	-7.37	-19.513	-13.41	-18.29	-7.85	-21.905	-14.108	7.6E-245	1.3E-166	3.1E-10
R-G_TV_3	-16.212	-7.16	-19.927	-13.473	-19.141	-7.49	-23.055	-14.494	0.0E+00	9.6E-166	9.7E-16
R-G_TV_4	-15.633	-7.41	-19.491	-12.842	-18.649	-7.98	-22.759	-14.468	0.0E+00	5.6E-175	1.3E-16
R-G_TV_5	-13.713	-20.93	-18.728	-1.821	-15.475	-30.28	-22.76	2.171	1.3E-52	1.1E-205	3.1E-29
R-B_TV_1	13.062	12.4	8.341	18.136	17.702	20.09	10.275	31.275	8.3E-163	8.9E-47	7.1E-12
R-B_TV_2	13.449	11.97	10.026	20.593	18.696	17.67	11.254	32.164	6.1E-219	6.9E-68	1.2E-14
R-B_TV_3	14.797	13.12	10.257	22.417	20.591	13.5	13.437	30.262	1.0E-287	1.4E-97	6.2E-18
R-B_TV_4	16.874	15.27	11.679	28.706	22.925	14.41	15.425	34.745	4.4E-295	1.1E-162	2.6E-14

R-B_TV_5	32.622	45.11	15.298	91.146	44.602	36.79	20.944	104.496	2.0E-129	6.5E-232	3.3E-20
(R-G)/(R+G+B)_TV_1	-0.083181	-4	-0.09177	-0.071287	-0.082993	-5.16	-0.094344	-0.067016	1.4E-01	8.8E-149	2.5E-16
(R-G)/(R+G+B)_TV_2	-0.081127	-3.82	-0.089075	-0.072043	-0.081449	-4.98	-0.090332	-0.065361	9.4E-03	1.3E-131	1.0E-21
(R-G)/(R+G+B)_TV_3	-0.076733	-4.15	-0.085501	-0.066598	-0.078653	-3.98	-0.086625	-0.066378	6.1E-55	1.2E-126	5.6E-11
(R-G)/(R+G+B)_TV_4	-0.070587	-5.4	-0.080199	-0.058111	-0.073338	-5.53	-0.084493	-0.058604	8.3E-87	2.1E-177	6.8E-07
(R-G)/(R+G+B)_TV_5	-0.049989	-29.87	-0.07194	-0.00384	-0.047833	-36.39	-0.073814	0.003582	5.0E-08	3.2E-249	4.6E-14
(G-B)/(R+G+B)_SV_1	0.12205	4.97	0.10216	0.13739	0.13417	5.46	0.11213	0.15344	8.7E-203	3.4E-84	3.2E-09
(G-B)/(R+G+B)_SV_2	0.11834	5.4	0.10063	0.13521	0.1308	5.99	0.11052	0.15806	4.8E-217	1.5E-116	3.1E-05
(G-B)/(R+G+B)_SV_3	0.11239	4.48	0.09671	0.12753	0.12331	5.77	0.10442	0.14949	1.4E-212	1.6E-99	3.8E-11
(G-B)/(R+G+B)_SV_4	0.10606	4.4	0.09301	0.12293	0.11404	5.17	0.09745	0.13872	8.2E-177	3.7E-101	3.8E-10
(G-B)/(R+G+B)_SV_5	0.10823	5.24	0.09007	0.13133	0.11486	6.36	0.08972	0.13935	2.6E-113	1.5E-106	9.0E-25
Ipca_SV_1	61.971	8.27	47.749	75.597	76.455	12.43	53.807	103.295	1.5E-192	8.1E-55	2.3E-10
Ipca_SV_2	61.836	7.78	47.916	77.794	78.376	11.3	56.382	104.126	7.1E-252	5.2E-71	3.7E-11
Ipca_SV_3	65.012	7.84	50.779	79.555	81.685	8.34	61.808	106.066	0.0E+00	4.8E-94	2.0E-21
Ipca_SV_4	67.247	8.04	52.074	83.547	81.976	7.32	60.599	103.757	0.0E+00	5.4E-142	3.0E-22
Ipca_SV_5	82.662	14.18	55.703	116.114	101.98	10.03	68.42	127.07	2.7E-265	8.7E-167	2.9E-28
ExB_SV_1	-0.015853	-45.66	-0.033932	0.008181	-0.03092	-28.94	-0.055144	-0.0048	6.6E-207	3.5E-81	9.8E-10
ExB_SV_2	-0.011142	-68.07	-0.030989	0.010362	-0.026727	-35.75	-0.060028	-0.002041	8.2E-223	2.4E-113	2.4E-05
ExB_SV_3	-0.004519	-131.41	-0.02229	0.014197	-0.018082	-47.14	-0.049767	0.003558	4.7E-219	2.2E-94	2.8E-12
ExB_SV_4	0.001866	297.39	-0.017443	0.018077	-0.00793	-89.42	-0.03751	0.012388	3.1E-179	1.3E-95	2.0E-11
ExB_SV_5	-0.00354	-196.06	-0.032007	0.013944	-0.011679	-74.06	-0.040113	0.014935	4.3E-108	9.8E-85	3.9E-28
ExG_SV_1	0.16261	6.02	0.13395	0.1881	0.17692	6.17	0.13923	0.20387	2.9E-151	2.5E-91	1.7E-06
ExG_SV_2	0.15902	6.62	0.13037	0.18732	0.17298	6.57	0.13878	0.20944	5.5E-158	2.3E-126	7.4E-06
ExG_SV_3	0.14625	6.5	0.11977	0.1733	0.1591	7.14	0.12314	0.19638	1.8E-155	9.8E-133	9.4E-07
ExG_SV_4	0.1276	8.03	0.09768	0.16133	0.13789	7.53	0.11153	0.17527	2.7E-122	6.1E-140	3.3E-08
ExG_SV_5	0.10982	17.28	0.04538	0.14675	0.11839	16.02	0.04494	0.16228	1.7E-55	6.7E-222	5.6E-15
Gray_TV_1	0.36673	0.4	0.36257	0.37221	0.3702	0.66	0.36435	0.37635	1.3E-167	6.3E-47	9.9E-11
Gray_TV_2	0.36572	0.41	0.36159	0.37052	0.36905	0.55	0.3637	0.37438	9.8E-208	2.9E-77	9.2E-11
Gray_TV_3	0.36506	0.36	0.36104	0.36857	0.36869	0.45	0.36427	0.37329	2.2E-272	4.2E-82	3.1E-11

Gray_TV_4	0.36477	0.39	0.36069	0.3694	0.36849	0.45	0.36355	0.37494	1.1E-289	3.5E-107	2.0E-08
Gray_TV_5	0.36634	0.51	0.36237	0.3725	0.36963	0.46	0.36388	0.37372	9.8E-229	5.3E-77	1.1E-56
Gray_SV_1	0.3583	0.41	0.35365	0.36203	0.36101	0.47	0.3557	0.36549	7.1E-194	5.4E-88	2.0E-08
Gray_SV_2	0.35751	0.43	0.35334	0.36162	0.36026	0.5	0.35556	0.36653	7.2E-206	9.1E-121	3.4E-05
Gray_SV_3	0.35594	0.35	0.35221	0.3597	0.35838	0.47	0.35361	0.36449	9.3E-201	4.9E-108	1.3E-09
Gray_SV_4	0.35407	0.33	0.35063	0.35835	0.35589	0.4	0.3521	0.36175	1.5E-168	1.2E-111	1.1E-08
Gray_SV_5	0.35374	0.44	0.34794	0.35897	0.35525	0.54	0.34823	0.36133	2.6E-110	2.2E-153	3.7E-19
SCOM_TV_1	6.2833	0.07	6.268	6.296	6.2893	0.09	6.2721	6.3037	9.1E-135	2.1E-115	8.0E-13
SCOM_TV_2	6.28	0.07	6.2679	6.2923	6.2862	0.08	6.2736	6.2995	2.3E-156	1.6E-119	2.0E-13
SCOM_TV_3	6.2757	0.06	6.2628	6.2859	6.2836	0.07	6.2723	6.2948	2.9E-223	1.4E-100	1.3E-07
SCOM_TV_4	6.2708	0.07	6.2596	6.2821	6.2794	0.08	6.2659	6.2941	6.7E-245	4.9E-126	7.7E-07
SCOM_TV_5	6.2589	0.15	6.225	6.2773	6.2632	0.22	6.219	6.2866	3.0E-42	2.6E-232	1.7E-23
PCA1_TV_1	-0.012521	-156.97	-0.064789	0.072296	0.05239	85.89	-0.03437	0.18008	1.1E-163	7.4E-20	2.1E-10
PCA1_TV_2	-0.022829	-88.55	-0.084938	0.049005	0.03723	98.72	-0.04592	0.15413	1.6E-206	1.6E-52	4.1E-12
PCA1_TV_3	-0.017425	-123.18	-0.078751	0.041176	0.0416	66.78	-0.03288	0.12704	6.9E-270	9.0E-81	8.0E-17
PCA1_TV_4	0.0016	1636.98	-0.06372	0.13038	0.05908	49.06	-0.01315	0.16146	4.2E-274	4.9E-133	6.0E-10
PCA1_TV_5	0.11131	73.23	-0.01797	0.38946	0.18056	36.84	0.03697	0.37702	3.7E-149	2.8E-203	6.5E-27
PCA1_SV_1	0.001657	893.07	-0.048188	0.043676	0.04208	58.28	-0.01554	0.1215	1.3E-198	1.4E-45	1.7E-12
PCA1_SV_2	-0.013065	-112.26	-0.061513	0.032153	0.03071	80.73	-0.02445	0.10927	8.4E-235	5.5E-75	3.6E-08
PCA1_SV_3	-0.014792	-103.94	-0.058554	0.034478	0.021405	89.36	-0.03222	0.089341	1.0E-239	7.1E-76	4.2E-24
PCA1_SV_4	-0.001175	-1814.61	-0.057039	0.080717	0.02242	91.88	-0.033426	0.103996	6.3E-129	6.2E-105	9.4E-23
PCA1_SV_5	0.06772	72.93	-0.0371	0.22631	0.08754	48.18	-0.01533	0.241	2.8E-35	3.8E-141	2.8E-32
PCA2_SV_1	41.585	9.28	31.743	56.806	52.401	15.44	35.657	79.471	1.3E-152	5.7E-30	1.8E-09
PCA2_SV_2	40.845	9.26	29.756	56.597	53.411	13.93	37.234	79.778	4.8E-216	1.6E-50	1.1E-11
PCA2_SV_3	45.642	11.68	30.838	63.512	58.092	9.68	41.332	78.21	5.9E-290	4.3E-116	2.8E-24
PCA2_SV_4	53.494	13.75	36.64	81.788	64.547	9.5	45.379	89.306	1.5E-240	3.6E-158	1.9E-27
PCA2_SV_5	81.5	28.5	40.97	147.93	98.304	21.5	54.344	160.212	5.8E-119	1.3E-215	1.5E-24
SLR1_TV_1	-2.198	-232.74	-20.83	14.534	11.755	83.47	-9.923	36.287	2.9E-160	1.6E-24	2.4E-13
SLR1_TV_2	-4.829	-114.7	-28.035	8.932	6.029	146.65	-19.066	35.66	2.4E-156	1.5E-74	7.9E-15

SLR1_TV_3	0.598	1162.78	-19.163	18.644	7.08	88.24	-12.244	28.255	2.2E-125	5.3E-141	4.5E-29
SLR1_TV_4	12.512	59.1	-7.183	41.493	14.55	44.06	-7.958	33.848	1.1E-23	1.1E-199	2.3E-12
SLR1_TV_5	35.867	21.97	15.979	61.873	31.261	19.52	14.446	53.83	1.5E-71	5.0E-152	1.9E-22
SLR1_SV_1	61.553	14.28	39.589	92.055	50.688	16.9	33.812	80.387	1.4E-162	6.3E-138	1.9E-09
SLR1_SV_2	59.915	15.15	34.897	89.559	48.935	16.54	29.436	78.83	2.7E-170	2.3E-141	2.1E-12
SLR1_SV_3	70.411	14.56	46.084	103.861	55.884	17.69	30.9	92.759	5.5E-198	2.1E-147	6.0E-08
SLR1_SV_4	94.249	14.16	56.697	137.943	76.562	16.11	43.26	107.962	2.0E-186	2.2E-145	3.0E-09
SLR1_SV_5	109.52	12.94	71.44	158.18	88.496	15.67	48.477	146.182	6.3E-201	2.4E-136	2.8E-15
SLR2_TV_1	16.301	23.16	-0.527	29.297	22.462	25.58	6.671	37.647	9.1E-120	6.8E-60	4.2E-12
SLR2_TV_2	13.659	32.6	-4.187	24.513	16.972	34.23	-2.007	39.346	3.4E-59	1.3E-124	7.3E-15
SLR2_TV_3	16.816	31.78	1.141	32.103	16.229	29.59	0.156	31.716	7.2E-05	1.4E-188	3.6E-22
SLR2_TV_4	25.083	22.22	7.016	45.902	21.148	24.56	3.133	37.412	8.7E-114	2.5E-221	6.5E-10
SLR2_TV_5	36.316	16.68	6.547	56.392	27.608	23.33	-4.384	46.823	9.6E-213	1.4E-176	1.2E-15
SLR2_SV_1	61.932	13.11	41.601	87.166	48.31	17.62	29.842	74.74	3.3E-240	4.8E-163	4.2E-13
SLR2_SV_2	59.567	12.8	38.446	80.799	44.877	17.17	25.154	68.952	9.3E-274	1.3E-156	2.1E-12
SLR2_SV_3	63.903	12.02	41.65	87.158	45.869	18.56	24.103	75.586	3.9E-288	3.7E-130	4.8E-09
SLR2_SV_4	79.101	12.86	52.112	111.984	58.254	18.33	25.344	86.912	3.7E-270	4.4E-143	1.2E-06
SLR2_SV_5	83.07	11.39	56.176	113.512	57.149	16.03	28.914	96.28	0.0E+00	2.5E-95	1.4E-09
SLR3_TV_1	32.527	4.36	28.025	36.175	35.595	5.13	30.125	39.651	8.0E-194	1.8E-50	1.7E-19
SLR3_TV_2	32.571	4.2	28.17	36.758	35.4	5.08	30.938	39.979	2.5E-200	3.6E-80	2.3E-17
SLR3_TV_3	34.484	5.05	29.568	39.418	36.357	3.29	31.623	39.774	1.0E-176	1.5E-141	1.4E-43
SLR3_TV_4	37.62	4.68	33.13	42.349	38.047	2.95	34.392	41.935	2.7E-23	2.8E-195	1.3E-28
SLR3_TV_5	41.477	6.42	25.169	48.069	39.183	6.79	26.37	45.417	9.2E-83	4.9E-99	1.5E-13
SLR3_SV_1	53.807	6.12	46.528	64.993	49.981	5.95	44.076	62.16	1.8E-132	6.3E-96	2.3E-08
SLR3_SV_2	54.687	6.87	46.125	66.401	51.012	6.35	43.245	62.851	3.1E-124	3.0E-127	1.1E-08
SLR3_SV_3	59.672	6.62	50.127	71.819	55.453	6.94	45.573	69.797	1.6E-137	9.9E-142	5.2E-07
SLR3_SV_4	67.663	6.4	54.21	81.975	63.109	6.4	50.325	74.999	1.1E-132	8.2E-131	3.5E-10
SLR3_SV_5	69.762	6.39	53.512	84.063	65.57	7.82	50.202	86.322	1.4E-93	7.4E-110	5.2E-28
SLR4_SV_1	52.153	11.3	39.555	72.664	47.696	11.5	36.598	72.489	2.9E-65	1.3E-84	4.9E-07

SLR4_SV_2	52.702	12.86	37.031	74.19	48.868	11.73	35.68	71.688	4.6E-53	1.2E-117	3.3E-11
SLR4_SV_3	62.513	12.59	45.152	85.418	57.136	12.14	42.292	84.056	2.3E-84	5.6E-158	1.4E-08
SLR4_SV_4	79.632	11.58	53.275	108.276	72.72	10.71	51.652	94.864	9.9E-95	1.3E-146	1.5E-12
SLR4_SV_5	91.248	11.57	65.3	127.624	84.683	12.66	59.06	130.228	6.6E-72	6.1E-172	1.3E-20
SLR5_TV_1	6.855	54.21	-4.451	19.444	17.189	37.43	2.505	31.736	2.7E-185	4.0E-29	3.0E-15
SLR5_TV_2	6.209	58.72	-6.56	18.476	15.818	37.04	2.366	31.302	9.2E-210	8.9E-63	7.1E-15
SLR5_TV_3	10.208	44.15	-3.422	21.917	18.009	22.33	4.677	30.001	1.8E-239	1.3E-115	1.6E-32
SLR5_TV_4	17.554	27.44	6.304	34.151	22.644	17.07	11.052	33.87	3.9E-181	2.6E-185	1.2E-19
SLR5_TV_5	34.343	16.92	19.557	48.284	35.641	10.72	24.001	49.441	2.3E-17	1.8E-171	3.0E-27
I2_TV_1	0.65387	2.22	0.60056	0.69432	0.60461	6.25	0.48588	0.67908	1.1E-147	1.4E-19	1.4E-10
I2_TV_2	0.65551	2.14	0.59999	0.698	0.6121	5.12	0.49427	0.67028	2.3E-180	6.8E-51	7.6E-15
I2_TV_3	0.63901	2.9	0.58835	0.68837	0.60137	3.65	0.52011	0.66268	1.1E-222	4.9E-95	2.7E-21
I2_TV_4	0.60799	3.89	0.48546	0.65779	0.57452	4.38	0.48904	0.63572	3.3E-203	1.8E-170	8.3E-11
I2_TV_5	0.48097	17.96	0.21638	0.60478	0.42984	18.4	0.22184	0.56759	1.3E-95	6.7E-233	2.0E-19
GMR_SV_1	10.654	10.22	7.207	13.896	12.536	11.64	8.017	16.214	2.1E-190	1.5E-132	2.1E-08
GMR_SV_2	10.99	9.63	8.08	14.297	13.021	10.53	8.749	17.373	9.8E-223	1.1E-137	2.0E-09
GMR_SV_3	10.06	12.34	5.915	13.555	12.228	12.87	6.944	17.241	1.9E-203	1.6E-138	1.9E-06
GMR_SV_4	6.9279	31.01	-0.9259	11.8346	8.8123	24.72	0.4552	14.576	9.9E-107	3.5E-153	1.1E-08
GMR_SV_5	-0.201	-3561.61	-23.338	9.609	0.996	738.23	-26.658	11.696	5.6E-10	2.3E-222	3.9E-17
G/R_SV_1	1.1169	1.11	1.0744	1.1469	1.1224	1.37	1.0616	1.1565	5.6E-18	9.8E-66	3.6E-06
G/R_SV_2	1.1177	1.21	1.0759	1.1541	1.121	1.28	1.0651	1.1588	2.5E-09	1.2E-101	8.9E-11
G/R_SV_3	1.0973	1.48	1.0504	1.1351	1.1022	1.34	1.0526	1.1354	8.3E-22	2.6E-167	5.3E-09
G/R_SV_4	1.061	1.98	0.9935	1.1132	1.0673	1.63	1.0031	1.1105	2.0E-22	1.3E-158	3.8E-15
G/R_SV_5	1.0056	4.43	0.8859	1.0857	1.0105	3.89	0.8787	1.0766	1.4E-05	4.5E-214	7.9E-22
G/B_TV_1	1.5912	2.07	1.5038	1.7278	1.6833	3.91	1.5421	1.8695	6.7E-161	3.6E-31	9.5E-10
G/B_TV_2	1.5698	2.1	1.4821	1.6831	1.6549	3.16	1.5267	1.8036	2.1E-205	8.4E-64	1.1E-10
G/B_TV_3	1.5613	1.91	1.4795	1.6431	1.6502	2.54	1.5414	1.7753	5.3E-271	1.2E-76	1.6E-12
G/B_TV_4	1.5648	2.18	1.4723	1.702	1.6553	2.53	1.5396	1.83	1.3E-286	1.2E-108	1.7E-08
G/B_TV_5	1.6459	4.43	1.518	1.9188	1.7416	3.14	1.5704	1.947	7.6E-202	4.3E-126	5.0E-40

AGR1	13328	16.48	5177	19460	10382	27.65	3960	19615	1.3E-92	3.6E-32	8.2E-13
AGR2	26252	36.87	4621	51970	17539	39.92	3201	42893	4.7E-131	2.6E-128	3.2E-38
AGR3	9232	76.64	-18262	42176	8973	49.53	-4703	25724	2.3E-01	2.5E-115	1.7E-19
AGR4	-1929	-302.14	-19943	14304	-2503	-185.09	-19477	12262	1.3E-03	8.9E-139	2.5E-20
AGR5	-13141	-60.12	-43398	10592	-11918	-66.74	-55232	-206	4.6E-05	2.8E-109	7.5E-13
RGR1	0.028633	37.79	0.005616	0.078435	0.024743	31.98	0.006112	0.048253	2.0E-31	2.0E-142	7.6E-19
RGR2	0.008836	78.13	-0.014953	0.044132	0.01137	46.04	-0.004632	0.026913	1.3E-24	4.8E-100	4.5E-11
RGR3	-0.001997	-273.19	-0.019583	0.013655	-0.00262	-201.43	-0.019714	0.015325	1.0E-03	2.6E-130	1.5E-13
RGR4	-0.013768	-69.9	-0.055814	0.010857	-0.015513	-61.04	-0.051912	-0.000242	4.4E-09	4.8E-176	2.6E-07
AWU_Diurnal	124.79	16.55	11.54	196.15	109.21	17.87	57.96	175.38	3.4E-58	8.8E-53	7.0E-23
AWU_Day	102.84	16.93	8.46	169.23	89.862	17.39	47.13	146.154	2.6E-57	9.7E-47	6.4E-22
AWU_Night	21.952	20.46	3.077	35.385	19.352	24.33	10	42.308	2.2E-36	1.3E-74	2.9E-11
PSA_TUE_Diurnal	6930	36.22	2318	53052	5975.8	22.9	2587.4	13244.5	9.6E-18	2.8E-19	7.2E-03
PSA_TR_Diurnal	0.000154	25.25	0.000019	0.000431	0.000177	24.99	0.000076	0.000386	1.8E-30	8.3E-49	4.0E-12
PSA_TUE_Day	8430	39.56	2906	72344	7256.5	22.79	3184.5	16006.1	2.3E-15	2.3E-14	2.2E-02
PSA_TR_Day	0.000127	25.6	0.000014	0.000344	0.000146	25.01	0.000062	0.000314	1.9E-29	3.4E-47	3.2E-12
PSA_TUE_Night	39902	31.52	11458	198945	34539	27.53	13800	76764	1.3E-24	4.5E-62	2.6E-04
PSA_TR_Night	0.000027	28.04	0.000005	0.000087	0.000031	28.78	0.000013	0.000072	2.0E-26	4.2E-56	3.5E-07
Foliage_TUE_Diurnal	0.09163	38.46	0.05028	0.78433	0.077276	23.81	0.033719	0.171832	1.1E-20	6.2E-24	1.3E-01
Foliage_TR_Diurnal	11.501	20.5	1.275	19.887	13.691	24.72	5.82	29.657	9.1E-67	9.8E-101	1.9E-10
Foliage_TUE_Day	0.1114	42.28	0.0589	1.06955	0.093795	23.46	0.0415	0.201802	1.9E-17	5.9E-17	2.1E-01
Foliage_TR_Day	9.4705	20.4	0.935	16.9794	11.269	24.63	4.955	24.096	4.2E-64	1.6E-92	2.4E-10
Foliage_TUE_Night	0.52933	32.67	0.24669	2.94125	0.44755	29.18	0.17983	1.157	4.1E-32	2.4E-78	7.6E-03
Foliage_TR_Day_1	2.0303	25.71	0.34	4.0537	2.4228	28.97	0.8643	5.5607	1.3E-52	1.7E-111	4.9E-05

ANNEXURE 5: Descriptive statistics and ANOVA of manual and semi-manual traits

	Control				Nitrogen				ANOVA_P-value		
Traits	Mean	CV	Min	Max	Mean	CV	Min	Max	Treatment	Genotype	G×E
Straw	11.122	18.66	5.89	17.77	8.407	27.73	3.36	16.49	3.59E-120	4.44E-60	2.72E-21
Total_Biomass	31.25	16.03	18.18	45.92	22.856	24.03	10.16	39.32	1.86E-153	6.53E-34	1.10E-24
TotalEar	8.8619	21.32	5	16	6.4971	22.99	3	11	3.04E-143	3.09E-63	4.05E-23
HI	0.47953	7.69	0.34792	0.59187	0.47647	7.81	0.36977	0.61232	7.53E-03	8.19E-167	3.89E-25
FLL	26.849	14.7	14.6	37.7	22.166	18.29	13.8	34.5	5.09E-99	4.75E-49	1.34E-06
FLW	1.8586	7.17	1.4	2.25	1.6774	9.47	1.2	2.1	2.23E-115	6.15E-63	1.61E-07
FLtoEar	11.2	43.39	0.6	24.5	11.479	47.73	0.3	27	2.08E-03	0.00E+00	5.98E-11
FLLWratio	14.462	13.76	7.684	20.286	13.211	15.58	8.353	21	2.39E-40	4.54E-73	1.88E-04
FLLtoEarRatio	2.3437	16.45	1.3971	3.6957	2.0559	17.81	1.1933	3.2292	5.52E-59	4.45E-76	1.77E-05
LNP	33.784	19.27	17	57.5	28.07	23.18	12	52.5	7.68E-66	1.84E-48	9.66E-12
TNP	8.9543	20.23	4	16	7.1852	25.68	3	14	8.88E-75	2.14E-45	5.11E-10
PH	73.873	16.73	40.5	104.5	73.43	17.92	38	106	2.43E-02	0.00E+00	8.94E-10
SPAD1	50.073	5.45	41.8	59.6	44.294	8.01	31.7	58.4	7.26E-180	1.07E-52	3.30E-06
SPAD2	49.397	7.74	34.5	58.8	42.824	10.74	23.6	59.5	3.19E-164	3.26E-78	5.07E-06
Phy3	12.687	15.24	8	20	12.682	12.93	10	18	9.20E-01	3.51E-208	1.62E-54
Phy4	8.2343	18.5	3	13	8.2762	16.72	4	11	2.91E-01	1.43E-191	4.07E-64
Phy5	4.9895	22.51	2	9	5.22	24.78	2	10	9.08E-23	6.81E-289	#######
DTG	9.8381	6.2	9	11	9.6619	5.94	9	11	3.86E-13	1.27E-87	1.76E-12
DTB	67.467	3.56	62	74	68.975	3.74	62	74	7.02E-78	2.54E-198	2.21E-12
DTA	76.674	3.62	71	82	77.519	3.7	71	82	9.83E-37	2.24E-272	3.83E-20
LC_SPAD1ratio	0.67631	19.66	0.34694	1.17325	0.63395	21.94	0.26316	1.14379	2.35E-11	4.38E-50	5.92E-10
LC_SPAD2ratio	0.68891	21.47	0.34836	1.23557	0.66722	29.37	0.26432	1.97034	4.92E-03	3.71E-60	1.30E-10
TC_SPAD1ratio	0.1793	20.82	0.08584	0.31765	0.16219	24.36	0.07143	0.30501	7.72E-21	1.06E-49	4.81E-09
TC_SPAD2ratio	0.18245	22.07	0.08507	0.33126	0.17021	29.82	0.06961	0.4661	8.95E-09	4.13E-50	1.35E-09
LER	8.6368	5.59	7	10.3333	8.726	4.98	7.6667	10.6667	8.60E-13	4.02E-196	2.30E-71

LER_DTBratio	7.834	6.19	6.5172	9.5714	7.9223	5.83	6.3	9.25	1.50E-11	3.28E-198	2.19E-51
LER_DTAratio	8.9046	6.48	7.4483	11	8.9047	6.03	7.1	10.1739	9.91E-01	3.34E-229	1.32E-61
SPADatio	0.98781	7.51	0.63536	1.37063	0.97041	11.06	0.50753	1.47003	1.15E-04	1.60E-44	2.14E-02
LPTveg	3.8039	10.04	2.7391	5.1	3.9581	11.22	2.7895	5.8333	1.25E-14	1.95E-51	5.22E-02
SPAD1total	1883.2	19.8	860.4	3262.3	1255.9	28.68	512.6	2478.8	3.93E-162	2.82E-43	9.57E-09
SPAD2total	1858.1	20.6	759.6	3274.4	1207.3	27.74	477.1	2805.9	2.09E-182	3.95E-56	7.37E-09
FLA	37.576	18.53	18	60.75	28.144	24.54	13.95	51.75	1.21E-119	4.33E-43	1.57E-07
PH_FLLratio	2.8025	20.92	1.4286	5.0904	3.4072	23.81	1.6441	5.9722	1.65E-89	6.11E-121	2.35E-09
SpikeLength	11.531	8.99	8.6	14.4	10.818	9.29	7.5	13.9	1.21E-79	3.26E-161	5.86E-07
SpikeletNo	19.977	8.72	16	24.5	20.166	8.24	16.5	24.5	1.58E-08	0.00E+00	1.07E-04
SSN	3.4576	52.17	0	9	2.8362	41.59	0.5	8.5	5.88E-26	4.30E-115	4.33E-11
GPS	2.6018	12.33	1.4419	3.7568	2.4419	13.35	1.3429	3.4324	7.28E-30	2.24E-86	5.88E-05
SpikeletDensity	1.8151	11.12	1.3834	3.1343	1.9546	10.66	1.4583	3.6154	2.29E-65	2.19E-132	1.33E-04
SFP	82.99	9.82	57.143	100	86.072	6.13	62.5	97.297	2.63E-27	9.23E-94	1.16E-11
SFI	77.641	13.78	32.704	109.649	82.362	13.91	30.882	121.25	5.89E-29	5.63E-122	2.94E-10
SpikeWt_ME	5.9709	12.81	3.7	8.19	5.4351	14.73	3.34	7.97	3.62E-55	2.87E-94	2.46E-09
SpikeWt_TE	14.158	22.77	6.84	24.03	9.004	32.95	2.53	16.97	1.95E-166	7.76E-39	3.88E-28
SpikeWt_AE	20.129	16.87	12.09	30.29	14.44	23.4	6.77	22.83	1.24E-165	5.24E-36	1.10E-26
GrainWt_ME	4.6225	14.16	2.59	6.55	4.2259	15.33	2.39	6.2	3.39E-47	2.04E-101	9.04E-09
GrainWt_TE	10.363	23.89	4.75	18.12	6.6319	33.74	1.52	12.72	4.12E-157	1.72E-38	1.10E-29
GrainWt_AE	14.986	17.83	8.53	23.03	10.858	23.75	5.13	17	4.50E-155	2.29E-38	2.33E-28
ChaffWt_ME	1.3484	13.28	0.86	1.89	1.2092	17.26	0.71	2.34	4.05E-57	5.24E-87	4.21E-09
ChaffWt_TE	3.7942	27.66	1.34	7.85	2.3725	39.23	0.35	5.03	1.64E-155	3.67E-73	3.57E-24
ChaffWt_AE	5.1426	20.98	2.61	9.55	3.5817	28.32	1.33	6.48	3.22E-160	6.58E-70	2.79E-22
TotalGrainNo_ME	103.54	12.06	52	139	98.196	13.5	47	130	1.96E-21	1.05E-79	1.99E-06
TotalGrainNo_TE	267.61	25.92	104	500	171.41	33.43	39	377	3.01E-171	1.16E-75	6.73E-32
TotalGrainNo_AE	371.16	19.75	172	608	269.61	23.6	116	490	6.86E-167	3.89E-77	2.86E-30
GPB_ME	15.095	19.03	7.946	25.618	19.258	21.38	11.213	35.382	1.69E-101	8.72E-50	1.42E-09
GPB_TE	32.858	11.76	22.045	44.91	28.413	15.6	11.008	38.142	1.23E-102	5.08E-75	4.22E-16

GPB_AE	47.953	7.69	34.792	59.187	47.671	7.73	36.977	61.232	1.24E-02	1.04E-169	3.92E-25
AGPB_ME	7.5474	19.03	3.9729	12.809	9.6288	21.38	5.6067	17.6912	1.69E-101	8.72E-50	1.42E-09
AGPB_TE	5.0657	22.86	2.5677	9.8255	6.7978	24.64	3.5743	13.4584	4.42E-101	5.72E-43	1.35E-08
AGPB_AE	5.6604	23.12	2.9148	10.5601	7.7467	25.34	4.1199	15.4634	3.46E-109	1.08E-46	4.26E-09
CPB_ME	4.4113	19.12	2.7404	6.8677	5.5038	22.14	3.1284	10.5642	1.74E-89	3.64E-55	6.72E-14
CPB_TE	12.054	19.88	5.574	22.032	10.207	25.99	2.159	19.227	1.28E-73	1.20E-120	3.41E-24
CPB_AE	16.465	14.38	10.047	26.803	15.711	16.44	8.534	24.639	1.26E-18	4.13E-140	2.26E-23
ACPB_ME	2.2056	19.12	1.3702	3.4338	2.7519	22.14	1.5642	5.2821	1.74E-89	3.64E-55	6.72E-14
ACPB_TE	1.8645	30.53	0.7787	5.3528	2.4973	41.8	0.5397	7.2909	4.16E-55	7.34E-58	2.34E-16
ACPB_AE	1.9403	25.87	0.8699	4.5547	2.558	30.84	1.2741	5.4563	9.27E-77	9.65E-58	4.93E-14
AvgSpikeWt_ME	2.9855	12.81	1.85	4.095	2.7176	14.73	1.67	3.985	3.62E-55	2.87E-94	2.46E-09
AvgSpikeWt_TE	2.122	18.22	1.1789	3.94	2.0348	19.44	1.1017	4.4967	2.51E-07	1.51E-74	1.71E-07
AvgSpikeWt_AE	2.3225	16.89	1.3009	3.7933	2.2487	17.04	1.2913	3.752	2.54E-06	7.50E-95	1.08E-06
AvgGrainWt_ME	2.3112	14.16	1.295	3.275	2.113	15.33	1.195	3.1	3.39E-47	2.04E-101	9.04E-09
AvgGrainWt_TE	1.5521	19.24	0.7456	2.8575	1.4924	20.03	0.7267	3.4067	6.77E-06	1.34E-66	6.80E-07
AvgGrainWt_AE	1.7299	18.06	0.8455	2.7867	1.6908	17.73	0.9	2.892	1.62E-03	7.17E-94	1.99E-06
AvgChaffWt_ME	0.67422	13.28	0.43	0.945	0.6046	17.26	0.355	1.17	4.05E-57	5.24E-87	4.21E-09
AvgChaffWt_TE	0.56987	25.71	0.24571	1.30833	0.54237	32.54	0.1075	1.195	4.58E-06	4.01E-112	3.23E-21
AvgChaffWt_AE	0.59267	20.75	0.30333	1.19375	0.55787	23.27	0.26286	0.97	1.10E-13	4.52E-119	3.38E-16
GWCWratio_ME	3.4541	13.19	1.6792	4.9688	3.5338	12.63	1.7692	4.7	2.64E-07	3.45E-145	1.76E-07
GWCWratio_TE	2.8511	25.95	1.1688	6.1163	3.0477	42.48	0.8686	15.093	6.49E-08	9.44E-120	4.03E-48
GWCWratio_AE	2.9889	19.53	1.424	5.0728	3.1411	22.76	1.5586	6.5412	2.89E-13	2.49E-155	2.26E-38
PHI_ME	0.77302	3.18	0.62676	0.83246	0.77714	3.06	0.63889	0.82456	4.36E-06	2.25E-122	1.29E-05
PHI_TE	0.73156	6.53	0.53891	0.85948	0.73515	8.66	0.46483	0.93786	7.03E-02	1.14E-119	1.10E-31
PHI_AE	0.7441	4.92	0.58747	0.83533	0.75194	5.24	0.60916	0.86739	8.08E-10	2.30E-142	9.26E-29
TKW_ME	44.841	11.82	25.827	64.198	43.165	10.36	28.868	58.763	2.99E-24	4.78E-157	1.45E-13
TKW_TE	39.361	14	21.115	58.786	38.828	11.92	23.256	62.627	9.46E-04	7.60E-166	3.58E-11
TKW_AE	40.897	12.94	22.444	58.655	40.473	10.73	26.347	56.276	1.37E-03	1.58E-210	1.87E-16
AvgGrainNo_ME	51.772	12.06	26	69.5	49.098	13.5	23.5	65	1.96E-21	1.05E-79	1.99E-06

AvgGrainNo_TE	39.58	15.12	13.222	59.25	38.461	16.47	19.167	89.333	8.41E-05	2.68E-57	1.31E-04
AvgGrainNo_AE	42.392	13.82	18.818	59.25	41.81	14.57	20.25	74.2	2.46E-02	6.54E-76	1.00E-03
SeedArea_TE	18.097	7.52	14.419	22.297	17.691	6.76	14.437	20.963	1.59E-24	9.66E-182	2.85E-16
SeedArea_ME	19.923	6.96	16.126	24.2	19.454	6.71	16.54	23.172	7.87E-22	5.97E-137	1.72E-05
SeedArea_AE	19.01	6.83	15.561	23.049	18.573	6.33	15.745	21.971	5.55E-32	9.86E-197	4.95E-14
SeedArea_Low_TE	13.43	13.54	7.763	19.39	13.969	11.53	9.252	18.463	4.98E-20	4.88E-152	7.37E-09
SeedArea_Low_ME	14.603	14.33	5.498	21.707	14.528	14.09	7.736	19.609	4.25E-01	1.17E-61	1.58E-03
SeedArea_Low_AE	14.016	12.08	8.713	20.131	14.248	11.18	9.654	18.802	8.66E-05	2.26E-131	4.66E-06
SeedArea_Top_TE	21.595	6.52	17.98	25.382	20.519	6.59	16.537	23.713	2.93E-90	3.54E-144	2.78E-22
SeedArea_Top_ME	23.213	6.5	18.833	27.781	22.597	6.47	18.995	26.757	2.33E-30	3.75E-142	2.31E-05
SeedArea_Top_AE	22.404	6.15	18.912	26.257	21.558	6.15	17.869	25.002	7.72E-74	3.19E-175	1.90E-16
SeedPerimeter_TE	21.633	3.83	19.872	24.129	21.254	3.73	19.189	23.436	9.69E-59	1.18E-222	9.96E-15
SeedPerimeter_ME	22.292	3.81	19.816	25.003	21.962	3.73	19.804	24.475	1.12E-31	1.67E-165	1.41E-03
SeedPerimeter_AE	21.962	3.64	19.854	24.566	21.608	3.53	19.497	23.443	2.36E-60	3.04E-238	2.37E-11
SeedPerimeter_Low_TE	19.053	6.05	15.926	22.648	19.209	5.64	14.797	22.462	2.86E-05	7.33E-152	1.13E-09
SeedPerimeter_Low_ME	19.337	7.91	11.836	23.825	19.305	7.62	14.004	29.667	6.59E-01	1.84E-44	8.85E-04
SeedPerimeter_Low_AE	19.195	5.95	15.673	23.004	19.257	5.64	16.002	24.384	1.44E-01	3.60E-113	1.34E-04
SeedPerimeter_Top_TE	23.181	3.65	20.955	25.55	22.619	3.72	20.182	24.872	7.26E-82	1.02E-176	2.30E-16
SeedPerimeter_Top_ME	23.844	4.28	20.709	31.039	23.465	4.2	20.93	28.617	2.86E-21	3.22E-108	4.73E-05
SeedPerimeter_Top_AE	23.513	3.62	21.154	26.7	23.042	3.68	20.807	25.829	6.13E-61	3.25E-177	1.17E-12
SeedLength_TE	7.1878	4.2	6.4123	8.1659	7.0549	4.2	6.2838	7.9263	4.96E-69	9.21E-270	1.84E-14
SeedLength_ME	7.4197	4.48	6.5268	8.4877	7.2887	4.29	6.4368	8.3311	1.33E-38	6.78E-192	5.42E-05
SeedLength_AE	7.3037	4.18	6.5364	8.2388	7.1718	4.07	6.3603	8.0222	5.89E-69	3.23E-272	1.99E-12
SeedLength_Low_TE	6.4419	5.84	5.1312	7.6899	6.4663	5.74	4.383	7.511	5.07E-02	1.59E-149	1.24E-08
SeedLength_Low_ME	6.4784	10.07	3.0884	8.2523	6.4265	8.85	3.6365	7.6477	8.18E-02	1.13E-41	4.28E-04
SeedLength_Low_AE	6.4601	6.69	4.9299	7.7808	6.4464	6.04	4.9636	7.4844	4.04E-01	2.26E-97	2.88E-05
SeedLength_Top_TE	7.5446	4.16	6.786	8.4787	7.4091	4.07	6.5582	8.2709	1.67E-54	9.99E-227	7.49E-14
SeedLength_Top_ME	7.8021	4.38	6.6449	8.7838	7.6782	4.39	6.4903	8.9997	1.53E-31	4.62E-187	5.10E-07
SeedLength_Top_AE	7.6733	4.07	6.7945	8.5511	7.5437	4.06	6.5242	8.614	2.15E-55	2.32E-245	1.38E-13

SeedWidth_TE	3.2062	5.5	2.4819	3.7164	3.1926	4.74	2.6213	3.646	7.90E-03	1.96E-170	3.30E-15
SeedWidth_ME	3.4155	4.85	2.7841	3.8589	3.3958	4.65	2.8165	3.8708	3.69E-04	2.07E-145	3.39E-06
SeedWidth_AE	3.3108	4.87	2.6723	3.7877	3.2942	4.42	2.7189	3.7584	1.66E-04	8.75E-196	1.53E-14
SeedWidth_Low_TE	2.6586	9.56	1.7722	3.3879	2.752	7.85	2.1503	3.3886	3.80E-31	7.27E-159	1.61E-08
SeedWidth_Low_ME	2.8749	8.28	2.1005	3.5158	2.8796	8.49	2.0487	3.5065	6.13E-01	3.07E-106	5.75E-03
SeedWidth_Low_AE	2.7667	8.08	2.1311	3.4456	2.8158	7.49	2.1466	3.3975	7.78E-13	2.16E-174	2.58E-07
SeedWidth_Top_TE	3.6575	4.37	3.025	4.0371	3.5381	4.41	2.9841	3.9498	1.59E-74	5.66E-116	3.43E-18
SeedWidth_Top_ME	3.7985	4.38	3.1722	4.2056	3.7578	4.33	3.2514	4.1417	2.68E-10	4.06E-108	9.85E-06
SeedWidth_Top_AE	3.728	4.03	3.0986	4.0929	3.648	4	3.1391	4.039	1.01E-48	7.08E-142	3.11E-13
SeedLWR_TE	2.2479	6.4	1.855	2.9749	2.2141	5.89	1.8608	2.778	7.63E-22	1.22E-241	3.24E-13
SeedLWR_ME	2.177	6.29	1.7865	2.7383	2.1506	5.94	1.8031	2.6709	4.68E-13	3.58E-216	3.14E-06
SeedLWR_AE	2.2124	6.11	1.8208	2.8372	2.1824	5.7	1.8385	2.7245	3.89E-23	2.68E-270	3.14E-13
SeedLWR_Low_TE	2.439	8.49	1.9439	3.2095	2.3599	7.54	1.5825	2.9299	6.95E-32	6.02E-154	1.12E-06
SeedLWR_Low_ME	2.2652	11.45	1.1706	2.9624	2.2431	10.21	1.1882	3.0145	3.63E-02	4.65E-75	1.92E-05
SeedLWR_Low_AE	2.3521	8.57	1.6748	3.0373	2.3015	7.8	1.679	2.9278	1.80E-14	4.67E-147	5.95E-07
SeedLWR_Top_TE	2.0663	5.68	1.7655	2.6327	2.0975	5.41	1.8064	2.5683	2.89E-18	1.70E-182	1.18E-07
SeedLWR_Top_ME	2.0577	5.99	1.7084	2.5999	2.0469	5.94	1.6913	2.5176	1.01E-02	3.96E-143	4.29E-07
SeedLWR_Top_AE	2.062	5.42	1.7511	2.6163	2.0722	5.29	1.7844	2.5033	1.19E-03	4.97E-202	2.18E-08

ANNEXURE 6: Variance components and genetic parameters of HTP traits

	Control					Nitrogen				
Parameters	**Gen_var**	**Res_var**	**Phen_var**	**h2mg**	**CVg**	**Gen_var**	**Res_var**	**Phen_var**	**h2mg**	**CVg**
Biovolume_1	2.47628E+14	3.4103E+14	5.88658E+14	0.69	16.48	3.62018E+14	4.48368E+14	8.10386E+14	0.71	28.82
Biovolume_2	4.32683E+14	5.03507E+14	9.36191E+14	0.72	15.70	6.10067E+14	7.6558E+14	1.37565E+15	0.71	27.90
Biovolume_3	5.0359E+14	4.88905E+14	9.92495E+14	0.76	15.25	6.8788E+14	9.17842E+14	1.60572E+15	0.69	25.68
Biovolume_4	7.56682E+14	4.63594E+14	1.22028E+15	0.83	19.34	6.05342E+14	7.41041E+14	1.34638E+15	0.71	25.46
Biovolume_5	1.42281E+15	2.73544E+14	1.69636E+15	0.94	35.42	5.95759E+14	2.97296E+14	8.93055E+14	0.86	36.18
PSA_1	7773915837	11773686610	19547602447	0.66	10.55	13384231803	20194517951	33578749754	0.67	17.73
PSA_2	10933331439	14140151059	25073482498	0.70	10.10	19224535211	28075196168	47299731380	0.67	17.61
PSA_3	12527871858	12835811591	25363683450	0.75	10.07	20475712045	30712376908	51188088953	0.67	16.63
PSA_4	18718271943	12022565258	30740837201	0.82	12.54	19033156806	25408555228	44441712034	0.69	16.57
PSA_5	29831468840	7678278252	37509747092	0.92	18.24	17334690677	13801323658	31136014334	0.79	18.76
2MPASA_TV_1	3.05586E+18	3.20613E+18	6.26199E+18	0.74	29.30	2.43733E+18	2.49899E+18	4.93633E+18	0.75	48.60
2MPASA_TV_2	6.05098E+18	5.53405E+18	1.1585E+19	0.77	26.44	4.90874E+18	5.46264E+18	1.03714E+19	0.73	43.57
2MPASA_TV_3	5.00059E+18	6.23935E+18	1.12399E+19	0.71	21.85	6.41798E+18	8.29825E+18	1.47162E+19	0.70	37.46
2MPASA_TV_4	8.31457E+18	7.5484E+18	1.5863E+19	0.77	29.01	5.7835E+18	7.637E+18	1.34205E+19	0.69	36.99
2MPASA_TV_5	9.82587E+18	4.62916E+18	1.4455E+19	0.86	59.66	3.27443E+18	1.69359E+18	4.96802E+18	0.85	63.86
2MPASN_TV_1	0.000227065	0.000553725	0.000780789	0.55	10.22	0.000114326	0.000533503	0.000647829	0.39	7.43
2MPASN_TV_2	0.000156893	0.000366457	0.00052335	0.56	8.95	0.000206478	0.000543822	0.0007503	0.53	10.10
2MPASN_TV_3	0.000106082	0.000370516	0.000476598	0.46	7.73	0.000140003	0.000611033	0.000751036	0.41	8.42
2MPASN_TV_4	0.000181433	0.000496965	0.000678398	0.52	9.27	5.55E-05	0.000804697	0.000860161	0.17	4.94
2MPASN_TV_5	0.01115012	0.013350581	0.024500701	0.71	54.88	0.025305198	0.039037151	0.064342349	0.66	75.97
Area_TV_1	902713942.5	1034949613	1937663556	0.72	15.12	1259221376	1510661255	2769882631	0.71	24.95
Area_TV_2	1134972979	1163431060	2298404039	0.75	13.19	1766045937	2256401699	4022447636	0.70	23.05
Area_TV_3	976185381.6	974374057.7	1950559439	0.75	11.35	1824662525	2637871080	4462533605	0.67	20.09
Area_TV_4	1883098606	982439273.5	2865537879	0.85	16.77	1589739335	1892613572	3482352907	0.72	19.77
Area_TV_5	5197001905	663020610.1	5860022515	0.96	42.33	2530608559	602900305.3	3133508864	0.93	40.82

BPC_TV_1	10298652.3	11906930.43	22205582.72	0.72	12.53	9532883.682	17442072.68	26974956.36	0.62	17.36
BPC_TV_2	14643238.09	9950408.297	24593646.39	0.82	13.17	9622962.593	18781754.94	28404717.53	0.61	15.70
BPC_TV_3	16456940.05	7997915.818	24454855.86	0.86	14.14	8208046.344	15572626.72	23780673.06	0.61	13.92
BPC_TV_4	22738985.15	11494538.46	34233523.61	0.86	15.75	8273870.98	11046973.23	19320844.21	0.69	14.43
BPC_TV_5	61266097.71	12260610.98	73526708.69	0.94	33.27	12797571.58	6247442.21	19045013.79	0.86	25.84
BPR_TV_1	555606.0075	245356.9701	800962.9776	0.87	21.99	153487.9496	263503.4775	416991.4272	0.64	17.25
BPR_TV_2	652489.123	186236.3424	838725.4654	0.91	23.86	120287.868	215231.9623	335519.8302	0.63	15.84
BPR_TV_3	736715.9096	185493.0158	922208.9254	0.92	27.90	102131.3018	141315.987	243447.2888	0.68	15.65
BPR_TV_4	859585.9383	333840.4338	1193426.372	0.89	25.47	88694.21646	131182.0154	219876.2319	0.67	14.78
BPR_TV_5	1183928.654	446148.3574	1630077.012	0.89	31.45	248926.4441	184645.8243	433572.2684	0.80	29.21
BPAR_TV_1	0.000345996	0.000122247	0.000468243	0.89	14.10	0.000178026	0.000166682	0.000344708	0.76	10.27
BPAR_TV_2	0.000261422	8.91E-05	0.000350559	0.90	13.98	0.000158028	0.000164649	0.000322677	0.74	11.14
BPAR_TV_3	0.000253021	8.50E-05	0.000338053	0.90	15.06	0.000126896	0.000149026	0.000275922	0.72	11.18
BPAR_TV_4	0.000304227	0.000110436	0.000414662	0.89	14.65	0.000106475	0.000165668	0.000272143	0.66	10.09
BPAR_TV_5	0.003049029	0.00123012	0.004279149	0.88	34.49	0.004357434	0.001769329	0.006126764	0.88	47.79
Compactness_TV_1	0.000597309	0.000694134	0.001291443	0.72	11.43	0.000442656	0.000695848	0.001138504	0.66	11.01
Compactness_TV_2	0.001006571	0.000776276	0.001782847	0.80	12.15	0.001019624	0.000757877	0.001777501	0.80	13.27
Compactness_TV_3	0.000642585	0.001006054	0.001648639	0.66	8.98	0.000612504	0.000948439	0.001560943	0.66	9.88
Compactness_TV_4	0.000723146	0.000819145	0.001542291	0.73	10.03	0.000466509	0.000970253	0.001436762	0.59	9.10
Compactness_TV_5	0.004076135	0.001477462	0.005553597	0.89	26.35	0.002766946	0.001782998	0.004549944	0.82	23.45
CHArea_TV_1	10516918042	13674882312	24191800354	0.70	11.01	13964306494	24654763684	38619070178	0.63	16.18
CHArea_TV_2	15900775612	11142081549	27042857160	0.81	12.78	18343767628	30142972544	48486740172	0.65	17.92
CHArea_TV_3	10385223861	13913050404	24298274265	0.69	10.35	18209869242	31639936245	49849805488	0.63	15.96
CHArea_TV_4	20439631361	15832370403	36272001764	0.79	14.69	18319249628	21896972715	40216222343	0.72	16.00
CHArea_TV_5	44568940071	19643138796	64212078867	0.87	30.83	37207304208	15650889862	52858194071	0.88	35.32
ObjectExtentY_TV_1	8310.222334	13288.0753	21598.29763	0.65	8.65	9822.626798	23014.19575	32836.82255	0.56	11.18
ObjectExtentY_TV_2	7393.34741	13392.99919	20786.3466	0.62	7.43	11234.63423	25843.92805	37078.56228	0.57	10.58
ObjectExtentY_TV_3	3246.363343	15491.11071	18737.47405	0.39	4.86	8787.329977	21561.01097	30348.34095	0.55	8.68
ObjectExtentY_TV_4	8642.114734	15804.67208	24446.78682	0.62	8.06	8275.041819	17800.59243	26075.63425	0.58	8.46

ObjectExtentY_TV_5	25020.35137	26533.20935	51553.56071	0.74	16.19	28261.49047	21581.644	49843.13447	0.80	19.10
MARA_TV_1	13010081626	22044480228	35054561854	0.64	9.09	18529907506	36901150847	55431058353	0.60	13.21
MARA_TV_2	26571457841	21414285808	47985743649	0.79	12.94	31635785723	49465515283	81101301006	0.66	18.05
MARA_TV_3	16727129838	26516406740	43243536579	0.65	10.32	29100184809	52833226726	81933411535	0.62	15.73
MARA_TV_4	33065516677	28499645707	61565162384	0.78	14.70	29273481023	35951277531	65224758555	0.71	15.84
MARA_TV_5	75822506642	35051135378	1.10874E+11	0.87	30.85	59812782860	29385566559	89198349419	0.86	34.20
AZR2M_TV_1	1.57897E+19	1.9286E+19	3.50757E+19	0.71	26.31	1.43038E+19	1.40418E+19	2.83456E+19	0.75	45.73
AZR2M_TV_2	3.07417E+19	2.71E+19	5.78334E+19	0.77	23.83	2.84346E+19	3.05331E+19	5.89678E+19	0.74	40.59
AZR2M_TV_3	2.87538E+19	2.74E+19	5.61549E+19	0.76	20.66	3.83732E+19	4.56379E+19	8.40111E+19	0.72	34.91
AZR2M_TV_4	5.09712E+19	3.87493E+19	8.97205E+19	0.80	27.52	3.65808E+19	3.77313E+19	7.43121E+19	0.74	34.89
AZR2M_TV_5	6.45713E+19	2.97375E+19	9.43088E+19	0.87	55.13	2.42821E+19	9.70229E+18	3.39844E+19	0.88	60.62
NZR2M_TV_1	0.002581635	0.001713246	0.004294881	0.82	13.46	0.001305623	0.002390657	0.00369628	0.62	9.44
NZR2M_TV_2	0.00113974	0.001443464	0.002583204	0.70	9.54	0.00145733	0.002191697	0.003649028	0.67	10.15
NZR2M_TV_3	0.000690115	0.001214872	0.001904987	0.63	7.72	0.001048944	0.002446501	0.003495445	0.56	8.56
NZR2M_TV_4	0.003032002	0.003564798	0.0065968	0.72	14.31	0.001291436	0.002746991	0.004038427	0.59	8.69
NZR2M_TV_5	0.827331431	8.252800851	9.080132282	0.23	112.24	1.50658688	1.872864421	3.379451301	0.71	157.57
2MPALA_SV_1	4.13157E+19	1.30044E+19	5.43201E+19	0.91	34.99	3.83097E+19	2.34159E+19	6.17256E+19	0.83	43.30
2MPALA_SV_2	1.15E+20	2.78547E+19	1.43E+20	0.93	35.40	1.09E+20	5.35424E+19	1.62E+20	0.86	45.55
2MPALA_SV_3	2.39E+20	4.49003E+19	2.84E+20	0.94	36.22	2.22E+20	1.03E+20	3.25E+20	0.87	45.41
2MPALA_SV_4	2.74E+20	3.86203E+19	3.13E+20	0.96	34.64	2.47E+20	8.87723E+19	3.35E+20	0.89	42.82
2MPALA_SV_5	2.63E+20	3.29773E+19	2.96E+20	0.96	35.14	2.14E+20	7.95217E+19	2.94E+20	0.89	41.80
2MPASA_SV_1	5.30225E+17	6.69509E+17	1.19973E+18	0.70	20.85	4.305E+17	4.98818E+17	9.29318E+17	0.72	30.10
2MPASA_SV_2	9.83428E+17	9.51507E+17	1.93493E+18	0.76	20.48	7.1873E+17	8.84305E+17	1.60303E+18	0.71	29.06
2MPASA_SV_3	9.94129E+17	9.41245E+17	1.93537E+18	0.76	18.24	9.97594E+17	1.23209E+18	2.22968E+18	0.71	27.67
2MPASA_SV_4	1.33117E+18	1.19329E+18	2.52447E+18	0.77	19.55	1.01205E+18	1.31031E+18	2.32236E+18	0.70	26.04
2MPASA_SV_5	1.56149E+18	8.91538E+17	2.45303E+18	0.84	26.75	6.34654E+17	5.53756E+17	1.18841E+18	0.77	27.94
2MPALN_SV_1	0.010551488	0.002615927	0.013167415	0.92	25.46	0.010267339	0.003288003	0.013555342	0.90	21.42
2MPALN_SV_2	0.018631589	0.003483576	0.022115165	0.94	30.42	0.01761703	0.005680383	0.023297413	0.90	24.36
2MPALN_SV_3	0.035107093	0.006445499	0.041552592	0.94	33.79	0.044999975	0.011102669	0.056102645	0.92	30.88

2MPALN_SV_4	0.041551512	0.008737516	0.050289028	0.93	32.28	0.062822953	0.0218104	0.084633353	0.90	30.23
2MPALN_SV_5	0.04622583	0.009191472	0.055417302	0.94	30.87	0.084046055	0.022171988	0.106218043	0.92	30.93
2MPASN_SV_1	0.000186295	8.23E-05	0.000268639	0.87	17.74	8.51E-05	0.000164417	0.000249519	0.61	12.37
2MPASN_SV_2	0.000146886	6.12E-05	0.0002081	0.88	17.00	9.61E-05	9.75E-05	0.000193582	0.75	13.87
2MPASN_SV_3	0.000117526	6.00E-05	0.000177572	0.85	15.37	0.00011652	9.59E-05	0.000212454	0.78	14.18
2MPASN_SV_4	0.000125273	0.000136102	0.000261376	0.73	14.57	0.000126879	0.000126864	0.000253744	0.75	13.04
2MPASN_SV_5	6.66E-05	0.000104	0.000170561	0.66	11.92	0.000142178	0.000278053	0.000420231	0.61	15.27
2MPAR_SV_1	4.305278711	1.018782003	5.324060714	0.93	36.45	4.196354034	1.158708699	5.355062733	0.92	30.30
2MPAR_SV_2	7.377522299	1.019562736	8.397085036	0.96	40.04	7.17815264	1.226496457	8.404649097	0.95	32.78
2MPAR_SV_3	11.53705745	1.691299465	13.22835692	0.95	40.50	12.35517986	2.042460268	14.39764013	0.95	36.77
2MPAR_SV_4	9.829329636	1.999217299	11.82854694	0.94	36.13	14.06297058	2.390199198	16.45316978	0.95	36.93
2MPAR_SV_5	14.01388739	4.326239462	18.34012685	0.91	34.61	20.76357174	5.182335884	25.94590763	0.92	35.18
Area_SV_1	440432755.3	686001200.2	1126433955	0.66	9.89	748476627.5	1212292664	1960769291	0.65	16.08
Area_SV_2	636398522.5	842498786.7	1478897309	0.69	9.70	1082103236	1637705761	2719808997	0.66	16.31
Area_SV_3	783465937.4	804804715.6	1588270653	0.74	10.05	1162593675	1744839190	2907432865	0.67	15.78
Area_SV_4	1064386788	751213880.4	1815600668	0.81	11.76	1119461572	1543423851	2662885423	0.69	15.91
Area_SV_5	1275497465	549852808.5	1825350274	0.87	13.80	978384474.5	1143882218	2122266692	0.72	16.22
ADAR_SV_1	2.34E-06	7.42E-06	9.77E-06	0.49	0.15	4.04E-06	2.22E-05	2.62E-05	0.35	0.20
ADAR_SV_2	1.51E-06	5.17E-06	6.68E-06	0.47	0.12	1.84E-06	1.64E-05	1.83E-05	0.25	0.14
ADAR_SV_3	1.06E-06	4.09E-06	5.15E-06	0.44	0.10	1.03E-06	1.33E-05	1.43E-05	0.19	0.10
ADAR_SV_4	1.28E-06	4.25E-06	5.53E-06	0.47	0.11	1.80E-06	1.34E-05	1.52E-05	0.29	0.14
ADAR_SV_5	1.18E-06	4.80E-06	5.98E-06	0.42	0.11	1.33E-06	1.50E-05	1.64E-05	0.21	0.12
BPC_SV_1	21113842.84	23010852.53	44124695.36	0.73	9.42	33991280.3	57227173.14	91218453.44	0.64	15.97
BPC_SV_2	30867024.2	26405815.96	57272840.16	0.78	9.28	53425134.12	72426612.61	125851746.7	0.69	16.87
BPC_SV_3	40419107.77	33092346.27	73511454.04	0.79	8.86	66407018.43	96472204.33	162879222.8	0.67	15.88
BPC_SV_4	79786286.68	37511785.26	117298071.9	0.86	11.20	67075495.56	89977015.83	157052511.4	0.69	14.72
BPC_SV_5	137831272.2	26264459.21	164095731.4	0.94	16.78	54001970.49	49404416.07	103406386.6	0.77	15.53
BPR_SV_1	2242337.932	1191629.012	3433966.944	0.85	13.24	2065979.45	3178043.752	5244023.202	0.66	18.18
BPR_SV_2	4176023.526	1508119.254	5684142.779	0.89	14.66	3487594.824	3801070.264	7288665.089	0.73	19.87

BPR_SV_3	6216147.731	2447916.084	8664063.815	0.88	13.34	5659926.363	6285670.496	11945596.86	0.73	19.30
BPR_SV_4	11245845.48	3611617.384	14857462.87	0.90	14.50	5719365.967	6374435.586	12093801.55	0.73	16.11
BPR_SV_5	17800828.05	2961994.527	20762822.58	0.95	22.09	3842798.895	2923259.388	6766058.283	0.80	16.74
BPAR_SV_1	0.000254394	0.000174874	0.000429268	0.81	6.89	0.000175859	0.000159467	0.000335327	0.77	6.16
BPAR_SV_2	0.000383636	0.000190873	0.000574509	0.86	8.44	0.000232039	0.00015054	0.000382579	0.82	7.06
BPAR_SV_3	0.000469833	0.00019637	0.000666204	0.88	8.34	0.000391944	0.000178344	0.000570288	0.87	8.29
BPAR_SV_4	0.000429191	0.00023404	0.00066323	0.85	7.16	0.000322623	0.000244526	0.000567149	0.80	6.73
BPAR_SV_5	0.000444206	0.000232536	0.000676743	0.85	7.79	0.000219299	0.000309732	0.000529031	0.68	5.98
Circumference_SV_1...123	3.45005E+11	7.46311E+11	1.09132E+12	0.58	55.70	2.23507E+11	2.85153E+11	5.0866E+11	0.70	70.52
Circumference_SV_2...124	2.64411E+11	5.37654E+11	8.02064E+11	0.60	37.54	87607266605	2.16673E+11	3.04281E+11	0.55	39.95
Circumference_SV_3...125	3.10684E+11	7.61667E+11	1.07235E+12	0.55	94.00	1.05609E+11	2.30102E+11	3.35711E+11	0.58	78.56
Circumference_SV_4...126	1.76937E+11	1.16682E+12	1.34376E+12	0.31	85.05	78397538707	4.25754E+11	5.04151E+11	0.36	107.03
Circumference_SV_5...127	5.22772E+11	2.13444E+12	2.65721E+12	0.42	99.81	48208603621	9.17486E+11	9.65695E+11	0.14	62.81
cmY_SV_1	3623.017586	730.4198073	4353.437394	0.94	1.92	3658.332148	2985.824602	6644.15675	0.79	1.91
cmY_SV_2	5438.321089	607.0196476	6045.340736	0.96	2.42	5278.590873	2971.661854	8250.252727	0.84	2.35
cmY_SV_3	7759.865394	630.737361	8390.602755	0.97	2.94	7910.931928	3112.954188	11023.88612	0.88	2.94
cmY_SV_4	8594.689612	589.907477	9184.597089	0.98	3.12	9445.979471	2170.214859	11616.19433	0.93	3.24
cmY_SV_5	9421.708538	625.9060686	10047.61461	0.98	3.26	10523.68557	2008.959922	12532.6455	0.94	3.42
Compactness_SV_1	0.001023285	0.000718144	0.001741429	0.81	10.92	0.000831946	0.000673699	0.001505645	0.79	10.52
Compactness_SV_2	0.001282621	0.00069011	0.00197273	0.85	12.23	0.000839166	0.000673486	0.001512652	0.79	11.01
Compactness_SV_3	0.001855453	0.000725222	0.002580675	0.88	14.91	0.001205874	0.00058867	0.001794544	0.86	14.10
Compactness_SV_4	0.002013285	0.000727848	0.002741133	0.89	16.10	0.00127295	0.000760405	0.002033354	0.83	15.57
Compactness_SV_5	0.002499374	0.000899113	0.003398487	0.89	16.92	0.001756253	0.001398107	0.003154361	0.79	17.49
CHArea_SV_1	9106571882	5299532985	14406104867	0.84	12.83	13694350639	10904785616	24599136255	0.79	18.35
CHArea_SV_2	13516208351	5979013183	19495221534	0.87	12.71	17714872771	14042591016	31757463788	0.79	16.95
CHArea_SV_3	20400380404	5126520024	25526900428	0.92	14.41	25699296373	16486695344	42185991718	0.82	17.92
CHArea_SV_4	25884184713	5894306032	31778490745	0.93	15.70	27538956896	10727446950	38266403846	0.89	17.73
CHArea_SV_5	28869748048	5570510605	34440258654	0.94	18.78	30470862366	7826676146	38297538512	0.92	21.04
Circumference_SV_1...143	92628.79407	34783.84242	127412.6365	0.89	8.86	119158.4901	71093.11118	190251.6013	0.83	10.71

Circumference_SV_2...144	110016.8087	37292.61318	147309.4219	0.90	8.68	127247.8245	75824.47148	203072.296	0.83	9.89
Circumference_SV_3...145	184793.2851	20317.67145	205110.9565	0.96	10.60	212204.8164	78458.004	290662.8204	0.89	11.91
Circumference_SV_4...146	191304.6111	17680.44295	208985.0541	0.97	10.54	230530.4399	44965.01446	275495.4544	0.94	11.94
Circumference_SV_5...147	224050.3523	17357.43115	241407.7835	0.97	11.85	262134.662	35695.29736	297829.9593	0.96	13.15
Excentricity_SV_1	0.019654968	0.003588166	0.023243135	0.94	31.21	0.010825415	0.003170387	0.013995802	0.91	20.06
Excentricity_SV_2	0.021590298	0.00263822	0.024228518	0.96	29.14	0.011066177	0.001915444	0.012981621	0.95	18.21
Excentricity_SV_3	0.021253923	0.002649189	0.023903112	0.96	25.66	0.014360536	0.001772659	0.016133195	0.96	19.48
Excentricity_SV_4	0.015962591	0.002254271	0.018216862	0.96	21.56	0.012862588	0.00149171	0.014354298	0.96	17.95
Excentricity_SV_5	0.011718743	0.002367434	0.014086176	0.94	16.68	0.01044214	0.001624529	0.012066669	0.95	14.70
ObjectExtentX_SV_1	4187.896234	3319.06401	7506.960244	0.79	7.91	5578.205973	5063.248381	10641.45435	0.77	10.31
ObjectExtentX_SV_2	2529.869136	2331.438566	4861.307703	0.77	5.67	4286.733943	5652.539796	9939.273739	0.69	8.31
ObjectExtentX_SV_3	2061.341311	2524.761503	4586.102814	0.71	5.19	2520.176054	5553.601263	8073.777316	0.58	6.12
ObjectExtentX_SV_4	2804.911536	3035.006451	5839.917987	0.73	5.97	2128.215585	4781.495705	6909.711291	0.57	5.44
ObjectExtentX_SV_5	4527.537933	3515.123624	8042.661557	0.79	8.66	3895.058366	4498.923156	8393.981521	0.72	8.29
ObjectExtentY_SV_1	26451.93086	9161.408826	35613.33968	0.90	13.04	28464.59715	15479.06152	43943.65866	0.85	14.30
ObjectExtentY_SV_2	34655.93149	9749.45139	44405.38288	0.91	13.19	30470.50631	16935.09677	47405.60308	0.84	12.87
ObjectExtentY_SV_3	59644.34354	5061.729337	64706.07288	0.97	15.74	59935.48355	15767.61889	75703.10244	0.92	16.42
ObjectExtentY_SV_4	56424.35008	3801.374396	60225.72448	0.98	14.94	64814.66005	8014.905138	72829.56519	0.96	16.21
ObjectExtentY_SV_5	59596.77915	4117.992238	63714.77139	0.98	15.76	68037.21429	8246.501741	76283.71603	0.96	17.01
PSCC_1_1	6638.623128	3093.660047	9732.283176	0.87	23.38	2043.835586	5253.037633	7296.873218	0.54	27.19
PSCC_1_2	7395.989119	3520.177735	10916.16685	0.86	18.95	4042.345519	7194.907225	11237.25274	0.63	28.10
PSCC_1_3	13226.13655	5525.026884	18751.16343	0.88	20.01	6745.494255	11650.31096	18395.80522	0.63	24.91
PSCC_1_4	33813.37753	18031.05635	51844.43388	0.85	21.26	14400.32262	22126.86776	36527.19038	0.66	24.75
PSCC_1_5	42787.0103	28658.36728	71445.37758	0.82	21.70	23442.3177	32858.75117	56301.06887	0.68	28.93
PSCC_2_1	31056.25835	13787.25463	44843.51298	0.87	22.94	9745.405932	23668.82754	33414.23347	0.55	26.90
PSCC_2_2	39135.28111	17343.19117	56478.47227	0.87	19.81	15711.04362	29342.57054	45053.61416	0.62	26.39
PSCC_2_3	85885.28818	28475.99278	114361.281	0.90	22.61	24933.12204	42322.97616	67256.0982	0.64	23.79
PSCC_2_4	264322.5978	84722.24256	349044.8403	0.90	25.01	58657.3032	83090.29485	141747.5981	0.68	24.74
PSCC_2_5	153961.5737	128193.1728	282154.7465	0.78	19.99	69590.02439	101974.2233	171564.2477	0.67	26.27

PSCC_3_1	159532.8531	84279.27242	243812.1255	0.85	21.13	60211.98566	126855.3883	187067.3739	0.59	29.27
PSCC_3_2	185370.5168	95153.13092	280523.6477	0.85	17.66	87520.37175	157361.9663	244882.3381	0.63	29.13
PSCC_3_3	319859.9173	154411.1042	474271.0214	0.86	17.64	148589.7622	222347.1045	370936.8667	0.67	28.10
PSCC_3_4	704473.0139	350948.1695	1055421.183	0.86	17.66	319603.7652	415155.3712	734759.1363	0.70	26.54
PSCC_3_5	610244.1281	550258.172	1160502.3	0.77	18.16	235472.3308	349330.6139	584802.9447	0.67	26.25
PSCC_4_1	234707.0442	198088.4259	432795.4702	0.78	12.75	285136.6883	592203.8926	877340.5809	0.59	27.79
PSCC_4_2	319514.2214	168157.7697	487671.9911	0.85	12.75	392023.6797	627796.3924	1019820.072	0.65	28.68
PSCC_4_3	384842.3039	277711.7236	662554.0274	0.81	11.48	532681.622	867412.2085	1400093.83	0.65	25.91
PSCC_4_4	901294.1135	1018964.355	1920258.468	0.73	12.87	942455.731	1481874.543	2424330.274	0.66	22.73
PSCC_4_5	1453843.789	2201919.045	3655762.834	0.66	15.06	1124292.307	1541275.871	2665568.179	0.69	28.27
PSCC_5_1	264604.0238	193212.5199	457816.5438	0.80	10.36	406117.6247	911909.2145	1318026.839	0.57	18.56
PSCC_5_2	412529.4195	204241.8293	616771.2488	0.86	11.41	640770.3087	935965.8612	1576736.17	0.67	20.96
PSCC_5_3	820042.1385	547065.4585	1367107.597	0.82	13.24	1184659.281	1843457.652	3028116.933	0.66	22.64
PSCC_5_4	3969479.931	4394409.714	8363889.645	0.73	19.08	3083868.889	4936038.949	8019907.839	0.65	24.23
PSCC_5_5	24197924.37	15569855.62	39767779.99	0.82	31.53	9670388.099	11573769.95	21244158.05	0.71	36.31
PSCC_6_1	275718.3109	194611.1653	470329.4762	0.81	10.11	354462.3205	552150.0764	906612.3969	0.66	13.61
PSCC_6_2	493584.9873	279342.409	772927.3963	0.84	11.40	729045.4324	760167.6042	1489213.037	0.74	16.65
PSCC_6_3	2035082.183	1355962.443	3391044.626	0.82	17.75	2562785.876	3049196.724	5611982.6	0.72	23.58
PSCC_6_4	11582953.93	10967001.3	22549955.23	0.76	23.95	10719038.61	14003491.15	24722529.76	0.70	29.17
PSCC_6_5	133983569.9	52374759.9	186358329.8	0.88	40.78	64540585.34	67210115.24	131750700.6	0.74	41.11
PSCC_7_1	285651.2654	273259.2907	558910.5561	0.76	9.72	408722.3318	470220.0461	878942.3779	0.72	12.88
PSCC_7_2	569586.1636	462029.4539	1031615.617	0.79	11.14	871570.3923	839069.277	1710639.669	0.76	15.35
PSCC_7_3	2335355.627	1542991.814	3878347.441	0.82	17.00	2502843.12	2974723.146	5477566.266	0.72	19.67
PSCC_7_4	6612583.379	8846195.16	15458778.54	0.69	17.72	9248663.816	11505112.79	20753776.6	0.71	24.03
PSCC_7_5	101515056.4	38599408.33	140114464.8	0.89	36.45	68932661.81	64658387.43	133591049.2	0.76	34.87
PSCC_8_1	795509.8804	1242762.786	2038272.666	0.66	12.67	1045826.329	1832138.869	2877965.198	0.63	15.71
PSCC_8_2	974118.8564	1801822.198	2775941.055	0.62	11.46	1459595.408	2423110.662	3882706.07	0.64	15.27
PSCC_8_3	3402091.642	3118870.896	6520962.538	0.77	16.71	2885709.812	4607465.475	7493175.286	0.65	17.26
PSCC_8_4	5681413.288	8455622.584	14137035.87	0.67	14.84	6967427.017	9737783.175	16705210.19	0.68	19.66

PSCC_8_5	63386286.25	23418931.66	86805217.9	0.89	29.98	52265604.75	41435082.15	93700686.9	0.79	32.50
PSCC_9_1	718647.2102	2532102.598	3250749.808	0.46	8.94	1161569.236	2655516.824	3817086.06	0.57	12.11
PSCC_9_2	1174764.682	3365594.778	4540359.46	0.51	9.52	1993989.777	3962744.509	5956734.286	0.60	13.01
PSCC_9_3	5136410.019	5315773.964	10452183.98	0.74	15.79	4002759.496	7309398.16	11312157.66	0.62	15.16
PSCC_9_4	3938378.039	6481347.549	10419725.59	0.65	10.68	5617361.353	9674177.193	15291538.55	0.64	14.93
PSCC_9_5	36380380.83	16786250.19	53166631.01	0.87	21.92	44848330.14	37348832.3	82197162.44	0.78	27.24
PSCC_10_1	440302.1473	823061.6639	1263363.811	0.62	7.14	727319.0549	1038988.782	1766307.837	0.68	9.80
PSCC_10_2	1152258.369	1387073.404	2539331.774	0.71	9.48	1709263.732	2533594.607	4242858.338	0.67	12.18
PSCC_10_3	2887812.551	2893569.05	5781381.601	0.75	11.68	3680068.72	5542097.861	9222166.581	0.67	14.50
PSCC_10_4	1874515.32	3189566.033	5064081.353	0.64	8.00	4432979.978	7082364.645	11515344.62	0.65	14.30
PSCC_10_5	28665151.64	12176615.9	40841767.54	0.88	21.45	44820706.49	37566108.81	82386815.29	0.78	27.71
PSCC_11_1	9686337.608	4928589.724	14614927.33	0.85	12.04	10655786.63	7835547.457	18491334.09	0.80	14.09
PSCC_11_2	12202111.29	6290996.812	18493108.1	0.85	11.44	13776587.29	12717115.78	26493703.07	0.76	13.55
PSCC_11_3	24524262.15	11302352.01	35826614.16	0.87	12.34	28238735.43	32022838.41	60261573.84	0.73	14.95
PSCC_11_4	21886701.54	13235195.53	35121897.07	0.83	10.07	33896361.01	37662893.95	71559254.96	0.73	14.45
PSCC_11_5	88466899.15	34473370.28	122940269.4	0.89	15.90	289957709.8	167753074.7	457710784.5	0.84	29.33
PSCC_12_1	809580.9629	927654.7206	1737235.683	0.72	10.06	1086508.071	1367824.717	2454332.788	0.70	13.44
PSCC_12_2	1955471.595	1803312.035	3758783.629	0.76	11.97	2800226.205	3454929.015	6255155.219	0.71	16.59
PSCC_12_3	3298628.55	3779485.827	7078114.378	0.72	11.45	4650655.17	7889126.289	12539781.46	0.64	16.13
PSCC_12_4	3094736.084	4910714.885	8005450.969	0.65	8.92	7041761.587	9919431.337	16961192.92	0.68	16.48
PSCC_12_5	35611032.5	23267700.92	58878733.43	0.82	19.90	31516181.98	40442163.13	71958345.11	0.70	22.17
PSCC_13_1	1309750.409	1749759.392	3059509.802	0.69	9.84	2246402.236	2172197.338	4418599.574	0.76	14.39
PSCC_13_2	3317975.134	3507386.381	6825361.515	0.74	11.94	5885734.05	5874415.156	11760149.21	0.75	17.73
PSCC_13_3	6214926.232	7089207.097	13304133.33	0.72	11.76	9279679.918	14016862.01	23296541.93	0.67	16.36
PSCC_13_4	7503157.665	10192407.89	17695565.55	0.69	10.00	18436786.97	21308781.66	39745568.63	0.72	18.32
PSCC_13_5	52330532.54	42444803.79	94775336.33	0.79	17.71	63258632.71	71094262.23	134352894.9	0.73	22.67
PSCC_14_1	3565553.584	5251409.499	8816963.084	0.67	9.50	8479523.59	5630058.14	14109581.73	0.82	14.38
PSCC_14_2	9768567.847	10295752.69	20064320.53	0.74	12.25	18256698.26	13776916.45	32033614.71	0.80	16.72
PSCC_14_3	17352593.85	18647995.53	36000589.38	0.74	11.84	26420250.08	31662392	58082642.08	0.71	15.25

PSCC_14_4	23161274.46	26327240.41	49488514.87	0.73	10.89	45590789.19	50140780.58	95731569.77	0.73	16.84
PSCC_14_5	205186050.8	62302798.52	267488849.3	0.91	26.66	206578667.6	101813831	308392498.6	0.86	31.37
PSCC_15_1	27840018.01	34155070.88	61995088.88	0.71	11.96	45783301.4	37478418.85	83261720.25	0.79	13.64
PSCC_15_2	40736224.91	49193576.85	89929801.77	0.71	12.07	72092794.93	57913182.13	130005977.1	0.79	14.60
PSCC_15_3	49535423.63	59893602.57	109429026.2	0.71	10.69	80817095.69	88463603.77	169280699.5	0.73	13.23
PSCC_15_4	86983470.09	72329976.09	159313446.2	0.78	13.12	98691493.44	107430259.5	206121753	0.73	14.84
PSCC_15_5	516805526.9	99289554.91	616095081.8	0.94	35.21	553948145.1	173512612.8	727460757.9	0.91	40.09
PSCC_16_1	323771725.3	310678183.5	634449908.8	0.76	15.26	376420003.7	459721278.2	836141281.9	0.71	16.29
PSCC_16_2	373507130	335926628.7	709433758.7	0.77	14.69	452382849	506172130.4	958554979.4	0.73	16.45
PSCC_16_3	269090157.7	256720081.8	525810239.4	0.76	12.39	443833266.9	544513042.9	988346309.8	0.71	16.25
PSCC_16_4	427175170	267807435.4	694982605.4	0.83	16.62	510485317.2	562287198.2	1072772515	0.73	18.95
PSCC_16_5	1693056228	227325783.3	1920382012	0.96	45.54	1462011303	273464873.6	1735476176	0.94	50.58
PSCC_17_1	788476349	897632196.6	1686108546	0.72	14.65	1299200318	2155643104	3454843421	0.64	26.81
PSCC_17_2	1234999015	961415559.3	2196414574	0.79	15.72	1433731154	2319408611	3753139765	0.65	23.84
PSCC_17_3	1046179523	705087759.9	1751267283	0.82	15.48	1326422210	1902542714	3228964924	0.68	22.57
PSCC_17_4	1252402673	563471965	1815874638	0.87	20.00	1123540732	1052883751	2176424483	0.76	25.35
PSCC_17_5	2567728960	283627300.7	2851356261	0.96	55.42	737104922.2	165418319.3	902523241.5	0.93	62.03
PSCC_18_1	284796825.5	356458922.9	641255748.3	0.71	16.41	339239218.6	621052153.3	960291371.9	0.62	36.58
PSCC_18_2	435621838.7	423353032.3	858974871.1	0.76	15.04	615065879.4	907393457	1522459336	0.67	34.93
PSCC_18_3	666575165	318542029.4	985117194.4	0.86	18.91	523263799.8	702546326.3	1225810126	0.69	31.50
PSCC_18_4	760502643.9	221243720.8	981746364.7	0.91	25.90	367769565	308877654.1	676647219.1	0.78	35.48
PSCC_18_5	652616524.6	70967975.54	723584500.2	0.97	59.91	73521092.42	21373817.85	94894910.28	0.91	58.39
PSCC_19_1	52415989.93	32021427.24	84437417.17	0.83	27.29	17118628.11	32625037.81	49743665.92	0.61	37.21
PSCC_19_2	85642222.6	64611192.12	150253414.7	0.80	20.85	57574714.75	77993955.57	135568670.3	0.69	39.82
PSCC_19_3	136713412.4	53741879.96	190455292.4	0.88	24.58	51419692.53	62353088.55	113772781.1	0.71	34.84
PSCC_19_4	138606070.9	35374003.94	173980074.9	0.92	30.92	34839706.09	30310160.78	65149866.87	0.78	34.46
PSCC_19_5	91294553.63	8549184.274	99843737.91	0.97	55.95	10539873.17	3056382.761	13596255.93	0.91	49.48
PSCC_20_1	7364473.989	3492091.265	10856565.25	0.86	28.33	1921908.187	3303670.376	5225578.563	0.64	28.58
PSCC_20_2	27514805.31	12831886.21	40346691.52	0.87	29.00	10431604.63	11391442.46	21823047.09	0.73	37.78

PSCC_20_3	37876267.62	11641793.72	49518061.34	0.91	28.32	10537616.05	11937159.91	22474775.96	0.73	31.36
PSCC_20_4	37368191.39	7914430.212	45282621.61	0.93	31.12	8897788.493	7607427.851	16505216.34	0.78	29.73
PSCC_20_5	31423457.09	2869033.779	34292490.86	0.97	50.98	4384576.598	1233165.682	5617742.279	0.91	44.64
No PSCC_1	5707031.53	4375849.842	10082881.37	0.80	14.88	5984149.895	7893435.977	13877585.87	0.69	21.74
No PSCC_2	26254371.3	11990785.61	38245156.91	0.87	20.38	13309151.95	17800645.38	31109797.33	0.69	23.28
No PSCC_3	36285736.96	14960565.47	51246302.43	0.88	18.35	15895113.22	23193757.18	39088870.4	0.67	20.16
No PSCC_4	58642652.21	13112074	71754726.21	0.93	23.14	17850922.68	17156301.53	35007224.21	0.76	21.38
No PSCC_5	85616252.66	7840348.44	93456601.1	0.97	43.29	17911527.85	4304022.551	22215550.4	0.93	39.70
NIR TV_1	8.041771323	2.63254023	10.67431155	0.90	2.16	16.14712741	9.743679468	25.89080688	0.83	3.12
NIR TV_2	14.94918822	2.368917444	17.31810566	0.95	2.68	22.69338303	5.748989142	28.44237217	0.92	3.31
NIR TV_3	67.75964492	2.082075702	69.84172062	0.99	5.97	76.85924787	2.237416286	79.09666416	0.99	6.28
NIR TV_4	5.742610029	1.417512714	7.160122743	0.92	1.99	4.758455112	1.690645557	6.449100669	0.89	1.79
NIR TV_5	9.222733824	2.508255179	11.730989	0.92	2.75	9.634629804	3.141959146	12.77658895	0.90	2.79
NIR SV_1	32.119532	2.987922457	35.10745445	0.97	4.47	29.2663373	2.223540838	31.48987814	0.98	4.25
NIR SV_2	29.23670001	3.672548354	32.90924836	0.96	4.03	29.66910447	2.837867547	32.50697202	0.97	4.01
NIR SV_3	20.15516439	3.529148228	23.68431262	0.94	3.48	20.69126056	3.067452947	23.75871351	0.95	3.44
NIR SV_4	18.7064311	4.442965137	23.14939623	0.93	3.29	13.38363648	3.592758329	16.97639481	0.92	2.70
NIR SV_5	18.32115977	4.326084632	22.64724441	0.93	3.68	11.46438288	3.317950834	14.78233371	0.91	2.85
IR TV_1	2.762757816	0.049875355	2.812633171	0.99	6.87	2.656461144	0.122174073	2.778635217	0.98	6.88
IR TV_2	1.279443169	0.033043849	1.312487018	0.99	4.71	1.177221608	0.081029618	1.258251226	0.98	4.57
IR TV_3	1.094582143	0.041031287	1.135613431	0.99	4.22	1.050499884	0.078304535	1.128804418	0.98	4.18
IR TV_4	1.76134943	0.048370892	1.809720322	0.99	5.36	1.679173737	0.061847794	1.74102153	0.99	5.27
IR TV_5	1.162686761	0.07142114	1.234107901	0.98	4.27	1.117399369	0.068072432	1.185471801	0.98	4.23
IR SV_1	8.097708445	0.01887651	8.116584955	1.00	14.26	8.110340691	0.022814178	8.13315487	1.00	14.31
IR SV_2	2.862235895	0.01740277	2.879638665	1.00	8.80	2.735101239	0.020853972	2.755955211	1.00	8.60
IR SV_3	3.703274487	0.020562968	3.723837455	1.00	9.32	3.805389143	0.02982059	3.835209732	1.00	9.46
IR SV_4	5.330172497	0.078146357	5.408318854	1.00	11.40	5.578423178	0.03473701	5.613160188	1.00	11.63
IR SV_5	2.921425042	0.031026193	2.952451235	1.00	7.96	3.035594747	0.034800328	3.070395075	1.00	8.11
Blue_TV_1	11.95540799	1.573811164	13.52921915	0.96	7.16	15.38252705	2.491791255	17.87431831	0.95	7.75

Blue_TV_2	12.61675288	1.717239773	14.33399266	0.96	6.85	15.75396717	4.261073409	20.01504058	0.92	7.03
Blue_TV_3	16.57667557	1.803343312	18.38001888	0.97	7.37	15.68782189	4.083770404	19.77159229	0.92	6.48
Blue_TV_4	22.06676297	2.228824424	24.29558739	0.97	8.16	21.66330763	3.213604981	24.87691262	0.95	7.34
Blue_TV_5	132.8586949	11.51122036	144.3699153	0.97	16.27	161.4889765	35.06456423	196.5535408	0.93	15.75
Green_TV_1	33.07142435	3.855814176	36.92723853	0.96	7.48	44.78155064	20.77398792	65.55553856	0.87	7.85
Green_TV_2	32.5878802	4.070112049	36.65799225	0.96	7.01	44.73810789	23.47402839	68.21213627	0.85	7.16
Green_TV_3	42.17321056	4.402481428	46.57569199	0.97	7.53	42.78073723	19.54092228	62.32165951	0.87	6.49
Green_TV_4	56.64034004	5.995102168	62.6354422	0.97	8.36	61.66695633	16.6874043	78.35436063	0.92	7.48
Green_TV_5	540.5036125	46.7888563	587.2924689	0.97	19.84	547.3404065	143.2325422	690.5729487	0.92	16.62
Red_TV_1	22.46460841	2.788253151	25.25286156	0.96	7.72	32.63066703	15.8388132	48.46948023	0.86	8.36
Red_TV_2	22.13697251	2.912642171	25.04961468	0.96	7.20	32.8754626	17.35607716	50.23153976	0.85	7.63
Red_TV_3	30.68649344	3.274329261	33.9608227	0.97	7.91	30.25854445	13.89486262	44.15340707	0.87	6.73
Red_TV_4	44.10244677	4.990296583	49.09274336	0.96	8.92	47.75087565	11.83867354	59.58954919	0.92	8.00
Red_TV_5	634.5677338	55.39802485	689.9657586	0.97	24.35	716.0967204	182.6089814	898.7057019	0.92	21.36
Blue_SV_1	14.41433685	9.959517059	24.37385391	0.81	5.43	15.6383259	28.27105176	43.90937766	0.62	5.20
Blue_SV_2	24.02616202	9.27952528	33.3056873	0.89	6.74	23.635325	22.02755989	45.66288488	0.76	6.02
Blue_SV_3	36.14621026	10.0558547	46.20206496	0.92	7.43	28.31190861	14.89243926	43.20434787	0.85	5.89
Blue_SV_4	37.53291567	10.1271442	47.66005986	0.92	6.94	27.89127952	12.60931083	40.50059035	0.87	5.36
Blue_SV_5	149.5656649	21.78590116	171.351566	0.95	11.96	130.0636392	21.60079217	151.6644314	0.95	9.70
Green_SV_1	33.21853422	16.53901366	49.75754788	0.86	5.65	43.37602512	78.23127565	121.6073008	0.62	5.69
Green_SV_2	43.86576435	14.20477864	58.07054299	0.90	6.32	51.75916641	59.59957223	111.3587386	0.72	5.93
Green_SV_3	66.44838071	14.38911698	80.83749769	0.93	7.11	48.42852382	34.45433685	82.88286066	0.81	5.25
Green_SV_4	69.71304809	15.07538255	84.78843064	0.93	6.79	49.35913009	23.90704543	73.26617552	0.86	4.99
Green_SV_5	296.2341173	40.62874172	336.862859	0.96	11.91	213.5114056	48.80143745	262.312843	0.93	8.61
Red_SV_1	27.03241734	17.58891007	44.62132741	0.82	5.69	35.8011287	75.30865822	111.1097869	0.59	5.80
Red_SV_2	40.07729045	15.3210642	55.39835466	0.89	6.75	46.66975164	56.06759078	102.7373424	0.71	6.31
Red_SV_3	69.91994055	16.01685779	85.93679834	0.93	8.00	49.13643255	30.7056957	79.84212825	0.83	5.83
Red_SV_4	85.01821461	19.97416971	104.9923843	0.93	7.94	52.9555695	22.6137785	75.569348	0.88	5.52
Red_SV_5	546.0537956	65.72516454	611.7789601	0.96	16.15	406.3018895	93.73924641	500.0411359	0.93	11.95

b_TV_1	8.94E-06	3.98E-06	1.29E-05	0.87	1.15	1.40E-05	4.03E-05	5.43E-05	0.51	1.51
b_TV_2	9.41E-06	4.29E-06	1.37E-05	0.87	1.17	1.47E-05	2.18E-05	3.64E-05	0.67	1.52
b_TV_3	9.97E-06	3.25E-06	1.32E-05	0.90	1.21	9.62E-06	1.24E-05	2.21E-05	0.70	1.24
b_TV_4	1.40E-05	4.29E-06	1.83E-05	0.91	1.44	1.25E-05	9.97E-06	2.25E-05	0.79	1.42
b_TV_5	0.000104887	1.55E-05	0.000120417	0.95	4.18	4.08E-05	2.66E-05	6.74E-05	0.82	2.73
g_TV_1	6.23E-06	2.66E-06	8.89E-06	0.88	0.61	8.10E-06	9.13E-06	1.72E-05	0.73	0.68
g_TV_2	6.04E-06	2.67E-06	8.71E-06	0.87	0.60	6.76E-06	5.77E-06	1.25E-05	0.78	0.63
g_TV_3	4.22E-06	2.07E-06	6.29E-06	0.86	0.50	4.61E-06	4.56E-06	9.17E-06	0.75	0.52
g_TV_4	5.31E-06	1.97E-06	7.28E-06	0.89	0.57	5.18E-06	4.36E-06	9.54E-06	0.78	0.55
g_TV_5	9.49E-06	3.23E-06	1.27E-05	0.90	0.77	2.87E-05	7.33E-06	3.61E-05	0.92	1.32
b_SV_1	6.83E-06	2.15E-06	8.98E-06	0.90	0.98	6.64E-06	1.14E-05	1.81E-05	0.64	1.00
b_SV_2	6.84E-06	2.52E-06	9.36E-06	0.89	0.98	1.00E-05	9.79E-06	1.98E-05	0.75	1.22
b_SV_3	4.19E-06	2.36E-06	6.56E-06	0.84	0.76	6.84E-06	6.44E-06	1.33E-05	0.76	0.99
b_SV_4	5.63E-06	3.00E-06	8.63E-06	0.85	0.88	6.05E-06	5.10E-06	1.11E-05	0.78	0.93
b_SV_5	2.67E-05	7.49E-06	3.42E-05	0.91	1.98	1.40E-05	1.44E-05	2.84E-05	0.75	1.45
r_SV_1	1.22E-06	1.34E-06	2.57E-06	0.73	0.32	2.72E-06	6.22E-06	8.94E-06	0.57	0.47
r_SV_2	1.52E-06	1.19E-06	2.70E-06	0.79	0.36	2.85E-06	4.26E-06	7.11E-06	0.67	0.48
r_SV_3	6.33E-06	1.77E-06	8.09E-06	0.91	0.72	3.16E-06	1.88E-06	5.05E-06	0.83	0.51
r_SV_4	1.40E-05	5.06E-06	1.91E-05	0.89	1.06	8.10E-06	3.70E-06	1.18E-05	0.87	0.80
r_SV_5	0.000101554	1.53E-05	0.000116864	0.95	2.74	5.70E-05	2.70E-05	8.40E-05	0.86	2.04
R-G_TV_1	1.247040598	0.169889123	1.416929722	0.96	-7.20	1.347316854	0.532269669	1.879586523	0.88	-6.87
R-G_TV_2	1.232920457	0.176844677	1.409765135	0.95	-6.90	1.335850911	0.730298496	2.066149407	0.85	-6.32
R-G_TV_3	1.161650082	0.186529935	1.348180018	0.95	-6.65	1.370203819	0.693256527	2.063460346	0.86	-6.12
R-G_TV_4	1.177120391	0.168127386	1.345247778	0.95	-6.94	1.522972388	0.697085695	2.220058083	0.87	-6.62
R-G_TV_5	6.874001591	1.390475629	8.26447722	0.94	-19.12	17.54034317	4.495569305	22.03591247	0.92	-27.06
R-B_TV_1	2.166018155	0.458548373	2.624566528	0.93	11.27	4.539942399	8.108741348	12.64868375	0.63	12.04
R-B_TV_2	2.091836792	0.502639548	2.59447634	0.93	10.75	4.950577807	5.995145267	10.94572307	0.71	11.90
R-B_TV_3	3.245641819	0.537268899	3.782910718	0.95	12.18	3.766559979	3.974586716	7.741146694	0.74	9.43
R-B_TV_4	5.592287454	1.069294359	6.661581813	0.94	14.01	7.360028857	3.57816521	10.93819407	0.86	11.83

R-B_TV_5	197.8269824	19.57795757	217.40494	0.97	43.12	207.7667338	62.32747633	270.0942102	0.91	32.32
(R-G)/(R+G+B)_TV_1	7.80E-06	3.05E-06	1.08E-05	0.88	-3.36	1.29E-05	5.26E-06	1.82E-05	0.88	-4.33
(R-G)/(R+G+B)_TV_2	6.85E-06	2.54E-06	9.39E-06	0.89	-3.23	1.09E-05	5.51E-06	1.64E-05	0.86	-4.05
(R-G)/(R+G+B)_TV_3	7.21E-06	2.73E-06	9.94E-06	0.89	-3.50	5.88E-06	3.89E-06	9.77E-06	0.82	-3.08
(R-G)/(R+G+B)_TV_4	1.13E-05	3.22E-06	1.45E-05	0.91	-4.75	1.20E-05	4.38E-06	1.64E-05	0.89	-4.72
(R-G)/(R+G+B)_TV_5	0.000203869	1.99E-05	0.000223766	0.97	-28.56	0.000243562	6.04E-05	0.000303988	0.92	-32.63
(G-B)/(R+G+B)_SV_1	2.69E-05	9.50E-06	3.64E-05	0.89	4.25	2.29E-05	3.05E-05	5.34E-05	0.69	3.57
(G-B)/(R+G+B)_SV_2	2.94E-05	1.07E-05	4.02E-05	0.89	4.58	3.43E-05	2.65E-05	6.08E-05	0.79	4.48
(G-B)/(R+G+B)_SV_3	1.59E-05	8.84E-06	2.47E-05	0.84	3.54	2.88E-05	2.09E-05	4.97E-05	0.81	4.35
(G-B)/(R+G+B)_SV_4	1.36E-05	7.78E-06	2.14E-05	0.84	3.48	1.99E-05	1.43E-05	3.41E-05	0.81	3.91
(G-B)/(R+G+B)_SV_5	1.84E-05	1.34E-05	3.18E-05	0.80	3.96	3.59E-05	1.71E-05	5.30E-05	0.86	5.22
Ipca_SV_1	21.26000539	5.099982712	26.3599881	0.93	7.44	32.78830732	57.58887793	90.37718525	0.63	7.49
Ipca_SV_2	19.06608123	4.176958335	23.24303956	0.93	7.06	33.91378678	44.74917447	78.66296125	0.69	7.43
Ipca_SV_3	22.68492284	3.407371392	26.09229423	0.95	7.33	21.31018899	25.17099733	46.48118633	0.72	5.65
Ipca_SV_4	24.82495958	4.482599405	29.30755898	0.94	7.41	21.34019483	14.62779484	35.96798967	0.81	5.64
Ipca_SV_5	117.0285224	20.75229315	137.7808156	0.94	13.09	65.47072807	39.11884713	104.5895752	0.83	7.93
ExB_SV_1	3.86E-05	1.32E-05	5.18E-05	0.90	-39.17	3.33E-05	4.64E-05	7.97E-05	0.68	-18.67
ExB_SV_2	4.16E-05	1.50E-05	5.66E-05	0.89	-57.88	5.02E-05	4.04E-05	9.06E-05	0.79	-26.50
ExB_SV_3	2.18E-05	1.25E-05	3.43E-05	0.84	-103.33	4.05E-05	3.09E-05	7.13E-05	0.80	-35.19
ExB_SV_4	1.89E-05	1.12E-05	3.01E-05	0.84	233.24	2.80E-05	2.13E-05	4.93E-05	0.80	-66.75
ExB_SV_5	2.74E-05	2.02E-05	4.76E-05	0.80	-147.91	4.51E-05	2.90E-05	7.41E-05	0.82	-57.52
ExG_SV_1	6.50E-05	2.94E-05	9.44E-05	0.87	4.96	5.56E-05	6.24E-05	0.000117983	0.73	4.21
ExG_SV_2	7.77E-05	3.10E-05	0.000108624	0.88	5.54	7.70E-05	5.04E-05	0.000127465	0.82	5.07
ExG_SV_3	6.21E-05	2.64E-05	8.86E-05	0.88	5.39	8.23E-05	4.45E-05	0.000126737	0.85	5.70
ExG_SV_4	7.36E-05	3.08E-05	0.000104457	0.88	6.73	7.14E-05	3.50E-05	0.000106457	0.86	6.13
ExG_SV_5	0.000299247	6.17E-05	0.000360913	0.94	15.75	0.000291554	6.89E-05	0.000360435	0.93	14.42
Gray_TV_1	1.51E-06	6.60E-07	2.17E-06	0.87	0.33	2.02E-06	3.92E-06	5.94E-06	0.61	0.38
Gray_TV_2	1.52E-06	6.92E-07	2.22E-06	0.87	0.34	1.86E-06	2.21E-06	4.07E-06	0.72	0.37
Gray_TV_3	1.19E-06	5.13E-07	1.71E-06	0.87	0.30	1.28E-06	1.49E-06	2.77E-06	0.72	0.31

Gray_TV_4	1.53E-06	5.41E-07	2.07E-06	0.89	0.34	1.40E-06	1.29E-06	2.70E-06	0.76	0.32
Gray_TV_5	2.49E-06	9.88E-07	3.47E-06	0.88	0.43	1.50E-06	1.35E-06	2.85E-06	0.77	0.33
Gray_SV_1	1.52E-06	5.68E-07	2.09E-06	0.89	0.34	1.28E-06	1.60E-06	2.88E-06	0.71	0.31
Gray_SV_2	1.70E-06	6.31E-07	2.33E-06	0.89	0.37	1.89E-06	1.38E-06	3.27E-06	0.80	0.38
Gray_SV_3	9.89E-07	5.17E-07	1.51E-06	0.85	0.28	1.69E-06	1.13E-06	2.82E-06	0.82	0.36
Gray_SV_4	8.86E-07	4.66E-07	1.35E-06	0.85	0.27	1.20E-06	7.78E-07	1.97E-06	0.82	0.31
Gray_SV_5	1.59E-06	7.86E-07	2.38E-06	0.86	0.36	2.74E-06	8.63E-07	3.61E-06	0.91	0.47
SCOM_TV_1	1.51E-05	6.27E-06	2.13E-05	0.88	0.06	2.01E-05	1.34E-05	3.35E-05	0.82	0.07
SCOM_TV_2	1.42E-05	6.02E-06	2.02E-05	0.88	0.06	1.61E-05	1.01E-05	2.63E-05	0.83	0.06
SCOM_TV_3	1.00E-05	5.00E-06	1.50E-05	0.86	0.05	1.05E-05	8.94E-06	1.94E-05	0.78	0.05
SCOM_TV_4	1.32E-05	4.72E-06	1.79E-05	0.89	0.06	1.35E-05	9.25E-06	2.28E-05	0.81	0.06
SCOM_TV_5	7.72E-05	1.15E-05	8.87E-05	0.95	0.14	0.000151098	3.41E-05	0.000185215	0.93	0.20
PCA1_TV_1	0.00026666	0.000118767	0.000385427	0.87	-130.42	0.000484008	0.001543852	0.002027861	0.48	41.99
PCA1_TV_2	0.000281052	0.000125926	0.000406978	0.87	-73.44	0.000531506	0.000823554	0.00135506	0.66	61.92
PCA1_TV_3	0.00036161	0.00010063	0.00046224	0.92	-109.13	0.000332291	0.000438158	0.000770449	0.69	43.82
PCA1_TV_4	0.000534706	0.000152326	0.000687033	0.91	1446.09	0.000496159	0.000341839	0.000837998	0.81	37.70
PCA1_TV_5	0.005923407	0.000744076	0.006667483	0.96	69.14	0.002973082	0.001454879	0.004427961	0.86	30.20
PCA1_SV_1	0.00016189	5.63E-05	0.000218223	0.90	767.90	0.000196592	0.000405563	0.000602155	0.59	33.32
PCA1_SV_2	0.000150928	6.32E-05	0.000214085	0.88	-94.03	0.000282833	0.000331753	0.000614586	0.72	54.76
PCA1_SV_3	0.00016241	7.24E-05	0.000234808	0.87	-86.16	0.000175159	0.000186691	0.00036185	0.74	61.83
PCA1_SV_4	0.000313683	0.000138619	0.000452302	0.87	-1507.62	0.000238988	0.000180946	0.000419935	0.80	68.95
PCA1_SV_5	0.002036969	0.000401901	0.002438871	0.94	66.65	0.000975145	0.00079676	0.001771905	0.79	35.67
PCA2_SV_1	9.88099961	5.028664781	14.90966439	0.85	7.56	18.85445282	46.68926993	65.54372275	0.55	8.29
PCA2_SV_2	10.317671	4.003639365	14.32131036	0.89	7.86	21.23524591	34.21132689	55.44657279	0.65	8.63
PCA2_SV_3	23.98864199	4.497901338	28.48654332	0.94	10.73	15.69654859	15.97241152	31.66896011	0.75	6.82
PCA2_SV_4	43.17716945	11.14029461	54.31746406	0.92	12.28	24.80031828	12.85601685	37.65633513	0.85	7.72
PCA2_SV_5	483.1025259	58.33231441	541.4348403	0.96	26.97	323.439747	124.1614536	447.6012007	0.89	18.29
SLR1_TV_1	17.03166021	9.114684001	26.14634421	0.85	-187.72	26.07402319	70.41838526	96.49240844	0.53	43.44
SLR1_TV_2	22.35029931	8.32568424	30.67598355	0.89	-97.91	36.62484704	41.80330522	78.42815227	0.72	100.37

SLR1_TV_3	39.308714	8.933689328	48.24240333	0.93	1048.16	22.88250366	16.21209066	39.09459432	0.81	67.56
SLR1_TV_4	43.98378282	10.75967396	54.74345678	0.92	53.00	31.79722097	9.368979563	41.16620053	0.91	38.75
SLR1_TV_5	46.66365673	15.63126872	62.29492544	0.90	19.05	25.52792879	11.762878	37.29080679	0.87	16.16
SLR1_SV_1	57.74611132	18.94608132	76.69219264	0.90	12.35	44.82738191	28.14928938	72.97667129	0.83	13.21
SLR1_SV_2	60.26726087	20.96413454	81.23139541	0.90	12.96	41.55335349	23.57105583	65.12440932	0.84	13.17
SLR1_SV_3	78.61261597	25.68453146	104.2971474	0.90	12.59	62.82287809	34.31239744	97.13527552	0.85	14.18
SLR1_SV_4	128.838182	49.34415166	178.1823336	0.89	12.04	101.8900445	49.62965611	151.5197006	0.86	13.18
SLR1_SV_5	132.8475485	68.39954878	201.2470973	0.85	10.52	138.5704543	53.95379544	192.5242497	0.89	13.30
SLR2_TV_1	9.954958563	4.296133339	14.2510919	0.87	19.36	13.08932801	20.00459597	33.09392398	0.66	16.11
SLR2_TV_2	15.84615789	4.002091924	19.84824982	0.92	29.14	19.86241687	13.99061149	33.85302836	0.81	26.26
SLR2_TV_3	23.33852736	5.115009751	28.45353711	0.93	28.73	16.92213621	6.211567891	23.1337041	0.89	25.35
SLR2_TV_4	25.6005145	5.467316988	31.06783149	0.93	20.17	21.84630389	5.212265433	27.05856932	0.93	22.10
SLR2_TV_5	27.86157307	8.943890886	36.80546396	0.90	14.53	31.66275973	9.945410521	41.60817025	0.91	20.38
SLR2_SV_1	56.58654381	9.327536124	65.91407994	0.95	12.15	45.03619336	27.21807334	72.25426669	0.83	13.89
SLR2_SV_2	48.08130979	9.649250614	57.7305604	0.94	11.64	36.73307341	22.71277019	59.4458436	0.83	13.51
SLR2_SV_3	46.06916018	12.82147702	58.8906372	0.92	10.62	41.82453786	30.74064323	72.56518109	0.80	14.10
SLR2_SV_4	77.02861039	26.67401435	103.7026247	0.90	11.10	73.62950415	40.39304083	114.022545	0.85	14.73
SLR2_SV_5	49.5517637	40.26833634	89.82010004	0.79	8.47	52.45555592	31.71590048	84.1714564	0.83	12.67
SLR3_TV_1	1.464683918	0.540897396	2.005581314	0.89	3.72	1.089125098	2.239306129	3.328431227	0.59	2.93
SLR3_TV_2	1.382010016	0.478595465	1.860605481	0.90	3.61	1.480997407	1.748240921	3.229238328	0.72	3.44
SLR3_TV_3	2.484249983	0.530510755	3.014760738	0.93	4.57	0.745441982	0.686798772	1.432240754	0.77	2.37
SLR3_TV_4	2.521077433	0.579193665	3.100271098	0.93	4.22	0.931355148	0.324047453	1.255402601	0.90	2.54
SLR3_TV_5	4.790185216	2.317840146	7.108025362	0.86	5.28	3.783128254	3.302663222	7.085791476	0.77	4.96
SLR3_SV_1	7.119073262	3.568269597	10.68734286	0.86	4.96	4.254449343	4.497059771	8.751509114	0.74	4.13
SLR3_SV_2	9.742183939	4.130010564	13.8721945	0.88	5.71	6.289346455	4.0627695	10.35211595	0.82	4.92
SLR3_SV_3	10.95430942	4.369351802	15.32366122	0.88	5.55	9.646140612	4.896650286	14.5427909	0.86	5.60
SLR3_SV_4	12.87708988	5.730289141	18.60737902	0.87	5.30	10.438384	5.668895955	16.10727995	0.85	5.12
SLR3_SV_5	11.11868805	8.561790521	19.68047858	0.80	4.78	18.7160154	7.36974545	26.08576085	0.88	6.60
SLR4_SV_1	21.22169887	12.98731255	34.20901141	0.83	8.83	13.97022908	15.85530662	29.8255357	0.73	7.84

SLR4_SV_2	30.76475232	14.3785724	45.14332472	0.87	10.52	19.19869888	13.19164931	32.39034819	0.81	8.97
SLR4_SV_3	45.32889416	15.84117757	61.17007173	0.90	10.77	33.11510449	14.28987324	47.40497773	0.87	10.07
SLR4_SV_4	60.80554966	23.92840867	84.73395833	0.88	9.79	41.42283529	18.66674755	60.08958284	0.87	8.85
SLR4_SV_5	79.23595713	32.10860848	111.3445656	0.88	9.76	91.63084076	23.20328718	114.8341279	0.92	11.30
SLR5_TV_1	9.903033509	3.888885495	13.791919	0.88	45.91	11.18274415	30.25640428	41.43914843	0.53	19.45
SLR5_TV_2	9.624788156	3.657082143	13.2818703	0.89	49.97	14.44590822	19.96051386	34.40642209	0.68	24.03
SLR5_TV_3	16.87211717	3.416045598	20.28816277	0.94	40.24	7.538199704	8.641645641	16.17984534	0.72	15.25
SLR5_TV_4	18.9763957	4.273601502	23.2499972	0.93	24.82	10.6159872	4.344910113	14.96089731	0.88	14.39
SLR5_TV_5	27.29597285	6.587212024	33.88318487	0.93	15.21	9.532349399	5.09115921	14.62350861	0.85	8.66
I2_TV_1	0.000148865	6.11E-05	0.000209996	0.88	1.87	0.000360446	0.001069108	0.001429554	0.50	3.14
I2_TV_2	0.000142975	5.36E-05	0.000196625	0.89	1.82	0.000405832	0.000577842	0.000983674	0.68	3.29
I2_TV_3	0.000284483	5.96E-05	0.000344095	0.93	2.64	0.000218395	0.000264124	0.000482519	0.71	2.46
I2_TV_4	0.000450497	0.000109823	0.00056032	0.92	3.49	0.000441256	0.000194016	0.000635272	0.87	3.66
I2_TV_5	0.006799754	0.000687746	0.007487499	0.97	17.14	0.004656496	0.001612672	0.006269168	0.90	15.88
GMR_SV_1	0.97515099	0.207917515	1.183068505	0.93	9.27	1.245925175	0.872284213	2.118209388	0.81	8.90
GMR_SV_2	0.900151426	0.212217432	1.112368858	0.93	8.63	1.146761279	0.729925959	1.876687238	0.82	8.22
GMR_SV_3	1.169792435	0.367534563	1.537326998	0.91	10.75	1.563217296	0.904337312	2.467554608	0.84	10.23
GMR_SV_4	3.361506806	1.269868992	4.631375798	0.89	26.46	3.333125718	1.413193541	4.74631926	0.88	20.72
GMR_SV_5	45.23970809	6.432270238	51.67197833	0.95	-3338.27	41.63306846	12.58806169	54.22113016	0.91	647.99
G/R_SV_1	8.75E-05	6.35E-05	0.000151011	0.81	0.84	9.92E-05	0.000134198	0.000233433	0.69	0.89
G/R_SV_2	0.000118628	6.08E-05	0.000179437	0.85	0.97	0.000112354	8.98E-05	0.00020218	0.79	0.95
G/R_SV_3	0.000200043	6.27E-05	0.000262755	0.91	1.29	0.000153514	6.21E-05	0.000215622	0.88	1.12
G/R_SV_4	0.000325551	0.000116645	0.000442197	0.89	1.70	0.000217431	8.44E-05	0.000301822	0.89	1.38
G/R_SV_5	0.001722289	0.000266617	0.001988906	0.95	4.13	0.001155545	0.000396985	0.00155253	0.90	3.36
G/B_TV_1	0.000743999	0.000333683	0.001077682	0.87	1.71	0.001226672	0.003106682	0.004333354	0.54	2.08
G/B_TV_2	0.000733995	0.00033821	0.001072206	0.87	1.73	0.001151416	0.001584124	0.002735541	0.69	2.05
G/B_TV_3	0.000641896	0.000247202	0.000889098	0.89	1.62	0.000786061	0.000965252	0.001751314	0.71	1.70
G/B_TV_4	0.0008708	0.000292489	0.001163288	0.90	1.89	0.000925957	0.00081698	0.001742938	0.77	1.84
G/B_TV_5	0.004373817	0.000961144	0.005334961	0.93	4.02	0.001421815	0.001554538	0.002976353	0.73	2.17

AGR1	1809374.013	2905391.272	4714765.285	0.65	10.09	3161938.042	5074166.012	8236104.055	0.65	17.13
AGR2	72282385.03	20448326.78	92730711.8	0.91	32.39	26549562.29	22064030.07	48613592.36	0.78	29.38
AGR3	34353874.46	15725786.45	50079660.91	0.87	63.49	11057549.54	8556272.598	19613822.14	0.79	37.06
AGR4	25155526.17	8919501.269	34075027.44	0.89	-260.07	13722524.81	7788750.212	21511275.03	0.84	-147.97
AGR5	42204380.54	19807521.15	62011901.69	0.86	-49.44	36375712.39	26798037.33	63173749.72	0.80	-50.60
RGR1	8.86E-05	2.83E-05	0.000116924	0.90	32.88	3.74E-05	2.45E-05	6.19E-05	0.82	24.72
RGR2	3.03E-05	1.72E-05	4.75E-05	0.84	62.32	1.46E-05	1.26E-05	2.72E-05	0.78	33.65
RGR3	2.20E-05	7.85E-06	2.98E-05	0.89	-234.91	1.70E-05	1.09E-05	2.79E-05	0.82	-157.24
RGR4	7.33E-05	1.94E-05	9.27E-05	0.92	-62.18	6.39E-05	2.59E-05	8.98E-05	0.88	-51.55
AWU_Diurnal	271.9853055	153.1958875	425.1811931	0.84	13.22	128.7379984	253.1850062	381.9230046	0.60	10.39
AWU_Day	184.1542309	117.531584	301.6858148	0.82	13.20	74.9250149	169.9324732	244.8574881	0.57	9.63
AWU_Night	12.48185224	7.726152312	20.20800455	0.83	16.09	10.06594105	12.16046593	22.22640698	0.71	16.39
PSA_TUE_Diurnal	1232198.228	5077359.581	6309557.808	0.42	16.02	799495.8153	1071172.234	1870668.049	0.69	14.96
PSA_TR_Diurnal	8.93E-10	6.17E-10	1.51E-09	0.81	19.43	6.58E-10	1.30E-09	1.96E-09	0.60	14.51
PSA_TUE_Day	1792201.791	9351191.235	11143393.03	0.37	15.88	1087702.326	1641634.384	2729336.709	0.67	14.37
PSA_TR_Day	6.29E-10	4.26E-10	1.05E-09	0.82	19.78	4.24E-10	9.04E-10	1.33E-09	0.58	14.14
PSA_TUE_Night	65353573.46	93021895.89	158375469.4	0.68	20.26	50288131.58	40285326.77	90573458.35	0.79	20.53
PSA_TR_Night	2.88E-11	2.86E-11	5.74E-11	0.75	19.86	3.42E-11	4.68E-11	8.10E-11	0.69	18.71
Foliage_TUE_Diurnal	0.000217975	0.001022819	0.001240794	0.39	16.11	0.000193589	0.000144674	0.000338263	0.80	18.01
Foliage_TR_Diurnal	3.818196739	1.740008948	5.558205687	0.87	16.99	6.430064217	5.02840792	11.45847214	0.79	18.52
Foliage_TUE_Day	0.000303141	0.001913893	0.002217034	0.32	15.63	0.000263305	0.000220738	0.000484044	0.78	17.30
Foliage_TR_Day...484	2.474777075	1.259135375	3.73391245	0.85	16.61	4.165126861	3.541344658	7.706471519	0.78	18.11
Foliage_TUE_Night	0.013017948	0.016865005	0.029882953	0.70	21.55	0.011128225	0.005913966	0.017042191	0.85	23.57
Foliage_TR_Day...486	0.177071067	0.095277363	0.272348431	0.85	20.73	0.295520883	0.196793858	0.492314741	0.82	22.44

ANNEXURE 7: Variance components and genetic parameters of manual and semi-manual traits

	Control					Nitrogen				
Parameters	**Gen_var**	**Res_var**	**Phen_var**	**h2mg**	**CVg**	**Gen_var**	**Res_var**	**Phen_var**	**h2mg**	**CVg**
Straw	2.57	1.67	4.25	0.82	14.43	2.40	3.02	5.43	0.70	18.44
Total_Biomass	14.25	10.63	24.88	0.80	12.08	9.90	20.25	30.15	0.59	13.77
TotalEar	2.26	1.31	3.57	0.84	16.95	0.81	1.42	2.23	0.63	13.82
HI	0.00	0.00	0.00	0.91	6.72	0.00	0.00	0.00	0.89	6.71
FLL	6.00	9.63	15.63	0.65	9.12	7.62	8.77	16.39	0.72	12.45
FLW	0.01	0.01	0.02	0.76	5.13	0.01	0.01	0.02	0.72	6.39
FLtoEar	21.11	2.55	23.66	0.96	41.02	28.40	1.72	30.12	0.98	46.42
FLLWratio	1.91	2.06	3.97	0.74	9.57	2.23	2.02	4.24	0.77	11.29
FLLtoEarRatio	0.07	0.08	0.15	0.75	11.60	0.07	0.06	0.13	0.78	13.11
LNP	18.69	23.44	42.13	0.71	12.80	18.87	23.42	42.30	0.71	15.48
TNP	1.36	1.90	3.25	0.68	13.02	1.48	1.92	3.40	0.70	16.92
PH	144.08	9.20	153.28	0.98	16.25	162.80	10.98	173.78	0.98	17.38
SPAD1	4.17	3.20	7.37	0.80	4.08	4.59	8.04	12.62	0.63	4.84
SPAD2	7.73	6.93	14.66	0.77	5.63	11.14	10.02	21.16	0.77	7.79
Phy3	3.06	0.69	3.75	0.93	13.78	2.22	0.47	2.70	0.93	11.76
Phy4	1.84	0.49	2.33	0.92	16.47	1.58	0.34	1.92	0.93	15.20
Phy5	1.11	0.16	1.27	0.95	21.10	1.57	0.11	1.68	0.98	23.97
DTG	0.20	0.17	0.37	0.79	4.60	0.19	0.13	0.32	0.82	4.54
DTB	4.75	1.03	5.77	0.93	3.23	5.06	1.61	6.67	0.90	3.26
DTA	6.84	0.91	7.75	0.96	3.41	7.07	1.17	8.24	0.95	3.43
LC_SPAD1ratio	0.01	0.01	0.02	0.69	12.77	0.01	0.01	0.02	0.72	14.83
LC_SPAD2ratio	0.01	0.01	0.02	0.75	15.07	0.02	0.02	0.04	0.73	20.20
TC_SPAD1ratio	0.00	0.00	0.00	0.68	13.39	0.00	0.00	0.00	0.72	16.42
TC_SPAD2ratio	0.00	0.00	0.00	0.71	14.79	0.00	0.00	0.00	0.70	19.63
LER	0.18	0.05	0.23	0.92	4.97	0.16	0.03	0.19	0.94	4.58

LER_DTBratio	0.18	0.05	0.24	0.91	5.45	0.18	0.03	0.21	0.94	5.36
LER_DTAratio	0.27	0.06	0.33	0.93	5.87	0.25	0.04	0.29	0.95	5.63
SPADatio	0.00	0.00	0.01	0.62	4.43	0.00	0.01	0.01	0.66	6.96
LPTveg	0.06	0.09	0.14	0.66	6.24	0.08	0.11	0.19	0.68	7.22
SPAD1total	54245.21	84890.95	139136.16	0.66	12.37	56247.21	72816.95	129064.16	0.70	18.88
SPAD2total	65881.47	81046.65	146928.12	0.71	13.81	53663.77	58136.40	111800.17	0.73	19.19
FLA	18.10	30.51	48.61	0.64	11.32	20.79	26.54	47.33	0.70	16.20
PH_FLLratio	0.20	0.14	0.34	0.81	16.12	0.45	0.21	0.66	0.86	19.61
SpikeLength	0.82	0.26	1.08	0.90	7.84	0.70	0.31	1.01	0.87	7.74
SpikeletNo	2.74	0.31	3.05	0.96	8.28	2.51	0.26	2.77	0.97	7.85
SSN	2.03	1.23	3.26	0.83	41.25	0.94	0.45	1.39	0.86	34.12
GPS	0.06	0.05	0.10	0.79	9.27	0.06	0.05	0.11	0.77	9.77
SpikeletDensity	0.02	0.02	0.04	0.81	8.55	0.03	0.01	0.04	0.89	9.17
SFP	38.23	28.41	66.64	0.80	7.45	17.18	10.63	27.82	0.83	4.82
SFI	75.99	38.84	114.83	0.85	11.23	84.80	46.75	131.54	0.84	11.18
SpikeWt_ME	0.37	0.21	0.59	0.84	10.22	0.34	0.30	0.64	0.78	10.81
SpikeWt_TE	6.43	3.92	10.36	0.83	17.91	2.53	6.27	8.79	0.55	17.65
SpikeWt_AE	7.06	4.42	11.48	0.83	13.20	3.32	8.10	11.42	0.55	12.62
GrainWt_ME	0.28	0.15	0.43	0.84	11.38	0.23	0.19	0.42	0.79	11.45
GrainWt_TE	3.81	2.31	6.12	0.83	18.84	1.43	3.57	5.00	0.55	18.04
GrainWt_AE	4.43	2.69	7.12	0.83	14.04	2.00	4.65	6.65	0.56	13.03
ChaffWt_ME	0.02	0.01	0.03	0.84	10.61	0.02	0.02	0.04	0.76	12.32
ChaffWt_TE	0.71	0.39	1.10	0.85	22.23	0.39	0.48	0.87	0.71	26.20
ChaffWt_AE	0.76	0.41	1.16	0.85	16.90	0.44	0.59	1.03	0.69	18.52
TotalGrainNo_ME	89.00	67.41	156.41	0.80	9.11	88.28	88.07	176.35	0.75	9.57
TotalGrainNo_TE	3501.17	1312.67	4813.85	0.89	22.11	1204.06	2074.28	3278.34	0.64	20.24
TotalGrainNo_AE	3979.94	1395.27	5375.21	0.90	17.00	1501.61	2544.98	4046.59	0.64	14.37
GPB_ME	4.81	3.41	8.22	0.81	14.53	6.29	10.64	16.92	0.64	13.02
GPB_TE	11.03	3.97	15.00	0.89	10.11	7.87	11.80	19.67	0.67	9.87

GPB_AE	10.38	3.20	13.58	0.91	6.72	10.16	3.46	13.62	0.90	6.69
AGPB_ME	1.20	0.85	2.06	0.81	14.53	1.57	2.66	4.23	0.64	13.02
AGPB_TE	0.77	0.57	1.34	0.80	17.31	0.93	1.88	2.81	0.60	14.19
AGPB_AE	1.02	0.69	1.71	0.82	17.87	1.35	2.50	3.85	0.62	15.01
CPB_ME	0.44	0.27	0.71	0.83	15.08	0.60	0.88	1.49	0.67	14.12
CPB_TE	3.91	1.85	5.76	0.86	16.40	4.67	2.40	7.06	0.85	21.16
CPB_AE	3.92	1.70	5.62	0.87	12.02	4.76	1.93	6.69	0.88	13.89
ACPB_ME	0.11	0.07	0.18	0.83	15.08	0.15	0.22	0.37	0.67	14.12
ACPB_TE	0.19	0.14	0.32	0.81	23.31	0.51	0.58	1.09	0.72	28.58
ACPB_AE	0.15	0.10	0.25	0.82	20.16	0.27	0.35	0.62	0.70	20.39
AvgSpikeWt_ME	0.09	0.05	0.15	0.84	10.22	0.09	0.07	0.16	0.78	10.81
AvgSpikeWt_TE	0.08	0.07	0.15	0.80	13.70	0.07	0.08	0.16	0.73	13.45
AvgSpikeWt_AE	0.09	0.06	0.15	0.82	13.12	0.08	0.07	0.15	0.79	12.69
AvgGrainWt_ME	0.07	0.04	0.11	0.84	11.38	0.06	0.05	0.11	0.79	11.45
AvgGrainWt_TE	0.05	0.04	0.09	0.78	14.24	0.04	0.05	0.09	0.70	13.26
AvgGrainWt_AE	0.06	0.04	0.10	0.82	14.00	0.05	0.04	0.09	0.78	13.15
AvgChaffWt_ME	0.01	0.00	0.01	0.84	10.61	0.01	0.01	0.01	0.76	12.32
AvgChaffWt_TE	0.01	0.01	0.02	0.84	20.46	0.02	0.01	0.03	0.85	26.42
AvgChaffWt_AE	0.01	0.01	0.02	0.85	16.81	0.01	0.01	0.02	0.85	18.86
GWCWratio_ME	0.15	0.06	0.21	0.87	11.05	0.14	0.06	0.20	0.87	10.55
GWCWratio_TE	0.38	0.17	0.55	0.87	21.51	1.17	0.51	1.68	0.87	35.57
GWCWratio_AE	0.25	0.09	0.34	0.89	16.72	0.39	0.13	0.51	0.90	19.76
PHI_ME	0.00	0.00	0.00	0.87	2.64	0.00	0.00	0.00	0.82	2.38
PHI_TE	0.00	0.00	0.00	0.86	5.36	0.00	0.00	0.00	0.86	7.14
PHI_AE	0.00	0.00	0.00	0.88	4.14	0.00	0.00	0.00	0.89	4.46
TKW_ME	20.06	8.15	28.20	0.88	9.99	14.98	5.10	20.09	0.90	8.97
TKW_TE	23.45	6.98	30.43	0.91	12.30	14.89	6.59	21.48	0.87	9.94
TKW_AE	22.80	5.31	28.11	0.93	11.67	15.10	3.81	18.91	0.92	9.60
AvgGrainNo_ME	22.25	16.85	39.10	0.80	9.11	22.07	22.02	44.09	0.75	9.57

AvgGrainNo_TE	17.36	18.58	35.94	0.74	10.53	16.76	23.46	40.22	0.68	10.64
AvgGrainNo_AE	17.63	16.82	34.44	0.76	9.90	18.95	18.26	37.21	0.76	10.41
SeedArea_TE	1.47	0.39	1.85	0.92	6.69	1.06	0.38	1.43	0.89	5.81
SeedArea_ME	1.25	0.67	1.93	0.85	5.62	1.21	0.50	1.71	0.88	5.65
SeedArea_AE	1.33	0.36	1.69	0.92	6.06	1.09	0.30	1.39	0.92	5.63
SeedArea_Low_TE	2.46	0.86	3.32	0.90	11.67	1.75	0.84	2.60	0.86	9.48
SeedArea_Low_ME	1.85	2.55	4.39	0.68	9.30	2.10	2.11	4.21	0.75	9.98
SeedArea_Low_AE	1.90	0.98	2.87	0.85	9.83	1.72	0.83	2.55	0.86	9.19
SeedArea_Top_TE	1.56	0.42	1.98	0.92	5.79	1.15	0.68	1.83	0.84	5.24
SeedArea_Top_ME	1.53	0.76	2.28	0.86	5.33	1.52	0.63	2.15	0.88	5.46
SeedArea_Top_AE	1.50	0.40	1.90	0.92	5.48	1.27	0.49	1.76	0.89	5.23
SeedPerimeter_TE	0.58	0.11	0.69	0.94	3.51	0.51	0.13	0.63	0.92	3.34
SeedPerimeter_ME	0.52	0.20	0.72	0.89	3.25	0.50	0.18	0.67	0.89	3.20
SeedPerimeter_AE	0.54	0.10	0.64	0.94	3.34	0.49	0.10	0.58	0.94	3.23
SeedPerimeter_Low_TE	0.99	0.35	1.33	0.90	5.21	0.80	0.37	1.18	0.87	4.66
SeedPerimeter_Low_ME	0.87	1.48	2.35	0.64	4.82	0.89	1.27	2.17	0.68	4.89
SeedPerimeter_Low_AE	0.81	0.50	1.31	0.83	4.68	0.74	0.44	1.18	0.83	4.47
SeedPerimeter_Top_TE	0.57	0.15	0.72	0.92	3.24	0.52	0.19	0.71	0.89	3.19
SeedPerimeter_Top_ME	0.62	0.42	1.05	0.82	3.31	0.61	0.37	0.97	0.83	3.32
SeedPerimeter_Top_AE	0.57	0.16	0.73	0.91	3.20	0.53	0.19	0.72	0.90	3.17
SeedLength_TE	0.08	0.01	0.09	0.96	3.94	0.07	0.01	0.09	0.94	3.88
SeedLength_ME	0.09	0.02	0.11	0.92	3.99	0.07	0.02	0.10	0.90	3.74
SeedLength_AE	0.08	0.01	0.09	0.96	3.93	0.07	0.01	0.09	0.95	3.77
SeedLength_Low_TE	0.10	0.04	0.14	0.89	4.99	0.09	0.04	0.14	0.87	4.76
SeedLength_Low_ME	0.15	0.27	0.43	0.63	6.05	0.13	0.19	0.32	0.67	5.64
SeedLength_Low_AE	0.11	0.08	0.19	0.80	5.04	0.09	0.06	0.15	0.82	4.69
SeedLength_Top_TE	0.08	0.02	0.10	0.94	3.79	0.07	0.02	0.09	0.93	3.68
SeedLength_Top_ME	0.09	0.02	0.12	0.92	3.89	0.09	0.03	0.11	0.90	3.80
SeedLength_Top_AE	0.08	0.01	0.10	0.95	3.79	0.08	0.02	0.09	0.93	3.68

SeedWidth_TE	0.02	0.01	0.03	0.91	4.85	0.02	0.01	0.02	0.88	4.01
SeedWidth_ME	0.02	0.01	0.03	0.85	3.95	0.02	0.01	0.02	0.89	3.99
SeedWidth_AE	0.02	0.01	0.03	0.92	4.32	0.02	0.00	0.02	0.92	3.93
SeedWidth_Low_TE	0.05	0.02	0.06	0.89	8.18	0.03	0.01	0.05	0.88	6.64
SeedWidth_Low_ME	0.03	0.02	0.06	0.80	6.24	0.04	0.02	0.06	0.84	6.75
SeedWidth_Low_AE	0.04	0.01	0.05	0.89	6.95	0.03	0.01	0.04	0.90	6.54
SeedWidth_Top_TE	0.02	0.01	0.03	0.90	3.77	0.01	0.01	0.02	0.79	3.29
SeedWidth_Top_ME	0.02	0.01	0.03	0.82	3.41	0.02	0.01	0.03	0.83	3.41
SeedWidth_Top_AE	0.02	0.01	0.02	0.90	3.47	0.01	0.01	0.02	0.85	3.24
SeedLWR_TE	0.02	0.00	0.02	0.94	5.91	0.01	0.00	0.02	0.93	5.36
SeedLWR_ME	0.02	0.00	0.02	0.93	5.70	0.01	0.00	0.02	0.92	5.32
SeedLWR_AE	0.02	0.00	0.02	0.95	5.72	0.01	0.00	0.02	0.95	5.29
SeedLWR_Low_TE	0.03	0.01	0.04	0.87	7.04	0.02	0.01	0.03	0.90	6.54
SeedLWR_Low_ME	0.03	0.04	0.07	0.73	7.87	0.03	0.02	0.05	0.80	7.73
SeedLWR_Low_AE	0.03	0.01	0.04	0.86	7.00	0.02	0.01	0.03	0.90	6.74
SeedLWR_Top_TE	0.01	0.00	0.01	0.92	5.04	0.01	0.00	0.01	0.89	4.66
SeedLWR_Top_ME	0.01	0.00	0.02	0.89	5.12	0.01	0.01	0.01	0.85	4.82
SeedLWR_Top_AE	0.01	0.00	0.01	0.93	4.91	0.01	0.00	0.01	0.91	4.63

ANNEXURE 8: Phenotypic and genotypic correlations of HTP traits under control and nitrogen deficiency condition

TraitID	Phenotypic Correlations	Genetic Correlations	TraitID	Phenotypic Correlations	Genetic Correlations
Biovolume_1	0.32	0.46	**Blue_TV_3**	0.86	0.91
PSA_1	0.27	0.41	**Green_TV_3**	0.77	0.85
2MPASA_TV_1	0.42	0.56	**Red_TV_3**	0.77	0.85
2MPASN_TV_1	0.28	0.61	**Blue_SV_3**	0.74	0.84
Area_TV_1	0.38	0.54	**Green_SV_3**	0.68	0.78
BPC_TV_1	0.21	0.31	**Red_SV_3**	0.71	0.81
BPR_TV_1	0.41	0.56	**b_TV_3**	0.51	0.64
BPAR_TV_1	0.69	0.83	**g_TV_3**	0.63	0.78
Compactness_TV_1	0.37	0.54	**b_SV_3**	0.48	0.59
CHArea_TV_1	0.37	0.55	**r_SV_3**	0.68	0.78
ObjectExtentY_TV_1	0.35	0.57	**R-G_TV_3**	0.76	0.84
MARA_TV_1	0.34	0.55	**R-B_TV_3**	0.56	0.67
AZR2M_TV_1	0.45	0.61	**(R-G)/(R+G+B)_TV_3**	0.70	0.83
NZR2M_TV_1	0.36	0.51	**(G-B)/(R+G+B)_SV_3**	0.65	0.79
2MPALA_SV_1	0.68	0.79	**Ipca_SV_3**	0.50	0.61
2MPASA_SV_1	0.37	0.52	**ExB_SV_3**	0.62	0.76
2MPALN_SV_1	0.84	0.92	**ExG_SV_3**	0.76	0.89
2MPASN_SV_1	0.58	0.80	**Gray_TV_3**	0.56	0.71
2MPAR_SV_1	0.88	0.95	**Gray_SV_3**	0.69	0.83
Area_SV_1	0.25	0.38	**SCOM_TV_3**	0.67	0.82
ADAR_SV_1	0.18	0.43	**PCA1_TV_3**	0.49	0.62
BPC_SV_1	0.27	0.39	**PCA1_SV_3**	0.40	0.49
BPR_SV_1	0.37	0.50	**PCA2_SV_3**	0.56	0.67
BPAR_SV_1	0.58	0.73	**SLR1_TV_3**	0.62	0.71
Circumference_SV_1	0.44	0.69	**SLR1_SV_3**	0.78	0.89
cmY_SV_1	0.74	0.86	**SLR2_TV_3**	0.76	0.84

Compactness_SV_1	0.64	0.80	**SLR2_SV_3**	0.73	0.85
CHArea_SV_1	0.64	0.79	**SLR3_TV_3**	0.58	0.69
Circumference_SV_1	0.74	0.86	**SLR3_SV_3**	0.77	0.89
Excentricity_SV_1	0.88	0.95	**SLR4_SV_3**	0.79	0.90
ObjectExtentX_SV_1	0.60	0.78	**SLR5_TV_3**	0.51	0.62
ObjectExtentY_SV_1	0.76	0.87	**I2_TV_3**	0.51	0.62
PSCC_1_1	0.31	0.46	**GMR_SV_3**	0.78	0.90
PSCC_2_1	0.31	0.45	**G/R_SV_3**	0.80	0.90
PSCC_3_1	0.31	0.45	**G/B_TV_3**	0.53	0.67
PSCC_4_1	0.22	0.33	**Biovolume_4**	0.36	0.47
PSCC_5_1	0.26	0.39	**PSA_4**	0.35	0.46
PSCC_6_1	0.47	0.65	**2MPASA_TV_4**	0.47	0.64
PSCC_7_1	0.55	0.74	**2MPASN_TV_4**	0.30	1.00
PSCC_8_1	0.54	0.85	**Area_TV_4**	0.46	0.58
PSCC_9_1	0.33	0.64	**BPC_TV_4**	0.31	0.41
PSCC_10_1	0.38	0.59	**BPR_TV_4**	0.32	0.41
PSCC_11_1	0.68	0.82	**BPAR_TV_4**	0.44	0.58
PSCC_12_1	0.36	0.51	**Compactness_TV_4**	0.34	0.52
PSCC_13_1	0.34	0.48	**CHArea_TV_4**	0.62	0.82
PSCC_14_1	0.47	0.64	**ObjectExtentY_TV_4**	0.46	0.77
PSCC_15_1	0.50	0.67	**MARA_TV_4**	0.61	0.82
PSCC_16_1	0.50	0.68	**AZR2M_TV_4**	0.53	0.68
PSCC_17_1	0.29	0.42	**NZR2M_TV_4**	0.29	0.44
PSCC_18_1	0.22	0.34	**2MPALA_SV_4**	0.77	0.83
PSCC_19_1	0.25	0.35	**2MPASA_SV_4**	0.38	0.51
PSCC_20_1	0.25	0.33	**2MPALN_SV_4**	0.83	0.90
No PSCC_1	0.31	0.42	**2MPASN_SV_4**	0.42	0.56
NIR TV_1	0.78	0.90	**2MPAR_SV_4**	0.91	0.97
NIR SV_1	0.95	0.98	**Area_SV_4**	0.31	0.42

IR TV_1	0.97	0.98	**ADAR_SV_4**	0.13	0.35
IR SV_1	1.00	1.00	**BPC_SV_4**	0.38	0.49
Blue_TV_1	0.87	0.92	**BPR_SV_4**	0.52	0.64
Green_TV_1	0.77	0.84	**BPAR_SV_4**	0.64	0.78
Red_TV_1	0.76	0.83	**Circumference_SV_4**	0.25	0.76
Blue_SV_1	0.48	0.67	**cmY_SV_4**	0.90	0.95
Green_SV_1	0.47	0.64	**Compactness_SV_4**	0.69	0.81
Red_SV_1	0.41	0.59	**CHArea_SV_4**	0.82	0.90
b_TV_1	0.23	0.35	**Circumference_SV_4**	0.90	0.94
g_TV_1	0.56	0.70	**Excentricity_SV_4**	0.94	0.98
b_SV_1	0.47	0.63	**ObjectExtentX_SV_4**	0.46	0.72
r_SV_1	0.25	0.39	**ObjectExtentY_SV_4**	0.93	0.96
R-G_TV_1	0.80	0.87	**PSCC_1_4**	0.46	0.61
R-B_TV_1	0.43	0.56	**PSCC_2_4**	0.49	0.63
(R-G)/(R+G+B)_TV_1	0.73	0.83	**PSCC_3_4**	0.47	0.60
(G-B)/(R+G+B)_SV_1	0.59	0.76	**PSCC_4_4**	0.36	0.52
Ipca_SV_1	0.48	0.62	**PSCC_5_4**	0.33	0.48
ExB_SV_1	0.58	0.74	**PSCC_6_4**	0.36	0.49
ExG_SV_1	0.66	0.83	**PSCC_7_4**	0.41	0.59
Gray_TV_1	0.40	0.55	**PSCC_8_4**	0.37	0.55
Gray_SV_1	0.62	0.78	**PSCC_9_4**	0.27	0.42
SCOM_TV_1	0.66	0.78	**PSCC_10_4**	0.26	0.41
PCA1_TV_1	0.17	0.26	**PSCC_11_4**	0.47	0.60
PCA1_SV_1	0.36	0.50	**PSCC_12_4**	0.17	0.26
PCA2_SV_1	0.31	0.46	**PSCC_13_4**	0.24	0.34
SLR1_TV_1	0.17	0.25	**PSCC_14_4**	0.29	0.40
SLR1_SV_1	0.75	0.86	**PSCC_15_4**	0.37	0.49
SLR2_TV_1	0.46	0.61	**PSCC_16_4**	0.47	0.61
SLR2_SV_1	0.76	0.86	**PSCC_17_4**	0.52	0.64

SLR3_TV_1	0.29	0.40	**PSCC_18_4**	0.58	0.68
SLR3_SV_1	0.66	0.83	**PSCC_19_4**	0.59	0.70
SLR4_SV_1	0.63	0.81	**PSCC_20_4**	0.66	0.77
SLR5_TV_1	0.18	0.26	**No PSCC_4**	0.57	0.68
I2_TV_1	0.18	0.27	**NIR TV_4**	0.78	0.86
GMR_SV_1	0.75	0.87	**NIR SV_4**	0.80	0.87
G/R_SV_1	0.57	0.77	**IR TV_4**	0.98	0.99
G/B_TV_1	0.31	0.45	**IR SV_4**	0.99	0.99
Biovolume_2	0.24	0.34	**Blue_TV_4**	0.89	0.92
PSA_2	0.23	0.33	**Green_TV_4**	0.84	0.89
2MPASA_TV_2	0.29	0.39	**Red_TV_4**	0.85	0.90
2MPASN_TV_2	0.25	0.45	**Blue_SV_4**	0.73	0.82
Area_TV_2	0.27	0.37	**Green_SV_4**	0.73	0.81
BPC_TV_2	0.19	0.27	**Red_SV_4**	0.74	0.82
BPR_TV_2	0.48	0.63	**b_TV_4**	0.70	0.83
BPAR_TV_2	0.60	0.74	**g_TV_4**	0.70	0.84
Compactness_TV_2	0.61	0.76	**b_SV_4**	0.51	0.63
CHArea_TV_2	0.33	0.45	**r_SV_4**	0.69	0.78
ObjectExtentY_TV_2	0.18	0.31	**R-G_TV_4**	0.77	0.85
MARA_TV_2	0.39	0.54	**R-B_TV_4**	0.77	0.85
AZR2M_TV_2	0.29	0.38	**(R-G)/(R+G+B)_TV_4**	0.83	0.92
NZR2M_TV_2	0.38	0.56	**(G-B)/(R+G+B)_SV_4**	0.65	0.78
2MPALA_SV_2	0.69	0.77	**Ipca_SV_4**	0.65	0.74
2MPASA_SV_2	0.30	0.40	**ExB_SV_4**	0.61	0.75
2MPALN_SV_2	0.86	0.94	**ExG_SV_4**	0.75	0.87
2MPASN_SV_2	0.66	0.81	**Gray_TV_4**	0.68	0.82
2MPAR_SV_2	0.90	0.94	**Gray_SV_4**	0.69	0.82
Area_SV_2	0.24	0.35	**SCOM_TV_4**	0.75	0.87
ADAR_SV_2	0.09	0.27	**PCA1_TV_4**	0.73	0.84

BPC_SV_2	0.35	0.47	**PCA1_SV_4**	0.53	0.64
BPR_SV_2	0.52	0.65	**PCA2_SV_4**	0.68	0.77
BPAR_SV_2	0.72	0.86	**SLR1_TV_4**	0.83	0.91
Circumference_SV_2	0.23	0.40	**SLR1_SV_4**	0.76	0.87
cmY_SV_2	0.79	0.87	**SLR2_TV_4**	0.86	0.93
Compactness_SV_2	0.68	0.83	**SLR2_SV_4**	0.78	0.89
CHArea_SV_2	0.62	0.75	**SLR3_TV_4**	0.82	0.90
Circumference_SV_2	0.75	0.86	**SLR3_SV_4**	0.72	0.83
Excentricity_SV_2	0.90	0.95	**SLR4_SV_4**	0.74	0.85
ObjectExtentX_SV_2	0.38	0.51	**SLR5_TV_4**	0.79	0.87
ObjectExtentY_SV_2	0.80	0.91	**I2_TV_4**	0.79	0.88
PSCC_1_2	0.45	0.62	**GMR_SV_4**	0.78	0.88
PSCC_2_2	0.43	0.58	**G/R_SV_4**	0.75	0.85
PSCC_3_2	0.44	0.60	**G/B_TV_4**	0.69	0.82
PSCC_4_2	0.36	0.48	**Biovolume_5**	0.74	0.83
PSCC_5_2	0.37	0.48	**PSA_5**	0.62	0.73
PSCC_6_2	0.54	0.69	**2MPASA_TV_5**	0.72	0.84
PSCC_7_2	0.59	0.76	**2MPASN_TV_5**	0.65	0.94
PSCC_8_2	0.49	0.78	**Area_TV_5**	0.86	0.91
PSCC_9_2	0.32	0.57	**BPC_TV_5**	0.68	0.76
PSCC_10_2	0.42	0.61	**BPR_TV_5**	0.13	0.16
PSCC_11_2	0.60	0.74	**BPAR_TV_5**	0.75	0.85
PSCC_12_2	0.42	0.56	**Compactness_TV_5**	0.77	0.90
PSCC_13_2	0.42	0.57	**CHArea_TV_5**	0.76	0.87
PSCC_14_2	0.51	0.66	**ObjectExtentY_TV_5**	0.66	0.86
PSCC_15_2	0.53	0.71	**MARA_TV_5**	0.74	0.86
PSCC_16_2	0.48	0.64	**AZR2M_TV_5**	0.75	0.85
PSCC_17_2	0.21	0.29	**NZR2M_TV_5**	0.46	1.00
PSCC_18_2	0.23	0.32	**2MPALA_SV_5**	0.79	0.85

PSCC_19_2	0.41	0.55	**2MPASA_SV_5**	0.52	0.65
PSCC_20_2	0.53	0.66	**2MPALN_SV_5**	0.86	0.92
No PSCC_2	0.38	0.49	**2MPASN_SV_5**	0.33	0.53
NIR TV_2	0.89	0.95	**2MPAR_SV_5**	0.84	0.92
NIR SV_2	0.93	0.97	**Area_SV_5**	0.44	0.56
IR TV_2	0.96	0.98	**ADAR_SV_5**	0.08	0.27
IR SV_2	0.99	0.99	**BPC_SV_5**	0.57	0.67
Blue_TV_2	0.85	0.90	**BPR_SV_5**	0.63	0.72
Green_TV_2	0.77	0.85	**BPAR_SV_5**	0.40	0.52
Red_TV_2	0.75	0.83	**Circumference_SV_5**	0.24	0.99
Blue_SV_2	0.64	0.78	**cmY_SV_5**	0.92	0.96
Green_SV_2	0.58	0.72	**Compactness_SV_5**	0.69	0.83
Red_SV_2	0.56	0.70	**CHArea_SV_5**	0.84	0.90
b_TV_2	0.47	0.62	**Circumference_SV_5**	0.92	0.95
g_TV_2	0.63	0.76	**Excentricity_SV_5**	0.91	0.96
b_SV_2	0.69	0.84	**ObjectExtentX_SV_5**	0.57	0.75
r_SV_2	0.36	0.50	**ObjectExtentY_SV_5**	0.94	0.97
R-G_TV_2	0.79	0.88	**PSCC_1_5**	0.40	0.54
R-B_TV_2	0.53	0.65	**PSCC_2_5**	0.32	0.44
(R-G)/(R+G+B)_TV_2	0.65	0.74	**PSCC_3_5**	0.21	0.29
(G-B)/(R+G+B)_SV_2	0.75	0.89	**PSCC_4_5**	0.25	0.37
Ipca_SV_2	0.56	0.70	**PSCC_5_5**	0.41	0.54
ExB_SV_2	0.74	0.88	**PSCC_6_5**	0.45	0.56
ExG_SV_2	0.75	0.88	**PSCC_7_5**	0.56	0.69
Gray_TV_2	0.56	0.71	**PSCC_8_5**	0.57	0.68
Gray_SV_2	0.75	0.89	**PSCC_9_5**	0.58	0.70
SCOM_TV_2	0.66	0.78	**PSCC_10_5**	0.57	0.69
PCA1_TV_2	0.44	0.58	**PSCC_11_5**	0.62	0.72
PCA1_SV_2	0.62	0.78	**PSCC_12_5**	0.50	0.66

PCA2_SV_2	0.45	0.59	**PSCC_13_5**	0.52	0.69
SLR1_TV_2	0.51	0.64	**PSCC_14_5**	0.74	0.83
SLR1_SV_2	0.73	0.84	**PSCC_15_5**	0.81	0.88
SLR2_TV_2	0.67	0.78	**PSCC_16_5**	0.85	0.90
SLR2_SV_2	0.76	0.86	**PSCC_17_5**	0.81	0.86
SLR3_TV_2	0.48	0.60	**PSCC_18_5**	0.80	0.85
SLR3_SV_2	0.74	0.87	**PSCC_19_5**	0.81	0.86
SLR4_SV_2	0.69	0.82	**PSCC_20_5**	0.82	0.87
SLR5_TV_2	0.44	0.57	**No PSCC_5**	0.82	0.87
I2_TV_2	0.43	0.55	**NIR TV_5**	0.84	0.92
GMR_SV_2	0.75	0.86	**NIR SV_5**	0.77	0.84
G/R_SV_2	0.63	0.77	**IR TV_5**	0.94	0.96
G/B_TV_2	0.51	0.66	**IR SV_5**	0.99	0.99
Biovolume_3	0.24	0.33	**Blue_TV_5**	0.86	0.91
PSA_3	0.23	0.33	**Green_TV_5**	0.84	0.89
2MPASA_TV_3	0.28	0.40	**Red_TV_5**	0.85	0.89
2MPASN_TV_3	0.16	0.36	**Blue_SV_5**	0.88	0.93
Area_TV_3	0.24	0.33	**Green_SV_5**	0.86	0.91
BPC_TV_3	0.20	0.28	**Red_SV_5**	0.86	0.91
BPR_TV_3	0.52	0.65	**b_TV_5**	0.73	0.83
BPAR_TV_3	0.54	0.67	**g_TV_5**	0.75	0.82
Compactness_TV_3	0.43	0.65	**b_SV_5**	0.46	0.56
CHArea_TV_3	0.35	0.52	**r_SV_5**	0.76	0.84
ObjectExtentY_TV_3	0.15	0.34	**R-G_TV_5**	0.84	0.90
MARA_TV_3	0.37	0.58	**R-B_TV_5**	0.83	0.88
AZR2M_TV_3	0.30	0.41	**(R-G)/(R+G+B)_TV_5**	0.88	0.93
NZR2M_TV_3	0.27	0.46	**(G-B)/(R+G+B)_SV_5**	0.54	0.65
2MPALA_SV_3	0.72	0.80	**Ipca_SV_5**	0.69	0.78
2MPASA_SV_3	0.27	0.37	**ExB_SV_5**	0.41	0.50

2MPALN_SV_3	0.88	0.94	**ExG_SV_5**	0.84	0.90
2MPASN_SV_3	0.66	0.81	**Gray_TV_5**	0.13	0.15
2MPAR_SV_3	0.91	0.96	**Gray_SV_5**	0.72	0.82
Area_SV_3	0.25	0.35	**SCOM_TV_5**	0.87	0.92
ADAR_SV_3	0.09	0.30	**PCA1_TV_5**	0.79	0.87
BPC_SV_3	0.29	0.40	**PCA1_SV_5**	0.61	0.71
BPR_SV_3	0.52	0.64	**PCA2_SV_5**	0.80	0.86
BPAR_SV_3	0.78	0.89	**SLR1_TV_5**	0.70	0.80
Circumference_SV_3	0.34	0.60	**SLR1_SV_5**	0.69	0.79
cmY_SV_3	0.86	0.92	**SLR2_TV_5**	0.77	0.85
Compactness_SV_3	0.75	0.86	**SLR2_SV_5**	0.63	0.78
CHArea_SV_3	0.71	0.82	**SLR3_TV_5**	0.60	0.73
Circumference_SV_3	0.83	0.89	**SLR3_SV_5**	0.52	0.61
Excentricity_SV_3	0.93	0.96	**SLR4_SV_5**	0.73	0.81
ObjectExtentX_SV_3	0.35	0.55	**SLR5_TV_5**	0.78	0.88
ObjectExtentY_SV_3	0.88	0.93	**I2_TV_5**	0.84	0.90
PSCC_1_3	0.47	0.63	**GMR_SV_5**	0.83	0.89
PSCC_2_3	0.48	0.63	**G/R_SV_5**	0.81	0.88
PSCC_3_3	0.44	0.57	**G/B_TV_5**	0.53	0.64
PSCC_4_3	0.27	0.37	**AGR1**	0.24	0.38
PSCC_5_3	0.42	0.57	**AGR2**	0.55	0.65
PSCC_6_3	0.55	0.71	**AGR3**	0.68	0.82
PSCC_7_3	0.53	0.69	**AGR4**	0.68	0.79
PSCC_8_3	0.47	0.66	**AGR5**	0.64	0.77
PSCC_9_3	0.35	0.52	**RGR1**	0.73	0.85
PSCC_10_3	0.32	0.45	**RGR2**	0.66	0.81
PSCC_11_3	0.53	0.67	**RGR3**	0.69	0.81
PSCC_12_3	0.29	0.43	**RGR4**	0.83	0.92
PSCC_13_3	0.32	0.46	**AWU_Diurnal**	0.27	0.38

PSCC_14_3	0.39	0.54	**AWU_Day**	0.24	0.35
PSCC_15_3	0.36	0.50	**AWU_Night**	0.53	0.69
PSCC_16_3	0.40	0.54	**PSA_TUE_Diurnal**	0.37	0.69
PSCC_17_3	0.29	0.39	**PSA_TR_Diurnal**	0.37	0.54
PSCC_18_3	0.30	0.39	**PSA_TUE_Day**	0.34	0.68
PSCC_19_3	0.40	0.51	**PSA_TR_Day**	0.36	0.52
PSCC_20_3	0.53	0.65	**PSA_TUE_Night**	0.60	0.82
No PSCC_3	0.35	0.46	**PSA_TR_Night**	0.50	0.70
NIR TV_3	0.99	1.00	**Foliage_TUE_Diurnal**	0.49	0.87
NIR SV_3	0.89	0.94	**Foliage_TR_Diurnal**	0.67	0.80
IR TV_3	0.96	0.98	**Foliage_TUE_Day**	0.44	0.88
IR SV_3	0.99	0.99	**Foliage_TR_Day**	0.64	0.78
			Foliage_TUE_Night	0.69	0.90
			Foliage_TR_Day	0.76	0.91

ANNEXURE 9: Phenotypic and genotypic correlations of manual and semi-automatic traits under control and nitrogen deficiency condition

TraitID	Phenotypic Correlations	Genetic Correlations	TraitID	Phenotypic Correlations	Genetic Correlations
Straw	0.33	0.43	**AvgSpikeWt_ME**	0.63	0.78
Total_Biomass	0.09	0.14	**AvgSpikeWt_TE**	0.58	0.76
TotalEar	0.35	0.49	**AvgSpikeWt_AE**	0.67	0.83
HI	0.69	0.77	**AvgGrainWt_ME**	0.66	0.81
FLL	0.47	0.69	**AvgGrainWt_TE**	0.56	0.75
FLW	0.53	0.73	**AvgGrainWt_AE**	0.67	0.83
FLtoEar	0.95	0.98	**AvgChaffWt_ME**	0.61	0.76
FLLWratio	0.63	0.84	**AvgChaffWt_TE**	0.58	0.69
FLLtoEarRatio	0.62	0.81	**AvgChaffWt_AE**	0.63	0.75
LNP	0.38	0.53	**GWCWratio_ME**	0.78	0.89
TNP	0.39	0.56	**GWCWratio_TE**	0.47	0.54
PH	0.96	0.98	**GWCWratio_AE**	0.60	0.67
SPAD1	0.51	0.71	**PHI_ME**	0.75	0.90
SPAD2	0.63	0.82	**PHI_TE**	0.54	0.62
Phy3	0.67	0.71	**PHI_AE**	0.61	0.70
Phy4	0.58	0.63	**TKW_ME**	0.76	0.85
Phy5	0.46	0.48	**TKW_TE**	0.80	0.90
DTG	0.57	0.72	**TKW_AE**	0.83	0.90
DTB	0.82	0.89	**AvgGrainNo_ME**	0.62	0.79
DTA	0.87	0.91	**AvgGrainNo_TE**	0.56	0.78
LC_SPAD1ratio	0.42	0.59	**AvgGrainNo_AE**	0.65	0.86
LC_SPAD2ratio	0.48	0.65	**SeedArea_TE**	0.78	0.87
TC_SPAD1ratio	0.43	0.62	**SeedArea_ME**	0.78	0.91
TC_SPAD2ratio	0.43	0.61	**SeedArea_AE**	0.82	0.89
LER	0.55	0.59	**SeedArea_Low_TE**	0.78	0.89
LER_DTBratio	0.63	0.68	**SeedArea_Low_ME**	0.60	0.84

LER_DTAratio	0.67	0.71	**SeedArea_Low_AE**	0.76	0.89
SPADatio	0.59	0.93	**SeedArea_Top_TE**	0.66	0.76
LPTveg	0.61	0.91	**SeedArea_Top_ME**	0.79	0.91
SPAD1total	0.39	0.58	**SeedArea_Top_AE**	0.77	0.85
SPAD2total	0.47	0.66	**SeedPerimeter_TE**	0.84	0.90
FLA	0.41	0.62	**SeedPerimeter_ME**	0.85	0.95
PH_FLLratio	0.75	0.90	**SeedPerimeter_AE**	0.87	0.93
SpikeLength	0.81	0.91	**SeedPerimeter_Low_TE**	0.77	0.87
SpikeletNo	0.95	0.98	**SeedPerimeter_Low_ME**	0.51	0.77
SSN	0.73	0.86	**SeedPerimeter_Low_AE**	0.74	0.89
GPS	0.66	0.84	**SeedPerimeter_Top_TE**	0.77	0.85
SpikeletDensity	0.79	0.92	**SeedPerimeter_Top_ME**	0.73	0.88
SFP	0.65	0.80	**SeedPerimeter_Top_AE**	0.79	0.88
SFI	0.70	0.82	**SeedLength_TE**	0.89	0.93
SpikeWt_ME	0.63	0.78	**SeedLength_ME**	0.87	0.95
SpikeWt_TE	0.10	0.15	**SeedLength_AE**	0.90	0.94
SpikeWt_AE	0.09	0.14	**SeedLength_Low_TE**	0.77	0.88
GrainWt_ME	0.66	0.81	**SeedLength_Low_ME**	0.49	0.74
GrainWt_TE	0.09	0.13	**SeedLength_Low_AE**	0.70	0.86
GrainWt_AE	0.10	0.14	**SeedLength_Top_TE**	0.85	0.91
ChaffWt_ME	0.61	0.76	**SeedLength_Top_ME**	0.84	0.93
ChaffWt_TE	0.38	0.49	**SeedLength_Top_AE**	0.87	0.93
ChaffWt_AE	0.38	0.50	**SeedWidth_TE**	0.77	0.86
TotalGrainNo_ME	0.62	0.79	**SeedWidth_ME**	0.79	0.90
TotalGrainNo_TE	0.34	0.45	**SeedWidth_AE**	0.81	0.88
TotalGrainNo_AE	0.36	0.47	**SeedWidth_Low_TE**	0.80	0.90
GPB_ME	0.44	0.61	**SeedWidth_Low_ME**	0.76	0.93
GPB_TE	0.47	0.61	**SeedWidth_Low_AE**	0.82	0.92
GPB_AE	0.70	0.78	**SeedWidth_Top_TE**	0.61	0.73

AGPB_ME	0.44	0.61	**SeedWidth_Top_ME**	0.71	0.87
AGPB_TE	0.41	0.59	**SeedWidth_Top_AE**	0.72	0.82
AGPB_AE	0.43	0.60	**SeedLWR_TE**	0.87	0.93
CPB_ME	0.40	0.54	**SeedLWR_ME**	0.88	0.95
CPB_TE	0.57	0.67	**SeedLWR_AE**	0.89	0.94
CPB_AE	0.64	0.73	**SeedLWR_Low_TE**	0.80	0.91
ACPB_ME	0.40	0.54	**SeedLWR_Low_ME**	0.62	0.81
ACPB_TE	0.43	0.57	**SeedLWR_Low_AE**	0.79	0.90
ACPB_AE	0.43	0.57	**SeedLWR_Top_TE**	0.83	0.92
			SeedLWR_Top_ME	0.77	0.89
			SeedLWR_Top_AE	0.85	0.92

ANNEXURE 10: QTLs identified for HTP traits under control condition

TraitID	Chromosome	Position	LeftMarker	RightMarker	LOD	PVE(%)	Add	LeftCI	RightCI
AreaDistributionAboveRelative_SV_3_C	**2A**	158	AX-94386216	AX-94466314	**5.07**	**17.37**	0.0002	157.5	158.5
BoundaryPointCount_TV_2_C	**2A**	24	AX-94386463	AX-94838306	**3.88**	**8.05**	-1166.2441	12.5	26.5
ObjectExtentY_TV_3_C	**2A**	28	AX-94386463	AX-94838306	**3.87**	**9.50**	-28.4117	23.5	34.5
AreaDistributionAboveRelative_SV_3_C	**2A**	52	AX-94391321	AX-94896508	**3.89**	**17.37**	-0.0001	51.5	53.5
Gray_TV_3_C	**3B**	189	AX-94393045	AX-94707424	**3.73**	**4.98**	-0.0003	188.5	192.5
R-G_TV_1_C	**4D**	167	AX-94393215	AX-94436391	**6.13**	**12.38**	-0.4319	165.5	173.5
Ipca_SV_1_C	**4D**	167	AX-94393215	AX-94436391	**5.24**	**5.16**	1.6147	165.5	171.5
I1_SV_1_C	**4D**	167	AX-94393215	AX-94436391	**4.95**	**4.83**	1.377	165.5	171.5
2ndMomentsPrincipalAxisRatio_SV_2_C	**4D**	167	AX-94393215	AX-94436391	**3.95**	**11.81**	0.682	165.5	172.5
Green_TV_3_C	**4D**	167	AX-94393215	AX-94436391	**5.93**	**12.05**	2.4358	165.5	171.5
Red_TV_3_C	**4D**	167	AX-94393215	AX-94436391	**5.08**	**10.45**	1.9412	165.5	171.5
R-G_TV_3_C	**4D**	168	AX-94393215	AX-94436391	**5.68**	**9.47**	-0.359	165.5	173.5
INT_TV_3_C	**4D**	167	AX-94393215	AX-94436391	**5.75**	**11.68**	1.9686	165.5	171.5
R-G_TV_4_C	**4D**	168	AX-94393215	AX-94436391	**5.14**	**8.61**	-0.3453	165.5	173.5
INT_TV_4_C	**4D**	167	AX-94393215	AX-94436391	**4.27**	**7.94**	1.9882	165.5	172.5
PSCC_1_3_C	**2A**	151	AX-94417025	AX-94521851	**24.53**	**9.89**	90.3668	149.5	151.5
PSCC_2_3_C	**2A**	151	AX-94417025	AX-94521851	**24.02**	**14.98**	222.5305	149.5	151.5
AreaDistributionAboveRelative_SV_3_C	**1D**	101	AX-94424092	AX-95204146	**3.82**	**17.37**	0.0003	99.5	101.5
PSCC_1_2_C	**7B**	273	AX-94427210	AX-94651564	**3.70**	**8.87**	27.1523	272.5	274.5
R-B_TV_2_C	**7B**	273	AX-94427210	AX-94651564	**3.65**	**8.99**	-0.4607	272.5	274.5
(R-G)/(R+G+B)_TV_2_C	**7B**	273	AX-94427210	AX-94651564	**3.65**	**8.99**	-0.4607	272.5	274.5
(G-B)/(R+G+B)_TV_2_C	**7B**	273	AX-94427210	AX-94651564	**3.65**	**8.99**	-0.4607	272.5	274.5
(G-B)/(R+G+B)_SV_2_C	**7B**	273	AX-94427210	AX-94651564	**3.65**	**8.99**	-0.4607	272.5	274.5
PCA2_SV_2_C	**7B**	273	AX-94427210	AX-94651564	**3.57**	**8.79**	-1.0386	272.5	274.5
BoundaryPointsToAreaRatio_SV_1_C	**6B**	77	AX-94444292	AX-95242894	**21.82**	**16.11**	0.0126	76.5	77.5
AreaDistributionAboveRelative_SV_3_C	**6B**	77	AX-94444292	AX-95242894	**6.84**	**17.37**	-0.0003	76.5	77.5

2ndMomentPrincipleAxisSmallNorm_SV_4_C	**3A**	21	AX-94449625	AX-94528394	**3.81**	**7.52**	0.0035	19.5	24.5
AreaDistributionAboveRelative_SV_3_C	**7A**	100	AX-94451998	AX-94910468	**3.94**	**8.69**	-0.0001	99.5	103.5
ObjectExtentY_SV_2_C	**5B**	160	AX-94453981	AX-94503623	**3.83**	**3.41**	49.4916	158.5	160.5
PSCC_5_4_C	**2D**	171	AX-94460743	AX-94404928	**4.68**	**6.98**	-841.5469	167.5	175.5
PSCC_1_5_C	**2D**	170	AX-94460743	AX-94404928	**4.63**	**7.81**	-76.1411	167.5	176.5
ObjectExtentX_SV_5_C	**4D**	96	AX-94465412	AX-94618351	**4.27**	**8.46**	-23.3079	94.5	97.5
AreaDistributionAboveRelative_SV_4_C	**7A**	8	AX-94468782	AX-94796013	**6.21**	**1.01**	0	7.5	8.5
Ipca_SV_1_C	**2A**	162	AX-94468973	AX-94538825	**5.36**	**5.24**	1.6198	161.5	162.5
I1_SV_1_C	**2A**	162	AX-94468973	AX-94538825	**5.15**	**4.98**	1.391	161.5	162.5
Ipca_SV_1_C	**2B**	195	AX-94472688	AX-94511149	**10.31**	**10.72**	-2.3175	194.5	197.5
PCA2_SV_1_C	**2B**	195	AX-94472688	AX-94511149	**11.88**	**1.90**	-1.6973	194.5	196.5
I1_SV_1_C	**2B**	195	AX-94472688	AX-94511149	**10.78**	**11.20**	-2.0882	194.5	196.5
PSCC_1_3_C	**3A**	67	AX-94474332	AX-94514642	**5.09**	**1.56**	35.9125	66.5	68.5
PSCC_2_3_C	**3A**	67	AX-94474332	AX-94514642	**5.09**	**2.43**	89.6296	66.5	68.5
AreaDistributionAboveRelative_SV_2_C	**2B**	264	AX-94478750	AX-94666770	**4.22**	**2.78**	-0.0003	262.5	264.5
2ndMomentPrincipleAxisSmallNorm_TV_2_C	**4B**	67	AX-94489678	AX-94573089	**3.55**	**5.27**	0.0049	64.5	67.5
g_TV_4_C	**4B**	67	AX-94489678	AX-94573089	**8.91**	**4.98**	-0.0011	65.5	67.5
PSCC_1_3_C	**4D**	146	AX-94492784	AX-95215056	**4.87**	**1.49**	-34.9236	145.5	149.5
PSCC_2_3_C	**4D**	146	AX-94492784	AX-95215056	**6.38**	**3.10**	-100.7683	145.5	149.5
PSCC_3_3_C	**4D**	146	AX-94492784	AX-95215056	**4.53**	**7.29**	-193.498	145.5	151.5
GMR_SV_3_C	**4D**	146	AX-94492784	AX-95215056	**3.85**	**9.75**	0.3455	145.5	151.5
G/R_SV_3_C	**4D**	146	AX-94492784	AX-95215056	**3.85**	**9.75**	0.3455	145.5	151.5
G/B_TV_3_C	**4D**	146	AX-94492784	AX-95215056	**3.85**	**9.75**	0.3455	145.5	151.5
AreaDistributionAboveRelative_SV_3_C	**3A**	239	AX-94495777	AX-94410925	**9.53**	**17.37**	0	237.5	239.5
BoundaryPointCount_SV_3_C	**5B**	156	AX-94510295	AX-95080881	**4.11**	**5.79**	1955.2227	151.5	157.5
BoundaryPointRoundness_SV_3_C	**5B**	156	AX-94510295	AX-95080881	**4.61**	**6.98**	769.8662	149.5	158.5
BoundaryPointsToAreaRatio_TV_1_C	**7A**	132	AX-94512826	AX-94777695	**3.50**	**7.44**	0.0054	131.5	141.5
g_TV_2_C	**7A**	136	AX-94512826	AX-94777695	**3.67**	**6.11**	-0.0009	129.5	143.5
PSCC_5_1_C	**7D**	351	AX-94524440	AX-95685070	**3.33**	**6.33**	-155.2634	350.5	352.5

AreaDistributionAboveRelative_SV_3_C	**5B**	262	AX-94534815	AX-94882207	**5.65**	**8.69**	0.0002	260.5	262.5
PSCC_13_1_C	**5D**	366	AX-94537215	AX-94555577	**3.58**	**9.14**	414.4614	362.5	368.5
PSCC_9_1_C	**5B**	235	AX-94545100	AX-95194941	**3.80**	**9.36**	377.563	231.5	236.5
PSCC_1_1_C	**4B**	92	AX-94545697	AX-94629926	**4.74**	**8.31**	28.9507	91.5	92.5
Blue_TV_3_C	**4B**	92	AX-94545697	AX-94629926	**5.95**	**11.29**	-1.5028	91.5	92.5
Green_TV_3_C	**4B**	92	AX-94545697	AX-94629926	**4.83**	**9.48**	-2.1803	91.5	92.5
Red_TV_3_C	**4B**	92	AX-94545697	AX-94629926	**4.61**	**9.24**	-1.8418	91.5	92.5
R-G_TV_3_C	**4B**	92	AX-94545697	AX-94629926	**7.20**	**11.23**	0.3943	91.5	92.5
SLR2_TV_3_C	**4B**	92	AX-94545697	AX-94629926	**3.85**	**7.66**	1.3556	91.5	92.5
INT_TV_3_C	**4B**	92	AX-94545697	AX-94629926	**5.08**	**10.04**	-1.8417	91.5	92.5
Compactness_SV_4_C	**4B**	92	AX-94545697	AX-94629926	**6.02**	**12.07**	0.0174	91.5	92.5
ConvexHullArea_SV_4_C	**4B**	92	AX-94545697	AX-94629926	**4.00**	**9.23**	-46305.375	91.5	92.5
R-G_TV_4_C	**4B**	92	AX-94545697	AX-94629926	**7.75**	**12.16**	0.414	91.5	92.5
SLR2_TV_4_C	**4B**	92	AX-94545697	AX-94629926	**6.80**	**11.76**	1.9185	91.5	92.5
Compactness_SV_5_C	**4B**	92	AX-94545697	AX-94629926	**9.56**	**14.91**	0.0232	91.5	92.5
AreaDistributionAboveRelative_SV_3_C	**2A**	182	AX-94555534	AX-94390510	**8.04**	**17.37**	0.0003	181.5	181.5
ConvexHullArea_TV_4_C	**4A**	47	AX-94582600	AX-94472012	**4.16**	**10.23**	-50981.0625	44.5	47.5
MinAreaRectangleArea_TV_4_C	**4A**	47	AX-94582600	AX-94472012	**3.74**	**10.07**	-59406.375	45.5	47.5
ObjectExtentX_SV_1_C	**4D**	65	AX-94584787	AX-94449728	**3.64**	**8.10**	20.7582	61.5	65.5
ObjectExtentY_TV_2_C	**4D**	65	AX-94584787	AX-94449728	**5.14**	**11.01**	35.0479	60.5	65.5
ObjectExtentX_SV_2_C	**4D**	65	AX-94584787	AX-94449728	**6.41**	**12.64**	20.5762	61.5	65.5
g_TV_4_C	**4D**	65	AX-94584787	AX-94449728	**15.60**	**9.63**	0.0015	62.5	65.5
AreaDistributionAboveRelative_SV_3_C	**1B**	52	AX-94605330	AX-94487937	**4.08**	**26.06**	0.0004	51.5	54.5
AreaDistributionAboveRelative_SV_3_C	**2D**	195	AX-94610157	AX-94664467	**5.65**	**8.69**	0.0001	194.5	200.5
AreaDistributionAboveRelative_SV_3_C	**7B**	36	AX-94622619	AX-94560940	**7.39**	**8.69**	0.0002	35.5	36.5
2ndMomentPrincipleAxisLargeNorm_SV_1_C	**4D**	161	AX-94632373	AX-94818797	**4.21**	**8.67**	0.0313	158.5	165.5
2ndMomentsPrincipalAxisRatio_SV_1_C	**4D**	161	AX-94632373	AX-94818797	**5.10**	**7.99**	0.6502	158.5	165.5
CenterOfMassY_SV_1_C	**4D**	162	AX-94632373	AX-94818797	**6.91**	**11.40**	-25.1797	158.5	164.5
Excentricity_SV_1_C	**4D**	162	AX-94632373	AX-94818797	**6.39**	**15.36**	0.0486	158.5	165.5

ObjectExtentY_SV_1_C	**4D**	161	AX-94632373	AX-94818797	**4.29**	**8.71**	55.6752	158.5	165.5
Green_TV_1_C	**4D**	162	AX-94632373	AX-94818797	**5.35**	**9.87**	2.199	158.5	165.5
Green_SV_1_C	**4D**	161	AX-94632373	AX-94818797	**4.31**	**8.84**	2.158	158.5	165.5
Red_SV_1_C	**4D**	160	AX-94632373	AX-94818797	**3.75**	**7.67**	1.8415	158.5	165.5
SLR2_TV_1_C	**4D**	161	AX-94632373	AX-94818797	**6.90**	**16.25**	-1.4469	158.5	164.5
INT_SV_1_C	**4D**	160	AX-94632373	AX-94818797	**4.00**	**8.24**	1.7741	158.5	165.5
2ndMomentPrincipleAxisLargeNorm_SV_2_C	**4D**	163	AX-94632373	AX-94818797	**3.77**	**6.90**	0.0388	158.5	165.5
CenterOfMassY_SV_2_C	**4D**	163	AX-94632373	AX-94818797	**4.07**	**7.47**	-21.4427	159.5	164.5
Blue_TV_2_C	**4D**	162	AX-94632373	AX-94818797	**6.68**	**12.64**	1.5121	158.5	164.5
Green_TV_2_C	**4D**	161	AX-94632373	AX-94818797	**6.49**	**11.23**	2.3488	158.5	164.5
Red_TV_2_C	**4D**	162	AX-94632373	AX-94818797	**5.45**	**10.41**	1.8442	158.5	165.5
SLR2_TV_2_C	**4D**	161	AX-94632373	AX-94818797	**6.77**	**15.32**	-1.6665	158.5	165.5
SLR2_SV_2_C	**4D**	161	AX-94632373	AX-94818797	**4.22**	**6.89**	-2.234	158.5	165.5
INT_TV_2_C	**4D**	162	AX-94632373	AX-94818797	**6.03**	**11.44**	1.8923	158.5	165.5
Compactness_SV_5_C	**4D**	162	AX-94632373	AX-94818797	**3.89**	**6.25**	-0.0148	158.5	164.5
SLR2_TV_5_C	**4D**	159	AX-94632373	AX-94818797	**5.26**	**8.43**	-1.7071	158.5	163.5
BoundaryPointsToAreaRatio_SV_1_C	**2B**	291	AX-94635171	AX-94568326	**5.82**	**3.39**	-0.0058	290.5	292
NormalisedZRotation2ndMoment_TV_2_C	**2B**	291	AX-94635171	AX-94568326	**3.91**	**9.57**	-0.0151	290.5	292
BoundaryPointsToAreaRatio_SV_2_C	**2B**	291	AX-94635171	AX-94568326	**5.57**	**12.90**	-0.0075	290.5	292
Compactness_TV_3_C	**2B**	291	AX-94635171	AX-94568326	**5.70**	**15.14**	0.0114	290.5	292
BoundaryPointsToAreaRatio_SV_3_C	**2B**	291	AX-94635171	AX-94568326	**4.86**	**12.08**	-0.0076	290.5	292
Gray_SV_3_C	**2B**	291	AX-94635171	AX-94568326	**3.78**	**7.61**	0.0003	290.5	292
Compactness_TV_4_C	**2B**	291	AX-94635171	AX-94568326	**5.09**	**12.81**	0.0111	290.5	292
BoundaryPointsToAreaRatio_SV_4_C	**2B**	291	AX-94635171	AX-94568326	**5.21**	**13.35**	-0.0073	290.5	292
AreaDistributionAboveRelative_SV_5_C	**2B**	6	AX-94642093	AX-94787319	**4.18**	**30.93**	0.0001	5.5	6.5
BoundaryPointsToAreaRatio_SV_1_C	**2D**	59	AX-94644557	AX-95630531	**5.37**	**3.09**	-0.0055	58.5	59.5
PSCC_1_3_C	**2B**	194	AX-94646108	AX-94472688	**6.15**	**1.94**	39.8645	192.5	195.5
PSCC_2_3_C	**2B**	194	AX-94646108	AX-94472688	**8.28**	**4.21**	117.406	192.5	195.5
PSCC_3_3_C	**2B**	194	AX-94646108	AX-94472688	**4.45**	**7.24**	192.7985	191.5	195.5

BoundaryPointRoundness_SV_3_C	**6B**	49	AX-94675561	AX-94909094	**3.97**	**5.80**	-696.3418	48.5	49.5
AreaDistributionAboveRelative_SV_5_C	**3A**	29	AX-94703603	AX-94568900	**9.57**	**15.46**	0.0003	28.5	29.5
PSCC_2_3_C	**3D**	0	AX-94704559	AX-94644333	**4.75**	**2.25**	86.652	0	0.5
AreaDistributionAboveRelative_SV_4_C	**1A**	20	AX-94705107	AX-95138946	**3.79**	**1.01**	0.0002	17.5	20.5
AreaDistributionAboveRelative_SV_3_C	**3B**	193	AX-94707424	AX-95074455	**3.90**	**8.69**	-0.0001	189.5	197.5
AreaDistributionAboveRelative_SV_5_C	**7A**	20	AX-94714854	AX-94461481	**4.66**	**15.46**	-0.0002	19.5	21.5
AreaDistributionAboveRelative_SV_3_C	**3B**	27	AX-94717736	AX-95144876	**4.08**	**8.69**	0.0001	23.5	27.5
PSCC_4_2_C	**4B**	100	AX-94722630	AX-95106107	**3.76**	**7.91**	-185.8872	98.5	100.5
ObjectExtentY_TV_1_C	**6B**	48	AX-94752965	AX-95242074	**3.38**	**5.52**	-27.9574	47.5	48.5
BoundaryPointsToAreaRatio_SV_1_C	**6A**	219	AX-94754448	AX-95111712	**14.76**	**9.89**	-0.0099	217.5	220.5
AreaDistributionAboveRelative_SV_3_C	**6A**	220	AX-94754448	AX-95111712	**3.86**	**17.37**	-0.0003	216.5	222.5
BoundaryPointsToAreaRatio_TV_2_C	**3B**	9	AX-94758693	AX-94411411	**3.65**	**9.00**	-0.0049	5.5	9.5
BoundaryPointsToAreaRatio_TV_3_C	**3B**	9	AX-94758693	AX-94411411	**3.71**	**7.83**	-0.0044	5.5	9.5
AreaDistributionAboveRelative_SV_3_C	**2A**	259	AX-94762364	AX-94912259	**4.93**	**8.69**	0.0001	258.5	262
AreaDistributionAboveRelative_SV_3_C	**5D**	158	AX-94797625	AX-95003025	**11.57**	**8.69**	0.0001	121.5	159.5
Blue_TV_1_C	**4D**	158	AX-94803237	AX-94762683	**5.24**	**11.54**	1.19	155.5	158.5
Red_TV_1_C	**4D**	158	AX-94803237	AX-94762683	**4.53**	**8.97**	1.5846	155.5	158.5
SLR1_TV_1_C	**4D**	158	AX-94803237	AX-94762683	**3.60**	**6.90**	-1.3264	155.5	158.5
INT_TV_1_C	**4D**	158	AX-94803237	AX-94762683	**4.95**	**9.84**	1.6114	155.5	158.5
Compactness_SV_4_C	**4D**	158	AX-94803237	AX-94762683	**3.78**	**7.51**	-0.0135	155.5	158.5
SLR2_SV_5_C	**4D**	157	AX-94803237	AX-94762683	**6.05**	**13.69**	-3.1077	155.5	158.5
NIRSV_1_C	**4D**	94	AX-94813788	AX-95134817	**5.39**	**9.96**	-2.0402	93.5	95.5
BoundaryPointRoundness_TV_1_C	**4D**	166	AX-94818797	AX-94393215	**4.19**	**6.43**	-210.3433	165.5	172.5
PSCC_2_1_C	**4D**	166	AX-94818797	AX-94393215	**3.66**	**6.70**	-56.0422	165.5	171.5
R-G_TV_2_C	**4D**	166	AX-94818797	AX-94393215	**6.22**	**12.64**	-0.4095	165.5	170.5
Compactness_SV_3_C	**4D**	166	AX-94818797	AX-94393215	**4.70**	**10.41**	-0.015	165.5	171.5
ConvexHullArea_SV_3_C	**4D**	166	AX-94818797	AX-94393215	**8.01**	**13.19**	60033.5312	165.5	170.5
ConvexHullCircumference_SV_3_C	**4D**	166	AX-94818797	AX-94393215	**4.82**	**13.42**	132.8406	165.5	173.5
Blue_TV_3_C	**4D**	166	AX-94818797	AX-94393215	**6.20**	**12.28**	1.5535	165.5	170.5

SLR2_TV_3_C	**4D**	166	AX-94818797	AX-94393215	**4.24**	**8.72**	-1.4344	165.5	170.5
Blue_TV_4_C	**4D**	166	AX-94818797	AX-94393215	**5.05**	**9.26**	1.6042	165.5	171.5
SLR2_TV_4_C	**4D**	166	AX-94818797	AX-94393215	**7.28**	**12.89**	-1.9912	165.5	169.5
SLR2_TV_5_C	**3A**	50	AX-94821666	AX-95190048	**4.74**	**7.91**	1.6691	49.5	50.5
PSCC_7_1_C	**5B**	272	AX-94825562	AX-95197417	**3.55**	**8.90**	182.1882	264.5	274.5
PSCC_8_1_C	**5B**	271	AX-94825562	AX-95197417	**4.70**	**11.80**	359.2092	266.5	274.5
AreaDistributionAboveRelative_SV_3_C	**2A**	175	AX-94835663	AX-94595993	**4.32**	**8.69**	0.0002	174.5	175.5
CenterOfMassY_SV_2_C	**4D**	138	AX-94852086	AX-94423396	**3.92**	**10.01**	-24.7592	127.5	144.5
ConvexHullArea_SV_2_C	**4D**	142	AX-94852086	AX-94423396	**4.09**	**8.58**	39245.7812	130.5	144.5
ConvexHullCircumference_SV_2_C	**4D**	142	AX-94852086	AX-94423396	**4.07**	**8.36**	112.5996	129.5	144.5
ObjectExtentY_SV_2_C	**4D**	139	AX-94852086	AX-94423396	**6.04**	**7.53**	73.1503	128.5	144.5
GMR_SV_2_C	**4D**	144	AX-94852086	AX-94423396	**4.51**	**7.16**	0.2928	131.5	144.5
G/R_SV_2_C	**4D**	144	AX-94852086	AX-94423396	**4.51**	**7.16**	0.2928	131.5	144.5
G/B_TV_2_C	**4D**	144	AX-94852086	AX-94423396	**4.51**	**7.16**	0.2928	131.5	144.5
BoundaryPointRoundness_TV_3_C	**4D**	144	AX-94852086	AX-94423396	**3.94**	**6.19**	-261.7369	132.5	144.5
BoundaryPointsToAreaRatio_TV_3_C	**4D**	144	AX-94852086	AX-94423396	**4.69**	**9.65**	-0.0049	130.5	144.5
2ndMomentsPrincipalAxisRatio_SV_3_C	**4D**	140	AX-94852086	AX-94423396	**6.38**	**17.83**	1.3626	129.5	144.5
CenterOfMassY_SV_3_C	**4D**	138	AX-94852086	AX-94423396	**5.41**	**13.84**	-33.0475	128.5	144.5
Excentricity_SV_3_C	**4D**	138	AX-94852086	AX-94423396	**6.97**	**19.05**	0.0651	130.5	144.5
ObjectExtentY_SV_3_C	**4D**	143	AX-94852086	AX-94423396	**5.14**	**14.34**	76.6265	130.5	144.5
R-G_TV_3_C	**4D**	137	AX-94852086	AX-94423396	**6.37**	**14.96**	-0.4489	126.5	144.5
SLR2_TV_3_C	**4D**	144	AX-94852086	AX-94423396	**4.14**	**8.36**	-1.3988	131.5	144.5
SLR2_SV_3_C	**4D**	144	AX-94852086	AX-94423396	**5.97**	**14.29**	-2.6784	133.5	144.5
BoundaryPointRoundness_TV_4_C	**4D**	144	AX-94852086	AX-94423396	**3.96**	**9.78**	-301.9166	133.5	144.5
BoundaryPointsToAreaRatio_TV_4_C	**4D**	144	AX-94852086	AX-94423396	**5.91**	**15.29**	-0.0071	137.5	144.5
2ndMomentPrincipleAxisLargeNorm_SV_4_C	**4D**	144	AX-94852086	AX-94423396	**4.36**	**6.21**	0.0591	132.5	144.5
CenterOfMassY_SV_4_C	**4D**	140	AX-94852086	AX-94423396	**5.72**	**21.24**	-31.063	130.5	144.5
ConvexHullCircumference_SV_4_C	**4D**	142	AX-94852086	AX-94423396	**8.03**	**21.10**	185.0216	132.5	144.5
Excentricity_SV_4_C	**4D**	140	AX-94852086	AX-94423396	**6.56**	**17.28**	0.0505	130.5	144.5

ObjectExtentY_SV_4_C	**4D**	141	AX-94852086	AX-94423396	**9.40**	**24.16**	109.8041	132.5	144.5
Green_TV_4_C	**4D**	136	AX-94852086	AX-94423396	**5.00**	**7.23**	3.3632	125.5	144.5
Red_TV_4_C	**4D**	135	AX-94852086	AX-94423396	**4.12**	**5.85**	2.7605	123.5	144.5
R-G_TV_4_C	**4D**	139	AX-94852086	AX-94423396	**5.75**	**12.76**	-0.4184	129.5	144.5
SLR2_SV_4_C	**4D**	144	AX-94852086	AX-94423396	**6.23**	**12.47**	-3.4898	136.5	144.5
2ndMomentsPrincipalAxisRatio_SV_5_C	**4D**	140	AX-94852086	AX-94423396	**4.38**	**10.02**	1.4603	129.5	144.5
CenterOfMassY_SV_5_C	**4D**	138	AX-94852086	AX-94423396	**5.19**	**21.69**	-34.3788	128.5	144.5
ConvexHullArea_SV_5_C	**4D**	140	AX-94852086	AX-94423396	**5.99**	**14.59**	65103.7188	131.5	144.5
ConvexHullCircumference_SV_5_C	**4D**	142	AX-94852086	AX-94423396	**9.07**	**23.96**	208.9017	133.5	144.5
Excentricity_SV_5_C	**4D**	140	AX-94852086	AX-94423396	**4.65**	**10.64**	0.0409	130.5	144.5
ObjectExtentY_SV_5_C	**4D**	139	AX-94852086	AX-94423396	**10.73**	**27.73**	129.5032	131.5	144.5
SLR4_SV_2_C	**2B**	292	AX-94852490	AX-95244768	**3.85**	**9.81**	-1.8347	291.5	292
AreaDistributionAboveRelative_SV_3_C	**7B**	86	AX-94861481	AX-94497402	**13.34**	**17.37**	-0.0001	75.5	88.5
AreaDistributionAboveRelative_SV_4_C	**4A**	98	AX-94880497	AX-95226266	**17.29**	**1.01**	0	95.5	98.5
AreaDistributionAboveRelative_SV_5_C	**7D**	263	AX-94883448	AX-94651589	**3.90**	**15.46**	-0.0002	260.5	263.5
NormalisedZRotation2ndMoment_TV_1_C	**6A**	93	AX-94893553	AX-94942005	**88.13**	**11.49**	0.1426	92.5	93.5
PCA2_SV_1_C	**6A**	93	AX-94893553	AX-94942005	**58.87**	**18.80**	5.3424	92.5	93.5
AreaDistributionAboveRelative_SV_3_C	**7A**	0	AX-94907627	AX-95199471	**11.29**	**17.37**	0	0	0.5
PSCC_18_1_C	**5B**	0	AX-94916379	AX-94889598	**3.55**	**8.67**	5930.4492	0	1.5
PSCC_19_1_C	**5B**	0	AX-94916379	AX-94889598	**4.47**	**7.54**	2485.9111	0	1.5
PSCC_20_1_C	**5B**	0	AX-94916379	AX-94889598	**3.69**	**8.01**	866.5229	0	1.5
b_SV_5_C	**5B**	0	AX-94916379	AX-94889598	**3.65**	**7.94**	-0.0015	0	1.5
PSCC_15_2_C	**7A**	84	AX-94934774	AX-94533089	**4.23**	**8.00**	2481.4219	78.5	90.5
AreaDistributionAboveRelative_SV_4_C	**6A**	3	AX-94940485	AX-94605333	**4.69**	**3.02**	0.0003	2.5	3.5
Excentricity_SV_2_C	**4D**	153	AX-94962854	AX-94803237	**6.58**	**15.58**	0.0509	152.5	158.5
ConvexHullArea_SV_4_C	**4D**	154	AX-94962854	AX-94803237	**6.35**	**15.69**	59594.4062	152.5	158.5
2ndMomentPrincipleAxisSmallNorm_TV_1_C	**4D**	70	AX-94988276	AX-95179517	**6.30**	**13.62**	0.0083	68.5	70.5
2ndMomentPrincipleAxisLargeNorm_SV_1_C	**4D**	70	AX-94988276	AX-95179517	**5.61**	**11.06**	-0.0354	69.5	70.5
2ndMomentPrincipleAxisSmallNorm_SV_1_C	**4D**	70	AX-94988276	AX-95179517	**14.30**	**24.72**	0.0077	68.5	70.5

Excentricity_SV_1_C	**4D**	70	AX-94988276	AX-95179517	**6.64**	**14.69**	-0.0475	68.5	70.5
BoundaryPointCount_TV_2_C	**4D**	70	AX-94988276	AX-95179517	**6.16**	**12.33**	1441.998	68.5	70.5
2ndMomentPrincipleAxisSmallNorm_SV_2_C	**4D**	70	AX-94988276	AX-95179517	**14.18**	**26.00**	0.0068	68.5	70.5
Excentricity_SV_2_C	**4D**	70	AX-94988276	AX-95179517	**6.96**	**15.74**	-0.0512	68.5	70.5
ObjectExtentY_SV_2_C	**4D**	70	AX-94988276	AX-95179517	**15.97**	**16.72**	-109.0002	69.5	70.5
2ndMomentPrincipleAxisLargeNorm_SV_3_C	**4D**	70	AX-94988276	AX-95179517	**7.06**	**13.13**	-0.0717	69.5	70.5
Excentricity_SV_3_C	**4D**	70	AX-94988276	AX-95179517	**6.91**	**11.72**	-0.0511	68.5	70.5
Excentricity_SV_4_C	**4D**	70	AX-94988276	AX-95179517	**6.95**	**13.39**	-0.0445	68.5	70.5
2ndMomentPrincipleAxisLargeNorm_SV_5_C	**4D**	70	AX-94988276	AX-95179517	**5.13**	**11.57**	-0.0745	68.5	70.5
2ndMomentsPrincipalAxisRatio_SV_5_C	**4D**	70	AX-94988276	AX-95179517	**5.05**	**8.53**	-1.3476	68.5	70.5
Excentricity_SV_5_C	**4D**	70	AX-94988276	AX-95179517	**6.03**	**10.15**	-0.04	68.5	70.5
AreaDistributionAboveRelative_SV_3_C	**6D**	71	AX-94998023	AX-94958771	**6.50**	**17.37**	-0.0002	60.5	71.5
Circumference_SV_5_C	**6B**	10	AX-95013982	AX-94448837	**3.97**	**10.06**	336494.8438	6.5	14.5
AreaDistributionAboveRelative_SV_3_C	**2B**	177	AX-95023698	AX-95207481	**4.81**	**8.69**	0.0001	176.5	177.5
AreaDistributionAboveRelative_SV_5_C	**1B**	133	AX-95080354	AX-95097993	**5.20**	**15.46**	0.0001	132.5	169.5
ObjectExtentY_SV_2_C	**4B**	101	AX-95106107	AX-94632604	**3.93**	**3.63**	-51.0251	99.5	105.5
2ndMomentPrincipleAxisLargeNorm_SV_1_C	**5B**	342	AX-95108331	AX-94457529	**3.32**	**6.36**	0.0269	341.5	342
MinAreaRectangleArea_TV_1_C	**6D**	113	AX-95115225	AX-94534520	**4.20**	**7.36**	-40241.5	110.5	116.5
b_TV_4_C	**2D**	373	AX-95125039	AX-94901587	**4.23**	**7.07**	-0.0013	365.5	375
Gray_TV_4_C	**2D**	374	AX-95125039	AX-94901587	**4.07**	**6.70**	0.0004	366.5	375
Gray_TV_3_C	**3A**	80	AX-95126297	AX-95217449	**6.87**	**8.54**	0.0004	79.5	80.5
Compactness_SV_3_C	**4D**	95	AX-95134817	AX-94465412	**4.15**	**9.11**	0.0141	93.5	95.5
NIRSV_3_C	**4D**	95	AX-95134817	AX-94465412	**8.06**	**12.99**	-1.9219	94.5	96.5
ConvexHullArea_SV_5_C	**4D**	95	AX-95134817	AX-94465412	**4.64**	**8.04**	-48956.2188	93.5	95.5
BoundaryPointRoundness_TV_1_C	**2B**	290	AX-95137042	AX-94494621	**4.97**	**7.75**	-229.9515	284.5	290.5
2ndMomentPrincipleAxisLargeNorm_SV_1_C	**2A**	23	AX-95142641	AX-94386463	**3.97**	**7.88**	0.0299	11.5	26.5
BoundaryPointCount_SV_3_C	**3B**	28	AX-95144876	AX-94450445	**5.13**	**7.37**	2195.125	26.5	30.5
2ndMomentPrincipleAxisSmallNorm_SV_4_C	**4D**	69	AX-95156869	AX-94988276	**4.82**	**9.67**	0.004	65.5	69.5
BoundaryPointsToAreaRatio_SV_1_C	**6D**	172	AX-95172977	AX-95143298	**3.36**	**1.96**	-0.0044	156.5	172.5

2ndMomentPrincipleAxisSmallNorm_TV_2_C	**6D**	168	AX-95172977	AX-95143298	**3.67**	**8.39**	-0.0062	154.5	172.5
BoundaryPointCount_TV_1_C	**4D**	77	AX-95179517	AX-94799212	**7.97**	**16.50**	1773.0674	71.5	82.5
BoundaryPointRoundness_TV_1_C	**4D**	77	AX-95179517	AX-94799212	**7.79**	**17.63**	347.3529	71.5	83.5
2ndMomentsPrincipalAxisRatio_SV_1_C	**4D**	78	AX-95179517	AX-94799212	**13.12**	**27.90**	-1.2134	72.5	83.5
BoundaryPointRoundness_TV_2_C	**4D**	76	AX-95179517	AX-94799212	**3.95**	**7.37**	279.4891	69.5	85.5
2ndMomentPrincipleAxisLargeNorm_SV_2_C	**4D**	78	AX-95179517	AX-94799212	**7.42**	**18.89**	-0.0641	71.5	86.5
2ndMomentsPrincipalAxisRatio_SV_2_C	**4D**	73	AX-95179517	AX-94799212	**7.04**	**25.24**	-0.9927	69.5	80.5
BoundaryPointRoundness_TV_3_C	**4D**	79	AX-95179517	AX-94799212	**3.55**	**8.20**	301.6279	70.5	90.5
2ndMomentPrincipleAxisSmallNorm_SV_3_C	**4D**	76	AX-95179517	AX-94799212	**10.62**	**23.26**	0.0063	71.5	82.5
2ndMomentsPrincipalAxisRatio_SV_3_C	**4D**	73	AX-95179517	AX-94799212	**7.23**	**17.92**	-1.3656	69.5	79.5
PSCC_1_3_C	**4D**	80	AX-95179517	AX-94799212	**3.87**	**1.83**	38.6711	69.5	91.5
2ndMomentPrincipleAxisLargeNorm_SV_4_C	**4D**	78	AX-95179517	AX-94799212	**10.68**	**21.97**	-0.1113	71.5	84.5
2ndMomentsPrincipalAxisRatio_SV_4_C	**4D**	74	AX-95179517	AX-94799212	**7.17**	**19.65**	-1.3055	69.5	80.5
CenterOfMassY_SV_4_C	**4D**	72	AX-95179517	AX-94799212	**5.89**	**17.59**	28.2678	69.5	80.5
ConvexHullCircumference_SV_4_C	**4D**	71	AX-95179517	AX-94799212	**4.96**	**10.83**	-132.4987	69.5	80.5
ObjectExtentY_SV_4_C	**4D**	71	AX-95179517	AX-94799212	**5.94**	**11.68**	-76.3084	69.5	79.5
ConvexHullArea_TV_5_C	**4D**	84	AX-95179517	AX-94799212	**4.08**	**9.30**	-90565.1562	75.5	93.5
MinAreaRectangleArea_TV_5_C	**4D**	83	AX-95179517	AX-94799212	**4.24**	**9.74**	-118949.2812	74.5	92.5
CenterOfMassY_SV_5_C	**4D**	72	AX-95179517	AX-94799212	**6.24**	**18.26**	31.5242	69.5	80.5
ConvexHullArea_SV_5_C	**4D**	71	AX-95179517	AX-94799212	**6.43**	**11.37**	-57478.1562	69.5	80.5
ConvexHullCircumference_SV_5_C	**4D**	71	AX-95179517	AX-94799212	**5.79**	**12.62**	-151.5073	69.5	80.5
ObjectExtentY_SV_5_C	**4D**	71	AX-95179517	AX-94799212	**6.20**	**10.55**	-79.8625	69.5	79.5
SLR2_TV_5_C	**4D**	78	AX-95179517	AX-94799212	**8.65**	**19.65**	2.6153	72.5	85.5
ObjectExtentY_SV_2_C	**4B**	61	AX-95196960	AX-94475207	**6.94**	**6.72**	69.0433	58.5	62.5
BoundaryPointCount_TV_1_C	**5B**	256	AX-95198219	AX-94534815	**3.45**	**4.73**	947.0469	255.5	260.5
BoundaryPointRoundness_SV_3_C	**5B**	260	AX-95198219	AX-94534815	**4.30**	**6.35**	729.3398	256.5	262.5
ConvexHullArea_TV_1_C	**4D**	64	AX-95211803	AX-94584787	**7.90**	**14.26**	46238.4688	61.5	65.5
ObjectExtentY_TV_1_C	**4D**	64	AX-95211803	AX-94584787	**7.46**	**13.23**	43.2643	60.5	65.5
MinAreaRectangleArea_TV_1_C	**4D**	63	AX-95211803	AX-94584787	**9.04**	**16.85**	60692.625	60.5	65.5

NIRSV_1_C	**4D**	150	AX-95215056	AX-94962854	**4.21**	**8.08**	1.8157	146.5	154.5
NIRSV_3_C	**4D**	149	AX-95215056	AX-94962854	**5.19**	**8.79**	1.5616	145.5	152.5
2ndMomentsPrincipalAxisRatio_SV_4_C	**4D**	151	AX-95215056	AX-94962854	**6.62**	**15.42**	1.1575	147.5	154.5
PSCC_2_4_C	**4D**	148	AX-95215056	AX-94962854	**5.39**	**7.75**	-198.7119	145.5	152.5
PSCC_11_4_C	**4D**	149	AX-95215056	AX-94962854	**4.10**	**6.31**	1612.5391	145.5	152.5
2ndMomentsPrincipalAxisRatio_SV_1_C	**5D**	98	AX-95216839	AX-94769595	**3.70**	**5.42**	0.5374	97.5	104.5
NIRTV_5_C	**5A**	85	AX-95220729	AX-94529089	**4.89**	**14.69**	-1.0503	84.5	86.5
AreaDistributionAboveRelative_SV_3_C	**5B**	248	AX-95239439	AX-94509500	**4.86**	**8.69**	0.0001	247.5	248.5
AreaDistributionAboveRelative_SV_2_C	**2D**	302	AX-95242359	AX-94470776	**4.47**	**2.78**	-0.0004	289.5	319.5
AreaDistributionAboveRelative_SV_5_C	**2D**	304	AX-95242359	AX-94470776	**4.25**	**30.93**	-0.0005	289.5	319.5
Gray_TV_3_C	**5D**	200	AX-95248671	AX-94775978	**3.79**	**5.69**	-0.0003	192.5	203.5
g_TV_4_C	**5D**	199	AX-95248671	AX-94775978	**4.24**	**2.83**	-0.0008	191.5	203.5
Gray_TV_4_C	**5D**	198	AX-95248671	AX-94775978	**3.70**	**7.44**	-0.0004	190.5	203.5
AreaDistributionAboveRelative_SV_3_C	**6B**	80	AX-95257962	AX-94883234	**4.38**	**17.37**	-0.0003	79.5	80.5
PSA_3angle_3_C	**2B**	46	AX-95258478	AX-94856684	**3.60**	**8.99**	-39648.25	45.5	47.5
Area_TV_3_C	**2B**	46	AX-95258478	AX-94856684	**3.66**	**9.19**	-11018.1719	45.5	47.5
PSCC_19_3_C	**2B**	46	AX-95258478	AX-94856684	**3.88**	**9.46**	-3891.5156	42.5	46.5
ConvexHullArea_TV_1_C	**6A**	48	AX-95628663	AX-94531473	**4.70**	**10.91**	-40481.9062	38.5	55.5
ObjectExtentY_TV_1_C	**6A**	48	AX-95628663	AX-94531473	**4.40**	**10.69**	-38.9517	40.5	56.5
ConvexHullArea_TV_2_C	**6A**	60	AX-95652375	AX-94490584	**4.13**	**9.79**	-38924.3438	58.5	60.5
MinAreaRectangleArea_TV_2_C	**6A**	60	AX-95652375	AX-94490584	**5.18**	**10.66**	-57036.3125	58.5	60.5
2ndMomentPrincipleAxisSmallNorm_SV_5_C	**6A**	60	AX-95652375	AX-94490584	**6.39**	**8.27**	-0.0035	59.5	60.5
PSCC_1_3_C	**2B**	170	AX-95652707	AX-94790270	**36.48**	**18.06**	-121.6707	167.5	171.5
BoundaryPointsToAreaRatio_SV_5_C	**2D**	338	AX-95683514	AX-95016766	**5.81**	**14.24**	-0.0086	330.5	342.5

ANNEXURE 11: QTLs identified for HTP traits under nitrogen deficiency condition

TraitID	Chromosome	Position	LeftMarker	RightMarker	LOD	PVE(%)	Add	LeftCI	RightCI
I1_SV_3_N	**4D**	170	AX-94393215	AX-94436391	**3.78**	**9.33**	1.5451	165.5	177.5
SLR2_TV_2_N	**5A**	83	AX-94410311	AX-94439079	**3.99**	**5.39**	1.4303	82.5	84.5
2ndMomentPrincipleAxisSmallNorm_SV_1_N	**6A**	192	AX-94431190	AX-94575839	**65.58**	**15.47**	-0.0222	190.5	192.5
2ndMomentPrincipleAxisSmallNorm_SV_4_N	**6A**	192	AX-94431190	AX-94575839	**4.83**	**9.24**	-0.0037	185.5	193.5
ConvexHullArea_TV_1_N	**4B**	58	AX-94455102	AX-94517912	**3.34**	**5.55**	36438.3438	57.5	58.5
BoundaryPointsToAreaRatio_SV_1_N	**2B**	143	AX-94464385	AX-94578476	**3.83**	**6.99**	-0.0041	138.5	143.5
2ndMomentPrincipleAxisSmallNorm_SV_4_N	**2B**	138	AX-94464385	AX-94578476	**5.09**	**10.11**	-0.0038	136.5	142.5
Compactness_SV_3_N	**4D**	97	AX-94465412	AX-94618351	**4.36**	**5.06**	0.0107	95.5	104.5
BoundaryPointsToAreaRatio_SV_5_N	**4D**	97	AX-94465412	AX-94618351	**3.80**	**8.95**	-0.0051	95.5	109.5
ConvexHullArea_SV_5_N	**4D**	96	AX-94465412	AX-94618351	**55.72**	**14.35**	250771.7188	95.5	96.5
2ndMomentPrincipleAxisSmallNorm_SV_2_N	**4B**	67	AX-94489678	AX-94573089	**9.62**	**20.24**	0.0052	64.5	67.5
NIRSV_1_N	**4D**	146	AX-94492784	AX-95215056	**3.98**	**7.39**	1.5796	145.5	146.5
Compactness_SV_3_N	**6D**	75	AX-94495622	AX-94589324	**4.57**	**5.38**	-0.0109	73.5	82.5
Compactness_SV_4_N	**6D**	75	AX-94495622	AX-94589324	**5.48**	**5.21**	-0.0123	73.5	82.5
Red_TV_3_N	**6D**	49	AX-94498408	AX-94909377	**3.81**	**5.54**	-1.5985	48.5	49.5
BoundaryPointsToAreaRatio_SV_4_N	**5B**	156	AX-94510295	AX-95080881	**5.13**	**8.74**	0.0060	148.5	157.5
ConvexHullArea_TV_1_N	**6D**	217	AX-94512033	AX-94416225	**3.33**	**5.53**	-36413.1250	216.5	217.5
BoundaryPointCount_SV_1_N	**7D**	107	AX-94533004	AX-94389584	**3.66**	**7.04**	2296.1953	101.5	111.5
BoundaryPointRoundness_SV_1_N	**7D**	109	AX-94533004	AX-94389584	**3.98**	**7.18**	510.5781	103.5	112.5
PSCC_6_1_N	**7D**	106	AX-94533004	AX-94389584	**3.50**	**7.04**	236.9910	99.5	111.5
PSCC_7_3_N	**7D**	104	AX-94533004	AX-94389584	**3.70**	**6.87**	673.3743	96.5	110.5
PSCC_8_3_N	**7D**	104	AX-94533004	AX-94389584	**3.76**	**8.19**	794.7261	97.5	111.5
PSCC_14_3_N	**7D**	105	AX-94533004	AX-94389584	**3.63**	**8.09**	2081.6475	97.5	111.5
PSCC_12_5_N	**7D**	105	AX-94533004	AX-94389584	**3.52**	**7.58**	2365.7480	98.5	111.5
2ndMomentPrincipleAxisSmallNorm_TV_4_N	**5A**	58	AX-94542868	AX-94637605	**6.76**	**8.65**	-0.0075	54.5	58.5
SLR2_TV_3_N	**4B**	92	AX-94545697	AX-94629926	**8.00**	**10.75**	1.7021	91.5	92.5

BoundaryPointCount_SV_4_N	**4B**	92	AX-94545697	AX-94629926	**3.99**	**7.64**	-2669.5840	91.5	92.5
BoundaryPointRoundness_SV_4_N	**4B**	92	AX-94545697	AX-94629926	**4.71**	**11.34**	-922.3579	91.5	92.5
ConvexHullArea_SV_4_N	**4B**	92	AX-94545697	AX-94629926	**5.22**	**11.01**	-55580.7500	91.5	92.5
PSCC_11_4_N	**4B**	92	AX-94545697	AX-94629926	**4.03**	**6.79**	-1888.9277	91.5	92.5
NoPSCC_4_N	**4B**	92	AX-94545697	AX-94629926	**3.77**	**9.20**	-1432.6934	91.5	92.5
SLR2_TV_4_N	**4B**	92	AX-94545697	AX-94629926	**6.19**	**12.02**	1.7578	91.5	92.5
ObjectExtentY_TV_5_N	**4B**	92	AX-94545697	AX-94629926	**4.59**	**11.07**	-61.7785	91.5	92.5
BoundaryPointCount_SV_5_N	**4B**	92	AX-94545697	AX-94629926	**4.97**	**11.93**	-2779.3184	91.5	92.5
BoundaryPointRoundness_SV_5_N	**4B**	92	AX-94545697	AX-94629926	**9.46**	**14.83**	-927.1914	91.5	92.5
BoundaryPointsToAreaRatio_TV_2_N	**2A**	126	AX-94567936	AX-94451172	**3.72**	**7.38**	-0.0040	125.5	126.5
Red_TV_3_N	**4B**	83	AX-94573089	AX-95629824	**4.92**	**11.63**	-2.3218	75.5	91.5
INT_TV_3_N	**4B**	85	AX-94573089	AX-95629824	**6.21**	**10.96**	-2.2907	77.5	91.5
Green_TV_4_N	**4B**	86	AX-94573089	AX-95629824	**5.56**	**11.01**	-3.1977	77.5	91.5
Red_TV_4_N	**4B**	87	AX-94573089	AX-95629824	**6.53**	**11.68**	-2.9292	78.5	91.5
INT_TV_4_N	**4B**	87	AX-94573089	AX-95629824	**6.16**	**11.88**	-2.6858	77.5	91.5
Blue_SV_4_N	**4D**	65	AX-94584787	AX-94449728	**3.84**	**8.25**	-1.5366	61.5	65.5
Blue_SV_4_N	**6B**	47	AX-94599546	AX-94406470	**3.76**	**8.15**	-1.5271	46.5	47.5
PSCC_16_3_N	**3B**	23	AX-94604586	AX-94712673	**3.78**	**6.96**	6760.2617	22.5	26.5
2ndMomentPrincipleAxisSmallNorm_TV_4_N	**1A**	34	AX-94605082	AX-95159844	**4.11**	**5.40**	0.0059	29.5	35.5
SLR3_TV_5_N	**6A**	258	AX-94616450	AX-95134269	**3.63**	**8.49**	0.6658	257.5	258
g_TV_4_N	**4D**	99	AX-94618351	AX-94852086	**3.98**	**8.27**	0.0009	95.5	106.5
Gray_TV_4_N	**4D**	100	AX-94618351	AX-94852086	**4.31**	**10.58**	0.0005	95.5	108.5
b_SV_5_N	**4D**	101	AX-94618351	AX-94852086	**3.52**	**7.53**	-0.0013	98.5	112.5
g_TV_1_N	**6B**	44	AX-94624138	AX-95160166	**4.16**	**9.04**	-0.0010	40.5	46.5
Gray_TV_1_N	**6B**	44	AX-94624138	AX-95160166	**4.29**	**9.23**	-0.0005	39.5	46.5
2ndMomentsPrincipalAxisRatio_SV_1_N	**4D**	161	AX-94632373	AX-94818797	**4.20**	**9.07**	0.5656	158.5	165.5
CenterOfMassY_SV_1_N	**4D**	161	AX-94632373	AX-94818797	**3.75**	**6.89**	-20.5803	158.5	165.5
Blue_TV_1_N	**4D**	159	AX-94632373	AX-94818797	**3.84**	**9.35**	1.2438	158.5	164.5
2ndMomentsPrincipalAxisRatio_SV_2_N	**4D**	160	AX-94632373	AX-94818797	**4.00**	**8.83**	0.7643	158.5	165.5

Blue_TV_2_N	**4D**	161	AX-94632373	AX-94818797	**7.55**	**13.59**	1.7575	158.5	163.5
Green_TV_2_N	**4D**	160	AX-94632373	AX-94818797	**5.22**	**11.06**	2.5416	158.5	164.5
Red_TV_2_N	**4D**	160	AX-94632373	AX-94818797	**4.52**	**9.03**	2.0513	158.5	164.5
R-G_TV_2_N	**4D**	160	AX-94632373	AX-94818797	**7.56**	**15.16**	-0.4915	158.5	163.5
SLR2_TV_2_N	**4D**	161	AX-94632373	AX-94818797	**5.89**	**9.18**	-1.8664	158.5	164.5
INT_TV_2_N	**4D**	160	AX-94632373	AX-94818797	**5.34**	**11.38**	2.0725	158.5	163.5
2ndMomentsPrincipalAxisRatio_SV_3_N	**4D**	161	AX-94632373	AX-94818797	**4.17**	**6.76**	1.0319	158.5	165.5
Compactness_SV_3_N	**4D**	162	AX-94632373	AX-94818797	**3.94**	**5.18**	-0.0107	158.5	165.5
ConvexHullArea_SV_3_N	**4D**	160	AX-94632373	AX-94818797	**3.65**	**6.86**	50722.7812	158.5	165.5
Excentricity_SV_3_N	**4D**	159	AX-94632373	AX-94818797	**4.27**	**9.40**	0.0323	158.5	164.5
Blue_TV_3_N	**4D**	161	AX-94632373	AX-94818797	**10.15**	**16.29**	1.9237	158.5	163.5
Green_TV_3_N	**4D**	162	AX-94632373	AX-94818797	**9.17**	**16.20**	3.0521	158.5	164.5
Red_TV_3_N	**4D**	162	AX-94632373	AX-94818797	**7.29**	**12.07**	2.3627	158.5	164.5
Green_SV_3_N	**4D**	160	AX-94632373	AX-94818797	**4.90**	**11.24**	2.4711	158.5	164.5
Red_SV_3_N	**4D**	159	AX-94632373	AX-94818797	**3.95**	**8.93**	2.1763	158.5	164.5
R-G_TV_3_N	**4D**	162	AX-94632373	AX-94818797	**10.34**	**19.72**	-0.5801	158.5	164.5
Ipca_SV_3_N	**4D**	161	AX-94632373	AX-94818797	**4.05**	**9.38**	1.6760	158.5	165.5
INT_TV_3_N	**4D**	161	AX-94632373	AX-94818797	**9.45**	**12.88**	2.4760	158.5	164.5
INT_SV_3_N	**4D**	159	AX-94632373	AX-94818797	**4.31**	**9.74**	2.0593	158.5	164.5
Blue_TV_4_N	**4D**	161	AX-94632373	AX-94818797	**7.90**	**11.57**	1.9647	158.5	164.5
Green_TV_4_N	**4D**	160	AX-94632373	AX-94818797	**7.09**	**11.24**	3.2194	158.5	164.5
Red_TV_4_N	**4D**	159	AX-94632373	AX-94818797	**6.19**	**8.78**	2.5291	158.5	163.5
Blue_SV_4_N	**4D**	159	AX-94632373	AX-94818797	**3.64**	**7.90**	1.5041	158.5	163.5
Green_SV_4_N	**4D**	159	AX-94632373	AX-94818797	**4.12**	**10.48**	2.1801	158.5	163.5
R-G_TV_4_N	**4D**	160	AX-94632373	AX-94818797	**6.07**	**9.83**	-0.4191	158.5	163.5
INT_TV_4_N	**4D**	160	AX-94632373	AX-94818797	**7.17**	**11.46**	2.6270	158.5	164.5
INT_SV_4_N	**4D**	159	AX-94632373	AX-94818797	**3.75**	**9.40**	1.9000	158.5	163.5
NIRSV_5_N	**4D**	159	AX-94632373	AX-94818797	**3.98**	**7.66**	1.0423	158.5	164.5
SLR2_TV_5_N	**4D**	159	AX-94632373	AX-94818797	**3.65**	**6.90**	-1.6705	158.5	162.5

2ndMomentPrincipleAxisSmallNorm_SV_2_N	**2D**	59	AX-94644557	AX-95630531	**3.71**	**7.22**	-0.0031	58.5	59.5
2ndMomentPrincipleAxisSmallNorm_SV_3_N	**2D**	59	AX-94644557	AX-95630531	**5.43**	**7.85**	-0.0037	58.5	59.5
IRTV_4_N	**4A**	3	AX-94665638	AX-94564822	**3.50**	**8.54**	-0.3883	2.5	4.5
SLR1_SV_4_N	**4A**	4	AX-94665638	AX-94564822	**4.12**	**6.51**	3.2279	2.5	8.5
GMR_SV_4_N	**4A**	4	AX-94665638	AX-94564822	**4.17**	**6.86**	-0.5930	2.5	8.5
G/R_SV_4_N	**4A**	4	AX-94665638	AX-94564822	**4.17**	**6.86**	-0.5930	2.5	8.5
G/B_TV_4_N	**4A**	4	AX-94665638	AX-94564822	**4.17**	**6.86**	-0.5930	2.5	8.5
BoundaryPointRoundness_SV_5_N	**7A**	66	AX-94666660	AX-95254589	**5.00**	**7.57**	653.4609	63.5	68.5
R-G_TV_2_N	**6B**	49	AX-94675561	AX-94909094	**4.26**	**7.74**	0.3508	48.5	49.5
Ipca_SV_3_N	**6B**	48	AX-94752965	AX-95242074	**5.10**	**10.96**	-1.8097	47.5	48.5
R-G_TV_4_N	**6B**	48	AX-94752965	AX-95242074	**6.01**	**9.42**	0.4100	47.5	48.5
2ndMomentPrincipleAxisSmallNorm_SV_3_N	**1D**	103	AX-94787613	AX-94723571	**4.81**	**7.04**	-0.0035	102.5	103.5
2ndMomentPrincipleAxisLargeNorm_SV_1_N	**4D**	158	AX-94803237	AX-94762683	**4.88**	**11.43**	0.0309	155.5	158.5
Excentricity_SV_1_N	**4D**	158	AX-94803237	AX-94762683	**5.27**	**12.63**	0.0319	155.5	158.5
SLR1_TV_3_N	**4D**	158	AX-94803237	AX-94762683	**5.14**	**8.72**	-1.8119	155.5	158.5
SLR2_TV_3_N	**4D**	158	AX-94803237	AX-94762683	**10.98**	**15.60**	-2.0226	155.5	158.5
NIRSV_4_N	**4D**	158	AX-94803237	AX-94762683	**3.58**	**8.01**	1.0751	155.5	158.5
SLR2_TV_4_N	**4D**	157	AX-94803237	AX-94762683	**5.99**	**11.81**	-1.7199	155.5	158.5
2ndMomentPrincipleAxisLargeNorm_SV_1_N	**4D**	94	AX-94813788	AX-95134817	**5.12**	**12.05**	-0.0321	93.5	95.5
CenterOfMassY_SV_3_N	**4D**	94	AX-94813788	AX-95134817	**4.60**	**10.34**	28.3678	93.5	95.5
ConvexHullArea_SV_5_N	**4D**	94	AX-94813788	AX-95134817	**68.02**	**21.17**	-305196.1250	93.5	94.5
R-G_TV_1_N	**4D**	166	AX-94818797	AX-94393215	**4.52**	**10.13**	-0.3843	165.5	174.5
Compactness_SV_1_N	**2A**	30	AX-94838306	AX-94391321	**4.05**	**8.93**	-0.0099	23.5	39.5
ConvexHullCircumference_SV_2_N	**4D**	143	AX-94852086	AX-94423396	**3.66**	**2.13**	109.4938	129.5	144.5
Excentricity_SV_2_N	**4D**	140	AX-94852086	AX-94423396	**5.06**	**11.97**	0.0372	130.5	144.5
ObjectExtentY_SV_2_N	**4D**	144	AX-94852086	AX-94423396	**4.07**	**3.03**	52.9177	131.5	144.5
ConvexHullCircumference_SV_3_N	**4D**	137	AX-94852086	AX-94423396	**4.39**	**6.96**	185.1349	126.5	144.5
ObjectExtentY_SV_3_N	**4D**	137	AX-94852086	AX-94423396	**5.24**	**15.04**	104.6397	127.5	144.5
2ndMomentsPrincipalAxisRatio_SV_4_N	**4D**	140	AX-94852086	AX-94423396	**4.63**	**7.18**	1.2586	128.5	144.5

CenterOfMassY_SV_4_N	**4D**	140	AX-94852086	AX-94423396	**7.25**	**22.99**	-40.7927	130.5	144.5
ConvexHullCircumference_SV_4_N	**4D**	138	AX-94852086	AX-94423396	**6.70**	**22.00**	217.1187	129.5	144.5
Excentricity_SV_4_N	**4D**	140	AX-94852086	AX-94423396	**5.29**	**8.10**	0.0398	129.5	144.5
ObjectExtentY_SV_4_N	**4D**	138	AX-94852086	AX-94423396	**7.51**	**23.66**	119.2919	130.5	144.5
2ndMomentsPrincipalAxisRatio_SV_5_N	**4D**	144	AX-94852086	AX-94423396	**3.60**	**7.22**	1.3655	131.5	144.5
CenterOfMassY_SV_5_N	**4D**	139	AX-94852086	AX-94423396	**6.86**	**22.12**	-43.0043	129.5	144.5
ConvexHullCircumference_SV_5_N	**4D**	139	AX-94852086	AX-94423396	**7.44**	**23.35**	231.7894	131.5	144.5
Excentricity_SV_5_N	**4D**	144	AX-94852086	AX-94423396	**3.55**	**7.30**	0.0289	132.5	144.5
ObjectExtentY_SV_5_N	**4D**	138	AX-94852086	AX-94423396	**7.82**	**24.04**	125.2825	130.5	144.5
g_TV_1_N	**2B**	292	AX-94852490	AX-95244768	**3.70**	**7.51**	0.0009	291.5	292
Gray_TV_1_N	**2B**	292	AX-94852490	AX-95244768	**4.18**	**8.75**	0.0005	291.5	292
PCA1_SV_1_N	**2B**	292	AX-94852490	AX-95244768	**4.67**	**11.88**	0.0059	291.5	292
Blue_TV_2_N	**2B**	292	AX-94852490	AX-95244768	**3.91**	**6.02**	1.1686	291.5	292
Green_TV_2_N	**2B**	292	AX-94852490	AX-95244768	**4.06**	**7.83**	2.1372	291.5	292
R-G_TV_2_N	**2B**	292	AX-94852490	AX-95244768	**5.01**	**9.12**	-0.3809	291.5	292
INT_TV_2_N	**2B**	292	AX-94852490	AX-95244768	**3.75**	**7.22**	1.6494	291.5	292
BoundaryPointsToAreaRatio_SV_3_N	**2B**	292	AX-94852490	AX-95244768	**3.68**	**9.10**	-0.0058	291.5	292
Excentricity_SV_1_N	**2B**	47	AX-94856684	AX-95633110	**3.47**	**8.47**	0.0262	46.5	47.5
PSCC_15_2_N	**2B**	37	AX-94901457	AX-94395539	**3.37**	**5.42**	-2562.5137	36.5	37.5
Area_SV_5_N	**2A**	116	AX-94903968	AX-94541515	**3.46**	**8.49**	10070.1094	103.5	117.5
NIRTV_5_N	**5B**	63	AX-94906481	AX-95091972	**4.35**	**10.56**	-1.0545	62.5	67.5
ConvexHullArea_TV_1_N	**1A**	246	AX-94935688	AX-94632377	**3.40**	**7.08**	-41245.6250	237.5	252.5
2ndMomentPrincipleAxisSmallNorm_SV_4_N	**4B**	66	AX-94938436	AX-94489678	**8.00**	**16.23**	0.0048	63.5	67.5
SLR2_SV_3_N	**4D**	154	AX-94962854	AX-94803237	**3.82**	**9.19**	-2.2621	152.5	158.5
SLR2_SV_4_N	**4D**	154	AX-94962854	AX-94803237	**4.45**	**8.24**	-3.0124	152.5	158.5
SLR2_SV_5_N	**4D**	155	AX-94962854	AX-94803237	**6.84**	**12.40**	-3.1495	153.5	158.5
AreaDistributionAboveRelative_SV_2_N	**5D**	274	AX-94964352	AX-95164232	**3.50**	**1.15**	-0.0003	273.5	307.5
NoPSCC_5_N	**4D**	12	AX-94970370	AX-95245862	**3.44**	**6.23**	-1211.4351	10.5	13.5
2ndMomentsPrincipalAxisRatio_SV_1_N	**4D**	70	AX-94988276	AX-95179517	**6.44**	**13.15**	-0.6805	68.5	70.5

Excentricity_SV_1_N	**4D**	70	AX-94988276	AX-95179517	**5.99**	**14.30**	-0.0340	68.5	70.5
2ndMomentPrincipleAxisLargeNorm_SV_2_N	**4D**	70	AX-94988276	AX-95179517	**6.37**	**12.40**	-0.0481	69.5	70.5
2ndMomentsPrincipalAxisRatio_SV_2_N	**4D**	70	AX-94988276	AX-95179517	**5.81**	**12.23**	-0.8993	68.5	70.5
ConvexHullCircumference_SV_2_N	**4D**	70	AX-94988276	AX-95179517	**19.73**	**13.03**	-270.7538	69.5	70.5
Excentricity_SV_2_N	**4D**	70	AX-94988276	AX-95179517	**6.63**	**11.47**	-0.0364	68.5	70.5
ObjectExtentY_SV_2_N	**4D**	70	AX-94988276	AX-95179517	**18.20**	**16.22**	-122.3262	69.5	70.5
2ndMomentPrincipleAxisLargeNorm_SV_3_N	**4D**	70	AX-94988276	AX-95179517	**7.20**	**12.00**	-0.0813	69.5	70.5
Excentricity_SV_3_N	**4D**	70	AX-94988276	AX-95179517	**6.58**	**14.76**	-0.0405	69.5	70.5
ObjectExtentY_SV_3_N	**4D**	70	AX-94988276	AX-95179517	**4.30**	**7.51**	-73.9625	69.5	70.5
NIRSV_4_N	**4D**	70	AX-94988276	AX-95179517	**3.76**	**8.36**	-1.0985	68.5	70.5
2ndMomentPrincipleAxisLargeNorm_SV_5_N	**4D**	70	AX-94988276	AX-95179517	**6.14**	**12.07**	-0.1097	69.5	70.5
2ndMomentsPrincipalAxisRatio_SV_5_N	**4D**	70	AX-94988276	AX-95179517	**5.94**	**12.15**	-1.7700	68.5	70.5
Compactness_SV_5_N	**4D**	70	AX-94988276	AX-95179517	**4.51**	**10.93**	0.0151	69.5	70.5
Excentricity_SV_5_N	**4D**	70	AX-94988276	AX-95179517	**5.62**	**11.73**	-0.0367	68.5	70.5
Green_SV_1_N	**6A**	191	AX-95010403	AX-94431190	**3.66**	**8.49**	-2.3347	184.5	193.5
Ipca_SV_1_N	**6A**	191	AX-95010403	AX-94431190	**4.14**	**9.60**	-2.1915	184.5	193.5
PCA2_SV_1_N	**6A**	191	AX-95010403	AX-94431190	**3.81**	**9.36**	-1.7318	184.5	193.5
I1_SV_1_N	**6A**	191	AX-95010403	AX-94431190	**4.17**	**9.71**	-2.0269	184.5	193.5
Blue_SV_2_N	**6A**	191	AX-95010403	AX-94431190	**4.72**	**9.56**	-1.6903	184.5	192.5
Green_SV_2_N	**6A**	191	AX-95010403	AX-94431190	**5.23**	**12.19**	-2.7694	185.5	192.5
Red_SV_2_N	**6A**	191	AX-95010403	AX-94431190	**4.80**	**11.36**	-2.5331	184.5	192.5
INT_SV_2_N	**6A**	191	AX-95010403	AX-94431190	**4.85**	**11.42**	-2.3016	184.5	192.5
Compactness_SV_3_N	**6A**	190	AX-95010403	AX-94431190	**10.13**	**13.39**	0.0172	186.5	192.5
Compactness_SV_4_N	**6A**	191	AX-95010403	AX-94431190	**11.38**	**11.73**	0.0184	186.5	192.5
PSCC_1_4_N	**6A**	191	AX-95010403	AX-94431190	**3.96**	**8.49**	42.8810	186.5	193.5
BoundaryPointsToAreaRatio_TV_2_N	**2D**	342	AX-95016766	AX-95654169	**5.59**	**11.67**	-0.0050	341.5	343.5
BoundaryPointsToAreaRatio_SV_2_N	**2D**	342	AX-95016766	AX-95654169	**8.23**	**18.58**	-0.0073	341.5	343.5
BoundaryPointsToAreaRatio_TV_3_N	**2D**	342	AX-95016766	AX-95654169	**5.70**	**10.30**	-0.0045	341.5	343.5
BoundaryPointRoundness_TV_4_N	**2D**	342	AX-95016766	AX-95654169	**5.18**	**13.35**	-125.0849	341.5	343.5

AreaDistributionAboveRelative_SV_2_N	**5A**	142	AX-95106872	AX-94935882	**3.68**	**1.15**	-0.0003	134.5	143.5
b_TV_4_N	**2D**	375	AX-95125039	AX-94901587	**4.37**	**9.05**	-0.0012	368.5	375
PCA1_TV_4_N	**2D**	375	AX-95125039	AX-94901587	**4.24**	**9.29**	0.0075	368.5	375
PSCC_15_1_N	**2B**	280	AX-95126899	AX-95137042	**5.18**	**12.33**	3193.8125	273.5	288.5
BoundaryPointsToAreaRatio_SV_4_N	**2B**	283	AX-95126899	AX-95137042	**4.52**	**8.49**	-0.0059	275.5	288.5
NIRSV_1_N	**4D**	95	AX-95134817	AX-94465412	**5.11**	**9.60**	-1.8235	93.5	95.5
NIRSV_3_N	**4D**	95	AX-95134817	AX-94465412	**5.90**	**10.72**	-1.6706	94.5	96.5
SLR1_TV_4_N	**4D**	95	AX-95134817	AX-94465412	**3.79**	**8.19**	1.7504	94.5	97.5
PSCC_15_2_N	**3A**	131	AX-95136924	AX-95630394	**3.48**	**5.61**	-2614.3750	130.5	131.5
b_SV_1_N	**2B**	288	AX-95137042	AX-94494621	**5.79**	**14.77**	-0.0012	284.5	290.5
ExG_SV_1_N	**2B**	286	AX-95137042	AX-94494621	**5.56**	**13.89**	0.0033	278.5	290.5
Gray_SV_1_N	**2B**	287	AX-95137042	AX-94494621	**6.45**	**15.73**	0.0006	279.5	290.5
SLR4_SV_1_N	**2B**	287	AX-95137042	AX-94494621	**4.58**	**9.05**	-1.4253	279.5	290.5
PSCC_16_2_N	**3B**	22	AX-95139631	AX-94604586	**3.38**	**6.77**	6653.6523	20.5	23.5
2ndMomentsPrincipalAxisRatio_SV_1_N	**2A**	22	AX-95142641	AX-94386463	**3.83**	**8.20**	0.5375	8.5	26.5
2ndMomentPrincipleAxisLargeNorm_SV_2_N	**2A**	20	AX-95142641	AX-94386463	**3.70**	**8.28**	0.0393	7.5	22.5
PSCC_16_1_N	**2A**	129	AX-95153321	AX-94417025	**3.59**	**8.69**	6089.3320	126.5	131.5
SLR4_SV_1_N	**2A**	129	AX-95153321	AX-94417025	**4.21**	**8.00**	-1.3398	126.5	131.5
2ndMomentPrincipleAxisSmallNorm_SV_1_N	**6B**	46	AX-95160166	AX-94829211	**57.33**	**11.96**	0.0195	45.5	46.5
b_TV_2_N	**6B**	46	AX-95160166	AX-94829211	**3.94**	**9.77**	0.0015	44.5	46.5
g_TV_2_N	**6B**	45	AX-95160166	AX-94829211	**3.88**	**9.62**	-0.0009	40.5	46.5
R-B_TV_2_N	**6B**	46	AX-95160166	AX-94829211	**3.80**	**9.90**	-0.7958	44.5	46.5
(R-G)/(R+G+B)_TV_2_N	**6B**	46	AX-95160166	AX-94829211	**3.80**	**9.90**	-0.7958	44.5	46.5
(G-B)/(R+G+B)_TV_2_N	**6B**	46	AX-95160166	AX-94829211	**3.80**	**9.90**	-0.7958	44.5	46.5
(G-B)/(R+G+B)_SV_2_N	**6B**	46	AX-95160166	AX-94829211	**3.80**	**9.90**	-0.7958	44.5	46.5
Ipca_SV_2_N	**6B**	46	AX-95160166	AX-94829211	**4.64**	**12.33**	-2.3027	44.5	46.5
Gray_TV_2_N	**6B**	46	AX-95160166	AX-94829211	**4.32**	**10.68**	-0.0005	44.5	46.5
PCA2_SV_2_N	**6B**	46	AX-95160166	AX-94829211	**4.61**	**11.86**	-1.8364	44.5	46.5
I1_SV_2_N	**6B**	46	AX-95160166	AX-94829211	**4.73**	**12.36**	-2.1407	44.5	46.5

Green_TV_3_N	**6B**	46	AX-95160166	AX-94829211	**4.34**	**6.81**	-1.9754	44.5	46.5
Blue_SV_3_N	**6B**	46	AX-95160166	AX-94829211	**4.85**	**10.73**	-1.7873	44.5	46.5
Green_SV_3_N	**6B**	46	AX-95160166	AX-94829211	**5.64**	**12.60**	-2.6146	44.5	46.5
Red_SV_3_N	**6B**	46	AX-95160166	AX-94829211	**5.11**	**11.82**	-2.5016	44.5	46.5
b_TV_3_N	**6B**	46	AX-95160166	AX-94829211	**5.79**	**12.73**	0.0014	44.5	46.5
g_TV_3_N	**6B**	46	AX-95160166	AX-94829211	**4.57**	**10.61**	-0.0008	44.5	46.5
R-G_TV_3_N	**6B**	46	AX-95160166	AX-94829211	**4.82**	**8.17**	0.3730	44.5	46.5
R-B_TV_3_N	**6B**	46	AX-95160166	AX-94829211	**5.47**	**13.81**	-0.7901	44.5	46.5
(R-G)/(R+G+B)_TV_3_N	**6B**	46	AX-95160166	AX-94829211	**5.47**	**13.81**	-0.7901	44.5	46.5
(G-B)/(R+G+B)_TV_3_N	**6B**	46	AX-95160166	AX-94829211	**5.47**	**13.81**	-0.7901	44.5	46.5
(G-B)/(R+G+B)_SV_3_N	**6B**	46	AX-95160166	AX-94829211	**5.47**	**13.81**	-0.7901	44.5	46.5
Gray_TV_3_N	**6B**	46	AX-95160166	AX-94829211	**5.12**	**12.46**	-0.0005	44.5	46.5
PCA1_TV_3_N	**6B**	46	AX-95160166	AX-94829211	**5.48**	**12.08**	-0.0079	44.5	46.5
PCA2_SV_3_N	**6B**	46	AX-95160166	AX-94829211	**4.96**	**11.59**	-1.5188	44.5	46.5
I1_SV_3_N	**6B**	46	AX-95160166	AX-94829211	**5.13**	**11.27**	-1.6883	44.5	46.5
INT_SV_3_N	**6B**	46	AX-95160166	AX-94829211	**5.16**	**11.94**	-2.2789	44.5	46.5
b_TV_4_N	**6D**	119	AX-95172977	AX-95143298	**4.35**	**8.85**	0.0012	117.5	135.5
PCA1_TV_4_N	**6D**	119	AX-95172977	AX-95143298	**3.91**	**8.49**	-0.0072	117.5	135.5
NoPSCC_5_N	**6D**	119	AX-95172977	AX-95143298	**3.52**	**6.64**	1257.8506	117.5	135.5
2ndMomentsPrincipalAxisRatio_SV_1_N	**4D**	93	AX-95179517	AX-94799212	**4.13**	**8.31**	-0.5470	82.5	93.5
2ndMomentsPrincipalAxisRatio_SV_2_N	**4D**	91	AX-95179517	AX-94799212	**4.86**	**12.51**	-0.9187	83.5	93.5
Excentricity_SV_2_N	**4D**	91	AX-95179517	AX-94799212	**7.07**	**14.54**	-0.0414	83.5	93.5
2ndMomentPrincipleAxisSmallNorm_SV_3_N	**4D**	76	AX-95179517	AX-94799212	**12.46**	**26.10**	0.0068	71.5	81.5
2ndMomentsPrincipalAxisRatio_SV_3_N	**4D**	81	AX-95179517	AX-94799212	**12.02**	**26.84**	-2.0561	73.5	88.5
Excentricity_SV_3_N	**4D**	93	AX-95179517	AX-94799212	**4.64**	**10.29**	-0.0342	83.5	93.5
2ndMomentPrincipleAxisLargeNorm_SV_4_N	**4D**	81	AX-95179517	AX-94799212	**9.81**	**17.27**	-0.1476	74.5	87.5
2ndMomentsPrincipalAxisRatio_SV_4_N	**4D**	81	AX-95179517	AX-94799212	**14.81**	**26.95**	-2.4426	75.5	87.5
CenterOfMassY_SV_4_N	**4D**	71	AX-95179517	AX-94799212	**6.17**	**14.67**	32.5546	69.5	79.5
Compactness_SV_4_N	**4D**	85	AX-95179517	AX-94799212	**8.14**	**10.96**	0.0179	77.5	91.5

ConvexHullArea_SV_4_N	**4D**	72	AX-95179517	AX-94799212	**3.72**	**8.43**	-48001.5000	69.5	81.5
ConvexHullCircumference_SV_4_N	**4D**	71	AX-95179517	AX-94799212	**5.05**	**10.52**	-150.1051	69.5	80.5
Excentricity_SV_4_N	**4D**	83	AX-95179517	AX-94799212	**15.84**	**28.62**	-0.0755	77.5	88.5
ObjectExtentY_SV_4_N	**4D**	71	AX-95179517	AX-94799212	**6.12**	**12.13**	-85.3937	69.5	79.5
R-G_TV_4_N	**4D**	77	AX-95179517	AX-94799212	**5.73**	**11.77**	0.4595	69.5	85.5
BoundaryPointCount_TV_5_N	**4D**	87	AX-95179517	AX-94799212	**3.52**	**7.83**	-1428.6514	77.5	93.5
ConvexHullArea_TV_5_N	**4D**	83	AX-95179517	AX-94799212	**5.95**	**13.71**	-92157.7188	74.5	90.5
MinAreaRectangleArea_TV_5_N	**4D**	83	AX-95179517	AX-94799212	**6.25**	**14.43**	-119673.7812	75.5	91.5
CenterOfMassY_SV_5_N	**4D**	71	AX-95179517	AX-94799212	**6.35**	**14.59**	34.9089	69.5	79.5
ConvexHullCircumference_SV_5_N	**4D**	71	AX-95179517	AX-94799212	**6.13**	**12.77**	-171.3809	69.5	79.5
ObjectExtentY_SV_5_N	**4D**	71	AX-95179517	AX-94799212	**6.55**	**12.48**	-90.2330	69.5	78.5
SLR1_TV_5_N	**4D**	77	AX-95179517	AX-94799212	**11.47**	**20.17**	3.0061	70.5	82.5
SLR2_TV_5_N	**4D**	76	AX-95179517	AX-94799212	**7.51**	**18.19**	2.7173	69.5	86.5
ObjectExtentY_SV_2_N	**4B**	61	AX-95196960	AX-94475207	**5.93**	**4.84**	66.7684	58.5	62.5
ConvexHullCircumference_SV_2_N	**4D**	64	AX-95211803	AX-94584787	**9.54**	**5.81**	180.7032	61.5	65.5
CenterOfMassY_SV_2_N	**4D**	148	AX-95215056	AX-94962854	**4.71**	**6.22**	-26.0614	145.5	152.5
CenterOfMassY_SV_3_N	**4D**	148	AX-95215056	AX-94962854	**5.63**	**13.82**	-32.4602	145.5	152.5
NIRSV_3_N	**4D**	149	AX-95215056	AX-94962854	**3.93**	**7.62**	1.3921	145.5	152.5
ConvexHullArea_SV_4_N	**4D**	149	AX-95215056	AX-94962854	**4.61**	**10.57**	53805.7500	145.5	152.5
PSCC_11_4_N	**4D**	150	AX-95215056	AX-94962854	**4.64**	**8.53**	2090.9102	146.5	154.5
BoundaryPointCount_SV_4_N	**3D**	302	AX-95245565	AX-95124939	**3.57**	**6.90**	-2507.4062	300.5	307.5
SLR2_TV_2_N	**5D**	201	AX-95248671	AX-94775978	**6.10**	**9.88**	-1.9488	195.5	204.5
BoundaryPointsToAreaRatio_SV_4_N	**4D**	51	AX-95253860	AX-94460894	**3.85**	**7.26**	-0.0054	43.5	52.5
Gray_SV_4_N	**4D**	52	AX-95253860	AX-94460894	**3.78**	**7.55**	0.0004	44.5	52.5
Gray_SV_5_N	**4D**	49	AX-95253860	AX-94460894	**4.07**	**6.32**	0.0006	42.5	52.5
b_TV_4_N	**6B**	30	AX-95652947	AX-94679349	**3.54**	**7.47**	0.0011	27.5	33.5
Gray_TV_4_N	**6B**	29	AX-95652947	AX-94679349	**4.30**	**7.76**	-0.0004	27.5	33.5
BoundaryPointRoundness_TV_1_N	**2D**	343	AX-95654169	AX-94976248	**6.68**	**15.93**	-182.0112	342.5	343.5
BoundaryPointsToAreaRatio_TV_1_N	**2D**	343	AX-95654169	AX-94976248	**6.62**	**15.16**	-0.0059	341.5	343.5

BoundaryPointsToAreaRatio_SV_1_N	**2D**	343	AX-95654169	AX-94976248	**10.86**	**22.29**	-0.0073	341.5	343.5
BoundaryPointRoundness_TV_2_N	**2D**	343	AX-95654169	AX-94976248	**7.32**	**16.07**	-161.3472	342.5	343.5
BoundaryPointRoundness_TV_3_N	**2D**	343	AX-95654169	AX-94976248	**9.17**	**21.83**	-170.5826	341.5	343.5
PSCC_13_1_N	**2D**	322	AX-95683514	AX-95016766	**3.50**	**8.64**	500.6719	321.5	332.5
PSCC_14_1_N	**2D**	327	AX-95683514	AX-95016766	**4.66**	**11.65**	1274.4971	321.5	335.5
PSCC_15_2_N	**2D**	326	AX-95683514	AX-95016766	**5.23**	**11.24**	3690.9258	321.5	333.5
Compactness_TV_3_N	**2D**	329	AX-95683514	AX-95016766	**6.00**	**14.57**	0.0124	321.5	335.5
PSCC_15_3_N	**2D**	322	AX-95683514	AX-95016766	**3.53**	**6.82**	2938.3379	321.5	331.5
Compactness_TV_4_N	**2D**	325	AX-95683514	AX-95016766	**5.03**	**9.66**	0.0102	321.5	332.5

ANNEXURE 12: QTLs identified for HTP traits under N:C ratio condition

TraitID	Chromosome	Position	LeftMarker	RightMarker	LOD	PVE(%)	Add	LeftCI	RightCI
2ndMomentsPrincipalAxisRatio_SV_2_CN	**4D**	171	AX-94393215	AX-94436391	**4.69**	**9.73**	-0.0938	167.5	176.5
PSCC_1_5_CN	**2A**	147	AX-94417025	AX-94521851	**3.73**	**4.51**	-0.0582	137.5	151.5
CenterOfMassY_SV_5_CN	**4D**	188	AX-94436391	AX-94791821	**3.55**	**7.32**	0.0045	178.5	192
BoundaryPointRoundness_TV_1_CN	**4B**	62	AX-94475207	AX-94709746	**6.46**	**5.56**	0.0578	61.5	62.5
NIRSV_1_CN	**6B**	75	AX-94531156	AX-94878401	**11.89**	**10.57**	-0.0074	74.5	75.5
BoundaryPointCount_TV_1_CN	**7D**	108	AX-94533004	AX-94389584	**3.29**	**7.96**	0.0482	100.5	111.5
BoundaryPointRoundness_TV_1_CN	**7D**	109	AX-94533004	AX-94389584	**3.78**	**3.46**	0.0457	102.5	111.5
ObjectExtentX_SV_1_CN	**7D**	108	AX-94533004	AX-94389584	**4.08**	**9.63**	0.0274	101.5	111.5
PSCC_7_1_CN	**7D**	105	AX-94533004	AX-94389584	**3.30**	**7.56**	0.0394	97.5	111.5
PSCC_8_1_CN	**7D**	108	AX-94533004	AX-94389584	**3.89**	**8.64**	0.0499	100.5	111.5
2ndMomentPrincipleAxisLargeNorm_SV_2_CN	**7D**	109	AX-94533004	AX-94389584	**4.64**	**11.16**	-0.0674	101.5	112.5
PSCC_7_2_CN	**7D**	103	AX-94533004	AX-94389584	**3.33**	**7.45**	0.0431	95.5	110.5
PSCC_8_2_CN	**7D**	105	AX-94533004	AX-94389584	**3.63**	**8.42**	0.0543	97.5	111.5
PSCC_8_3_CN	**7D**	105	AX-94533004	AX-94389584	**4.13**	**9.08**	0.0675	98.5	111.5
BoundaryPointRoundness_TV_5_CN	**7D**	95	AX-94533004	AX-94389584	**5.07**	**10.71**	0.0780	93.5	103.5
PSCC_12_5_CN	**7D**	108	AX-94533004	AX-94389584	**3.41**	**8.21**	0.0654	99.5	113.5
Red_SV_2_CN	**6B**	47	AX-94599546	AX-94406470	**3.54**	**8.80**	-0.0225	46.5	47.5
b_TV_2_CN	**6B**	47	AX-94599546	AX-94406470	**4.07**	**9.89**	0.0050	46.5	47.5
r_SV_2_CN	**6B**	47	AX-94599546	AX-94406470	**4.36**	**11.10**	-0.0018	46.5	47.5
PCA2_SV_2_CN	**6B**	47	AX-94599546	AX-94406470	**4.11**	**10.08**	-0.0409	46.5	47.5
SLR3_TV_2_CN	**6B**	47	AX-94599546	AX-94406470	**3.71**	**9.78**	-0.0126	46.5	47.5
I2_TV_2_CN	**6B**	47	AX-94599546	AX-94406470	**3.71**	**9.44**	0.0102	46.5	47.5
NIRTV_4_CN	**6D**	51	AX-94626852	AX-94618570	**3.31**	**9.26**	-0.0038	50.5	51.5
Excentricity_SV_2_CN	**4D**	163	AX-94632373	AX-94818797	**3.76**	**8.27**	-0.1089	158.5	166.5
2ndMomentsPrincipalAxisRatio_SV_1_CN	**6B**	0	AX-94636827	AX-94537957	**3.55**	**7.35**	-0.0693	0	0.5
NIRSV_1_CN	**6D**	184	AX-94643574	AX-94672976	**4.29**	**3.46**	0.0042	181.5	190.5

NormalisedZRotation2ndMoment_TV_1_CN	**6D**	185	AX-94672976	AX-95159098	**3.50**	**7.89**	0.0440	181.5	193.5
SLR2_TV_4_CN	**7B**	237	AX-94696807	AX-94844630	**3.48**	**7.63**	0.0292	236.5	240.5
PSCC_3_4_CN	**6D**	50	AX-94704491	AX-94626852	**3.35**	**8.33**	0.0374	49.5	51.5
Excentricity_SV_2_CN	**4B**	100	AX-94722630	AX-95106107	**4.76**	**9.54**	0.1173	99.5	104.5
2ndMomentPrincipleAxisSmallNorm_TV_4_CN	**3B**	119	AX-94732225	AX-94993758	**3.53**	**6.37**	0.0471	114.5	119.5
NIRSV_1_CN	**6A**	224	AX-94751435	AX-94648279	**6.68**	**5.78**	0.0055	221.5	231.5
PSCC_3_2_CN	**6B**	48	AX-94752965	AX-95242074	**3.53**	**7.66**	0.0413	47.5	48.5
Ipca_SV_2_CN	**6B**	48	AX-94752965	AX-95242074	**3.68**	**9.04**	-0.0292	47.5	48.5
Gray_TV_2_CN	**6B**	48	AX-94752965	AX-95242074	**3.47**	**8.76**	-0.0011	47.5	48.5
I1_SV_2_CN	**6B**	48	AX-94752965	AX-95242074	**3.90**	**9.51**	-0.0338	47.5	48.5
PSCC_3_3_CN	**6B**	48	AX-94752965	AX-95242074	**3.75**	**9.11**	0.0396	47.5	48.5
PSCC_4_3_CN	**6B**	48	AX-94752965	AX-95242074	**4.20**	**10.02**	0.0503	47.5	48.5
Green_TV_3_CN	**6B**	48	AX-94752965	AX-95242074	**3.73**	**9.20**	-0.0176	47.5	48.5
Red_TV_3_CN	**6B**	48	AX-94752965	AX-95242074	**3.72**	**9.15**	-0.0185	47.5	48.5
b_TV_3_CN	**6B**	48	AX-94752965	AX-95242074	**5.17**	**12.72**	0.0048	47.5	48.5
R-B_TV_3_CN	**6B**	48	AX-94752965	AX-95242074	**4.36**	**10.89**	-0.0517	47.5	48.5
(R-G)/(R+G+B)_TV_3_CN	**6B**	48	AX-94752965	AX-95242074	**4.36**	**10.89**	-0.0517	47.5	48.5
(G-B)/(R+G+B)_TV_3_CN	**6B**	48	AX-94752965	AX-95242074	**4.36**	**10.89**	-0.0517	47.5	48.5
(G-B)/(R+G+B)_SV_3_CN	**6B**	48	AX-94752965	AX-95242074	**4.36**	**10.89**	-0.0517	47.5	48.5
Gray_TV_3_CN	**6B**	48	AX-94752965	AX-95242074	**4.14**	**10.60**	-0.0010	47.5	48.5
I2_TV_3_CN	**6B**	48	AX-94752965	AX-95242074	**4.93**	**11.93**	0.0097	47.5	48.5
Green_TV_4_CN	**6B**	48	AX-94752965	AX-95242074	**3.42**	**8.56**	-0.0158	47.5	48.5
Red_TV_4_CN	**6B**	48	AX-94752965	AX-95242074	**3.28**	**8.08**	-0.0159	47.5	48.5
R-B_TV_4_CN	**6B**	48	AX-94752965	AX-95242074	**3.85**	**9.43**	-0.0392	47.5	48.5
(R-G)/(R+G+B)_TV_4_CN	**6B**	48	AX-94752965	AX-95242074	**3.85**	**9.43**	-0.0392	47.5	48.5
(G-B)/(R+G+B)_TV_4_CN	**6B**	48	AX-94752965	AX-95242074	**3.85**	**9.43**	-0.0392	47.5	48.5
(G-B)/(R+G+B)_SV_4_CN	**6B**	48	AX-94752965	AX-95242074	**3.85**	**9.43**	-0.0392	47.5	48.5
Gray_TV_4_CN	**6B**	48	AX-94752965	AX-95242074	**3.58**	**9.08**	-0.0009	47.5	48.5
2ndMomentsPrincipalAxisRatio_SV_1_CN	**4D**	70	AX-94988276	AX-95179517	**3.39**	**6.99**	0.0677	68.5	70.5

Excentricity_SV_3_CN	**4B**	101	AX-95106107	AX-94632604	**3.34**	**8.07**	0.0621	99.5	106.5
CenterOfMassY_SV_1_CN	**6B**	46	AX-95160166	AX-94829211	**3.42**	**9.01**	-0.0042	44.5	46.5
PSCC_4_1_CN	**6B**	46	AX-95160166	AX-94829211	**3.54**	**9.28**	0.0512	44.5	46.5
PSCC_5_1_CN	**6B**	46	AX-95160166	AX-94829211	**3.71**	**9.24**	0.0476	44.5	46.5
CenterOfMassY_SV_2_CN	**6B**	46	AX-95160166	AX-94829211	**4.11**	**10.78**	-0.0051	44.5	46.5
PSCC_4_2_CN	**6B**	46	AX-95160166	AX-94829211	**4.51**	**11.05**	0.0524	44.5	46.5
PSCC_5_2_CN	**6B**	46	AX-95160166	AX-94829211	**4.63**	**11.01**	0.0505	44.5	46.5
PSCC_18_2_CN	**6B**	46	AX-95160166	AX-94829211	**3.45**	**8.88**	0.0651	44.5	46.5
BoundaryPointsToAreaRatio_TV_3_CN	**6B**	46	AX-95160166	AX-94829211	**3.97**	**9.66**	-0.0404	44.5	46.5
Compactness_TV_3_CN	**6B**	46	AX-95160166	AX-94829211	**3.28**	**8.86**	0.0317	44.5	46.5
PSCC_18_3_CN	**6B**	46	AX-95160166	AX-94829211	**4.13**	**10.28**	0.0671	44.5	46.5
PSCC_17_4_CN	**6B**	46	AX-95160166	AX-94829211	**3.61**	**9.20**	0.0587	44.5	46.5
PSCC_18_4_CN	**6B**	46	AX-95160166	AX-94829211	**5.18**	**11.77**	0.0586	44.5	46.5
PSCC_19_4_CN	**6B**	46	AX-95160166	AX-94829211	**3.36**	**7.61**	0.0422	44.5	46.5
b_TV_4_CN	**6B**	46	AX-95160166	AX-94829211	**4.04**	**10.18**	0.0036	44.5	46.5
I2_TV_4_CN	**6B**	46	AX-95160166	AX-94829211	**3.93**	**9.73**	0.0072	44.5	46.5
BoundaryPointRoundness_TV_1_CN	**4D**	71	AX-95179517	AX-94799212	**13.22**	**12.46**	-0.0866	69.5	76.5
BoundaryPointsToAreaRatio_TV_5_CN	**7B**	40	AX-95203420	AX-94718892	**3.47**	**7.14**	0.0649	37.5	40.5
PSCC_3_3_CN	**1B**	56	AX-95631420	AX-94662545	**3.48**	**8.71**	-0.0388	54.5	56.5
PSCC_4_3_CN	**1B**	56	AX-95631420	AX-94662545	**3.33**	**8.06**	-0.0451	54.5	56.5
2ndMomentsPrincipalAxisRatio_SV_5_CN	**6A**	60	AX-95652375	AX-94490584	**3.80**	**9.57**	-0.0635	59.5	60.5

ANNEXURE 13: QTLs identified for manual and semi-automatic traits under control, N stress and N:C ratio condition

QTL clusture	No of traits in QC	Trait Name	Chromosome	Position	LeftMarker	RightMarker	LOD	PVE(%)	Add	LeftCI	Right CI
1	2	DTB_C	2A	25	AX-94386463	AX-94838306	5.76	11.61	-0.848	17.5	28.5
1		DTA_C	2A	26	AX-94386463	AX-94838306	4.69	10.48	-0.8252	23.5	35.5
2	3	Spikeletno._C	2B	45	AX-94395539	AX-95258478	13.37	13.41	-0.6274	40.5	46.5
2		FL:Ear_C	2B	44	AX-94395539	AX-95258478	3.35	5.41	0.0836	37.5	46.5
2		DTA_N	2B	43	AX-94395539	AX-95258478	5.39	11.84	-1.005	37.5	46.5
3		AvgChaffWt_ME_N	5A	146	AX-94406550	AX-95158257	3.34	5.22	0.0213	144.5	147
4	3	AvgSpikeWt_AE_C	5D	372	AX-94407210	AX-95152512	3.40	8.67	0.0877	367.5	378.5
4		AvgGrainWt_AE_C	5D	374	AX-94407210	AX-95152512	3.66	7.30	0.0758	367.5	379.5
4		Length_Top30_TE_N	5D	379	AX-94407210	AX-95152512	3.64	5.57	0.0673	374.5	383.5
5	6	AvgGrainWt_AE_CN	5A	44	AX-94408726	AX-94386305	3.77	7.12	0.0339	42.5	44.5
5		SpikeWt_ME_CN	5A	44	AX-94408726	AX-94386305	3.69	6.50	0.0249	42.5	44.5
5		GrainWt_ME_CN	5A	44	AX-94408726	AX-94386305	3.85	8.10	0.0293	42.5	44.5
5		AvgSpikeWt_ME_CN	5A	44	AX-94408726	AX-94386305	4.10	7.21	0.0261	42.5	44.5
5		AvgGrainWt_ME_CN	5A	44	AX-94408726	AX-94386305	4.89	9.38	0.0315	42.5	44.5
5	1	UI_TotalPlant_NC	5A	43	AX-94408726	AX-94386305	3.32	8.95	0.0364	39.5	44.5
6	2	ChaffWt_ME_C	1A	66	AX-94414832	AX-94633764	4.36	8.86	0.0681	55.5	74.5
6		AvgChaffWt_ME_C	1A	67	AX-94414832	AX-94633764	4.95	10.30	0.0326	55.5	75.5
8		AvgGrainNo_AE_CN	5A	64	AX-94419728	AX-94656347	3.93	6.30	0.0242	62.5	65.5
9	2	LWR_TE_N	5B	168	AX-94423826	AX-94721005	3.94	4.60	-0.0294	167.5	168.5
9		LWR_Top5_AE_N	5B	168	AX-94423826	AX-94721005	4.80	2.63	-0.0245	167.5	168.5
12		Length_ME_C	6B	15	AX-94448837	AX-94849484	5.59	9.35	-0.0991	12.5	15.5
13	2	ChaffWt_ME_CN	2A	128	AX-94451172	AX-95153321	4.84	9.94	0.032	126.5	131.5
13		AvgChaffWt_ME_CN	2A	128	AX-94451172	AX-95153321	4.13	8.44	0.0289	126.5	131.5
14		Length_TE_C	7D	178	AX-94451889	AX-94533316	3.50	5.41	-0.0728	172.5	182.5
14		Area_Top30_TE_C	3A	61	AX-94454033	AX-94504504	4.43	10.36	-0.4102	59.5	62.5
14		Perimeter_Low5_AE_C	3B	162	AX-94460311	AX-95142468	3.86	10.57	-0.3775	147.5	173.5

14		**SpikeletDensity_C**	**2D**	177	AX-94460743	AX-94404928	**5.17**	**7.96**	-0.0533	171.5	177.5
15	**4**	**SpikeWt_ME_CN**	**2B**	137	AX-94464385	AX-94578476	**5.26**	**9.16**	0.0295	136.5	141.5
15		**GrainWt_ME_CN**	**2B**	137	AX-94464385	AX-94578476	**4.61**	**9.64**	0.032	136.5	140.5
15		**AvgSpikeWt_ME_CN**	**2B**	137	AX-94464385	AX-94578476	**4.14**	**7.06**	0.0258	136.5	141.5
15		**AvgGrainWt_ME_CN**	**2B**	137	AX-94464385	AX-94578476	**3.88**	**7.13**	0.0275	136.5	140.5
16		**Phy1_N**	**2D**	321	AX-94470776	AX-94529866	**3.36**	**5.50**	-0.4191	319.5	321.5
17		**LWR_Low30_TE_CN**	**2B**	195	AX-94472688	AX-94511149	**32.63**	**8.42**	-0.0468	194.5	196.5
20	**3**	**SpikeWt_ME_C**	**5B**	264	AX-94476767	AX-94825562	**4.53**	**8.95**	0.2038	262.5	268.5
20		**GrainWt_ME_C**	**5B**	265	AX-94476767	AX-94825562	**3.81**	**7.74**	0.1653	262.5	269.5
20		**AvgSpikeWt_ME_C**	**5B**	264	AX-94476767	AX-94825562	**3.80**	**7.42**	0.0892	262.5	268.5
21	**4**	**Flagleaflength(cm)_C**	**2B**	263	AX-94478750	AX-94666770	**4.65**	**10.41**	-1.0129	260.5	264.5
21		**FL:Ear_C**	**2B**	263	AX-94478750	AX-94666770	**7.72**	**12.03**	-0.1251	260.5	264.5
21		**FlagleafareaxSPAD2_C**	**2B**	263	AX-94478750	AX-94666770	**3.45**	**8.35**	-90.4409	260.5	264.5
21		**Phy2_N**	**2B**	264	AX-94478750	AX-94666770	**4.02**	**6.90**	0.3906	260.5	264.5
23		**Length_Top5_ME_N**	**3A**	63	AX-94485622	AX-94676774	**4.02**	**7.12**	-0.0797	61.5	63.5
25	**2**	**FL:Ear_C**	**4B**	67	AX-94489678	AX-94573089	**4.82**	**7.12**	-0.0955	65.5	67.5
25		**Straw_N**	**4B**	67	AX-94489678	AX-94573089	**14.76**	**12.95**	-1.0385	65.5	67.5
26		**Length_Low30_TE_N**	**4D**	146	AX-94492784	AX-95215056	**3.41**	**6.28**	-0.0819	145.5	152.5
27		**FlagleafareaxSPAD1_C**	**6D**	77	AX-94495622	AX-94589324	**4.47**	**4.91**	-79.5227	73.5	77.5
28		**Spikeletno._C**	**5B**	163	AX-94503623	AX-94512154	**5.22**	**4.61**	0.3685	160.5	163.5
29	**24**	**Spikeletno._C**	**3A**	62	AX-94504504	AX-94485622	**5.85**	**5.19**	0.393	61.5	63.5
29		**Area_TE_C**	**3A**	62	AX-94504504	AX-94485622	**3.63**	**8.88**	-0.3798	60.5	62.5
29		**Area_ME_C**	**3A**	62	AX-94504504	AX-94485622	**4.52**	**10.95**	-0.3924	60.5	62.5
29		**Area_AE_C**	**3A**	62	AX-94504504	AX-94485622	**4.01**	**11.05**	-0.374	60.5	62.5
29		**Area_Top5_ME_C**	**3A**	62	AX-94504504	AX-94485622	**4.46**	**10.87**	-0.404	60.5	62.5
29		**Area_Top5_AE_C**	**3A**	62	AX-94504504	AX-94485622	**4.87**	**11.08**	-0.417	60.5	62.5
29		**Perimeter_TE_C**	**3A**	62	AX-94504504	AX-94485622	**3.41**	**8.46**	-0.2069	60.5	62.5
29		**Perimeter_ME_C**	**3A**	62	AX-94504504	AX-94485622	**4.05**	**10.11**	-0.226	60.5	62.5
29		**Perimeter_AE_C**	**3A**	62	AX-94504504	AX-94485622	**3.96**	**9.68**	-0.2142	59.5	62.5

29		**Area_TE_N**	**3A**	62	AX-94504504	AX-94485622	**5.59**	**13.42**	-0.4033	60.5	62.5
29		**Area_ME_N**	**3A**	62	AX-94504504	AX-94485622	**5.87**	**13.07**	-0.4319	60.5	62.5
29		**Area_AE_N**	**3A**	62	AX-94504504	AX-94485622	**5.97**	**14.18**	-0.4048	60.5	62.5
29		**Area_Top30_TE_N**	**3A**	62	AX-94504504	AX-94485622	**6.73**	**15.08**	-0.4752	60.5	62.5
29		**Area_Top5_ME_N**	**3A**	62	AX-94504504	AX-94485622	**5.46**	**10.79**	-0.4238	61.5	63.5
29		**Area_Top5_AE_N**	**3A**	62	AX-94504504	AX-94485622	**6.71**	**13.42**	-0.445	60.5	62.5
29		**Perimeter_TE_N**	**3A**	62	AX-94504504	AX-94485622	**4.64**	**11.30**	-0.2486	60.5	62.5
29		**Perimeter_ME_N**	**3A**	62	AX-94504504	AX-94485622	**5.02**	**10.21**	-0.2461	60.5	62.5
29		**Perimeter_AE_N**	**3A**	62	AX-94504504	AX-94485622	**5.21**	**11.58**	-0.2433	60.5	62.5
29		**Perimeter_Top30_TE_N**	**3A**	62	AX-94504504	AX-94485622	**6.03**	**10.37**	-0.252	60.5	62.5
29		**Perimeter_Top5_ME_N**	**3A**	62	AX-94504504	AX-94485622	**5.10**	**9.22**	-0.2626	61.5	63.5
29		**Perimeter_Top5_AE_N**	**3A**	62	AX-94504504	AX-94485622	**5.28**	**9.03**	-0.2406	60.5	62.5
29		**Length_TE_N**	**3A**	62	AX-94504504	AX-94485622	**3.52**	**8.23**	-0.0783	60.5	62.5
29		**Length_AE_N**	**3A**	62	AX-94504504	AX-94485622	**3.49**	**7.32**	-0.0735	59.5	62.5
29		**Length_Top5_AE_N**	**3A**	62	AX-94504504	AX-94485622	**5.47**	**6.64**	-0.0773	61.5	63.5
30		**AvGrainNo_TE_N**	**2A**	0	AX-94514957	AX-95164135	**4.32**	**9.01**	-1.3773	0	0.5
31		**SPAD1_C**	**3B**	106	AX-94518428	AX-94886619	**4.27**	**8.18**	-0.6774	104.5	106.5
33	**3**	**Width_TE_CN**	**3B**	239	AX-94532414	AX-95241932	**4.22**	**7.74**	-0.0103	237.5	240
33		**Width_AE_CN**	**3B**	239	AX-94532414	AX-95241932	**3.53**	**6.42**	-0.0079	237.5	240
33		**LWR_TE_CN**	**3B**	239	AX-94532414	AX-95241932	**4.50**	**8.27**	0.0092	237.5	240
34	**5**	**SeedCount_TE_CN**	**7D**	105	AX-94533004	AX-94389584	**4.28**	**10.54**	0.0763	96.5	111.5
34		**SpikeWt_AE_CN**	**7D**	105	AX-94533004	AX-94389584	**3.66**	**8.88**	0.0548	96.5	111.5
34		**GrainWt_AE_CN**	**7D**	104	AX-94533004	AX-94389584	**4.06**	**9.75**	0.0627	96.5	111.5
34		**SpikeWt_TE_CN**	**7D**	105	AX-94533004	AX-94389584	**3.63**	**8.89**	0.068	96.5	111.5
34		**GrainWt_TE_CN**	**7D**	104	AX-94533004	AX-94389584	**3.85**	**9.96**	0.0744	96.5	111.5
35	**2**	**TKW_ME_N**	**3D**	263	AX-94541792	AX-94796463	**3.80**	**9.56**	-1.3049	261.5	265.5
35		**Width_ME_N**	**3D**	263	AX-94541792	AX-94796463	**4.44**	**8.97**	-0.0462	261.5	265.5
36	**8**	**Area_ME_C**	**6A**	172	AX-94552086	AX-94819583	**3.68**	**9.10**	-0.3545	162.5	173.5
36		**Area_Low5_ME_C**	**6A**	172	AX-94552086	AX-94819583	**4.61**	**8.21**	-0.5082	164.5	173.5

36		**Perimeter_Low5_ME_C**	**6A**	172	AX-94552086	AX-94819583	**4.08**	**9.10**	-0.3525	164.5	173.5
36		**Perimeter_Low5_AE_C**	**6A**	172	AX-94552086	AX-94819583	**4.71**	**7.13**	-0.3106	164.5	173.5
36		**Length_TE_C**	**6A**	172	AX-94552086	AX-94819583	**4.00**	**5.86**	-0.0753	161.5	173.5
36		**Length_AE_C**	**6A**	170	AX-94552086	AX-94819583	**4.56**	**8.26**	-0.089	161.5	173.5
36		**Length_Low5_ME_C**	**6A**	172	AX-94552086	AX-94819583	**4.01**	**9.90**	-0.1588	164.5	173.5
36		**Length_Low5_AE_C**	**6A**	172	AX-94552086	AX-94819583	**5.03**	**9.71**	-0.1232	164.5	173.5
37		**SPAD1_CN**	**2A**	182	AX-94555534	AX-94390510	**3.18**	**7.81**	-0.0128	177.5	182.5
38		**AvgChaffWt_ME_N**	**5D**	369	AX-94555577	AX-94407210	**3.61**	**5.31**	0.0214	367.5	375.5
39	**3**	**LC1:SPAD1_C**	**7B**	202	AX-94556413	AX-94920594	**3.62**	**7.12**	0.0335	192.5	206.5
39		**LC1:SPAD2_C**	**7B**	201	AX-94556413	AX-94920594	**3.48**	**6.91**	0.035	191.5	206.5
39		**TC1:SPAD2_C**	**7B**	204	AX-94556413	AX-94920594	**3.53**	**8.04**	0.0102	193.5	209.5
40		**LWR_TE_N**	**6A**	105	AX-94557166	AX-95180977	**8.50**	**10.78**	0.0447	104.5	106.5
42	**2**	**TC1:SPAD1_C**	**4A**	12	AX-94564822	AX-94965732	**3.75**	**7.57**	0.009	5.5	13.5
42		**TC1:SPAD2_C**	**4A**	11	AX-94564822	AX-94965732	**4.07**	**8.87**	0.0108	4.5	13.5
43	**2**	**Area_Top5_ME_N**	**7D**	375	AX-94582171	AX-94688812	**3.94**	**7.61**	0.3523	374.5	375.5
43		**Width_Top5_ME_N**	**7D**	375	AX-94582171	AX-94688812	**4.24**	**9.06**	0.0409	374.5	375.5
44	**7**	**Perimeter_Top5_AE_C**	**3B**	225	AX-94591588	AX-94847389	**4.14**	**8.68**	0.2213	224.5	228.5
44		**Length_ME_C**	**3B**	225	AX-94591588	AX-94847389	**3.99**	**6.91**	0.085	224.5	228.5
44		**Length_AE_C**	**3B**	225	AX-94591588	AX-94847389	**3.78**	**5.99**	0.0758	224.5	230.5
44		**Length_Top5_ME_C**	**3B**	225	AX-94591588	AX-94847389	**4.13**	**6.43**	0.082	224.5	228.5
44		**Length_Top5_AE_C**	**3B**	225	AX-94591588	AX-94847389	**3.90**	**7.01**	0.0756	224.5	228.5
44		**Length_Top5_AE_N**	**3B**	225	AX-94591588	AX-94847389	**3.51**	**4.35**	0.0621	224.5	229.5
44		**LWR_Top5_AE_N**	**3B**	227	AX-94591588	AX-94847389	**26.14**	**21.32**	0.0691	224.5	229.5
45		**SeedCount_TE_N**	**6B**	47	AX-94599546	AX-94406470	**16.66**	**9.11**	28.4237	46.5	47.5
46		**LWR_Low5_AE_C**	**1B**	52	AX-94605330	AX-94487937	**3.46**	**6.95**	-0.0499	51.5	52.5
47	**2**	**AvgGrainWt_AE_CN**	**3D**	254	AX-94611921	AX-94542553	**5.23**	**9.89**	-0.0399	252.5	256.5
47		**AvgGrainWt_TE_CN**	**3D**	254	AX-94611921	AX-94542553	**4.93**	**10.47**	-0.0482	252.5	256.5
47	**2**	**AvgGrainNo_AE_C**	**4D**	98	AX-94618351	AX-94852086	**4.30**	**9.63**	1.5378	95.5	107.5
47		**AvgGrainNo_ME_C**	**4D**	98	AX-94618351	AX-94852086	**4.71**	**10.59**	1.8309	95.5	107.5

48		**Area_Low5_ME_C**	**3A**	51	AX-94621725	AX-94840749	**4.17**	**7.16**	-0.4759	50.5	54.5
49		**LWR_Top5_AE_N**	**3A**	19	AX-94626189	AX-94769054	**16.88**	**11.16**	-0.05	18.5	20.5
50		**AvgSpikeWt_ME_CN**	**1A**	250	AX-94632377	AX-94929285	**4.68**	**8.33**	-0.0281	241.5	253.5
51	**2**	**TotalEar_C**	**1D**	287	AX-94633263	AX-95242859	**3.30**	**7.92**	-0.4792	281.5	290.5
51		**AvGrainNo_TE_C**	**1D**	285	AX-94633263	AX-95242859	**3.53**	**10.18**	1.6248	281.5	288.5
52	**10**	**LWR_ME_C**	**2B**	291	AX-94635171	AX-94568326	**9.10**	**16.34**	-0.0539	290.5	292
52		**LWR_AE_C**	**2B**	291	AX-94635171	AX-94568326	**8.13**	**14.45**	-0.0503	290.5	292
52		**LWR_Top5_AE_C**	**2B**	291	AX-94635171	AX-94568326	**5.82**	**11.74**	-0.0374	290.5	292
52		**Width_ME_N**	**2B**	291	AX-94635171	AX-94568326	**6.67**	**12.87**	0.0551	290.5	292
52		**Width_AE_N**	**2B**	291	AX-94635171	AX-94568326	**4.85**	**12.47**	0.0461	290.5	292
52		**Width_Top30_TE_N**	**2B**	291	AX-94635171	AX-94568326	**4.05**	**10.60**	0.0413	290.5	292
52		**LWR_TE_N**	**2B**	291	AX-94635171	AX-94568326	**8.08**	**9.94**	-0.0429	290.5	292
52		**LWR_ME_N**	**2B**	291	AX-94635171	AX-94568326	**9.96**	**18.00**	-0.0479	290.5	292
52		**LWR_AE_N**	**2B**	291	AX-94635171	AX-94568326	**8.25**	**15.02**	-0.0452	290.5	292
52		**LWR_Top5_AE_N**	**2B**	291	AX-94635171	AX-94568326	**7.32**	**4.16**	-0.0305	290.5	292
53		**AvgGrainNo_ME_CN**	**2A**	125	AX-94639372	AX-94773990	**3.44**	**7.69**	0.0237	124.5	125.5
54		**FLL:FLW_C**	**2B**	267	AX-94666770	AX-95126899	**4.50**	**10.59**	-0.5361	262.5	268.5
55		**Perimeter_Top5_AE_C**	**3A**	57	AX-94674841	AX-94531680	**3.51**	**6.84**	-0.1972	56.5	57.5
56	**4**	**PHI_AE_N**	**7D**	53	AX-94691513	AX-95113410	**5.06**	**8.79**	0.0124	49.5	56.5
56		**PHI_TE_N**	**7D**	53	AX-94691513	AX-95113410	**3.41**	**8.49**	0.0177	49.5	57.5
56		**Perimeter_ME_N**	**7D**	60	AX-94691513	AX-95113410	**3.38**	**6.80**	0.1988	54.5	62.5
56		**Length_ME_N**	**7D**	58	AX-94691513	AX-95113410	**3.51**	**6.22**	0.0786	52.5	62.5
57		**LWR_Top5_AE_N**	**6A**	110	AX-94693461	AX-95110918	**3.76**	**2.04**	-0.0214	108.5	110.5
58		**AvGrainNo_TE_C**	**3A**	69	AX-94709825	AX-95166499	**3.51**	**7.54**	1.4041	68.5	70.5
59		**AvgGrainWt_TE_N**	**1B**	219	AX-94716176	AX-94564758	**4.20**	**5.23**	-0.0676	209.5	220.5
60		**PHI_ME_N**	**5D**	353	AX-94731801	AX-94460698	**3.70**	**1.45**	-0.005	352.5	353.5
61	**2**	**LWR_Top30_TE_CN**	**5A**	39	AX-94740353	AX-94408726	**3.63**	**9.11**	-0.0082	37.5	41.5
61		**LWR_Top5_AE_CN**	**5A**	40	AX-94740353	AX-94408726	**3.41**	**7.17**	-0.0077	36.5	42.5
62	**3**	**Area_Low5_AE_C**	**3A**	132	AX-94756965	AX-94525583	**4.11**	**7.39**	-0.4378	131.5	137.5

62		**SterileSpikelets_N**	**3A**	132	AX-94756965	AX-94525583	**4.95**	**10.39**	-0.3285	131.5	139.5
62		**Grains/Spikelet_N**	**3A**	132	AX-94756965	AX-94525583	**4.95**	**10.39**	-0.3285	131.5	139.5
63		**FlagleafareaxSPAD1_C**	**3B**	96	AX-94769061	AX-95071165	**3.52**	**3.66**	-68.5305	95.5	96.5
64	**1**	**UI_TotalPlant_C**	**7D**	170	AX-94788229	AX-94451889	**3.43**	**8.67**	-1.5209	145.5	174.5
65	**2**	**SPAD1_C**	**4D**	158	AX-94803237	AX-94762683	**4.51**	**8.72**	-0.6995	155.5	158.5
65		**SPAD1_N**	**4D**	156	AX-94803237	AX-94762683	**3.27**	**8.00**	-0.764	152.5	158.5
66		**Length_Top30_TE_N**	**4A**	40	AX-94807421	AX-95121822	**4.30**	**7.61**	-0.079	38.5	41.5
67		**LWR_TE_CN**	**2D**	23	AX-94816778	AX-94529210	**3.79**	**6.95**	0.0084	21.5	23.5
68	**2**	**Perimeter_Low30_TE_N**	**6A**	173	AX-94819583	AX-95164366	**5.05**	**7.95**	-0.2918	167.5	173.5
68		**Length_Low30_TE_N**	**6A**	173	AX-94819583	AX-95164366	**4.62**	**8.67**	-0.0965	167.5	173.5
69		**LWR_Low30_TE_CN**	**2B**	21	AX-94820757	AX-94387250	**3.36**	**0.58**	-0.0123	18.5	23.5
70	**3**	**LWR_TE_N**	**4A**	37	AX-94823192	AX-94460475	**5.55**	**6.64**	-0.0352	35.5	37.5
70		**LWR_AE_N**	**4A**	37	AX-94823192	AX-94460475	**4.02**	**6.97**	-0.0308	35.5	37.5
70		**LWR_Low30_TE_N**	**4A**	37	AX-94823192	AX-94460475	**3.43**	**8.09**	-0.0465	35.5	37.5
71	**3**	**Phy5avg_C**	**1D**	292	AX-94824351	AX-94710221	**3.37**	**7.57**	-0.1271	291.5	292
71		**AvgSpikeWt_AE_N**	**1D**	292	AX-94824351	AX-94710221	**4.02**	**7.94**	0.0868	291.5	292
71		**AvgGrainWt_TE_N**	**1D**	292	AX-94824351	AX-94710221	**8.31**	**11.21**	0.098	291.5	292
72		**Length_Top5_AE_N**	**7B**	74	AX-94824813	AX-94478773	**5.61**	**6.96**	0.0784	69.5	75.5
73		**LWR_Low30_TE_CN**	**3B**	240	AX-94828707	AX-94772233	**5.28**	**0.93**	0.0156	239.5	240
74	**2**	**SterileSpikelets_C**	**2A**	30	AX-94838306	AX-94391321	**3.68**	**6.48**	-0.4325	23.5	39.5
74		**Grains/Spikelet_C**	**2A**	30	AX-94838306	AX-94391321	**3.68**	**6.48**	-0.4325	23.5	39.5
75	**3**	**PHI_ME_N**	**3A**	56	AX-94840749	AX-94674841	**5.93**	**2.53**	-0.0067	52.5	57.5
75		**Spikeletno._N**	**3A**	56	AX-94840749	AX-94674841	**6.08**	**5.96**	0.3963	52.5	57.5
75		**Perimeter_Low5_ME_N**	**3A**	53	AX-94840749	AX-94674841	**3.37**	**7.89**	-0.3232	50.5	56.5
76		**PHI_ME_N**	**3A**	153	AX-94846213	AX-94633808	**4.34**	**1.72**	0.0055	152.5	153.5
77	**8**	**FLtoEarlength_C**	**4D**	144	AX-94852086	AX-94423396	**6.66**	**8.90**	1.5045	134.5	144.5
77		**PH_C**	**4D**	138	AX-94852086	AX-94423396	**8.93**	**22.08**	6.0543	130.5	144.5
77		**LeafNo./Plant_C**	**4D**	138	AX-94852086	AX-94423396	**8.93**	**22.08**	6.0543	130.5	144.5
77		**TillerNo./Plant_C**	**4D**	138	AX-94852086	AX-94423396	**8.93**	**22.08**	6.0543	130.5	144.5

77		**FLtoEarlength_N**	**4D**	138	AX-94852086	AX-94423396	**7.92**	**13.11**	2.4715	131.5	144.5
77		**PH_N**	**4D**	136	AX-94852086	AX-94423396	**9.42**	**28.51**	6.9793	129.5	144.5
77		**LeafNo./Plant_N**	**4D**	136	AX-94852086	AX-94423396	**9.42**	**28.51**	6.9793	129.5	144.5
77		**TillerNo./Plant_N**	**4D**	136	AX-94852086	AX-94423396	**9.42**	**28.51**	6.9793	129.5	144.5
78	**8**	**AvgSpikeWt_AE_C**	**2B**	292	AX-94852490	AX-95244768	**4.84**	**10.48**	0.0964	291.5	292
78		**AvgSpikeWt_TE_C**	**2B**	292	AX-94852490	AX-95244768	**4.61**	**9.75**	0.097	291.5	292
78		**AvgGrainWt_TE_C**	**2B**	292	AX-94852490	AX-95244768	**5.95**	**11.40**	0.0839	291.5	292
78		**SpikeLength_C**	**2B**	292	AX-94852490	AX-95244768	**3.43**	**10.11**	0.2588	291.5	292
78		**Earlength(cm)_C**	**2B**	292	AX-94852490	AX-95244768	**5.41**	**15.40**	0.3497	291.5	292
78		**Width_TE_C**	**2B**	292	AX-94852490	AX-95244768	**3.94**	**9.81**	0.0523	291.5	292
78		**Spikeletno._N**	**2B**	292	AX-94852490	AX-95244768	**10.85**	**10.81**	0.5307	291.5	292
78		**Earlength(cm)_N**	**2B**	292	AX-94852490	AX-95244768	**3.39**	**10.36**	0.2559	291.5	292
79	**7**	**LWR_ME_C**	**5B**	171	AX-94854507	AX-95093991	**3.28**	**5.50**	-0.0318	169.5	171.5
79		**Perimeter_Top5_ME_N**	**5B**	171	AX-94854507	AX-95093991	**4.13**	**7.43**	-0.2371	169.5	171.5
79		**Perimeter_Top5_AE_N**	**5B**	171	AX-94854507	AX-95093991	**4.92**	**8.42**	-0.2335	169.5	171.5
79		**Length_ME_N**	**5B**	171	AX-94854507	AX-95093991	**4.33**	**6.85**	-0.0839	169.5	171.5
79		**Length_Top5_ME_N**	**5B**	171	AX-94854507	AX-95093991	**5.57**	**9.93**	-0.0944	169.5	171.5
79		**Length_Top5_AE_N**	**5B**	171	AX-94854507	AX-95093991	**6.51**	**8.11**	-0.0859	170.5	171.5
79		**LWR_Top5_ME_N**	**5B**	171	AX-94854507	AX-95093991	**3.49**	**6.93**	-0.0275	169.5	171.5
80		**DTB_N**	**2B**	47	AX-94856684	AX-95633110	**5.14**	**10.73**	-0.8365	45.5	47.5
81	**2**	**TKW_AE_N**	**3D**	261	AX-94860226	AX-94475547	**4.39**	**10.43**	-1.4208	259.5	262.5
81		**TKW_TE_N**	**3D**	261	AX-94860226	AX-94475547	**3.95**	**10.60**	-1.3741	258.5	262.5
82	**2**	**DTA_C**	**3A**	49	AX-94877647	AX-94430043	**3.39**	**6.95**	0.6749	48.5	49.5
82		**DTA_N**	**3A**	49	AX-94877647	AX-94430043	**3.42**	**6.74**	0.7597	48.5	49.5
83	**2**	**AvgSpikeWt_AE_N**	**5B**	263	AX-94882207	AX-94476767	**3.46**	**6.63**	0.0794	262.5	267.5
83		**AvgSpikeWt_TE_N**	**5B**	263	AX-94882207	AX-94476767	**3.44**	**7.74**	0.0876	262.5	266.5
84	**3**	**Area_Low30_TE_N**	**3D**	274	AX-94891378	AX-94417156	**3.60**	**8.01**	-0.4235	271.5	280.5
84		**Area_Low5_AE_N**	**3D**	274	AX-94891378	AX-94417156	**4.11**	**8.92**	-0.453	271.5	281.5
84		**Width_Low5_AE_N**	**3D**	274	AX-94891378	AX-94417156	**3.90**	**7.71**	-0.0608	271.5	282.5

87	**2**	**Straw_N**	**2A**	114	AX-94903968	AX-94541515	**3.32**	**2.93**	0.4938	101.5	117.5
87		**Total_Biomass_N**	**2A**	114	AX-94903968	AX-94541515	**3.26**	**7.96**	1.1564	102.5	117.5
88	**1**	**NUtE_C**	**7A**	119	AX-94910468	AX-95081294	**3.76**	**9.59**	-0.7343	110.5	120.5
89		**LWR_Top5_AE_N**	**4D**	3	AX-94916236	AX-94952403	**4.84**	**2.75**	0.0248	0	3.5
90		**PHI_ME_N**	**6D**	118	AX-94917195	AX-95172977	**5.28**	**2.12**	-0.0061	117.5	132.5
91	**2**	**Perimeter_ME_C**	**3A**	17	AX-94927331	AX-95116867	**3.34**	**8.40**	0.2046	13.5	18.5
91		**Length_TE_C**	**3A**	17	AX-94927331	AX-95116867	**3.85**	**5.65**	0.0738	13.5	17.5
92	**3**	**SpikeWt_ME_CN**	**1A**	249	AX-94935688	AX-94632377	**4.88**	**8.53**	-0.0285	241.5	253.5
92		**ChaffWt_ME_CN**	**1A**	247	AX-94935688	AX-94632377	**3.92**	**9.34**	-0.0311	239.5	252.5
92		**AvgChaffWt_ME_CN**	**1A**	247	AX-94935688	AX-94632377	**3.89**	**9.33**	-0.0305	239.5	252.5
94	**3**	**SpikeWt_ME_CN**	**2A**	181	AX-94940052	AX-94555534	**3.42**	**5.95**	-0.0238	176.5	182.5
94		**AvgSpikeWt_ME_CN**	**2A**	181	AX-94940052	AX-94555534	**3.71**	**6.41**	-0.0246	176.5	182.5
94		**LWR_Low30_TE_CN**	**2A**	177	AX-94940052	AX-94555534	**43.52**	**13.40**	0.059	176.5	177.5
96		**Flagleaflength(cm)_N**	**1A**	152	AX-94977486	AX-95211442	**3.40**	**11.92**	-1.9554	138.5	168.5
97		**FL:Ear_C**	**3D**	154	AX-94979815	AX-94711591	**4.43**	**7.24**	-0.0963	147.5	155.5
98	**2**	**SpikeletFertilityPercent_C**	**4B**	49	AX-94985380	AX-94926956	**3.52**	**7.87**	1.9783	41.5	52.5
98		**LWR_Low5_AE_N**	**4B**	41	AX-94985380	AX-94926956	**3.49**	**6.77**	0.0523	37.5	46.5
99	**4**	**PH_C**	**4D**	70	AX-94988276	AX-95179517	**5.99**	**9.17**	-3.9021	68.5	70.5
99		**LeafNo./Plant_C**	**4D**	70	AX-94988276	AX-95179517	**5.99**	**9.17**	-3.9021	68.5	70.5
99		**TillerNo./Plant_C**	**4D**	70	AX-94988276	AX-95179517	**5.99**	**9.17**	-3.9021	68.5	70.5
99		**PH:FlagleaftoEar_N**	**4D**	70	AX-94988276	AX-95179517	**5.20**	**10.03**	3.1103	68.5	70.5
100	**9**	**Spikeletno._C**	**7A**	130	AX-95011176	AX-94512826	**25.36**	**31.15**	-0.9531	128.5	130.5
100		**SterileSpikelets_C**	**7A**	130	AX-95011176	AX-94512826	**8.30**	**14.35**	-0.6435	126.5	134.5
100		**Grains/Spikelet_C**	**7A**	130	AX-95011176	AX-94512826	**8.30**	**14.35**	-0.6435	126.5	134.5
100		**SpikeletDensity_C**	**7A**	129	AX-95011176	AX-94512826	**11.55**	**20.60**	-0.0858	126.5	132.5
100		**SpikeletFertilityPercent_C**	**7A**	130	AX-95011176	AX-94512826	**4.49**	**9.69**	2.197	125.5	135.5
100		**Spikeletno._N**	**7A**	130	AX-95011176	AX-94512826	**26.52**	**35.14**	-0.957	127.5	133.5
100		**SterileSpikelets_N**	**7A**	130	AX-95011176	AX-94512826	**4.89**	**11.39**	-0.3432	125.5	138.5
100		**Grains/Spikelet_N**	**7A**	130	AX-95011176	AX-94512826	**4.89**	**11.39**	-0.3432	125.5	138.5

100		**SpikeletDensity_N**	**7A**	129	AX-95011176	AX-94512826	**7.85**	**17.53**	-0.0802	125.5	132.5
101	**2**	**LWR_Top5_ME_C**	**2D**	342	AX-95016766	AX-95654169	**5.68**	**11.25**	-0.0384	334.5	342.5
101		**Flagleafwidth(cm)_N**	**2D**	342	AX-95016766	AX-95654169	**4.56**	**11.49**	0.0395	341.5	343.5
102	**2**	**AvgGrainWt_AE_N**	**2B**	0	AX-95017401	AX-95235145	**4.52**	**2.93**	-0.0664	0	4.5
102		**AvgGrainWt_TE_N**	**2B**	2	AX-95017401	AX-95235145	**3.36**	**4.49**	-0.0625	0	4.5
103	**2**	**Flagleaflength(cm)_N**	**6D**	32	AX-95075969	AX-95090440	**3.44**	**3.16**	1.0066	20.5	33.5
103		**FLL:FLW_N**	**6D**	32	AX-95075969	AX-95090440	**4.28**	**10.34**	0.5861	29.5	34.5
104	**2**	**LWR_ME_N**	**5B**	167	AX-95078721	AX-94387859	**4.43**	**7.49**	-0.031	166.5	167.5
104		**LWR_AE_N**	**5B**	167	AX-95078721	AX-94387859	**3.87**	**6.72**	-0.0304	166.5	167.5
105		**FlagleafareaxSPAD1_C**	**1B**	138	AX-95080354	AX-95097993	**5.30**	**8.47**	-104.3693	132.5	151.5
106	**3**	**SterileSpikelets_C**	**5B**	157	AX-95080881	AX-94968540	**3.70**	**5.96**	0.4179	150.5	158.5
106		**Grains/Spikelet_C**	**5B**	157	AX-95080881	AX-94968540	**3.70**	**5.96**	0.4179	150.5	158.5
106		**Spikeletno._N**	**5B**	158	AX-95080881	AX-94968540	**4.26**	**4.01**	0.3266	156.5	159.5
107		**Perimeter_Top5_ME_N**	**5B**	115	AX-95091972	AX-94541687	**3.48**	**6.30**	0.2166	103.5	115.5
108	**2**	**Perimeter_Low5_AE_N**	**3D**	217	AX-95098689	AX-94383394	**3.78**	**11.71**	-0.5225	201.5	230.5
108		**Length_Low5_AE_N**	**3D**	218	AX-95098689	AX-94383394	**3.47**	**6.78**	-0.2121	203.5	231.5
109	**3**	**Perimeter_Top30_TE_N**	**5A**	93	AX-95112161	AX-94596250	**3.33**	**5.58**	-0.1829	92.5	93.5
109		**Length_Top30_TE_N**	**5A**	93	AX-95112161	AX-94596250	**4.57**	**6.98**	-0.0753	92.5	93.5
109		**LWR_Top5_AE_N**	**5A**	93	AX-95112161	AX-94596250	**3.61**	**1.97**	-0.021	92.5	93.5
110	**4**	**Area_Top5_ME_N**	**7D**	61	AX-95113410	AX-94716438	**4.24**	**8.31**	0.3685	56.5	62.5
110		**Area_Top5_AE_N**	**7D**	62	AX-95113410	AX-94716438	**3.62**	**7.06**	0.3195	54.5	62.5
110		**Perimeter_Top5_ME_N**	**7D**	62	AX-95113410	AX-94716438	**4.97**	**9.34**	0.2618	60.5	62.5
110		**Perimeter_Top5_AE_N**	**7D**	62	AX-95113410	AX-94716438	**4.24**	**7.30**	0.2144	60.5	62.5
111	**24**	**Perimeter_Top30_TE_C**	**1D**	149	AX-95123147	AX-94623039	**3.36**	**7.99**	0.205	147.5	150.5
111		**Length_TE_C**	**1D**	149	AX-95123147	AX-94623039	**6.63**	**9.83**	0.0976	147.5	150.5
111		**Length_ME_C**	**1D**	149	AX-95123147	AX-94623039	**3.77**	**6.23**	0.0808	147.5	150.5
111		**Length_AE_C**	**1D**	149	AX-95123147	AX-94623039	**5.62**	**8.65**	0.0911	147.5	150.5
111		**Length_Top30_TE_C**	**1D**	149	AX-95123147	AX-94623039	**4.60**	**9.93**	0.0921	147.5	150.5

111		**Length_Top5_ME_C**	**1D**	149	AX-95123147	AX-94623039	**4.04**	**6.05**	0.0796	147.5	150.5
111		**Length_Top5_AE_C**	**1D**	149	AX-95123147	AX-94623039	**5.19**	**8.98**	0.0856	147.5	150.5
111		**LWR_TE_C**	**1D**	149	AX-95123147	AX-94623039	**3.45**	**6.49**	0.0345	147.5	150.5
111		**LWR_ME_C**	**1D**	149	AX-95123147	AX-94623039	**5.32**	**9.20**	0.0406	147.5	150.5
111		**LWR_AE_C**	**1D**	149	AX-95123147	AX-94623039	**4.38**	**7.50**	0.0363	147.5	150.5
111		**LWR_Top30_TE_C**	**1D**	149	AX-95123147	AX-94623039	**5.00**	**8.28**	0.0352	147.5	150.5
111		**LWR_Top5_ME_C**	**1D**	149	AX-95123147	AX-94623039	**5.14**	**10.02**	0.0363	147.5	150.5
111		**LWR_Top5_AE_C**	**1D**	149	AX-95123147	AX-94623039	**5.19**	**10.53**	0.0355	147.5	150.5
111		**Perimeter_Top30_TE_N**	**1D**	149	AX-95123147	AX-94623039	**4.76**	**8.18**	0.2223	147.5	150.5
111		**Length_TE_N**	**1D**	149	AX-95123147	AX-94623039	**3.47**	**8.11**	0.0772	147.5	150.5
111		**Length_Top30_TE_N**	**1D**	149	AX-95123147	AX-94623039	**6.36**	**10.11**	0.0909	147.5	150.5
111		**Length_Top5_ME_N**	**1D**	149	AX-95123147	AX-94623039	**3.81**	**6.66**	0.0763	147.5	150.5
111		**Length_Top5_AE_N**	**1D**	149	AX-95123147	AX-94623039	**5.12**	**6.28**	0.0747	147.5	150.5
111		**LWR_TE_N**	**1D**	149	AX-95123147	AX-94623039	**5.94**	**7.25**	0.0367	147.5	150.5
111		**LWR_ME_N**	**1D**	149	AX-95123147	AX-94623039	**4.34**	**7.44**	0.0309	147.5	150.5
111		**LWR_AE_N**	**1D**	149	AX-95123147	AX-94623039	**4.97**	**8.86**	0.0348	147.5	150.5
111		**LWR_Top30_TE_N**	**1D**	149	AX-95123147	AX-94623039	**5.10**	**9.99**	0.0341	147.5	150.5
111		**LWR_Top5_ME_N**	**1D**	149	AX-95123147	AX-94623039	**5.66**	**11.62**	0.0351	147.5	150.5
111		**LWR_Top5_AE_N**	**1D**	149	AX-95123147	AX-94623039	**9.49**	**5.62**	0.0356	147.5	150.5
112	**2**	**Length_Top5_ME_C**	**7D**	63	AX-95129629	AX-94829914	**6.57**	**10.06**	0.1026	62.5	65.5
112		**Length_Top5_AE_C**	**7D**	63	AX-95129629	AX-94829914	**4.80**	**8.27**	0.082	62.5	65.5
113		**Area_Low5_ME_C**	**3A**	131	AX-95136924	AX-95630394	**4.40**	**7.57**	-0.4884	130.5	131.5
114	**6**	**Width_Top5_ME_C**	**2B**	290	AX-95137042	AX-94494621	**3.79**	**9.30**	0.0451	284.5	290.5
114		**AvgSpikeWt_TE_N**	**2B**	285	AX-95137042	AX-94494621	**5.75**	**13.24**	0.1147	278.5	289.5
114		**AvgGrainWt_TE_N**	**2B**	287	AX-95137042	AX-94494621	**6.79**	**9.40**	0.0897	280.5	290.5
114		**Width_Top5_ME_N**	**2B**	289	AX-95137042	AX-94494621	**4.95**	**11.29**	0.0457	284.5	290.5
114		**Width_Top5_AE_N**	**2B**	289	AX-95137042	AX-94494621	**4.68**	**12.42**	0.043	284.5	290.5
114		**LWR_Top5_ME_N**	**2B**	290	AX-95137042	AX-94494621	**5.25**	**10.79**	-0.0337	286.5	290.5
115	**2**	**LC1:SPAD1_N**	**2A**	22	AX-95142641	AX-94386463	**3.59**	**8.72**	-0.0306	8.5	28.5

115		**TC1:SPAD1_N**	**2A**	20	AX-95142641	AX-94386463	**5.83**	**10.34**	-0.0118	12.5	27.5
116		**HI_N**	**4D**	69	AX-95156869	AX-94988276	**3.67**	**6.66**	0.0102	65.5	69.5
118	**5**	**FlagleafareaxSPAD1_C**	**2B**	262	AX-95164994	AX-94478750	**7.22**	**7.97**	-102.0405	260.5	264.5
118		**FlagLeafArea(cm2)_C**	**2B**	262	AX-95164994	AX-94478750	**4.57**	**6.92**	-1.7445	260.5	264.5
118		**LeafNo./Tiller_C**	**2B**	262	AX-95164994	AX-94478750	**4.57**	**6.92**	-1.7445	260.5	264.5
118		**PH/FLL_C**	**2B**	262	AX-95164994	AX-94478750	**4.57**	**6.92**	-1.7445	260.5	264.5
118		**Length_Low30_TE_N**	**2B**	261	AX-95164994	AX-94478750	**4.65**	**8.79**	-0.0977	254.5	262.5
119		**Perimeter_ME_CN**	**1D**	132	AX-95172164	AX-94458693	**3.45**	**8.63**	-0.0054	131.5	132.5
120		**Length_ME_C**	**7B**	96	AX-95176438	AX-94498748	**3.30**	**5.35**	0.0747	95.5	98.5
121	**9**	**HI_C**	**4D**	79	AX-95179517	AX-94799212	**3.78**	**9.74**	0.0128	69.5	91.5
121		**FLtoEarlength_C**	**4D**	75	AX-95179517	AX-94799212	**17.49**	**31.59**	-2.8338	69.5	80.5
121		**PH:FlagleaftoEar_C**	**4D**	71	AX-95179517	AX-94799212	**6.38**	**14.60**	2.5265	69.5	86.5
121		**Perimeter_Low5_AE_C**	**4D**	93	AX-95179517	AX-94799212	**4.50**	**6.64**	-0.3022	82.5	93.5
121		**Length_Low5_AE_C**	**4D**	93	AX-95179517	AX-94799212	**3.69**	**6.83**	-0.1043	82.5	93.5
121		**FLtoEarlength_N**	**4D**	80	AX-95179517	AX-94799212	**17.07**	**28.40**	-3.6445	74.5	85.5
121		**PH_N**	**4D**	71	AX-95179517	AX-94799212	**6.61**	**10.80**	-4.2912	69.5	79.5
121		**LeafNo./Plant_N**	**4D**	71	AX-95179517	AX-94799212	**6.61**	**10.80**	-4.2912	69.5	79.5
121		**TillerNo./Plant_N**	**4D**	71	AX-95179517	AX-94799212	**6.61**	**10.80**	-4.2912	69.5	79.5
122	**6**	**Area_Top30_TE_C**	**5B**	237	AX-95194941	AX-94547339	**4.04**	**9.15**	0.3847	233.5	241.5
122		**Area_Top5_AE_C**	**5B**	237	AX-95194941	AX-94547339	**4.00**	**8.98**	0.3735	233.5	241.5
122		**AvgChaffWt_AE_N**	**5B**	240	AX-95194941	AX-94547339	**4.39**	**10.00**	0.041	235.5	246.5
122		**AvgChaffWt_TE_N**	**5B**	240	AX-95194941	AX-94547339	**3.62**	**8.63**	0.0548	234.5	247.5
122		**SpikeletFertilityIndex_N**	**5B**	237	AX-95194941	AX-94547339	**4.54**	**10.74**	-3.2018	234.5	244.5
122		**Grainwt./ChaffWt._N**	**5B**	237	AX-95194941	AX-94547339	**4.54**	**10.74**	-3.2018	234.5	244.5
123		**Straw_N**	**4B**	61	AX-95196960	AX-94475207	**6.92**	**5.78**	0.6938	58.5	62.5
124	**5**	**Perimeter_Top30_TE_C**	**5B**	256	AX-95198219	AX-94534815	**3.82**	**9.20**	0.219	255.5	259.5
124		**Perimeter_Top5_ME_C**	**5B**	257	AX-95198219	AX-94534815	**4.36**	**9.38**	0.2636	255.5	260.5
124		**Perimeter_Top5_AE_C**	**5B**	256	AX-95198219	AX-94534815	**4.33**	**8.62**	0.2201	255.5	260.5

124		**Length_Top5_ME_C**	**5B**	256	AX-95198219	AX-94534815	**6.07**	**9.19**	0.0978	255.5	259.5
124		**Length_Top5_AE_C**	**5B**	256	AX-95198219	AX-94534815	**3.76**	**6.38**	0.0718	255.5	259.5
125		**LWR_TE_CN**	**6B**	122	AX-95205691	AX-94439435	**3.28**	**5.94**	-0.0078	117.5	122.5
126		**SeedCount_TE_N**	**6B**	50	AX-95210974	AX-95126184	**8.82**	**4.32**	-19.5908	49.5	50.5
128		**Length_TE_C**	**4D**	152	AX-95215056	AX-94962854	**5.39**	**7.90**	-0.0872	147.5	154.5
129	**3**	**Perimeter_Low30_TE_N**	**2B**	260	AX-95217512	AX-95164994	**4.52**	**7.34**	-0.2819	253.5	262.5
129		**Perimeter_Low5_AE_N**	**2B**	260	AX-95217512	AX-95164994	**3.35**	**2.75**	-0.2554	253.5	262.5
129		**Length_Top5_AE_N**	**2B**	260	AX-95217512	AX-95164994	**3.91**	**4.89**	-0.0662	252.5	262.5
130		**Length_Top5_ME_N**	**5A**	91	AX-95235763	AX-95112161	**3.70**	**6.91**	-0.0775	86.5	93.5
130		**Length_Top5_AE_N**	**5A**	91	AX-95235763	AX-95112161	**4.80**	**6.23**	-0.0742	86.5	93.5
131		**Perimeter_Top5_ME_C**	**3D**	302	AX-95245565	AX-95124939	**4.35**	**8.96**	0.2582	300.5	305.5
134		**Spikeletno._N**	**2B**	46	AX-95258478	AX-94856684	**9.82**	**9.66**	-0.5038	41.5	46.5
135		**DTA_C**	**4A**	199	AX-95630121	AX-94419673	**3.50**	**7.20**	0.6844	198.5	199.5
136	**2**	**Phy5:DTB_C**	**7A**	60	AX-95630495	AX-94724955	**3.42**	**8.69**	0.1285	58.5	63.5
136		**Phy5:DTA_C**	**7A**	59	AX-95630495	AX-94724955	**3.71**	**8.27**	0.1593	57.5	60.5
137	**5**	**AvgSpikeWt_AE_CN**	**1B**	56	AX-95631420	AX-94662545	**4.19**	**8.51**	-0.0376	53.5	56.5
137		**AvgGrainWt_AE_CN**	**1B**	56	AX-95631420	AX-94662545	**4.46**	**9.03**	-0.0381	53.5	56.5
137		**AvgSpikeWt_TE_CN**	**1B**	56	AX-95631420	AX-94662545	**3.73**	**9.58**	-0.0443	53.5	56.5
137		**AvgGrainWt_TE_CN**	**1B**	56	AX-95631420	AX-94662545	**4.56**	**10.42**	-0.0481	54.5	56.5
137		**Width_Top5_AE_CN**	**1B**	55	AX-95631420	AX-94662545	**3.51**	**6.92**	-0.0081	52.5	56.5
138		**LWR_ME_N**	**4A**	36	AX-95631860	AX-94823192	**3.73**	**6.28**	-0.0284	35.5	37.5
139		**Perimeter_AE_CN**	**1D**	130	AX-95633085	AX-94746478	**3.40**	**8.76**	-0.005	126.5	130.5
140	**1**	**GrainN%_C**	**1A**	0	AX-95652677	AX-94542766	**3.35**	**8.45**	0.1027	0	0.5
141	**3**	**Flagleafwidth(cm)_C**	**2D**	343	AX-95654169	AX-94976248	**7.38**	**17.53**	0.0444	341.5	343.5
141		**PHI_ME_N**	**2D**	343	AX-95654169	AX-94976248	**37.38**	**24.10**	-0.0204	341.5	343.5
141		**Width_TE_N**	**2D**	343	AX-95654169	AX-94976248	**3.78**	**9.72**	0.0422	342.5	343.5
142	**2**	**Length_ME_C**	**2D**	341	AX-95683514	AX-95016766	**4.71**	**7.76**	-0.09	334.5	342.5
142		**Length_AE_C**	**2D**	341	AX-95683514	AX-95016766	**3.96**	**5.92**	-0.0752	332.5	342.5
143	**2**	**AvgChaffWt_ME_N**	**7D**	353	AX-95685070	AX-95155766	**5.66**	**8.76**	0.0276	350.5	361.5

143		**Perimeter_Top5_AE_N**	**7D**	371	AX-95685070	AX-95155766	**4.02**	**6.76**	0.206	360.5	373.5